Lecture Notes in Civil Engineering

Ranjith Dissanayake · Priyan Mendis · Kolita Weerasekera · Sudhira De Silva · Shiromal Fernando *Editors*

ICSECM 2019

Proceedings of the 10th International Conference on Structural Engineering and Construction Management

Springer

Lecture Notes in Civil Engineering

Volume 94

Lecture Notes in Civil Engineering (LNCE) publishes the latest developments in Civil Engineering - quickly, informally and in top quality. Though original research reported in proceedings and post-proceedings represents the core of LNCE, edited volumes of exceptionally high quality and interest may also be considered for publication. Volumes published in LNCE embrace all aspects and subfields of, as well as new challenges in, Civil Engineering. Topics in the series include:

- Construction and Structural Mechanics
- Building Materials
- Concrete, Steel and Timber Structures
- Geotechnical Engineering
- Earthquake Engineering
- Coastal Engineering
- Ocean and Offshore Engineering; Ships and Floating Structures
- Hydraulics, Hydrology and Water Resources Engineering
- Environmental Engineering and Sustainability
- Structural Health and Monitoring
- Surveying and Geographical Information Systems
- Indoor Environments
- Transportation and Traffic
- Risk Analysis
- Safety and Security

To submit a proposal or request further information, please contact the appropriate Springer Editor:

– Mr. Pierpaolo Riva at pierpaolo.riva@springer.com (Europe and Americas);
– Ms. Swati Meherishi at swati.meherishi@springer.com (Asia - except China, and Australia, New Zealand);
– Dr. Mengchu Huang at mengchu.huang@springer.com (China).

All books in the series now indexed by Scopus and EI Compendex database!

More information about this series at http://www.springer.com/series/15087

Ranjith Dissanayake · Priyan Mendis ·
Kolita Weerasekera · Sudhira De Silva ·
Shiromal Fernando
Editors

ICSECM 2019

Proceedings of the 10th International Conference on Structural Engineering and Construction Management

Springer

Editors
Ranjith Dissanayake
Department of Civil Engineering
University of Peradeniya
Kandy, Sri Lanka

Kolita Weerasekera
Department of Civil Engineering
The Open University of Sri Lanka
Nugegoda, Sri Lanka

Shiromal Fernando
Civil and Structural Engineering
Consultants (Pvt) Ltd.
Rajagiriya, Colombo, Sri Lanka

Priyan Mendis
Department of Infrastructure Engineering
University of Melbourne
Parkville, VIC, Australia

Sudhira De Silva
Department of Civil and Environmental
Engineering
University of Ruhuna
Galle, Sri Lanka

ISSN 2366-2557 ISSN 2366-2565 (electronic)
Lecture Notes in Civil Engineering
ISBN 978-981-15-7221-0 ISBN 978-981-15-7222-7 (eBook)
https://doi.org/10.1007/978-981-15-7222-7

This Springer imprint is published by the registered company Springer Nature Singapore Pte Ltd.
The registered company address is: 152 Beach Road, #21-01/04 Gateway East, Singapore 189721, Singapore

Preface

It is with great pleasure that we present the Proceedings of the 10th International Conference on Structural Engineering and Construction Management (ICSECM) 2019. This is the ninth consecutively organized conference following a series of International Conferences since 2010, keeping its tradition of adhering to engineering excellence.

Taking a step forward from the last nine events, the coverage of specialty areas in this conference has been diversified. This book contains the manuscripts of research work from many different sub-specialties. These manuscripts were presented at parallel sessions from 13th to 14th December 2019 at ICSECM 2019.

We would like to express our appreciation to all keynotes lecturers for their invaluable contribution for the development of a sustainable world. We are also very grateful to the authors for contributing research papers of high quality. The manuscripts in this proceeding book have been reviewed by a panel of academic and professional experts who have vast expertise in their respective fields. The enormous work carried out by these reviewers is gratefully appreciated as well. We are also pleased to acknowledge the advice and assistance provided by the members of the international advisory committee and members of the editorial committee along with many others who volunteered to assist in order to make this very significant event a success. Furthermore, we acknowledge the financial sponsorship provided by many organizations that have been extremely supportive towards the success of this international conference.

It is the earnest wish of the editors that this proceeding book would be used by the research community and practicing engineers who are directly or indirectly involved in studies related to structural engineering and construction management.

Editorial Committee

The 10th International Conference on Structural Engineering and Construction Management (ICSECM)2019

Kandy, Sri Lanka	Prof. Ranjith Dissanayake
Parkville, VIC, Australia	Prof. Priyan Mendis
Nugegoda, Sri Lanka	Prof. Kolita Weerasekera
Galle, Sri Lanka	Dr. Sudhira De Silva
Rajagiriya, Colombo, Sri Lanka	Eng. Shiromal Fernando

Contents

Element Level Bridge Inspection in the U.S.—Challenges for Assessing Specific Distress Type, Location and Progression

A. R. M. H. B. Amunugama and U. B. Attanayake

Abstract Collapse of the Silver Bridge over Ohio river between West Virginia and Ohio in 1967, which killed over 40 people, highlighted the need of conducting frequent safety inspections. Consequently, the Federal-Aid Highway Act of 1968 was passed that required the U.S. Secretary of Transportation to establish the National Bridge Inspection Standards (NBIS) to ensure the safety of the traveling public. The Act directed the States to maintain an inventory of bridges in the Federal-aid highway system. This Act was amended several times and the Federal Highway Administration (FHWA) revised its regulations to develop the current version of the Standards. The National Bridge Inspection Standards provide guidelines on the types of bridges that are required to be inspected, inspection frequency, qualification of bridge inspectors, and documenting observations and maintenance of bridge inventories. As per the Standards, bridge components are classified into three major groups: bridge deck, superstructure, and substructure. A rating between 0 and 9 is assigned to these three components based on their condition at the time of inspection. Due to several drawbacks associated with the NBIS rating procedures, in early 1990s, element level bridge inspection method was introduced. The AASHTO Manual for Bridge Element Inspection provides the procedures and guidelines for element level inspection. This manual provides two element classifications: National Bridge Elements (NBEs) and Bridge Management Elements (BMEs). Also, highway agencies can define and incorporate additional elements into their databases as Agency-Developed Elements (ADEs). Four levels of condition states are defined with guidance statements for inspectors. This article describes the evolution of bridge inspection procedures, challenges for effective use of data, and the required changes to address specific conditions for improving inspection data accuracy, quality, and usefulness.

Keywords Bridge · Cracking · Distress · Element · Inspection · Standards

A. R. M. H. B. Amunugama (✉) · U. B. Attanayake
Western Michigan University, Kalamazoo, MI, USA
e-mail: a.amunugama@wmich.edu

R. Dissanayake et al. (eds.), *ICSECM 2019*, Lecture Notes in Civil Engineering 94,
https://doi.org/10.1007/978-981-15-7222-7_1

1 Introduction

The U.S. Federal-Aid Highway Act of 1968 was enacted following the historic collapse of Silver Bridge over Ohio river in 1967. The bridge was located between West Virginia and Ohio in the U.S., and the collapse resulted over 40 casualties. The Act required the U.S. Secretary of Transportation to establish the National Bridge Inspection Standards (NBIS) to ensure safety of travelling public [2]. The NBIS establishes minimum qualifications of inspectors, identifies the types of bridges to be inspected, defines inspection frequency and the information to be collected and reported. Finally, load rating is included as part of the NBIS to ensure safety [4]. The revisions were needed to address perceived ambiguities in the NBIS by clarifying the NBIS language, reorganizing the NBIS into a more logical sequence; and making the regulation easier to read and understand [2]. Inspection procedures, rating systems, and documentation process evolved throughout years to enhance bridge management decisions. The current practice is to use component-level inspection, element-level inspection, or a hybrid version of those two methods.

Bridge deck, superstructure, and substructure are the three primary components rated during component-level inspection to report to the Federal Highway Administration (FHWA) for analysis of bridge condition on a national scale, and record in the National Bridge Inspection (NBI) database. A rating scale of 9 (excellent and/or new condition) to 0 (failed condition and/or out-of-service) is used. The respective rating is decided based on the severity of deteriorations at the time of inspection [6]. The outcome is used for asset management purposes. Due to the involvement of large-scale functional and geometric characteristics, use of component-level inspection data at Federal level for decision making activities has eventually become a challenging task. Further, the NBI data is not comprehensive enough to provide adequate information to make performance-based assessment and decisions including the selection of cost-effective repair, rehabilitation, or replacement alternatives. Thus, highway agencies included additional components in their bridge management databases. In addition to assigning a rating, inspectors include a description of observations in their reports. As an example, Michigan Department of Transportation (MDOT) bridge management database includes inspector comments recorded since early 1990s. However, additional refinements to the data collection, documentation, and rating procedures are needed to improve the effectiveness of bridge management decisions and evaluating inter-dependency of bridge elements on distress initiation and rate of deterioration. Based on the positive experience of several Departments of Transportation (DOTs) that included additional bridge components into their management databases, the element level inspection concept, procedures, and guidelines are developed. This article describes the evolution of bridge inspection procedures, challenges for effective use of data, and the required changes to address specific conditions for improving inspection data accuracy, quality, and usefulness.

2 Evolution of Bridge Element Inspection

The condition ratings (0–9) defined as per the National Bridge Inspection Standards were limited to bridge deck, superstructure, and substructure. A rating was assigned without identifying the deterioration process or the extent of deterioration. A significant variability was observed between the ratings assigned by bridge inspectors since a rating was decided based on multiple distress symptoms observed on a component or a localized problem. Also, the NBIS data was primarily used at the Federal level to indicate large-scale functional and geometric characteristics of bridges to present an overall performance within a state or among states rather than using such data for bridge management purposes at the state level. Since the data collected following NBIS is inadequate for making maintenance decisions or conducting research, Pontis Bridge Management System (BMS) was developed by FHWA and Caltrans during 1990–91 period by incorporating a menu of 160 elements with a greater level of details. Utilizing the experience by early adopters of Pontis BMS, the task force created in 1993, under the patronage of FHWA, developed a new standard called the Commonly Recognized (CoRe) elements with a set of 108 standardized elements [5].

The development of the CoRe element manual and adoption of it in 1995 as an official AASHTO manual is significant, since the manual incorporates the definitions of each element, the unit of measurement, definition of a set of standardized condition states, and a list of typical feasible actions for each condition state. Since the condition states defined from CoRe element inspection are different from the NBIS rating, FHWA developed and accepted a translator algorithm in 1997 to convert CoRe element condition data into NBIS condition rating for Federal level analysis. The CoRe element specification allows adding sub-elements and non-CoRe elements. [5] list the guidelines for consideration when defining sub-elements and non-CoRe elements.

In 1998, AASHTO Guide for Commonly Recognized Structural Elements was published. This guide included a total of 98 CoRe elements and eight Smart Flags. The first edition of the Manual for Bridge Element Inspection (MBEI) was published in 2013, with an interim update in 2015 [1]. MBEI provides two element types identified as National Bridge Elements (NBEs) or Bridge Management Elements (BMEs), as well as guidance for defining Agency-Developed Elements (ADEs), with or without ties to the elements defined in the manual. The latest edition of the manual includes deck, superstructure, substructure, culverts, bearings, and bridge rail as NBEs; joints, protective systems, and approach slabs as BMEs. In addition, material defects are listed under steel, prestressed concrete, reinforced concrete, timber, other materials, masonry, wearing surfaces, concrete reinforcing steel, steel protective coatings, and concrete protective coatings. The manual defines four Condition States (CSs) for NBEs, BMEs, and material defects with descriptions of defects that bridge inspectors can use for deciding a specific condition state of an element or a material defect. As an example, Fig. 1 shows the condition state definitions for various defects observed on Element 109: Pre-stressed concrete open girder/beam. Further, the manual lists

3.3.1.6—Element 109—Prestressed Concrete Open Girder/Beam

Description: Pretensioned or post-tensioned concrete open web girders regardless of protective system.

Classification: NBE **Units of Measurement**: ft

Quantity Calculation: Sum of all the lengths of each girder.

Condition State Definitions

Defects	Condition States			
	1	2	3	4
	GOOD	FAIR	POOR	SEVERE
Delamination/Spall/ Patched Area (1080)	None.	Delaminated. Spall 1 in. or less deep or 6 in. or less in diameter. Patched area that is sound.	Spall greater than 1 in. deep or greater than 6 in. diameter. Patched area that is unsound or showing distress. Does not warrant structural review.	The condition warrants a structural review to determine the effect on strength or serviceability of the element or bridge; OR a structural review has been completed and the defects impact strength or serviceability of the element or bridge.
Exposed Rebar (1090)	None.	Present without measurable section loss.	Present with measurable section loss but does not warrant structural review.	
Exposed Prestressing (1100)	None.	Present without section loss.	Present with section loss but does not warrant structural review.	
Cracking (PSC) (1110)	Width less than 0.004 in. or spacing greater than 3 ft.	Width 0.004–0.009 in. or spacing 1.0–3.0 ft.	Width greater than 0.009 in. or spacing less than 1 ft.	
Efflorescence/Rust Staining (1120)	None.	Surface white without build-up or leaching without rust staining.	Heavy build-up with rust staining.	
Damage (7000)	Not applicable.	The element has impact damage. The specific damage caused by the impact has been captured in Condition State 2 under the appropriate material defect entry.	The element has impact damage. The specific damage caused by the impact has been captured in Condition State 3 under the appropriate material defect entry.	The element has impact damage. The specific damage caused by the impact has been captured in Condition State 4 under the appropriate material defect entry.

Fig. 1 Condition state definitions for various defects observed on Element 109: Prestressed concrete open girder/beam (Adapted from [1])

feasible actions by material type under each condition state defined for material defects. However, the actions listed in the manual are not explicit and need further research to develop lists of comprehensive action plans for each type and extend of deterioration.

3 Recording Bridge Element Inspection

Condition state (CS) of each element is decided based on the severity of distress. Since documenting specifics on distress types and extent of deterioration are not mandatory, agencies follow their own policies and procedures while assigning a condition state. However, necessary guidance is provided to bridge inspectors with pictures and additional information on specific distress types as footnotes of the CS tables. As an example, Fig. 2 shows the Michigan Department of Transportation (MDOT) CS Table for Prestressed Concrete Elements. Even though this table does not provide crack width and spacing details similar to AASHTO MBEI manual tables, the follow-up pages of the Michigan Bridge Element Inspection Manual [3] provides pictorial descriptions of distress types and a description on the significance of crack widths to support bridge inspectors make informed decisions to assign a CS for a specific element. AASHTO MBEI manual procedures are developed with a much broader vision. As an example, documentation of crack widths, spacing, intensity, etc., can be accomplished in future with the availability of Unmanned Aerial Vehicles (UAV) and artificial intelligence (AI) enabled inspection systems. On the other hand, MDOT needs to have practically implementable procedures since it is not practical for inspectors to document distress type and extent at the level described in the AASHTO MBEI during biennial inspection.

CS TABLE 2 – PRESTRESSED CONCRETE

Defects	Condition State 1	Condition State 2	Condition State 3	Condition State 4
	GOOD	FAIR	POOR	SEVERE
Spalls/ Delaminations/ Patch Areas (1080)	None.	Delaminated. Spall 1 in. or less deep or less than 6 in. diameter. Patched area is sound.	Spall greater than 1 in. deep or greater than 6 in. diameter. Patched area is unsound or showing distress. Does not warrant structural review.	The condition warrants a structural review to determine the effect on strength or serviceability of the element or bridge; OR a structural review has been completed and the defects impact strength or serviceability of the element or bridge.
Exposed Rebar (1090)	None.	Present without section loss.	Present with section loss that does not warrant structural review.	
Exposed Prestressing (1100)	None.	Present without section loss.	Present with section loss that does not warrant structural review.	
Cracking [1] - PSC (1110)	Insignificant cracks or moderate-width cracks that have been sealed.	Unsealed moderate-width cracks or unsealed moderate pattern (map) cracking.	Wide cracks or heavy pattern (map) cracking.	
Efflorescence / Rust Staining (1120)	None.	Surface white without build-up or leaching without rust staining.	Heavy build-up with rust staining.	
Settlement - Substructure (4000)	None.	Exists within tolerable limits or arrested with effective actions taken to mitigate.	Exceeds tolerable limits but does not warrant structural review.	
Scour - Substructure (6000)	None.	Exists within tolerable limits or arrested with effective countermeasures.	Exceeds tolerable limits but is less than the limits determined by scour evaluation, and does not warrant structural review.	
Damage (7000)	Not applicable.	The element has minor damage caused by vehicular or vessel impact.	The element has moderate damage caused by vehicular or vessel impact.	The element has severe damage caused by vehicular or vessel impact.

Fig. 2 Condition state definitions for various defects observed on prestressed concrete elements (Adapted from [3])

4 Limitations of the Current Procedures

As discussed previously, the element level inspection procedures allow defining ADEs. As an example, Fig. 3 shows few ADEs in the Michigan Bridge Element Inspection Manual [3]. Even though it is advantageous to have ADEs, use of just the CSs for further analysis and decision making are challenging since all possible distress types are not included and quantitative data is not collected. As an example, beam end deterioration (826) shown in Fig. 3 as an ADE does not document end cracking.

Another limitation of the current procedures is observed with respect to documentation of distress location and quantity. Figure 4 shows longitudinal cracking observed on the bottom flange of fascia beams. Typically, these cracks are observed on the exterior face of the fascia beams. As shown in the figure, Bridge 1 had cracking only on one of the approach spans while Bridge 2 had cracking along all 3 spans. Since such distresses on bridge girders are documented in terms of length with respect to the total length of all the girders, the percent of cracking of girders will be very small. Further, without ADEs for fascia beams, the location of such cracks cannot be located. With such limitations in data collection and documentation, the only option available is to analyse bridge inspector comments documented in the Structure Inventory Appraisal (SIA) reports.

CS TABLE 9 – BEAM END (Deterioration, Contact, Temp Support)

	Condition State 1	Condition State 2	Condition State 3	Condition State 4
Defects	**GOOD**	**FAIR**	**POOR**	**SEVERE**
Beam End Deterioration (826)	Section loss to element has been repaired.	Section loss exists and has not been repaired. Structural analysis is not yet warranted.	Measurable section loss that warrants detailed inspection to determine remaining section.	The condition warrants a structural review to determine the effect on strength or serviceability of the element. A request for action (RFA) should be submitted requesting a structural evaluation and/or repairs.
Beam End Contact (844)	Beam ends have been modified to address contact.	Beam ends are in contact. No visible distress observed.	Beam ends are in contact, distress is observed.	
Beam End Temporarily Supported (845 SH, 846 FH)	Temporary support(s) in place and functioning as designed.	Minor section loss on temporary support.	Moderate section loss on temporary support.	

Fig. 3 An example of ADEs (Adapted from [3])

(a) Bridge 1 (b) Bridge 2

Fig. 4 Longitudinal cracking on fascia beams

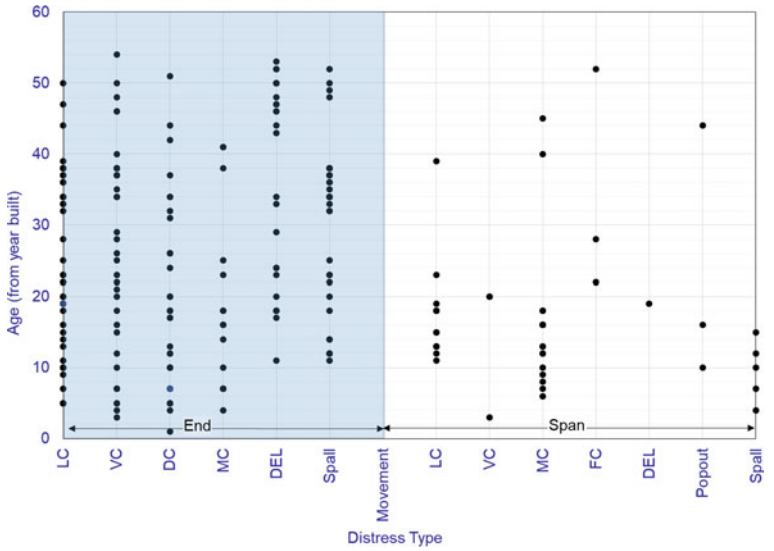

Fig. 5 Age of PC beam and type and location of distress

As an example, bridge inspector comments of 127 prestressed concrete girder bridges were reviewed and the type and location of distress (LC—longitudinal cracking, VC—vertical cracking, DC—diagonal cracking, MC—map cracking, DEL—delamination, spall, movement, and popout) were documented. As shown in Fig. 5, a large number of beams had end cracking but were unable to identify from element inspection data. Analysis of inspector comments also had several challenges. The most significant challenge was due to inconsistent terminology and format.

5 Summary, Conclusions, and Recommendations

Evolving bridge inspection procedures were reviewed. Element level inspection procedures show a significant improvement compared to the National Bridge Inspection Standards. However, practical implementation challenges are observed with regards to collecting quantitative data and documenting distress types and locations. Another challenge was to have all bridge inspectors using consistent terminology for the comments recorded in the Structure Inventory and Appraisal reports. The following recommendations are derived from the work presented in this article:

1. Expand the current version of pictorial guidance provided in the inspection manuals to include every distress type allowing the inspectors to select appropriate pictures to describe observations rather than providing comments.

2. Develop additional ADEs for fascia girders and specific distress types.
3. Calculate percent of distress per girder or end region length to identify the significance of distress.

References

1. AASHTO (2015) Manual for bridge element inspection, with 2015 Interim, 444 North Capitol Street, NW Suite 249, Washington, DC 20001, USA
2. FR (2004) Federal register—rules and regulations, vol 69, no 239, pp 74419–74439, December 14, 2004
3. MDOT (2015) Michigan bridge element inspection manual. Michigan Department of Transportation, 425 W. Ottawa St., P.O. Box 30050, Lansing, MI 48909
4. Ryan TW, Mann JE, Chill ZM, Ott BT (2012) Bridge Inspector's Reference Manual (BIRM). Report No. FHWA NHI 12-049, the Federal Highway Administration, National Highway Institute, 1300 N. Courthouse Road, Arlington, Virginia 22201, USA
5. Thompson PD, Shepard RW (2000) AASHTO commonly-recognized bridge elements, Successful applications and lessons learned. The handout prepared for the national workshop on Commonly Recognized Measures for Maintenance. http://www.pdth.com/images/coreelem.pdf. Last accessed 20 Oct 2019
6. Washer G, Hammed M, Brown H, Fogg J, Salazar J, Leshko B, Conner R, Koonce J, Karper C, Jansen P (2019) Guidelines to improve the quality of element-level bridge inspection data. NCHRP Report 259, the National Cooperative Highway Research Program, the National Academies of Sciences, Engineering, and Medicine, Washington, DC 20001, USA

A Multi-scale Model for Predicting the Compressive Strength of Ordinary Portland Cement (OPC)

S. Krishnya, Y. Yoda, and Y. Elakneswaran

Abstract Realistic prediction of mechanical properties and performance of the Ordinary Portland Cement (OPC) is frequently required, as the OPC plays the key role in concrete material that is broadly used in construction industry. This paper aims to predict the compressive strength of hydrated cement paste by a multi-step approach incorporating thermodynamic and multi-scale models in two subsequent steps. In step 1, the thermodynamic model developed in PHREEQC platform was amended and extended to predict the volume fraction of hydration products. In the consequent step, the multi-scale analytical model was developed to predict the compressive strength of the cement paste. This step comprises three hierarchical levels, initiates the model at nano-scale to the way up to micro-scale, which are sequentially C-S-H globule, C-S-H foam (includes capillary porosity) and the cement paste (consist of hydration products, porous and unhydrated cement). In this approach, as a key concept, the formation of calcium silicate hydrate (C-S-H) was distinctly considered in low and high-density states to an accurate prediction. The results obtained from the previous step was implemented to the subsequent step, and by the end of each step, the predictions were successfully verified with the experimental data reported in the literature. The comparison of model outcomes suggests high predictive capability of the model; however, the proposed model can be possibly valid to the conditions used herein, and to generalize the model, further verifications are highly recommended, left for the future work.

Keywords Hydration products · Volumetric prediction · Calcium-silicate-hydrate (C-S-H) · Compressive strength · Multi-scale model

S. Krishnya (✉) · Y. Elakneswaran
Division of Sustainable Resources Engineering, Faculty of Engineering, Hokkaido University, Sapporo, Japan
e-mail: krishnya@eis.hokudai.ac.jp

Y. Yoda
Center for Construction Engineering, Shimizu Corporation, Shimizu Institute of Technology, Tokyo, Japan

R. Dissanayake et al. (eds.), *ICSECM 2019*, Lecture Notes in Civil Engineering 94,
https://doi.org/10.1007/978-981-15-7222-7_2

1 Introduction

Mechanical properties of OPC such as compressive strength, Poisson's ratio and Young's modulus are significant parameters used in structural designs and analyses. Hydration products and porosity take a leading role in determining the microstructure of hardened cement, hence results in the evolution of the mechanical properties [8, 17]. Up to the date, several macro-scale investigations have been aimed to describe the progression of mechanical properties based on various concepts including degree of hydration, maturity concept and percolation theory. However, such approaches provide insufficient information regarding the progression mechanism of strength at fine scales (nano-micro), and henceforth, they are considered only as the preliminary step towards a comprehensive material-to-structural design approach. Few studies have attempted to deal with porosity or gel-space ratio to assess the progression of strength [2, 13]. However, the Connectiveness between micro and macromechanics i.e. the deep understanding of the nano-microstructure of cement, hydration products and how they are related to the mechanical properties, is still missing.

The nano-microstructures of the cement pastes are very complicated, and that have not been completely understood yet. Typically, several products are formed during the hydration process of the OPC, and the product that contributes substantially to the strength is C-S-H which has a high specific surface area with a complex pore structure [16]. During the early stages of hydration, production of C-S-H nucleates at the surface of unreacted cement grains, leading to the development of soft outer products with low density. While outer products are continuously formed, fresh C-S-H matrix would start forming within the space confined by the existing C-S-H layer, and this newly formed C-S-H has higher density.

The aim of this paper is to predict the compressive strength of the OPC paste from the volumetric prediction of hydration products. The volumetric fractions of hydration products were predicted by extending the thermodynamic model developed in coupled PHREEQC platform, followed by the multi-scale model to evaluate the compressive strength. The originality of the proposed approach relies on the multi-scale model that starts at nano level of the C-S-H matrix, along with a distinct consideration of low density C-S-H (LD C-S-H) and high density C-S-H (HD C-S-H) at the assessment.

2 Model Description

Several studies have demonstrated that chemical thermodynamic modelling, coupled with thermodynamic databases, could reliably predict hydrated cement phase assemblages and chemical compositions. As such, the coupled thermodynamic model (combination of both PHREEQC module and Excel) proposed by Elakneswaran et al. [4] was employed in this study to model the assemblage of OPC hydrates by weight. Previously, this model has been investigated on various cements such as OPC,

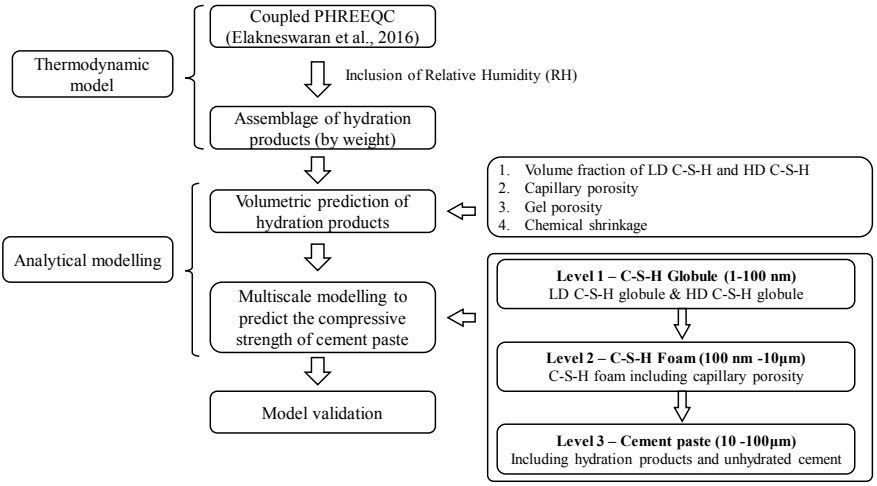

Fig. 1 Flow chart of the model design

slag cement, lime cement and ferrite-rich cement and have verified to the accurate prediction of weight fractions of the hydrates as a function of hydration time [4, 5]. The flow chart outlining all the steps carried out in this study is presented in Fig. 1. As the first step, the coupled thermodynamic model was amended by the inclusion of relative humidity (Fig. 1). The method is described in Sect. 2.1.

2.1 Inclusion of Relative Humidity (RH)

The RH phenomenon is one of the crucial factors that significantly vary during the hydration process, in particular, the external drying and self-desiccation cause the decrease in humidity [15]. However, the existing model does not incorporate the decrease in pore RH caused by hydration. Therefore, this study attempted to modify the existing model slightly by integrating the RH phenomenon to accurately reflect hydration assemblage. The empirical relationships that have been experimentally developed in the previous studies [11, 12, 15] were adopted. Equations (1) and (2) are based on w/c ratio of the cement paste: high and low w/c ratios i.e. $w/c > 0.4$ and $w/c \leq 0.4$ respectively.

$$\text{for } w/c > 0.4,\ RH(\%) = 100t^{\left(0.07\left(\frac{w}{c}\right)-0.0435\right)} \tag{1}$$

$$\text{for } w/c \leq 0.4,\ RH(\%) = 100t^{\left(-4.5\left(\frac{w}{c}\right)^2+3.471\left(\frac{w}{c}\right)-0.6859\right)} \tag{2}$$

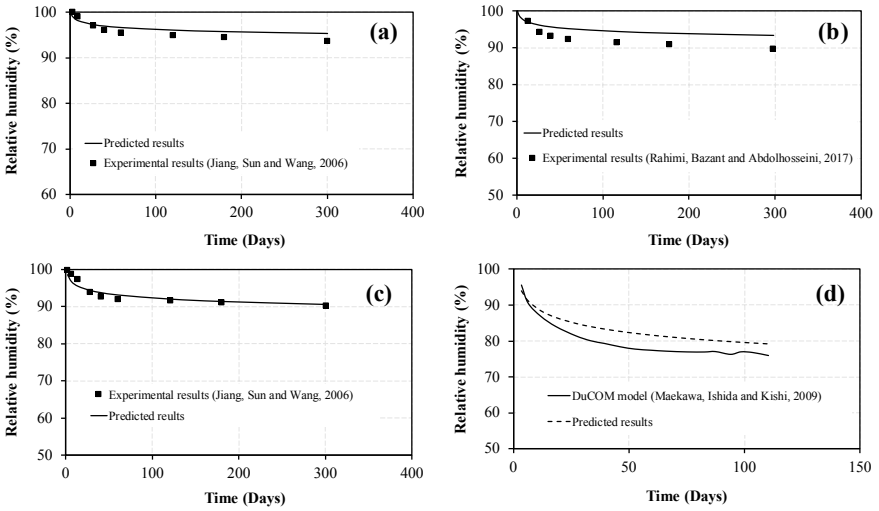

Fig. 2 Predictive capacity of developed RH's relationships **a** w/c of 0.5, **b** w/c of 0.45, **c** w/c of 0.4, and **d** w/c of 0.3

The predictive capabilities of the *RH*'s relationships are shown in Fig. 2 in the form of a plot of predicted versus experimental results for two random w/c ratios for each equation; w/c ratios of 0.5 and 0.45 for Eq. (1) (Fig. 2a, b) and w/c ratios of 0.4 and 0.3 for Eq. 2 (Fig. 2c, d). It can be seen that both of the relationships accurately predict the *RH* of the cement paste.

2.2 Volumetric Prediction of Hydration Products

2.2.1 Volume Fraction of C-S-H

The concept of two types of C-S-H (HD C-S-H and LD C-S-H) were introduced at this step of the model. The weight of the total C-S-H predicted at the previous step (coupled thermodynamic model) was further sorted into HD C-S-H and LD C-S-H by using the relationship (Eq. 3) proposed by Tennis and Jennings [16]. Each type of C-S-H contains a specific amount of gel porosity, leading to different densities i.e. the densities of HD C-S-H and LD C-S-H are 2000 kg/m^3 and 1700 kg/m^3 respectively [10].

$$M_r = 3.017.\frac{w}{c}.\alpha - 1.347.\alpha + 0.538 \tag{3}$$

where, M_r is ratio of the mass of LD C-S-H to the total mass of C-S-H, *w/c* is water cement ratio and α is degree of hydration.

2.2.2 Capillary Porosity

Capillary porosity is one of the most important factors that determines the mechanical properties of the cement paste, and that presents depending on the degree of hydration and w/c ratio. The percentage of the sum of capillary porosity and chemical shrinkage was calculated as follows (Eq. 4). As the effect of chemical shrinkage is relatively negligible, it has not been considered in the analysis reported by previous researchers [16]. However, the effect of chemical shrinkage is taken into the model reported herein.

$$V_c = V_i - \left(V_p + V_{rr}\right) \tag{4}$$

where, V_c is volume of sum of capillary porosity and chemical shrinkage, V_i is initial volume of cement paste, V_p is volume of products and V_{rr} is volume of remaining reactants. As mentioned earlier, each type of C-S-H contains a specific amount of gel porosity. The gel porosity in LD C-S-H is 36% and 26% for HD C-S-H [10].

2.2.3 Chemical Shrinkage

Theoretically, the chemical shrinkage is caused by the volume change during hydration process. The coefficients of chemical shrinkage proposed by Bentz, Lura and Roberts [1] for every phase of the clinker as shown in Table 1 were used in the analysis. During the analysis, the capillary porosity was calculated by deducting the chemical shrinkage from the porosity reported in (Eq. 4), which comprised of capillary and chemical shrinkage.

Table 1 Coefficients for chemical shrinkage

Cement phase	Coefficient/(g water/g solid cement phase)
C_3S	0.0704
C_2S	0.0724
C_3A (Convert all C_3A to ettringite)	0.171
C_3A (Convert all C_3A to Monosulfoaluminate)	0.115
C_4AF (Convert all C_4AF to ettringite)	0.117
C_4AF (Convert all C_4AF to Monosulfoaluminate)	0.086

2.3 Hierarchical Modelling

For predicting the compressive strength, the microstructure of hardened cement paste was contemplated in three levels of hierarchical modelling as illustrated in Fig. 1. Each level of the model represents the cement material at different scales i.e. the scale of the matrix ranges from nano to micro. It should be noted that the volume of C-S-H considered in this multiscale model includes the gel porosity.

Level 1: Bottommost level of this hierarchical model, which focuses only the C-S-H globules with two different densities (high and low) as explained earlier. The characteristic scale of this level bounds between 1 nm and 100 nm. The volume fraction of HD C-S-H (Φ_{CSH-HD}) existing in total C-S-H was computed by using Eq. (5), in which the results obtained at the volumetric prediction of hydration products was used (see Sect. 2.2).

$$\Phi_{CSH-HD} = \frac{V_{HDCSH}}{V_{TotalCSH}} \tag{5}$$

where, V_{HDCSH} is volume fraction of HD C-S-H and $V_{TotalCSH}$ is volume fraction of total C-S-H. From Eq. (6), the actual packing density of C-S-H globule (η_{glob}) was interpolated. The packing density of LD C-S-H (η_{CSH-LD}) and HD C-S-H (η_{CSH-HD}) were 0.63 and 0.76 respectively [3].

$$\eta_{glob} = \eta_{CSH-LD} + (\eta_{CSH-HD} - \eta_{CSH-LD})\Phi_{CSH-HD} \tag{6}$$

The relationship between the packing density and tensile strength of C-S-H globule ($f_{t,CSH}$) was given in Eq. (7) [14]. As reported by Hlobil, Šmilauer and Chanvillard [7], the apparent tensile strength of C-S-H globule ($f_{t,glob}$) was considered as 320 MPa.

$$f_{t,CSH} = f_{t,glob} \exp\left(\frac{1.293\left(\eta_{glob}^{13.011} - 1\right)}{\eta_{glob}}\right) \tag{7}$$

The tensile strength of C-S-H globule ($f_{t,CSH}$) which has been calculated by using the above relationship (Eq. 7) was used to estimate the compressive strength of C-S-H globule ($f_{c,CSH}$). The popular relationship proposed in Griffith model i.e. uniaxial compressive strength to tensile strength ratio equals to 8, was used for the above prediction [6].

Level 2: C-S-H foam including C-S-H globule and capillary porosity was considered in this level, and the scale of this level can be defined within the range from 100 nm-10 μm. The C-S-H space ratio (Υ_{CSH}) proposed by Hlobil et al. [7] was considered in this level (Eq. 8). Volume fraction of C-S-H (Φ_{CSH}) and capillary porosity (Φ_{cap}) were obtained from the volumetric prediction model (See Sect. 2.2).

$$\Upsilon_{CSH} = \frac{\Phi_{CSH}}{\Phi_{CSH} + \Phi_{Cap}} \tag{8}$$

Compressive strength of C-S-H foam ($f_{c,CSHfoam}$) was computed using the $f_{c,CSH}$ obtained in the previous level (Level 1) by Eq. (9) [7]. β is the C-S-H distribution factor, and the applicable range of β for the Eqs. (10) and (11) has been defined to be between 0.4 and 1.0. C_1 and D_1 are the parameters as a function of β. It should also be noted that the lower β value represents denser C-S-H distribution.

$$f_{c,CSHfoam} = f_{c,CSH}\exp\left(-\frac{C_1\left(1-\Upsilon_{CSH}^{D_1}\right)}{\Upsilon_{CSH}}\right) \tag{9}$$

$$C_1 = 1.101\exp\left(-\frac{0.296(\beta-1)}{\beta}\right) \tag{10}$$

$$D_1 = -11.058\beta^{1.987} + 16.191\beta \tag{11}$$

Level 3: This final level incorporates the C-S-H foam, unhydrated clinker and other hydration products, extending the model to the cement paste. The characteristic scale of this level ranges 10–100 μm. The compressive strength of the cement paste ($f_{c,cp}$) was eventually predicted from Eq. (12) [7]. The volume fraction of solids other than C-S-H ($\Phi_{inclusion}$) was derived from the volumetric prediction model (Sect. 2.2).

$$f_{c,cp} = f_{c,CSHfoam}(0.758 + (1-0.758)\exp(-29.3\Phi_{inclusion})) \tag{12}$$

Finally, the predicted results from this model were successfully validated with the available experimental results found in the literatures.

3 Results and Discussion

3.1 Volumetric Prediction of Hydration Products

The extended model for the prediction of volume fraction for hydrates were validated for capillary porosity and the chemical shrinkage. The capillary porosity and chemical shrinkage verses the hydration period is presented in Fig. 3, comparing the results obtained from this extended model with the experimental results reported by Igarashi and Maruyama [9] for the w/c of 0.4 (Fig. 3a, b respectively).

The comparison shows a very good agreement of predicted results with experimental data for capillary porosity and chemical shrinkage. For the w/c of 0.4, the predicted capillary porosity (Fig. 3a) after 1 day and 320 days are 37.08% and

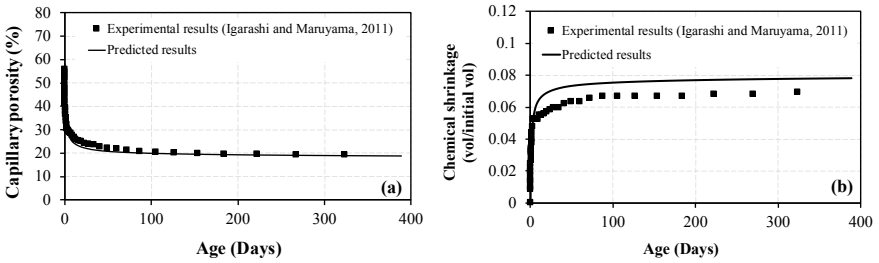

Fig. 3 Comparison of predicted results with experimental results for **a** capillary porosity and **b** chemical shrinkage of w/c of 0.4

19.05% respectively while the experimental results are 38 and 19.2%. The observation suggests the exponential increase of chemical shrinkage with increasing hydration period (in Fig. 3b). After 320 days, the experimental and predicted chemical shrinkage of the cement (w/c of 0.4) are 0.0692 and 0.0777 respectively.

Figure 4 presents the overall volumetric prediction of hydration products at the given phase composition (C_3S 65.6%, C_2S 11.7%, C_3A 8.1% and C_4AF 9.6% blaine surface area 343 m^2/kg and density 3.16 g/cm^3) for w/c ratio of 0.4 and the temperature at 20 °C as the reference. It can be seen that the predicted hydrates consist of C-S-H, portlandite, monosulphate and ettringite phases, with a small content of hydrotalcite-like phase and iron-bearing hydrogarnets. Due to the presence of small quantity of calcite, the model has predicted the formation of hemicarboaluminate and monocarboaluminate in OPC. The volumetric prediction also indicates that the formation of C-S-H (41%) is considerably higher compared to the other hydration products at the end of 1000 days. By that time, the predicted chemical shrinkage, capillary porosity and gel porosity are 8.2%, 10.6% and 12.7% respectively.

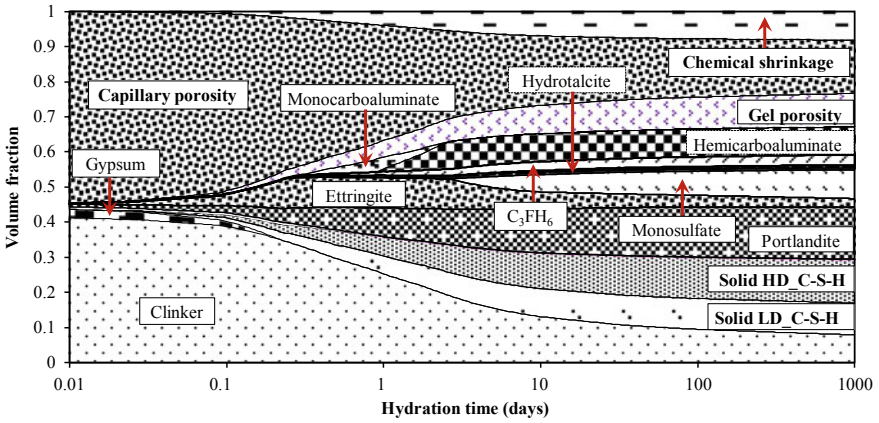

Fig. 4 Volumetric prediction of hydration products as a function of hydration period for OPC w/c 0.4

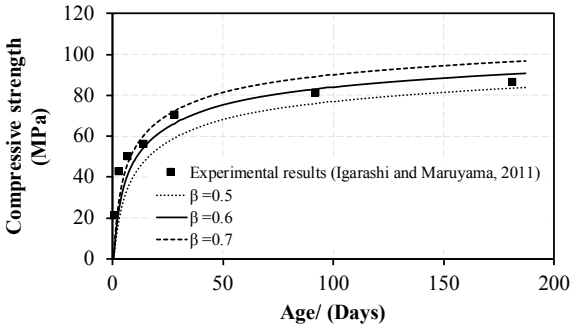

Fig. 5 Comparison of development of compressive strength from experimental results and predicted results of cement paste with w/c 0.4

3.2 Prediction of Compressive Strength

Figure 5 shows the predictive capabilities of the model, comparing the compressive strength from the proposed model with independent set of experiment results found in the literature. The results show that the compressive strength increase with the increase in hydration period. The experimental results, from Igarashi and Maruyama [9], at w/c of 0.4, shows a better agreement with predicted results at β of 0.6. The predicted compressive strength after 28 days is 67 MPa (experiment result of 72 MPa), and the prediction and experiment results after 91 days are 82.3 MPa and 81 MPa respectively. The attained β values fall within the range (0.4–1.0) recommended by Hlobil et al. [7].

4 Conclusions

In this study, the prediction of compressive strength of OPC was successfully demonstrated using a multi-step approach. In the first step, the validated PHREEQC model (prediction of weight assemblage) reported previously was amended to predict the volume fraction of hydrates, particularly the LD C-S-H, HD C-S-H, capillary porosity, chemical shrinkage and gel porosity. The results showed an accurate predictability with the comparison of the experimental results. In the second step, the multi-scale analytical modelling was performed to predict the compressive strength, initiating from C-S-H globule to the way up to the cement paste with the aid of the predicted volume fraction of hydrates in previous step. Finally, the model outcomes of the compressive strength of OPC were verified with w/c ratio of 0.4 using the experimental results. Although its agreement with the experimental data appears to be good, it is only valid under the conditions used, and further validations are required to generalize the model.

References

1. Bentz BYDP, Lura P, Roberts JW (2005) Mixture proportioning for internal curing. Concrete Int 35–40
2. Bentz DP (1999) CEMHYD3D: a three-dimensional cement hydration and microstructure development modeling package
3. Constantinides G, Ulm F-J (2007) The nanogranular nature of C-S–H. J Mechan Phys Solid Pergamon 55(1):64–90
4. Elakneswaran Y, Owaki E, Miyahara S, Ogino M, Maruya T, Nawa T (2016) Hydration study of slag-blended cement based on thermodynamic considerations. Constr Build Mater 124:615–625
5. Elakneswaran Y, Noguchi N, Matumoto K, Morinaga Y, Chabayashi T, Kato H, Nawa T (2019) Characteristics of ferrite-rich portland cement: comparison with ordinary portland cement. Front Mater 1–11
6. Griffith A (1924) Theory of rupture. In: Biezeno C, Burgers J (eds) First international congress for applied mechanics, Delft, pp 55–63
7. Hlobil M, Šmilauer V, Chanvillard G (2016) Micromechanical multiscale fracture model for compressive strength of blended cement pastes. Cem Concr Res 83:188–202
8. Hu C, Hanb Y, Gaob Y, Zhangb Y, Li Z (2014) Property investigation of calcium–silicate–hydrate (C–S–H) gel in cementitious composites. Mater Charact 95:129–139
9. Igarashi G, Maruyama I (2011) Relationship between mechanical properties and phase composition of hardened cement phase (In Japanes). J Struct Constr Eng 76(660):213–222 (in Japanes)
10. Jennings HM, Thomas JJ, Gevrenov JS, Constantinides G, Ulm F (2007) A multi-technique investigation of the nanoporosity of cement paste. Cem Concr Res 37(3):329–336
11. Jiang Z, Sun Z, Wang P (2006) Internal relative humidity distribution in high-performance cement paste due to moisture diffusion and self-desiccation. Cement and Concrete Re Pergamon 36(2):320–325
12. Maekawa K, Ishida T, Kishi T (2009) Multi-scale modeling of structural concrete. Taylor & Francis
13. Maruyama I, Igarashi G (2014) Cement reaction and resultant physical properties of cement paste. J Adv Concr Technol 12(6):200–213
14. Němeček J, Šmilauer V, Němeček J, Kolařík F, Maňák J (2018) Fracture properties of cement hydrates determined from microbending tests and multiscale modeling. In: Computational modelling of concrete structures. CRC Press, pp 113–119
15. Rahimi-Aghdam S, Bažant ZP, Qomi MJA (2017) Cement hydration from hours to a century controlled by diffusion through barrier shells of C-S-H
16. Tennis PD, Jennings HM (2000) A model for two types of calcium silicate hydrate in the microstructure of Portland cement pastes. Cement and Concrete Res Pergamon 30(6):855–863
17. Wang X, Subramaniam KV (2011) Ultrasonic monitoring of capillary porosity and elastic properties in hydrating cement paste. Cement and Concrete Compos 33(3):389–401

Construction of Working Platforms on Expansive Soils Using Recycled Concrete and Stabilizers: A Case Study

H. Karami, D. Robert, S. Costa, F. Tostovrsnik, B. O'donnell, and S. Setunge

Abstract Expansive clay soils are distributed worldwide, and are a source of damages to infrastructure, building foundations and roads due to its low strength, high compressibility and high level of volumetric changes. Due to excessive soil movement, uplift pressure can induce swelling pressure on foundations and shrinkage of clay can result substantial foundation settlements. In order to mitigate such adverse behaviour on structures, underlying clay needs to be improved prior to supporting the structural foundations. This study investigates the capability of enzymatic cement stabilization with recycled concrete to improve soil stability in the application to building foundations. Firstly, a series of experiments was conducted to characterise the Expansive clays obtained from the construction site. Then the experiments were performed on the basis of stabilized soils to investigate the improvement in strength and hydraulic behaviour of expansive soil. Stabilizing mix design obtained from lab tests was applied to construct building foundation on in situ clay base. Structural monitoring of the constructed foundation reveals minimal displacements during drying and wetting periods across 10 years after construction. Results from the current study will assist to derive a new standardized approach for constructing capping layer for buildings and roads using recycled materials and innovative soil stabilization methods.

Keywords Expansive soil · Stabilization · Recycled concrete · Building foundations · Enzyme

H. Karami · D. Robert (✉) · S. Setunge
Civil Engineering Department, School of Engineering, RMIT University, Vic 3001, Australia
e-mail: dilan.robert@rmit.edu.au

S. Costa
School of Engineering, Deakin University, Vic, Australia

F. Tostovrsnik
Site Geotechnical Pty Ltd, Vic, Australia

B. O'donnell
Center for Pavement Excellence Asia Pacific, Melbourne, Australia

R. Dissanayake et al. (eds.), *ICSECM 2019*, Lecture Notes in Civil Engineering 94,
https://doi.org/10.1007/978-981-15-7222-7_3

1 Introduction

Infrastructure damage due to expansive soils is commonly reported in many countries such as in Australia, Canada, England, China, India, and the United States. In the United States alone, expansive soils cause $2.3 billion in damage to houses, buildings, roads, pipelines, and other structures. This is often considered more than twice the damage from floods, hurricanes, tornadoes, and earthquakes [1]. The significant distribution of expansive soils across Victoria (50% of the surfaces of land area [2], also enhances the risk of infrastructure damage in significant terms. Moisture susceptible volume change characteristics of expansive soils always cause costly damages to buildings in terms of inclined cracks in claddings and instability of footings at the corners. Over designing of foundations and slabs to address this problem incur excessive expenses in addition to the overuse of natural resources.

Expansive soils are identified as clay soils which reveal significant volume changes because of change in soil water and wetness. Montmorillonite is the most important mineral in these soils which gives them high swell-shrink potential [3]. Constructing foundations on soils with high amount of montmorillonite has risk of uplift, sinking forces caused by swelling, and consequently heaving and cracking of foundations and structural members [4]. Key engineering characteristics for these soils are the soil moisture content, plasticity, swelling behaviour and dry density which need careful assessment for identifying possible remediation actions. The local conditions that need to be considered for evaluation of expansive soil impact are the amount of clay fraction, initial moisture conditions, and confining pressure [5]. However, the single most important characteristic for expansive soils is the volume change which is a major cause of natural disasters, since they cause extensive damages to the structures and infrastructure built on top of them [6–10]. Additives such as cement, lime, fly ash or their mixtures have been used for elimination of the expansive upward force or swelling of the active soils. However, these approaches are not largely cost effective and some have been noted as not being environment-friendly [11]. Other investigated materials with stabilizing effects are corncob bash, blast furnace slag, steel slag, recycled basanite, marble dust, microbe-inspired cementing, and rice husk ash. Lime and other alkaline stabilizers have a corrosive effect and a negative environmental impact [12, 13].

In recent years, enzymes have been tested as sustainable as well as an environmentally friendly soil stabilizer [14]. Enzyme is considered as a non-traditional stabilizer whereas cement and lime based products belong to traditional category of stabilization. Eko-Soil has been identified as one of the commonly adopted enzymes to stabilize soils in Victoria. In stabilization process of the expansive soil, Eko-soil based stabilization is effective to reduce the plasticity of the soil and increase the overall strength and durability [15]. Modification of the expansive soils with Eko-soil can be used as a sub-base for road embankment material [16].

This paper discusses the efficiency of enzymatic cement combined stabilization and use of recycled concrete in the construction of stabilized working platform which was adopted on highly expansive soils. The foundation of expansive

Table 1 The identification and qualitative classification of soil expansiveness including in situ soil properties

Expansive Nature	Liquid Limit	Plasticity Index	PI<0.425mm	Potential swell(%)
very high	>70	>45	>3200 ☒	>5.0
High ☒	>70 ☒	>45	2200-3200	2.5-5.0
moderate	50-70	25-45 ☒	1200-2200	0.5-2.5 ☒
low	<50	<25	<1200	<0.5

soil was stabilised using three additives: enzymes, blended cement and recycled concrete. The purpose of the stabilization has been considered on improving the mechanical properties which are of interest in foundation design and elimination of the swelling and shrinkage behaviour of soils. Number of onsite/lab experiments were conducted to characterise the plasticity, optimum moisture content (OMC), maximum dry density (MDD), unconfined compressive strength (UCS) and California bearing ratio (CBR) of the stabilized mix. The experiments were part of an actual civil engineering work with a view to use the stabilization approach as a capping layer for building foundations.

2 Materials

2.1 Soil Description

The soil used in this investigation was based on natural soil on the site. Based on the index properties, the expansive nature of the in situ soil can be classified as "high" as demonstrated in Table 1 which shows the criteria for expansive classification according to Australasian road transport and traffic agencies [17]. Based on the index properties, the soil can be classified as silty clay of high plasticity based on the Table 1.

2.2 Stabilizers

The enzymes used for stabilization were sourced from an enzyme based product called Eko-Soil. This commercially available product is brown in colour and has a sweet ferment odour. Store condition for Eko-Soil is between 10 and 40 °C. The characteristics of the enzyme are listed in Table 2.

Eko-Soil is an effective natural material produced by water (20%), non-ironic surfactants (20%) and sugar cane (60%). It reacts with clay particles by organic encapsulation to result densified and aggregated clay structure. This mechanism is capable of producing high strength surface and a stronger structure with a high load bearing capacity and low permeability.

Table 2 Properties of Eko-Soil [18]

Properties	Value
Specific gravity	1.05
Boiling point	100 °C
Evaporation rate	Same as Water
Vapour pressure	Same as Water
Melting point	N/A
Appearance	Brown Colour
Odour	Slight Ferment

In the industry applications, dilution mass ratio (DMR) of 1:500 and application mass ratio (AMR) of 1% have been specified [18]. DMR is the dilution ratio of the product in water whereas AMR is the ratio of mass of the product to the dry soil mass. The proposed treatment with enzymes for expansive soil is an anti-expansive treatment to reduce the expansiveness of the clayey soil.

The cement used in the experiments is general purpose blended cement. A proportion of 3% blended general-purpose cement was used in the stabilization process adopted in the current study.

2.3 Recycled Concrete

Use of recycled concrete material has been identified as a sustainable, cost effective and environment friendly application in many construction projects. Recycled concrete used in this project was sourced from a local landfill in Victoria for constructing the stabilized working platform. A proportion of 20% recycled concrete was used in the stabilization mix.

3 Site Location and Classification

The area map of the location is shown in Fig. 1 with approximate test locations. The site covers an area of approximately 5000 m^2 (part of the estimated 36,600 m^2 of retailing area), predominantly rectangular in shape and is situated in the eastern suburbs of Melbourne. The soil profile encountered at this site is considered consistent with the geology of the area, mainly comprising of silty fine sands which overlie high plasticity silty clay.

The proposed working platform on the soil subgrade is identified as 300 mm thick stabilised layer overlying the clay subgrade as shown in Table 3.

The ground profile obtained from site investigation is shown in Table 4. This information along with the geology/climatic information of the area reveal that the

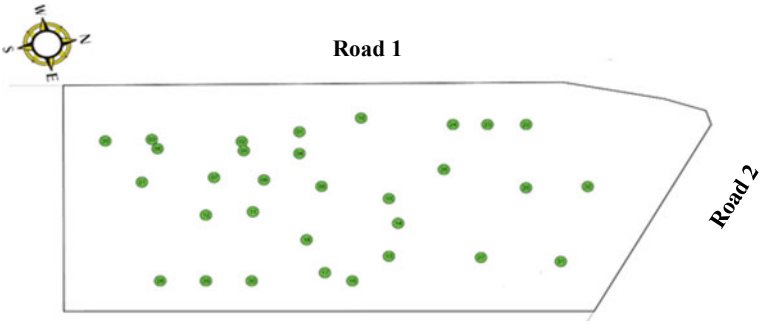

Fig. 1 Site plan with approximate 32 test locations

Table 3 Site profile up to 300 mm depth

Layer 1 (Working Platform)	Layer 2 (Subgrade)
Crushed Recycled Concrete Blended GP Cement Enzyme (Eko–Soil)	Silty CLAY of high plasticity

site can be subjected to soil movements as identified from Australian Standard [19] residential slabs and footings, which characterises the reactivity as Class M[1] [19]. i.e. the site consists of moderately reactive clay or silt with potential seasonal differential surface movement and ground movements due to moisture changes (i.e. surface movement of 20 mm to 40 mm according to [19].

4 Testing Program

A series of experiments was conducted, first to characterise the materials and then to evaluate the efficiency of in situ clay stabilization in terms of mechanical and hydraulic behaviour. These include index tests (i.e. density, specific gravity, liquid limit, plastic limit, plasticity index, compaction limits), mechanical tests (i.e. California bearing ratio (CBR) and unconfined compressive strength (UCS)) and hydraulic tests (i.e. permeability). The time dependent efficacy of stabilization has also been evaluated by testing the samples at various curing times (i.e. 3, 7, 14 and 28 days). Tests were conducted in accordance with Australian standards and brief description of the test methods are discussed below.

- The rapid Hilf compaction test was conducted using standard compaction effort. The results were used to compare with field density data and to determine the

[1]Moderately reactive clay or silt sites, which may experience moderate ground movement from moisture changes.

Table 4 Field classification summary

Depth (m)	Field Description of Materials	Sample depth (m)		In situ Moisture
		From	To	
0.150	GW, Sandy, Medium Gravel FILL Brown/grey			
0.300	GC, Clayey, Medium Gravel trace Sand FILL Brown, Moist Well Graded	0.200	0.300	MC = 18.6%
0.450	CI, Gravelly, Clay trace Sand FILL (of medium plasticity) Brown Firm			
0.780	CI, Silty, Clay with Gravel FILL (of medium plasticity) Orange/red Soft	0.550	0.600	MC = 25.3%
0.850	CI, Clay trace Gravel, FILL (of medium plasticity) Orange grey and red Firm Becoming stiff at 0.8 m depth	0.800	0.850	MC = 28.6%

density ratio for the purposes of compaction control of the soil. The test was conducted in accordance with AS 1289.5.7.1 [20].

- UCS tests were conducted on the basis of in situ stabilised and re-compacted samples. Specimens were compacted using standard compaction energy and cured for 3 and 7 day periods according to AS 5101.4 [21].
- CBR tests were conducted on the representative samples from in situ stabilised soil in accordance to AS 1289.6.1.1 [22]. The specimen was prepared using standard compaction energy followed by 2-day curing and 4-day soaking period.
- Permeability tests were carried out on in situ stabilised, re-compacted samples after a 6-day curing period in accordance with AS 1289.6.7.3 [23].

5 Results and Discussion

Results of laboratory experiments conducted on the basis of stabilized and non-stabilized samples are first presented and discussed. Having identified the efficacy of clay stabilization using the proposed approach, in situ clay soil stabilization was then performed to enhance the strength of working platform. Finally, the results of in situ density tests were presented to ascertain the effectiveness of the stabilization application in the field.

5.1 Unconfined Compressive Strength (UCS)

Initial trial tests were conducted using lime in place of blended cement. The reason for adding lime was to assist drying out the subgrade and improve performance under the prevailing wet conditions. This trial mixture consisted of 3% lime, 20% recycled concrete, 1% Eko-soil enzyme and clay. The UCS strength determined from this mixture returned a value of 0.2 MPa after 7 Days. Then a second trial mixture was prepared replacing lime with cement. This mixture contained a combination of additives with 3% blended general-purpose cement, 20% recycled concrete, 1% Eko-soil enzyme and clay. The second mixture returned a UCS strength of 0.7 MPa after 7 Days. Based on these UCS results, general purpose blended cement was used instead of lime in the working platform construction.

UCS results (Fig. 2) based on final stabilized mix (i.e. recycled aggregate, cement, Eko-Soil and clay) indicate a high level of performance exceeding conventional unbound granular material. It is important to note that there was no intention to

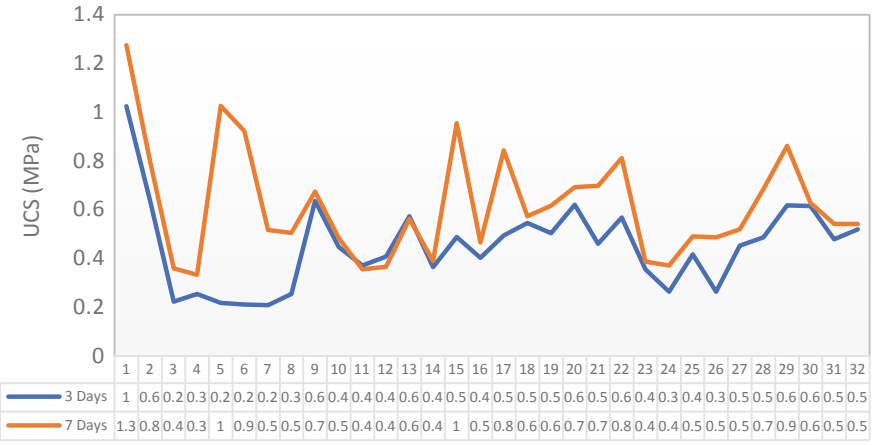

Fig. 2 UCS test result for the stabilized clay with mix of crushed recycled concrete, cement and Eko-enzyme

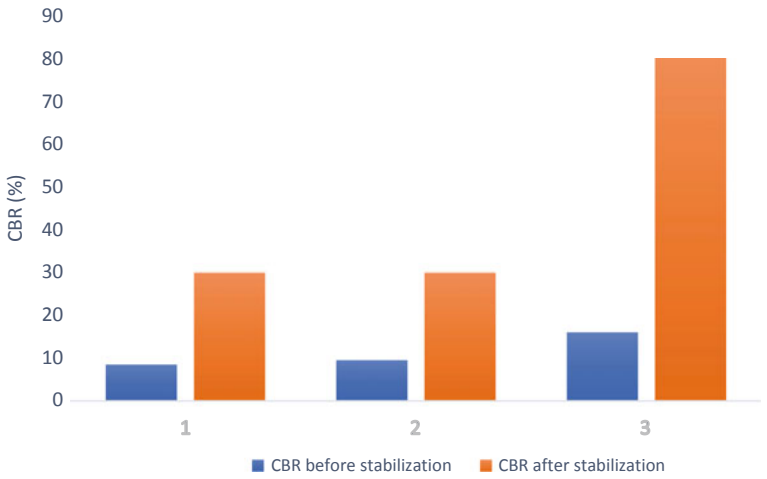

Fig. 3 CBR test results based on recycled concrete, clay and Eko-enzyme

produce a cemented base course product in the modification process. Cemented base course layers are susceptible to shrinkage and fatigue cracking. They also require a strategy to mitigate the effect of early shrinkage cracking and eventual fatigue cracking. A maximum 28-day UCS of 1 MPa (0.7 MPa for 7-day UCS) is a reasonable achievement for a modified material. During the investigation, it was found that the stabilised material possesses a compressive strength of 0.79 MPa (Fig. 3).

5.2 California Bearing Ratio (CBR)

Laboratory soaked CBR values were obtained from three samples for both in situ soil and stabilised soil. The stabilised soil has resulted a CBR values between 30 and 80% while the CBR of natural soil was between 8 and 16%. The increase in CBR in stabilised soil therefore accounts for 250% to nearly 400% which is a significant contribution for overall strength of the working platform.

5.3 Permeability

Results of permeability tests are summarised in Table 5 for both non-stabilized and stabilized samples. Stabilized samples revealed a permeability of 1.0×10^{-8} cm/sec, which is considered appropriate for the impervious materials. In average, the permeability characteristics of stabilized samples dictate two-fold improvement in hydraulic behaviour compared to that in non-stabilized samples (i.e.in situ clay).

Table 5 Permeability test results

Sample Number	Coefficient of Permeability	
	Before Stabilisation (m/s)	After Stabilisation (m/s)
1	4.0E-07	1.0E-08
2	6.0E-07	–

Table 6 Stages of site works

Stage 1	Mixing of the top 300 mm of soil with 20% recycled crushed concrete
Stage 2	Continue mixing the top soil with addition of 3% GP cement and 1% Eko-enzyme (1:500 dilute with water)
Stage 3	Compaction process and perform in situ tests

5.4 In Situ Stabilisation

Having characterised the stabilization behaviour, in situ stabilization of on-site clay (up to 300 mm thickness) was performed using recycled concrete, cementitious blended binder and the enzyme (Eko-Soil) for providing the required working platform and to support the subsequent rigid concrete pavement construction. Onsite stabilization was conducted in three stages as shown in Table 6.

5.5 Density Testing

A total of 32 density control tests together with proof rolling and visual assessment were conducted (including falling weight reflectometer testing) after the in situ stabilization was completed. Results indicate that the in situ density achieved a density ratio of at least 95% (Standard Compaction) throughout the controlled working platform layer area. Field densities measured at all the sampling locations are shown in Fig. 4. These results revealed that the required density was well maintained in the field and hence the required strength was achieved from the stabilized working platform.

5.6 Discussion

Results from the lab and field experiments showed that the addition of stabilizers along with the recycled concrete have well improved the expansive soil characteristics in favour of a sustainable working platform. They revealed that small amounts of additives with waste concrete have been cost effective to mitigate the problematic responses of expansive soil which are of typically in high moisture contents.

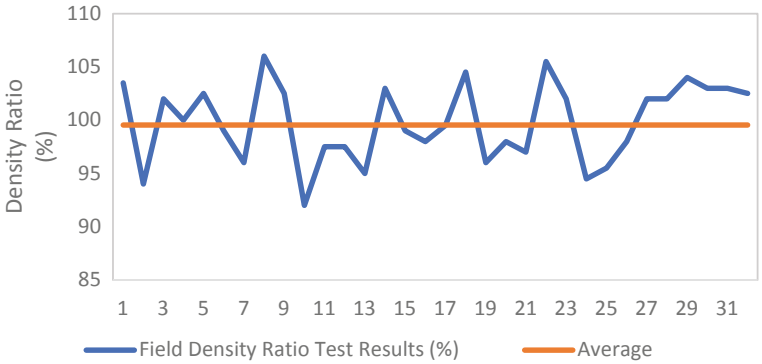

Fig. 4 Field density results after stabilization with recycled concrete, clay and Eko-enzyme

The stabilization has enhanced the strength of working platform while reducing the permeability in substantial terms. The effectiveness and durability of stabilization approach has been reflected by the excellent condition of the infrastructure constructed on the stabilized working platform even after 10 years of construction as noted by present day images (Fig. 5).

The stabilization approach has been cost effective due to the use of recycled concrete and small dosages of stabilizers. The cost of such a subgrade improvement will usually be only a small component of the total construction cost. Nevertheless, it is important to adopt such approaches mainly for lightly-loaded pavements due to substantial reduction in the construction costs compared to fully imported subbase

Fig. 5 Site with servicing infrastructure as at present time (Sept 2019)

considerations which may result costly over-designs in most cases. The approach can also replace building thick capping layers/slabs of concrete which are highly uneconomical in practice.

The soil modification by stabilisation is increasingly being applied in Victoria and worldwide. This is because of its potential use of in situ material and recycled materials (such as recycled concrete in this project) which result cost effective and durable constructions. Further, such approaches of stabilization can claim eco-friendly nature as of its minimum/no use of cement-based products along with no harming additives to the environment. It will also preserve natural resources (i.e. new quarried products) which would otherwise be used in constructing working platforms/capping layers.

It is also expected that the use of stabilised capping layer would have minimised associated weakening of underlying subgrade, in contrast to the Class 2 fill material [24]. The stabilized layer has the ability to retain water without allowing it to permeate the underlying subgrade soil due to very low permeability characteristics of the stabilized material. This has assisted to protect the weak subgrade, thus enabled to enhance the overall performance of the working platform in significant terms.

6 Conclusion

This study investigated the possibility of using recycled concrete for constructing a working platform in conjunction with a novel stabilization approach for in situ clay soils. It showed that the waste materials can be effectively utilised to support building foundations when appropriately treated with the sustainable additives. In situ expansive clay soils have been uniformly mixed with recycled concrete, cement and enzymes to construct the working platform which is operating well to-date without exceeding serviceability performance. The systematic characterization of stabilization using number of physical, chemical, mechanical and hydraulic tests at the laboratory has assisted to yield the optimum benefits of stabilization application in the field context. Study revealed that the uniform mixing of in situ soils with 20% crushed concrete, 3% blended GP cement and 1% enzyme layer has been effective to result a durable and sustainable working platform. Low permeability, low swelling and high CBR/UCS results of stabilized soils indicate that the adopted construction approach would be well suited to provide an effective capping layer for road pavement as well as building foundations using environment friendly and recycled materials.

References

1. Lee D, Jones IJ (2012) Expansive soils. ICE manual of geotechnical engineering. Volume 1, geotechnical engineering principles, problematic soils and site investigation. British Geological Survey: ICE Publishing
2. Xi Sun JL, Gang Ren (2017) Residential footing design on expansive soils: a review of Australian practice. Electronic J Geotech Eng [Online] 22. Accessed 2017
3. Chen FH (1975) Foundations on expansive soils, Elsevier
4. Mohamed M (2012) Prediction of swelling characteristics of expansive soils. Sudan Eng Soc J 58:8
5. Sabtan AA (2005) Geotechnical properties of expansive clay shale in Tabuk, Saudi Arabia. Asian Earth Sci 25:10
6. Arya Assadi Langroudi SSY (2009) A micro-mechanical approach to swelling behavior of unsaturated expansive clays under controlled drainage conditions. Appl Clay Sci 45:8–1, 45, 12
7. Avsar E, Ulusay R, Sonmez H (2009) Assessments of swelling anisotropy of Ankara clay. Eng Geol 105:8
8. Chen L, Yin Z, Zhang P (2007) Relationship of resistivity with water content and fissures of unsaturated expansive soils. China Univ Mining Technol 17:4
9. Ferber V, Auriol JC, Cui YJ, Magnan JP (2009) On the swelling potential of compacted high plasticity clays. Eng Geol 104:11
10. Huang R, Wu L (2007) Stability analysis of unsaturated expansive soil slope 2007. Earth Sci Frontiers 14:5
11. Akinwumi IU (2015) Soil modification by addition of cactus mucilage. Geomech Eng 8:13
12. Little DN (1995) Stabilization of pavement subgrades and base courses with lime, Dubuque, IA, Kendal/Hunt Publishing Company
13. Najmiah ABAR (2007) Effect of lime on California bearing ratio (CBR) of soft soils. B.E. thesis, Universiti Teknologi Petronas
14. Shankar HKR, Mithanthaya RI (2009) Bio-enzyme stabilised laterite soil as a highway material. J Indian Roads Congress 9
15. Pooni J, Robert FGD, Setunge S, O'Donnell B (2019) Durability of enzyme stabilized expansive soil in road pavements subjected to moisture degradation. Transp Geotechnics 21
16. Kushwaha SS, Dindorkar DKN (20180 Stabilization of expansive soil using Eko soil enzyme for highway embankment. Mater Today Proc 5:13
17. Austroads (2004) Technical basis of Austroads pavement design guide, Australasian road transport and traffic agencies
18. EKOSOIL (2015) Eko Soil Manual. Melbourne, Australia
19. AS2870 1996. Residential slabs and footings. AS 2870—1996. Sydney, NSW 2001, Australia: SAI Global Limited
20. Australian Standard (2006) Methods of testing soils for engineering purposes—soil compaction and density tests—compaction control test—Hilf density ratio and Hilf moisture variation (rapid method). AS 1289.5.7.1-2006
21. Australian Standard (2008) Methods for preparation and testing of stabilized materials—unconfined compressive strength of compacted materials. AS 5101.4-2008
22. Australian Standard (1998) Methods of testing soils for engineering purposes—soil strength and consolidation tests—determination of the California bearing ratio of a soil—standard laboratory method for a remoulded specimen. AS 1289.6.1.1
23. Australian Standard (1999) Methods of testing soils for engineering purposes—soil strength and consolidation tests—determination of permeability of a soil—constant head method using a flexible wall permeameter. AS 1289.6.7.3
24. Vicroads RAB (2013) Earthworks. VicRoads

Damage Assessment of Geopolymer Aggregate Concrete Using Numerical Modeling

C. Seneviratne, D. Robert, C. Gunasekara, M. Wimalasiri, D. Law, and S. Setunge

Abstract Production of alternative aggregates is an area of study that is contributing to achieve the goal of producing sustainable concrete. However, a thorough understanding of the material is required prior to its application in construction for sustainable practice. While laboratory experiments can facilitate the understanding of new material, it is always challenging to use lab tests for damaged response evaluation and in particular failure assessment of its applications. State-of-art numerical modeling approaches with advanced material modeling can facilitate minimizing those challenges when they are calibrated/benchmarked using measured data. This study investigates for a suitable modeling approach to capture the damage response of a new material (i.e. Geopolymer) based coarse aggregate (GPA) concrete. Modeling was conducted by adopting the standard continuum modelling method. Unconfined strength test was simulated by considering Concrete Damage Plasticity (CDP) model in an explicit platform. Laboratory experiments such as stress-strain tests and compressive strength tests were also performed to calibrate and benchmark the results from the numerical model. The effect of mesh sensitivity has been identified in the outcome of damage prediction for GPA concrete. Results from the verified numerical models have been related to assess the permeability degradation of GPA. Outcomes from the study are important to predict structural/damage response using the new Geopolymer based aggregate concrete and facilitate the evaluation of structural response under loading.

Keywords Concrete damage · Continuum modelling · Concrete damage plasticity model · Geopolymer aggregate concrete · Laboratory experiments

C. Seneviratne · D. Robert (✉) · C. Gunasekara · M. Wimalasiri · D. Law · S. Setunge
RMIT University, Melbourne, VIC 3000, Australia
e-mail: dilan.robert@rmit.edu.au

R. Dissanayake et al. (eds.), *ICSECM 2019*, Lecture Notes in Civil Engineering 94,
https://doi.org/10.1007/978-981-15-7222-7_4

1 Introduction

The recent statistical reports on concrete production have estimated that concrete is being produced at a rate of over 16 billion metric tons per year making it the single most widely used material in the world [9]. However, the growth in concrete production has caused many environmental concerns including the emission of significant carbon footprint. Furthermore, the aggregates in concrete occupy at least three quarters of the volume of concrete [22] which contribute to a worldwide production of aggregates at a rate of 4.5 billion tons per year. Since a substitute material for concrete is not yet been produced, reducing the carbon intensity of concrete production by the invention of novel sustainable constituents has become an imperative among the scientific community.

The term "Alternative Coarse Aggregates" can be used to define both by-product based aggregates and recycled coarse aggregates based on their source [39]. Both aggregate types have been subjected to significant developments in the past decade. Consequently, the utilization of recycle coarse aggregates in structural applications has become a common practice. However, associated negative impacts such as poor workability has refrained recycle aggregates from becoming more adoptable.

With the development of the mechanical processes such as pelletizing, sintering & expanding processes that can produce artificial aggregates, the studies relating by-product based manufactured aggregates have become more popular. Over recent years, researchers have used materials such as bottom ash [15, 47], fly ash [3, 45, 49], blast furnace slag [42] and clay [26, 48] to prepare these artificial aggregates. Moreover, mean compressive strength achieved using these artificial aggregates in concrete varies in the range of 27–74 MPa. However, a large amount of energy is required for the manufacturing of most of these lightweight aggregates as they require curing at higher temperatures ranging from 1000 to 1300 °C for the sintering process [37].

Geopolymer aggregate (GPA) is a novel type of a coarse aggregate produced from low calcium class F flash, with an alkaline activator by employing high-pressure agglomeration. Concrete with 100% GPA was reported to obtain a mean compressive strength of up to 37 MPa at 28 days [20], Gunasekera et al. [21]. However, there is a clear gap in the literature on how this novel type of aggregate based concrete responds under stress/loading. Such studies are vital towards understanding and comparing the performance of this novel aggregates to conventional aggregate concrete before using them for structural applications.

Numerical modelling has been extensively used in previous studies to understand key mechanical properties and structural properties of concrete [43, 54]. Furthermore, damage response can be evaluated more preciously using the concepts of numerical modeling approaches in comparison to laboratory experiments. These studies have utilized Finite Element Method (FEM) to demonstrate the required characteristics of concrete. Existing studies on modelling the behavior of concrete under compressive loading have been performed in general using two main approaches; multi-phase mesoscale modelling and macroscale continuum modelling.

In multi-phase mesoscale models, the concrete structure is represented in phases such as cement mortar, interfacial transition zone (ITZ), and coarse aggregates. Changes to the properties of each phase affect the overall mechanical properties, stress levels, stiffness and many other properties of the macro-scale structure. In literature, nanoindentation technique with in-place scanning probe microscope imaging has been used to determine the hardness and modulus of elasticity of the ITZ, cement paste and the aggregates of the mesoscale models [46, 53].

In macroscale continuum models, minimum size for an element is considered. Moreover, the average values of the mass, density, acceleration & velocity of the entire element or over the surface of the element is considered for the analysis. The discrete atomic structure of the element is smeared out into a continuum element [27]. However, this element should be in an appropriate size for the heterogeneities to be replaced by homogenized average values of the required properties. Therefore, the continuum models could be accurate when simulating the behavior at a microscale in comparison to multi-phase mesoscale models.

Prior research on numerical modelling of alternative aggregate concrete has been conducted in the recent years with mainly focusing on recycle aggregate concrete [25, 32, 50]. Most of these studies have used mesoscale approach to model the behavior of recycle aggregate concrete. This is mainly because of the influence of the two new phases (Adhered mortar, ITZ between recycled aggregates and adhered mortar) in the microscale recycle aggregate concrete structure. However, Gambarelli [19] highlighted that macroscopic analysis is principally capable of demonstrating major effects related to dynamic fracture of concrete by analyzing the differences between mesoscale and macroscale approaches for modelling dynamic fracture of concrete in compression. Recent studies by Gunasekera et al. [21] showed that, in the case of GPA concrete, the meso-structure of concrete behaves similar to conventional aggregate concrete as there are no additional phases generated.

In the present paper, macroscale 3D continuum models of GPA concrete have been studied to understand the damage response under compressive loading using the Concrete Damage Plasticity Model (CDPM) in ABAQUS explicit platform. Laboratory tests including unconfined compressive strength tests and stress-strain tests were conducted at 28 days to benchmark and validate the results of the numerical models. In addition, sensitivity of the input parameters and capabilities of the CDPM were discussed. Furthermore, mesh sensitivity analysis was conducted by comparing the stress- strain response of the plasticity models against the input parameters to obtain mesh size independent modeling approach. Results from the validated numerical models were utilized to predict the permeability degradation of GPA concrete prepared at various grades.

2 Research Significance

This study reports the damage response of a newly introduced fly ash based geopolymerised coarse aggregate concrete. The aim of this study is to evaluate and build a suitable numerical modelling approach to demonstrate the damage of manufactured aggregate concrete (GPA concrete) under uniaxial compressive loading. This understanding could help to encourage the use of alternative aggregates such as GPA in concrete as it facilitates for further evaluation of its applications. The production of GPA utilizes class F low calcium fly ash deposited in ash ponds adding value to an environmentally unsafe pollutant due to contamination with groundwater, surface water, and nearby soils [29, 33]. Furthermore, the use of GPA aggregate in concrete has the capability to reduce the strong dependence on natural quarried aggregates for manufacturing concrete. The reported studies relating to simulating damage of concrete has focused mainly on normal concrete and recycle aggregate concrete. This study will investigate a modelling approach to simulate the damage response of GPA based concrete using the CDP model in the ABAQUS. Modelling parameters are determined based on a series of laboratory experiments for the calibration and verification of the model. A verified modelling methodology is a critical step forward when understanding the loading response of GPA concrete which has immense potential for various applications in future. Hence, this study aims for developing a robust model that can be utilized for evaluating the structural response of GPA concrete applications.

3 Laboratory Experiments for Parameter Identification

The Identification of mechanical properties of GPA concrete are vital towards simulating its damage response using the CDP model. The compressive strength of concrete is regarded as the main parameter that governs most of the other mechanical and durability properties of concrete. The relationship between compressive strength and other properties such as elasticity are well defined in both the literature and in the standard documents such as AS 3600 [5]. However, in the context of GPA concrete, these relationships are still unknown. Therefore, each of the parameters are required to calibrate first and then verify the model predictions by comparing with the experimental data. Thus, following experimental setup was adopted for identifying the essential parameters for model calibration.

As the first step, suitable mix design for GPA concrete was produced on the basis of the absolute volume method. At the same time, a concrete mix design with similar mix proportions were produced with conventional Basalt Coarse Aggregates (BCA) as a control mix to compare the performance of GPA concrete with conventional coarse aggregate concrete. Coarse aggregates used for the GPA concrete mixes consisted of 100% GPAs whereas for the control mix, 100% basalt crushed coarse aggregate of 10 mm was used. Water/binder ratios were kept to 0.35 and used high range water

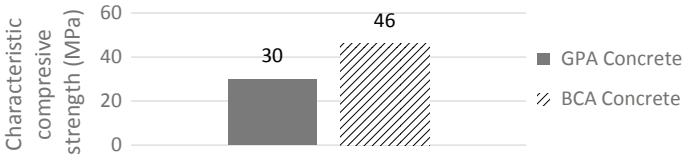

Fig. 1 28-day characteristic compressive strength

reducing admixture to counter consistency losses. However, different superplasticizer contents were used to recompense for the different water absorption of the two aggregate types.

Both mixes were mixed using a 120-litre concrete pan mixer under laboratory conditions using the standard mixing procedures. Compaction of the specimens were conducted in accordance with AS 1012.8.1 [6] using a vibrating table to obtain homogeneous mixes. After the initial curing period of 24 h, these specimens were stripped from their moulds and standard moist curing was adopted in compliance with the same standard. Following the curing process, the compressive strength test was conducted by following AS 1012.9 [7] to determine the compressive strength at 28-day period for GPA concrete and conventional BCA concrete. The observed characteristic compressive strength was 30 MPa for GPA concrete in contrast to 46 MPa for BCA concrete as shown in Fig. 1. The difference in the compressive strength could be due to the lower strength of the GPAs [20]. (i.e. Crushing value of GPAs were 34.1% in contrast to 23.2% for BCAs; higher the aggregate crushing value, the lower the strength of coarse aggregates).

The density of concrete is another material property that is required in the FE model. Therefore, with the laboratory experiments conducted in accordance with AS 1012.12.2 [8], this was observed to be 2096 kg/m^3. Furthermore, the Modulus of Elasticity (MOE) and Poisson's ratio are two other critical parameters required for the modelling purposes. These properties were also identified for GPA concrete based on laboratory experiments conducted by following AS 1012.17 [4]. The MOE of GPA concrete was observed to be 18.2 GPa whilst the Poisson's ratio was 0.1. Stress-strain response from compression loading was obtained for the purpose of implementing and calibrating CDP model. Strain readings were recorded by monitoring the readings of data acquisition rig which was attached to the electrical resistance strain gauges fixed to the either end of the specimens subjected to the compressive loading. Results of stress-strain relationship are shown in Fig. 2. This test was conducted in the form of load control test instead of a strain-controlled test. Therefore, the post peak behavior of the stress- strain diagram was not recorded in this experiment. The difference in the stress-strain could be due to the different modulus of elasticity observed for two concrete types.

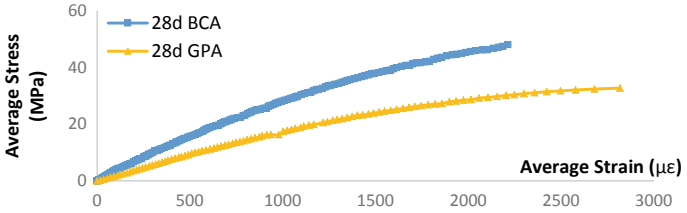

Fig. 2 Stress-strain curve at 28-day period

4 Finite Element Modeling

4.1 Model Description

Three-dimensional continuum finite element models were performed using Abaqus V 6.14 to investigate the modelling capability of GPA using the continuum approach. A prism specimen with the dimensions of 100 mm × 100 mm × 100 mm was used to simulate the unconfined compressive strength test of concrete. Three dimensional, 8-node linear brick, reduced integration elements (C3D8R) were used to represent GPA concrete with the behavior simulated using concrete damage plasticity model. The size of the model was chosen to reduce the effects on boundary conditions on the model response [51, 52]. The compressive load was applied to the cube using two rigid plates which were tied to the top and bottom surface of the cube specimen for reducing the effect of stress localization. However, the dimensions of these plates were slightly larger at 152 mm × 152 mm to avoid the excessive distortions that could occur in the solid continuum elements at the edges of the cube. Translations in the bottom plate were restricted in both horizontal directions (X, Z) and vertical direction (Y), while the translations of the top plate in the horizontal directions (X, Z) were restricted. Furthermore, the compressive load of 35 MPa was applied over a time period of 0.01 s with a smooth loading amplitude. The correct modelling approach was devised by evaluating the damage response on the basis of five models having different mesh discretization Fig. 3.

4.2 Concrete Damage Plasticity Model (CDPM)

Concrete damage plasticity model available in the Abaqus was used to simulate the behavior of GPA concrete. The model uses the concepts of isotropic damage while considering the elastic stiffness degradation induced by plastic straining. It considers the failure criteria of either tensile cracking or compressive crushing in response to tension and compression applied on concrete [2]. Figure 4 represents uniaxial compression and tensile behavior which was assumed to be influenced by concrete damage plasticity. This assumption is regarded as the basis of the CDP model. The

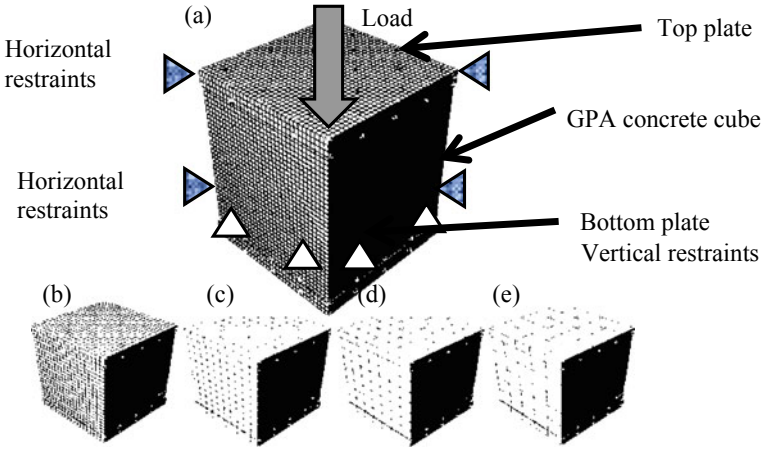

Fig. 3 Mesh discretization's **a** 3 mm **b** 5 mm **c** 10 mm **d** 15 mm **e** 20 mm

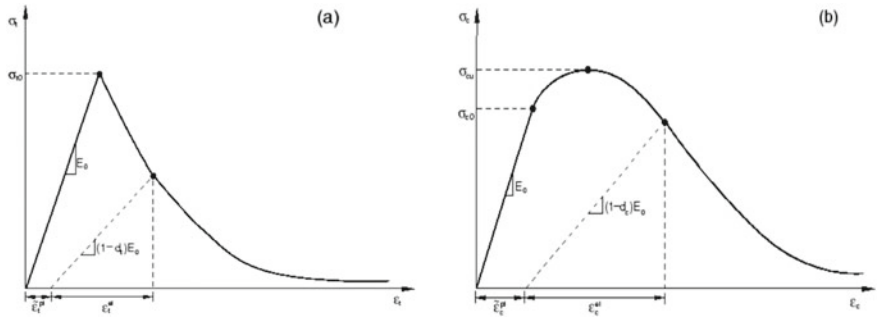

Fig. 4 σ − Ɛ in tension and compression for CDP model

yield criterion is adopted from the yield function of Lubliner et al. [34] with the modifications proposed by Lee and Fenves [30] to account for different degradation in tension and compression. The plastic flow rule adopted in CDP model is described by flow potential of Drucker- Prager hyperbolic function.

Due to the versatility of the CDP model, it has been used extensively in the literature for the numerical analysis of various concrete related studies. Chen and Andrawes [13] has used CDP model to predict the behavior of shape memory alloy spiral confined concrete under monotonic compression and verified the results with experimental results. Dulinska and Jasinska [18] used CDP model for seismic analysis of steel pipeline with concrete coating to investigate the inelastic behavior of the material. Labibzadeh [28] has used CDP model to investigate carbon fiber reinforced polymer sheets as a retrofitting approach for reinforced concrete slab with central opening. Demir et al. [16] utilized CDP model to investigate the behavior

of reinforced concrete deep beams under static and dynamic loads. Mohamad and Chen [36] investigated the shear behavior of self-insulating concrete masonry system using a simplified micro-modeling technique. Djeddi et al. [17] has used CDP model to predict the load deflection response and the failure modes of reinforced concrete beams with hybrid FRP systems. Huang et al. [24] used CDP model damage predictions to demonstrate the shear behavior of reinforced and prestressed concrete structures. Bahij et al. [10] has investigated the shear behavior of ultra- high performance concrete beams with high strength rebars and steel stirrups. Othman and Marzouk [40] has reported the use of CDP with ABAQUS/Explicit to simulate ultra-high performance fiber reinforced concrete material under impact loading. Nehdi and Ali [38] has conducted a numerical investigation on cementitious composite made of hybrid shape memory alloy and polyvinyl alcohol short fibers with drop weight impact loading using CDP model to study energy dissipation capability and penetration depth. Raza et al. [44] has conducted FEA using CDP model to simulate the load carrying capacity of Glass Fiber-Reinforced Polymer (GFRP) reinforced concrete columns.

4.3 Input Parameters

Identification of representing parameters such as modulus of elasticity, stress, cracking strain & damage parameter are essential to simulate the tension stiffening of the concrete using the CDP model. These parameters depend on the compressive strength of concrete, hardness and other properties of the constituents such as aggregates. The input parameters of CDP model used in the current study are shown in Table 1 and Fig. 5. The parameters are either obtained on the basis of the experiments conducted on GPA concrete or from reported data.

Stress-strain behavior required for the modelling of GPA concrete was based on experimental data obtained from GPA concrete with the post-peak behavior simulated using similar grade concrete with natural aggregate. Inelastic strains required for the modelling were obtained using the total strains on the basis of Eq. 1 and 2 for compression and tensile loading conditions respectively.

$$\varepsilon_c^{\text{in}} = \varepsilon_c - \varepsilon_{0c}^{\text{el}}, \text{ where } \varepsilon_{0c}^{\text{el}} = \sigma_c / E_o \tag{1}$$

$$\varepsilon_t^{\text{ck}} = \varepsilon_t - \varepsilon_{0t}^{\text{el}}, \text{ where } \varepsilon_{0t}^{\text{el}} = \sigma_t / E_0 \tag{2}$$

Table 1 Input parameters for G30 GPA concrete CDP model

Dilation angle (β)	20° [35]
Eccentricity (m)	0.1 [2]
f (fb0/fc0)	1.16 [2]
ϒ (K)	0.667 [2]

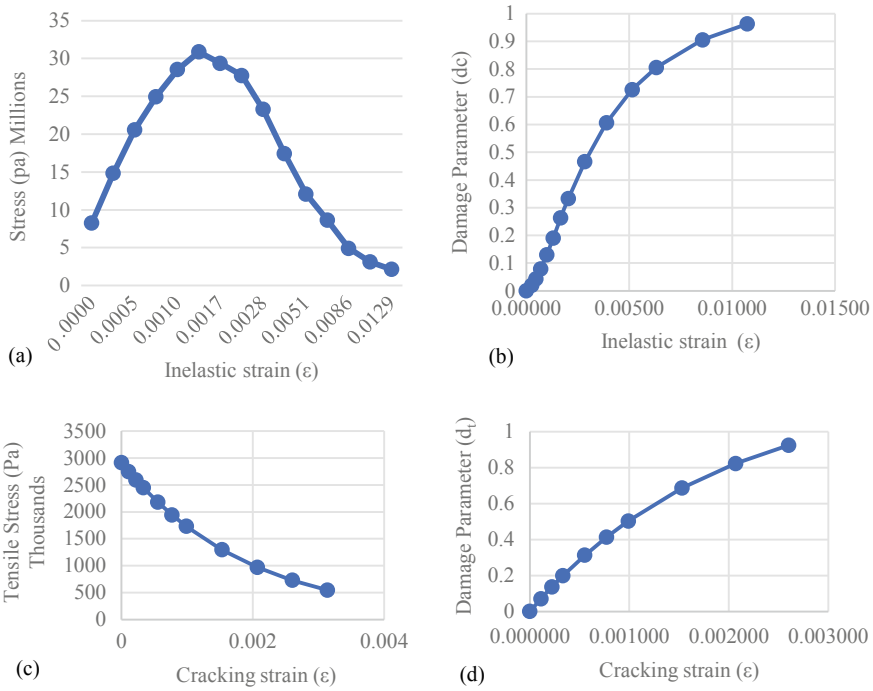

Fig. 5 Tabular input parameters for G30 GPA CDP model **a** Compressive stress versus inelastic strain, **b** Compressive damage versus Inelastic strain **c** Tensile stress versus cracking strain, **d** Tensile damage versus cracking strain

where ε_c^{in} is the inelastic strain in compression; ε_c is the total strain in compression; ε_{0c}^{el} is the elastic strain in compression; σ_c is the ultimate compressive stress; ε_t^{ck} is the cracking strain in tension; ε_t is the total strain in tension; ε_{0t}^{el} is the elastic strain in tension; σ_t is the ultimate tensile stress; $\mathbf{E_0}$ is the initial (undamaged) elastic stiffness of the material.

5 Results and Discussion

The model developed for simulating GPA concrete damage was verified using the results obtained from laboratory experiments. The failure modes between the experiment and the modelling after application of 35 MPa compression loading are compared in Fig. 6. It can be seen that the failure mode predicted from the modelling show a close resemblance to the experimental damage of CDP concrete. It has also been observed that the CDP concrete failure mode is similar to the semi-explosive failure commonly observed in conventional aggregate concrete.

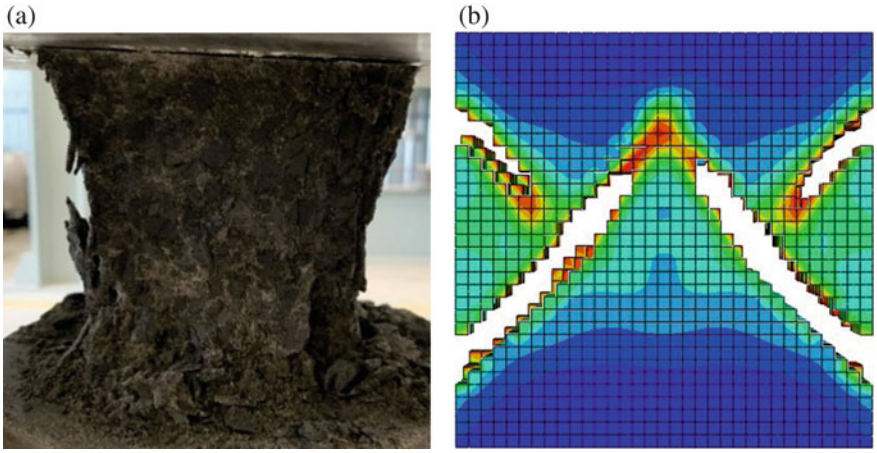

Fig. 6 Failure mode of G30 GPA Concrete **a** Experimental **b** CDP model (with deleted elements of damage > 0.95)

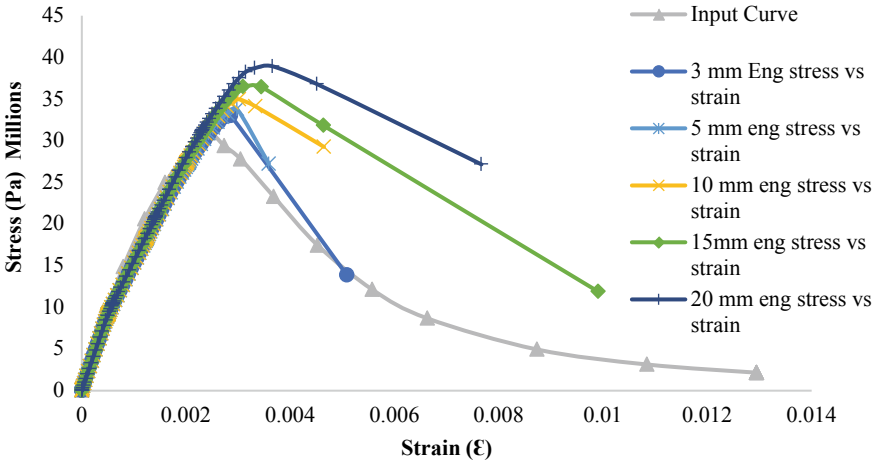

Fig. 7 Eng. stress-Eng. strain response of various element sizes

The observed damages between the model and experiments have been quantified using the damaged volume after the failure. The cube damage analyzed from the experiment was estimated to be approximately 350 cm^3, reflecting a volume proportion of 35%. On the other hand, the volume proportion having a compression damage parameter (d_c) of more than 0.95 is 42% at the time of the failure in the numerical model. This difference between the model prediction and experimental observation is only less than 7%.

Results of the mesh sensitivity analyses are showed in Fig. 7 in terms of the variation in Engineering stress versus engineering strain. Engineering stresses were

calculated by using reaction forces of the bottom plate attached to the model. Engineering strains were determined using the translation values of the top most elements in the cube (i.e. vertical displacement/model height). Results showed that the model predictions are highly sensitive for the element size selected. i.e. Decrease in the size of the elements can reach the ultimate strength of the cube as observed from the experiment. Element size of 20 mm over-estimated the compressive strength by 26% compared to the experimental results. On the other hand, the modelling with element size of 3 mm reduces the over-estimation up to 7%. It should also be noted that the higher ultimate compressive stresses from the model prediction is due to the sustained hydrostatic compressive stresses of the failed elements that have not been removed from the mesh. In order for them to be deleted (i.e. removed from stress calculations), the damaged variables of the elements must reach maximum degradation value of 1 [1]. However, the maximum damage parameters utilized in the current modelling is 0.95 to minimize the computational errors during the modelling. Hence, slightly higher ultimate stresses are expected in the model output due to sustained hydrostatic compressive stresses, but this difference can be elevated with the increase in mesh size in the model. Hence, the adopted element size of 3 mm can provide reasonable model predictions with minimum meshing influence.

A substantial CPU time difference was observed when the mesh size was reduced from higher to a lower size. For example, the approximate CPU time taken for the analyses with 20 mm and 3 mm models are 5 min and 200 min respectively using a computer having 128 GB of RAM with 28 cores (each core having 2.4 GHz of speed). Considering acceptable results of 3 mm mesh model (given some hidden difference due to the use of 0.95 peak damage value) and the extensive computational expense at smaller size mesh model, the model having 3 mm mesh was selected to proceed for further analysis. It is also to be noted that the observed stress-strain variation due to the changes in mesh size is similar to the findings reported by Chaudhari and Chakrabarti [12] for CDP model.

Results of the analyses conducted for different grades of GPA concrete are showed in Fig. 8a–c at the failure points (i.e. applied stresses of 32.9 MPa, 27.3 MPa and 22.1 MPa respectively) of G30, G25 and G20 GPA concrete respectively. The elements with damage over 0.95 were removed from the model to represent the damage caused due to applied stress. The shape of the failure observed from all the

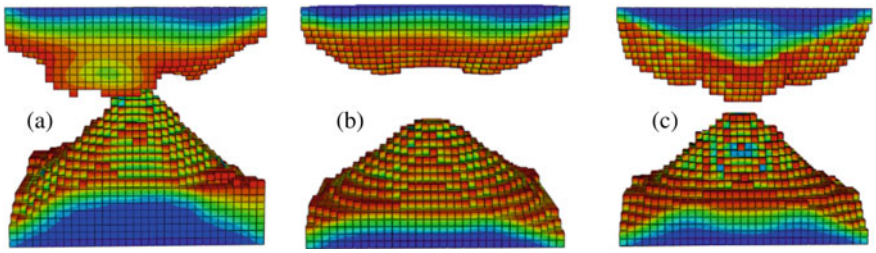

Fig. 8 3D view of the failure using 3 mm mesh model **a** G30 **b** G25 **c** G20

grades are similar. However, the G25 and G20 cubes represent more explosive failure pattern. Furthermore, the stress- strain behavior reported in the Fig. 9 is also similar except for the changes due to the modulus of elasticity and ultimate compressive stress differences between the grades. The volume proportions having a compression damage parameter (dc) of more than 0.95 are 42%, 56% and 48% for G30, G25 & G20 respectively at the failure load. The observed ultimate compressive strength from the output was 32.9 MPa, 27.3 MPa, 22.1 MPa for G30, G25 and G20 GPA concrete respectively. These values indicate variations of 7%, 9.2% and10.5% with the ultimate strength of their respective grades.

Having estimated the damage for different grades of GPA concrete, the verified model was used to determine how the damage can lead for the degradation of hydraulic characteristics (i.e. permeability). The water permeability of concrete is a critical parameter that affects the durability and serviceability of concrete structures subjected to aggressive environments [31]. The factors such as w/c ratio, age of curing, cement content, properties of the cement and permeability of the aggregates influence the permeability of concrete [39]. Furthermore, concrete permeability can also be affected by the applied stress to the concrete due to the propagation of cracks in the meso-structure [23]. Hence, it is important to estimate the permeability damage of GPA concrete using the verified model under externally applied stress levels.

Evolution of damage at the mid-level of the prism was considered for the determination of permeability variance at respective grades. Furthermore, Eq. 3 [14] has been used in the current study to relate the damage by applied stress to the permeability of GPA concrete in the direction of the applied load.

$$k_D = k_0\left[1 + (\alpha D)^{\beta} + \frac{(\alpha D)^{2\beta}}{2} + \frac{(\alpha D)^{3\beta}}{6}\right] \tag{3}$$

where k_D is the current permeability coefficient; k_0 is the initial permeability coefficient; D is the overall damage variable; α and β are two parameters defined by Picandet et al. [41] to 11.3 and 1.64 respectively.

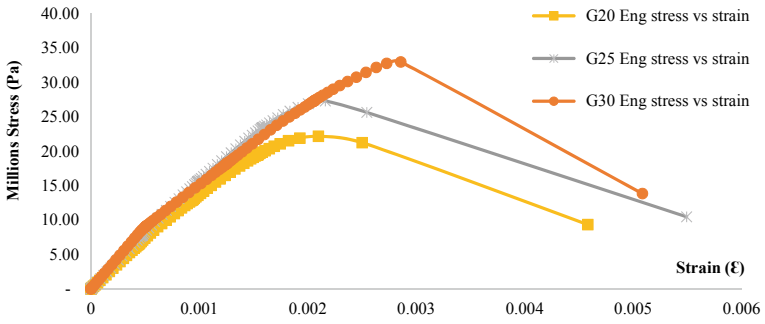

Fig. 9 Eng. stress versus Eng. strain response of various concrete grades

However, the values of k_0 at reported grades for GPA concrete was not available for the analysis. Therefore, the percentage difference of permeability [P(%)] caused by the applied stress is considered by modifying the Eq. 3 to the form of Eq. 4 as reported in Fig. 10a at different grades of GPA concrete. Figure 10b reports the same comparison by using the Eq. 3 with the assumed values for the k_0 from the literature. Based on the water/cement ratio of GPA concrete mixes (i.e. water/cement ratio of G30, G25 and G20 concrete was 0.35, 0.4, 0.45 respectively) the coefficient of permeability were assumed for G30, G25, G20 as 0.024e-11, 0.8e-11 and 1.91e-11 respectively from the results reported by Bamforth [11].

$$P(\%) = \left[(\alpha D)^{\beta} + \left((\alpha D)^{2\beta}/2\right) + \left((\alpha D)^{3\beta}\right)/6\right] \times 100 \tag{4}$$

Overall, results showed that the permeability of GPA concrete is highly sensitive to the applied stress level. i.e. application of 80% of ultimate load would increase the permeability of G30 GPA concrete as much as by 155%. This percentage increment is much higher in comparison to the 99% increment observed in G30 BCA concrete due to the increased damage at the same stress level. The percentage difference [P (%)] observed for G25 and G20 GPA concrete is 23% and 32% respectively, which is lower compared to G30 GPA and G30 BCA concrete. Although a significant increment in the K value was observed due to elevated stress levels, there is a clear difference between K values of different grades (i.e. K at 0.8 stress level for G30 is less than K value of G25 at 0 stress level). Lab experiments are currently being conducted to further verify the model predictions of permeability variations with applied stresses for GPA concrete.

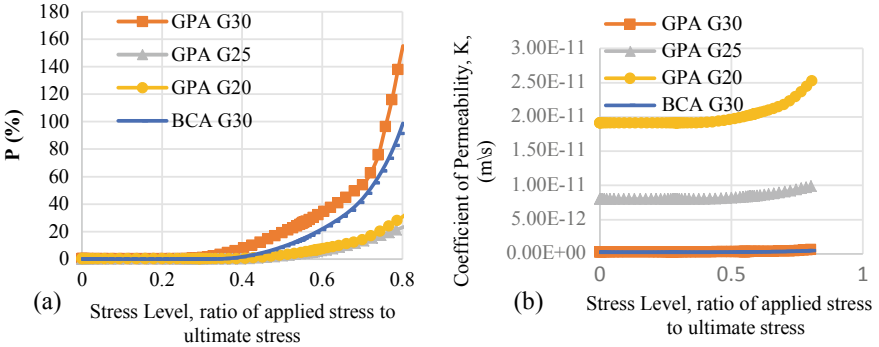

Fig. 10 Effect on applied stress on permeability **a** Percentage change in the permeability **b** Coefficient of permeability

6 Conclusion

This study presented a verified modeling approach to capture the damage response of a new material (i.e. Geopolymer) based coarse aggregate (GPA) concrete. Three-dimensional continuum finite element model was developed to demonstrate the unconfined compressive strength test in order to quantify the stress induced damage in GPA concrete. Series of laboratory experiments were conducted using GPA concrete sample cubes to calibrate the developed model. The response of the continuum model was verified by comparing with the experimental data in terms of damage modes and stress-strain responses. Results revealed that the response predicted from the model is highly sensitive to the size of the mesh adopted in the modelling. Damage responses of different grade GPA concrete depict characteristic changes due to the differences in the concrete capacity. The application of the modeling outcome has been demonstrated by evaluating the permeability degradation which is a key design parameter in assessing the whole-of-life cycle assessments of concrete structures. The verified modeling approach presented in this study can be efficiently utilized for understanding the loading response of GPA concrete that has broad applications in future engineering.

Acknowledgements The authors wish to express their gratitude to Polyagg Pty Ltd for supplying the geopolymer coarse aggregates. Technical assistance provided to conduct the laboratory experiments by the Heavy Structures laboratory of Civil and Infrastructure Engineering, RMIT University is also acknowledged. Furthermore, postgraduate research scholarship provided by RMIT University is gratefully acknowledged.

References

1. Abaqus (2005) Lecture 9: material damage and failure
2. Abaqus (2009) Abaqus/standard user's manual. Simulia
3. Abdullah A., Ku Yin KAR, Al Bakri Abdullah MM, Hussin K, Tran MV (2015) Comparison of mechanical properties of fly ash artificial geopolymer aggregates with natural aggregate. Appl Mech Mater 754–755:290–295
4. As 1997. As 1012.17-1997 (R2014) Methods of testing concrete determination of the static chord modulus of elasticity and Poisson's ratio of concrete specimens. Standards Australia
5. As 2009. As 3600—Concrete structures. Design for durability. Standards Australia, Sydney
6. As 2014a. As 1012.8.1:2014. Methods of testing concrete method for making and curing concrete—compression and indirect tensile test specimens. Standards Australia
7. As 2014b. As 1012.9:2014. Methods of testing concrete compressive strength tests—concrete, mortar and grout specimens. Standards Australia
8. As 2014c. As 1012.12.2. Methods of testing concrete determination of mass per unit volume of hardened concrete-water displacement method. Standards Australia
9. Ashby MF (2013) Materials and the environment eco-informed material choice, 2nd edn. Butterworth-Heinemann, Waltham, Mass
10. Bahij S, Adekunle SK, Al-Osta M, Ahmad S, Al-Dulaijan SU, Rahman MK (2018) Numerical investigation of the shear behavior of reinforced ultra-high-performance concrete beams. Struct Concrete 19:305–317

11. Bamforth PB (1991) The water permeability of concrete and its relationship with strength 43:233–241
12. Chaudhari V, Chakrabarti A (2012) Modeling of concrete for nonlinear analysis using finite element code Abaqus. Int J Comput Appl 44:14–18
13. Chen Q, Andrawes B (2012) 3D finite element modeling to study the behavior of shape memory alloy confined concrete. In: Proceedings of the 15th World conference on earthquake engineering, Lisbon, Portugal, September
14. Choinska M, Dufour F, Pijaudier-Cabot G (2007) Matching permeability law from diffuse damage to discontinuous crack opening
15. Cioffi R, Colangelo F, Montagnaro F, Santoro L (2011) Manufacture of artificial aggregate using Mswi bottom ash. Waste Manage 31:281–288
16. Demir A, Ozturk H, Dok GJDS (2016) Engineering 2016. 3D numerical modeling of RC deep beam behavior by nonlinear finite element analysis 2:13–18
17. Djeddi F, Ghernouti Y, Abdelaziz Y, Alex L (2016) Strengthening in flexure-shear of RC beams with hybrid FRP systems: experiments and numerical modeling. J Reinforced Plastics Compos 35:1642–1660
18. Dulinska JM, Jasinska D (2013) Performance of steel pipeline with concrete coating (modeled with concrete damage plasticity) underseismic wave passage. Appl Mech Mater 459:608–613
19. Gambarelli S (2019) Dynamic fracture of concrete in compression: 3D FE analysis at macro and meso scale. Ia-Framcos
20. Gunasekara C, Setunge S, Law DW, Willis N, Burt T (2018) Engineering properties of geopolymer aggregate concrete. J Mater Civil Eng 30:04018299
21. Gunasekera C, Law D, Setunge S (2018) Effect of geopolymer aggregate on strength and microstructure of concrete. ACI Mater J 115:899–908
22. He H, Stroeven P, Pirard E, Courard L (2015) The shape simulation of aggregate and cement particles in a DEM system 2015:1–7
23. Hoseini M, Bindiganavile V, Banthia N (2009) The effect of mechanical stress on permeability of concrete: a review 31:213–220
24. Huang Z, Grip N, Sabourova N, Bagge N, Tu Y-M, Elfgren L (2016) Modelling of damage and its use in assessment of a prestressed bridge, Luleå Tekniska Universitet
25. Jayasuriya A, Adams MP, Bandelt MJ (2018) Understanding variability in recycled aggregate concrete mechanical properties through numerical simulation and statistical evaluation. Constr Build Mater 178:301–312
26. Kang SG, Kim YS (2015) A comparative study on the physical properties of artificial aggregates made from acid clay and dredged soil. Mater Sci Forum 804–804:81–84
27. Kelly P (2015) Solid mechanics part I: an introduction to solid mechanics
28. Labibzadeh M (2015) The numerical simulations of the strengthened RC slabs with CFRPS using standard CDP material model of Abaqus code 19:1268–1287
29. Latimer G (2017) Hazardous waste in Australia 2017. Department of the Environment and Energy
30. Lee J, Fenves GLJJOEM (1998) Plastic-damage model for cyclic loading of concrete structures 124:892–900
31. Li X, Xu Q, Chen S (2016) An experimental and numerical study on water permeability of concrete. Constr Build Mater 105:503–510
32. Li W, Luo Z, Sun Z, Hu Y, Duan WHJMOCR (2017) Numerical modelling of plastic-damage response and crack propagation in RAC under uniaxial loading 70:459–472
33. Lokeshappa Dikshit, Kumar A (2012) Behaviour of metals in coal fly ash ponds. APCBEE Proc 1:34–39
34. Lubliner J, Oliver J, Oller S, Oñate E (1989) A plastic-damage model for concrete. Int J Solids Struct 25:299–326
35. Mander JB, Priestley MJN, Park R (1988) Theoretical stress-strain model for confined concrete. J Struct Eng 114:1804–1826
36. Mohamad AE, Chen Z (2016) Experimental and numerical analysis of the compressive and shear behavior for a new type of self-insulating concrete masonry system 6, 245

37. Nadesan MS, Dinakar P (2017) Structural concrete using sintered flyash lightweight aggregate: a review. Constr Build Mater 154:928–944
38. Nehdi M, Ali M (2019) Experimental and numerical study of engineered cementitious composite with strain recovery under impact loading. Appl Sci 9:994
39. Neville AM (2012) Properties of concrete. Prentice Hall
40. Othman H, Marzouk HJIJOIE (2018) Applicability of damage plasticity constitutive model for ultra-high performance fibre-reinforced concrete under impact loads 114:20–31
41. Picandet V, Khelidj A, Bastian G (2001) Effect of axial compressive damage on gas permeability of ordinary and high-performance concrete 31:1525–1532
42. Raffaele C, Francesco C (2013) Use of Cement Kiln Dust, Blast Furnace Slag and Marble Sludge in the manufacture of sustainable artificial aggregates by means of cold bonding pelletization. Materials 6:3139–3159
43. Ramesh G, Sotelino E, Chen WJC, Research C (1996) Effect of transition zone on elastic moduli of concrete materials 26:611–622
44. Raza A, Khan QUZ, Ahmad A (2019) Numerical investigation of load-carrying capacity of GFRP-reinforced rectangular concrete members using CDP model in Abaqus. Adv Civil Eng 2019:1–21
45. Razak RA, Al Bakri Abdullah MM, Hussin K, Ismail KN, Hardjito D, Yahya Z (2016) Performances of Artificial Lightweight Geopolymer Aggregate (ALGA) in OPC concrete. Key Eng Mater 673–673:29–35
46. Shah SP, Konsta-Gdoutos MS, Metaxa ZS, Mondal P (2009) Nanoscale modification of cementitious materials. Springer, Heidelberg
47. Tang P, Florea MVA, Brouwers HJH (2017) Employing cold bonded pelletization to produce lightweight aggregates from incineration fine bottom ash. J Cleaner Prod 165:1371–1384
48. Tay J, Hong S, Show K, Chien C, Lee D (2003) Manufacturing artificial aggregates from industrial sludge and marine clay with addition of sodium salt 47:173–178
49. Terzić A, Pezo L, Mitić V, Radojević Z (2015) Artificial fly ash based aggregates properties influence on lightweight concrete performances. Ceram Int 41:2714–2726
50. Wang Y, Peng Y, Kamel MM, Ying LJ (2019a) Mesomechanical properties of concrete with different shapes and replacement ratios of recycled aggregate based on base force element method
51. Wang Y, Peng Y, Kamel MMA, Ying L (2019) 2D numerical investigation on damage mechanism of recycled aggregate concrete prism. Constr Build Mater 213:91–99
52. Wimalasiri M, Robert D, Qing Li C (2016) New method to investigate the permeability of stressed concrete. In: Hong Hao CZ (ed) Mechanics of structures and materials: advancements and challenges Perth. CRC Press, Australia
53. Xiao J, Li W, Sun Z, Lange DA, Shah SPJC, Composites C (2013) Properties of interfacial transition zones in recycled aggregate concrete tested by nanoindentation 37:276–292
54. Zhu W, Tang CJC, Materials B (2002) Numerical simulation on shear fracture process of concrete using mesoscopic mechanical model 16:453–463

Quantification of Benefits of Soil Stabilized Pavement Layers for Sustainable Road Infrastructure

Dheeraj Bonagiri, Veeraragavan Amirthalingam, and Srinivas Vallabhaneni

Abstract The service life and performance of pavements depend mainly on the quality of the materials used for construction. Naturally available materials such as soil, stone aggregates, sand etc. and some of the processed materials like bitumen are conventionally used for road construction. But they are depleting fast and results in higher procurement and processing cost. Therefore, alternative materials such industrial wastes, chemical products are considered for road construction. If these materials can be suitably utilised in highway construction, the pollution and scarcity of aggregates problems may be partly reduced. In the present study, a soil stabilizer produced by the Stabilroad is investigated for its application in pavement layers. The Stabilroad stabilizer should be used along with cement which can be mixed with the existing soil. This makes the pavement layers to have good compressive strength as well as flexible and waterproof. The StabilRoad allows the agencies to stabilize different soils and build roads using locally available soil without the need to extract new material from the mines. Different dosages of cement and Stabilroad are mixed with the available soil and their geotechnical characteristics are evaluated. The focus was to study the strength characteristics of untreated and stabilized soil samples by Unconfined compressive strength and resilient behaviour under cyclic loading conditions using cyclic triaxial test procedure as per AASHTO T-307 protocol. Typical Red soil was collected for present study investigation. The optimal dosage of cement and stabilizer was determined based on laboratory studies. The strength properties of stabilized soils were determined at optimum dosage. Using the results, alternative pavements were designed according to IRC guidelines and validated using KENLAYER software. The critical strains were found to decrease with stabilized subgrades as compared to natural soil as subgrade. A cost comparison analysis is carried out to assess the financial benefit of using the Stabilroad. The reduction

D. Bonagiri · V. Amirthalingam (✉)
Transportation Engineering Division, Indian Institute of Technology Madras, Chennai, India
e-mail: av@iitm.ac.in

D. Bonagiri
e-mail: bonagiri.dheeraj@gmail.com

S. Vallabhaneni
Vishwasamudra Engineering Pvt Ltd, Hyderabad, India

R. Dissanayake et al. (eds.), *ICSECM 2019*, Lecture Notes in Civil Engineering 94,
https://doi.org/10.1007/978-981-15-7222-7_5

in virgin aggregates consumption due to the use of stabilized pavement layer is presented. Typical Red soil was collected for the present investigation.

Keywords Stabilroad stabilized soil · Cement · Unconfined compressive strength · Resilient modulus · Cost analysis · Sustainable pavements

1 Need and Importance

Indian road industry faces several capacity issues and other constraints. The availability of good quality naturally occurring aggregates is considered as one of the major problems faced by the road construction industry now. So due to the scarcity of the naturally occurring good quality materials, removal and replacement of problematic soil become both costly and time consuming. Therefore, it is important to look for innovative pavement design techniques such as stabilization or in situ ground improvement techniques to reduce the thickness of granular pavement layers to achieve reduction in quantity of stone aggregates.

Stabilization is an important technique of improving the soil properties which has been used traditionally from long time. But the type of stabilizer used is changing from period to period considering economy and suitability. Initially stabilization technique was used only for improving the poor soils, but now a days the motto of stabilization is to increase subgrade strength and reduce the usage of virgin aggregates in upper layers. Different waste materials produced from the industry are used as stabilizers for subgrade soils, but their suitability is confined to certain type of soils. So, the corporate sector started research on producing organic materials which can be suitable to all type of soils.

2 Stabilroad

Recently a new stabilizer (manufactured in Germany) is introduced in India called Stabilroad. The stabilizer is a whitish powder made of 100% natural minerals, which should be used along with cement. The stabilizer had been successfully used for nearly 20 years in all climatic zones. The most important feature of this technology is that by using the Stabilroad additive, the construction process can be accelerated (by enhancing cement hydration process), cost of the work can be reduced, and at the same time a very strong, elastic, waterproof and frost-proof surface can be achieved. All these can be achieved by reusing locally available soil.

3 Objective

The research is aimed to investigate the suitability of Stabilroad additive for stabilization of locally available soil and study the effectiveness in terms of improved performance of highway pavement and quantify the benefits of reduced virgin aggregate consumption.

The scope of the work is limited to:

- Stabilization of locally available Red soil with Stabilroad soil stabilizer.
- Evaluation of the strength characteristics of soils by conducting UCS tests and Resilient Modulus tests.
- Pavement design using IRC 37 and analysis by KENPAVE software.
- Assessment of economic and social benefits on the usage of Stabilroad over the traditional materials.

4 Review of Earlier Work

As the stabilizer (Stabilroad) used is a new technology, no earlier work is carried out on it. To investigate it, research related to cement stabilization is studied as the Stabilroad is used along with cement. Work related to optimum dosage of stabilizer, evaluation of cement stabilized layers, pavement design with stabilized layers, cost analysis is studied to carryout current research on Stabilroad additive.

5 Materials

5.1 Soils

For the experimental program of this study two different soil samples were collected from Chennai namely red soil and clay. Particle size distribution of the soils were investigated following the Indian Standard (IS) test method and results are presented in Fig. 1. According to the Unified Soil Classification System (USCS), clay soil was classified as high-plasticity clay (CH) and red soil as clayey sand (SC). Atterberg limits tests were also conducted and found that clay soil has high plasticity index than red soil.

Moreover, compaction properties of the soils were determined and are presented in Table 1. The geotechnical properties of soil (such as compressive strength, CBR, permeability, and compressibility etc.) are dependent on the moisture and density at which the soil is compacted. Higher level of compaction enhances the geotechnical parameters of the soil; therefore, achieving desired degree of relative compaction is necessary to meet desired strength of the soil.

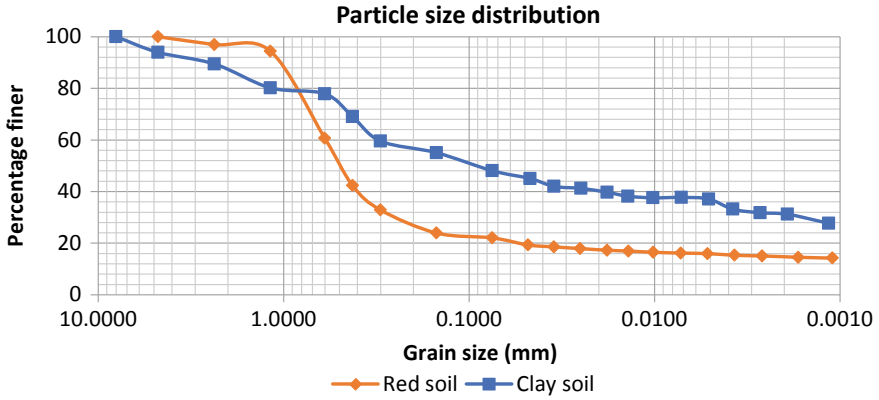

Fig. 1 Particle size distribution of red and clay soils

Table 1 Basic properties of clay and red soil

Soil property	Clay	Red soil
Liquid limit (LL)	86%	27.40%
Plastic Limit (PL)	17.90%	12.80%
Plasticity index (PI)	68.10%	14.60%
Shrinkage limit (SL)	10.20%	11.70%
Specific gravity (G_s)	2.682	2.647
Gravel	6%	3%
Sand	42%	78%
Silt	19%	5%
Clay	33%	14%
Soil Classification (According to USCS)	Highly compressible clay (CH)	Clayey sand (SC)
Swelling index	130%	12%
Optimum moisture content (OMC)	17.60%	8.80%
Maximum dry density, kN/m^3	16.9	19.8
CBR	–	8%

5.2 Stabilizer

The stabilizers used for the present study are Ordinary Portland Cement (OPC) and Stabilroad (Whitish powder). Different dosages of cement and Stabilroad were mixed with soil and the respective tests were carried out to characterize the properties of stabilized soil.

5.3 Experimental Investigation

Laboratory testing was conducted to characterize the soils. The testing program was conducted at the Geotechnical Laboratory at IIT Madras. Soil samples with and without the stabilizer were subjected to different tests to determine their physical properties, compaction characteristics, unconfined compressive strength, CBR and resilient modulus.

As the clay soil property (High plasticity) is not suitable for cement stabilization. Red soil only is considered for stabilroad stabilization.

6 Stabilization of Soil

6.1 Tests on Soil with Cement

Red soil is considered for stabilization with cement as its properties are suitable for it i.e. less plasticity index value. Two different dosages of cement 10% and 12% are added to soil and the samples were prepared with optimum moisture content for testing. The samples were wrapped, and the unconfined compressive strength is determined at different time periods as the strength varies with curing time. Variation of UCS with cement dosage and curing time is shown in Fig. 2 which shows increase in strength with dosage. 12% cement dosage was chosen as optimum dosage as 7 day UCS value of it lies within the range given by Indian Road Congress IRC-37 i.e. 28–35 kg/cm^2

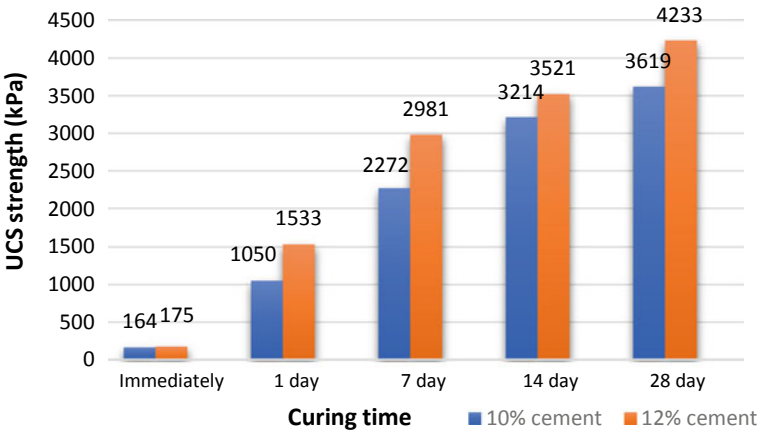

Fig. 2 Variation in UCS with curing time

6.2 Tests on Soil with StabilRoad Additive

The Stabilroad stabilizer is added to soil in addition to the cement to increase the strength of the soil further. The dosages of the stabilizer considered are 1, 2, 3% of cement content as suggested by the supplier.

6.3 Methods

To evaluate the effects of different dosages of stabilizers, strength properties of the stabilized soils were determined for varied amount of stabilizer (i.e. 1%, 2%, 3% of Stabilroad)

6.4 Unconfined Compressive Strength (UCS)

IS 2720-10 (Standard test method for unconfined compressive strength of cohesive soil) was followed to conduct UCS tests on each specimen. The loading rate was 0.625 mm/min. Material proportions were measured gravimetrically and mixed thoroughly, and then compacted such that height to diameter ratio is 2 at optimum moisture content. The UCS tests on untreated soil specimens were conducted immediately after compaction, whereas the treated/stabilized soil specimens were cured in a humid room for 7 days or 28 days prior to testing. Unconfined compressive strength determined for different dosages of stabilizer was shown in Fig. 3.

6.5 Repeated Loaded Triaxial Testing (RLT)

In order to characterize the resilient and permanent deformation behaviour of the treated/stabilized subgrade soils, RLT tests were performed to determine the resilient modulus (Mr) according to AASTHO T307 (Standard method for determining the resilient modulus of subgrade soils). The RLT tests were conducted by applying a repeated axial cyclic stress of a fixed magnitude, load duration, and cycle duration to a cylindrical test specimen for a certain number of cycles. The cyclic loading consists of haversine shaped load pulse. The resilient modulus is found to increase with stabilization, variation can be clearly seen in Table 2.

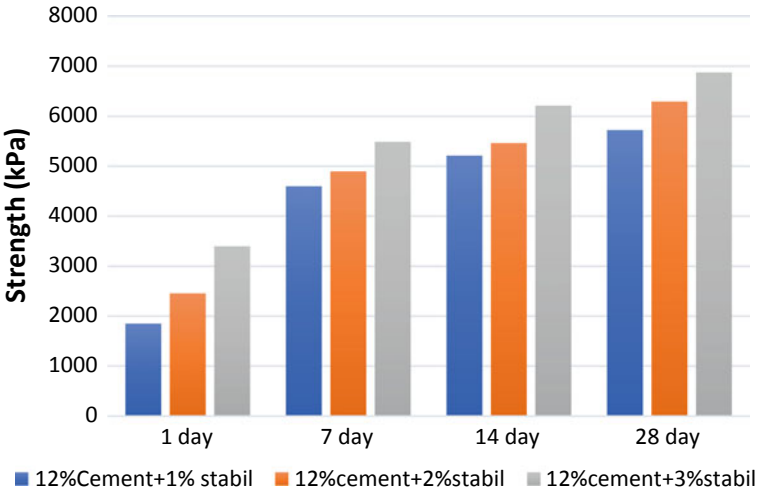

Fig. 3 Variation in UCS with time with Stabilroad

Table 2 Resilient modulus values for different cycles

Sequence	Confining Pressure(kPa)	Maximum Stress (kPa)	Resilient modulus (MPa)		
			Natural red soil	With 12% Cement	With 12% Cement + 3% Stabilroad
0	41.4	27.6	105.33	263.69	133.37
1	41.4	13.8	121.25	151.67	92.94
2	41.4	27.6	84.56	210.71	130.18
3	41.4	41.4	104.49	275.95	222.31
4	41.4	55.2	111.65	297.7	339.55
5	*41.4*	*68.9*	*121.13*	*256.52*	*370.98*
6	27.6	13.8	78.41	202.88	201.63
7	27.6	27.6	101.05	288.11	225.01
8	27.6	41.4	108.06	329.2	285.07
9	27.6	55.2	119.08	353.01	355.85
10	27.6	68.9	123.07	345.99	362.64
11	13.8	13.8	79.46	233.24	213.31
12	13.8	27.6	102.55	266.29	234.25
13	13.8	41.4	106.26	277.78	257.54
14	13.8	55.2	108.1	305.56	288.68
15	13.8	68.9	108.54	305.66	452.74

Table 3 Thickness of pavement alternatives

Layer	Thickness (mm)	Mr (MPa)	Damage ratio
Untreated soil			
BC	150	3000	0.92
GSB	450	208	n/a
Subgrade	500	66.7	0.015
Cement treated soil			
BC	100	3000	0.98
AIL	100	450	n/a
CTB	300	250	0.42
Subgrade	500	67	0.015
Stabilroad treated soil			
BC	90	3000	0.911
AIL	100	450	n/a
STB	280	350	0.61
Subgrade	500	67	0.006

6.6 Pavement Design

Using the results of Unconfined compressive strength and resilient modulus from experimental investigation, alternate pavement was designed (considering traffic of 30 msa) as per the guidelines of IRC 37. KENLAYER analysis was carried out to validate the design. The final designed thickness is given in Table 3. In present study three alternatives were considered. They are untreated red soil, cement treated (12% cement) and Stabilroad treated (12% cement + 3% stabilroad additive).

The pavement thickness was found to be reduced due to the stabilization of subgrade, especially the thickness of bituminous layer was reduced which helps in saving natural resources (bitumen and aggregates).

6.7 Cost Analysis

Cost analysis is a process of evaluating the total economic worth of the project, which can be adopted to decide the best alternative.

The cost analysis was carried out for one-km of a four lane divided highway with 3.5 m lane width (Table 4). The rate analysis for the different layers were considered based on the Schedule of Rates, 2019, followed by the road agencies.

Table 4 Cost analysis of alternative pavements

1. Conventional natural soil (CBR = 8%) subgrade			
Pavement layer type	Optimized thickness (mm)	Unit cost (Rs/m^3)	Cost/layer/m^2
BC + DBM	150	8859	1329
GSB	450	1647	742
SUBGRADE	500	100	50
Total cost (Rs/m^2) 2120			
Total cost for 4-lane divided highway will be Rs.2.97 crores/km			
2. Cement stabilized layers			
Pavement layer type	Optimized thickness (mm)	Unit cost (Rs/m^3)	Cost/layer/m^2
BC + DBM	100	8859	322
AIL	100	2423	219
CTB	300	1301	390
SUBGRADE	500	100	50
Total cost (Rs/m^2) 1569			
Total cost for 4-lane divided highway will be Rs. 2.2 crores/km			
3. Stabilroad stabilized layers			
Pavement layer type	Optimized thickness (mm)	Unit cost (Rs/m^3)	Cost/layer/m^2
BC + DBM	90	8859	797
AIL	100	2423	242
STB	280	1523	426
SUBGRADE	500	100	50
Total cost (Rs/m^2) 1515			
Total cost for 4-lane divided highway will be Rs. 2.1 crores/km			

6.8 Aggregate Consumption

The aggregate requirement for the three alternative pavements are shown in Table 4. The data on aggregate requirement for different types of pavement layers are worked out. The aggregate requirements for StabilRoad pavement is nearly one third of the requirements of conventional pavements. The use of StabilRoad will result in sustainable pavements.

7 Conclusions

- Unconfined compressive strength of cement stabilized soil (7-day curing) is found to be 15 times higher than the natural soil, whereas StabilRoad stabilized soil's strength is found to be 34 times higher.

Table 5 Aggregate consumption calculation per km (4-lane)

Pavement alternative	Layer	Thickness	Quantity to be executed/cum	Aggregate in MT per cum	Aggregates required in MT
Conventional pavement	BC	150	21,000	2.3	48,300
	GSB	450	63,000	1.62	102,060
	SUBGRADE	500	70,000	0	0
					150,360
Cement Stabilized soil	BC	100	14,000	2.3	32,200
	AIL	100	14,000	2.11	29,540
	CTB	300	42,000	0	0
					61,740
Stabilroad stabilized soil	BC	90	12,600	2.3	28,980
	AIL	100	14,000	2.11	29,540
	STB	280	39,200	0	0
					58,520

(BC—Bituminous Concrete, GSB—Granular subbase AIL—Aggregate Interlayer, CTB—Cement treated soil, STB—Stabilroad treated base)

- Resilient modulus of stabilized soil is found to increase significantly with curing time when treated with stabilizer.
- The thickness of conventional pavement is 600 mm; the thickness of the pavement with cement stabilized pavement layers is 500 mm and with Stabilroad stabilized layer is 470 mm.
- The construction cost of traditional pavement is Rs.2.97 Cr (0.421 US$ million)/km, cement stabilized soil is Rs.2.2 Cr (0.321 US$ million)/km and Stabilroad stabilized soil is Rs.2.1 Cr (0.297 US$ million)/km which concludes that using the stabilized layers in pavement construction, the cost can be reduced. The use of stabilized pavement layers reduces the transportation of aggregates over long distances.
- The aggregate consumption for stabilized layer pavement is three times lesser than conventional pavement. Thus, use of Stabilroad stabilizer ensures sustainable pavements and the pavement can be constructed saving natural resources, significantly.

References

1. AASHTO T307-99 (2003) Standard method of test for determining the resilient modulus of soils and aggregate materials. American Association of State Highway and Transportation Officials, Washington DC
2. IRC- SP-89-Part 2-2018 Indian Road Congress code, Guidelines for design of stabilized pavements

3. IRC-37 2018 Indian Road Congress code, Guidelines for the design of flexible pavement (fourth revision)
4. IS: 2720 (Part 4)-1985: Indian Standard code of practice for method of test for soils—grain size analysis
5. IS: 2720 (Part 5)-1985: Indian Standard code of practice for method of test for soils—determination of liquid and plastic limit
6. Mahedi M, Cetin B, White DJ (2018) Performance evaluation of cement and slag stabilized expansive soils. Transp Res Rec J Transp Res Board 036119811875743. https://doi.org/10.1177/0361198118757439
7. Mallela J, Quintus HV, Smith K (2004) Consideration of lime-stabilized layers in mechanistic-empirical pavement design. The National Lime Association
8. Rashidi M, Ashtiani RS, Si J, Izzo RP, McDaniel M (2018) A practical approach for the estimation of strength and resilient properties of cementitious materials. Transp Res Rec 2672(52):152–163. https://doi.org/10.1177/0361198118769900
9. Saxena P, Tompkins D, Khazanovich L, Balbo JT (2010) Evaluation of characterization and performance modeling of cementitiously stabilized layers in the mechanistic-empirical pavement design guide. Transp Res Rec 2186(1):111–119. https://doi.org/10.3141/2186-12
10. Theyse HL, De Beer M, Rust FC (1996) Overview of South African mechanistic pavement design method. Transp Res Rec 1539(1):6–17. https://doi.org/10.1177/0361198196153900102
11. Wen H, Edil T (2008) Characterisation of Cement stabilized layer linked to pavement design & analysis. NCHRP project 4-36

Impact of Contractor's Overhead and Profit Factor on Price Fluctuation Calculated Using CIDA Price Fluctuation Formula

A. S. Samarakoon and L. S. S. Wijewardena

Abstract The inevitability of price fluctuations is highly demanded topic all over the world. When it comes to the construction industry, the fluctuations of the prices of the construction inputs i.e. materials, labour, plant and equipment should be particularly studied since they are biasing to the contract sum in millions, billions range in major projects. The Price Adjustment (PA) technique is introduced by the Construction Industry Development Authority (CIDA) [formerly Institute of Construction Training and Development (ICTAD)] known as the "CIDA formula method for adjustment to contract price due to fluctuation in prices" has a constant of 0.966 based on a 15% fixed profit percentage according to the derivation of the formula. But the contractor's overhead and profit margin vary widely and neither be fixed for all projects nor for each and every construction contractor. Generally, it can vary according to the type of construction project and according to the contractor. Hence, the price escalations rendering from the CIDA formula are not the true fluctuations for a particular project or a contractor. Therefore, this study was carried out to investigate the degree of accuracy of the CIDA price fluctuation formula method compared to the conventional method with the aid of an automated spreadsheet. Furthermore, it discusses and interprets the deviation of the price escalation generated from CIDA formula and the actual modified CIDA formula for contractor's profit percentage. As interpreted by the study, it shows the true escalation to a high-end contractor should be lower than the current escalation calculated by the CIDA formula for a particular project whereas low-end contractor should be paid more than the current amount calculating from the CIDA formula. Therefore the current CIDA formula is not giving the true price escalation in point of view from the contractor's profit percentage.

Keywords Cost adjustment factor · Overhead and profit · CIDA formula method · Input percentage · Price escalation

A. S. Samarakoon (✉) · L. S. S. Wijewardena
Department of Civil Engineering, The Open University of Sri Lanka, Nawala, Nugegoda 11222, Sri Lanka
e-mail: ashini.shalima@gmail.com

R. Dissanayake et al. (eds.), *ICSECM 2019*, Lecture Notes in Civil Engineering 94,
https://doi.org/10.1007/978-981-15-7222-7_6

1 Introduction

In the construction industry, contractors need to be compensated for the fluctuations of the prices of the construction inputs i.e. materials, labour and plant and equipment since they are biasing to the contract sum in millions, billions range in major projects. Price escalation is the change in cost or price of specific goods or services in a given economy over a period. The escalation in price of units reflects the inflationary trends in the economy [2]. Methods for calculation of price adjustments can be categorized into two approaches. First one is the FIDIC formula for Price adjustment calculation [4]. Asian countries, such as, India and Pakistan, are also practicing a PA formula similar to the FIDIC formula which is the second approach. Central Public Works Department is the responsible authority in India [3]. In 1973, the National Economic Development Office in UK (NEDO) established systematic PAFs, namely Baxter Formula for civil engineering works, Osborne Formula for other building works and Bespoke formula used for the specialist engineering installations [1]. The Construction Industry Development Authority (CIDA) [formerly Institute of Construction Training and Development (ICTAD)] in Sri Lanka has been able to resolve the problem up to some extent by adjusting the effect of price fluctuations using a price fluctuation formula introduced by them. It is commonly known as the 'CIDA Formula Method' as published by the CIDA in January 1993. They have derived two formulae as;

1. The formula for the contracts not exceeding 10 million (Simplified Formula) and
2. The formula for the contracts exceeding 10 million.

The general formula (contract value more than 10 Million Rupees) for price adjustment reference to the "CIDA formula method for adjustments to contract price due to fluctuation in prices" is as follows in Eq. (1), [5].

$$F = \frac{0.966(V - V_{\text{na}})}{100} \sum_{\text{All inputs}} P_x \frac{(I_{xc} - I_{xb})}{I_{xb}} \tag{1}$$

In the derivation of the CIDA formula, it has taken the cost adjustment factor (K) as 15% and the rest adjustment factor (R) as 10%. The value of K used in the derivation of this formula has a fixed value of 15% which allows for the profit and overheads of the contractor. But this margin ranges generally up to 35% and cannot be fixed for every project [7]. Jayasinghe, et al. has shown the need of adjusting the CIDA formula in order to account for the variation of the profit and the overhead margin of contractors.

2 Methodology

The selected building project consists of 321 BOQ items which include Excavation, Concreting, Formwork, Reinforcement, Brick work, Rubble Masonry, Roof Works, Cement Rendering, Doors, Windows, Plastering and Painting as major trades. The total contract sum of the project with 15% overhead and profit margin is Rs. 133, 500,098.58.

A. Adjusting the overhead and profit margin up to 35% of the selected project which is exceeding 10 million of contract sum and the project duration exceeding 1 year.
B. Collection of work norms for BOQ items and the calculation of input percentages.
C. Collection of prices for materials, labour and plant.
D. Collection of Interim Payments (Monthly Bills)
E. Calculation of Price Escalations for each of the interim payment bill according to the CIDA Formula Method [6].
F. Calculation of Price Escalations for each of the interim payment bill according to the conventional method.
G. Determination of the closeness of CIDA formula to the true fluctuation amount obtained by conventional method.
H. Analysis of the variance of Price Escalations calculated by the modified fixed coefficient for the current CIDA formula and the existing CIDA formula.

Work norms of the each BOQ items are fed to the spreadsheet to auto generate the budget rate and hence BOQ rate. Calculation of the input percentages has been done by referring the ICTAD Formula Method (ICTAD/ID/07)

An automated spreadsheet was developed for adjusting the overhead and profit margin up to 35%. The BOQ rates of the selected project are rearranged with a uniform overhead and profit margin. Automated spreadsheet can calculate BOQ rates for any given overhead and profit percentage. The BOQ is separated to identify the non-adjustable elements and dis-regarding items according to the CIDA Formula Method. Figure 1 shows a flow chart of calculating input percentages as described in the ICTAD Formula Method (ICTAD/ID/07).

Total of Non-Adjustable elements (LKR)	24,883,695.15
BOQ Total (LKR)	133,500,098.58
% of Non-Adjustable elements from the BOQ	18.64%
Adjusted BOQ Total (LKR)	108,616,403.43
Total of Dis-regarding items (LKR)	1,644,700.00
% of Dis-regarded items from the BOQ	1.23%
Total, Less non-adjustable elements & Dis-regarded items (LKR)	106,971,703.43

The formula considered 90% of the inputs directly while the balance 10% of inputs are considered indirectly. Less cost significant items (less than 1% contribution)

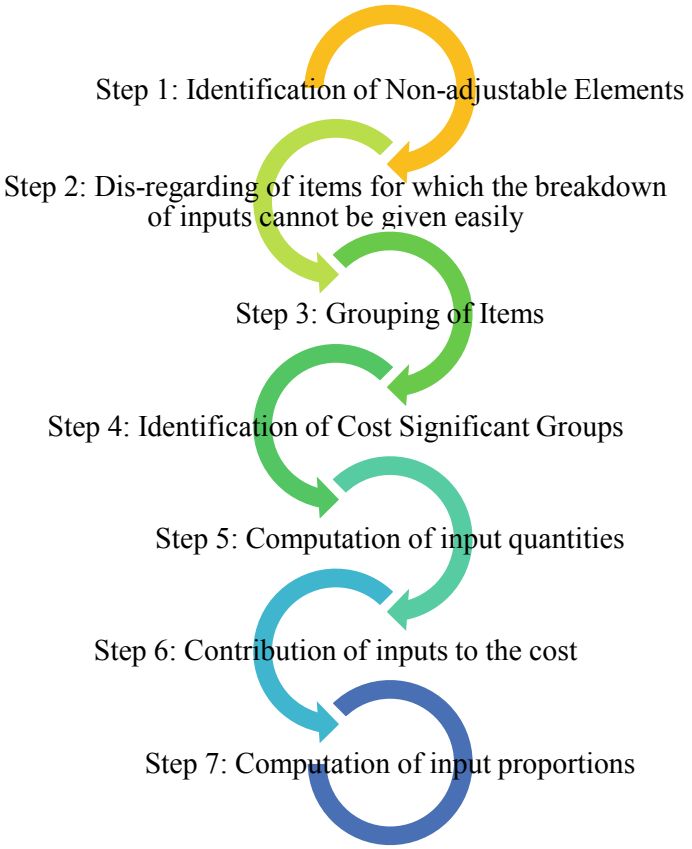

Fig. 1 Flowchart—calculation of input percentages

are eliminated from the final computation and the balance items only are shown in Table 1. The total amount of cost significant inputs is computed as Rs. 56,904,102.17. According to the concepts of the formula this should represent only 90% of the cost inputs. Hence the total cost of inputs estimated as Rs. 63,226,780.19 by dividing the 90% of cost by 0.9. The input percentages of each input are then calculated in relation to the total cost of inputs. The final input proportions together with the reference indices are shown in Table 1.

Table 1 Contribution of inputs to the cost—arranged in descending order (with insignificant items assigned under rest)

Input	Indices Reference	Amount	Percentage
Unskilled Labour	L3	13,557,584.04	21.44
Skilled labour	L1	12,566,887.94	19.88
R/F steel	M13	8,690,283.84	13.74
Cement	M4	8,130,675.74	12.86
Bricks	M9	4,884,300.00	7.73
Sand	M8	3,498,898.12	5.53
Wall paint	M27	2,985,560.00	4.72
Metal	M7	1,813,494.41	2.87
F/Work Timber	M21	776,418.09	1.23
Rest		56,904,102.17	90.00
		6,322,678.02	10.00
		63,226,780.19	100.00

3 Results and Discussion

3.1 Variation of Price Escalations with the Change of Overhead and Profit Margin

Price escalations calculated for each of the interim bill of the selected project shows an exponential growth with the increase of the Overhead of Profit margin of the contractor. Results given by first six project interim bills (IPC 01 to IPC 06) are shown in Fig. 2.

The graph in the Fig. 3 is plotted to interpret the first 5 IPC numbers for the price fluctuations calculated by conventional method (Blue Color), price fluctuations calculated by CIDA formula for the BOQ with 15% overhead and profit (Green Color) and for the price fluctuations calculated by CIDA formula for the BOQ with 35% overhead and profit (Yellow Color). It can be clearly seen that there is a considerable difference when the contractor's overhead and profit percentage varying from 15% to 35%. Hence, there is a significant effect on the fluctuations calculated by CIDA formula.

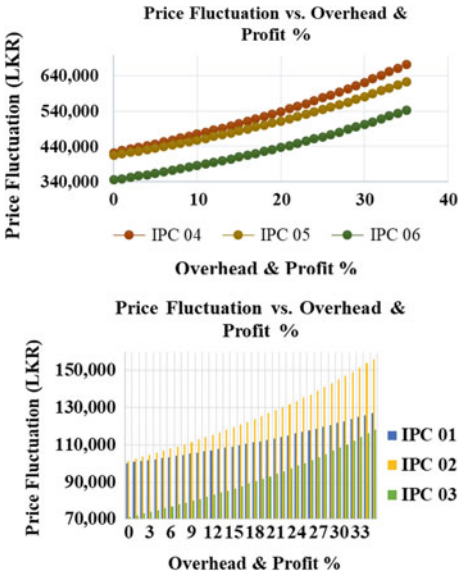

Fig. 2 Price fluctuation versus overhead & Profit% for first six project interim bills

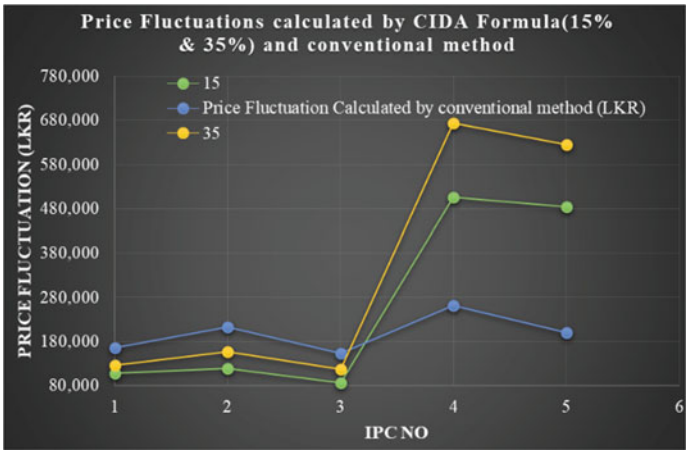

Fig. 3 Deviation of price fluctuations calculated by CIDA formula (15% & 35%) from the conventional method

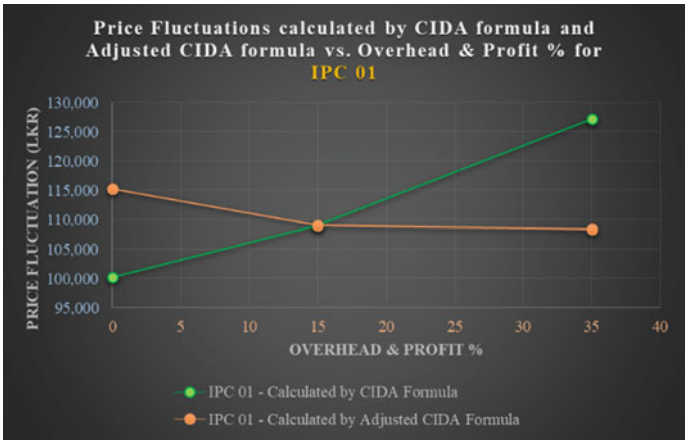

Fig. 4 Variance between the price fluctuations calculated by CIDA formula (up to 35%) and adjusted CIDA formula for IPC 01

3.2 Price Fluctuations Calculated by CIDA Formula and Adjusted CIDA Formula

Figure 4 interprets the output generated for IPC 01 from the current CIDA Formula and the adjusted CIDA Formula. The actual Overhead and Profit margin has been used in the adjusted CIDA Formula.

4 Discussion

The fixed coefficient 0.966 of CIDA formula represent the contractor's cost adjustment factor as (K) 15% and the inputs not listed for price adjustment under the contract (Rest) as (R) 10%. In this study, the price fluctuations are calculated using the CIDA formula for a BOQ of a building project by varying the overhead and profit percentage up to 35%. In Sri Lanka, there are contractors in different grades which has different overhead scales. Therefore, it is not fair to treat all the contractors with the formula derivate by the same overhead and profit factor of $K = 15\%$. Because it is unfair for the contractors who has small scale overheads.

On the other hand, prices of the resources i.e. material, labour and plants are depending on the area of purchasing. It is required to check the prices that are taken to generate the ICTAD price indices bulletin since it is affecting the difference from the price fluctuations calculated by the CIDA formula and the conventional method. The collection of prices to the study came across the following scenarios.

1. When the contractor purchasing materials in a bulk amount the contractor has purchased resources for a discounted rate from suppliers. The discounted price is less than the market price
2. The contractor has purchased materials in a bulk amount for a higher price than the market price but to a longer credit periods
3. In special circumstances the contractor has purchased materials through petty cash
4. For small tools contractor has used company owned small tools which have completely depreciated already
5. Some small tools are hired or newly purchased for the project
6. There are subcontractors who have left the job and the new subcontractors coming are completing the job to a higher demand
7. There can be stock transfers from the other projects.

Due to above concerns, gathering of data such as prices of each and every resources for calculating of true price fluctuations is impractical. The best method is to find the resource rates which are based on ICTAD price indices that published in monthly bulletin.

5 Conclusion

The main objective of the study is to evaluate the effect of contractor's profit percentage on price fluctuation calculated using CIDA price fluctuation formula. To achieve this aim, objectives are set as to find the relationship between ICTAD price adjustments and true price adjustments, to estimate the accuracy of the ICTAD formula method for the PAs by the conventional method and the CIDA formula method and to evaluate the variation between the price escalations calculated from the adjusted CIDA formula and the current CIDA formula.

According to the derivation of the CIDA formula, it has taken the contractor's profit and overhead factor, K as 15%. Therefore, in the equation there is constant as 0.966 together with a rest adjustment factor, R as 10%. The issue arises basically because of having different overhead and profit percentages to contractor. This is usually varies according to the project such as building, road, water, etc. even within the same contractor. But in the practice at the present, the CIDA formula which has been derived by substituting the overhead and profit factor, K as 15 is used by the contractors to calculate price escalations for any kind of project.

The conclusions arrived are as follows.

1. The price escalations calculated from the CIDA formula is providing a higher escalation claim to the contractors with higher overhead and profit margins than the actual claim there should be. This can be clearly observed from the graphs plotted in the results. And also has explained mathematically simply in the discussion. When the contractor's overhead and profit margin, $K = 15\%$, the constant in the CIDA formula is 0.966. As in the calculation of the discussion, the constant

becomes a lower value of 0.823 from 0.966, if 35% substituted for K. Since the constant is in the numerator the actual price escalation calculated should be multiplied by the lower value of 0.823. Hence the actual escalation claim which should be claim by the contractors with higher overhead and profit are always getting a lower amount than the price escalation calculated by the current CIDA formula.

2. The price escalations calculated from the CIDA formula is providing a lesser escalation claim to the contractors with lower overhead and profit margins than the actual claim there should be. This can be clearly observe from the graphs plotted in the results. And also has explained using mathematically using the CIDA formula simply as in the discussion. When the contractor's overhead and profit margin, $K = 15\%$, the constant in the CIDA formula is 0.966. As in the calculation of the discussion, the constant rises to a higher value of 1.111 from 0.966, if 0% substituted for K. Since the constant is in the numerator the actual price escalation calculated should be multiplied by the higher value of 1.111. Hence the actual escalation claim which should be claim by the contractors with lower overhead and profit are always getting a higher amount than the price escalation calculated by the current CIDA formula.

6 Recommendations

According to the CIDA price fluctuation formula, to calculate the actual price escalations it is necessary to use the actual overhead and profit margin or in other words cost adjustment factor K. But it will not be successful since there is no practice or standards of representing the overhead and profit margin by any contractor. Therefore it is recommended to use estimates for K values according to the ICTAD grading of construction companies. According to the ICTAD guidelines there are 11 grades for main grades from the lowest grade as C9 to the highest grade CS2. Therefore it is recommended to suggest K factors based on the ICTAD grades by considering the financial limits of the contractors. However, it would be necessary to carry out the future studies by analysing the range of construction companies for different ICTAD grades and evaluating of K values for each grade.

The variation of project resource prices in different areas is the other perspective that should be emphasized. At the present there is only one price indices bulletin is publishing for each month for the whole country by CIDA. But the resource prices are not equal within the country. It will be changing depending on the demand, ease of access, transportation, etc. Therefore, the price indices have to be varied depending on the prices of resources in different areas of the country.

References

1. Abeysekara WVMK (1997) Construction contracts and claims-Project Report, OUSL
2. Chaphalkar NB, Sandbhor SS (2012) Wholesale price index and its effect on price escalation of materials for Indian construction industry. IJERT, Maharashtra
3. CPWD (2007) CPWD works manual. CPWD, New Delhi
4. FIDIC (2005) Conditions of contract for construction: for building and engineering works designed by the employer, 2005th edn. FIDIC, Geneva
5. ICTAD (2008) ICTAD formula method for adjustments to contract price due to fluctuation in prices, 2008th edn. Ministry of Housing and Development, Colombo
6. ICTAD (2018) ICTAD statistical bulletin. ICTAD, Colombo
7. Jayasinghe B, Alahakoon C, Wijewardena S (2015) Sensitivity of the ICTAD price fluctuation formula procedure for the true material price fluctuations in construction industry. J Eng Technol Open Univ Sri Lanka 3(1):2279–2627

Assessing Applicability of Structural Measures for Enhancing Flood Management in Sri Lanka

Rusiru Ernst, Udayangani Kulatunga, and Pavithra Rathnasiri

Abstract Floods can be identified as one of the most devastating natural disasters all over the world which brings a considerable amount of social, economic and environmental impacts. Therefore, it is important to focus on adequate knowledge, strategies and decision makers in order to prevent these floods from becoming disasters. Different measures are taken in order to respond to the prevailing disaster situations and those measures can be categorized as structural measures as well as non-structural measures. Among them, substantial attention should be paid for adopting structural measures for flood mitigation. Structural measures can be defined as different types of facilities which are permanently constructed with the aim of reducing potential risk at an event of a flood. The study provides literature synthesis addressing the importance of structural measures in flood mitigation process, different types of structural measures and their impact regarding Sri Lankan context.

Keywords Disasters · Floods · Flood management · Structural measures

1 Introduction

Floods can be occurred due to different reasons such as heavy rainfalls, inadequate capacity of rivers to discharge excessive water, poor permeability of the soil and inadequate drainage to carry away the excessive rainwater [40]. Different types of floods such as flash floods, river floods, coastal floods and inland floods are occurred due to above reasons. These will lead to serious risks to millions of people and public property in any country [45]. Hence it is obvious that there is a higher need of flood management to mitigate the problems associated with flooding [56]. According to Institute for Water Resources [IWR] [24], flooding is one of the main natural hazards within the world and 520 million people are affected by floods in every year as well as between 50 and 60$ billion global economic losses are occurred. Therefore with the rapid increase of social, environmental and economic losses due to floods, nowadays

R. Ernst (✉) · U. Kulatunga · P. Rathnasiri
Department of Building Economics, University of Moratuwa, Moratuwa, Sri Lanka
e-mail: rusiruernst@gmail.com

R. Dissanayake et al. (eds.), *ICSECM 2019*, Lecture Notes in Civil Engineering 94,
https://doi.org/10.1007/978-981-15-7222-7_7

the world tends to get proper steps in order to prevent, protect and mitigate the flood disasters all over the world [14].

When it comes to the Sri Lankan context, Sri Lanka can be identified as one of the flood prone countries because of its unique geographical location and topography [64]. Floods can be identified as one of the most destructive natural disasters in Sri Lanka and can have a considerable impact on human lives and national economy of the country in different ways [48]. Currently, different types of methods for flood management are available in Sri Lanka with the purpose of reducing the impact of it [26]. Those methods include both structural and non-structural measures and the influence of them for flood mitigation differ from one another [13].

Accordingly, through a comprehensive literature review, Hence, this paper evaluates the importance of structural measures in flood management process and the negative impacts of them within the context of Sri Lanka.

2 What Is Flood Management

Floods can be identified as one of the natural phenomena which can occur at any time in any area. However, it is important to focus on adequate knowledge, strategies and decision making in order to prevent these floods from becoming disasters [11]. This section pays the attention on flood management and its importance.

Flood management can be defined as the process of managing floods properly with the aim of reducing the flood risks on human lives and natural environment [37]. Flood management focuses on considerable amount of issues as well as tasks ranging from prediction of flood hazards to reduction of flood risks. Further, the study has stated that because of this wide array of issues and tasks, flood management needs systematization and integration.

According to Sayers et al. [52], different steps are included in flood management process in order to reduce and control the flood risk in an event of flood such as gathering information, risk analysis, evaluation of the risk, appraisal of options, decision making, implementing the decisions and reviewing decisions [52].

2.1 Importance of Flood Management

Flooding is a natural phenomenon which the world is adversely affected over the last few decades [8]. Therefore, many countries tend to follow flood risk management procedure to reduce the risk of flood events. According to Hooijer et al. [22], the main goal of flood management can be identified as to minimize flood risks through implementing different types of measures. Further, goal of flood management includes both reducing the probability of flooding as well as minimizing the potential damage (Table 1).

Table 1 Flood mitigation measures

Flood mitigation measures	
Structural measures	Non-structural measures
• Dams • Reservoirs • Levees • Channel improvements • Flood walls	• Flood warning and evacuation • Flood plain land use • Flood proofing • Flood insurance

Adapted from [38]

3 Methods of Flood Management

Both preparedness for floods as well as prevention of floods are included in the term of flood management [59]. Further, a balanced approach in between these two areas should be considered in flood management. Accordingly, different flood mitigation measures can be identified covering these areas and those measures can be categorized as structural measures as well as non-structural measures [33]. Structural measures can be identified as protection actions while the nonstructural measures can be identified as vulnerability reduction actions [23]. Minea and Zaharia [35] have stated that when applying these measures proper interaction should be developed between both structural and non-structural measures. Some examples for structural and non-structural measures are listed in Table 2.

When considering the flood management measures, substantial attention should be paid for the order which these measures are applied [2]. Accordingly, developing public awareness comes first while proposing risk reducing measures comes second and finally training is carried out. Both structural and nonstructural measures as flood risk reducing measures are separately discussed in following sub sections respectively.

Table 2 Classification of reservoirs

Classification of reservoirs	
According to the location	According to water storage
• On stream (by constructing a dam across a river) • Off stream (by enclosing waterproof banks partially or completely)	• Dry reservoir (storage area is free of water during dry weather conditions) • Wet reservoir (has a permanent pool)

Adapted from (Hettiarachchi 2011)

3.1 Structural Measures

Structural measures can be defined as different types of facilities which are permanently constructed with the aim of reducing potential risk at an event of flood [6]. Most government actions of any country tend to improve these structural measures because the risk and damage of floods can be reduced and mitigated in a considerable level through these measures [30]. These structural measures include different types of constructions such as dams, river dikes, levees, channel improvements, flood ways and internal drainage systems which are constructed based on the concept of urban disaster prevention and urban planning approach [56]. Although floods are prevented in a considerable level by these structural measures, they cannot be identified as environmentally sustainable because they can lead to severe environmental issues such as environmental degradation and loss of wetlands and animal habitats [53].

3.2 Nonstructural Measures

Non-structural measures can be defined as methods which can be used to reduce the damages from floods not involving physical construction but implementing different types of precautions [7]. These measures include flood forecasting and warning, establishing laws and regulations, flood risk management, reconstruction and rehabilitation planning, flood insurance system and flood related databases [30]. These measures directly focus on reducing losses of human lives as well as property damages [2]. Although these non-structural measures are highly effective, proper interaction is needed in between both structural and non-structural measures as they may become less effective without structural measures [19]. Furthermore, Kundzewicz [32] has comprehensively disclosed that non-structural measures are indispensable for risk mitigation in floods but the most appropriate solution is applying mix of structural and non-structural measures.

4 Importance of Structural Measures

As per the above mentioned factors, both structural and nonstructural measures are used for flood mitigation all over the world. Improving these structural and nonstructural measures lead to successful flood risk management [56]. Among them, importance of adopting structural measures is discussed in following section.

Structural measures can be identified as traditionally known methods which are used for flood mitigation in most of the flood prone areas [19]. In addition, although the nonstructural measures can be identified as effective methods for flood management, without improving structural measures, they would be less effective. Variety of structural measures are used in flood mitigation and inundation of floodplain areas

is prevented in different ways using these different structural measures [38]. The study has further revealed that idea by giving examples namely reducing peak flows using reservoirs, limiting the water flow using levees and flood walls and reducing peak stages using channel improvements. Structural measures can be identified as constructed permanent facilities while the nonstructural measures are temporary methods which are used for flood mitigation [43].

Accordingly, many advantages can be identified in structural measures when adopting them in flood prone areas with the aim of flood mitigation as shown follows [3].

1. Delaying water runoff
2. Increasing of infiltration
3. Controlling ground water
4. Controlling downstream discharge
5. Flood attenuation.

Plessis and Viljoen [44] have comprehensively disclosed that the priority should be given for keeping floodwater out of developed floodplains. Further, it can be accomplished by developing structural measures rather than implementing nonstructural measures. According to Salvesen [49], structural measures seek to reduce the impact of floods while nonstructural measures seek to keep people away from the flood. Therefore, rather than keeping people away from the hazard, it is better to move or tame the water flow up to considerable level that reduces the risk.

According to Hooijer et al. [22], prevention and mitigation are two different terms in flood management which can be used to describe structural and nonstructural measures as prevention of floods is done by nonstructural measures while the mitigation of floods is done by structural measures. The study has further emphasized that although prevention of floods is done, floods can be occurred at any time due to any reason. Therefore, mitigation is more important and as a result structural measures play a vital role in flood management. The same idea is further revealed in a recent study by Velasco et al. [57] by stating that nonstructural measures are only focusing on vulnerability reduction while the structural measures are focusing on reduce the impact in an event of flood.

Kousky and Walls [31] have given an example relating Meramec river which joins Mississippi river in order to emphasize the importance of structural measures for flood management. The authors have mentioned that floods which can be lead to seasonal flooding are occurred in Meramec river due to lack of structural protection around the river. Another example is given by a recent study by Grelot, Bailly and Lavergne [18] stating that flood events are controlled in a considerable level in Orb river at France where only structural measures are considered. Therefore, it is obvious that flood events are efficiently controlled and reduced through structural measures compared to nonstructural measures.

5 Types of Structural Measures

Although nonstructural measures are implemented in flood mitigation, they can be less effective without structural measures [19]. Different types of structural measures which are developed nowadays for flood management can be listed as follows.

- **Dams**

Dams can be identified as an effective alternative when the land uses and other nonstructural measures are restricted in any area [5]. In generally, dams are constructed with the purpose of irrigation, power generation and flood mitigation [1]. Further, when considering the flood mitigation, excess rainwater is stored in order to release in a proper way and therefore, floods are prevented in the presence of heavy inflow to the dams. In addition, Himsley [21] has disclosed that dams are constructed across streams as well as flow paths to store and release excessive water properly without making any hazard when there is heavy water inflows to the dams. Also the author has further emphasized that the way of mitigating the flooding includes operation of dam gates as well as pre-releasing water from dams. Berga et al. [5] has identified in his study that there is a special type of dams for flood mitigation which are called as Flood Mitigation Dams (FMD). According to the author, the reservoir of these dams is usually empty and only filled normally during flood events.

- **Reservoirs**

Reservoirs also can be identified as one of the important structural measures which are constructed for flood mitigation. According to Zhou et al. [63], the main purpose of these reservoirs is to prevent damages from flood events as well as safety of the reservoir itself. Reservoirs have the ability of storing large flow volumes, modifying flood routing and reducing peak flows [5]. Therefore, water is managed by these reservoirs properly during high flow periods by reducing the amount that goes downstream and lowering flood peaks [17]. Moreover, Zhou et al. [63] has disclosed that sometimes a single reservoir may not have the enough storage capacity for control certain flood events. Hence, cascade reservoirs can be used to operate together to provide protection at such flood events.

- **Levees**

Federal Emergency Management Agency [FEMA] [16] has defined a levee as a man-made structure which can be identified as an earthen embankment which is designed and constructed to provide protection against floods. Further, these levees are constructed parallel to a body of water to divert the flow of water with the purpose of protecting from temporary flooding. The author has mentioned that levees provide protection against floods up to a some extent and it is further emphasized in a recent study by Hui [23] which states that levees can decrease the flood risk by providing partial protection but cannot eliminate the risk. Levees can be constructed along one

or both sides of a waterway with suitable height and width in order to prevent rising floodwaters from inundating land [41]. Further, normally they are made of soil and are sloped on both sides. Accordingly, levees can be constructed from levees with simple berms to super levees which provide protection for largest floods. Generally, levees can be identified as one of the most suitable structural measures which can be used for flood risk management in urban areas by providing protection against flood events along coasts, rivers and artificial waterways [8]. The study has comprehensively disclosed that many urban areas would be uninhabitable without constructing levees because as per the above factor, they are a vital part of modern flood management. Although levees can be identified as effective flood control measures, flood risk can be considerably amplified if they are improperly installed [62]. Therefore, it is important to install these levees in areas where they are highly needed.

- **Floodwalls**

Floodwalls can be identified as another main structural measure as same as the levees but they are constructed vertically to a waterway [16]. The study has further mentioned that these floodwalls are also mostly constructed in urban areas using stone or concrete. Opperman [41] has identified these floodwalls as a traditional responsive method for flood risk management. According to the author, it generally provides a barrier in order to prevent rising of floodwater and entering into the area behind the floodwall. Further, less space is taken for floodwalls than levees and therefore they can be identified as the most suitable structural measure for urban areas than levees for flood mitigation (Fig. 1).

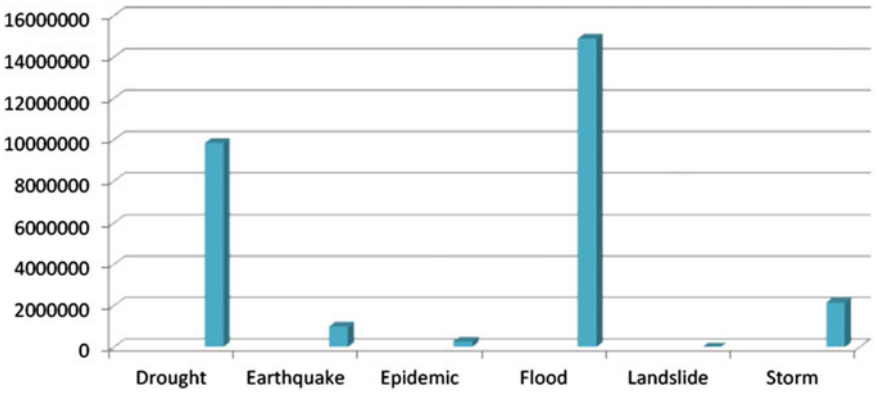

Fig. 1 Number of people affected by different disasters in Sri Lanka Adapted from: [29]

- **Diversions**

Diversions can be identified as one of the best alternative for flood management. Flood events are controlled by these diversions by reducing flood peak discharge in the river immediately after diversion point [19]. Kingsford (2000) has stated that floods are controlled through diversions by reducing sediment erosion, retaining runoff and encouraging groundwater infiltration. The author has further mentioned that after a rainfall, the amount of water which reach to the floodplain areas are governed by the diversions in flood controlling. Different types of structures such as water traps and transverse dikes are used in order to divert flood water for water supply augmentation purposes [19].

- **Drainage systems**

It is obvious that constructing structural flood control measures in urban areas is difficult because the space available for them is very limited [46]. Hence, the author has disclosed that improving drainage systems with suitable control measures like gates is a practical as well as financially viable option for flood mitigation in urban areas. According to Verworn [58], runoff components through an urban drainage system can be categorized into two types namely waste water and storm water. Waste water comes from domestic and industrial developments while storm water is produced by rain or any other cause which can leads for a flood event. Accordingly, the author has further mentioned that drainage systems can be used as an effective flood mitigation measure in urban areas which minimize the adverse impact on human lives, environment and properties (Fig. 2).

- **Channel Improvements**

Modifications which are made for river channels can be identified as channel improvements [41]. The study has identified different ways of modifications such as dredging and straightening of channels to increase the speed of flood within the channel as well as to change the way of water flow. Normally these channel improvements are designed with the purpose of increasing the carrying capacity of a reach of river [28, 41]. According to the authors, it is done by enlarging the cross sectional flow area of the channel. When channels are straightened, artificial straight channels are constructed to cut out the meanders [15]. Therefore, water can be move out from the area quickly and as a result, floods risk can be reduced by constructing channel improvements.

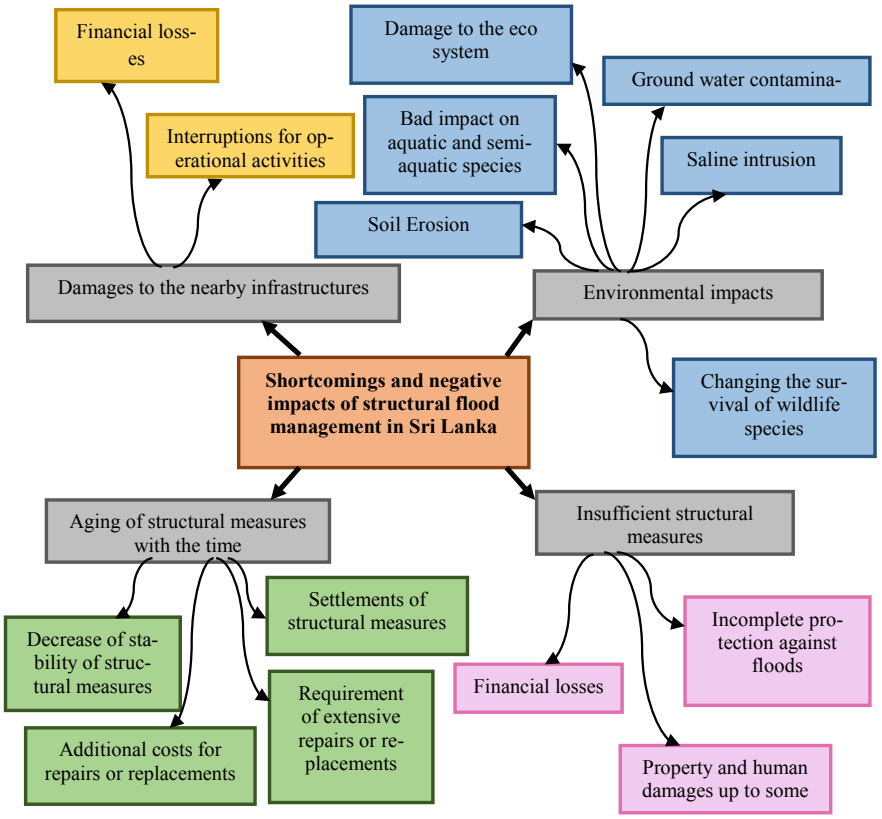

Fig. 2 Impact of structural flood management in Sri Lanka

6 Floods in Sri Lanka

Sri Lanka is prone to various natural disasters such as floods, drought, landslides etc. which leads large number of losses of human lives as well as property damages from past to present [27].

According to the above statistical data, it is clear that majority of people are affected by floods in Sri Lanka. It is further emphasized in a study by Palliyaguru and Amaratunga [42] where states that major deaths are reported every year in Sri Lanka because of floods. Wickramaratne et al. [60] have stated that 103 river basins can be identified in Sri Lanka which cause annual floods throughout the country. Further, Mahaweli, Kelani, Kalu, Gin and Nilvala rivers are the main river basins among them which leads major floods in the country. In Sri Lanka, floods are occurred during two monsoon seasons, which affect for the country throughout the year [27].

Further, when considering the areas, which are at the risk of flooding, southern and Sabaragamuwa provinces are mostly affected during south-west monsoon while eastern, northern and north central provinces are more vulnerable during north-east monsoon. The frequency of occurring floods has highly increased through the past decades in Sri Lanka and it is further revealed by providing an example which states that a steady increase can be seen in flood occurrence in Colombo area from 2005 onwards [20]. Different reasons affect for occurring floods in Sri Lanka can be listed such as heavy rainfalls, filling in of low lands, erection of unauthorized structures, lack of maintenance of drainage systems, earthquakes, landslides etc. [60, 54].

7 Existing Structural Flood Management Measures in Sri Lanka

Different initiatives were taken by Sri Lankan government with the aim of mitigating the damages due to floods and under structural measures, different methods namely reservoirs, dams, diversions, channel improvements and levees have been adopted throughout the country [27, 54]. According to Sivakumar [54], these measures have been developed to modifying the flood by keeping flood water away from populated areas.

When considering the dam construction in Sri Lanka, it is not new to the country because a great hydraulic civilization is owned by Sri Lanka [61]. The dam network consists of 350 medium and large dams as well as 12,000 small dams [50]. Further, construction of dams varies in design, age and construction and these dams brings multiple benefits in flood management. Currently, large number of dams are constructed within the country and examples can be given as Kotmale, Randenigala, Rantambe, Victoria, Kantale, Deduru Oya, Kalu Ganga, Moragahakanda, Laxapana, Gal Oya etc. [27].

Reservoir construction is another structural measure of flood controlling which are adopted in Sri Lanka. It is prevailed from the past within the country and they can be identified as built structures for water storage which can be beneficial in flood controlling [10]. Hettiarachchi (2011); Wijesundara and Dayawansa [61], have provided some examples for reservoir construction namely Sembuwatta, Inginimitiya, Parakrama Samudraya, Senanayake Samudraya, Kandalama, Deduru Oya, Beire Lake etc.

Levee construction is also a similar construction for dams which are adopted in Sri Lanka as structural measures for flood management [16]. Examples for existing levee systems which are constructed in Sri Lanka can be identified as levee systems in Gin river, Nilwala river and Maduru oya [25].

When considering the diversions for flood mitigation, some existing examples can be given as follows. 23 km long trans-basin diversion option is implemented in order to divert Uma oya water to Kirindi oya basin [12]. Moreover, according to Sampath and Mishra [51], flood mitigation is increased in parts of North Western Province

by diverting Deduru oya water through two main canals. Elahera and Angamedilla diversion, Gurugoda oya mini hydro diversion and Madiwela canal diversion are some other examples for existing diversion projects in Sri Lanka [34]. Moreover, currently somewhat improved drainage systems have been constructed in urban areas with the purpose of waste water disposal and flood management as well [55]. As per the above factors, it is obvious that variety of structural measures are adopted as flood management initiatives up to considerable extent in Sri Lanka.

8 Shortcomings and Negative Impact of Existing Structural Measures

Although these structural measures play a vital role in flood management, different shortcomings and negative aspects can be identified which leads different types of problems and it is mainly focused through following section.

When considering the structural flood management, major issue, which relates to it is severe environmental impact caused by existing structural measures [4]. That means, serious environmental problems such as loss of wetlands and animal habitats, soil erosion and environmental degradation in downstream areas are occurred due to implementing structural measures in flood management all over the world. Moreover, another impact can be identified as aging of existing structural measures [39]. An example is given by the study for that prevailing issue as sustainable improvements or replacements are needed for the existing structural flood control measures, which are adopted in Mississippi and lower Missouri river basins. Also, inadequate structural measures lead more damages in flood events in many countries. As an example, considerable amount of damages due to floods are reported in last few decades in Vietnam, which is located within a tropical monsoon zone [9].

When it comes to the Sri Lankan context, major problem which can be identified with these existing structural measures itself is aging with the time and insufficient structural measures for flood management [25]. The study has further clarified that those flood control structures badly need replacements or rehabilitations in order to ensure their functions in an event of flood as most of them were implemented before 1980s. According to JICA [25], flood control measures in Kelani, Gin and Nilwala rivers can be identified as examples for the structures which need replacements. Another critical negative aspect is damage to the eco system due to constructing these flood control structures [47]. The study has clearly mentioned that it has become a great threat due to different activities such as excavations, rock blasting, cut and fill etc. by taking Uma oya multipurpose project as an example. [36] has further revealed this environmental impact of flood control structures by stating that different types of environmental issues such as soil erosion, ground water contamination, bad impact on aquatic and semiaquatic species, changing the survival of wildlife species, saline intrusion for the water etc. are occurred due to Mahaweli reservoir construction project. Another negative impact due to structural measures can be identified as

damages to the infrastructures in nearby areas [47]. The 1author has given an example that adverse impacts on specially water wells and walls are occurred due to Uma oya project and tunneling activities.

Adapted from: [4, 39, 25, 47].

According to the above diagram, different shortcomings and negative impacts can be comprehensively identified regarding Sri Lankan context. Therefore, structural measures should be implemented as proper flood management measures by reducing these negative impacts in Sri Lanka.

References

1. Abraham M (2018) How dams can control floods. New Delhi. Retrieved from http://nwda.gov.in/upload/uploadfiles/files/DAM(1).pdf
2. Andjelkovic I (2001) Guidelines on non-structural measures in urban flood management. Technical Documents Hydrol (50). Retrieved from http://lib.riskreductionafrica.org/bitstream/handle/123456789/607/3613.Guidelinesonnon-structuralmeasuresinurbanfloodmanagement.pdf?sequence=1
3. Anita J (2013) Structural and non-structural approaches as flood protection strategy in Muara Angke settlement, North Jakarta, pp 1–9. Retrieved from http://lib.itenas.ac.id/kti/wp-content/uploads/2013/12/Microsoft-Word-SIBE-Juarni-Anita-2013_noPW.pdf
4. Bechtol V, Laurian L (2005) Restoring straightened rivers for sustainable flood mitigation. Disaster Prevention Manage Int J 14(1):6–19. https://doi.org/10.1108/09653560510583806
5. Berga L, Galeati G, Lundquist D, Asman I, Scott C, Riha J (2010) Dams and floods in Europe: role of dams in flood mitigation. Europe. Retrieved from http://cnpgb.apambiente.pt/IcoldClub/jan2012/EWG FLOODS FINAL REPORT.pdf
6. Bons K (2010) Comparing structural & Non-structural measures. In: Comparing Structural & Non-Structural Measures. Retrieved from http://www.gfdrr.org/sites/gfdrr/files/%28SESSION_1%29_Kees_Bons_%28Deltares%29_Structural_and_Non-structural_Measures.pdf
7. Bridges D (2014) Non-structural measures for water management problems. In: S. P. Simonovic (ed), Proceedings of the International Workshop, pp 471–475. https://doi.org/10.1007/978-94-007-6809-3_62
8. CIRIA (2013) The international levee handbook. London. Retrieved from http://webissimo.developpement-durable.gouv.fr/IMG/pdf/A_The_International_Levee_Handbook_C731__cle7f8a33.pdf
9. Chau V, Holland J, Cassells S (2014) Institutional structures underpinning flood management in Vietnam. Int J Disaster Risk Reduction 10:341–348
10. Climate Change Adaptation Technologies for Water [CCATW] (2015) Surface reservoirs. In: Water adoptation technology Brief. Retrieved from https://www.ctc-n.org/sites/www.ctc-n.org/files/resources/surface_reservoirs.pdf
11. De Bruijn KM (2004) Resilience and flood risk management. Water Policy 6:53–66. https://doi.org/10.2166/wp.2004.0004
12. Dharmasena GT (2017, October 13) Reality of the Uma Oya diversion project. Retrieved from http://www.island.lk/index.php?page_cat=article-details&page=article-details&code_title=173248
13. Du Plessis LA, Viljoen MF (1999) Determining the benefits of flood mitigation measures in the lower Orange River: A GIS application. University of the Orange Free State
14. European Union (2003) Best practices on flood prevention, protection and mitigation. Ec.Europa.Eu. Copenhagen. Retrieved from http://ec.europa.eu/environment/water/flood_risk/pdf/flooding_bestpractice.pdf

15. Evans S (2014) Channel straightening. Retrieved March 11, 2019, from https://getrevising.co.uk/grids/channel_straightening
16. Federal Emergency Management Agency [FEMA] (2012) Levees - frequently asked questions. Washington. Retrieved from https://www.fema.gov/media-library-data/20130726-1803-25045-4819/st_broomelv.pdf
17. Grand River Conservation Authority [GRCA] (2014) Dams and flood management. Retrieved from https://www.grandriver.ca/en/learn-get-involved/resources/Documents/GRCA_factsheet_Dams.pdf
18. Grelot F, Bailly J, Lavergne C (2013) Ranking sources of uncertainty in flood damage modelling: a case study on the cost-benefit analysis of a flood mitigation project in the Orb Delta, France. J Flood Risk Manage 1–16. https://doi.org/10.1111/jfr3.12068
19. Heidari A (2009) Structural master plan of flood mitigation measures. Natural Hazards Earth Syst Sci 9(1):61–75. https://doi.org/10.5194/nhess-9-61-2009
20. Hettiarachchi M, Athukorale K, Wijekoon S, & De Alwis A (2014) Urban wetlands and disaster resilience of Colombo , Sri Lanka. Int J Disaster Resilience Built Environ 5(1):79–89. https://doi.org/10.1108/IJDRBE-11-2011-0042
21. Himsley N (2011) Dams and flood mitigation. Sydney. Retrieved from https://actuaries.asn.au/library/events/Other/2011/Norm Himsley.pdf
22. Hooijer A, Klijn F, Bas G, Pedroli M, Os ADGVAN (2004) Towards sustainable flood risk management in the Rhine and Meuse river basins. River Res Appl 20:343–357. https://doi.org/10.1002/rra.781
23. Hui R (2013) Optimal design of levee and flood control systems. University of California. Retrieved from https://watershed.ucdavis.edu/shed/lund/students/HuiDissertation2014.pdf
24. Institute for Water Resources [IWR] (2011) 2011-R-08. In: Flood risk management Approaches. Retrieved from https://www.iwr.usace.army.mil/Portals/70/docs/iwrreports/2011-R-08.pdf
25. Japan International Cooperation Agency [JICA] (2013) Data Collection Survey on disaster management program in Sri Lanka. Retrieved from http://open_jicareport.jica.go.jp/pdf/12111894.pdf
26. Japan International Cooperation Agency (2009) Comprehensive study on disaster management in Sri Lanka
27. Jayawardane AKW (2005) Disaster mitigation initiatives in Sri Lanka. University of Moratuwa. Retrieved from https://iiirr.ucalgary.ca/files/iiirr/Kochifullpaper-final.pdf
28. Johnson WK, Davis DW (1975) Analysis of structural and nonstructural flood control measures using computer program HEC-5C. Retrieved from https://www.hec.usace.army.mil/publications/TrainingDocuments/TD-7.pdf
29. Kafle, S. K. (2017). Disaster risk management systems in South Asia: Natural hazards, vulnerability, disaster risk and legislative and institutional frameworks. J Geogr Nat Disasters 7(3). https://doi.org/10.4172/2167-0587.1000207
30. Kang S, Lee S, Lee K (2018) A Study on the implementation of non-structural measures to reduce urban flood damage - focused on the survey results of the experts. https://doi.org/10.3130/jaabe.8.385
31. Kousky C, Walls M (2014) Floodplain conservation as a fl ood mitigation strategy: examining costs and benefits. Ecol Econ 104:119–128. https://doi.org/10.1016/j.ecolecon.2014.05.001
32. Kundzewicz ZW (2009) Non-structural flood protection and sustainability. Water Int 27(1):3–13. https://doi.org/10.1080/02508060208686972
33. Lumbroso D, Ramsbottom D, Spaliveiro M (2008) Sustainable flood risk management strategies to reduce rural communities' vulnerability to flooding in Mozambique. J Flood Risk Manage 1(1):34–42. https://doi.org/10.1111/j.1753-318X.2008.00005.x
34. Mahaweli Development Board (2008) Mahaweli Ganga development Sri Lanka. Retrieved from http://mahaweli.gov.lk/en/pdf/Library/Mahaweli Ganga Development Sri Lanka.pdf
35. Minea G, Zaharia L (2011) Structural and non-structural measures for flood risk mitigation in the bâsca river catchment (Romania). Forum Geografic 10(1):157–166. https://doi.org/10.5775/fg.2067-4635.2011.034.i

36. Moonasingha AD (1991) The environmental impacts of Mahaveli river engineering and reservoir construction project. In: IWEM Conference. Birmingham. Retrieved from https://moonasingha.yolasite.com/anand---iwem---impacts-of-mahaweli-project.php
37. Murray A (2017) Natural flood management adopting ecosystem approaches to managing flood risk. Dublin 2. Retrieved from https://www.heritageweek.ie/content/images/natural_flood_management_a_study_for_friends_of_the_earth_february_2017.pdf
38. Musgrave WF, Thampapillai DJ (1985) Flood damage mitigation: A review of structural and nonstructural measures. Water Resources Res 21(4):411–424. https://doi.org/10.1029/WR021i004p00411
39. Myers MF, White GF (2010) The challenge of Missippi flood. Environ Sci Policy Sustain Dev 35(10):37–41. https://doi.org/10.1080/00139157.1993.992913
40. National Institute of Disaster Management [NIDM] (2007) Hydro meteorological disasters characteristics of flood. In: India: Ministry of home affairs. Retrieved from http://nidm.gov.in/PDF/Disaster_hymet.pdf
41. Opperman JJ (2014) A flood of benefits. In: The Nature Conservancy. Arlington, Virginia. Retrieved from https://www.conservationgateway.org/ConservationPractices/Freshwater/HabitatProtectionandRestoration/Documents/A Flood of Benefits - J.Opperman - May 2014.pdf
42. Palliyaguru R, Amaratunga D (2008) Managing disaster risks through quality infrastructure and vice versa. Struct Surv 26(5):426–434. https://doi.org/10.1108/02630800810922766
43. Petry B (2002) Coping with floods: complementarity of structural and non-structural measures. In: Flood defence, pp 60–70. Retrieved from https://fenix.tecnico.ulisboa.pt/downloadFile/3779571681931/keynote lecture - coping with floods.pdf
44. Plessis LA, Viljoen MF (2000) Determining the benefits of flood mitigation measures in the lower Orange River: a GIS application, vol 25. Bloemfontein
45. Rabalao RT (2010) The social, psychological and economic impact of flooding in Ga-Motla and Ga-Moeka communities of Moretele district in North West Province, South Africa. University of Free State
46. Rai PK, Dhanya CT, Chahar BR (2017) Flood control in an urban drainage system using a linear controller. Water Pract Technol 12(4):942–952. https://doi.org/10.2166/wpt.2017.102
47. Rathnayake U, Suratissa DM (2016) Uma Oya multi purpose development project, Sri Lanka. In: Flood management and social impacts. Retrieved from https://www.researchgate.net/publication/301889687_Uma_Oya_multi-purpose_development_project_Sri_Lanka_flood_management_and_social_impacts
48. Ratnayake U, Herath S (2005) Changing rainfall and its impact on landslides in Sri Lanka. J Mountain Sci 2(3):218–224. https://doi.org/10.1007/BF02973195
49. Salvesen D (2010) Structural approaches to flood and coastal hazard mitigation; assessing structural approaches. In: Breaking the disaster cycle: future directions in natural hazard mitigation, vol 6. Retrieved from https://www.hsdl.org/?view&did=471126
50. Samarajiva R, Goswami D, Ennen R (2006) Concept paper for a dam-related hazard warning system in Sri Lanka. Retrieved from https://www.lirneasia.net/wp-content/uploads/2006/01/DamSafety_2.0.pdf
51. Sampath DS, Mishra BK (2014) Analysis of the diversion requirements from the Deduru Oya reservoir in Sri Lanka. Int J Surf Groundwater Manag 1(2). Retrieved from https://www.researchgate.net/publication/277775468_Analysis_of_the_Diversion_Requirements_from_the_Deduru_Oya_Reservoir_in_Sri_Lanka
52. Sayers P, Galloway G, Penning-rowsell E, Yuanyuan L, Fuxin S (2014) Strategic flood management: ten golden rules to guide a sound approach. Int J River Basin Manage 13(2). https://doi.org/10.1080/15715124.2014.902378
53. Shaw R (2006) Critical issues of community based flood mitigation. J Sci Cult Spec Issue Flood Disaster Risk Reduction in Asia 72(1–2):1–17. Retrieved from http://drr.upeace.org/english/documents/References/Topic 5-Risk Management and Adaptation to Climate Change/Shaw 2006 Critical Issues of Community Based Flood Mitigation.pdf

54. Sivakumar SS (2015) Flood mitigation strategies adopted in Sri Lanka: a review. Int J Sci Eng Res 6(2):607–611. Retrieved from https://www.researchgate.net/publication/274193595_Flood_Mitigation_Strategies_Adopted_in_Sri_Lanka_A_Review
55. Tamura T (2009) Greater Colombo flood control and environmental improvement project (II) (III). Retrieved from https://www2.jica.go.jp/en/evaluation/pdf/2008_SL-P50_4.pdf
56. Tingsanchali T (2012) Urban flood disaster management. Procedia Eng 32:25–37. https://doi.org/10.1016/j.proeng.2012.01.1233
57. Velasco M, Russo B, Cabello À, Termes M, Sunyer D, Malgrat P (2016) Assessment of the effectiveness of structural and nonstructural measures to cope with global change impacts in Barcelona. J Flood Risk Manag. https://doi.org/10.1111/jfr3.12247
58. Verworn H (2002) Advances in urban-drainage management and flood protection. R Soc 1451–1460. https://doi.org/10.1098/rsta.2002.1009 Advances
59. WMO (2015) Effectiveness of flood management measures. In: Integrated Flood Management Tools Series, vol 21. Retrieved from https://www.floodmanagement.info/publications/tools/Tool_21_Effectiveness_of_Flood_Management_Measures.pdf
60. Wickramaratne S, Ruwanpura J, Ranasinghe U, Durage SW, Adikariwattage V, Wirasinghe SC (2012) Ranking of natural disasters in Sri Lanka for mitigation planning. Int J Disaster Resilience Built Environ 3(2):115–132. https://doi.org/10.1108/17595901211245198
61. Wijesundara CJ, Dayawansa NDK (2011) Construction of large dams and their impact on cultural landscape: a study in Victoria reservoir and the surrounding area. Trop Agric Res 22(1):211–219. Retrieved from https://tar.sljol.info/article/10.4038/tar.v22i2.2830/galley/2280/download/%0A
62. Yen BC (1995) Hydraulics and effectiveness of levees for flood control. In: Hydrometeorology, impacts, and management of extreme floods, pp 1–12. https://doi.org/10.1.1.508.1875
63. Zhou C, Sun N, Chen L, Ding Y, Zhou J, Zha G, Luo G (2018) Optimal operation of cascade reservoirs for flood control of multiple areas downstream: a case study in the upper Yangtze river basin. Water 10(9). https://doi.org/10.3390/w10091250
64. Zubair L, Ralapanawe V, Tennakoon U, Yahiya Z, Perera R (2006) Natural disaster risks in Sri Lanka: mapping hazards and risk hotspots. In: Natural disaster hotspots case studies, pp 109–136. https://doi.org/10.1596/978-0-8213-6332-4

Experimental Study on the Flexural and Shear Behaviour of Precast Prestressed Hollow Core Slab

R. Sagadevan and B. N. Rao

Abstract In general, the total cost of the building is mainly influenced by the self-weight of structural members. In particular, the self-weight of the floor slab is a key parameter which restricts its span. The hollow core slab (HCS) is being developed as an alternate to the conventional solid slab and results in self-weight reduction up to 50%. However, the reduction in the cross-sectional area increases the flexural deflection, which can be overcome by prestress technology. In this study, the flexural behaviour of precast prestressed HCS made of Styrofoam, with 10 m span, was examined experimentally. Two specimens were tested, one with screed (topping) concrete and other without screed concrete. The influence of screed concrete on the flexural and creep behaviour was investigated. It is found that the screed concrete reduces the flexural and creep deflection significantly. The applicability of HCS system to industrial buildings was investigated by adopting a service load as per Indian standard, IS 875 (Part 2): 1987, and subsequently found that the HCS satisfies the code requirements related to strength and serviceability (deflection and crack). Additionally, it was observed that the voids significantly influences the shear capacity of precast prestressed HCS.

Keywords Precast · Prestress · Concrete slab · Hollow core slab · Flexural behaviour · Shear capacity

1 Introduction

The increase in structural and architectural demand leads to research in innovative slab systems in building structures. The slab systems are classified as one- and two-way slabs based on its structural behaviour. The various types of conventional slab systems are wall-supported, beam-supported, grid beam-supported, ribbed, flat plate, and flat slab [9]. These slab systems have few disadvantages over its many advantages, such as dead load per unit area and span limitation. These limitations were reduced

R. Sagadevan (✉) · B. N. Rao
Structural Engineering Laboratory, Civil Engineering Department, Indian Institute of Technology Madras, Chennai, Tamil Nadu 600036, India
e-mail: sagadevan.ceg@gmail.com

R. Dissanayake et al. (eds.), *ICSECM 2019*, Lecture Notes in Civil Engineering 94,
https://doi.org/10.1007/978-981-15-7222-7_8

by introducing prestress in slab systems. Usually the dead weight of slabs higher than that of the live load acting on it, this leads to an increase in overall material consumption and cost as well. Past research evidenced that the voided slab systems (one-way and biaxial) can be an alternative to the conventional slab systems. The one-way voided slab are the slabs with voids in one direction, whereas the biaxial voided slabs are produced with voids in both lateral and longitudinal directions [13, 16]. The voids usually placed where the stress in concrete is minimum, generally on the tension side. The voided slabs render the self-weight up to 50% without a significant reduction in its load-carrying capacity [10, 15]. However, the initial flexural stiffness of biaxial voided slab was observed to be lesser than that of solid slab. Few studies showed that:

- The volume ratio of voids have a significant influence on the initial and secant stiffness [6];
- The flexural stiffness of spherical voided slab was 80–90% of solid slab having equal depth, however, its flexural strength was the same as that of solid slab [7];
- The flexural stiffness of the voided slab was about 50% lesser in comparison with the solid slab of identical dimensions and reinforcement at yield stage [11].
- In biaxial cuboid void slab, the one-way flexural capacity of the voided slab was approximately 90% of solid slab and the secant stiffness (at yield) of the void slab was about 60% of solid slab [12].
- The two flexural capacity of biaxial sphere void slab was observed to the same as that of the solid slab with 37% reduction in initial flexural stiffness. However, the secant stiffness corresponding to the yield load of voided and solid slab specimens were comparable [14].

The reduction in the flexural stiffness of voided slab usually reduced by prestressing the slab. In addition, the prestressed voided slab with without concrete topping (screed concrete) being used in the precast buildings due to its numerous advantageous [2, 18]. The topping concrete is mainly adopted to obtain smooth and even floor finish. If the concrete topping and the HCS act compositely during service, then the surface conditions such as texture and moisture of the HCS may affect the overall strength of the slab [1, 2]. The experiments demonstrated substantial shear strength capabilities for HCS when used in conjunction with 50 mm concrete topping [17]. Experiments evidence that the influence of deflection of the supporting beams on the shear resistance of the HCS was observed to be significant [8]. There are several problems related to concrete topping construction were reported, such as interface shear stress, debonding, direct tension, differential shrinkage, prestress strand relaxation, and creep [2]. These problems influence the load-carrying capacity and failure mode of the HCS with concrete topping.

In the current study, one-way flexural experiments were carried out to understand the effect of screed concrete on the load-carrying capacity and creep deflection of prestressed precast HCS. Two identical one-way HCS specimens of 10 m span with and without screed concrete were tested. The applicability of the HCS system to industrial buildings was investigated by adopting a service load as per Indian standard 875 (IS 875 - Part 2 [5]. The flexural behaviour is studied by means of

load-deflection relation, cracking & ultimate load, and creep deflection recovery. Furthermore, the influence of voids on the shear capacity of the prestressed precast HCS was investigated through experiments.

2 Experimental Program

2.1 Details of Test Specimens

Full scale prestressed HCS specimens were tested, which is part of a precast industrial building as shown in Fig. 1. The dimension of the slab specimen was 10 m × 1.2 m × 0.265 m and the screed concrete thickness was 50 mm. The voids are created by Styrofoam and the cross-section details are shown in Fig. 2. The photographs of various stages of prestressed HCS specimen casting is shown in Fig. 3. The properties of materials such as concrete and prestress strand are summarised in Table 1. M60 grade of concrete confirming to Indian standard 1343 [3] was adopted in this study. Uncoated stress relieved low relaxation seven-wire (ply) strand of class 2 confirm to Indian standard 14268 [4] was adopted as a prestressing strand. For the purpose of conducting shear test the specimens were cut from the original specimen with the size of 2 m × 0.6 m × 0.265 m.

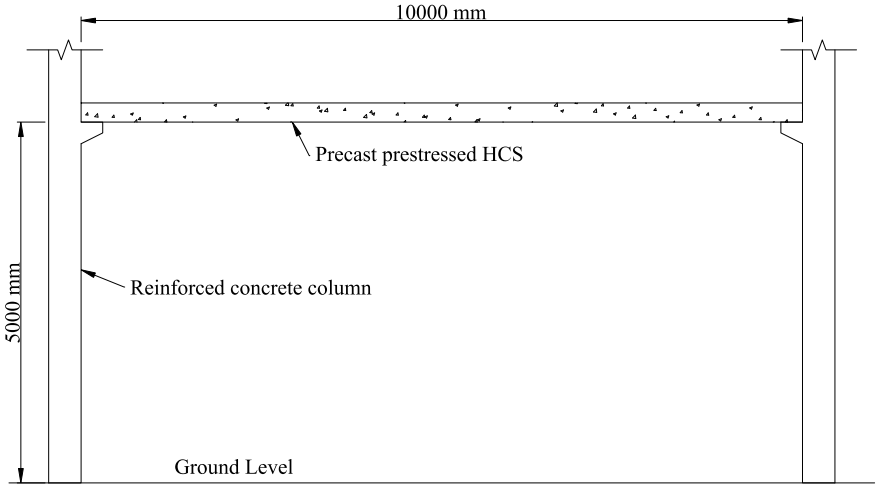

Fig. 1 Typical details of a precast industrial building

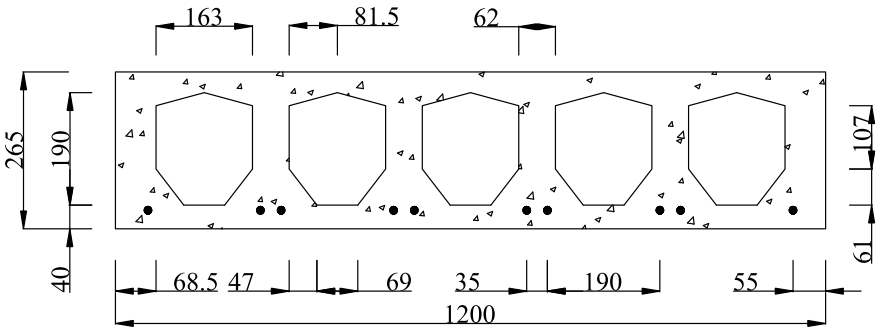

(a) Specimen without screed concrete

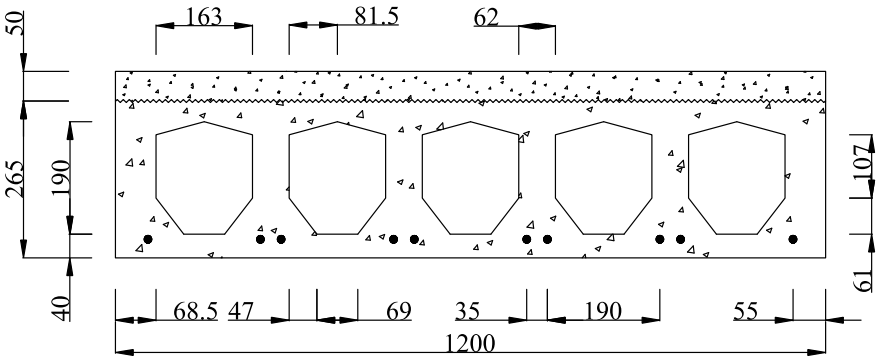

(b) Specimen with screed concrete

All dimensions are in mm

Fig. 2 Cross-section of specimens

Fig. 3 Various stages of prestressed HCS specimen casting

Table 1 Specimen details

Description	Details
Dimension	10 m × 1.2 m × 0.265 m
Screed thickness	50 mm
Grade of concrete at transfer (f_{ci})	40 N/mm^2
Grade of concrete at 28 days (f_{ck})	60 N/mm^2
No. of strands	10
Dia. of strand (ϕ)	12.7 mm
Clear cover to strand	25 mm
Breaking strength of strand (f_p)	183.7 kN
Yield strength of strand, f_y	165.3 kN
Actual breaking strength of strand (f_{pm})	193.0 kN
Actual yield strength of strand (f_{ym})	173.7 kN
Applied pre-tension ($\approx 0.5 f_p$)	100.0 kN/strand

2.2 Experimental Test Set-up and Instrumentation

2.2.1 Flexural Test

The specimens were tested with simple supports (125 mm width) at both ends. The loads (concrete blocks) were placed on top of the specimens as shown in Fig. 4. The schematic arrangement of loads at various stages are shown in Fig. 4a. The photograph of the test set-up is shown in Fig. 4b. The initial camber was measured after setting up the slab specimens in position (prior to loading). The vertical deflection at a distance of 2.5 m, 5.0 m, and 7.5 m from an end were measured by using linear variable differential transformers (LVDTs) with a measuring range of ± 100 mm. Total station technique was used to measure the deflection beyond service load. The crack width at each increment of the loading stage was measured by using microscope.

As per IS 875 (Part 2), for the work areas of an industrial building with machinery/equipment (medium duty), the minimum design service load is 7.0 kN/m^2 and ultimate load is 10.5 (= 1.5 × 7.5) kN/m^2. However, in this study, the load was adopted conservatively as described below.

Loading pattern for Specimen 1 (without screed concrete)

Initially, the specimen was loaded up to 90 kN (design service load of 7.5 kN/m^2) and measured the creep effect for an hour. The load was completely removed and measured the immediate creep (elastic) recovery in terms of deflection. Then, the specimen was loaded up to 155 kN (ultimate load of ≈ 12.92 kN/m^2). The load was retained for 15 h and measured the creep effect. After that, the specimen was loaded up to 204.5 kN (≈ 17 kN/m^2) and the effect of creep was measured after 23 h. Finally,

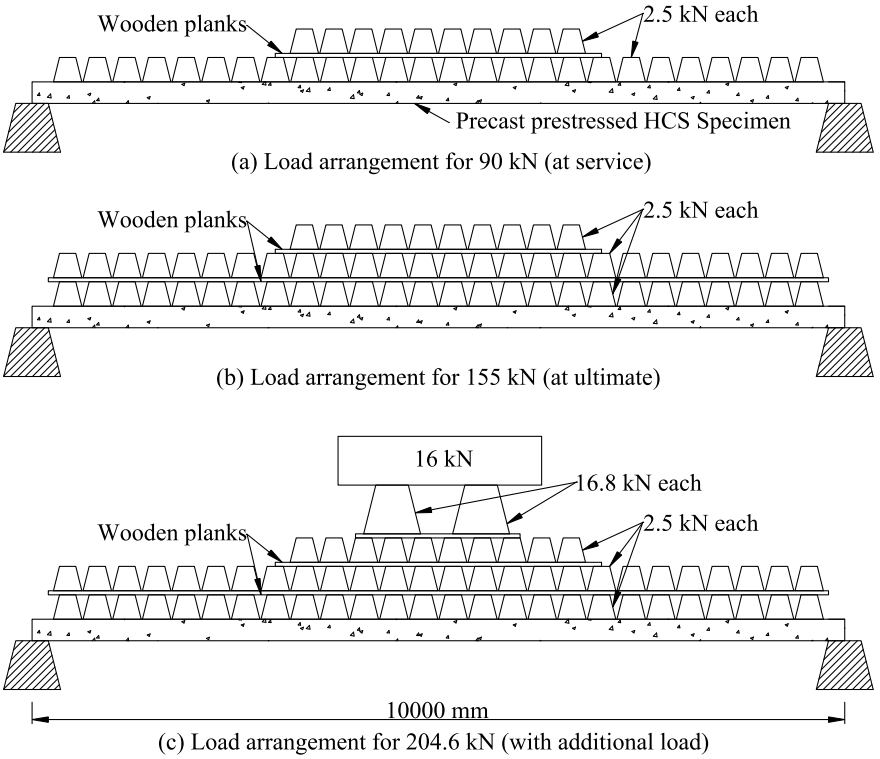

(a): Schematic arrangement of the flexural test set-up

(b): Photograph of flexural test set-up (at service load – specimen without screed concrete)

Fig. 4 a Schematic arrangement of the flexural test set-up. b Photograph of flexural test set-up (at service load- specimen without screed concrete)

all the loads were removed completely and measured the immediate creep recovery in terms of deflection.

Loading pattern for Specimen 2 (with screed concrete)

Initially, the specimen was loaded up to 90 kN (design service load of 7.5 kN/m^2) and measured the creep effect for an hour. Then, the specimen was loaded up to 155 kN (design ultimate load of $\approx$ 12.92 kN/m^2). The load was retained for 15 h and measured the creep effect. After that, the specimen was loaded up to 204.5 kN ($\approx$ 17 kN/m^2) and the effect of creep was measured after 23 h. Finally, all the loads

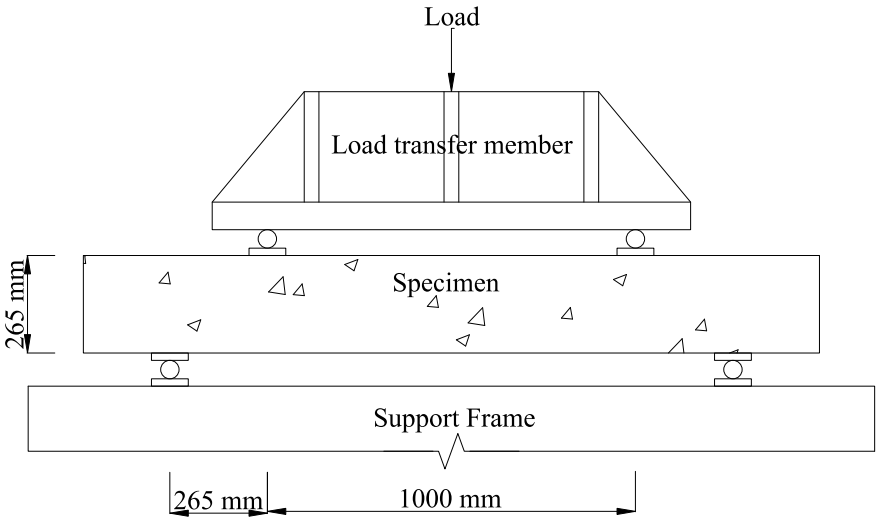

Fig. 5 Schematic arrangement of the shear test set-up

were removed completely and measured the immediate creep recovery in terms of deflection.

2.2.2 Shear Test

Four-point bending test was carried out. The specimens (without screed concrete) were supported by a hinge at one side and roller at another side of specimen. Loading positions arrived such that the specimen fails by shear, i.e., shear span equals to the effective depth of slab. The schematic test set-up is shown in Fig. 5. Load controlled test was performed.

3 Experimental Results and Discussions

3.1 Flexure

The observed load versus mid-span deflection of tested specimens is shown in Fig. 6. The camper is denoted with a positive sign and the observed deflection (downward) is denoted with a negative sign. The observation evidenced that the 50 mm thickness screed concrete is having a significant effect on structural behaviour of prestressed hollow core slab. The immediate creep recovery of the specimen without screed concrete was observed to be almost five times lesser in comparison with the specimen with screed concrete. The observed load versus deflection behaviour, up to service

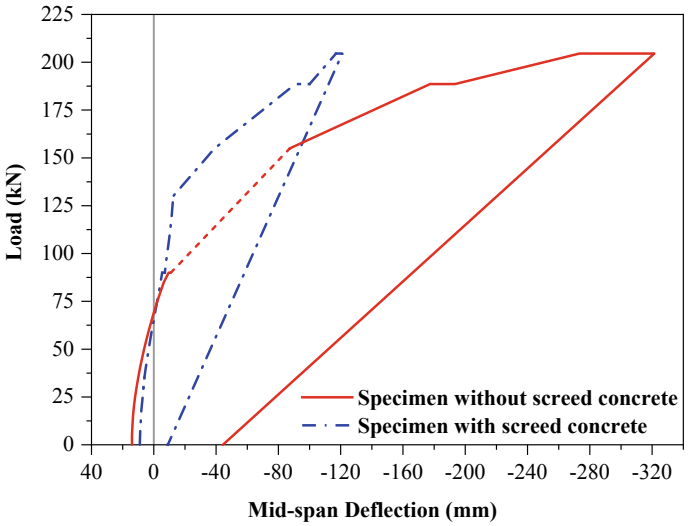

Fig. 6 Load versus mid-span deflection behaviour

load of 90 kN for both the specimens are shown in Fig. 7. For the specimen without screed concrete the creep effect was recorded with service load by unloading the specimen (Fig. 8). Flexural cracks were observed in mid-span of the specimens. The observed load versus crack width is shown in Fig. 9. The key observations are summarised in Table 2. The deformed shape of specimen is shown in Fig. 10.

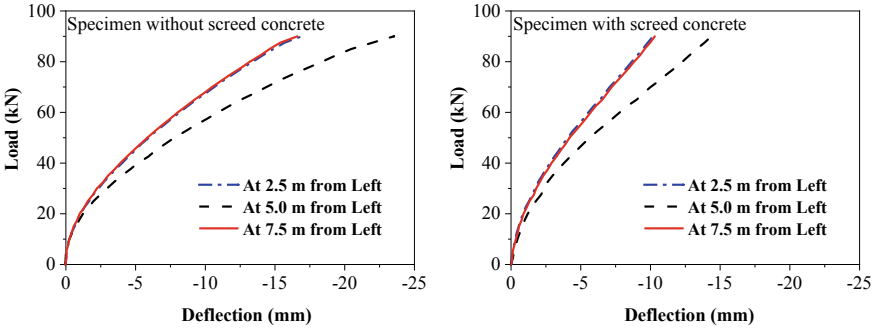

Fig. 7 Load versus deflection behaviour (up to 90 kN load-service load)

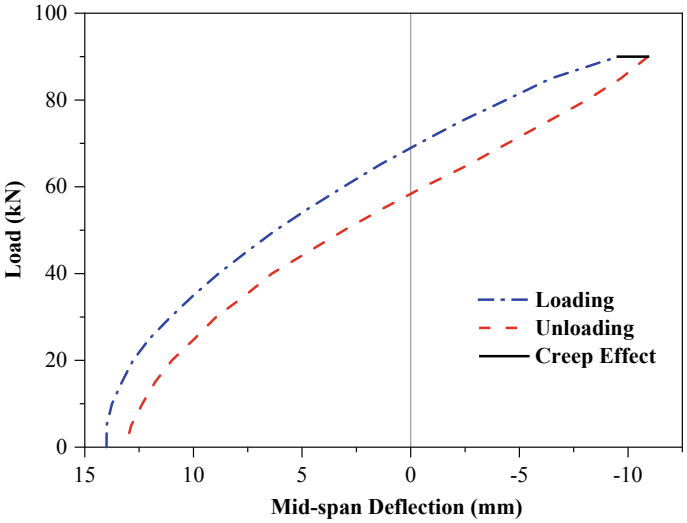

Fig. 8 Load versus mid-span deflection behaviour of the specimen without screed concrete

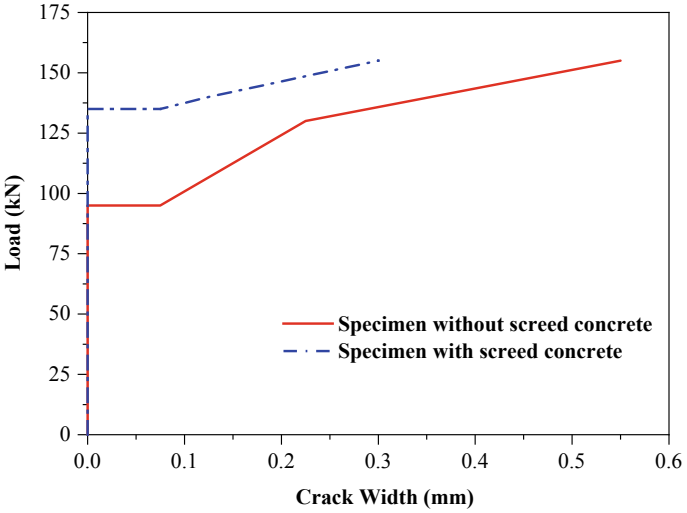

Fig. 9 Load versus crack width

3.2 Shear

The tested specimens under point bending were failed by shear. The tested specimens with the observed cracks are shown in Fig. 11. The observed failure load is summarised in Table 3. The observed mean shear stress was 3.45 N/mm^2.

Table 2 Experimental results – one-way flexure

Description	Specimen without screed (S1)	Specimen with screed (S2)	Ratio, S1/S2
Self-weight	42.41 kN	57.12 kN	0.74
Load at first crack	92.50 kN	137.50 kN	0.67
	Deflection at mid-span (mm)		
Initial camber	+14.00	+9.00	1.56
At service load (90 kN)	−9.53	−5.38	1.77
After 1 h with service load (90 kN)	−10.92	−7.05	1.55
After removal of service load (90 kN)	+13.13	–	–
At design ultimate load (155 kN)	−87.35	−39.00	2.24
At 188.6 kN load	−177.35	−91.00	1.95
After 15 h with 188.6 kN load	−193.35	−100.00	1.93
At 204.5 kN load	−273.35	−117.00	2.34
After 23 h with 204.5 kN load	−321.35	−121.00	2.66
After removal of 204.5 kN load	−44.35	−9.00	4.93

Fig. 10 The deformed shape of the specimen with screed concrete

Theoretically, solid slab with the same ultimate shear stress can carry 47% higher load than that of the voided slab. The reduction in the shear capacity of the hollow core slab is attributed to the reduction of concrete area due to the presence of voids.

Fig. 11 Tested specimens with shear cracks

Table 3 Experimental results-shear

ID	Failure load (V), kN	Shear load at an end (V_u), kN	Effective concrete area (A_e), mm^2	Shear Stress (τ_u), N/mm^2
SP1	548	274	74,415	3.68
SP2	478	239	74,415	3.21

4 Conclusions

The following conclusions are drawn based on the experimental investigation of precast prestressed one-way hollow core slab. This study verifies the applicability of slab system to carry the floor load of an industrial building specified in IS 875 (Part 2). In this study, one-way flexure and shear parameters were investigated. Structural behaviour of the voided slab specimens with and without screed concrete, were studied considering parameters such as load versus deflection behaviour, crack pattern, load-carrying capacity, and creep effect.

1. The hollow core slab specimens showed the typical flexural mode of failure under one-way bending. The screed concrete showed a significant effect on the structural behaviour of prestressed hollow core slab. In addition, interface delamination of the screed concrete was not observed, i.e., slab and screed concrete showed composite action for the entire period of loading.
2. The observed deflection of the specimen with screed concrete was almost half the deflection of the specimen without screed concrete. Also, the immediate creep recovery of the specimen without screed concrete was observed to be almost five times lesser in comparison with the specimen with screed concrete.

3. The cracking load of hollow core slab specimen without screed concrete was 67% of the specimen with screed concrete. Further, the crack width of the specimen without screed concrete was observed to be almost twice that of the specimen with screed concrete.
4. The estimated shear capacity of the solid slab was observed to be 47% higher than that of the voided slab. The reduction in shear capacity of hollow core slab is attributed to the reduction of concrete area due to the presence of voids.

Acknowledgements This work was supported by Department of Science & Technology, India (SR/S3/MERC/0040/2012) and M/s Consolidated Construction Consortium Limited (CCCL), Chennai, Tamil Nadu, India. The authors wish to acknowledge the assistance and facilities offered by Technical Staff, Structural Engineering Laboratory, IIT Madras, Chennai, Tamil Nadu, India.

References

1. Haruna SI (2014) Flexural behavior of precast prestressed concrete hollow core slabs with cast-in-place concrete topping. Department of Civil Engineering, Atilim University, Turkey
2. Ibrahim IS et al (2016) Experimental study on the shear behaviour of precast concrete hollow core slabs with concrete topping. Eng Struct 125:80–90. https://doi.org/10.1016/j.engstruct.2016.06.005 (Elsevier Ltd)
3. IS 1343 (2012) Prestressed concrete—code of practice. Bureau of Indian Standards, New Delhi
4. IS 14268 (2017) Uncoated stress relieved low relaxation seven-wire (ply) strand for prestressed concrete—specification. Bureau of Indian Standards, New Delhi
5. IS 875—Part 2 (1987) Code of practice for design loads (other than earthquake) for buildings and structures—Part 2: imposed loads. Bureau of Indian Standards, New Delhi
6. Kim SH (2011) Flexural behavior of void RC and PC slab with polystyrene forms. Key Eng Mater 452–453:61–64. https://doi.org/10.4028/www.scientific.net/KEM.452-453.61
7. Midkiff CJ (2013) Plastic voided slab systems: applications and design. MS Thesis, Kansas State University, Manhattan
8. Pajari M (2010) Prestressed hollow core slabs supported on beams—finnish shear tests on floors in 1990–2006
9. Pillai SU, Menon D (2012) Reinforced concrete design, 3rd edn. Tata McGraw Hill, New Delhi
10. Sagadevan R, Rao BN (2017) Analytical studies on flexural capacity of biaxial hollow slab. In: Proceedings, international conference on composite materials and structures, Hyderabad, India
11. Sagadevan R, Rao BN (2019) Effect of void former shapes on one-way flexural behaviour of biaxial hollow slabs. Int J Adv Struct Eng 11(3):297–307. https://doi.org/10.1007/s40091-019-0231-7
12. Sagadevan R, Rao BN (2019) Evaluation of one-way flexural behaviour of biaxial voided slab. Indian Concr J 98(5):7–16
13. Sagadevan R, Rao BN (2019) Experimental and analytical investigation of punching shear capacity of biaxial voided slabs. Structures 20:340–352. https://doi.org/10.1016/j.istruc.2019.03.013
14. Sagadevan R, Rao BN (2019d) Experimental and analytical investigations on two-way flexural capacity of biaxial voided slab. In: Proceedings, national conference on advances in structural technologies, pp 635–648
15. Sagadevan R, Rao BN (2019e) Numerical study on flexural capacity of biaxial hollow slab. In: Rao ARM, Ramanjaneyulu K (eds) Recent advances in structural engineering, Volume 1.

Select Proceedings of SEC 2016. Springer, Singapore, pp 97–105. https://doi.org/10.1007/978-981-13-0362-3_8
16. Sagadevan R, Rao BN (2019) Prediction of punching shear capacity of biaxial voided slab. J Struct Eng Manage 6(2):24–33
17. Scott NL (1973) Performance of precast prestressed hollow core slab with composite concrete topping. PCI Journal (March–April), pp 64–77
18. Wariyatno NG, Haryanto Y, Sudibyo GH (2017) Flexural behavior of precast hollow core slab using PVC pipe and styrofoam with different reinforcement. Proc Eng 171:909–916. https://doi.org/10.1016/j.proeng.2017.01.388

Gas Diffusivity Based Characterization of Stabilized Solid Waste from Kurunegala Open Dump Disposal Site

M. Shanujah, T. K. K. Chamindu Deepagoda, M. C. M. Nasvi, A. K. Karunarathna, V. Shreedharan, and G. L. S. Babu

Abstract Open dumps are complex ecosystems with respect to Greenhouse Gas (GHG) emission which occurs as a consequence of anaerobic decomposition of organic substances typically available in Municipal Solid Waste (MSW). Subsurface soil conditions (e.g. soil texture, structure) and atmospheric boundary conditions (e.g. wind, temperature) are the major key factors which affect the water retention characteristics, gas diffusivity, and hence the subsurface transport of GHGs. In this study, we characterized the stabilized "soil-like" fraction sampled from an open dumpsite located in Kurunegala, Sri Lanka to investigate subsurface landfill gas (CO_2) transport behaviour. The MSW, collected at 2.5–5 m depth was screened to separate the stabilized "soil-like" fractions and proportioned into two groups (0–4.75 mm, 4.75–9.5 mm) for the particle-size based characterization. Soil-gas diffusivity (D_p/D_o, where D_p and D_o are gas diffusion coefficients in soil air and free air, respectively) and soil–water characteristic (SWC) of the stabilized waste were measured and parameterized using existing and modified parametric models. The results revealed that the investigated material exhibited two-region porosity (i.e., inter-aggregate pore region and intra-aggregate pore regions) which, in turn, affected the water retention and gas transport properties. We further experimentally investigated CO_2 gas transport originated from a point source buried in medium bench-scale emission tank under the dry condition and the observed subsurface methane profiles were simulated using the multiphase transport simulator TOUGH2-EOS7CA. In addition, potential effects of atmospheric boundary controls, wind (1.5 and 3 ms^{-1}) and temperature (26 and

M. Shanujah (✉) · T. K. K. Chamindu Deepagoda · M. C. M. Nasvi
Department of Civil Engineering, Faculty of Engineering, University of Peradeniya, Peradeniya 20400, Sri Lanka
e-mail: dilshanujah@eng.pdn.ac.lk

A. K. Karunarathna
Department of Agricultural Engineering, Faculty of Agriculture, University of Peradeniya, Peradeniya 20400, Sri Lanka

V. Shreedharan
Government College of Engineering, Kannur, India

G. L. S. Babu
Indian Institute of Science, Bangalore, India

R. Dissanayake et al. (eds.), *ICSECM 2019*, Lecture Notes in Civil Engineering 94,
https://doi.org/10.1007/978-981-15-7222-7_9

34 °**C**), were also examined based on a series of controlled bench-scale experiments using bench-scale emission tank interfaced with a wind tunnel at the dry condition. Results showed the pronounced effects of particle size and wind and, to a lesser degree, of temperature on soil-landfill gas migration.

Keywords Greenhouse gases (GHG) · Municipal solid waste (MSW) · Stabilized waste · Soil-gas diffusivity · Inter-aggregate · Intra-aggregate

1 Introduction

Open dumps are considered as an important global source of GHGs due to the inadequate gas collection system and unplanned heaps of uncovered wastes disposed with no protection of environmental consideration. Previous studies predicted that the MSW generation per capita in Sri Lanka will be reaching 1.0 kg/cap/day by 2025 [1, 2]. There are nearly 236 large-scale waste dumps disposal sites available in Sri Lanka (Ministry of Environment) and the predominant MSW is (~56%) biodegradable [1]. Biodegradable waste disposed in open dumps undergo anaerobic degradation, which leads to the production of biogas consisting of methane (CH_4), carbon dioxide (CO_2) and trace gases and these landfill gases (LFG) can potentially migrate from the deep subsurface of the dumpsites to the atmosphere. The main environmental hazards related to these landfill gas are believed to be the explosion hazards, the global climate effects and indoor/outdoor air pollution [3].

Stabilized waste from an old open dump normally consists 50–60 wt% of fine-grained degraded matter ("soil-like" fractions) which is the result of the humification process of MSW [4] and makes up a considerable portion of the total stabilized waste. Diffusion is the primary mechanism which controls subsurface gas migration [5]. It is described by the dimensionless soil-gas diffusivity (D_p/D_o; where D_p and D_o are gas diffusing coefficients [m^2s^{-1}] in soil and free air, respectively). Soil-gas diffusivity and soil–water characteristic (SWC) are strongly linked to the soil texture and structure [6]. Moreover, the wind or temperature-induced near-surface fluctuation may also affect the subsurface gas migration [7].

Despite the presence of several studies in the literature investigating the surface landfill gas migration and emission, subsurface landfill gas migration in an old open dump disposal site has not been studied yet. Although many studies focusing the effect of soil condition on subsurface gas transport in porous media are available (e.g., [8–10]), studies specifically focused on the effect of atmospheric conditions on subsurface gas transport characteristics in soil are limited in the literature [11–13].

Stabilized waste from an old open dump disposal site located in Kurunegala, Sri Lanka was selected for this study. The "soil-like" fractions were separated from the stabilized waste sampled at 2.5–5 m depth and proportioned into two groups (0–4.75 mm, 4.75–9.5 mm) to characterize for particle size distribution, gas diffusivity, soil–water retention. We further experimentally measured CO_2 gas concentration originated from a point source buried in medium bench-scale emission

tank under the dry condition and the observed subsurface methane concentrations were compared with the simulated result using the multiphase transport simulator TOUGH2-EOS7CA. In addition, potential effects of atmospheric boundary controls, wind (1.5 and 3 ms^{-1}) and temperature (26 and 34 °C), were also examined based on a series of controlled bench-scale experiments with the same emission tank coupled with a wind tunnel.

2 Methodology

2.1 Materials and Methods

Kurunegala open dump disposal site was selected for this study. It is one of the largest and oldest waste disposal site in North Western Province, Sri Lanka with an average waste collection of 55 MT/day and is being dumped in 12.5 acres. Suitable locations (Pit 01; 7° 30′ 49.8′ N, 80° 21′ 22.3′ E, Pit 02; 7° 30′ 51.0′ N, 80° 21′ 23.2′ E, Pit 03; 7° 30′ 48.3′ N, 80° 21′ 22.8′ E) at old dumping yard area of this disposal site were excavated using crawler excavator. The stabilized waste was extracted at the depth of 2.5–5 m from the surface of the sampling pits and air-dried for two days. Of this stabilized waste, we obtained 55–60% of "soil-like" fraction while the remaining fraction included plastic, metal, stones, paper, glass, textile, and other inerts. The "soil-like" fractions were proportioned into two groups by manual sieving (smaller fraction; 0–4.75 mm, larger fraction; 4.75–9.5 mm) to investigate particle size based diffusivity characteristics. The particle size distribution of each fraction was analysed using mechanical sieving and hydrometer method. Basic physical properties of both fractions are shown in Table 1.

Soil–water characteristic was measured using the Tempe cell apparatus [14]. The cell was connected to 200 cm water reservoir in which the water level was gradually lowered to mimic a drainage cycle. A dielectric soil moisture sensor (ECH2O EC-5) was installed in the Tempe cell and ADC (Analog-to-Digital Converter) counts for

Table 1 Physical properties of "soil-like" fraction

Physical properties						
Fractions	Size range mm	D_{50}£mm	Bulk density kg/m^{-3}	Total porosity cm^3cm^{-3}	Particle densityζ kg/m^{-3}	Hydraulic conductivity cms^{-1}
Smaller	0–4.75	0.8	1025	0.54	2400(0.018)	0.00 €
Bigger	4.75–9.5	6.1	973	0.56	2400(0.018)	0.013₽

£ Taken from the particle size gradation curve
ζStandard deviation of the results are given in parentheses
€ Measured by falling head permeability test method
₽ Measured by constant head permeability test method

each matric potential were taken. Volumetric water content at stable stage of each matric potential was calculated using two-point α-mixing model [15].

One-chamber diffusion apparatus was used to measure the diffusion coefficient [16]. "Soil-like" fractions were individually packed in 100 cm^3 sample cores with constant packing energy. Measurements were started at in-situ moisture condition as well as fully saturated condition and continued for several air-dry steps. Different moisture conditions were achieved by stepwise evaporation of saturated samples. At each step, gas diffusivity was measured by the method adopted by Moldrup et al. [17]. An oxygen sensor (KE-12, Figaro Inc., Japan), mounted at the top of the chamber was able to monitor changes in oxygen concentration inside the chamber continuously. This information was used to calculate soil gas diffusivity as per the method developed by Taylor [18] and Currie [16].

A medium bench-scale Plexiglass tank (hereafter referred to as emission tank) of dimensions 0.5 m (length) × 0.3 m (depth) × 0.1 m (width) was fabricated. A diffusive gas source (2 μm filter element) was placed at the bottom in the mid-section of the emission tank. Smaller and bigger "soil-like" fractions were individually packed in the emission at dry condition. A steady-state atmosphere was created around the emission tank by avoiding wind and sun radiation effects. CO_2 (100%) gas was injected through the gas source at 0.4 l/min flow rate for a period of six hours. Gas samples were extracted at steady state and stored in pre-evacuated 6 ml vials. Collected samples were analysed to obtain percentages of CO_2 along the depth of emission tank using gas chromatograph (Shimadzu, CG-2014).

We used multiphase transport simulator TOUGH2 and EOS7CA [19, 20] for numerical simulation which can simulate subsurface flow and transport of liquid and gas phases [i.e., H_2O, brine, non-condensable gas (e.g., CO_2), gas tracer, and air] under isothermal or non-isothermal conditions. A 2-D Cartesian numerical domain (with the same dimension of emission tank) was divided into 221 elements for simulation. Top boundary is considered as an open boundary for gas and heat flow whereas the left, right boundaries and the bottom boundary of the domain were set as no-gas flow condition (Neumann-type) and adiabatic for heat transport. CO_2 source was created at a single point in the mid of the domain. We used measured soil–water characteristic and soil-gas diffusivity for the simulation. Simulations were carried out for fully dry condition at atmospheric temperature (26 °C). Results of numerical simulations were converted to a graphical format using Tecplot 360 EX 2017 R2 software. Finally, simulated concentrations of CO_2 were compared with the experimental concentration.

A series of controlled bench-scale laboratory experiments were conducted using a wind tunnel interfaced with the emission tank as illustrated schematically in Fig. 1. The tank was packed uniformly with the smaller fraction (we used only the smaller fraction for this series of experiments). Experiments were conducted at two wind velocities (1.5 and 3 ms^{-1}) and two temperature conditions (26 and 34 °C). To generate and control the wind velocity, the wind tunnel was installed with the wind blower (BW-3, 3-inches) connected with a variable velocity controller. Wind velocity was measured using a hot wire anemometer (TECPEL, AVM-714). The wind tunnel was also attached to the heater system near the wind blower to channel the heated

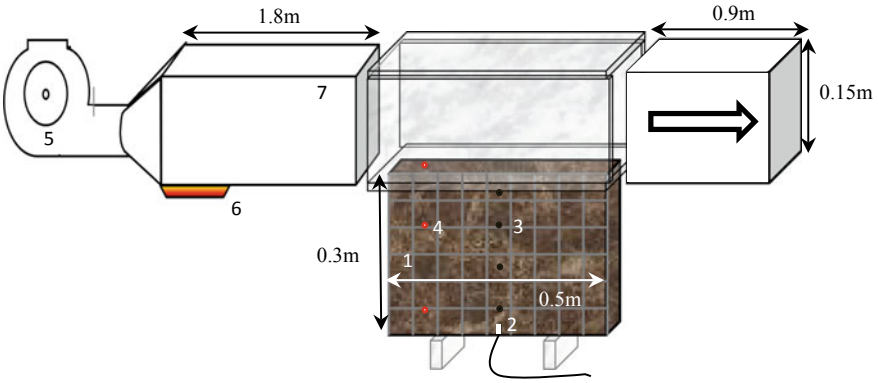

1. Emission tank packed with "soil-like" fraction
2. CO_2 gas source
3. Gas extraction points
4. Temperature sensors
5. Wind blower
6. Heater assembly
7. Galvanized steel duct

Fig. 1 Schematic of the experimental set-up (not to scale). The arrow shows the wind direction

airflow across the test section. CO_2 (100%) gas was injected through the gas source at 0.4 l/min flow rate for a period of six hours at the bottom mid of the emission tank. Gas samples were extracted at steady stage and stored in pre-evacuated 6 ml vials and CO_2 concentrations were determined using gas chromatography.

2.2 Parametric Functions

We used Duner (1994) bimodal function which could adequately describe the continuous relationship between matric suction (ψ) and the volumetric water content (θ). The ψ-θ Model can be presented as:

$$\boldsymbol{\theta}(\Psi) = \boldsymbol{\theta_r} + (\boldsymbol{\theta_s} - \boldsymbol{\theta_r})\left[\mathbf{w}\left(\frac{1}{1+|\boldsymbol{\alpha}_1\Psi|^{\mathbf{n}_1}}\right)^{\mathbf{m}_1} + (1-\mathbf{w})\left(\frac{1}{1+|\boldsymbol{\alpha}_2\Psi|^{\mathbf{n}_2}}\right)^{\mathbf{m}_2}\right] \quad (1)$$

where θ_s ($cm^3\,cm^{-3}$) and θ_r ($cm^3\,cm^{-3}$) are the saturated and residual water contents, respectively, α_1 and α_2 are model scaling factors (cm^{-1}) and n_1, n_2, m_1 and m_2 ($m_1 = 1–1/n_1$, $m_2 = 1–1/n_2$) are model shape factors. The subscript 1 and 2 indicate region 1 and region 2, respectively.

We modified pervious bimodal functions (e.g., [21–23]) by introducing gas percolation threshold (ε_p) which can adequately describe the relationship between air-fill porosity (ε) and soil-gas diffusivity (D_p/D_o) in inter-aggregate pore region. The modified model takes the form of:

Region 1: inter-aggregate pore region

$$\frac{\mathbf{D_p}}{\mathbf{D_o}} = \frac{\alpha_1}{(\mathrm{w} - \varepsilon_\mathbf{p})^{\beta_1}} \left[\frac{\varepsilon - \varepsilon_p}{\emptyset}\right]^{\beta_1} \quad \varepsilon < \mathbf{w}\emptyset \tag{2}$$

Region 2: intra-aggregate pore region

$$\alpha_1 + \frac{\alpha_2}{(1-\mathbf{w})^{\beta_2}} \left[\frac{\varepsilon - \mathrm{w}\emptyset}{\emptyset}\right]^{\beta_2} \quad \varepsilon < (1-\mathbf{w})\emptyset \tag{3}$$

where, $\emptyset$ ($cm^3\ cm^{-3}$) is the total porosity, w is the weighing factor to numerically distinguish the two-regions, ε_p ($cm^3\ cm^{-3}$) is the air-filled pore space percolation threshold, subscripts 1 and 2 indicates the two regions of the pore size distribution. Note here that, α_1 and α_2 are the predicted gas-diffusivity at $\varepsilon = \mathrm{w}\,\emptyset$ and $\varepsilon = (1-\mathrm{w})\emptyset$, respectively.

3 Results and Discussion

3.1 Soil Water Characteristic (SWC)

The water characteristic and associated air-entry potentials, together with the best-fit parameterized Durner [24] model (Eq. 1), are shown in Fig. 2. Results also show that the "soil-like" fractions exhibit a distinct bimodal shape, commonly observed for dual-porosity media. Systematic decline in saturated moisture content (θ_s) indicates decrease in total porosity with decreasing particle size. However, the effect of particle size in SWC is less evident at low matrix potentials. Note that the air-entry matric suction; required for the onset of desaturation remains the same (~1.75 kPa) and comparatively low for both fraction, suggesting rapid drainage of water available in the inter-aggregate pore region. Mesopore (ie., pore radius 0.01–15 μm) distribution

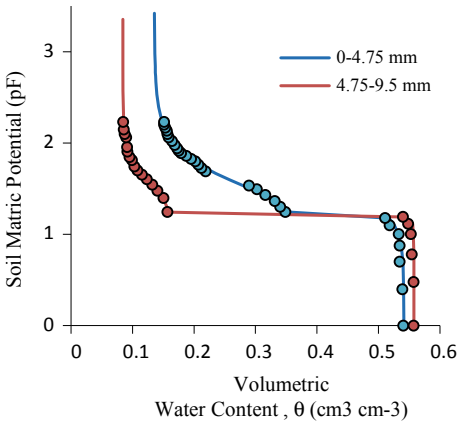

Fig. 2 Volumetric soil–water content (θ, $cm^3\ cm^{-3}$) as a function of soil metric potential (pF, solid circles) together with parameterized Durner [24] bimodal function, Eq. 1 (solid lines)

is dominant in smaller fraction, resulting larger air-filled pore space as compared to the larger fraction under the same suction level. Water retention under matric suction is controlled by adsorptive and capillary forces among soil particles as well as the surface area of the soil particles. Since water retention characteristic reflects the pore size distribution of the two fractions, it provides a useful insight of soil-gas diffusivity in subsurface gas migration.

3.2 Soil Gas Diffusivity

Gas diffusivity of both fractions plotted against air-filled porosity is shown in Fig. 3, along with the parameterized newly developed bimodal function. Note that there were no sufficient D_p/D_o measurements in bigger size fraction, typically observed for porous media with large aggregates [21] as the inter-aggregate region was already drained and air-filled. We developed a two-region gas diffusivity function based on the previous models to estimate gas diffusivities for media with distinct inactive pore space in the inter-aggregate pore region. Notably, the gas percolation threshold increases with increasing particle size (gas percolation for smaller and bigger fractions are 0 and 0.1 $cm^3\ cm^{-3}$, respectively) as also evidenced in the literature [21]. Apparently, particle size effect is not evident in gas diffusivity through air-fill pore space. Note the linear increase (with the same gradient) in gas diffusivity within the intra-aggregated region in both fractions, implying comparable pore size distribution. Additionally, mean particle size, derived from the particle-size distribution (not shown) of the bigger fraction ((D_{50} = 6.14 mm) was nearly eightfold larger than that of the smaller fraction (D_{50} = 0.78 mm), suggesting a marked difference in soil particle networks, and hence the pore network that facilitates gas-diffusivity in subsurface. Moreover, soil moisture induced additional tortuosity and discontinuity within a gaseous pore network, making D_p/D_o strongly related to volumetric water content (see Fig. 2).

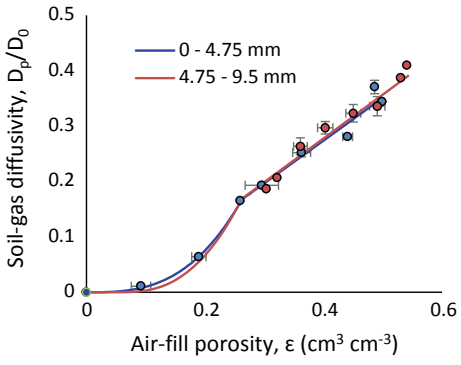

Fig. 3 Soil-gas diffusivity, D_p/D_0, as a function of air-fill porosity (solid circles) together with newly established D_p/D_0 bimodal function (Eg. 2 and 3, solid lines). Error bars indicate one standard deviation about the mean (n = 3)

3.3 *Depth-Wise Carbon Dioxide (CO_2) Concentration Profile—Comparison of Experimental and Numerical Results*

Figure 4a and c shows the steady-state CO_2 concentration profiles of both fractions at the dry condition of the soils. Notably, upward-bulging CO_2 profile can be seen at both fractions due to pressure-driven advective flow from gas source to the atmosphere. Diffusive movements (lateral and downward) are virtually same in all directions in both fractions. But it is very low in larger fraction due to high diffusivity at dry condition, resulting fast movement of CO_2 in both lateral and outward directions. Furthermore, smaller size fraction constrains gas movement due to the low porosity, slightly smaller diffusion coefficient and low permeability. Figure 4 b and d shows the comparison between measured and simulated CO_2 concentration across the depth of the emission tank. Notably, measured CO_2 concentration profiles could be adequately simulated in both fractions, implying the applicability of TOUGH2/EOS7CA multi-phase transport simulator as also evidenced in the previous studies (e.g., [12], hence proved to be promising numerical tool to estimate subsurface methane migration in the absence of direct concentration measurements.

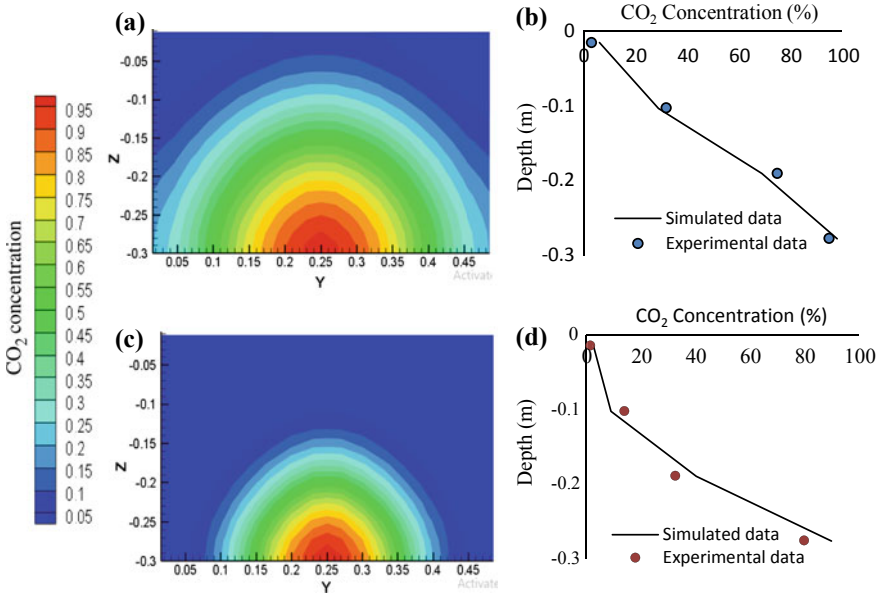

Fig. 4 **a** Simulated steady-state CO_2 concentration profile for smaller fraction, **b** Comparison between measured and simulated CO_2 concentration profile for smaller fraction, **c** Simulated steady-state CO_2 concentration profile for larger fraction, **d** Comparison between measured and simulated CO_2 concentration profile for larger fraction. The y and z in this Figure indicate the width and depth of the emission tank, respectively

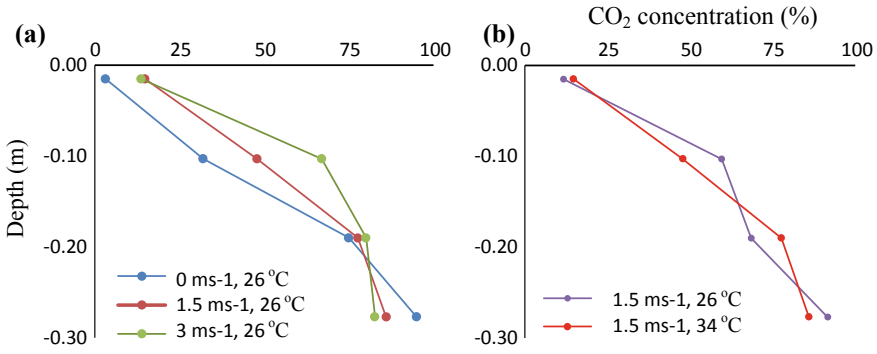

Fig. 5 Depth-wise wind **a** and temperature **b** effect on CO_2 concentration

3.4 Depth-Wise Carbon Dioxide (CO_2) Concentration Profile—Wind and Temperature Effects

Figure 5 shows the steady-state CO_2 concentration profiles of the smaller fraction with near-surface atmospheric wind velocity (a) and temperature (b) variations. Note that the three profiles shown in Fig. 5a correspond to the three wind velocities (0, 1.5, 3 ms^{-1} where the temperature remained unchanged, 26 °C) and two profiles shown in Fig. 5b correspond to two temperatures (26 °C, 34 °C) where the wind speed remained unchanged at 1.5 ms^{-1}. Evidently, wind has made noticeable control on near subsurface migration of methane whereas no distinct effect of wind is observed at the depth below 12 cm. Similar observation was also made by Ishihara et al. [25] who invoked the research on the influence of turbulent surface wind on subsurface water vapor transfer, suggesting that the turbulent diffusivity close to the surface is much larger than the molecular diffusivity, so that barometric pressure variations near the surface constrain the water vapour movement as we observed an increased CO_2 concentration with the increased surface wind velocity (0–12 cm). Notably, atmospheric temperature-induced effect on subsurface CO_2 migration is negligible as evidenced in Fig. 5b.

4 Conclusions

This study characterized soil-gas diffusivity (D_p/D_o) to examine the CO_2 transport in differently-proportioned "soil-like" fractions extracted at 2.5–5 m depth from an open dumpsite located in Kurunegala, Sri Lanka. The mean particle size of the two fractions (smaller; 0.8 mm, larger; 6 mm) are markedly different, thus suggesting a significant difference in particle size and pore networks for gas migration. Measured soil–water characteristic (SWC) exhibited marked variation in both two size fractions thus giving a useful fingerprint of pore size distribution. However, despite

the observed differences in SWC, the measured diffusivity in two fractions are not distinct. Measured SWC and gas diffusivity were successfully parameterized using available and modified parametric functions. The results revealed that the investigated material exhibited two-region porosity (i.e., inter-aggregate pore region and intra-aggregate pore regions). Furthermore, measured (CO_2) concentration profiles in differently proportionated "soil-like" fraction under dry condition were simulated using TOUGH2/EOS7CA, thereby proving the applicability of the numerical simulator for landfill gas emissions. In addition, pronounced effects of wind and, to a lesser degree, of temperature on soil-landfill gas migration was observed. Other environmental aspects such as saturation, porous media anisotropy, and methane oxidation need to be accounted for more realistic simulations.

Acknowledgements The authors gratefully acknowledge the financial support for this research from the Indian-Sri Lankan Inter Governmental Science and Technology Co-operation Programme (Grant No: MTR/TRD/AGR/3/2/17).

References

1. Menikpura SNM, Gheewala SH, Bonnet S (2012) Sustainability assessment of municipal solid waste management in Sri Lanka: problems and prospects. J Mater Cycles Waste Manag. 14(3):181–192 (Dordrecht)
2. World Bank (1999) What a waste: Solid waste management in Asia. In: Hoornweg D, Thomas L (eds) Urban Development Sector Unit (UDSU), East Asia and pacific Region., Washington DC, USA
3. Kjeldsen P (1996) Landfill gas migration in soil. In: Landfilling of waste: biogas
4. Krook J, Svensson N, Eklund M (2012) Landfill mining: a critical review of two decades of research. Waste Manag 32:513–520
5. Buckingham E (1904) Contributions to our knowledge of the aeration of soils. Bur Soil Bull 25. U.S. Government Print Office, Washington, DC
6. Ding F, Sun W, Huang Y (2018) Net N2O production from soil particle size fractions and its response to changing temperature. Sci Total Environ 650:97–104
7. Poulsen TG, Moldrup P, Christophersen M, Kjeldsen P (2003) Relating landfill gas emissions to atmospheric pressure using numerical modelling and state-space analysis. Waste Manage Res 21:356–366
8. Currie JA (1984) Gas diffusion through soil crumbs: the effects of compaction and wetting. J Soil Sci 1984(35):1–10
9. Fujikawa T, Miyazaki T (2005) Effects of bulk density and soil type on the gas diffusion coefficient in repacked and undisturbed soils. Soil Sci 170:892–901
10. Chamindu Deepagoda TKK, Elberling B (2015) Characterization of diffusivity-based oxygen transport in Arctic organic soil. Eur J Soil Sci 66:983991
11. Basirat F, Sharma P, Fagerlund F, Niemi A (2015) Experimental and modeling investigation of CO_2 flow and transport in a coupled domain of porous media and free flow. Int J Greenhouse Gas Control 42:461–470
12. Chamindu Deepagoda TKK, Smits KM, Oldenburg CM (2016) Effect of subsurface soil moisture variability and atmospheric conditions on methane gas migration in shallow subsurface. Int J Greenhouse Gas Control 55:105–117
13. Chamindu Deepagoda TKK, Mitton M, Smits K (2017) Effect of varying atmospheric conditions on methane boundary-layer development in a free flow domain interfaced with a porous media domain. Science and Technology, Greenhouse Gases

14. Smits KM, Sakaki T, Howington SE, Peters JF, Illangasekare TH (2013) Temperature dependence of thermal properties of sands across a wide range of temperatures (30–70°C). Vadose Zone J 12(1):vzj2012.0033.
15. Sakaki T, Limsuwat A, Smits KM, Illangasekare TH (2008) Empirical twopoint a-mixing model for calibrating the ECH2O EC-5 soil moisture sensor in sands. Water Resour Res 44 W00D08
16. Currie JA (1960) Gaseous diffusion in porous media. Part 2—dry granular materials. Br J Appl Phys 11:318–324
17. Moldrup P, Olesen T, Gamst J, Schjonning P, Yamaguchi T, Rolston DE (2000) Predicting the gas diffusion coefficient in repacked soil: water induced linear reduction model. Soil Sci Soc Am J 64:1588–1594
18. Taylor SA (1949) Oxygen diffusion in porous media as a measure of soil aeration. Soil Sci Soc Am Proc 14:55–61
19. Oldenburg CM (2015) EOS7CA version 1.0: TOUGH2 module for gas migration in shallow subsurface porous media systems. Lawrence Berkeley National Laboratory Report LBNL-175204
20. Pruess K, Oldenburg CM, Moridis GJ (1999) TOUGH2 user's guide version 2. E.O. Lawrence Berkeley National Laboratory Report, LBNL-43134
21. Chamindu Deepagoda TKK, Moldrup P, Jensen MP, Jones SB, de Jonge LW, Schjønning P, Scow K, Hopmans JW, Rolston DE, Kawamoto K, Komatsu T (2012) Diffusion aspects of designing porous growth media for earth and space soils. Soil Sci Soc Am J 76:1564–2157
22. Moldrup P, Olesen T, Yoshikawa S, Komatsu T, Rolston DE (2005) Predictive descriptive models for gas and solute diffusion coefficients in variably saturated porous media coupled to pore size distribution: III. Inactive pore space interpretations of gas diffusivity. Soil Sci 170:867–880
23. Resurreccion AC, Kawamoto K, Komatsu T, Moldrup P, Sato K, Rolston DE (2007) Gas diffusivity and air permeability in a volcanic ash soil profile: effects of organic matter and water retention. Soil Sci 172(6):432–443
24. Durner W (1994) Hydraulic conductivity estimation for soils with heterogeneous pore structure. Water Resour Res 30(2):211–223
25. Ishihara Y, Shimojima E, Harada H (1992) Water vapor transfer beneath bare soilwhere evaporation is influenced by a turbulent surface wind. J Hydrol 131:63–104
26. Second National Communication on Climate Change (2011) Ministry of Environment. Democratic Socialist Republic of Sri Lanka. (Report submitted to the UNFCCC secretariat)

Investigation of the Relationship Between Densities Versus Mechanical Properties of Sri Lankan Timber Species

C. K. Muthumala, Sudhira De Silva, K. K. I. U. Arunakumara, and P. L. A. G. Alwis

Abstract The aim of this study was to investigate the relationships among wood density, modulus of rupture (MOR), modulus of elasticity (MOE), compression parallel to grain (CNP) and compression perpendicular to grain (CPG) in 32 timber species grown in Sri Lanka. Defects free stem section from each timber was taken at the breast height and samples were prepared according to BS 373: 1957 standard. The tests for mechanical properties were performed through the Universal Testing Machine (UTM 100 PC). Linear Regression Analysis was done for interpreting the effectiveness of the relationship in wood density with other mechanical properties (MOR, MOE, CPG, CNG). The relationship between wood density and mechanical strength properties were analyzed by regression models. Wood density showed strong positive relationship with CPG and MOR. Results in the regression test revealed a significant relationship ($P = 0.001$) among wood density and other mechanical properties such as MOR, MOE, CNP and CPG. These results can be used for developing effective timber classification system in Sri Lanka.

Keywords Density · Mechanical properties · Timber classification

C. K. Muthumala (✉)
Research, Development and Training Division, State Timber Corporation, Battaramulla, Sri Lanka
e-mail: ck_muthumala@yahoo.com

S. De Silva
Department of Civil and Environmental Engineering, Faculty of Engineering, University of Ruhuna, Galle, Sri Lanka

K. K. I. U. Arunakumara
Department of Crop Science, Faculty of Agriculture, University of Ruhuna, Kamburupitiya, Sri Lanka

P. L. A. G. Alwis
Department of Agricultural Engineering, Faculty of Agriculture, University of Ruhuna, Kamburupitiya, Sri Lanka

R. Dissanayake et al. (eds.), *ICSECM 2019*, Lecture Notes in Civil Engineering 94,
https://doi.org/10.1007/978-981-15-7222-7_10

1 Introduction

Wood is considered to be an excellent material for furniture, interior decorations and construction purposes. Density is very important physical character for consideration in selecting wood for numerous uses, such as furniture manufacturing, construction of frame, bridge, building structures, sporting goods, measuring instruments, musical instruments and decorative surfaces etc. The density of a material is the mass per unit volume at some specified condition. For a hydroscopic material such as wood, density depends on two factors: the weight of the wood structure and moisture retained in the wood.

Density is the single most important indicator of strength in wood and may therefore predict such characteristics as hardness, ease of machining and nailing resistance [1].

Wood has a relatively high strength in relation to its density when compared with other materials used in construction. The strength properties of wood depend upon its density and structure, which assist us in selecting a suitable type of wood for a particular use [2].

Mechanical properties of wood indicate the ability of wood to resist various types of external forces, static or dynamic, which may act on it. Mechanical properties are particularly considered when timber is used for constructional and structural purposes. These properties not only vary with species, with reference to the nature of their fibre structure but also with the moisture content, temperature and defects of wood. Quantitative characteristics of wood and its behaviour to external influences other than applied forces depend on mechanical properties. These properties are important because they can significantly influence the performance and strength of wood used in structural applications [3].

Mechanical property values are given in terms of stress (force per unit area) and strain (deformation resulting from the applied stress) [4].

The strength of a timber depends on its species and the effects of certain growth characteristics [5]. Different wood species have different strength characteristics, and also within a species these characteristics may also vary. Therefore, in practice, a classification system of strength classes is used. There is no proper timber classification system applicable for timber industry in Sri Lanka, the present study focused on developing a classification system for selected 32 timber species based on their strength properties. In this study, the relationships among wood densities and mechanical properties of 32 timber species grown in Sri Lanka have been evaluated.

Table 1 Selected timber species

Common name	Scientific name	Common name	Scientific name
1. Albizia	*Albizia molucana*	17. Mango‘	*Mangifera indica*
2. Cypress	*Cypressus macrocarpa*	18. Margosa	*Azadirachta indica*
3. Ebony	*Diospyros ebenum*	19. Mi	*Modhuca longifolia*
4. Ehela	*Cassia fistula*	20. Micro	*Eucalyptus microcorys*
5. Ginisapu	*Michelia champaca*	21. Milla	*Vitex pinnata*
6. Grandis	*Eucalyptus grandis*	22. Na	*Mesua ferrea*
7. Halmilla	*Berrya cordifolia*	23. Nedun	*Pericopsis mooniana*
8. Havarinuga	*Alstonia macrophylla*	24. Palu	*Manilkara hexandra*
9. Hora	*Dipterocarpus zeylanicus*	25. Paramara	*Samanea saman*
10. Jack	*Artocarpus heterophyllus*	26. Pine	*Pinus caribaea*
11. Khaya	*Khaya senegalensis*	27. Robusta	*Eucaliptus robusta*
12. Kolon	*Adina cordifolia*	28. Rubber	*Hevea brasiliensis*
13. Kumbuk	*Terminalia arjuna*	29. Satin	*Chloroxylon swietenia*
14. Lunumidella	*Melia dubia*	30. Suriyamara	*Albizia odoratissima*
15. Madan	*Syzygium cumini*	31. Teak	*Tectona grandis*
16. Mahogany	*Swietenia macrophylla*	32. Welang	*Pterospermum suberifolium*

2 Materials and Methods

2.1 Wood Samples

The study was conducted with 32 timber species available in Sri Lanka. Trees of 30–40 years-old with straight trunks, normal branching and no disease or pest symptoms were selected and felled. Stem section from each tree was taken at the breast height (Table 1).

2.2 Sample Preparation

The wood species were machined and trimmed to standard size of 20 mm × 20 mm × 60 mm for determination of density, 20 mm × 20 mm × 300 mm for bending tests, 20 mm × 20 mm × 60 mm for compression parallel to grain tests and 50 mm × 50mm × 50 mm for compression perpendicular to grain tests. The samples were replicated five times [6].

2.3 Determination of Density

To avoid the effect of the weight of water in the wood, use oven-dry weight for standard measurements of density. The samples were dried in an oven at 100 ± 2 °C for 24 h. The samples were then removed and transferred to a desiccators and allowed to reach equilibrium temperature in the laboratory before the oven-dry weight was obtained. This procedure was repeated until a substantially constant weight was obtained. Equation 1 was used to determine the density based on the oven-dry weight and water displacement method was used in determining the density.

$$\text{Density} = \frac{\text{Weight of oven dried wood (kg)}}{\text{Volume of wood } \left(\text{m}^3\right)} \tag{1}$$

2.4 Mechanical Tests

Mechanical tests conducted on the wood species included modulus of rupture and modulus of elasticity (MOR and MOE). The tests were performed on a Universal Testing Machine (UTM) at the wood laboratory of State Timber Corporation, Battaramulla, Sri Lanka.

MOR and MOE were calculated using the Eq. 2 and 3 as stated below.

The load was applied at a constant speed of 2 mm/s at UTM.

$$MOR = \frac{3\text{PL}}{2\text{bd}^2} \tag{2}$$

where:

MOR = Modulus of rupture
P = Maximum Load (N)
L = Length of sample (mm)
b = width of the sample (mm)
h = thickness of the sample (mm)

$$MOE = \frac{\text{PL}^3}{4\text{bd}^3\Delta} \tag{3}$$

where:

P = Maximum load at proportionate stage (N)
L = Length of sample (mm)
b = Width of the sample (mm)

d = Thickness of the sample (mm)
△ = Slope of the graph

Compression parallel to grain and Compression perpendicular to grain values were calculated using the following Eq. (4).

The load was applied at a constant speed of 0.5 mm/s at UTM.

$$\text{Serviceability compressive strengthof the specimen} = \frac{\text{Maximum Load at Serviceability state}}{\text{Load acting area}} \quad (4)$$

3 Results and Discussions

Variations in wood densities and mechanical properties are given in Table 2.

Variations in wood density and mechanical properties have also been reported by several researchers [7, 8, 9]. As the data were normally distributed, the Pearson correlation test was done and positive correlations among densities with other variables were evident at the results. To find out the relationship between density with other mechanical properties, Linear regression test was done.

Following scatter plots show the relationship between density (kg/m^3) and mechanical strength (N/mm^2) properties of 32 timber species grown in Sri Lankan conditions (Figs. 1, 2, 3 and 4).

Among other predictors, CPG showed the highest value of R^2value (0.576), indicating the best goodness of fit for the density. The effectiveness order of other predictors for the dependent variable of density is CPG > MOR > CNG > MOE as indicated in the scatter plots (See Figs. 1–4).

As shown by Table 3, results show a significant relationship ($p = 0.000$) between dependant variable of density with the independent variables of other mechanical properties.

Table 4 represents the correlation between density with other mechanical properties and the strength relationship among mechanical properties. Strong correlations (0.745 and 0.759 respectively for density with MOR and density with CPG were observed. While other two variables (MOE and CNG) showed moderate correlations (0.609 and 0.646 respectively) with wood density.

Multicolliniarity relationships among the independent variables were not evident as indicated with low VIF values (less than 5)and high Tolerance values (higher than 0.25) of the regression test.

Table 2 Density values (kg/m^3) and mechanical strengths (N/mm^2)of timber species

Timber species	Density	Com. Para. to grain	Com. Per. to grain	MOE	MOR
Albizia	525	10.433	3.504	1939.81	17.360
Cypress	502	24.918	3.408	4491.91	53.133
Ebony	1120	52.902	20.970	8676.39	136.050
Ehela	960	37.639	12.657	9928.79	107.960
Ginisapu	570	28.305	9.003	5336.39	65.723
Grandis	570	47.225	4.920	8026.14	68.482
Halmilla	796	43.841	8.775	8141.7	91.140
Havarinuga	651	40.058	8.528	9836.82	84.564
Hora	806	44.361	15.463	13603.9	83.033
Jack	645	42.750	14.480	5872.66	63.927
Kaya	600	37.092	11.775	8879.29	81.501
Kolon	708	34.125	6.167	6196.25	66.455
Kumbuk	756	34.562	8.743	5719.41	60.585
Lunumidella	400	16.708	3.797	4206.02	25.608
Madan	720	23.718	9.620	5211.13	48.870
Mahogany	570	29.875	8.560	6140.01	66.221
Mango	600	28.964	10.101	5033.35	55.923
Margosa	733	48.000	12.255	7438.61	76.755
Mi	973	37.063	10.247	5810.99	64.165
Micro	910	62.478	11.469	14919.8	127.34
Milla	892	51.241	16.973	6736.23	74.760
Na	1087	56.368	10.685	12175.2	140.654
Nedun	795	34.216	12.753	8715.65	111.880
Palu	1100	53.095	17.213	11349.9	82.719
Paramara	650	29.936	4.992	3974.98	38.419
Pinus	465	48.500	4.108	6910.6	69.864
Robusta	775	38.221	7.363	9723.76	98.847
Rubber	680	29.596	5.711	7911.07	75.785
Satin	980	45.187	16.000	11489.6	142.660
Suriyamara	840	43.742	11.950	5454.79	102.795
Teak	720	49.312	10.080	8478.26	90.766
Welan	640	26.490	7.313	5760.22	59.880

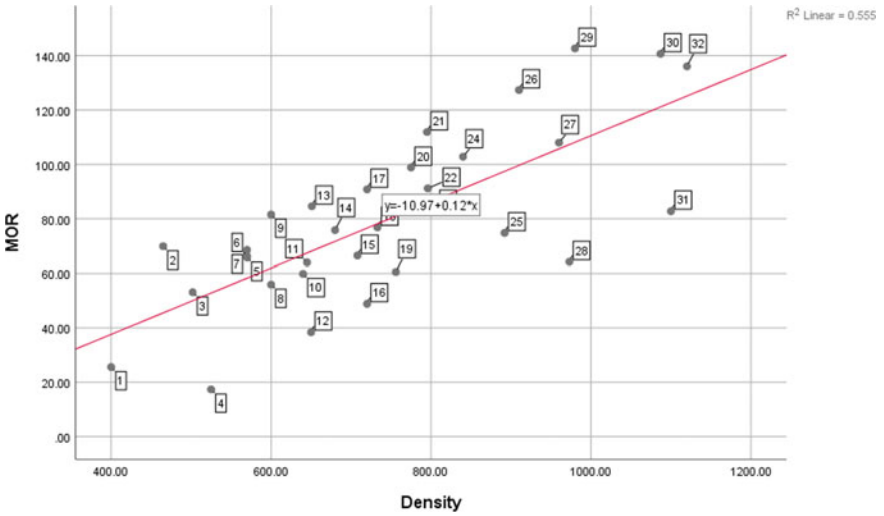

Fig. 1 The relationship between wood density (kg/m^3) versus modulus of rupture (MOR) (N/mm^2)

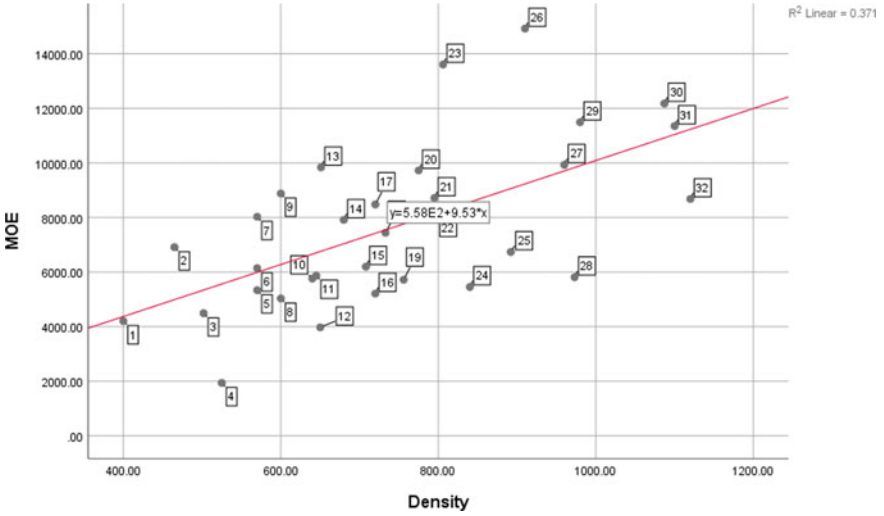

Fig. 2 The relationship between wood and density (kg/m^3) and modulus of elasticity (MOE) (N/mm^2)

4 Conclusion

Inadequate length of sawn timber material is also reported to be a limiting factor for fully utilization of timbers. Finger joint, a method which connects two small pieces of timber together is identified as a sound technique to minimize the wastage. As

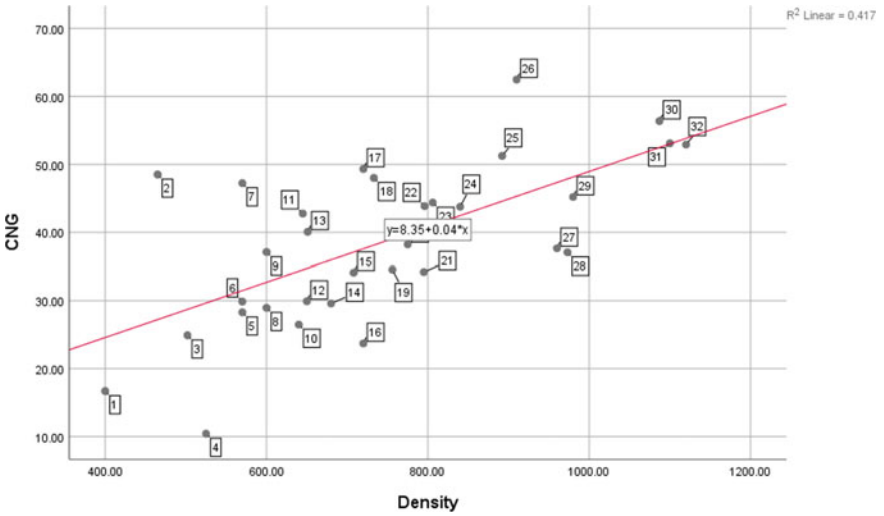

Fig. 3 The relationship between wood density (kg/m^3) versus compression parallel to grain (CNG) (N/mm^2)

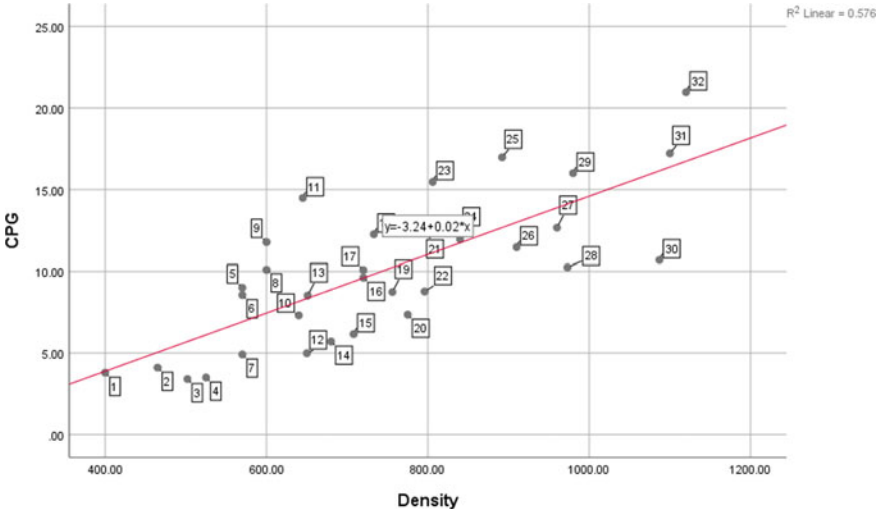

Fig. 4 The relationship between wood density (kg/m^3) versus compression perpendicular to grain (CPG) (N/mm^2)

there is no timber classification system applicable for finger joint technique in Sri Lanka. In the present research study is focused to evaluation the relationship between wood density and mechanical properties of 32 wood species. These results can be used for developing effective timber classification system in Sri Lanka.

The following conclusions were drawn from the study:

Table 3 ANOVA test results in linear regression

Model		Sum of squares	df	Mean square	F	Sig
1	Regression	761305.973	4	190326.493	15.677	0.000[b]
	Residual	327798.246	27	12140.676		
	Total	1089104.219	31			

b indicates significant

Table 4 Relationship between density versus mechanical properties

Model		95.0% Confidence interval for B		Correlations			Collinearity statistics
		Lower bound	Upper bound	zero-order	Partial	Part	Tolerance
1	(Constant)	167.868	447.025				
	MOR	0.049	4.975	0.745	0.374	0.221	0.291
	MOE	−0.024	0.024	0.609	−0.002	−0.001	0.322
	CNG	−4.823	6.760	0.646	0.066	0.036	0.354
	CPG	7.713	32.127	0.759	0.542	0.354	0.570

- The mechanical properties (MOR, MOE & CPG, CNG)showed positive relationship with the wood density.
- CPG showed the highest value for R^2 (coefficient determination) of 0.576 expressing the best goodness of fit for the density.
- The order of independent variables of CPG > MOR > CNG > MOE showed the goodness of fit to the model which could predict the effectiveness of the dependent variable of density.
- MOR and CPG showed strong correlation with density with the value of 0.746 and 0.759 respectively while other two variables showed moderate correlation as 0.609 and 0.646 for MOE and CNG respectively.
- Significant relationship ($P = 0.001$) between wood densities, and mechanical properties of CPG, MOR, CNP and MOE was recorded.
- Independent variables didn't show the multicollinearity relationship. Therefore, the relationship between mechanical properties and density can be used for the developing of an effective timber classification system in Sri Lanka.

References

1. Hoadley RB (2000) Understanding wood: a craftsman's guide to wood technology. The Taunton Press, Newtown, USA
2. Reinprecht L (2016) Wood deterioration, protection and maintenance. Wiley Blackwell Publishing house, West Sussex, United Kingdom

3. Winandy JE (1994) Effects of long-term elevated temperature on CCA-treated Southern Pine lumber. Forest Prod J 44(6):49–55
4. American Society for Testing and Materials (1991). Annual Book of Standards, Vol. D.09 Wood. Philadelphia, PA. https://www.fpl.fs.fed.us/documnts/pdf1994/winan94a.pdf
5. Yeomans D (2003) Strength grading historic timbers. Cathedral Communications Limited 2010. https://www.buildingconservation.com/articles/gradingtimbers/gradingtimbers.ht
6. BS 373:1957 (1999) Methods of testing small clear specimens of timber. British Standards Institution. London, 1
7. Zhang SY (1997) Wood specific gravity-mechanical property relationship at species level. Wood Sci Technol 31:181–191
8. Zobel BJ, Sprague J (1998) Juvenile wood in trees. Springer, New York
9. Zobel BJ, Van Buijtenen JP (1989) Wood variation, its causes and control. Springer-Verlag, Berlin, p 363

A Guide for Structural Health Monitoring of Buildings in Sri Lanka

R. C. Loganathan

Abstract Structural Health Monitoring (SHM) of a building, also known as a 'Structural Audit', is a method of ascertaining the performance of the building in its operational condition. SHM has been in existence for a long time under different names. In the past, it was practice for a professional to be called upon to make a structural assessment of the structure if the building was about to change hands, had to undergo structural changes, or even to observe distress points. However after few building failures around the world especially the collapse of an eight storied building in Dhaka in 2013, the trend (especially in Asia) changed and building operators found the need for a structural audit at a regular basis. Major multinational operating in south Asian countries has made it mandatory to check the structural stability of the buildings (especially factory buildings) on an annual basis in order to have a continued business. SHM of a building is a specialised job, and an experienced professionally qualified civil/structural engineer is usually tasked with this function. This paper is structured according to the three main categories of SHM (1) Observation and Non Destructive Testing (NDT) under operational condition; (2) analysing data to check performance of the structure under the present condition; and (3) recommendations and remedial action, if required. In Sri Lanka, it has been a practice to issue a report on visual observation of the building. This paper seeks to set out a methodical manner in conducting inspections for SHM within the Sri Lankan context.

Keywords Structural health monitoring · Structural audit · Guidelines

1 Introduction

Structural Health Monitoring is undertaken to check the adequacy of a structure in its operational condition for present and future use. Although SHM can be performed in many structures (buildings, bridges, underground structures, dams etc.) this paper is particularly concerned with concrete framed buildings. It has become necessary

R. C. Loganathan (✉)
Perigon Lanka Pvt Ltd, 8, Stubbs Place, Colombo 00500, Sri Lanka
e-mail: loga@perigonlanka.com

R. Dissanayake et al. (eds.), *ICSECM 2019*, Lecture Notes in Civil Engineering 94,
https://doi.org/10.1007/978-981-15-7222-7_11

to check the structural health condition of a building due to different reasons. They are change of ownership, undergo structural changes, observation of defects and to assurance of structural stability for continued use. Also with sustainability taking centre stage in the drive towards a greener world, it has become important to look at the re-use of existing buildings for continued usage. SHM is carried out usually in two stage. The first is visual and the second is the strength investigation. Also it may be necessary to get the service of the sub consultants to check chemical composition of certain building materials and building service.

2 Literature Review

Structural Health Monitoring has been in existence for a long time under different names. Conditional assessment, structural audit or periodic structural inspection are the terms used for the exercise. However in Sri Lanka, except for papers submitted at different conferences or annual sessions of The Institution of Engineers Sri Lanka, so far proper guidelines has not been set down by any agency. Leading countries have laid down guide lines for carrying out structural health monitoring. Periodic Structural Inspection is carried out in Malaysia within five to ten years (Building and Construction Authority of Malaysia [1]). A good document I reviewed for this paper was a publication by Institution of Structural Engineers UK [2]. The publication is particularly concerned with buildings. After the inspection and testing of samples the one has to make a decision on future course of action as given in TR69 [3]. Once the decision to repair is taken its good to follow the principles given in TR 69 with reference to BS EN 1504 [3].

3 Terms of Reference

The first step of SHM is the establishment of Terms of Reference. Few clients are unaware of the SHM process and try to give instruction verbally. Further they expect the engineer to perform the process in a day or two and give a report immediately. It is wise for clients to let their own facilities manager or a Project Management company to establish a TOR for the SHM process. If an intermediator is not present it would be better if the engineer prepares a TOR and explain it to the client. It is always better to make a site visit before finalising a TOR. The Terms of Reference should contain the physical boundaries of investigations any investigations to be done with help of testing houses and if the services of sub consultants are utilised. It should be a live document so that it can be updated (along with the commercial conditions) with the consent of the client.

4 Health and Safety

Structural inspections can be as dangerous as construction. The building subject to structural inspection may have elements that are not safe. The engineer in charge of the assignment must ensure the safety of the all those who may be affected, including the occupants and surrounding structures. Before entering a building a general assessment of the condition of the structure should be made and entry should be made only if the building appears to be adequately safe. At certain establishments the visiting team may have to attend a safety induction programme.

5 Stages of SHM

5.1 Desk Study

It would be very helpful if document on the design, drawings, construction, structural changes and soil reports are available before making a site visit. If drawings are not available it is best to get an as-built drawing done by a specialist company. By studying the documents, an experienced engineer will understand the structural system of the building, recognise critical aspects where inspection should be carried out and identify allowable imposed loads. The clients representative should be forewarned about the need for opening up any area (e.g. inside ceiling void) before the visit.

5.2 Visual Inspection

The purpose of having visual inspection is to identify structural defects, check material deterioration, identity structural distress and check for addition and alteration. A photographic record should be taken before commencement of visual inspection. Usually visual inspection will include Checking Dimensions Checking Structural Arrangement, Checking the type of Materials used and Checking the Condition of the Structure.

5.2.1 Checking of Dimensions

From the available drawings critical dimensions should be checked. Levels of key structural elements should be taken. Changes made from the initial construction must be noted down. Verticality of columns and structural wall should be checked with a plumb-bob. In this regard if the engineer feels that floor to columns are not in alignment, the services of specialist surveyor should be obtained to verify it.

5.2.2 Checking Structural Arrangement and Materials

Find out the materials used and the structural framing system of the building. Identify critical members such as transfer beams or floating columns, long span members, joint details, crossing ducts through beams, etc. Changes to structural system from the original drawings should be identified. There will be cases where new mezzanine floors or new lifts has been installed. Also identify deviation from the intended use which may result in overloading.

5.2.3 Checking the Condition of the Structure

This is a key part of the SHM. Experience in inspection of similar structures will be very helpful. The condition should be recorded so that it can be reviewed later with the rest of the team.

Some of the general conditions to look for are deformation, distortion to members, bowing of beams ties or bracing in steel structure, vibration, corrosion, settlement in walls and floors deflection and cracks in retaining walls, settlement of foundation etc.

For concrete in particular one should look for cracking, rust stains, cracks at intervals, random diagonal cracking in beams, spalling, and water penetration at cracks, joint behaviour etc.

For timber structures its best to consult specialist literature before a check is carried out.

5.3 Testing

At the desk study and the visual inspection stage the engineer can conclude if there is a need for testing. If the structure has performed well so far without any apparent defects and the structure can be inspected fully, one can conclude there is no need for any testing. Defects of any sort, or overloading of the structure will require further testing of the structure. Cost may decide the number of test to be performed. It's wise to discus with the client the pros and cons of performing the number of tests.

Some of the most commonly available tests in Sri Lanka are listed below.

5.3.1 Concrete Strength and Quality

See Table 1.

Table 1 Test for strength

Rebound hammer test	Measure the surface hardness of the concrete. Used primarily for making a comparative assessment of quality of concrete
Ultrasonic pulse velocity test	To establish the quality of concrete. It can be assessed by measuring the velocity of ultrasonic pulse through the concrete
Core test	To determine the compressive strength and density of concrete from 100 mm or 150 mm core samples taken from the structure

Table 2 Test for durability

Cover meter test	To measure the actual cover orientation and distribution of the reinforcement
Carbonation test	Also known as Phenolphthalein test. This is to determine the carbonation from a core sample taken from a structural element
Half cell potential test	To assess the level of corrosion of reinforcement
Chemical test	Determination of Chloride, Sulphate contents and pH of concrete

5.3.2 Durability of Concrete

See Table 2.

5.4 Structural Analysis—Capacity Evaluation

If the initial brief or the TOR permits a structural analysis will help on the final recommendation of the assignment. Based on the physical properties of the structural elements and the imposed loading a finite element computer modelling can be carried out. For the loading it is best to use the current actual loading. But in a case where the change of building usage is anticipated the new loading can be used (only if it's higher than the present loading). From the calculations the structural capacity of main structural elements can be calculated. The results can be compared with the NDT tests to confirm that the relevant structural element is adequate to carry the required load.

6 The Report

A SHM report contains the condition of the building and the remedial action to be taken. When writing reports the engineer should consider potential readers. The report should be as simple as possible. However it must be technically accurate. Abbreviations should be avoided unless it is a common familiar one. Photographs are useful but any included should be referred to in the text. The report should

include appropriate background information to allow a stranger to the structure to become aware of the full situation by reading the report. The conclusions should be definite, reasoned, engineering judgments, reached after careful consideration of the information obtained. Recommendations should be based on the conclusions. They may include remedial work, regular maintenance work, monitoring, inspections, or if the report is only for first stage what's to be done at the next stage.

One of the important item that should contain in the report are information to prepare a cost estimate by a quantity surveyor. It would be helpful if alternate remedial options are given so that the client can exercise economic choices. Adequate warnings should be given on the use of cheaper alternative, which may significantly more expensive in the long term.

7 Post Actions

Based on the findings and recommendations different measures of repairs and strengthening has to be carried out. Once recommendations are given TR69 'Repair of concrete structures with reference to BS EN 1504′ gives six options for repair of concrete for the client to decide.

1. Do nothing, but monitor.
2. Reanalyse the structural capacity of the weakened element.
3. Prevent or reduce further deterioration.
4. Improve, strengthen or refurbish all or part of the structure.
5. Replace all or part of the structure.
6. Demolish, completely or partially.

Once the decision to repair is taken its good to follow the principles given in BS EN 1504 (Table 3).

Strengthening of concrete may require due to several reasons.

- Demand of the structural member exceeds the capacity of the member due to increased loading conditions.
- The structural member no longer to carry the loads due to deteriorations.
- Poor design and construction methods.
- Settlement or ground movement.
- Impact (Due to a vehicle).
- Fire.

Different Strengthening methods are available according to the element and the location. Some of them are adding extra reinforcement and enlarging the section, bonding Fibre Reinforced Polymer Sheets (FRP), Structural Grouting or even adding new member to work with the existing members (steel beam under an existing beam).

Table 3 Repair principles (BS EN 1504)

Principles related to defects in concrete	
Principle 1	Protection against ingress
Principle 2	Moisture control
Principle 3	Concrete restoration
Principle 4	Structural strengthening
Principle 5	Increasing physical resistance
Principle 6	Increasing resistance to chemicals
Principles related to reinforcement corrosion	
Principle 7	Preserving or restoring passivity
Principle 8	Increasing resistivity
Principle 9	Cathodic control
Principle 10	Cathodic protection
Principle 11	Control of anodic areas

8 Conclusion

Structural Health Monitoring, Structural Appraisal or Structural Auditing is an activity different from Structural Design. In SHM the actual conditions are known as opposed to design where the actual structure has not been built. Correct assessment of the structural condition, interpretation and adoption of the test results are the most important factors one should follow. If the condition of the structure is assessed properly two questions can be answered.

1. Is the structure adequately safe now and will it remain so in the future?
2. Can it be used for its intended purpose now and in the future?

While answering the above questions one should make a mature engineering judgment to make the building a safe place live or work. As mentioned in Sect. 6 the conclusions should be definite, reasoned, engineering judgments, reached after careful consideration of the information obtained.

9 Recommendation

It is best to introduce regulations for buildings over 15 years to be to be assessed periodically. India and Malaysia doing this. In addition to regulations, proper guide lines should be prepared for SHM so that the inspection, testing and recommendation can be done in a professional manner. As more and more multi-national companies insists on a report on the condition of the local factories, having regulations and guidelines for the use of professionals and building operators will be very helpful.

References

1. Periodic Structural Inspection of Existing Buildings—Guidelines For Structural Engineers—Building and Construction Authority of Malaysia
2. Appraisal of existing structures (Third edition)—Institution of Structural Engineers (UK)
3. Technical Report 69—Repair of concrete structures with reference to BS EN 1504

A Review on Mechanical Properties and Morphological Properties of Concrete with Graphene Oxide

A. M. B. Chandima and S. P. Guluwita

Abstract This paper contains a comprehensive review carried out on the literature of performance of cementitious composites of Graphene oxide (GO) and cement. During the past decay, various types of Nanomaterials introduced to the cement to achieve the durability and higher strength. For the substantial improvement of the construction industry are using Silica fume as a mineral admixture. This gives very high and ultra-high strength concrete. Even though cement–silica composite has high performance, intrinsic brittleness nature of cement is a limitation for some application which can overcome by using nanomaterials. There are few common nanomaterials which, are used for concrete Nano silica, nano titanium, carbon nanotube (CNT), carbon fiber and graphene. As a composite material, chemically oxidized graphene which is graphene oxide is extensively used in favour of its bulk production and good dispersion properties. Graphene could combine into the cement paste or mortar and strengthen the bonds of the cement hydrates. As a result, the essential properties of cement and especially its tensile and compressive strength could be improved. The Graphene Oxide and Ordinary Portland Cement (OPC) composite are normally produced by dispersing GO sheets in water. For this purpose, did not use surfactant, dispersant or stabilizing agents. The compositions produced by adding GO at the time of mixing the cementitious materials, course and fine aggregates and water. Research works show that very low quantity of GO is needed to improve flexural strength of an OPC matrix. It also improves the ductility and reduces the risk of catastrophic damage due to the extreme loads. The addition of GO improves the pore structure of concrete and decrease the total porosity.

Keywords Nanomaterials · Cement · Composites · Graphene

A. M. B. Chandima · S. P. Guluwita (✉)
Department of Material Science and Engineering, University of Moratuwa, Moratuwa, Sri Lanka
e-mail: sguluwita@materials.mrt.lk

R. Dissanayake et al. (eds.), *ICSECM 2019*, Lecture Notes in Civil Engineering 94,
https://doi.org/10.1007/978-981-15-7222-7_12

1 Introduction

In ancient time to till the most common materials used for the construction industry are cement aggregate, water and admixtures. In the modern construction field, people are researching for the new materials without compromising on performance. Due to the blooming of nanotechnology, people use the materials at nanoscale which offers the enhanced properties of concrete structure. On the other hand, the carbon footprint in cement production, which be achieved by lowering the clinker content of cement. Sustainable production of cement can be achieved by utilizing mineral admixture, industrial waste, Nanomaterials and this result, improves the performance of either cement product or enhances the durability of concrete structure.

This review papers dispute on the nanomaterials use in concrete, especially graphene oxide. Nanomaterials are defined as material with at least one-dimensional structure range approximately from 1 to 100 nm. The requirement of high-performance concrete in the construction industry rises day by day and the requirement of novel material has been developed steeply. Then the researcher focused more on nanomaterials since the properties of nanoparticles have diversified from the same materials at the macro or the micro scale. The types of nanomaterials used in concrete and cement are nano silica, nano alumina, carbon nano tube (CNT), polycarboxylates, titanium oxide, nano kaolin, nano clay and etc.

1.1 Structure of Cement

Ordinary Portland cement is the composed of various mineral oxides and cement products which represents the particular crystal structures and impurities. There are different solid phases associated with cement chemistry and main solid phases are named as Alite (C3S), Belite (C2S), Aluminate and Ferrite.

During the cement production the final step is the grinding of clinker mixed with gypsum to the fine powder which are in a wide range of sizes from 10 to 90 μm. Cement particles are reacted extensively with water and liberated heat while forming a “C-S-H” gel as the main hydration product which has a structure of very small internal pores. There is a major drawback in the cement structure which is the crack formation and results in the degradation of concrete structure. There are various research projects, conducting to overcome this issue. Cement based nano-composite played a vital role to give strength and durability of the concrete.

1.2 Nanomaterials for Construction

The usage of nanotechnology concept in cement composites is drastically growing during the past decays. Nanomaterials used in the cement industry as a reinforcing

agent which provides a much higher specific surface area for interaction with the cement matrix in nanoscale. Even though, the most of the research works is based on the application of nanotechnology in cement composites for enhancement of mechanical properties, but some research works focus on usage of nanoparticles in cement industries such as Nanosilica (SiO_2), Alumina (Al_2O_3), Titanium dioxide (TiO_2) nanoparticles, nano-clay nano-calcium particles carbonate ($CaCO_3$), Carbon Nano Tubes (CNT), Graphene oxide, etc.

1.3 Graphene Oxide

Among all the nanomaterials one of the nanofibrous material; Graphene oxide (GO) exhibits pozzolanic characteristics which can enhance the internal matrix properties and interface structure. There are several methods for the preparation of GO. Graphene oxide is a compound made out of carbon, hydrogen and oxygen molecules. Graphite oxide is produced by chemically treated the graphite with conc. Sulphuric acid. This strong acid is reacted with the graphite and removed an electron during the chemical reaction which is known as redox reaction. Graphene oxide is a by-product of this oxidation process as when the oxidising agents react with graphite, the interplanar space of the graphite sheet is increased. The completely oxidised compound then disperses in a base solution which is water, and graphene oxide obtained as a result [1]. Since GO has versatile properties, it is an ideal filler of nano level for the modification of cementitious materials [2]. The drawbacks of usage of graphene are difficult to synthesis and very expensive [3]. Even though GO is expensive researchers investigate various amazing outcomes whiles incorporate this nanomaterial into cementitious materials [4].

2 Production of Graphene Oxide

Graphene oxide is typically produced from the chemical oxidation and exfoliation of graphite. GO forms as hexagonal 2D sheet layers with several nanometres levels thick and several hundred manometers long. GO has ranges of reactive oxygen functional groups, and those are incorporated with cementitious materials during hydration for the formation of microstructure [3]. Graphene can be functionalized with three different methods as below [5]. Noncovalent attachment of large/small aromatic-containing molecules through stacking, grafting molecules on the basal plane of graphene and the chemical reactions between the functional groups on GO and other molecules, together with subsequent or simultaneous chemical reduction.

Nandhini and Padmanaban [6] mentioned the preparation of Graphene oxide by modifying Hummers method. Graphite flakes were mixed with $NaNO_3$, $KMnO_4$ and with conc. H_2SO_4 to prepare the dispersion of GO solution [6].

Fakhim et al. [7] group of researchers used exfoliation of graphite oxide for the synthesis of GO through a colloidal suspension route which was first investigated by Stankovich et al. [8]. During the synthesis process natural graphite powder mixed with $NaNO_3$ and Conc. H_2SO_4 in an ice bath and $KMnO_4$ added as strong oxidizing agent. The product was graphite oxide slurry and it was exfoliated by ultrasonication to generate graphene oxide nanoflakes. The resulted mixture was then filtered and washed with diluted HCl solution to remove metal ions and finally, the product was washed with DI water to remove the acid [7].

2.1 Composite of Graphene Oxide and Cement

It is required to obtain a properly dispersed graphene matrix to have good interfacial interaction in between the graphene oxide nanoparticles and cement. It gives high mechanical strength to the cement motor or concrete mixture. GO contains functional groups which are hydrophilic and highly dispersible in the aqueous medium. This unique property of GO is the reason for the better combination with cement to form composites while enhancing the mechanical properties.

Fakhim et al. [7] mentioned the dispersion of Carbon Nanostructures within Cement Matrix. The bundle of GO was added gradually to water mixed with polycarboxylate ether (PCE) superplasticizer and the sonicated to obtained properly disperse individual GO flakes. Then Ordinary Portland cement, OPC was added to the dispersed GO at required water/cement ratio.

Jinwoo et al. [9] mentioned that for wet-mix design required more energy to sonicate the GO with water to obtain a good dispersion sample. Therefore, they tested both wet-mix design and dry-mix designs. Even though wet-mix design requires more energy for sonication it exhibits higher compressive and flexural strengths than Dry-mix designs. Well-dispersion GONF-cement composite indicate the higher strengths. In practically dry-mix design will be easy to perform.

3 Properties of GO-Cement Composite

3.1 Mechanical Properties

3.1.1 Tensile Strength

Tensile strength of cement motor is generally used to have an indirect indication of the compressive strength of cement. Although it is specified by ASTM C307-03 standard, the direct tension test does not provide useful insight rather than compression strength. Therefore, most of the researchers measured tensile stresses indirectly by a spitting tension test or a flexural strength test. However, few researchers reported

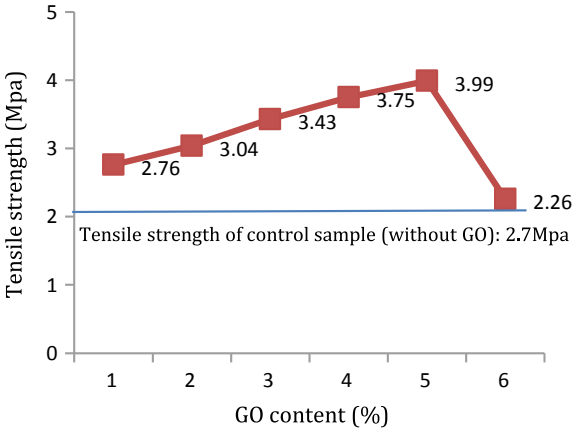

Fig. 1 Tensile strength results of cement motor specimens with different GO content [7]

tensile strength as one of mechanical property. Kim et al., indicated that the 11% and 17% increase of tensile strength after 7 days and 28 days of casting respectively with 0.5% of GO flakes with 0.2% polycarboxylate ether superplasticizer [10].

Jinchang et al. investigated that, the bending strength of the GO reinforced cement based composite material and it is reported that the increase of the bending strength 23.82% was the highest value obtained for the content of GO was 0.03%.

Fakhim et al., reported that, the tensile strength of the specimens was increased gradually until it reached to the percentage of nano-GO 1.5% which was 47.8% compared with the specimens without GO flakes [7] (Fig. 1).

3.1.2 Flexural Strength

Flexural Strength (modulus of rupture) is a measure of tensile strength in bending. Abrishami et al., revealed the effect of the dispersing agent of GO flakes such as graphene–water suspension and NH_2-functionalized GO.

As in Table 1 it is indicated that, the flexural strength of the cement-GO composites which was NH_2-functionalized GO gave better flexural strength after 14 days of casting with compared to pure GO-cement composite motor [11].

Devasena et al., indicated that addition of GO increased the flexural strength. However, there was the optimum quantity to achieve maximum tensile and flexural strength of concrete. 0.05, 0.1, 0.2% of cement content were added GO to the composite and 0.1% GO-cement composite showed 4.2 and 2.34% enhancement of flexural strength for 14 days and 28 days respectively [12].

Wang et al., investigated the flexural strength of hardened cement paste and motor and reported the flexural strength of harden cement paste were increased by 86.1%, 68.5% and 90.5% after 3, 7 and 28 days, respectively, and for the hardened motor the corresponding increased are 69.4%, 106.4% and 70.5%.

Table 1 Comparison of flexural strength with specimens without GO (%)

Graphene–water	NH_2 functionalized GO	Flexural strength %
0.05		8.9
0.1		23.5
0.15		20.8
0.20		4.7
0.25		3.0
	0.05	67.70
	0.10	70.9
	0.15	54.1
	0.20	40.7
	0.25	35.7

3.1.3 Compressive Strength

There are varieties of samples used to measure the compressive strength of cement motor or concrete. Researchers used cubes or cylinder for concrete while others used prism mould or cube for cement motor test. The compressive strength development of cement motor or concrete is evaluated from previous research works.

Kim et al. found that the average cube and cylinder strength were increased by 10% and 29% respectively when 0.5% GO flakes were incorporated [10].

Shareef et al. reported that the compressive strength of M25 concrete by replacing cement with 1% and 2% GO increased 7% and 17% respectively for 28 days [13].

Abrishami et al., revealed that the NH_2-functionalized GO reported higher compressive strength for 14 days of casting with compared to pure GO-cement composite motor. It increased by 39.1% of compressive strength with compared to without GO [11].

Krystek [14] studied the compressive strength of cement motor reinforced with the 0.03% of GO. This enhanced compressive strength of cement motor by 23% and by 28% for the cubic compressive and uniaxial cylindrical compressive strength respectively [14].

Devasena et al., indicated that 0.1% GO-cement composite showed 14% and 10% enhancement of compressive strength for 14 days and 28 days respectively [12].

Wang et al., investigated the compressive strength of hardened cement paste and motor and reported the compressive strength of harden cement paste were increased by 52.4%, 46.5% and 40.4% after 3, 7 and 28 days, respectively, and for the hardened motor the corresponding increased are 43.2%, 33% and 24.4%.

Jinchang et al., studied the compressive strength of cement motor by addition of GO. The mass fraction of GO was set as 0.01%, 0.03% and 0.05% and the water cement ratio was set as 0.35, 0.4, 0.45 and 0.5. The outcome of the research works was stated as below. It was found that the compressive strength was maximum with 0.03% of GO and the growth rate of compressive strength was 10.86%. As per Fig. 2b showed that the variation of compressive strength of cement motor under

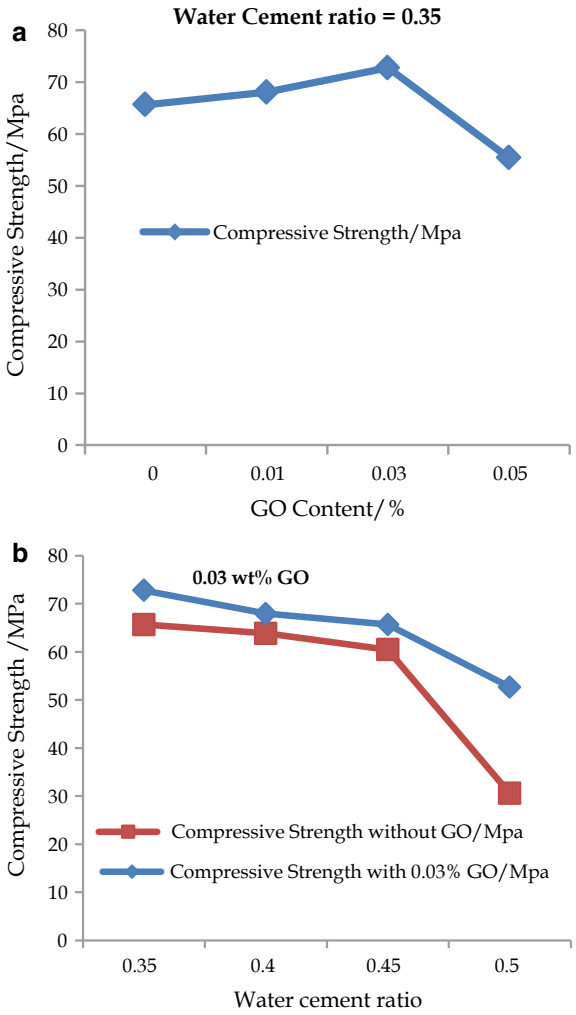

Fig. 2 The variation of the compressive strength of GO reinforced cement based composite material [15]

different water cement (w/C) ratio and reported the larger the w/c ratio, the lower the compressive strength [15].

3.2 The Pore Structures

In all types of phases in cement-based composites contain enormous pores. The strong influence on mechanical properties and durability is based on the pore structure.

Table 2 Pore structure of GNP/cement composites [16]

Samples (% of GO)	Total intrude volume (ml/g)	Median volume pore diameter (nm)	Porosity (%)
G0: 0%	0.1454	35.9	27.1
G1: 0.05%	0.1052	33.2	19.9
G2: 0.01%	0.1105	29.2	20.7
G3: 0.15%	0.1261	35.9	23.4

Wang et al. studied about the pore parameters and morphology of the cement-based composites doped with graphene nanoplates through mercury intrusion porosimetry (MIP) and an ultra-high-resolution field emission scanning electron microscopy (FE-SEM). As per Table 2 this study revealed that the addition of GNPs reduces the value of porosity and median volume pore diameter compared with the composite without GNPs.

Lv et al. indicated in their research work that, GO nanosheets have an important effect on the pore structure of GON-cement composites. These samples were prepared via doping with GO with cement composite. The outcome of this research work was interesting and the out of different pore diameters, median pore diameter and the average pore diameter were showed similar values which concluded that the pore diameter were uniform. The results indicated that GONs can enhance the formation of ordered network of micro structures due to this homogeneous distribution of pores. This property helps to increase the strength and toughness of cement [17] (Table 3).

Li et al. investigated that the workability of cement paste was reduced due to formation of the GO agglomerates. On the other hand, it was accelerated the hydration process by providing nucleation sites which act as seeding material in the cement paste. They addressed that the emerging of GO refined the pore structure of the cement paste. As per their research found that the major impact of GO was on macropores than on large and small mesopores [18].

Table 3 Pore structure of GON/cement composites [17]

Specimens	Total pore area (m^3/g)	Median pore diameter (nm)	Average pore diameter (nm)	Porosity (%)
Control	25.64	28.43	19.92	23.56
Sample 1	13.38	12.27	10.66	9.32
Sample 2	12.45	12.25	11.27	9.56
Sample 3	13.36	11.68	10.67	8.34
Sample 4	12.78	12.03	11.54	8.69

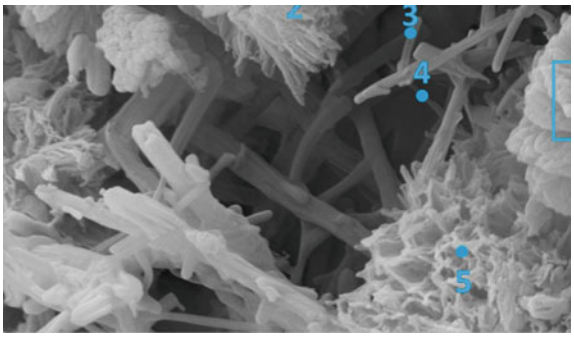

Fig. 3 The images of SEM analysis (GONF-combined cement paste with 0.05% GONF at 7 days) [9]

3.3 Morphology Properties

SEM (scanning electron microscope) was preferred by the researchers to investigate microstructure of cement hydration products when GO is introduced into the cement matrix. Figure 3 reveals several needle-shaped ettringite projecting into the pores and the amorphous morphology of C-S-H can be clearly seen. According to the research evident of Jinwoo et al. [9] confirmed that, the GONFs were inside the products of cement hydration which were surrounded by C-S-H which evident that GONF's act as nano-reinforcing and nano-filling ingredients.

Jinchang and Yeming [15] revealed that, GO affect the distribution and the formation of cement hydration product and it provides better filling effect, hydration effect and nucleation effect. GO has large specific surface area which provides better growth space for the hydration products. Since GO reduced the porosity results high strength and ductibility cement motor [15] (Fig. 4).

Fakhim et al. [7] research team used ultra-high-resolution field emission scanning electron microscopy (FE-SEM) to observe the fracture surface of samples containing 1.5 wt% GO. It was indicated that the nano-GO flakes were well dispersed in the cement matrix, and it can be observed that the good bonding between the GO surfaces and the surrounding cement matrix (Fig. 5).

4 Conclusion

The microstructural properties and mechanical properties of GO with cementitious materials have been reviewed and discussed in brief in this article. It is implied by all the researchers' that the main reason for the high bond strength is influence of GO to the hydration process of cement at the molecular level. It is required to have better disperse GO to react with cement matrix. Therefore, researchers investigated different dispersion methods to achieve this target. It is revealed that dry mix of the

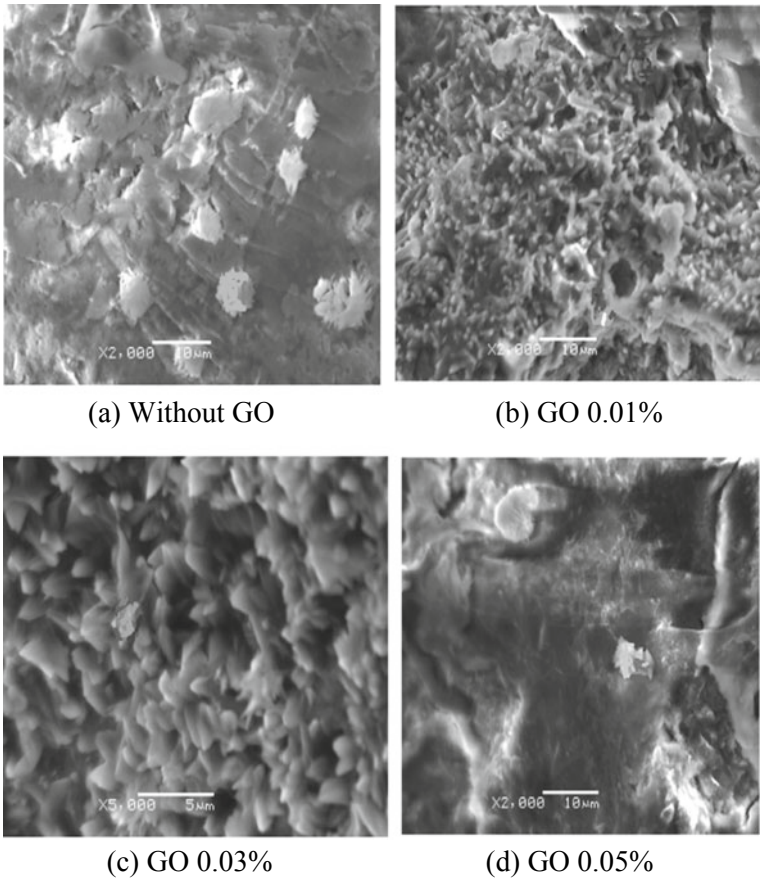

(a) Without GO (b) GO 0.01%

(c) GO 0.03% (d) GO 0.05%

Fig. 4 The test specimens under different mixing amount of graphene oxide under SEM [15]

GO did not give higher bonding strength. A variety of liquid solutions used to disperse GO nano-flakes by creation of non-valent bond with surfactants through chemical alteration of the surface of GO. Polycarboxylate superplasticizer was commonly used for this purpose. Following is a list of areas where improvement of structural and mechanical properties of graphene cement composite:

(1) Addition of GO accelerate the hydration process of cement which helps to decrease pore volume by proper reinforcing the structure resulted the increase the mechanical properties of both the hardened cement paste and motor. It is indicated that the pore structure of composites is enhanced with smaller pore size and the uniform pore distribution. The incorporation of GO reduced total pore volume of the cement mortar by 6.9% for 28 days. Properly distributed pore structure resulted with the increase of the percentage of GO to 0.03% and reduced the large pores (>100 nm) of the hardened cement composite by

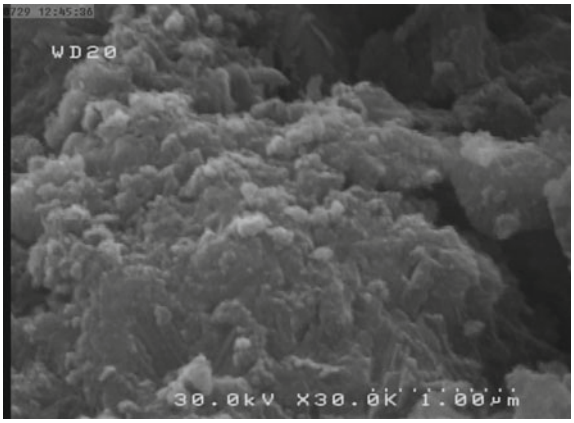

Fig. 5 FE-SEM images of cement motor with 1.5 wt% showing C-S-H gel in the form of a dense sponge matrix that gradually spread, merge, and adhere to GO, strengthening the cement and reducing its permeability [7]

48.7%, while the number of small pores (10–100 nm) increased by 127% with comparison to the cement mortar without GO [19].

(2) The addition of GO improved the high mechanical strength of hardened cement motor after 03 days and 7 days, but has less effect on 28 days. Findings of the research works revealed that the addition of GO could greatly enhance the flexural and compressive strength up to 13% and 23% of 0.03 wt% GOCC compared to the without GO for 28 days [14]. Wang et al. revealed the highest enhancements of compressive strength and flexural strength with the addition of GO (0.05%). It revealed that for the harden cement mortar, the compressive strength increases were 43.2, 33 and 24.4% after 3, 7 and 28 days, respectively, and the corresponding flexural strength was greater by 69.4, 106.4 and 70.5%.

(3) SEM or FE-SEM used to observe the surface of samples and it is indicated that the nano GO flakes were properly dispersed in the matrix and there was good bonding between the GO interface and with the cement matrix.

References

1. Chen D, Feng H, Li J (2012) Graphene oxide: preparation, functionalization, and electrochemical applications. Chem Rev 112(11):6027–6053
2. Tong T, Fan Z, Liu Q et al (2016) Investigation of the effects of graphene and graphene oxide nanoplatelets on the micro- and macro-properties of cementitious materials. Constr Build Mater 106:102–114
3. Zheng Q, Han B, Cui X, Yu X, Ou J (2017) Graphene-engineered cementitious composites: small makes a big impact. Nanomater Nanotechnol 7:1–18
4. Zhu Y, Murali S, Cai W et al (2010) Graphene and graphene oxide: synthesis, properties, and applications. Adv Mater 22:3906–3924

5. Sideri S (2014) Feasibility study of functionalized graphene for compatibility with cement hydrates and reinforcement steel. Master's thesis, Chalmers University of Technology, Gothenburg, Sweden
6. Nandhini S, Padmanaban I (2016) Experimental investigation on graphene oxide composites with fly ash concrete. Int J Earth Sci Eng 09(03):515–519
7. Fakhim B, Hassani A, Rashidi A, Ghodousi P (2014) Preparation and mechanical properties of graphene oxide. Sci World J
8. Stankovich S, Dikin DA, Piner RD et al (2007) Synthesis of graphene-based nanosheets via chemical reduction of exfoliated graphite oxide. Carbon 45(7):1558–1565
9. Jinwoo A, Matthew M, Wonseok C, Boo H (2018) Feasibility of using graphene oxide nanoflake (GONF) as additive of cement composite. Admixture (additive) for cement composites
10. Kim B, Taylor L, Troy A, McArthur M, Ptaszynska M (2018) The effects of graphene oxide flakes on the mechanical properties of cement mortar. Comput Concr 21(3):261–267
11. Abrishami ME, Zahabi V (2016) Reinforcing graphene oxide/cement composite with NH_2 functionalizing Group. Bull Mater Sci 39(4):1073–1078
12. Devasena M, Karthikeyan J (2015) Investigation on strength properties of graphene oxide concrete. Int J Eng Sci Invent Res Dev
13. Shareeff KRM, Rawoof SA, Sowjanya K (2017) A feasibility study on mechanical properties of concrete with graphene oxide. IRJET 04(23)
14. Krystek M (2019) Mechanical properties of cement motor with graphene oxide. Archit Civ Eng Environ
15. Jinchang P, Yeming W (2018) Graphene oxide on the microstructure and mechanical properties of cement based composite material
16. Wang B, Zhao R, Zhang T (2018) Pore structure and durability of cement-based composites doped with graphene nanoplatelets. Mater Express 8(2)
17. Lv S, Zhang J, Zhu L, Jia C (2016) Preparation of cement composites with ordered microstructures via doping with graphene oxide nanosheets and an investigation of their strength and durability. Materials
18. Li X, Yan ML, Li WG, Li CY, Sanjayan JG, Duan WH, Li Z (2017) Effects of graphene oxide agglomerates on workability, hydration, microstructure and compressive strength of cement paste. Constr Build Mater 145:402–410
19. Wang Y, Yang J, Ouyang D (2019) Effect of graphene oxide on mechanical properties of cement mortar and its strengthening mechanism. Materials 12:3753
20. Geim AK, Novoselov KS (2007) The rise of graphene. Nat Mater 6:183–191
21. Lv S, Ma Y, Qiu C, Sun T, Liu J, Zhou Q (2013) Effect of graphene oxide nanosheets of microstructure and mechanical properties of cement composites. Constr Build Mater 49:121–127
22. Qureshi ST, Panesar DK (2017) A review: the effect of graphene oxide on the properties of cement-based composites. Leadership in Sustainable Infrastructure
23. Špitalský Z, Kratochvíla J, Csomorová K, Krupa I, Graça MPF, Costa LC (2015) Mechanical and electrical properties of styrene-isoprene-styrene copolymer doped with expanded graphite nanoplatelets. J Nanomater
24. Wang Q, Wang J, Chun-Xiang L, Bo-Wei L, Zhang K, Chong Z (2015) Influence of graphene oxide additions on the microstructure and mechanical strength of cement. New Carbon Mater 30(4):349–356
25. Kjaernsmo H, Kakay S, Fossa KT, Gronil J (2018) The effect of graphene oxide on cement motor. IOP Conf Ser Mater Sci Eng 362:012012

Hydraulic Characteristics of Ballast Subjected to Particle Degradation Using Parallel Gradation Technique

G. Thanushan, K. Milojan, and L. C. Kurukulasuriya

Abstract Rail tracks are positioned on ballast for the reasons including high load bearing capacity, economy and rapid drainage. It is essential to maintain proper drainage in the ballasted track in order to reduce the pore water pressures during loading that would result in reduced shear strength. The clean and fresh ballast particle assemblage has adequate porosity to facilitate drainage. However, the ballast becomes fouled due to the intrusion of fines either from the subgrade or particle breakage which impairs track drainage as a result of reduced porosity. The degradation (fouling) of ballast can be mainly categorized into two, which are internal particle breakage and subgrade particle intrusion (mud pumping). The aim of this research is to analyse the variation of hydraulic conductivity of ballast subjected to particle degradation by inter particle breakage and fouled with subgrade soil separately. Breakage index is used to state the level of fouling in ballast sample which is fouled with broken down particles and volume based percentage is used to state the level of fouling in ballast fouled with subgrade material in this study. Several constant head hydraulic conductivity tests were conducted with Rowe cell apparatus and parallel gradation technique is adopted to accommodate sufficient amount of ballast sample inside the Rowe cell. The study revealed that, the hydraulic conductivity decreased as the percentage of fouling increased due to the presence of fine particles between the ballast particles.

Keywords Ballast · Hydraulic conductivity · Ballast fouling · Parallel gradation · Rowe cell

1 Introduction

Sri Lankan railway department widely uses ballasted railway tracks for the railway transportation. A typical ballasted track consists of superstructure (ties, fasteners, and rails) and substructure (ballast, sub-ballast, and subgrade layers). One of the most

G. Thanushan (✉) · K. Milojan · L. C. Kurukulasuriya
University of Peradeniya, Peradeniya, Sri Lanka
e-mail: gthanushan93@gmail.com

R. Dissanayake et al. (eds.), *ICSECM 2019*, Lecture Notes in Civil Engineering 94,
https://doi.org/10.1007/978-981-15-7222-7_13

Fig. 1 Degraded ballast railway track

important physical property of ballast is drainage capacity. Railroad ballast usually contains uniformly graded material that creates sufficiently large pore structure to facilitate rapid drainage. When it is degraded and aged drainage capacity is reduced. Several rock types such as limestone, basalt, and slag are used for ballast all over the world. Aggregates obtained from crushing rocks are the widely used ballast material in Sri Lanka, which can get deteriorated during its service life due to particle breakage and subgrade intrusion primarily among other forms of degradation possible.

Ballast particles are gradually degraded with and drainage capacity reduced due to the cyclic loading imposed with the passage of trains and also due to atmospheric conditions. This research study analyses the effect of particle degradation on the hydraulic conductivity of ballast. There are two major mechanisms involved in ballast degradation. First one is due to the abrasion between ballast particles while it is undergoing cyclic load will produce finer particle and that will finally fill the voids reducing effective porosity of ballast [1]. This will result in a reduction in average ballast particle size (D50) also. The other way is migration of subgrade particles into the ballast layer named as mud pumping, which will be filled in the ballast voids leading to a reduced void ratio. Mostly in Sri Lanka, this process is induced by the increase in pore water pressure due to cyclic loading by the train and where, wet subgrade particles are the fouling agent [2] (Fig. 1).

2 Literature Review

Ballast Gradation is a primary factor affecting the stability and drainage of tracks [3]. Sri Lankan railway tracks are designed and built according to the Indian standard which shows considerably higher shear strength than other standard gradations [4]. Indian standard also fulfils the drainage criteria and has the highest performance in load bearing characteristics and stability [5].

Constant head hydraulic conductivity test is more suitable to analyse the hydraulic properties of the ballast and fouled ballast. However, as the sizes of the aggregates are relatively large and angular, it is impossible to conduct the constant head hydraulic conductivity test using the conventional permeability test apparatus. Therefore, parallel gradation technique which was proposed by Lowe [6] is used for this study.

Several tests were carried out on field sample in order to analyse the hydraulic conductivity with fouling. Su et al. [7] carried out a research to study the relationship between permeability and fouling volume percentage of ballast fouled with fine sand and coarse sand. Rahman et al. [8] carried out a study to obtain a correlation between permeability and resistivity for the ballast and sub ballast layer. Clay and crushed ballast were used as the fouling materials.

Selig and Waters [9] proposed two methods to quantify the level of ballast fouling. The first method is by defining a fouling index, which is the sum of the percent by weight of ballast sample passing the 4.75 mm sieve plus the percent passing the 0.075 mm sieve. The second method is the percentage of fouling, which is the ratio of the dry weight of the material passing the 9.5 mm sieve to the dry weight of total sample.

A constant head permeability test and a middle scale direct shear test of railway subballast were conducted in the research by Jing et al. [10], aiming to investigate the subballast permeability and shear characteristics. Four different designed gradations within the standards were subjected to the investigation in order to study the effect of particle size distribution on permeability characteristics of subballast.

3 Materials and Methods

3.1 Ballast Subjected to Particle Breakage

Ballast (specific gravity = 2.730) was collected from a stock pile near to the Gampola town. First collected ballast sample was sieved with BS 1377:1990 sieves (75 mm, 63 mm, 50 mm, 37.5 mm, 28 mm, 20 mm, 14 mm, 10 mm, 6.3 mm, and 5 mm) and categorized according to size ranges.

The parallel gradation technique was used to prepare samples for the experiments and a modified Rowe cell apparatus was used to conduct constant head hydraulic conductivity tests.

A reduction factor of 3 was selected and new parallel graded curve was prepared by scaling down the upper bound of the Indian standard gradation curve to represent the gradation of fresh ballast. Parallel graded fresh ballast sample was prepared according to the new gradation curve (Fig. 2).

State of fouling for the ballast fouled with internal particle breakage was represented in terms of Marsal Particle breakage index (BI). The particle breakage was induced on the parallel graded fresh ballast sample by subjecting the ballast sample

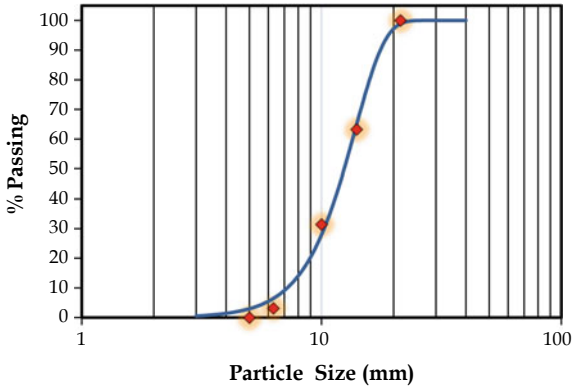

Fig. 2 Gradation curve of parallel graded ballast

to a predetermined number of revolutions in a Los Angeles Abrasion Value (LAAV) testing machine.

Shihana et al. [4] conducted several trial tests on LAAV testing machine and obtained the breakage indices corresponding to the number of revolutions applied as shown in the Fig. 3.

Then she plotted the gradation curves of those samples which are shown in Fig. 4.

Since they used a factor of 8 for parallel gradation, these plots correspond with a parallel gradation factor of 8. Therefore, these plots were adjusted for a parallel gradation factor of 3 and re-plotted for this study to determine the breakage index value of the particles degraded in the LAAV testing machine. Three parallel graded ballast samples were degraded in the LAAV testing machine by applying 150, 400 and 600 revolutions. Gradation curves of these degraded samples were plotted and breakage indices of these samples were determined by comparing with the modified reference plot (Fig. 5).

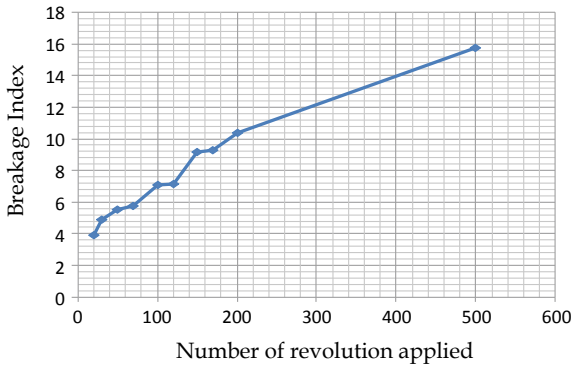

Fig. 3 Variation of induced ballast breakage and number of revolution of drum

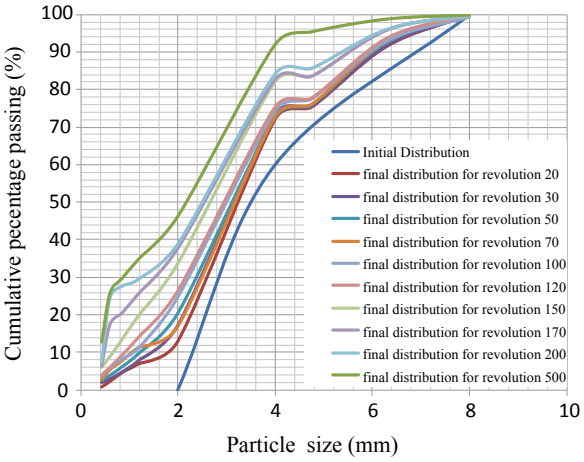

Fig. 4 Particle size distribution of different revolution samples

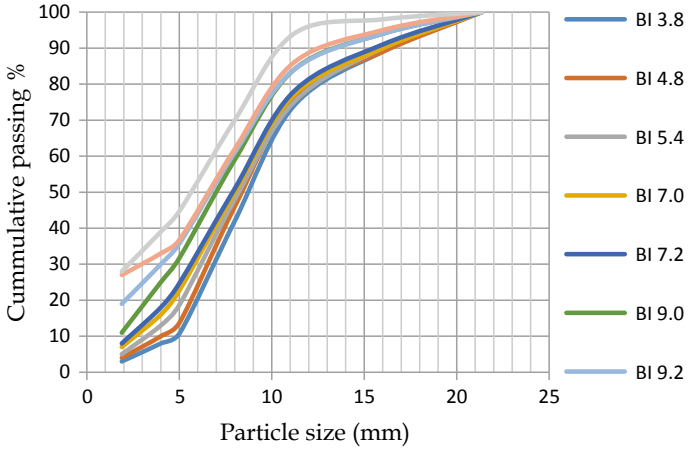

Fig. 5 Gradation curves with pre-determined BI values

Accordingly, corresponding to the number of revolutions of 150, 400 and 600, the Marsal breakage indices were 4.8, 5.4 and 7.2 respectively.

3.2 Pumped Up Subgrade Material

Pumped up subgrade material (specific gravity = 2.679) was collected from the railway track near to the Peradeniya railway station. At first the sample was dried

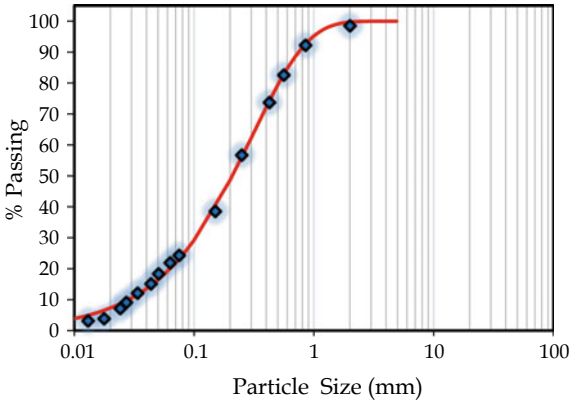

Fig. 6 Particle size distribution of subgrade material

and sieved with BS 1377:1990 sieves (2 mm, 850 μm, 560 μm, 425 μm, 250 μm, 150 μm, 75 μm and 63 μm). Particles passing through the 63 μm were used for the hydrometer analysis from which the particle size gradation curve of the subgrade material was plotted (Fig. 6).

3.3 Experiment

A series of constant head hydraulic conductivity tests were conducted in order to evaluate the hydraulic conductivity of the fresh ballast (parallel graded), fresh ballast fouled with subgrade material and ballast fouled with broken down particles. Rowe cell apparatus, having an internal diameter of 254.20 mm and a height of 127.60 mm was slightly modified to conduct the hydraulic conductivity tests (Fig. 7). Sample was filled inside the Rowe cell in layers and compacted by tapping the Rowe cell surface with a rubber mallet. The mass of the sample used was recorded and packing density was calculated. A constant head water flow was supplied to the Rowe cell through the lower part and the discharge was collected from the upper section of the Rowe cell. Two adjustable clips placed in the inlet tube and discharge tube were used to control the flow rate. The inlet total head and discharge total head were measured through the manometers connected near to the inlet and outlet.

After the manometers' readings have become constant, the input head, discharge head, discharge volume and time taken were recorded. Flow rate was varied to obtain the variation of flow rate with head difference from which the hydraulic conductivity was calculated.

The degree of fouling of ballast by the subgrade material was defined by the percentage of voids filled by the fouling agent. For this study, ballast with fouling percentages of 5, 10 and 15 were used.

Fig. 7 **a** Slightly modified Rowe cell, **b** hydraulic conductivity test setup

4 Results

Figures 8, 9, 10, 11, 12, 13 and 14 show the variation of flow rate with the hydraulic gradient for the fresh ballast and for the ballast degraded by particle breakage or subgrade intrusion.

In order to apply the Darcy's law, flow of water should be in laminar region. Therefore, the hydraulic conductivity was evaluated using the initial linear variation region that represents the laminar flow regime. Figure 15 shows the variation

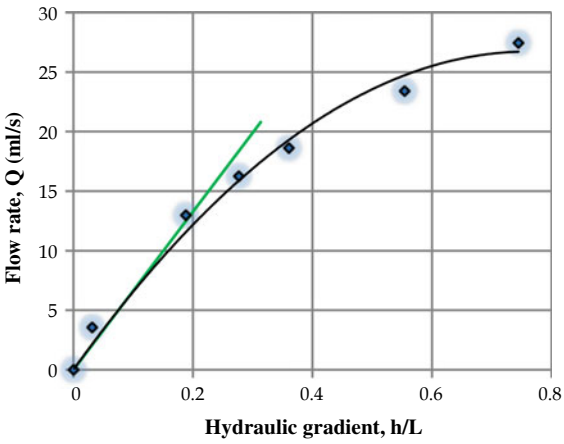

Fig. 8 Q versus h/L for the fresh ballast

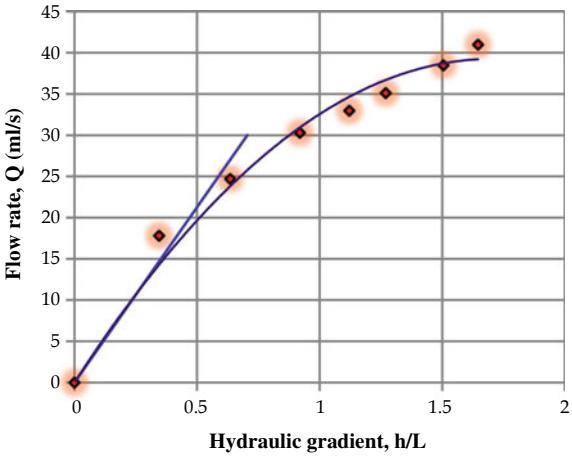

Fig. 9 Q versus h/L for the BI = 4.8 ballast

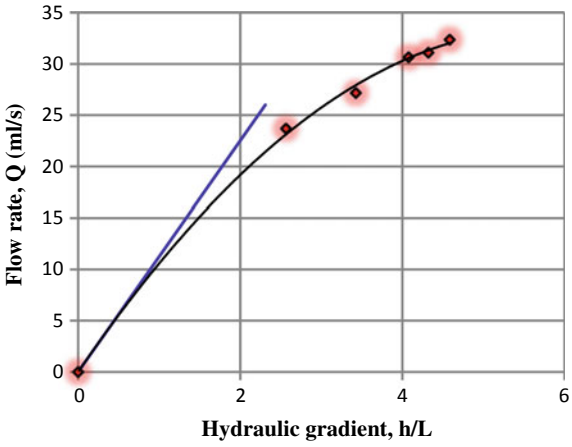

Fig. 10 Q versus h/L for the BI = 5.4 ballast

of hydraulic conductivity with breakage index and Fig. 16 shows the variation of hydraulic conductivity with fouling percentage of subgrade material.

They show a decrease in hydraulic conductivity with the increase in breakage index or fouling percentage of subgrade material. Figure 17 shows the effect of ballast breakage or subgrade fouling on the limiting value of hydraulic gradient for laminar flow regime. With the degree of fouling, it can also be shown that the laminar region increases with the increase in the degree of ballast contamination or subgrade fouling.

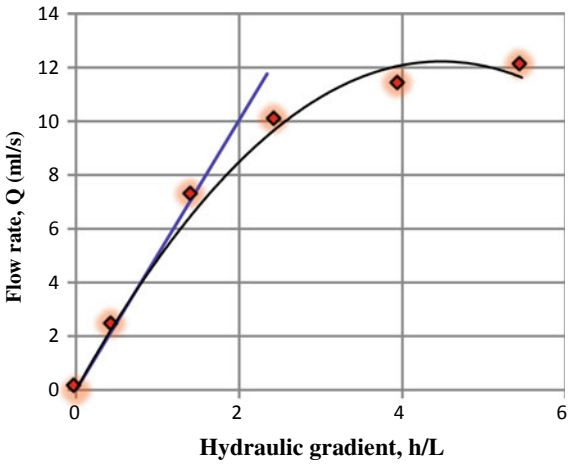

Fig. 11 Q versus h/L for the BI = 7.2 ballast

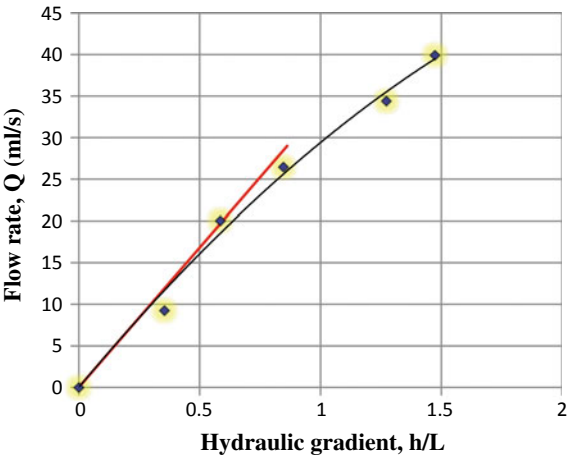

Fig. 12 Q versus h/L for the 5% fouled ballast

5 Discussion

The breakage of ballast causes to produce small size particles that will move into void spaces thereby diminishing the free flow of water through the ballast assemblage. This is associated with increased density due to increased well gradedness as compared with the fresh ballast assemblage which is uniformly graded. In reality, particle breakage results in track settlement. In case of subgrade intrusion into the ballast assemblage, although a track settlement cannot be anticipated, the clogging of void spaces within the fresh ballast assembly would take place thereby decreasing the hydraulic conductivity in both cases.

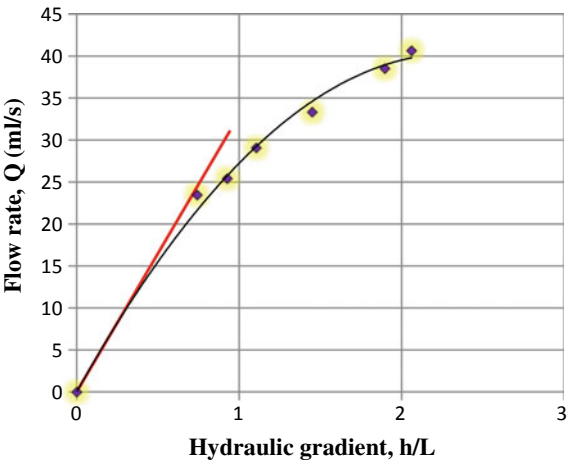

Fig. 13 Q versus h/L for the 10% fouled ballast

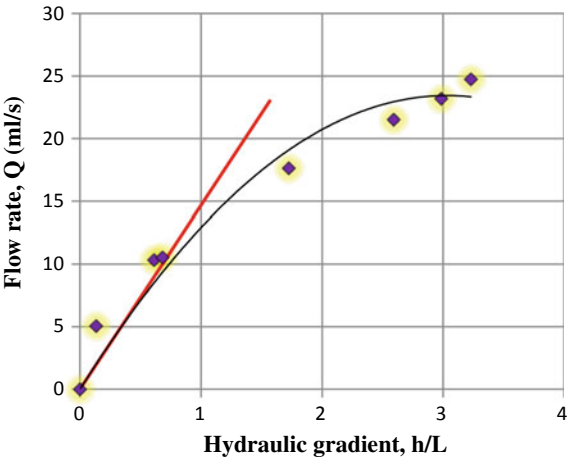

Fig. 14 Q versus h/L for the 15% fouled ballast

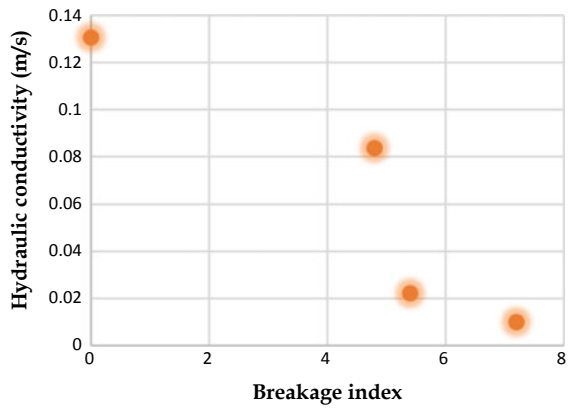

Fig. 15 Hydraulic conductivity versus breakage index

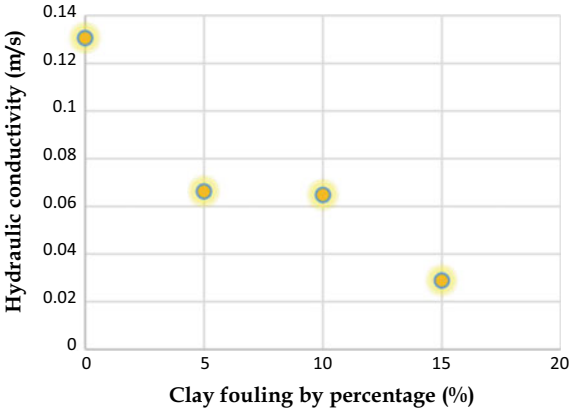

Fig. 16 Hydraulic conductivity versus fouling percentage

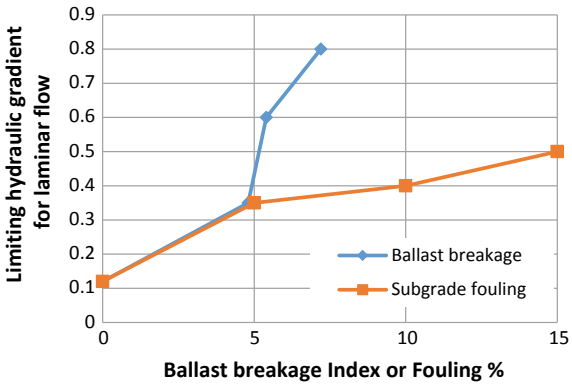

Fig. 17 Limiting hydraulic gradient for laminar flow

However, presence of such small sized particles cause the closing of the large voids in the particle assembly. This creates an increase in resistance to the flow thus causing the reduction in hydraulic conductivity. However, the flow would be more streamlined, thereby causing the limiting hydraulic gradient of laminar flow regime to increase under both ballast breakage and subgrade material intrusion.

6 Conclusion

From the study of the influence of ballast breakage or subgrade material pumping into the ballast particle assemblage, the following conclusions can be made.

1. The hydraulic conductivity decreases with the increase in either the ballast breakage index or the percentage fouling due to subgrade material intrusion.
2. The limiting hydraulic gradient of laminar flow regime increases under both ballast breakage and subgrade material intrusion.

References

1. Selig ET, Collingwood BI and Field SW (1988) Causes of fouling in track. Area bulletin 717
2. Tennakoon N, Indraratna B, Rujikiatkamjorn C, Nimbalkar S (2012) Assessment of ballast fouling and its implications on trackdrainage, 11th Australia - New Zealand Conference on Geomechanics: Ground Engineering in a Changing World, pp 421–426
3. Anbazhagan DP (2013) Characterization of rail track ballast fouling using ground penetration radar and field sampling
4. Shihana AM, Vasan V, Kurukulasuriya LC (2016) Shear strength characteristics of ballast subjected to particle breakage and mud pumping using parallel gradation technique. ICSBE 2016-Submission 173
5. Pakalavan V, Nirvekala B, Kurukulasuriya LC (2015) Shear strength characteristics of different gradations of ballast using parallel gradation technique. In: Proceedings, 6th international conference on sustainable built environment (ICSBE 2015)
6. Lowe J (1964) Shear strength of coarse embankment dam material. In: Proceedings, 8th congress on large dams, pp 745–761
7. Su Z, Huang H, Jing G (2015) Experimental analysis permeability characteristics of fouling railway ballast. Metallurgical and Mining Industry, Issue 9
8. Rahman AJ, Parsons R, Han J (2012) Properties of fouled railroad ballast (phase 1). Mid-America Transportation Center, Performing Organization Report No. 25-1121-0001-465
9. Selig ET, Waters JM (1994) Track geotechnology and substructure management. Thomas Telford Ltd., London
10. Jing G, Wang Z, Huang H, Wang Y (2015) Permeability and direct shear tests characteristics of railway subballast. Open Civ Eng J 9

Rapid Conversion of Domestic Organic Waste and Sewerage into Organic Fertiliser to Minimise the Hassle and the Cost of Organic Waste Handling and Sewerage Treatment in Condominiums, Tall and Green Buildings

S. A. S. Perera and M. F. H. M. Aadhil

Abstract Household Organic solid waste (HOSW) disposal is a hassle to the house holder and a high cost operation for the local authorities, where it has to be manually collected, transported in garbage trucks and disposed at solid waste dumps located a long distance away. At present, most dump sites have become Garbage Mountains, filled to the brim and at the verge of collapsing and submerging human habitats located in their vicinity, like the "Meethotamulla Municipal Solid Waste Dump Disaster". In condominiums and tall buildings, where a large number of people live in a small area, the problem is more sever, since a large number of houses are located and HOSW has to be carried manually in lifts or by climbing down large numbers of steps to the round level and dumped into garbage containers, which is collected once in 2–3 days by garbage collectors and disposed at dump sites. In Condominiums, design, construction and operation of sewerage treatment systems, mainly consisting of aerobic and anaerobic microbial digestion has a very high capital cost and a high operational cost. After treatment, the waste water should meet CEA approved parameter values for disposal to the city sewerage system. The paper discusses and provides results of a research project carried out by the author, where HOSW and sewerage were converted into low cost, germ free, odourless, organic fertiliser containing high C, H, O, N, P, K, Ca, Mg by using Delta-D Technology, as a solution to the problems described above. Delta-D Technology is a patented technology developed by the author to rapidly convert all types of organic waste into organic fertiliser.

Keywords Solid waste · Waste in high-rise · Organic waste

S. A. S. Perera (✉) · M. F. H. M. Aadhil
Department of Chemical and Process Engineering, University of Moratuwa, Moratuwa, Sri Lanka
e-mail: anulperera@yahoo.com

R. Dissanayake et al. (eds.), *ICSECM 2019*, Lecture Notes in Civil Engineering 94,
https://doi.org/10.1007/978-981-15-7222-7_14

1 Introduction

In the past decade the Sri Lankan real estate market and infrastructure growth has been at record highs due to the post war investor confidence. The rapid urbanization and growth in densely populated spaces closer to the city has resulted in various implications in terms of waste management, logistics related to waste, transportation pollution etc. Currently, there are over 900 apartment complexes in the country having over 15,000 residential units while another 300 condominium projects are in pipeline with over 17,000 residential units [17]. They are expected to be completed within the next three-four year. Among that approximately 90% of condominiums are located within Colombo and its suburbs exerting a positive impact on the Sri Lankan economic outlook. However, the sustainability of these projects have been challenged due to the volume of domestic organic waste and sewerage generated on a daily basis from these domiciles.

2 Research Problem

At a national level only 20% of households relied on local authorities for solid waste disposal. Over 40% burnt their own solid waste and 7–8% resorted to composting their organic solid waste. However the viable options for high-rise buildings and condominiums seem to be to rely on local authorities. However on average condominium homes produce 0.7 kg of wet organic waste per person per day. If this waste can be converted into a valuable fertilizer, this will result in benefits in multiple ways [18].

3 Methodology

3.1 Sample Collection

Organic waste samples were collected from several condominium properties in the western province and mixed as the sample considered in the study. The waste contained primarily food wastes such as cooked rice, meat, vegetables etc. Additionally peels of fruits and vegetables, waste of meat and fish, egg shells, waste tea leaves could be observed.

Dried, mixed sewerage sludge was obtained from a domestic property with the help of the Dehiwala-Mount Lavinia Municipal council.

3.2 Sample Preparation and Experimentation

Perera [14, 16] noted that, the Delta-D Technology is a patented process, by which, plant wastes [7–10], such as, leaves, saw dust, tea waste, straw, paddy husk, salvinia, weeds, fruit peels [7–10], seeds and animal wastes [12, 13], such as, offal, feathers, bones, skin, (in other words any type of organic waste) etc., can be converted into organic fertilizer, with a high content of Nitrogen (N), Phosphorous (P) and Potassium (K), within 1–2 days.

Domestic organic waste and sewerage sludge was analysed to determine the presence of nutrients that are useful for plant growth and soil preparation. The analysis was expanded to determine toxic or components that should not enter the food chain. The components analysed were, total Nitrogen (N), Phosphorous (P), Potassium (K). Additionally, Organic Carbon (C), Sodium (Na), Magnesium (Mg), Lead (Pb), Nickel (Ni), Copper (Cu), Iron (Fe), Chromium (Cr), Zinc (Zn), Mercury (Hg) Cadmium (Cd) and Arsenic (As). The results of which is presented in Table 1.

1 L of Delta-D solution was diluted with water to 1:1 ratio and added to 15 kg of mixed organic waste consisting of cooked food waste, fruits and vegetable peels and waste, fish and meat waste, processed organic food waste and other biodegradable forms of domestic organic waste sample. The slurry was then stirred using a wooden pole to ensure even distribution of the Delta-D solution [14, 16].

The sewerage sludge was mixed with saw dust at 1:1 ratio to form a 20 kg mixture. 2.5 L of Delta-D solution was added to the mixture and let to rest for 48 h. After two days due to the low Phosphorous (P) content in the original sewerage sludge 3 kg of Eppawala Rock Phosphate (ERP) was added since the content of P_2O_5 in ERP ranges between 12 and 42% and is indefinite. Two days later 4 kg of Dolomite was added and the mixture was left closed for 5 days to obtain a nutrient rich fertilizer with lesser moisture content.

Table 1 Testing standards used for microbial testing

Parameter	Test method
Total coliform	ISO 4831: 2006/SLS 516 Part 3 Section 1: 2013
Fecal coliforms	ISO 7251: 2005/SLS 516 Part 12 Section 1: 2013
Escherichia coli	ISO 7251: 2005/SLS 516 Part 12 Section 1: 2013
Salmonella spp.	ISO 6579: 2002/Amd 1: 2007, SLS 516 Part 5: 2013

3.3 Characteristics and Toxicity of the Fertilizer

The final samples were analysed for the above nutrients and adulterant parameters to determine the quality of the fertiliser using Inductive coupled plasma-optical emission spectroscopy (ICP-OES). The fertiliser was applied on plants to evaluate the plant growth aspects such as the height increase of the shoot, branching, increase in number of leaves, leaf size and leaf density. An acute toxicology test as per the test guideline number 203 by the Organisation for Economic Co-operation and Development was carried out to determine the acute toxicity of the leachate produce from the fertiliser [4].

14 samples of approximately 3 g each of fertiliser was mixed in one of the tanks over 14 days increasing the concentration of nutrients in the water. The dissolution of over 50 g in 20 L of water has to be validated prior to the toxicology experiment to ensure the components dissolved or remain as a suspension in the fish tank. The experiment was triplicated.

3.4 Determination of Pathogenic Nature of the Produced Fertiliser

The total coliform of the produced fertilizer was analyzed as the raw material sludge was detected with coliform. Further fecal coliforms, *Escherichia coli* and *Salmonella* spp. was analyzed. The following standards were used for each of the parameters as given in Table 1.

4 Results and Discussion

4.1 Characterization of the Produced Fertiliser

The produced fertilizer is of indefinite composition and an ultimate analysis need not be undertaken. The nutrients, micro nutrients and heavy metals of concern were analysed. The analysis report is presented in Table 2.

The ultimate analysis of the fertilizer produced using sewerage sludge is given by Table 3.

The allowable maximum levels of harmful components are listed in Table 4 as per the National fertilizer secretariat [1].

As disclosed by the analysis of the components of the fertilizer the produced fertilizer is accepted within the guidelines of fertilizers. Given the high carbon content, the fertilizer can be categorized as an organic fertilizer. However, it has to be understood that the waste composition may vary with changes in lifestyle and many other factors.

Table 2 Nutrient and heavy metal constituent composition of the fertilizer produced using organic waste

No.	Parameter	Result	LOQ	Unit	Test method
1	Total Nitrogen (N)	0.43	–	% by mass	SLS 645: Part 1: Section C: 2009
2	Phosphorous (P)	1.3	–	% by mass	SLS 645: Part 5:1985
3	Potassium (K)	37	–	mg/kg	EPA3051 A with ICP-OES
4	Organic Carbon (C)	17.8	–	% by mass	SLS 1246: Appendix D:2003
5	Sodium (Na)	0.4	–	g/kg	EPA3051 A with ICP-OES
6	Magnesium (Mg)	1.1	–	g/kg	EPA3051 A with ICP-OES
7	Lead (Pb)	ND	0.04	mg/kg	EPA3051 A with ICP-OES
8	Nickel (Ni)	ND	0.04	mg/kg	EPA3051 A with ICP-OES
9	Copper (Cu)	16	–	mg/kg	EPA3051 A with ICP-OES
10	Iron (Fe)	0.1	–	g/kg	EPA3051 A with ICP-OES
11	Chromium (Cr)	ND	–	mg/kg	EPA3051 A with ICP-OES
12	Cadmium (Cd)	ND	0.04	mg/kg	EPA3051 A with ICP-OES
13	Zinc (Zn)	7	–	mg/kg	EPA3051 A with ICP-OES
14	Arsenic (As)	ND	0.04	mg/kg	EPA3051 A with ICP-OES
15	Mercury (Hg)	ND	0.04	mg/kg	EPA3051 A with ICP-OES

Note mg/kg: milligrams per kilogram, ND: not detected, g/kg: grams per kilogram, LOQ: limit of quantification, ICP-OES: inductive coupled plasma-optical emission spectroscopy, EPA: environmental protection agency

Therefore, these values have to be understood to ensure that no harmful components are added and plant nutrients and soil fertilizing ingredients are rich.

4.2 Plant Growth and Suitability

The plant agronomy aspects of application of the produce fertilizer was studied in comparison with 5 samples supplied with either of the fertilizer, one sample without any fertilizer, one sample with regular compost fertilizer brought from plant shops and one sample supplied with albert's solution synthetic fertilizer.

Sample 1—Delta-D fertilizer produced from kitchen waste;
Sample 2—Regular compost Fertilizer;
Sample 3—Synthetic Fertilizer;
Sample 4—No fertilizer;
Sample 5—Delta-D fertilizer produced from sewerage sludge (Figs. 1 and 2).

When examining the agronomy of various plant species the knowledge regarding factors affecting its growth is paramount. It is important for the plant roots to have

Table 3 Nutrient and heavy metal constituent composition of the fertilizer produced using sewerage sludge

No.	Parameter	Result	LOQ	Unit	Test method
1	Total Nitrogen (N)	2.09	–	% by mass	SLS 645: Part 1: Section C: 2009
2	Phosphorous (P)	2.1	–	% by mass	SLS 645: Part 5:1985
3	Potassium (K)	30	–	mg/kg	EPA3051 A with ICP-OES
4	Organic Carbon (C)	19.2%	–	% by mass	SLS 1246: Appendix D:2003
5	Sodium (Na)	0.67	–	g/kg	EPA3051 A with ICP-OES
6	Magnesium (Mg)	7.1	–	g/kg	EPA3051 A with ICP-OES
7	Lead (Pb)	ND	0.04	mg/kg	EPA3051 A with ICP-OES
8	Nickel (Ni)	ND	0.04	mg/kg	EPA3051 A with ICP-OES
9	Copper (Cu)	11	–	mg/kg	EPA3051 A with ICP-OES
10	Iron (Fe)	0.3	–	g/kg	EPA3051 A with ICP-OES
11	Chromium (Cr)	ND	–	mg/kg	EPA3051 A with ICP-OES
12	Cadmium (Cd)	ND	0.04	mg/kg	EPA3051 A with ICP-OES
13	Zinc (Zn)	6	–	mg/kg	EPA3051 A with ICP-OES
14	Arsenic (As)	ND	0.04	mg/kg	EPA3051 A with ICP-OES
15	Mercury (Hg)	ND	0.04	mg/kg	EPA3051 A with ICP-OES

Table 4 Maximum allowable levels of harmful components

No.	Parameter	Maximum concentration (mg/kg)
1	Lead (Pb)	30
2	Chromium (Cr)	50
3	Cadmium (Cd)	3
4	Arsenic (As)	50
5	Mercury (Hg)	1

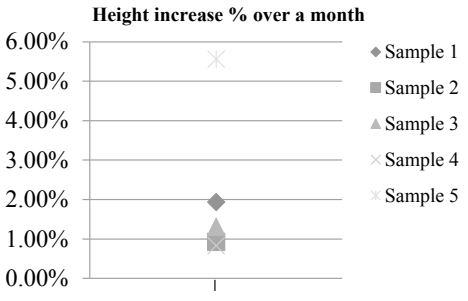

Fig. 1 Net increase % over a month

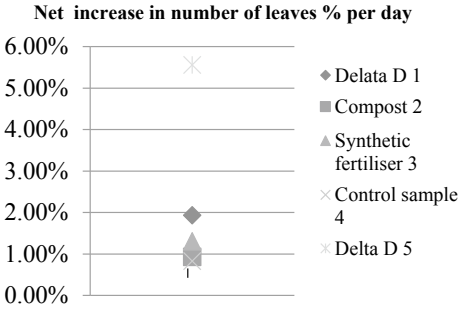

Fig. 2 Net increase in number of leaves % over a month

access to adequate amounts of nutrients in a balanced ratio. However the nutrient requirement is dependent on many factors. It was observed that the samples supplied with fertilizer produced using the Delta-D technology had a greater growth rate than comparative samples as seen in Figs. 1 and 2. The reason for this may be due to the higher nutrient uptake as a result of the Delta-D digestion process [15].

An important parameter in the characterization of a fertilizer, is the Nitrogen to Phosphorous to Potassium ratio. In the used sample the ratio was 23:70:1. Therefore this product is a high Phosphorous fertilizer and is more suitable for crops with high phosphorous demand. The value can be adjusted by limiting the addition of the Eppawala rock phosphate and achieve the standard recommended N:P:K ratio of 2:1:3. Phosphorous is involved with energy transfer, maintenance and has direct effect on tree health and yield in fruiting plants. Legumes also require high amounts of available phosphorous in soil [14, 16].

Figures 3 and 4 display the growth comparison of the produced fertilizer when compared with other fertilizers applied to the same species of plants of same origin and ages.

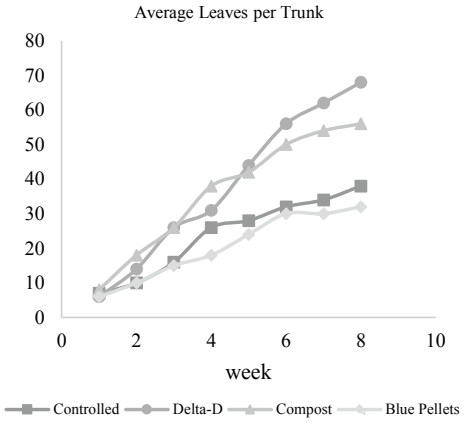

Fig. 3 Average leaves count per trunk

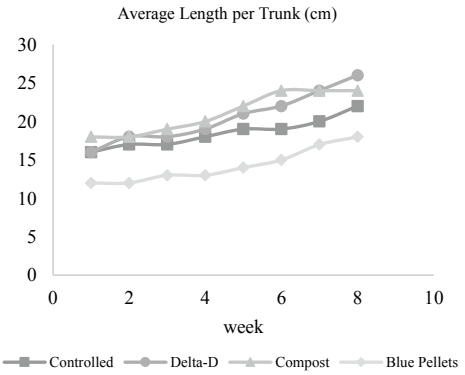

Fig. 4 Average length per trunk

4.3 Acute Aquatic Toxicology Test Results

The tanks were inhabited with 3 species of freshwater fish with 5 each of each of two species and 4 from the remaining. None of the species died during the experiment (Table 5). Therefore it could be determined that the acute toxicity of the fertilizer is none harmful for freshwater fish as deduced by the results based on the Organisation for Economic Cooperation and Development (OECD) test no. 203 [2].

Table 5 Results of fish tank test

Test day/observation	1	2	3	4	5	6	7	8	9
Approx. time from start of test (h)	12	36	60	84	108	132	156	180	204
No of live fish in tank for scoring	14	14	14	14	14	14	14	14	14
No of morbid fish removed after scoring	–	–	–	–	–	–	–	–	–
No. dead removed	–	–	–	–	–	–	–	–	–
Abnormal horizontal orientation	–	–	–	–	–	–	–	–	–
Abnormal vertical orientation	–	–	–	–	–	–	–	–	–
Loss of buoyancy control	–	–	–	–	–	–	–	–	–
Hypoactivity	–	–	–	–	–	–	–	–	–
Hyperactivity	–	–	–	–	–	–	–	–	–
Irritated skin behaviour	–	–	–	–	–	–	–	–	–
Hyperventilation	–	–	–	–	–	–	–	–	–
Hypoventilation	–	–	–	–	–	–	–	–	–
Skin pigmentation	–	–	–	–	–	–	–	–	–
Faecal casts (anal)	–	–	–	–	–	–	–	–	–
Mucus secretion	–	–	–	–	–	–	1	1	–

Table 6 Microbial test results

Parameter	Result of sludge and waste mixture	Result of fertilizer	Unit
Total coliform	550	ND	MPN/g
Fecal coliforms	440	ND	MPN/g
Escherichia coli	10	ND	MPN/g
Salmonella spp.	Absent	Absent	In 25 g

4.4 Microbial Count of the Two Produced Fertilizer Samples as a Mixed Sample

The pathogenic nature of the feed sludge and the produced fertilizer were compared by carrying out microbial tests on the feed sludge and the produced fertilizer according to the standards mentioned in the methodology Table 1. The comparison revealed that although the feedstock contained high microbial counts the final product was free from any form of microbes. Table 6 contains the results.

The Delta-D process inhibits all pathogenic microbes and results in the fertilizer being pathogen free. When the fertilizer is applied to the earth, microbial digestion takes place from microorganisms in the earth further digesting any large molecules present in the fertilizer and break it down to smaller fractions to be able to be absorbed into the plants.

5 Conclusions and Recommendations

- Delta-D Technology is a low cost, sustainable solution [7–11] for conversion of household organic waste (OW) and human sewerage (HS) into pathogen free organic fertilizer (OF) that could be used for agriculture [5].
- ICP-OES results indicate that the heavy metal contents and other harmful elements are within the accepted range for fertilizers.
- Results of agricultural experiments carried out, show that OF produced from OW using Delta-D technology has a positive impact on yield [5].
- Results of Fish Tank Tests, show that the acute toxicology of the fertilizer does not harm aquatic life therefore the leachate produced from the application of the fertilizer is non-threatening to aquatic and marine environments [11, 15].
- It can be done in each house, so that, there is no need for collection and transport of perishable OW for disposal at main solid waste dumps or sanitary landfills which is becoming challenging specially in tall buildings with large number of domicile units in one space.
- Tall buildings and condominiums, with a large number of houses and a very large human population, generate large amounts of organic waste (OW), of which,

collection and disposal is a challenging task. If each household uses Delta-D Technology to convert OW into OF, the burden can be reduced.

- At the planning and design stage, each condominium and tall building can plan for a Delta-D Based Organic Fertiliser Production Plant, which rapidly converts all the OW produced into OF, which can be sold at a price to residents for domestic agriculture, as well as, used in lawns, gardens and parks within each complex.
- In many countries in the world, human sewerage is directly used as organic fertilizer, in small scale and large scale agriculture. One main problem associated with this method is that pathogens are not destroyed and could spread disease to plants, animals and humans.
- Each Condominium and Tall Building, at its design and planning stage, has to accommodate an extremely complicated and expensive sewerage treatment systems, which needs large extents of land as well. Moreover, in many cases, such systems discharge waste into the ocean. This causes pollution of marine eco-system as well. If a Delta-D Based Sewerage to OF plant is accommodated, then, it becomes a low cost, sustainable solution, which nutrients used as fertilizer in agriculture is recycled back as OF.
- The direct application of sewerage fertilizer is practiced in many parts of the world and can have negative impacts such as eutrophication and algal bloom in fresh water sources resulting in negative impacts to aquatic eco-systems [3]. By stopping direct disposal of sewerage to aquatic environments, harmful impacts of which can be stopped and the nutrients can be used in agriculture by means of converting to a valuable fertilizer.

References

1. National Fertilizer Secretariat (2017) https://www.nfssrilanka.org/fertilizer-guideline. [Online] Available at: https://www.nfssrilanka.org. Accessed 2017.
2. OECD (2019) Test no. 203: fish, acute toxicity test, OECD guidelines for the testing of chemicals, section 2, OECD Publishing, Paris
3. Ongley ED (1996) Fertilizers as water pollutants. In: Control of water pollution from agriculture—FAO irrigation and drainage. Food and Agriculture Organization of the United Nations, Rome, p 55
4. Organisation for Economic Co-operation and Development (2017) Test guideline No 203: fish, acute toxicity testing. s.l.:OECD.org
5. Perera S (2001) Is anaerobic digestion of market garbage to produce biogas technically and economically feasible. Engineering Research Unit, University of Moratuwa, Moratuwa
6. Perera S (2002) Influence of organic fertiliser fortified with Eppawela rock phosphate on the cultivation of spinach. In: Proceedings of the international seminar on the engineer in sustainable, social and economic development—regional contribution towards agenda 21, organised by The Institution of Engineers Sri Lanka (IESL), Colombo, World Federation of Engineering Organisations
7. Perera S (2007) Delta-D initiated microorganic digestion of saw dust into organic fertiliser—a technically, economically and environmentally feasible solution to the saw dust problem in Sri Lanka. Journal of The Institution of Engineers, Colombo, Sri Lanka

8. Perera S (2007) Delta-D technology, a technically, economically and environmentally feasible solution to the urban solid waste (USW) problem and the fertiliser problem in Sri Lanka. Annual Transactions of IESL, Colombo
9. Perera S (2007) Manufacture of organic fertiliser from vegetable market garbage (VMG) using Eppawela rock phosphate and its' effects on rice cultivation. In: The proceedings of the 22nd international conference on solid waste technology and management, Philadelphia
10. Perera S (2007) Patented process for rapid digestion of all types of biomass into organic fertiliser, a solution to the urban solid waste (USW) and to the fertiliser problem in Sri Lanka. In: The proceedings of the of the 22nd international conference on solid waste technology and management, Philadelphia
11. Perera S (2008) Delta-D technology—a patented technology that could be used to prevent emission of green house gases from urban solid waste, agricultural waste and farm waste. UNESCO and the Punjab State Council, Chandigarh
12. Perera S (2009) Conversion of coconut water waste produced in desiccated coconut mills into liquid organic fertiliser using Delta-D technology. In: The proceedings of the 24th international conference on solid waste technology and management, Philadelphia
13. Perera S (2009) Manufacture of organic fertiliser from poultry slaughterhouse waste rendering plant sludge using Delta-D technology. In: 24th International conference on solid waste technology and management, Philadelphia
14. Perera S (2012) Delta-D technology—a green solution to unsorted urban solid waste (USW) disposal problems in Sri Lanka. In: International conference on sustainable built environment, Kandy
15. Perera S, Aadhil M (2017) Environmental impacts of organic fertilizer produced from industrial zone central effluent treatment plant sludge using the Delta-D technology. In: The proceedings of the 111th annual session of the Institute of Engineers, Colombo, Sri Lanka
16. Perera SAS (2012) Delta D technology—a patented process for rapid digestion of all types of organic wastes into organic fertiliser in 1 day, an ideal solution to the urban solid waste problem and the fertiliser problem in Sri Lanka. In: Delta-D technology, p 3
17. Prathapasinghe D, Perera M, Ariyawansa R (2018) Evolution of condominium market in Sri Lanka: a review and predict. In: 2nd international conference on real estate management and valuation 2018, Colombo
18. Waidyasekara W, Jayamal K (2008) Opinion study on garbage disposal system for condominiums using quality function deployment. In: CIB International conference on building education and research, Kandalama

Investigation of Functionality of Landfill Liner Systems Under Wet Zone Climatic Conditions in Sri Lanka

H. M. W. A. P. Premarathne and L. C. Kurukulasuriya

Abstract Engineered land filling is one of the most environmentally friendly methods to dispose municipal solid waste. Bottom liner and top capping are two basic elements of engineered landfill. Bottom liner is expected to prevent contamination of the adjacent environment by leachate. In this study, the performance of two types of clay liners is examined under wet zone climatic conditions in field scale lysimeters. Two 1.5 m diameter and 5 m high lysimeters were constructed to represent an engineered landfill with emphasis to monitor the performance of the liner material placed. In one lysimeter, a 1 m thick liner was placed at maximum dry density using an expansive soil obtained from Moragahakanda area in the central province of Sri Lanka and in the other lysimeter, the liner thickness was reduced to 0.6 m but with the addition of 5% bentonite by weight of the expansive soil. The lysimeters were instrumented to monitor the leachate head generated above the liner and the head developed in the leachate leakage detection pipe. The period of monitoring was extended to include both dry and wet seasons. Based on the monitoring data and using the laboratory measured values performance of the two types of liners were investigated. Geo Slope SEEP/W model was developed to investigate the seepage through both liner types. Based on the actual rainfall values numerical analysis was done to predict the leaked leachate volume through the liner. Those results obtained from numerical analysis were compared with the actual field scale data. The clay liner with 5% bentonite is three times effective in reducing leachate flow rate through the liner when compared with that of control lysimeter. The numerical analysis showed that an increase in liner thickness will reduce the rate of seepage through the liner reaching a limiting value.

Keywords Municipal solid waste · Landfill · Lysimeter · Bottom liner

H. M. W. A. P. Premarathne (✉) · L. C. Kurukulasuriya
Department of Civil Engineering, University of Peradeniya, Peradeniya, Sri Lanka
e-mail: wapiumika@gmail.coma

R. Dissanayake et al. (eds.), *ICSECM 2019*, Lecture Notes in Civil Engineering 94,
https://doi.org/10.1007/978-981-15-7222-7_15

1 Introduction

Municipal Solid Waste (MSW) is the waste generated from the domestic, commercial and construction activities by human and which is collected and treated by municipalities. Increasingly affluent lifestyles, continuing industrial and commercial growth in many countries around the world in the past decade has been accompanied by rapid increases in both the municipal and industrial solid waste production. The huge amount of MSW generation is not only an environmental threat but also a health risk for all living beings. Therefore, proper management of MSW is needed to be implemented. MSW management practices employed in the different countries so far are landfilling, incineration, composting, recycling or recovery from waste. In both developed and developing countries, landfills are used as the main disposal method of MSW. In Sri Lanka also, priority is being given to dispose the solid waste in an environmentally friendly manner but still engineered landfills are not being used for the disposal of solid waste. Only recycling, reusing and composting are being practiced in a small scale.

Central Environmental Authority (CEA) of Sri Lanka has published technical guideline for the design of landfill facilities [1]. As per the CEA technical guideline, landfill liner constructed using clay should be 100 cm of minimum liner thickness having maximum hydraulic conductivity of 1×10^{-7} cm/s. The maximum leachate head that can exist above the clay liner is 30 cm. If the clay liner is constructed using soil-bentonite mixture (more than 5% bentonite), the maximum allowable hydraulic conductivity is 5×10^{-10} cm/s and the liner thickness should be greater than 60 cm. Very less amount of work has been reported on the suitability of locally available expansive soil for the construction of liners. Expansive clay deposits occur in the arid and semi-arid regions of Sri Lanka. Sri Lanka has been divided in to three clay mineral zones depending on the major clay mineral in each zone, namely wet zone clay mineral province, dry zone clay mineral province and intermediate zone clay mineral province [2]. It has been revealed that dry zone clay mineral province mainly consists of kaolinite-montmorillonite clays while intermediate clay mineral province consists of kolinite with low proportions of gibbsite and montmorillonite. Hydraulic conductivity of a clay liner depends on the properties of clay as well as properties of pore fluid. Usually soils with high clay content which contain kaolinite clay minerals are used for the construction of compacted clay liners. When the clay content is not sufficient to achieve required level of hydraulic conductivity, soil is mixed with different admixtures such as bentonite.

Wanigarathna [6] has studied four types of local soil combinations to find the best material for the liner through a laboratory study. Wanigarathna [6] used soil from Moragahakanda area (Soil M), Soil M amended by 5% bentonite and soil M amended by 10% bentonite. During this research, soil classification tests, consolidation tests and hydraulic conductivity tests were carried out for these soil combinations. Accordingly, Moragahakanda soil was classified as Sandy Clay of Intermediate Plasticity (CIS). Research has concluded that Moragahakanda soil amended by 5% bentonite

Table 1 Soil properties of Moragahakanda soil and those amended by bentonite (after Wanigarathna [6])

Test	Soil M	Soil M + 5%	Soil M + 10%
Liquid limit (%)	44	49	70
Plastic limit (%)	19	21	25
Plasticity index (%)	25	28	45
Specific gravity	2.640	2.46	2.28
Swell pressure (kPa)	126.1	267.7	357.0
pH	8.06	8.20	8.34
EC (ms/cm)	0.027	0.161	0.322

was the most economical and technically viable option for the liner. Soil properties of the Moragahakanda soil and those amended by bentonite are given in Table 1.

Raziful et al. [3] has carried out a research on lysimeter study in Bangladesh to investigate the performance of both the base and cap liners. In this research, for protection of leaching, both the cap and base liners made from compacted clay liner (CCL) were used in landfill lysimeter. One aerobic lysimeter and two anaerobic type of lysimeters were used in this study. This study reveals that rapid leachate production occurred in the aerobic cell of lysimeter-A than that of the other two anaerobic lysimeters-B and C which indicates the importance of the barrier layer of CCL and the cover materials selection in landfill design. It is interesting to note that anaerobic lysimeter with an extra CCL shows the lowest settlement than that of aerobic lysimeters indicating the importance of the compaction density as well as the cap and base liners in solid waste landfill.

There is a research gap in developing landfill liner systems utilizing locally available materials in developing countries which brings economic benefits for those countries. Objectives of this research are to evaluate the use of locally available material as a liner material for solid waste landfills and to develop a numerical model to estimate an economically viable thickness of the liner to be used that will minimise the leachate flow rate when using the locally available material.

2 Methodology

Two lysimeters were constructed at Gampola, Sri Lanka (7° 8′ 33.62″ N, 80° 34′ 42.69″ E) in a field scale study site. Performance of two liners made out of two local materials was investigated in this research. Functionality of these locally available liner materials is to be assessed through the proper characterization of material and MSW as well as the generated and leached volume of leachate from lysimeters.

Lysimeters used in this study were cylindrical concrete tanks with the dimension of 1.5 m in diameter and 5 m in height. In one lysimeter 100 cm thick compacted clay liner prepared according to CEA guidelines was placed using Moragahakanda soil which was identified as the control lysimeter. In the second lysimeter, 60 cm thick liner was placed using Moragahakanda soil amended by 5% bentonite which was identified as the experimental lysimeter. Schematic diagram of the control and experimental lysimeters are shown in Fig. 1. Lysimeters were made out of reinforced concrete to avoid contamination of the surrounding environment, similar to a study done by Rafizul et al. [4]. At the bottom, 125 mm thick concrete layer was placed as an impermeable layer, so that the leachate leaking through the liner is diverted to the leakage collection pipe. On top of that layer, 50 mm internal diameter perforated PVC pipe network was placed as the bottom drainage layer. This pipe was covered with a geotextile to reduce rapid clogging by the sediments of the waste. This pipe was located in an aggregate layer having d_{50} between 6 and 10 mm. Bottom drainage pipe was connected to a vertically fixed 110 mm diameter PVC pipe, which acts as a leachate detection pipe (Fig. 1). The liner was placed on top of the bottom drainage layer. Thickness and the composition of the liners were

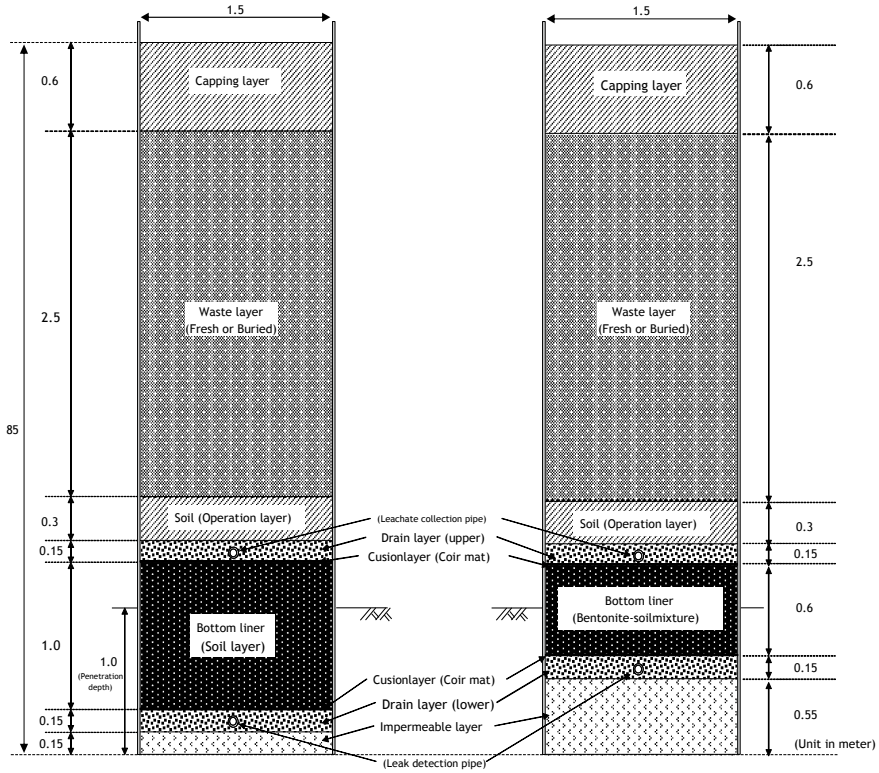

Fig. 1 Schematic diagram of the lysimeter

different between two lysimeters. The liner of the control lysimeter was prepared using Moragahakanda soil compacted to 100% maximum dry density (1.52 g/cm^3 at 19.3% moisture content). The experimental liner was prepared using Moragahakanda soil amended by 5% bentonite compacted to 1.45 g/cm^3 at 15.9% optimum moisture content.

Leachate collection pipe network was laid on top of the both liners. This network also consisted of 50 mm PVC pipe network covered with geo textile layer. This pipe network was within an aggregate layer of 150 mm thickness with d_{50} between 6 and 10 mm. This leachate collection pipes were connected to a leachate collection tank. A sand layer of 30 cm in height was placed above the upper drainage layer as an operation layer. Locally available river sand was used for this purpose.

Waste layer was then placed on the operation layer. Fresh organic waste was placed for a height of 2.5 m. Waste was obtained from Gampola Urban Council. Solid waste composition in Sri Lanka consists of 62% biodegradable waste, 6.5% paper, 6% polythene and plastic, 6% of wood and 2% glass [7]. It reveals that the Sri Lankan municipal solid waste consists of a large proportion of compostable materials. Biodegradable waste which is packed in the lysimeters had moisture content of 68% at the fresh state.

Waste was compacted layer wise having the control of compaction energy (kJ/m^3) using a hand tamper for compacting each layer. The hand tamper consisted of a concrete cylinder of 30 cm diameter with a weight of 10 kg. For each layer, number of tamping was counted to have uniform packing of each layer. A 110 mm perforated PVC pipe was placed while the waste was being compacted above the top drainage layer to facilitate monitoring of the leachate level above the liner.

Finally, a capping layer was placed on top of the waste layer which had a height of 60 cm and consisted of local soil. Typically, reddish brown latosolic and red yellow podosolic soils were used for the capping layer.

2.1 Instrumentation

Diver sensors were installed in perched water detection pipes to detect the height of the perched water column layer inside the waste. Divers establish the height of a water column by measuring the water pressure using the built-in pressure sensor and also the temperature within the waste. Mini Divers manufactured by Van Essen Instruments were installed in the lysimeters.

Table 2 Monthly rainfall of the study area

Month	Number of rainy days	Rainfall (mm)
December 2015	19	296.3
January 2016	2	12.3
February 2016	3	5.0
March 2016	7	112.4
April 2016	8	73.7
May 2016	27	738.7

2.2 Numerical Analysis of Seepage Through Lysimeters

Numerical analysis for the field scale lysimeter units were carried out using the GeoStudio 2007 (SEEP/W) software. The purpose of the numerical analysis of this was to compare the leaked leachate volume through the liner between the field scale and at SEEP/W models.

3 Results and Discussion

Construction, operation and monitoring of landfill lysimeters were carried out from June, 2015 to June 2016. Diver sensor data, water head over the liner and rainfall data were used to evaluate the liner performance.

3.1 Rainfall Data of the Study Area

Daily rainfall data for the study area was obtained from the weather station at Peradeniya which was operated by Department of Agriculture. Table 2 shows the monthly rainfall in the study area during the period of study. Rainfall was almost constant throughout the period except in May 2016 which experienced an enormous increase of rainfall.

3.2 Water Head Development Above the Liner at Lysimeters

The temperature within the waste was initially varying around 30 °C and towards the latter part of the study period it showed a reduction in temperature. Since the ambient temperature in Gampola area is around 25–27 °C, elevated temperature at initial stages is an indication of anaerobic digestion of fresh waste within the lysimeter. Control lysimeter had developed a water head up to a level of 10–12 cm

above the liner as shown in Fig. 2. Figure 3 shows the water head and temperature in the experimental lysimeter. Temperature variation is similar in both lysimeters. It can be seen that the water head above the liner had followed the same variation as that in the control lysimeter which in turn was similar to that of rainfall variation.

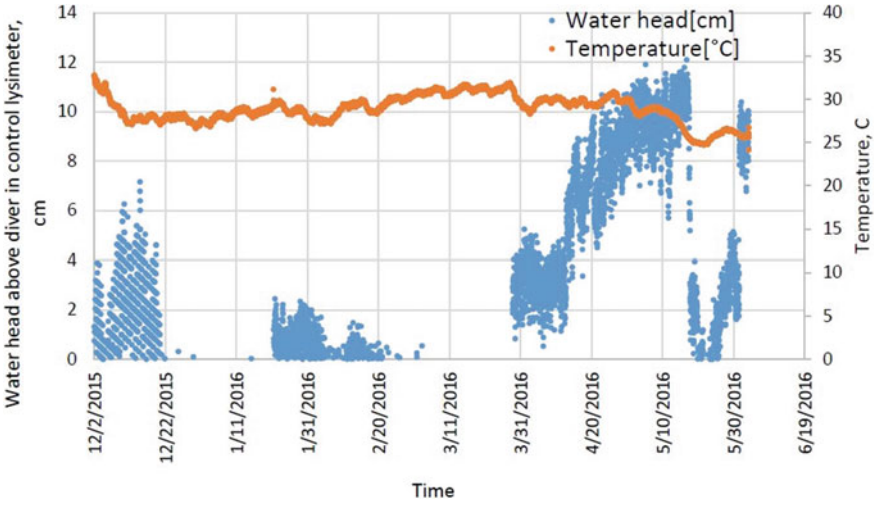

Fig. 2 Variation of water head development and temperature in control lysimeter

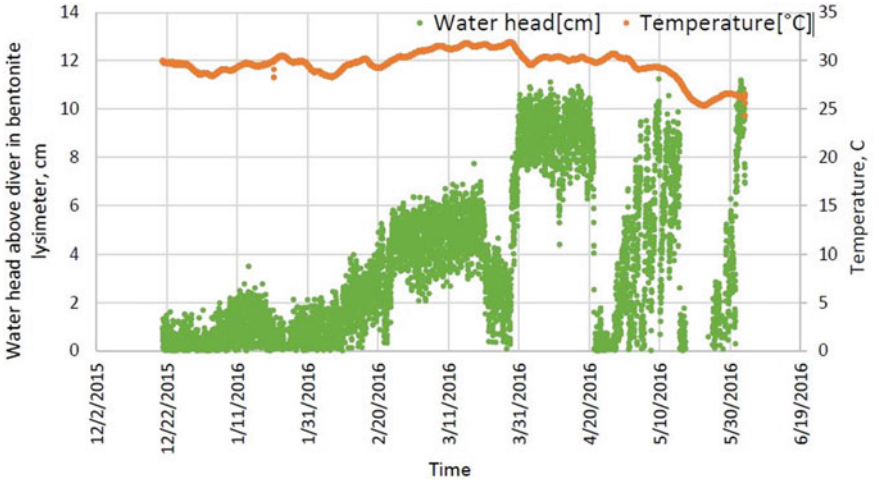

Fig. 3 Variation of water head and temperature in bentonite lysimeter

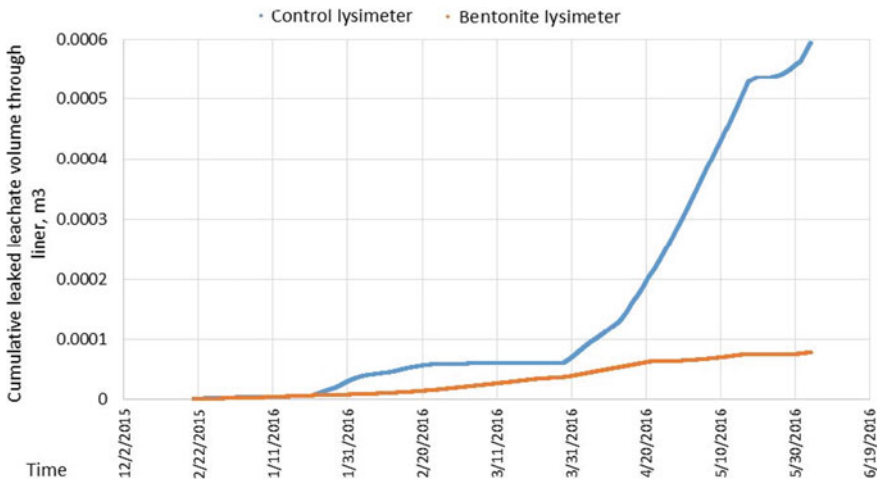

Fig. 4 Cumulative leaked leachate volume through liners in control and bentonite lysimeters

3.3 Leachate Leakage Through the Liner

Leachate flow through liners was calculated using Darcy's law. Difference of the water head above the liner and the water head in the leachate detection pipe was considered to govern the flow through the liner.

From Fig. 4 the rate of leakage of leachate through the liner can be obtained from which it can be seen that the Bentonite liner shows a uniform rate of leachate seepage while the control lysimeter shows a significant increase after a certain period of time. Development of permanent flow paths may have led to this situation in control lysimeter. However, the bentonite lysimeter was able to sustain its permeability characteristics regardless of the water head developed above the liner or the period of operation.

3.4 Numerical Analysis of Seepage Through Lysimeters

Both bentonite and control lysimeters were modelled using the SEEP/W software under steady state condition. The analyses were performed by simulating the rainfall as an infiltration applied as a unit flux (expressed in m/s) on the top of the capping layer. The magnitude of the unit flux was calculated based on the monthly rainfall data assuming that four hours of rain occurred in a rainy day.

Two extreme scenarios of the liner were used to verify the accuracy of the numerical model developed. The liner was considered to be of high permeability as one such extreme scenario and for the other, it was considered as almost impermeable.

Figure 5 shows the seepage flow lines for the highly permeable and highly impermeable liners. According to these results obtained for both these scenarios, model could be verified for use for the actual condition.

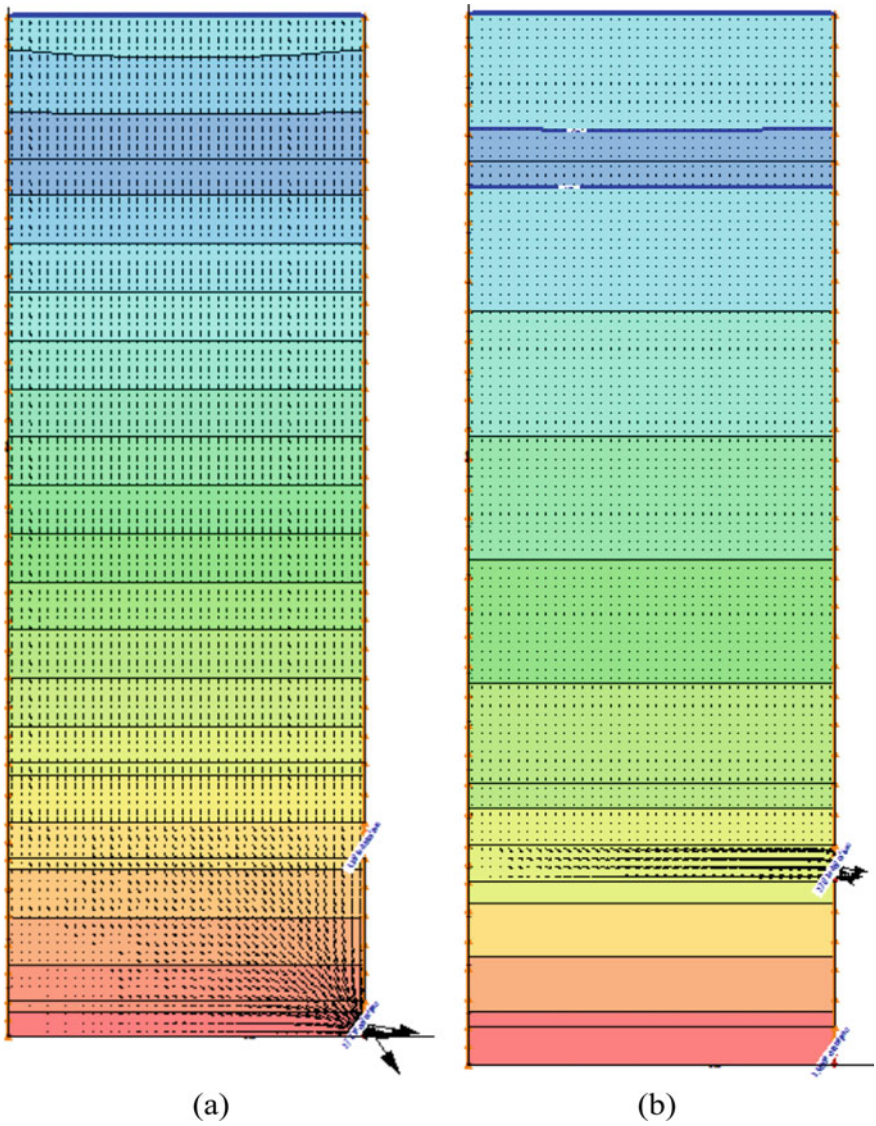

Fig. 5 Seepage flow lines for **a** highly permeable and **b** highly impermeable liner

Table 3 Results of numerical analysis of seepage for control lysimeter

Month	Unit flux (mm/s) (assuming 4 h rain in each day)	Flow through the drain layer above the liner (m^3/s)	Flow through the drain layer below the liner (m^3/s)
December 2015	1.805E−07	2.648E−07	8.624E−10
January 2016	7.147E−08	1.054E−07	8.625E−10
February 2016	1.929E−08	2.904E−08	8.625E−10
March 2016	1.858E−07	2.726E−07	8.625E−10
April 2016	1.066E−07	1.567E−07	8.625E−10
May 2016	3.167E−07	4.640E−07	8.625E−10

Table 4 Results of numerical analysis of seepage for bentonite lysimeter

Month	Unit flux (mm/s) (assuming 4 h rain in each day)	Flow through the drain layer above the liner (m^3/s)	Flow through the drain layer below the liner (m^3/s)
December 2015	1.805E−07	2.643E−07	2.812E−10
January 2016	7.147E−08	1.048E−07	2.813E−10
February 2016	1.929E−08	2.848E−08	2.813E−10
March 2016	1.858E−07	2.720E−07	2.812E−10
April 2016	1.066E−07	1.562E−07	2.812E−10
May 2016	3.167E−07	2.720E−07	2.813E−10

3.4.1 Results of Control Lysimeter

Results of the seepage analysis of control lysimeter are given in Table 3.

3.4.2 Results of Bentonite Lysimeter

Results of the seepage analysis of bentonite lysimeter are given in Table 4.

It can be seen that the flow through the liner in experimental lysimeter is less than three times the flow through that in control lysimeter.

3.4.3 Comparison of Field and Seep/W Model Results

Comparison of seepage rate between field observations and numerical analyses are given in Table 5. Difference between the numerical analysis derived values and field values of the leaked leachate flow can be due to following reasons.

Table 5 Comparison of leaked leachate flow between field scale observations and numerical model outputs

Month	Control lysimeter		Bentonite lysimeter	
	Calculated leaked leachate flow using field data (m^3/s)	Flow through the drain layer below the liner (m^3/s)	Calculated leaked leachate flow using field data (m^3/s)	Flow through the drain layer below the liner (m^3/s)
January 2016	1.11E−11	8.625E−10	2.31E−12	2.813E−10
February 2016	1.10E−11	8.625E−10	4.46E−12	2.813E−10
March 2016	5.49E−11	8.625E−10	7.65E−12	2.812E−10
April 2016	9.30E−11	8.625E−10	9.58E−12	2.812E−10
May 2016	9.78E−11	8.625E−10	4.28E−12	2.813E−10

- Finite element model of the lysimeter was considered under plane strain conditions. The section in field scale however is circular in plan with a diameter of 1.5 m.
- Settlement of the layers (especially waste layer) was not considered in the model that can affect the permeability as the time progresses.
- Degree of compaction can vary due to the non-homogenous composition of the waste layer, thus resulting in non-uniform permeability coefficients.

Numerical analysis of lysimeters can be used to optimise the design of liners. Spatial variations of the materials may be required to be included in the model to obtain results with better quantitative accuracy.

3.4.4 Effect of Liner Thickness on Seepage Flow Rate

Figure 6 shows the variation of seepage flow through the liners with the liner thicknesses. When the liner thickness increases seepage flow decreases fitting well into a

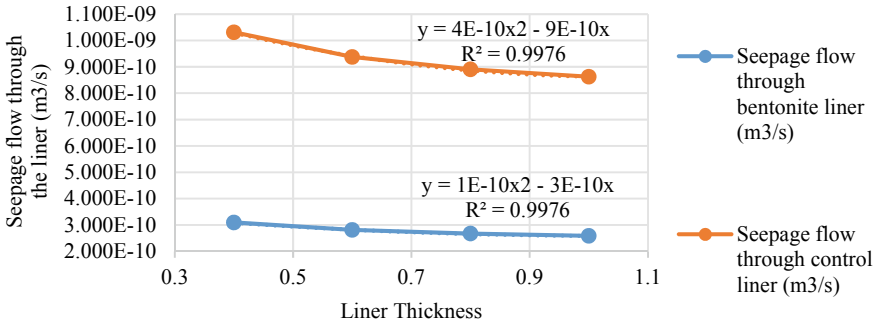

Fig. 6 Variation of seepage flow through the liner with liner thickness

second order polynomial variation. Control liner shows higher seepage flow reduction rate for lower liner thicknesses compared to that for the bentonite liner. Increase in liner thickness will reduce the rate of seepage through the liner reaching a limiting value. Using Fig. 6, a cost effective liner thickness to achieve the minimum leakage of leachate can be identified.

4 Conclusions

Functionality of liner was investigated under the wet zone climatic conditions in Sri Lanka. Both control and bentonite liners were investigated using experimental setup and numerical analyses.

From the above studies following conclusions can be made.

- The clay liner with 5% bentonite is three times effective in reducing leachate flow rate through the liner when compared with that of control lysimeter.
- The numerical analysis showed that an increase in liner thickness will reduce the rate of seepage through the liner reaching a limiting value.

Acknowledgements Financial support for this research was extended by the SATREPS Project for Waste Landfill Sites taking into account Geographical Characteristics in Sri Lanka.

References

1. Central Environmental Authority (2007) Technical guidelines on solid waste management in Sri Lanka, vol 1, pp 20–27
2. Herath NW (1993) Identification and behavior of expansive soils in Sri Lanka
3. Raziful IM, Howlader MK, Alamgir M (2012) Waste management, vol 32, pp 2068–2079, September
4. Rafizul IM, Howlader MK, Alamgir M (2012) Construction and evaluation of simulated pilot scale landfill lysimeter in Bangladesh. J Waste Manage 32:2068–2079
5. Renou S, Givaudan JG, Poulain S, Dirassouyan F, Moulin P (2008) Landfill leachate treatment: review and opportunity. J Hazard Mater 150(3):468–493
6. Wanigarathna D (2012) Characterization of locally available soil as a liner material for solid waste landfills in Sri Lanka. MSc thesis, University of Peradeniya, Sri Lanka
7. Wijerathna DMCB, Jinadasa KBSN, Herath GBB, Mangalika L (2012) Solid waste management problem in kandy municipal council-a case study. SAITM Research Symposium on Engineering Advancements. Available from: https://www.saitm.edu.lk/fac_of_eng/RSEA/SAITM

Feasibility of Using Mobile Apps in Communication and Dissemination Process of Multi-hazard Early Warning (MHEW) Mechanism in Sri Lankan Context

P. L. A. I. Shehara, C. S. A. Siriwardana, D. Amaratunga, R. Haigh, and T. Fonseka

Abstract The alerts given accurately on time via Early Warning mechanisms can save thousands of lives as well as can minimize the level of damage to the Critical Infrastructure to a greater extent. With the rapid occurrence of natural hazards day by day, more emphasis on Disaster Risk Reduction strategies are concerned in order to minimize the disaster-related economic losses and damages. The concept of Multi-Hazard Early Warning emerged with the implementation of Disaster Risk Reduction strategies over the world to work under different global frameworks, mainly with the initiation of the Sendai Framework for Disaster Risk Reduction 2015–2030. Communication and dissemination component of the Multi-Hazard Early Warning mechanism can be considered more significant in terms of reducing the damages and losses over lives and properties. Science and technological applications can be vividly incorporated to enhance the efficiency of delivering Multi-Hazard Early Warning messages from upstream, interface phases towards the downstream community level. With the proper delivery of Early Warning information through technological applications, the efforts on minimizing the damage extent on Critical Infrastructures can be undertaken. This concern is mainly elaborated as one of the seven targets in Sendai Framework for Disaster Risk Reduction 2015–2030. Under this research study, different mobile apps using in different countries are overviewed with the special focus on the comparison of mobile apps that are currently using in Sri Lanka, Maldives and Indonesia. With these concerns, the feasibility of using mobile apps in disaster Early Warning mechanism in Sri Lankan context was examined using a questionnaire survey which was conducted within 10 Grama Niladari divisions. Under this, community responses were collected from 323 responses and these were analyzed using Fuzzy logic approach to identify the decision making scores of the community on level of importance and level of usefulness of the mobile apps.

P. L. A. I. Shehara (✉) · C. S. A. Siriwardana · T. Fonseka
University of Moratuwa, Moratuwa, Sri Lanka
e-mail: ishanishehara@gmail.com

D. Amaratunga · R. Haigh
Global Disaster Resilience Hub, University of Huddersfield, Huddersfield, UK

R. Dissanayake et al. (eds.), *ICSECM 2019*, Lecture Notes in Civil Engineering 94,
https://doi.org/10.1007/978-981-15-7222-7_16

Keywords Multi-hazard early warning (MHEW) · Disaster risk reduction (DRR) · Technology · Mobile apps · Fuzzy logic approach

1 Introduction

Disasters that trigger natural hazards have impacted 2.5 million lives and costs more than US$1.5 billion over the past 35 years in history [22]. From the disaster incidents in the recent history, the Indian Ocean Tsunami in 2004, 2010 Haiti earthquake and 2011 Great East Japan (Tohoku) earthquake are some such catastrophic incidents that have made huge calamities in the countries [5]. Among those incidents, 2004 Indian Ocean Tsunami has devastated 228,000 casualties from 14 countries over the world, where the lack of delivery of proper Early Warning (EW) mechanism and lack of community on such experiences were at its highest consideration [16, 18].

In order to mitigate the disaster impact over the lives and properties of the vulnerable communities, different implementations and initiations have considered so far with the aim of reducing the disaster risk by 2030 along with the Sendai Framework for Disaster Risk Reduction (2015–2030) [14]. Concerning the global context, this vulnerable community is mostly neglected in delivering EW disaster alerts. Further, reaching this community is considered as more challenging in this concern [25].

As one of the precautions to this challenging behavior of the natural hazards that trigger disasters, innovative and technology-driven approaches such as crowdsourcing and participatory sensing have been evolved [10]. Under this, adopted technology-mediated approaches like mobile applications and social media platforms have evolved more increasingly with the time passage [23].

Mobile technology has become a core communication platform that can be used in reaching the vulnerable community in disaster situations [15]. With the increasing nature of disasters over the world, the need for the application of mobile technology to reach the vulnerable community has become a more important phenomenon. Under recent research studies, mobile phones have been identified as the most reliable, effective and affordable mode in reaching the last mile communities [21]. For this, the smartphone usage level needs to be focused more considerably. Accordingly, the number of smartphone users in 2019 records as 3.2 billion in the global context [26]. Smart phone-based applications were recognized as an elegant solution which emerged as an alternative to conventional detection and warning mechanism [9].

With the rapid acceleration of disasters over the world, the new breed of disaster warning alert apps acts as a lifeline before, during and after disaster situations [33]. Recent research studies denote that mobile apps play a major role during each phase of the disaster management cycle, preparedness stage, emergency response stage, recovery stage and mitigation stage [29]. Among all these stages, the use of mobile apps plays a key role mainly in the preparedness stage and the emergency response stages [17].

The general use of mobile apps during disasters with the interaction of the users are summarized in Table 1 [29].

Table 1 Interaction with users and general purpose of apps

Interaction	General-purpose apps
One to one	Personal messaging apps
One to many	News apps from news agencies Weather apps from meteorological agencies
Many to many	Social media apps like Facebook, Twitter

When considering the user interaction with the purpose of the apps, it can be clearly concluded, the use of dedicated disaster warning apps can reach the vulnerable community using a verified authority. These dedicated disaster warning alert apps can be incorporated towards the evacuation mechanism of the community as well. The location-based delivery of disaster Early Warning (EW) alerts and customization of the app features to view the evacuation routes are considered more advanced functions of these apps [12].

Mobile-based dedicated apps for disasters mainly focus on delivering evidence-based information and alerts to the community at risk [6]. As identified, the function of MHEW is considered to be defined as a systematic approach of conveying information to the community level who are vulnerable to the risk of an identified hazard in advance of physical effects [20]. Under this mechanism, the use of disaster dedicated apps today revolutionizes disaster communication by enhancing the information flow from the interface to downstream level components in the Early Warning mechanism [27].

In the global context, the usage level of mobile apps in delivering the disaster EWs was examined using the literature. Under this, the usage level was determined through the number of app downloads that have marked in the android play store. The result summary is denoted under Table 2 [2, 7, 8, 30, 31].

Accordingly, the aforementioned app download variation mainly denotes the usage range variation in the globally identified mobile apps. Further, this denotes

Table 2 Overview of disaster early warning alert apps

Download range	Disaster early warning alert apps
100–1000	Emergency alert PDMA KP, Weather and Alert
1000–10,000	Disaster Management (Earthquakes, Weather Alerts), DEWN, Alertable Emergency Alerts, GDACS (Global Disaster Alert Coordination System), Hazards—IFRC, NDWC, TSP Indonesia, Global monitoring
10,000–100,000	Saskatchewan Emergency Alert, Natural Disaster Monitor, SERVIR, Alberta Emergency alert, Indian Ocean Tsunami Alert, Alert 5, Safety tips
100,000–1,000,000	Disaster Alert, CSEM-EMSC LastQuake, Earthquakes tracker, eQuake, Volcanoes & Earthquakes, CSEM-EMSC LastQuake
1,000,000–10,000,000	Earthquake Alert, Earthquake Network—Realtime alerts
10,000,000 above	Weather Radar Live and Alerts

that the disaster EW alert apps with a higher range indicating the downloads of more than 1,000,000 are identified as very much low. The community exposure on mobile app usage is more delivered upon this representation.

An overview of the existing disaster management mobile applications that are currently using in the disaster emergency response stage was identified globally and app features were recognized in the recent research studies [24]. Under this, the focus was directed towards identification of the recently developed mobile platforms and their usage level variations obtaining twitter usage as the main example.

The android app development over the world denotes that the community trust level is more generating towards the delivery of the warning through mobile apps. Different disaster dedicated apps are currently being developed to address the emergency information needs of the public and authorities [13]. All stakeholders should be aware of and exposed to such tools even before a disaster. If these disaster dedicated apps are to be useful during disasters, the app must be supported and endorsed by authorities and also promoted to and accepted by the public as a preparedness tool. Efforts must then be carried out in the preparedness phase to facilitate the access, knowledge, and use of technology for disaster situations [4]. It is a challenge to gain the interest of both the authorities and the public. On the one hand, the authorities must overcome possible challenges in adapting to new technologies and be invested enough to put their resources behind a complex information communication channel. Further, these apps also need to be attractive enough to the public to achieve critical mass for maximum impact.

Under this research study, the community level response on the applicability of the mobile applications in the Sri Lankan context was examined after reviewing the global context overview. Further, using the field questionnaire survey done in the selected Grama Niladari divisions in Sri Lanka, the feasibility of the application of mobile app technology is further studied. For this to be determined, the fuzzy logic approach is considered to determine the level of importance and level of usefulness.

2 Overview of Dedicated Early Warning Mobile Applications in Sri Lanka, Maldives and Indonesia

Dedicated mobile applications in terms of dissemination of disaster EW alerts to reach the vulnerable community has become more important with time. Concerning the past disaster incidents, the Indian Ocean Tsunami which happened in 2004 is remarked as the most catastrophic incident in the South Asian region. Under this, the most crucial damages that have impacted in terms of the number of deaths and damage contents were recorded as Sri Lanka, Indonesia and Maldives [19]. This was more revealed through the impact that has triggered the country Gross Domestic Product (GDP) value of 83.6% of Maldives, 7.6% of Sri Lanka and 2% of GDP in Indonesia. With this concern from the Tsunami impact, the influence of the usage of modern technology platforms and community exposure on disaster EW apps are

Table 3 Overview of dedicated apps using in Sri Lanka, Indonesia and Maldives

Parameters	Sri Lanka	Maldives	Indonesia
Mobile app	DEWN	Moosun	Info BMKG
Developed authority	Dialog Axiata PLC, Dialog-University of Moratuwa, Microimage, Disaster Management Center (DMC)	Maldives Meteorological Service (MMS)	Meteorological, Climatological and Geophysical agency
Developed year	2009	2019	2016
Interface appearance	Textorial	Pictorial	Prictorial
The functions	Weather forecast, landslide information	Weather forecast Maldives islands, earthquake updates, radar and satellite images	Weather forecast, earthquake information
Mobile phone applicability	Android, iOS	Android, iOS	Android, iOS
Android app downloads	5000+	10,000+	5,000,000+
Nature of the alert received on 2nd August 2019	No Tsunami threat	Tsunami alert	Tsunami alert
Time variation (h)	1930	1805	1805

examined below. The review of the dedicated mobile applications currently using in Indonesia, Sri Lanka and the Maldives are represented in Table 3.

Under the review of these apps, it can be clearly seen that the user level of the apps has a higher rating in Indonesia with an increase in disaster frequency.

During the recent Tsunami alert warning which happened on 2nd August 2019, the time duration variation of the alert receiving from the three aforementioned apps was examined. Accordingly, the warning received through the mobile app in Sri Lanka was a verified one which mentioned that not having a Tsunami threat though it took about a one-hour time gap compared with the other two apps. This basically denotes the importance of the level of accuracy and the timely delivery of information to the vulnerable community which is the key enablers of effective EW mechanism.

3 Examining the Feasibility Level in the Sri Lankan Context

The community response in the Sri Lankan context was examined through a field survey conducted in selected 10 Grama Niladari divisions based on the hazard level

from floods, tsunami and landslides. The population densities of the selected Divisional Secretariate divisions are listed under Table 4. These collected responses were analyzed based on urban and rural level comparisons to present a better overview of the responses.

Accordingly, as the areas where the population density exceeds 500 persons per km^2 are considered urbanized in the Sri Lankan context. From the selected study locations, Colombo and Wattala Divisional Secretariat (DS divisions) are considered as urbanized and Bulathsinhala DS division is considered as rural in the context of population density [1].

Under this field survey study, as one major part, the community response towards the dissemination of the disaster EW alerts through the mobile applications was tested. Mainly, the level of importance of mobile applications in the dissemination of EW alerts and the level of use of mobile applications in terms of dissemination of EW alerts were considered. The demographic features of the selected Grama Niladari divisions are denoted under Table 5.

Under this data collection, the reliability of the collected responses was checked using the software named IBM SPSS 22 software. In this software, the reliability was measured using a parameter named Cronbach alpha. This representation of

Table 4 Population densities

Location	Area (km^2)	Population	Population density
Bulathsinhala	206	64,600	313
Wattala	54	175,525	3250
Colombo	18	323,257	17959

Table 5 Demographic background of the responders

Variable	Category	Percentage (%)
Gender	Male	47
	Female	53
Age	Below 18	4
	18–24 years	8
	25–39 years	29
	40–60 years	44
	Over 60 years	15
Occupation category	Government sector	6
	Private sector	17
	Self-employed	25
	Student (school)	5
	Student (university)	2
	Others (no job, retired)	45

Table 6 Case processing summary results

Case processing summary			
		N	%
Cases	Valid	295	91.3
	Excluded	28	8.7
	Total	323	100.0
Cronbach alpha	0.704		

Cronbach alpha is denoted under Eq. 1. When the Cronbach alpha is less than 0.3, the data is considered as not suitable for further analysis as the reliability level of data is considered as low. When the Cronbach alpha is more than 0.7, data is considered as suitable for further analysis as the reliability level is considered high [28].

$$\alpha = \frac{Nc}{v + (N-1)c} \tag{1}$$

$\propto$ Cronbach alpha
N Number of items (responses)
c Average of all covariance between items
v Average variance of each item

The case processing summary of the results is denoted under Table 6.

As the obtained results for the parameter are greater than 0.7, the collected data could be considered for further analysis. For the results obtained through the field community survey, the Fuzzy logic approach was used in the determination of the most biased community response for the considered parameters.

3.1 Application of Fuzzy Logic Approach

The fuzzy logic approach was considered in the determination of the Likert scale responses to reach the highly biased community response over the adaptation of community towards dedicated disaster mobile apps. Under this, the Likert scale scoring was considered to determine the level of importance and level of use of these dedicated apps. The fuzzy rating scale was considered in quantifying the human scale decisions on the Likert scale to obtain more biased human perception [11]. Triangular fuzzy number X can be represented based on the triplet ($\times 1$, $\times 2$, $\times 3$) which is determined from the three value judgment for a considered response concerning minimum possible value $\times 1$, kernel value $\times 2$ and most possible value $\times 2$ and maximum possible value $\times 3$ [3].

Accordingly, fuzzy correspondences were defined based on the past studies conducted on converting Likert scale score to fuzzy score which is represented under Table 7 [32].

Table 7 Fuzzy correspondences

Variable	Fuzzy correspondences
Unlikely	(1.0, 1.0, 2.0)
Somewhat unlikely	(1.0, 2.0, 3.0)
Moderate	(2.0, 3.0, 4.0)
Somewhat likely	(3.0, 4.0, 5.0)
Extremely likely	(4.0, 5.0, 5.0)

3.2 Level of Importance of Mobile Applications in Early Warning Alert Dissemination

The community-level response on assessing the level of importance of using disaster warning alert mobile applications was determined using the 5 points Likert scale, where the score was categorized based on "most important", "important", "moderate", "less important" and "not important". The sample frequencies obtained for this scale from the community survey are represented under Table 8.

Accordingly, the average weighted score for the fuzzy triangular number was determined which is represented under Table 9.

The obtained Kernel value of 4.5 denotes the biasness of the responses received over the level of importance of mobile applications under the rating scale on the Likert scale. This denotes, the overall response towards this parameter of the level of importance was obtained as higher than the rating of importance. This depicts the favorable nature of the community towards adapting to the new approaches in the dissemination of EW alerts.

Further, the obtained responses were analyzed using the fuzzy logic approach in comparison of the urban and rural level community perspectives over the level of importance of disaster warning alert apps. The comparison is represented in Table 10.

From the obtained results, when compared to the triangular fuzzy numbers obtained for urban and rural level responses, the rural level response on the level

Table 8 Sample frequency table for the level of importance

Score	1	2	3	4	5
Frequency	1	7	20	62	225

Table 9 Average weighted score

Parameter	Value
Average weighted score for fuzzy triangulation number	((1.0, 1.0, 2.0) * 1 + (1.0, 2.0, 3.0) * 7 + (2.0, 3.0, 4.0) * 20 + (3.0, 4.0, 5.0) * 62 + (4.0, 5.0, 5.0) * 225)/323
	(3.2, 4.5, 4.7)

Table 10 Decision matrix for the urban and rural levels

Parameter	Urban level					Rural level				
Likert scale score	1	2	3	4	5	1	2	3	4	5
Frequency	0	3	13	37	124	1	4	8	21	66
Average weighted score for fuzzy triangulation number	(1.0, 1.0, 2.0) * 0 + (1.0, 2.0, 3.0) * 3 + (2.0, 3.0, 4.0) * 13 + (3.0, 4.0, 5.0) * 37 + (4.0, 5.0, 5.0) * 124/187					(1.0, 1.0, 2.0) * 1 + (1.0, 2.0, 3.0) * 4 + (2.0, 3.0, 4.0) * 8 + (3.0, 4.0, 5.0) * 21 + (4.0, 5.0, 5.0) * 66/100				
	(3.3, 4.1, 4.4)					(3.5, 4.5, 4.8)				

of importance of using mobile apps is more biased towards the mediator between most important and important levels which the Kernel value is 4.5 of the Likert scale. In the same manner, the urban level fuzzy triangulation number of 4.1 denotes that the level of importance of using mobile apps is more biased towards important level score 4 of the Likert scale. When comparing both the responses, there is a high perception of rural level community towards adapting to mobile-based apps in the dissemination of EW alerts.

3.3 Level of Usefulness of Mobile Applications in Early Warning Alert Dissemination

The level of use of mobile apps was tested using a Likert scale with a rating of five score scale. Under this, the scale rating was defined as "not useful", "somewhat useful", "moderately useful", "useful" and "extremely useful". The frequency of the responses received for each of the Likert scale scores is represented under Table 11.

From the frequency of the responses received for each score on the Likert scale, the average weighted fuzzy score was determined. The obtained triangular fuzzy value is represented under Table 12.

Table 11 Sample frequency table for the level of usefulness

Score	1	2	3	4	5
Frequency	1	6	31	67	209

Table 12 Average weighted score

Parameter	Value
Average weighted score for fuzzy triangulation number	((1.0, 1.0, 2.0) * 1 + (1.0, 2.0, 3.0) * 6 + (2.0, 3.0, 4.0) * 31 + (3.0, 4.0, 5.0) * 67 + (4.0, 5.0, 5.0) * 209)/323
	(3.4, 4.4, 4.7)

Table 13 Decision matrix for urban and rural level responses

Parameter	Urban level					Rural level				
Likert scale score	1	2	3	4	5	1	2	3	4	5
Frequency	0	3	13	37	124	1	4	8	21	66
Average weighted score for fuzzy triangulation number	(1.0, 1.0, 2.0) * 0 + (1.0, 2.0, 3.0) * 3 + (2.0, 3.0, 4.0) * 19 + (3.0, 4.0, 5.0) * 38 + (4.0, 5.0, 5.0) * 117/177					(1.0, 1.0, 2.0) * 1 + (1.0, 2.0, 3.0) * 3 + (2.0, 3.0, 4.0) * 12 + (3.0, 4.0, 5.0) * 22 + (4.0, 5.0, 5.0) * 61/99				
	(3.5, 4.5, 4.9)					(3.4, 4.4, 4.8)				

From the results obtained for the weighted average of the fuzzy triangulation number, the kernel value of 4.4 represents that the community response on the level of usefulness of the mobile apps is more biased towards the mediator between useful and extremely useful.

The comparison of the triangulation fuzzy numbers in the comparison of the urban and rural level community are represented under Table 13.

When comparing the triangular fuzzy numbers obtained for urban and rural level responses, the rural level response on the level of use of using mobile apps is more biased towards the mediator between the most useful and useful levels which the Kernel value is 4.4 of the Likert scale. In the same manner, the urban level fuzzy triangulation number of 4.5 denotes that the level usefulness of mobile apps is more biased towards the mediator between the extremely useful and useful of the Likert scale. When comparing the responses, both the urban and rural level perceptions towards adapting to mobile-based apps in the dissemination of EW alerts represent a favorable response.

4 Conclusion

Science and technology have influenced the DRR mechanism in the global perspective and the use of mobile technology under this plays a vital role. Accordingly, the dedicated apps which are targeted at reaching the vulnerable community during disasters were overviewed. The dedicated mobile apps using in Sri Lanka, Maldives and Indonesia were examined in order to identify the applicability of mobile app technology in disaster situations. Moreover, the feasibility of the application of dedicated mobile apps for disasters in Sri Lanka was tested as a part of a field questionnaire survey that was conducted in 10 GN divisions in the country.

From the community responses obtained, the level of importance and level of use of these dedicated apps in the Sri Lankan context were examined. For this, the Fuzzy logic approach was used to determine the biasness of the Likert scale community response on the tested parameters of level of importance and level of usefulness.

From the results obtained through the Fuzzy Logic approach, the kernel value of the fuzzy triangular value of 4.5 for the level of importance of using mobile apps denotes that the community response is more biased towards somewhat higher than the important level of using apps. This denotes the community expectation towards the willingness of adaptability to dedicated mobile apps. In the comparison of urban and rural level perceptions, there is a more favorable adaptation on a rural level community than the urban level community in terms of determination of level of importance.

Further, under the Fuzzy logic analysis, the kernel value of the fuzzy triangulation number of 4.4 denotes that the biasness of the Likert scale response on the level of usefulness of the mobile apps. The kernel value is more biased towards a little more than the useful score on the Likert scale. In comparison to the urban and rural level community perceptions, both have favorable adaptation towards mobile apps in terms of the level of usefulness.

Acknowledgements The authors here gratefully acknowledge Erasmus+ Capacity Building for Higher Education Grant, CApacity Building in Asia for Resilience EducaTion (CABARET) for providing funds and expertise in carrying out this research study.

References

1. (14) (PDF) Re-Defining Urban Areas in Sri Lanka. [WWW Document] (n.d.) ResearchGate. URL: https://www.researchgate.net/publication/314257911_Re-Defining_Urban_Areas_in_Sri_Lanka. Accessed 8 Nov 19
2. 10 Free Disaster Apps to Have in Your Pocket | PreparednessMama [WWW Document] (n.d.) URL: https://preparednessmama.com/disaster-apps/. Accessed 26 Nov 19
3. Anandan V, Uthra G (2014) Defuzzification by area of region and decision making using Hurwicz criteria for fuzzy numbers. Appl Math Sci 8:3145–3154. https://doi.org/10.12988/ams.2014.44294
4. Antoniou N (n.d.) IAC-13.E5.5.3 Social media in the disaster cycle—useful tools or mass distraction? 10
5. Asian Development Bank (2018) Understanding disaster risk for advancing resilient development
6. Buus N, Juel A, Haskelberg H, Frandsen H, Larsen JLS, River J, Andreasson K, Nordentoft M, Davenport T, Erlangsen A (2019) User involvement in developing the MYPLAN mobile phone safety plan app for people in suicidal crisis: case study. JMIR Ment Health 6. https://doi.org/10.2196/11965
7. Content, T.F.T.F. has 30+ years' professional technology support experience H. writes troubleshooting, Lifewire, is the G.M. of (n.d.) The 7 Best Emergency Alert Apps of 2019 [WWW Document]. Lifewire. URL https://www.lifewire.com/best-emergency-apps-4769340. Accessed 26 Nov 19
8. Disaster Alert™ App | Pacific Disaster Center [WWW Document] (n.d.) URL: https://www.pdc.org/apps/disaster-alert/. Accessed 26 Nov 19
9. Fildes N (2018) Mobile phones and AI vie to update early disaster warning systems [WWW Document]. Financial Times. URL: https://www.ft.com/content/4949829c-1293-11e8-a765-993b2440bd73. Accessed 26 Nov 19

10. Frisiello A, Nguyen QN, Rossi C (2017) Gamified crowdsourcing for disaster risk management. In: 2017 IEEE international conference on big data (big data), pp 3727–3733. https://doi.org/10.1109/BigData.2017.8258370
11. Gil MÁ, Lubiano MA, de la Rosa de Sáa S, Sinova B (2015) Analyzing data from a fuzzy rating scale-based questionnaire. A case study. Psicothema 27:182–191. https://doi.org/10.7334/psicothema2014.268
12. Gughan N, Samuel BJ, Kirubanandasarathy N (2015) Disaster alert notification and rescue management through smart phones using GPS. Int J Appl Eng Res
13. Lien Y, Jang H, Tsai T (2009) A MANET based emergency communication and information system for catastrophic natural disasters. In: 2009 29th IEEE international conference on distributed computing systems workshops. Presented at the 2009 29th IEEE international conference on distributed computing systems workshops, pp 412–417. https://doi.org/10.1109/ICDCSW.2009.72
14. Lipat ANM (n.d.) Sendai framework disaster risk reduction 2015–2030
15. Mobile Technology [WWW Document] (2016) Global disaster preparedness center. URL: https://www.preparecenter.org/activities/mobile-technology. Accessed 16 Nov 19
16. Perera C, Jayasooriya D, Jayasiri G, Randil C, Bandara C, Siriwardana C, Dissanayake R, Hippola S, Sylva K, Kamalrathne T, Kulatunga A (2020) Evaluation of gaps in early warning mechanisms and evacuation procedures for coastal communities in Sri Lanka. Int J Disaster Resilience Built Environ 11(3):415–433
17. Phys.org [WWW Document] (n.d.) Mobile phones help transform disaster relief. URL: https://phys.org/news/2018-03-mobile-disaster-relief.html. Accessed 17 Nov 19
18. Rathnayake DK, Kularatne D, Abeysinghe S, Shehara I, Fonseka T, Mudiyanselage SDJE, Kamalrathne WGCT, Siriwardana C, Appuhamilage CSBAM, Dissanayake R (2020) Barriers and enablers of coastal disaster resilience – lessons learned from tsunami in Sri Lanka. Int J Disaster Resilience Built Environ 11(2):275–288
19. Reliefweb (2005) Indonesia, Maldives, Sri Lanka: earthquake and tsunami OCHA Situation Report No. 18—Indonesia
20. Samarajiva R (2005) Policy commentary: mobilizing information and communications technologies for effective disaster warning: lessons from the 2004 tsunami. New Media Soc 7:731–747. https://doi.org/10.1177/1461444805058159
21. Samarajiva R, Waidyanatha N (2009) Two complementary mobile technologies for disaster warning. info 11:58–65. https://doi.org/10.1108/14636690910941885
22. SciDev.Net (2019) Early warning of disasters: facts and figures [WWW Document]. SciDev.Net. URL: https://www.scidev.net/index.cfm?originalUrl=/global/earth-science/feature/early-warning-of-disasters-facts-and-figures-1.html. Accessed 9 Nov 19
23. See L, Mooney P, Foody G, Bastin L, Comber A, Estima J, Fritz S, Kerle N, Jiang B, Laakso M, Liu H-Y, Milčinski G, Nikšič M, Painho M, Pődör A, Olteanu-Raimond A-M, Rutzinger M (2016) Crowdsourcing, citizen science or volunteered geographic information? The current state of crowdsourced geographic information. ISPRS Int J Geo-Inf 5:55. https://doi.org/10.3390/ijgi5050055
24. Shehara I, Siriwardana C, Amaratunga D, Haigh R (2019) An overview of existing digital platforms in disaster emergency response stage. In: Presented at the SBE19 Malta international conference, Malta
25. Shehara PLAI, Siriwardana CSA, Amaratunga D, Haigh R (2019) Application of social network analysis (SNA) to identify communication network associated with multi-hazard early warning (MHEW) in Sri Lanka. 2019 Moratuwa Engineering Research Conference (MERCon), Moratuwa, Sri Lanka, 2019, pp 141–146. https://doi.org/10.1109/MERCon.2019.8818902
26. Statista [WWW Document] (2019) Statista. URL: https://www.statista.com/statistics/330695/number-of-smartphone-users-worldwide/. Accessed 16 Nov 19
27. Sukhwani V, Shaw R (2020) Operationalizing crowdsourcing through mobile applications for disaster management in India. Prog Disaster Sci 5:100052. https://doi.org/10.1016/j.pdisas.2019.100052

28. Taber KS (2018) The use of Cronbach's alpha when developing and reporting research instruments in science education. Res Sci Educ 48:1273–1296. https://doi.org/10.1007/s11165-016-9602-2
29. Tan ML, Prasanna R, Stock K, Hudson-Doyle E, Leonard G, Johnston D (2017) Mobile applications in crisis informatics literature: a systematic review. Int J Disaster Risk Reduction 24:297–311. https://doi.org/10.1016/j.ijdrr.2017.06.009
30. The best emergency apps for hurricanes, earthquakes, and other disasters—CNET Download.com [WWW Document] (n.d.) URL: https://download.cnet.com/news/the-best-emergency-apps-for-hurricanes-earthquakes-and-other-disasters/. Accessed 26 Nov 19
31. Three apps to warn travellers of natural disasters—how good are they? [WWW Document] (2017) South China Morning Post. URL: https://www.scmp.com/lifestyle/travel-leisure/article/2113386/three-free-apps-warn-travellers-natural-disasters-near-and. Accessed 26 Nov 19
32. Vonglao P (2017) Application of fuzzy logic to improve the likert scale to measure latent variables. Kasetsart J Soc Sci 38:337–344. https://doi.org/10.1016/j.kjss.2017.01.002
33. Yeoh N (n.d.) A surprising solution to surviving natural disasters: mobile apps [WWW Document]. Forbes. URL: https://www.forbes.com/sites/neilyeoh/2019/05/23/a-surprising-solution-to-natural-disasters-mobile-apps/. Accessed 26 Nov 19

Conceptual Compilation of Activity Criteria During the Post-disaster Stage of a Fire Hazard in Hospitals

W. D. M. Kularatne, H. H. H. Hasalanka, C. S. A. Siriwardana, W. K. D. Rathnayake, and H. T. V. Fonseka

Abstract The occurrence of fire hazards can cause disastrous consequences in any place and such consequences can be particularly severe in hospitals where a large number of the present population are highly vulnerable in disastrous events. It is also possible that, even after the fire hazard is neutralized, the hospital may remain in a risky position. For example, damages caused due to the electricity framework in the building can cause cascading effects later on by disrupting the power supply of the hospital. Therefore, it is important to seriously consider and undertake the necessary post-disaster activities after a fire. This paper tries to look at all activities necessary to effectively get through the post-disaster stage of a fire-hazard in a hospital so that it can build up its resilience to future fire hazards. This compilation of activities will include post-disaster inspection and cause identification, transfer of patients if necessary and the involvement of insurance agencies. A comprehensive list of activities has been produced separated under five categories of people, buildings and critical infrastructure systems, equipment, hospital material stores, and post-fire administrative and managerial work. Here, it is also discussed which of these activities should be applied to a scenario depending on the impact level of the fire hazard.

Keywords Fire hazards · Post-disaster stage · Disaster recovery · Hospital safety

1 Introduction

Fires have the propensity to reach an uncontrollable stage very quickly and in its uncontrollable stage can have very disastrous effects on everything it touches. According to the 2004 World Health Report, approximately 312,000 deaths due to fire have been recorded in 2002 [25]. Smoke, which is a bi-product of fire, is

W. D. M. Kularatne (✉) · H. H. H. Hasalanka · C. S. A. Siriwardana · H. T. V. Fonseka
Department of Civil Engineering, University of Moratuwa, Moratuwa, Sri Lanka
e-mail: devmini.kularatne@gmail.com

W. K. D. Rathnayake
Department of Civil Engineering, University of Peradeniya, Peradeniya, Sri Lanka

R. Dissanayake et al. (eds.), *ICSECM 2019*, Lecture Notes in Civil Engineering 94,
https://doi.org/10.1007/978-981-15-7222-7_17

equally as dangerous, as it includes narcotic gases such as carbon dioxide, carbon monoxide, and hydrogen cyanide, irritants like nitrogen monoxide, nitrogen dioxide, ammonia, hydrogen fluoride, hydrogen bromide, Sulphur dioxide and hydrogen chloride, volatile organic compounds such as isocyanates, phenol and styrene and carcinogenic compounds such as benzene, polycyclic aromatic hydrocarbons and dioxins [5]. In addition to the deaths, fires have also caused around 11,471,000 recorded cases of diseases in 2002.

Even in institutions as respected and trusted as hospitals, fire disasters can occur, causing damage to people, buildings, critical infrastructures such as electrical systems and fuel supply, hospital equipment and medical stocks. The likelihood of a fire occurring in a building can vary with the functions occurring in the building [16]. Therein, it can be deduced that hospitals run a high risk of fires occurring in their buildings as they contain substantial quantities of combustible material such as flammable chemicals and medical gases, electrical generators and large networks of electrical wiring. This can be evidenced by past fire disasters that occurred in hospitals around the globe. The 2008 fire in the Royal Marsden Hospital in London caused the entire hospital to be evacuated from the buildings and also caused damage worth 500 million Great British Pounds [2]. The 2011 hospital fire in AMRI hospital in Calcutta, India caused 89 deaths [15, 18] while in 2013, the fire in the Ramenskyon Psychiatric Hospital in Moscow, Russia caused 38 deaths [21]. A fire in 2018 in the Sejong Hospital in South Korea caused 37 deaths, mainly from smoke inhalation and caused another 130 persons to be injured [6].

With the introduction of frameworks such as the Hyogo Framework in 2005 and its successor, the Sendai Framework in 2015, many institutions including hospitals, have come to understand the need for concepts such as Disaster Risk Reduction (DRR) and Build Back Better (BBB) [1]. As such, hospitals globally, have begun to operate programs such as risk assessments of the hospital, disaster training of hospital staff and disaster and emergency management [10, 12, 13, 24]. Disaster management can't be described as a linear process as it is continuous and therefore can be depicted as a cyclic process consisting of the phases prevention, preparedness, response, mitigation and recovery [3].

When dealing with DRR, it is necessary to give equal importance to the recovery process. When hazards occur, it is not always possible to prevent disastrous results affecting the community. Therefore, being prepared to take the necessary action after the disaster is mitigated is also a significant part of the DRR process.

When specifically considering fire disasters in hospitals, it can be clearly reasoned that the extinguishment of the fire will not end the work that is needed to be done to prevent more loss and damage to the hospital. This study seeks to compile a list of post-disaster activities that need to be conducted after a fire has occurred in a hospital in order to Build Back Better.

2 Post-disaster Frameworks

A disaster is most often a sudden and unforeseen event, which overwhelms local capacity and requires external assistance. These events can cause significant damage, destruction and human suffering [9]. Administrators often find that working to recover from a disaster can be a challenge, as there is much greater pressure on them than during a non-disaster period. This is due to factors such as the need for rapid reaction and quick results, media attention, and the involvement of external stakeholders such as local and international aid agencies. This pressure can be increased when there is also a lack of experience and capacity in handling the work amount necessary [3]. Complete recovery from the disaster will include restoration of not only the physical structures but also the social stability of the affected community. Recovery after a disaster includes a large range of activities and these work for recovery and coordination can be categorized into the following modules; Institutional arrangements for recovery, Post-disaster needs assessment, Recovery planning, Managing recovery, Building Back Better and managing residual risks and Resource mobilization [3].

It is understandable that the method of disaster recovery can vary considering the factors relevant to each disaster, such as the type of disaster, its impacted population and the significance of the damage on persons and properties. The guide to developing disaster recovery frameworks published by the GFDRR has its own separate modules that can be customized to suit the needs of the target audience. These six modules can be named as follows: Conducting post-disaster damage and needs assessment, Policy, and strategy-setting for recovery, Institutional framework for recovery, Financing for recovery, Implementation arrangements and recovery management, and Strengthening recovery systems in governance [9].

The recovery plan which would be successful in the long term would be a plan where the divisions of Finance, Regulation, and Administration work cohesively and concurrently so that all financial, technical and human resources available can be used for recovery, reconstruction and risk management.

It is evident from historical incidents that disasters affect poverty-stricken families much more harshly, effectively paralyzing the production and income of families. In such a case, it is important that low-income victims of disasters are compensated fairly, considering both their injuries and losses as well as their predictable future losses due to the disaster. A major requirement here is ensuring the victims' job stability [22].

Vulnerability to disasters increases due to the weak environment and weak disaster management [14]. In order to build back better, it is important to not just restore the status of the institution to the pre-disaster state but to improve further. An institution's disaster management plan should not be allowed to stagnate but should be constantly improved, by taking lessons from past disasters [24].

According to the Disaster Preparedness and Response Division, Ministry of Health of Sri Lanka, there are several key indicators of the recovery plans of the health sector [14]. They are as follows.

a. The hospital being repaired and functional to their full capacities
b. Reconstruction of hospital structures incorporating disaster resilient features and following the Safe Hospital guideline given by the WHO and PAHO
c. Preparedness of healthcare systems to respond to disasters
d. Having conducted disaster drills
e. Number of households being covered under health insurance schemes.

Post-disaster recovery planning means the development of a number of strategies to bring back the community or institution to where it was before the disaster and continue further to improve its state. These strategies can include the development and implementation of the following; Post-disaster recovery plan, Recovery ordinances, Continuity plan, Post-disaster buildable lands inventories, Utility recovery and reconstruction plans, Temporary shelter plan and Establishment of a coordinating organization and guiding principles for reconstruction [19].

There have been defined Standard Operating Procedures (SOPs) for hospitals themselves regarding emergency and disaster management. It can be seen in these guidelines, that hospitals must be concerned with external disasters occurring outside the hospital in the community as well as disasters that may occur within the hospital [20, 23]. The guidelines themselves are mostly concerned with the preparedness for disasters in hospital and are less descriptive regarding the recovery stage and the activities to be done. However, post-disaster follow-up and critique of actions during disasters have been mentioned to be a critical path of disaster management in hospitals [17]. This includes event analysis and incident reporting [11]. There are three main goals regarding protection from fire in hospitals, safety of life, protection of property, and continuous operation of the facility [11]. Disaster management in hospitals, which are institutions with already complex work, becomes even more complex [4]. Therefore, the actions taken must be careful, thorough and well-planned.

3 Methodology

The aim of this study was to develop a compilation of activities that can be proposed for a post-disaster situation after a fire has occurred in a hospital. As part of the study, fire safety and management in nine governmental hospitals in Sri Lanka were studied. These hospitals included various tiers of government hospitals in the country, starting from Tertiary hospitals such as District General hospitals and Teaching hospitals to Secondary hospitals such as Base hospitals and Divisional hospitals and Primary medical care units.

In considering the post-disaster stage of a hospital in the case of a fire hazards, the following factors were identified through the hospital survey.

a. Aspects of hospitals that could suffer losses from fire hazards such as patients and staff, equipment and infrastructure.
b. Essential areas of management in a post-disaster situation in a hospital such as patient handling and patient care.

c. Stages of a fire hazard in a hospital and probable effects in the hospital from each level of hazard.
d. Short-term and long-term effects from a fire hazard in a hospital.

Along with the exposure gained through these surveys, a thorough literature review and peer discussions were done to compile a comprehensive and thorough list.

In this compilation, the categorization of activities was partially adopted from the Hospital Safety Index (HSI) Guide [24], where the major modules are structural safety, non-structural safety, and emergency and disaster management. Fire hazards can affect people and property. In hospitals property can be divided into three as buildings and critical infrastructure systems, equipment and materials. Post-disaster activities for a fire hazard will be needed for people and property both. There will also be management activities needed to be done to manage to aftermath of the disaster. The categorization for the activity list for post-disaster fire situation was done as follows.

1. People
2. Buildings and critical infrastructure systems
3. Equipment
4. Hospital material stores
5. Post-fire managerial and administrative work.

It was also deduced that the number and type of activities would differ according to the impact and magnitude of the fire. Therefore, the next part of the study included analyzing how to assign the activities according to the impact of the fire and the aspects of the hospital which could be affected by the fire.

4 Compilation of Proposed Post-Disaster Activities After a Fire in a Hospital

As mentioned earlier, fires in hospitals can leave devastating results, and after the fire is extinguished, there remains a number of actions that must be taken, in order, to first, prevent damage that has occurred from spreading further. Next, action must be taken so that the recovery of the hospital is efficient and comprehensive, where the concept of Build Back Better (BBB) is fully adopted.

A disaster such as a fire can affect various aspects of the hospital. We can categorize the aspects that be affected into four major areas; people, buildings and critical infrastructure systems, equipment and material stocks in the compilation of the activity list, each of these four aspects has been considered and activities that will be needed for each aspect of the hospital have been described.

4.1 People

When considering the people in hospitals, it must be realized that there are various types of people within a hospital. They include hospital patients, patient' visitors and hospital staff such as medical staff, supportive staff, administrative staff, and external service providers [12, 13]. After the fire, it is important that all persons who were in the fire-affected area are given a thorough medical examination, including those who do not show any physical trauma. This is because, in the occurrence of a fire, in addition to being burned, a person can be negatively impacted due to the bi-products of fire such as smoke and soot [8]. After the fire, it is important to confirm the safety of the affected area and do necessary investigation and cleanup before letting people come back into the buildings. Sometimes, the evacuated persons will have to be moved to another building in the area, or to another hospital entirely. In any case, there should be arranged a place of shelter where the evacuated persons can stay until a permanent arrangement is made. As there could be a need for hospital patients and victims of the fire to be transferred to another hospital, transportation systems such as ambulances from the hospital should be prepared to be used if necessary.

During the initial medical examination, the affected persons will be identified. After providing emergency medical care, the victims of the fire must be admitted for further medical care. This could be done in the same hospital if possible, or in the next nearest hospital that can provide sufficient medical care. Similarly, any hospital patients who were evacuated during the fire should be similarly transferred to another area of the hospital, which was unaffected by the fire, or to the nearest hospital which can fulfill the medical requirements of the patients.

A large disaster can cause a situation where there will be people missing after the fire. In this case, first, a list of all people missing must be compiled by the hospital administration staff in cooperation with relevant authorities such as the police force and the firefighting department. Search operations for the missing persons should be arranged and conducted.

In some cases, victims may be found deceased. In this case, usually, most countries' police force or other relevant authorities have a process of action that must be taken. In general, the following work must be done; the deceased victims should be identified, if possible, and after possible investigation on the site of the fire has been concluded, the deceased victim must then be transferred to an examination area to perform an autopsy. After the investigative and medical work has been concluded, the body may be released to the deceased's family [7].

Another action that must be taken is to recruit staff in order to replace any staff member who might have been affected by the fire and will be needing some recuperating time [24].

Finally, there is some long-term recovery-related work that needs to be done, for the people who were affected by the fire as well as for their families. In addition to suffering from injuries and loss of property, they may also suffer from loss of income revenue due to the losses incurred. Therefore, it is necessary that the hospital provide compensation to the victim or the victim's family. For the fire-impacted persons, who

are seeking to claim from personal insurance policies, the hospital should be efficient in arranging the necessary documentation for the insurance companies. Finally, as to ascertain the wellness of the affected populations' emotional stability, the hospital should arrange and offer counseling for the people.

4.2 Buildings and Critical Infrastructure Systems

As mentioned before, it is unwise to enter the fire-affected buildings immediately after the fire has been extinguished. The buildings that were affected directly by the fire as well as indirectly through the bi-products of fire like smoke should be given an initial check to confirm whether the area is safe to be entered. This should be done by a trained professional such as a firefighter. The critical infrastructure systems in the affected area should also be checked to ensure that the extinguished fire would not cause cascading disasters through the systems. These systems will include electrical, water supply, medical gas, fuel supply, heating, ventilation, and air conditioning, waste management and elevator systems. Another action that must be taken is to clear the paths and routes within the hospital that may have been blocked during the fire, so that patient translocations that are needed can be done easily and safely.

In case of severe damage, the next step is to contact the insurance agency of the hospital. This step is to be taken if the hospital has been insured. The damages in the affected area must be assessed by the responsible authorities such as the insurance agents, firefighters, and police officers. The assessed damages must thus be documented. After the assessment and documentation have been completed by all parties responsible, the affected area should be thoroughly cleaned up, which will include the toxic products that will have been left by the fire, like toxic gases, smoke, and soot.

Before the fire-affected area of the hospital can rebegin to operate, the necessary retrofitting and reparation of damages can be done. This should be planned methodically and thoroughly.

During the fire, fire detectors and fire alarms, firefighting equipment such as sprinkler systems and fire hose reels and portable fire extinguishers could have been used. Afterward, the hospital should take care to replace any fire extinguishers used. Also, all the systems including fire detection and alarms and sprinkler systems should be assessed and any damage incurred should be repaired as soon as possible.

4.3 Hospital Equipment

Hospitals have many kinds of equipment, including medical equipment, laboratory equipment and other equipment such as kitchen equipment. If the fire-affected area has any type of equipment present, certain steps should be taken. First, equipment in

the area should be checked to see if any damage has been incurred during the fire. If so, the hospital must contact the insurance agency if the equipment has been insured.

The damage to the equipment should be assessed and documented and necessary reparations or replacements of the equipment should be done.

4.4 Hospital Material Stores

Hospitals are required to have storage spaces for various items. Usually, there are general supply stores, medical stores, surgical equipment stores, blood banks and other miscellaneous item stores (recycle items storage, kitchen supply storage, etc.). In the occurrence of these storage spaces being affected by the fire, the following actions must be taken. An initial check must be carried out to assess if any serious damage has been caused by the fire. If the damaged store items have been insured, the insurance agency must be contacted and notified. Then the damage should be assessed and documented and finally, the stores must be restocked if needed.

4.5 Post-fire Managerial and Administrative Work

It is important, that after any type of disaster, the administration takes action so that the institution is not only restored to its pre-disaster status but improved even further. Here, the paper discusses the summary of the actions that the hospital's administrative division should take so that in the future, the hospital's resilience is increased through principles of Build Back Better (BBB).

As soon as possible after the fire is extinguished, the fire-affected areas must be secured until the investigative and restorative work is completed. The police force must be contacted, and the cause of fire should be investigated.

Working with media institutions is an important part of post-disaster recovery. In order to prevent the propagation of misinformation and unnecessary panic, it is important that the administration of the hospital prepare and present a statement regarding the fire disaster to the media at the earliest possible time.

Another important factor is the continuity of the administrative work after the fire. In case the fire caused administrative office facilities to be affected, temporary office facilities should be arranged until restorative work is completed.

A vital element of post-disaster activities is the Disaster Recovery Plan (DRP). The administration should prepare a customized DRP, put it into operation and monitor and evaluate the outcomes. After a disaster, institutions have to be prepared to manage donations and other kinds of funding that will come through to the institution. The management of the funding flow should also be included in the disaster recovery plan.

The next significant item of action is the updating of the hospital disaster management plan. In order to BBB and increase resilience, it is important that the disaster

management plan is updated from the "Lessons Learnt" from the past disasters that occurred. It is therefore important to review the actions of the hospital staff during the fire and analyze the weaknesses of the current action plan. Thereby, the hospital disaster management plan can be reviewed and modified to better suit the institution.

4.6 Summarization of the Proposed Activity List

The developed list of proposed activities to be conducted after a fire disaster occurs in a hospital is has been summarized in tabulated form in Table 1.

5 Discussion

Although the compiled list of activities is vast and comprehensive, it must be realized that not all of the activities will be needed to be done in each and every occurrence of a fire hazard. As we can see in Fig. 1, the area affected by fire can depend on the time taken to stop the fire. If the time taken to extinguish the fire increases, the fire can spread from point of origin to the complete room and adjacent rooms to the other floors in the building and then to other buildings in the vicinity. With the level of impact, the impacted aspects of the healthcare institution can vary.

A fire can be extinguished almost immediately after it starts, resulting in no losses being incurred on any people, buildings or equipment. There can be some instances, where no people are harmed, but the equipment is severely damaged. There can also be instances where a large portion of the hospital is damaged, meaning there are losses incurred in all aspects of the hospital.

In Figs. 2, 3, 4, and 5, it has been identified how the activities needed to be done after varying levels of impacts of fire can be chosen from the list that has been compiled.

6 Conclusion

Fire hazards, unlike natural hazards, can be prevented from occurring, through good practices of fire safety and fire risk management. An aspect of good fire risk management is incorporating lessons learned into the overall risk management plan.

However, there will be instances wherein spite of all precautions, a fire can occur in a hospital, causing the need for post-disaster action to be taken. Therefore, the presence of an action plan for post-disaster recovery is necessary, especially for a large institution such as a hospital.

The aspects that be affected by a fire hazard in a hospital include people, buildings and critical infrastructure systems, equipment and material stores. These effects

can be short-term or long-term and therefore, the hospital administration must be prepared to deal with both kinds of effects. In addition to handling the negative effects on these aspects, the hospital will need to deal with other stressful activities such as communication with media and recovery fund raising work. As mentioned in literature regarding post-disaster frameworks, recovery planning is an important aspect in

Table 1 Proposed post-disaster activities to be conducted in a hospital after a fire

People	Building and critical infrastructure systems
A 1. Provide medical attention to all persons who were in the affected area 2. Provide a shelter space for all persons who were evacuated from the affected area **B** 3. Arrange transportation systems such as ambulances in preparation to transfer patients **C** 4. Admit the victims affected by the disaster a. To the same hospital if suitable b. To the next hospital which fulfils the medical requirements of the patients **D** 5. Transfer the evacuated patients a. To an unaffected part of the hospital if suitable b. To the nearest hospital which fulfils the medical requirements of the patients **E** 6. Provide compensation to victims affected by the fire or the victims' families 7. Provide validating documentation for victims claiming personal insurance 8. Arrange counselling for disaster victims **F** 9. Identify missing persons 10. Arrange search operations for missing persons **G** 11. When a victim is found diseased a. Identify victims (if possible, through visual inspection) b. Conduct onsite examination of the body c. Transfer the body to an examination area d. Perform autopsy e. Release body to victims' families **H** 12. Mobilization and recruitment of new hospital staff	**I** 1. Conduct initial check by trained professionals to confirm whether the area is safe to enter 2. Conduct check of infrastructure systems to confirm operational capability a. Electrical systems b. Water supply systems c. Medical gas supply d. Fuel supply e. HVAC system f. Waste management systems g. Elevator systems 3. Clearing paths and routes within the hospital **J** 4. Contact hospital insurance company 5. Assess damages and document the damages **K** 6. Clean area affected by the fire and dispose of toxic products of the fire **L** 7. Retrofitting and reparation of damages in the affected area **M** 8. Restock the equipment used for fire fighting

(continued)

Table 1 (continued)

People	Building and critical infrastructure systems
Hospital Equipment	**Hospital Material Stores**
N 1. Initial check to see whether the equipment is damaged or safe to use **O** 2. Contact insurance company 3. Assess the damage of the equipment 4. Reparation or replacement of damaged equipment	**P** 1. Contact insurance company 2. Assessment of damage 3. Restock stores if needed
Post-fire Managerial and Administrative Work	
1. Secure the areas affected by the fire until restoration is completed 2. Contact Police and start the investigation of the fire and its cause of origin 3. Prepare and present a statement regarding the disaster event to the media 4. Provide temporary office facilities in case administrative buildings are affected 5. Disaster recovery plan a. Prepare plan b. Operate the plan c. Monitor and evaluate outcomes 6. Hospital disaster management plan a. Review hospital actions during the fire b. Deduce weaknesses in the current plan of action c. Review the plan of action during a disaster and modify 7. Manage funding and donations given for reparations	

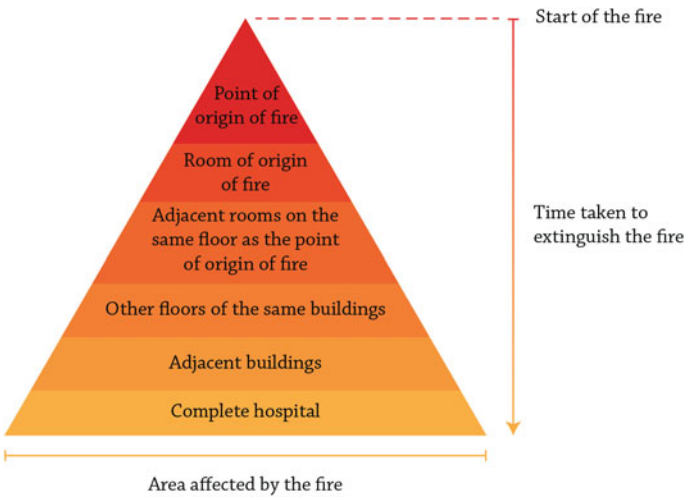

Fig. 1 Variation of the impact of fire with time

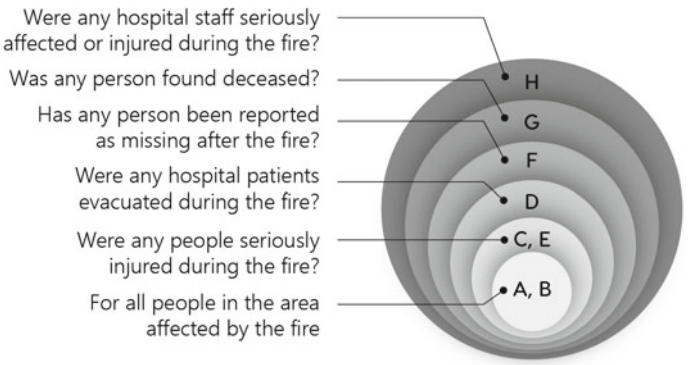

Fig. 2 Activity categorization according to the level of impact on people

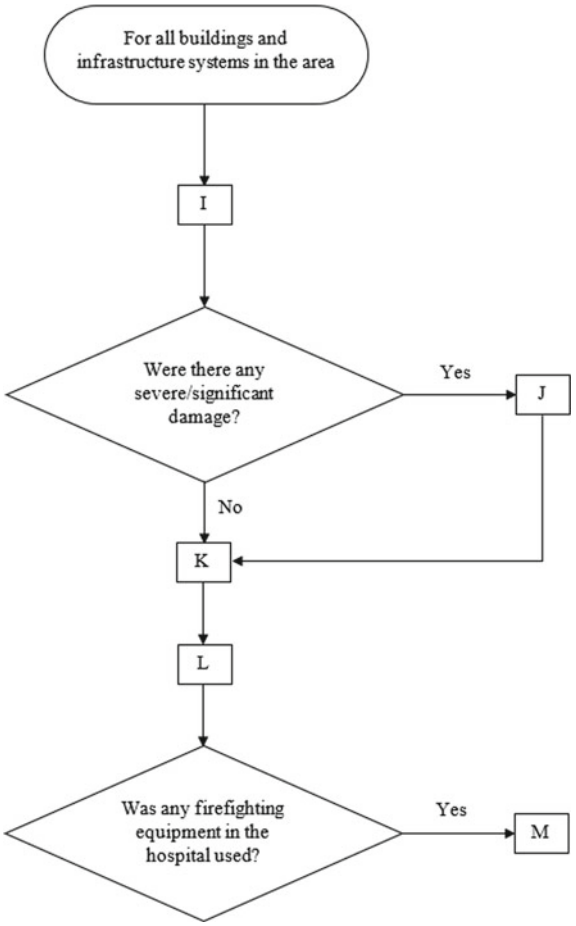

Fig. 3 Activity sequence for buildings and critical infrastructure in the fire-affected area

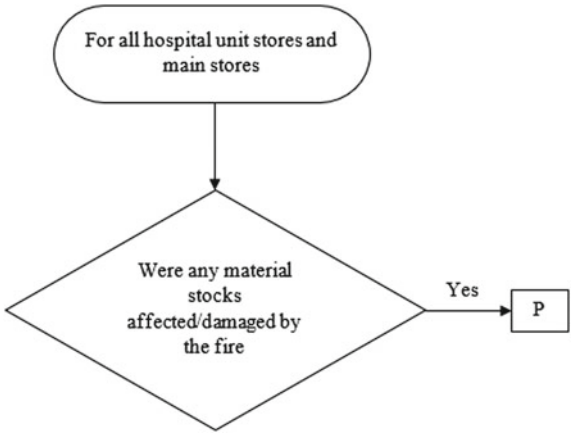

Fig. 4 Activity sequence for material stores in the fire-affected area

Fig. 5 Activity sequence for equipment in the fire-affected area

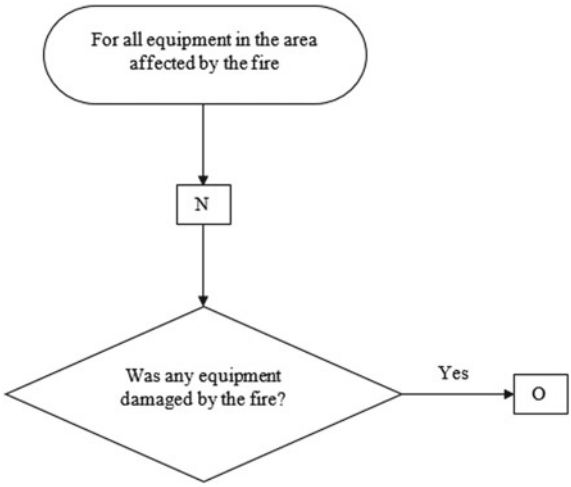

disaster recovery. When a healthcare institution has a prepared basic recovery plan ready at the time of the disaster, the recovery planning phase in the post-disaster stage can be completed quickly and recovery can be accelerated.

It must be noted that the results of each fire hazard can be different and therefore, the recovery plan for each hazard must also be different. With this developed list of criteria, it is hoped that healthcare systems can use the list as a foundation on which to build a comprehensive and customized criteria list according to the nature and scale of the fire hazard that has occurred.

This study is part of a larger project in building a fire risk management framework for hospitals for the Sri Lankan aspect. The next step in this study is to validate this compiled list of activities through an expert opinion survey.

Acknowledgements The authors would like to thank the Disaster Preparedness and Response Division of the Ministry of Health, Sri Lanka for their help in this project as well as the staff of the hospitals that were studied for their help and cooperation.

References

1. Aitsi-Selmi A, Egawa S, Sasaki H, Wannous C, Murray V (2015) The Sendai framework for disaster risk reduction: renewing the global commitment to people's resilience, health, and well-being. Int J Disaster Risk Sci 6:164–176. https://doi.org/10.1007/s13753-015-0050-9
2. Allen N, Cockroft L, Borland S (2008) £500m Royal Marsden blaze cripples services
3. Arenas A, Missal R, Mellucci C, Murshed Z, Vatsa K, Trujillo M, Olson L (2016) National post-disaster recovery planning and coordination. United Nations Development Programme (UNDP), New York
4. Belmont E, Fried BM, Gonen JS, Murphy AM, Sconyers JM, Zinder SF (2006) Emergency preparedness, response & recovery checklist beyond the emergency management plan. In: Hospital preparation for bioterror. Elsevier, Amsterdam, pp 295–331. https://doi.org/10.1016/B978-012088440-7/50026-4
5. Blomqvist P (2005) Emissions from fires, consequences for human safety and the environment. Doctoral thesis, Lund University
6. British Broadcasting Corporation (2018) Dozens die in South Korea hospital fire. BBC News
7. Corbitt-Dipierro C (n.d.) Fatalities at the fire scene: simple steps for strong results [WWW Document]. Inter Fire Online. URL: https://www.interfire.org/features/fatalities.asp. Accessed 11.8.19
8. Federal Emergency Management Agency (2019) After the fire
9. GFDRR (2015) Guide to developing disaster recovery frameworks. Global Facility for Disaster Reduction and Recovery (GFDRR)
10. Hasalanka HHH, Siriwardana CSA, Wijesekara NWANY, Kodituwakku KALC (2018) Development of a tool to assess structural safety of Sri Lankan hospitals under disaster conditions. Presented at the International Conference on Sustainable Built Environment, Kandy, Sri Lanka
11. International Finance Corporation (2017) Good practice note—OFC life and fire safety: hospitals
12. Kularatne D, Siriwardana C, Hasalanka H (2019) Evaluating the applicability of the "Hospital Safety Index Guide" for the Sri Lankan context. In: 2019 Moratuwa engineering research conference (MERCon). Presented at the 2019 Moratuwa engineering research conference (MERCon). IEEE, Moratuwa, Sri Lanka, pp 406–411. https://doi.org/10.1109/MERCon.2019.8818932
13. Kularatne WDM, Siriwardana CSA, Hasalanka HHH (2018) Investigation of emergency and disaster management of hospitals in Sri Lanka; a pilot study. Presented at the International Conference on Sustainable Built Environment, Kandy, Sri Lanka

14. Ministry of National Policies and Economic Affairs, Ministry of Disaster Management (2017) Post-disaster recovery plan for the floods and landslides of May 2017
15. NDTV (2011) Kolkata: 89 killed in AMRI hospital fire; six board members arrested [WWW Document]. NDTV.com. URL https://www.ndtv.com/india-news/kolkata-89-killed-in-amri-hospital-fire-six-board-members-arrested-566913. Accessed 11.8.19
16. Nimlyat PS, Audu AU, Ola-Adisa EO, Gwatau D (2017) An evaluation of fire safety measures in high-rise buildings in Nigeria. Sustain Cities Soc 35:774–785. https://doi.org/10.1016/j.scs.2017.08.035
17. Occupational Safety and Health Administration (2008) Hospitals and community emergency response: what you need to know
18. Pal I, Ghosh T (2014) Fire incident at AMRI Hospital, Kolkata (India): a real time assessment for urban fire. J Bus Manag 3:6
19. Partnership for Disaster Resilience (2007) Post-disaster recovery planning forum: how-to guide. University of Oregon's Community Service Centre, Oregon
20. Spieler SS, Singer MP, Cummings L (2008) Emergency preparedness in public hospitals
21. The Guardian (2013) Moscow psychiatric hospital fire kills 38. The Guardian
22. United Nations Development Programme (2011) Methodological guide for post-disaster recovery planning processes. United Nations Development Programme, Ecuador
23. United Nations Development Programme (2008) Guidelines for hospital emergency preparedness planning
24. World Health Organization, Pan American Health Organization (2015) Hospital safety index guide for evaluators, 2nd ed. World Health Organization
25. World Health Organization (WHO) (ed.) (2004) Changing history. The world health report, Geneva

Development of a Hospital Safety Assessment for Tsunami in the Sri Lankan Context

H. H. H. Hasalanka, C. S. A. Siriwardana, and W. D. M. Kularatne

Abstract In the context of disasters, hospitals act as a safe place for both patients, victims and several other stakeholders. The 2004 Indian Ocean Tsunami could be identified as one of the most disastrous events which significantly impacted the coastal region in Sri Lanka. Many infrastructure and buildings were affected and destroyed due to the extremity of the event including hospitals located in the coastal line. Hence, it is necessary to assess the level of safety of existing hospitals in the coastal region in the event of a tsunami. Therefore, a hospital safety assessment tool should be developed for Tsunami under the Sri Lankan context. Since, the structural condition of buildings, functional and operational aspects, as well as the emergency management aspects, are vital to ensure the safety of hospitals under tsunami, all of these were included in the assessment tool. The most cost-effective and efficient method to obtain the level of structural safety of hospitals is the Rapid Visual Screening (RVS) method. It is because the safety level could be obtained through a sidewalk survey. In other words, the level of safety could be obtained with the RVS method through visual observations with the naked eye, without using any equipment. Also, the functional, operational and emergency management aspects could also be easily assessed through observations, reviews of documentation and structured interviews. As the developed assessment tool is expected to be used to assess the level of safety of existing hospitals, the Rapid Visual Screening (RVS) method along with the reviews of documentation and the methods of structured interviews were adapted to the assessment tool. As the initial step of developing the assessment tool, an attribute list was developed considering the available literature. For RVS structural safety assessments, the Papathoma Tsunami Vulnerability Assessment (PTVA) model and FEMA guidelines are widely used. Among these two guidelines, the PTVA model is specifically developed for tsunami while FEMA guidelines are developed for cyclones, seismic activities, floods, etc. Furthermore, the Hospital Safety Index (HSI) guide published by the World Health Organization (WHO) includes a comprehensive assessment tool related to functional, operational and emergency management categories. The developed attribute list was used to assess selected hospitals in the southern coast of Sri Lanka, in order to obtain the

H. H. H. Hasalanka (✉) · C. S. A. Siriwardana · W. D. M. Kularatne
University of Moratuwa, Katubedda 10400, Sri Lanka
e-mail: hhhhasalanka@gmail.com

R. Dissanayake et al. (eds.), *ICSECM 2019*, Lecture Notes in Civil Engineering 94,
https://doi.org/10.1007/978-981-15-7222-7_18

applicability of the developed attributes. This paper discusses the development procedure of the initial attribute list to assess the level of safety of a hospital in Sri Lanka under a Tsunami. After that, a comprehensive assessment tool could be developed through the feedback obtained through the study along with the experts' opinions.

Keywords Hospital safety · Tsunami · Hospitals · Coastal region · Rapid visual screening

1 Introduction

Hospitals are identified as one of the major service units in society and therefore the safety of hospitals is significantly important [1, 2]. The World Health Organization (WHO) has identified this need and has developed a safe hospital guideline to assess the level of safety of hospitals with the collaboration of Pan American Health Organization (PAHO) [17]. This guideline consists of hazard identification, structural safety, non-structural safety, and emergency and disaster management. This was developed for the Latin American context where earthquakes and cyclones were considered as the mainly occurring hazards under structural safety. Hasalanka et al. [1, 2] and Kularatne et al. [3] discuss the limitations of the above guideline when applying in the Sri Lankan context and its adaptability [1–3].

Sri Lanka is one of the countries that provide free healthcare services to the community. There are 1736 governmental healthcare facilities in the country including National Hospital (NH), Teaching Hospitals (TH), Provincial General Hospitals (PGH), District General Hospitals (DGH), Base Hospitals (BH), District/Divisional Hospitals (DH) and Primary Medical Care Units (PMCU). These hospitals are exposed to different types of hazards based on their location [1]. Among them, the hospitals located in the coastal region are exposed to Tsunami and storm surges. During the 2004 Indian Ocean Tsunami (IOT), many of the infrastructures were completely or partially destroyed including hospitals such as TH Mahamodara. In the case of hospitals, not only the hospital building but the functionality was affected as well including critical areas such as theatres, maternity units, etc. and the critical systems such as water supply system, HVAC system, and transportation system. Even though the return period of a tsunami is higher, the impact of the event is extremely high. Apart from that, the storm surges are constantly affecting the infrastructure in the coastal region which includes the hospitals. Therefore, when considering the safety of hospitals in the coastal region, integration of the structural safety of the building as well as the safety of critical areas and systems along with emergency planning should be considered. In order to identify the existing level of safety of hospitals in the coastal region against tsunami and storm surges, a method of assessment is required which discusses the above-mentioned areas.

Apart from the Safe Hospital guideline developed by the WHO and PAHO, there are other guides and models developed in order to assess the structural safety of buildings with respect to various hazards. FEMA guidelines [4–6] and PTVA-4 model

[7] could be identified as the most widely used guides for assessing the structural safety of buildings. FEMA guidelines were developed for earthquakes, floods, fire, cyclones, etc. whereas the PTVA model was specifically developed for Tsunami. The specialty of all these guidelines is that they are applicable to assess the level of structural safety of existing structures by means of Rapid Visual Screening (RVS). This is a sidewalk survey method where the safety level could be evaluated through visual observations without using any equipment. This method is widely used to assess the structural safety of buildings where a basic idea about the existing level of safety could be obtained through a time-saving and cost-effective manner. Each attribute has been given a relative safety score which is known as a basic score that represents the level of safety in a numerical manner and the attributes were given relative importance as weights. Then, the existing level of safety has been presented as a safety score which is the weighted average of basic scores and weights of each attribute.

Papathoma et al. [8] published the initial PTVA method to assess the tsunami vulnerability of building structures through sidewalk surveys. This was published even before the 2004 IOT had occurred. Since then, the original model has been revised several times and the PTVA-4 model [7] was published as the latest version of tsunami vulnerability assessment methods. This model includes structural vulnerability attributes categorized into the building vulnerability and the surrounding vulnerability. These attributes discuss aspects such as the construction material, soil type, building orientation, perimeter walls and fencing, and movable objects, which illustrate the building and surrounding characteristics that make buildings vulnerable to tsunami. In Sri Lanka, several studies have been carried out related to the topic of tsunami vulnerability of buildings, after the IOT occurred. Researchers have demonstrated the lessons learned from the Tsunami damage in Sri Lanka where the structural damages caused by, 2–5 m high wavelengths from the foundation level, under static and dynamic loads were described [9]. Under that, the necessary specifications that single storey buildings, multi storey structures, water tanks, boundary walls should include and the effect on transportation infrastructure were addressed. Dias et al. developed the tsunami vulnerability functions for single storey unreinforced masonry residential structures using the Monte Carlo simulation for Sri Lanka [10]. Then the vulnerability curves were developed to represents the damage percentage with respect to the submerged height. Bandara and Dias developed a method to include the wave loading at the design stage of structures in the coastal region [11]. Velocity of waves, hydrostatic pressure generated, hydrodynamic pressure, impulsive pressure and other possible forces were considered in developing this method. Apart from that, the National Building Research Organization (NBRO) published a hazard resilient housing construction manual [12] which includes the structural requirements to make a single storey or two storey house resilient against Tsunami.

All the above-mentioned guides, models and publications include structural vulnerability measures of building structures and additionally the WHO and PAHO Safe Hospital guideline contains the functional, operational and emergency management measures specifically developed for hospitals. In this research, it is intended to

identify the attributes through the above-mentioned literature, field experience, and experts' opinion, in order to assess the safety of hospitals in the coastal region in Sri Lanka in the event of a tsunami. The main aim of this study is to identify the key parameters that describe the safety of hospitals under structural safety, functional safety and emergency and disaster management preparedness, in the Sri Lankan context.

2 Methodology

This paper contributes to the Disaster Risk Reduction (DRR) process of hospitals in Sri Lanka, considering tsunami. Moreover, the intention of this paper is to develop an attribute list that shows the level of safety of hospitals in the country, considering the occurrence of a tsunami. Since the existing hospitals are to be assessed, the RVS method is preferred for assessments, as it is a more cost-effective and time-efficient way to obtain the level of safety of hospitals. Furthermore, the outcome of such an assessment justifies the need for thorough analysis whenever needed.

For the development of the attribute list, a comprehensive literature survey was carried out and the findings were combined with experts' opinions and the field experience obtained through the visits of selected hospitals situated on the southern coast in Sri Lanka. In the expert opinion survey, the experts in the structural engineering field, medical field and emergency and disaster management field were interviewed for their opinions. Field experience was gained through pilot surveys done in six hospitals, namely; TH Mahamodara, DGH Matara, BH Balapitiya, BH Tangalle, DH Unawatuna and PMCU Mirissa. These hospitals were selected by considering the distance from the coast, elevation from MSL, the effect from the 2004 IOT and also considering a proper representation across the types of governmental hospitals in Sri Lanka. The respective distances from the coast and their status during the IOT are mentioned in Table 1. These field surveys were carried out in order to observe the specific safety measures in a hospital under the structural, functional and emergency and disaster management aspects.

Table 1 Details of hospitals surveyed in the southern coast of Sri Lanka

Hospital	Distance from the coast (m)	Status during the 2004 IOT
TH Mahamodara	140	Highly affected
DGH Matara	600	Slightly affected
BH Balapitiya	220	Not affected
BH Tangalle	400	Not affected
DH Unawatuna	850	Not affected
PMCU Mirissa	160	Moderately affected

The attribute list has been mainly divided into structural safety, functional safety, and emergency and disaster management. Structural safety criteria include the integration of structural elements that contribute to the load transfer mechanism in buildings as well as the additional structural safety provided by its surroundings. Functional safety section includes the criteria related to the critical systems that are required to function the hospital properly in a Tsunami disaster. Emergency and disaster management criteria include factors that illustrate the level of preparedness of a hospital against a Tsunami.

The structural safety is sub-categorized into the building attributes and hospital attributes as in the PTVA-4 model. Along with the applicable attributes given in the PTVA-4 model, necessary specific attributes for hospitals in Sri Lanka have been included in the structural safety section according to the expert's opinion and the field surveys. Building attributes include the specific structural measures of the structural elements in a building. Since most governmental hospitals in Sri Lanka are most commonly found as a group of buildings, the structural safety measures related to a group of buildings are included in the hospital attributes. This section is expected to be applied for each building to obtain the level of structural safety. The functional safety section includes all the necessary critical systems that are required for the functioning of the hospital. All the necessary emergency planning procedures and capacity measures of the hospital will be included in the emergency and disaster management section. The summary of the methodology is shown in Fig. 1.

The development procedure of the attribute list is to be discussed hereafter.

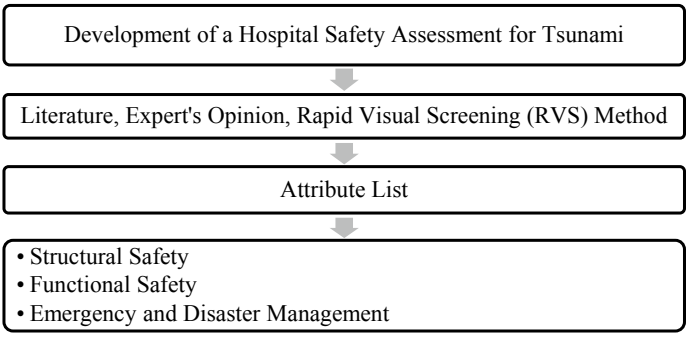

Fig. 1 Summary of the methodology

3 Development of the Attribute List

3.1 Development of Structural Safety Attributes

Under this section, the integrity of structural elements of buildings and the structural condition of them along with the structural safety measures provided by the surrounding are discussed.

3.1.1 Attributes Related to a Building

In this section, the structural integrity of the structural elements of buildings is thoroughly discussed. This is the ability of structural elements to deal with the design loads without failure and to hold together as an integral part.

Buildings are subjected to overturning or sliding in a tsunami due to the lateral loads created by hydrostatic pressure, hydrodynamic pressure as well as the impulsive action [9, 11]. Higher the number of storeys in a building increases the weight of the structure, thus, the sliding and overturning may reduce.

Under the aspect ratio, the ratio of the see facing side to the other side is considered. Safety against tsunami loads increases as the aspect ratio lowers. It is preferred that the shorter side of the building faces the direction of the sea, as it will lower the aspect ratio considered here. It is also recommended that the aspect ratio be less than 3 [12].

The ratio between the area of openings in the sea-facing direction and the wall area in the sea-facing direction is considered as the void ratio [12]. This is to reduce the impact on the structure from tsunami impact action by allowing water to flow through the structure [7]. Therefore, it is ideal to keep the ground floor free from the critical units in a hospital and place them on the upper floors if the hospital under the consideration is situated in a tsunami-prone location. The level of safety will increase with the increase of the void ratio.

If the elevation of buildings is not regular, stress concentrations may be generated and also overturning can take place during the impact of a tsunami [17]. Thus, it is preferred that the elevation of buildings be geometrically regular.

If the short columns are present, they will be subjected to excessive damages as the stiffness is higher. Under the impulsive action of a tsunami, these columns will absorb a higher amount of energy and thereby, eventually lead to failure. It is preferred that no short columns are present.

Reinforced concrete framed structures are preferred for the structural system as the structural stability is much higher in this case with respect to masonry structures [7]. Furthermore, the structure would be tied down to the foundation which will resist the pulling and overturning action against tsunami [11, 17]. Along with that, it would provide the necessary protection against storm surges as well. Reinforced concrete columns with masonry infills are more common in Sri Lankan hospitals and these structures are more stable than the masonry structures.

As tsunami and storm surge exert an excessive lateral load on the structure, a proper lateral load resisting mechanism should be there to resist that [9, 11]. Shear walls, staircases, and infill masonry walls behave as such where shear walls are much better than the others.

The coastal region is highly exposed as far as the hazard of tsunami is concerned. Along with that, high winds can make a huge impact on the structures nearby, making roof structures highly vulnerable, as they are located at a higher elevation, lightweight, and contains sharp corners and eves [12]. Thus, the structural integrity of roof structures should be taken into consideration under this study [17].

Plinth beams will ensure the structural integrity of the elements in the building and also will avoid the propagation of cracks to the superstructure in case there is a movement at the foundation level. Since scouring occurs during a tsunami, it can cause the foundation to be deformed or settled. Thus, the integration of the elements such as columns through plinth beams is very important to the structural safety of the buildings.

It is necessary that the building structures are being held tightly to the ground by preventing sliding and overturning at the same time the load is being transferred to the ground without settling down. Therefore, the foundation has significant importance towards the safety of the structure against any type of hazard [7]. However, the scouring during a tsunami could lead to a failure in the foundation. Thus the type of foundation will contribute to the level of structural safety of buildings.

Even though a building is built as a reinforced concrete framed structure, if the reinforcements are exposed and there is a significant amount of deterioration, the building will not perform as expected. Therefore, the condition of the building must be included as a measure of the structural safety of buildings [7].

Gutter discharge and soil type represent the scouring effect near the foundation. This is necessary for the stability of the foundation [7, 12].

Shielding from surrounding buildings is referred to as the "building raw" by Dall'Osso et al. [7]. This reduces the impact loading induced by the tsunami and therefore it is necessary to be included in the measurement of the structural stability of a building structure.

A governmental hospital, which is usually a group of buildings in Sri Lanka, has many parking spaces near the building structures. Furthermore, there are often container structures present nearby, being used for storage purposes. These objects will be subjected to floating in a tsunami inundation and therefore, the nearby structures could get damaged as a result. Therefore, in a hospital, the availability of large movable objects could be identified as a variable, which increases the vulnerability of nearby structures as the number of objects increases [7].

3.1.2 Attributes Related to a Building Complex (Hospital)

Under this section, the factors applicable to the whole hospital and related to the structural safety of each building are described.

Table 2 Summary of structural safety attributes

Attribute	Obtained from
Number of storeys	Dias [9], PTVA-4 [7]
Aspect ratio	NBRO [12]
Void ratio	NBRO [12], PTVA-4 [7]
Vertical geometric irregularities	WHO and PAHO [17]
Availability of short columns	Field observation
Structural system	PTVA-4 [7], WHO and PAHO [17]
Lateral load resisting system	Dias [9], Field observation
Safety of roof structure	NBRO [12], WHO and PAHO [17]
Plinth beams	NBRO [12]
Safety of foundation	PTVA-4 [7]
Condition of the building	PTVA-4 [7], WHO and PAHO [17]
Gutter discharge and soil type	PTVA-4 [7], NBRO [12], Field observations
Shielding from surrounding buildings	PTVA-4 [7], Field observations
Large movable objects	PTVA-4 [7], Field observations
Protective vegetation and natural barriers	PTVA-4 [7], Field observations
Sea walls	PTVA-4 [7]
Perimeter walls	Field observations

Protective vegetation or any other natural barriers [7] such as mountains can provide shielding to the hospital complex by reducing the level of exposure which will reduce the risk of the hospital against a tsunami.

Sea walls will behave as barriers against tsunami waves by reducing the energy carried with the waves [7]. Therefore, the effect on the buildings nearby will decrease.

As most governmental hospitals in Sri Lanka consist of a group of buildings, there are perimeter walls that provide protection to hospitals. These can behave as barriers against tsunami and provide shielding.

Even though the hospital under consideration is located away from the coastal line, the proximity of waterways connected to the sea could be identified as an important factor, as the hospital could get inundated, due to the flooding of the waterways caused by a tsunami.

The summary of structural safety attributes is shown in Table 2.

3.2 Development of Functional Safety Attributes

This section discusses the necessary measures for the functionality of a hospital that are not related to structural safety, such as services and critical systems.

Table 3 Summary of functional safety attributes

Attribute	Obtained from
Location of critical units	Field observation/Experts' opinion
Power supply system and backup	WHO and PAHO [17]
HVAC system	WHO and PAHO [17]
Water supply system and backup	WHO and PAHO [17]
Fire protection system	WHO and PAHO [17]
Medical gases storage	WHO and PAHO [17]
Fuel reserves	WHO and PAHO [17]

Maternity units, theatres, pediatric units, ICUs (Intensive Care Units), etc. could be identified as the critical units in a hospital, as they shelter a set of most vulnerable patients in a hospital. Since the tsunami is concerned, it is preferred that these critical units are located at a higher elevation. Therefore, the location of critical units should be identified as a measure of the level of risk in a hospital against a tsunami.

Both the condition of the existing power supply system and the availability of backup systems are important factors to the continuing functioning of the hospital as power failures could occur during a tsunami [17].

The HVAC system is necessary for ICUs, theatres, etc. and therefore, the condition of these system units is essential for the functionality of the above-mentioned units in a hospital [17].

The availability of a water supply system and its backup system to satisfy the required demand is a necessary aspect to function a hospital. Furthermore, fire protection systems, medical gas storage, fuel reserves for generators are identified as the necessary requirements for a hospital for better functionality in an emergency. The summary of the functional safety attributes is shown in Table 3.

3.3 Development of Emergency and Disaster Management Attributes

Capacity measures and emergency and disaster management measures that illustrate the level of preparedness of a hospital against the Tsunami disaster, that are necessary for the safety of hospitals are discussed in this section.

Bed Occupancy Rate (BOR) is the ratio between the number of admissions to the number of available beds. When the BOR gets higher than 100%, the risk gets higher as there is an inadequacy of beds in the hospital. Therefore, it is preferred that the BOR is maintained at a lower value than 100%. Furthermore, the population to bed ratio in the country should be kept within acceptable values so that people get the maximum out of healthcare services in the country [13–16].

Along with that, the ratio of medical staff, nurses to the population in the serving region of a hospital interprets the preparedness to provide healthcare services in a disaster and therefore it is necessary to maintain these ratios at an acceptable level [15]. Furthermore, ambulance services are also necessary during emergency situations.

Apart from that, the disaster management trainings, tsunami drills, knowledge of first aid basic life support and first aid advanced life support, availability of evacuation plans, evacuation signs, vertical evacuation methods, and disaster response plans, evacuation route conditions, evacuation shelters, availability of disaster cupboards, adequate drugs backup, preparedness for dead body management, blood reserves could be identified as some key parameters that describe the level of preparedness of a hospital against such disaster [14, 15]. Furthermore, the distance to the next closest hospital and availability of early warning methods would be added advantages towards the emergency and disaster management over a hazard like a tsunami.

The summary of the emergency and disaster management attributes is shown in Table 4.

Table 4 Summary of emergency and disaster management attributes

Attribute	Obtained from
Bed occupancy rate	Munasinghe and Matsui [14], Experts' opinion
Ratio of medical staff/Nurses to the population	Experts' opinion, Annual Health Bulletin of Sri Lanka [15]
Disaster management trainings	Experts' opinion, Munasinghe and Matsui [14]
Tsunami drills	Experts' opinion
Knowledge of first aid basic life support	Experts' opinion
Knowledge of first aid advanced life support	Experts' opinion
Evacuation plans	Experts' opinion
Evacuation signs	Experts' opinion
Vertical evacuation	Experts' opinion
Disaster response plans	Experts' opinion, Munasinghe and Matsui [14]
Evacuation route condition	Experts' opinion
Evacuation shelter	Experts' opinion
Disaster cupboards	Experts' opinion
Drugs backup	Experts' opinion, Munasinghe and Matsui [14]
Preparedness for the dead body management	Experts' opinion, Munasinghe and Matsui [14]
Blood reserves	Experts' opinion, Munasinghe and Matsui [14]
Distance to the nearest hospital	Experts' opinion
Early warning methods	Experts' opinion

4 Conclusion

In this research, the main focus was to identify the key attributes that describe the safety levels of hospitals in Sri Lanka against Tsunami, under the structural safety, functional safety and emergency and disaster management. Under the structural safety, the attributes related to the structural elements in a building as well as the attributes related to the whole hospital (by considering a group of buildings), that improve the structural safety of each building, have been identified. Under the functional safety, the location of critical units, as well as the critical systems, were considered. Furthermore, the emergency and disaster management section consists of attributes related to the emergency and disaster management preparedness and capacity of the hospital in a tsunami. The integration of these attributes in an effective manner would represent the level of safety of the hospital in a tsunami. Therefore, these findings are utterly important towards the development of a framework for risk analysis, disaster preparedness, and response planning, etc. in a hospital located in a tsunami-prone area.

In the development of attributes that describe the safety of hospitals against tsunami in Sri Lanka, all the necessary parameters were identified under the categories of structural safety, functional safety, and emergency and disaster management. By using these attributes, the safety level of a hospital against tsunami could be defined as safety indices. For that, criteria have to be defined for each attribute which shows the level of safety and they should be given respective scores. Then, the relative importance of each attribute can be obtained through an expert survey thus, the weights for each attribute can be defined. After that, the safety indices for under each category of structural safety, functional safety and emergency and disaster management can be obtained in an effective manner.

Acknowledgements The authors wish to thank the Disaster Preparedness and Response Division (DPRD), Ministry of Health, Sri Lanka, for granting permission to access hospitals in the southern coastal line in Sri Lanka. Furthermore, the project HEARTS-SL team and the directors and administrative staff in each hospital are also acknowledged for their immense support throughout the project.

References

1. Hasalanka HHH et al (2019) A framework to develop multi-hazard maps to identify the natural hazards which affect the safety of Sri Lankan hospitals. In: 2019 Moratuwa engineering research conference (MERCon). IEEE, pp 418–423. https://doi.org/10.1109/mercon.2019.8818863
2. Hasalanka HHH et al (2018) Development of a tool to assess structural safety of Sri Lankan hospitals under disaster conditions
3. Kularatne D, Siriwardana C, Hasalanka HHH (2019) Evaluating the applicability of the "hospital safety index guide" for the Sri Lankan context. In: 2019 Moratuwa engineering research conference (MERCon). IEEE, pp 406–411. https://doi.org/10.1109/mercon.2019.8818932

4. Fema P-154, ATC-21 (1988) Rapid visual screening of buildings for potential seismic hazards: a handbook. Applied Technology Council, Redwood City, FEMA 145, January, p 388. https://doi.org/10.4231/D3M90238V
5. FEMA-155 (2002) FEMA-155: rapid visual screening of buildings for potential seismic hazards: supporting documentation. Federal Emergency Management Agency, January. https://doi.org/10.4231/D3M90238V
6. FEMA (2015) Reducing flood risk to residential buildings that cannot be elevated, FEMA P-1037. https://doi.org/10.5114/aoms.2013.38674
7. Dall'Osso F et al (2016) Revision and improvement of the PTVA-3 model for assessing tsunami building vulnerability using "international expert judgment": introducing the PTVA-4 model. Nat Hazards 83(2):1229–1256. https://doi.org/10.1007/s11069-016-2387-9
8. Papathoma M et al (2003) Assessing tsunami vulnerability, an example from Herakleio, Crete. Nat Hazards Earth Syst Sci 3(5):377–389. https://doi.org/10.5194/nhess-3-377-2003
9. Dias P (2006) Lessons learned from tsunami damage in Sri Lanka, May, pp 74–81. https://doi.org/10.1680/cien.2006.159.2.74
10. Dias WPS, Yapa HD, Peiris LMN (2009) Civil engineering and environmental systems tsunami vulnerability functions from field surveys and Monte Carlo simulation, 6608. https://doi.org/10.1080/10286600802435918
11. Bandara KMK, Dias WPS (2012) Tsunami wave loading on buildings: a simplified approach 40(3):211–219. https://doi.org/10.4038/jnsfsr.v40i3.4695.
12. National Building and Research Organization (NBRO) (2015) Hazard resilient housing construction manual
13. Kaier K, Mutters NT, Frank U (2012) Bed occupancy rates and hospital-acquired infections-should beds be kept empty? Clin Microbiol Infect 18(10):941–945. https://doi.org/10.1111/j.1469-0691.2012.03956.x
14. Munasinghe NL, Matsui K (2019) Examining disaster preparedness at Matara District General Hospital in Sri Lanka. Int J Disaster Risk Reduction 101154. https://doi.org/10.1016/j.ijdrr.2019.101154
15. Ministry of Health, Sri Lanka (2016) Annual health bulletin of Sri Lanka 2016. Available at: www.health.gov.lk
16. Tiwary NK, Urfi AJ (2016) Spatial variations of bird occupancy in Delhi: the significance of woodland habitat patches in urban centres. Urban Forest Urban Greening 20:338–347. https://doi.org/10.1016/j.ufug.2016.10.002
17. World Health Organization & Pan American Health Organization (2015) Hospital safety index: guide for evaluators, 2nd ed. World Health Organization. https://apps.who.int/iris/handle/10665/258966

Effect of Corner Strength Enhancement on Shear Behaviour of Stainless Steel Lipped Channel Sections

D. M. M. P. Dissanayake, K. Pologanathan, S. Gunalan, K. D. Tsavdaridis, and N. Degtyareva

Abstract During the cold-forming process of manufacturing, stainless steel sheets undergo plastic deformations, in particularly around corner regions of press braked sections. These plastic deformations lead to significant changes in material properties of stainless steel compared to its flat sheet properties. Consequently, yield strength and ultimate strength increments can be envisaged and this process is termed as cold working. Stainless steel exhibits significant level of strain hardening under plastic deformations. This is the main reason for these strength enhancements. In the structural design process of stainless steel sections, these strength increments are required to be considered to harness the benefits arising from it. Therefore, previous research proposed predictive models for these strength enhancements. In this context, the effect of corner strength enhancement on press-braked stainless steel lipped channel sections under shear was examined in this paper. 120 finite element models were developed. Different corner radii and section thicknesses were taken into account. Results highlighted that the effect of cold working on the shear capacity of stainless steel lipped channel sections is more significant in compact sections compared to slender sections where up to 9% increment was observed. Further analysis was conducted using 40 finite element models to highlight the inelastic reserve capacity available in compact stainless steel lipped channel sections in shear. From the results, it was concluded that when web slenderness is less than 0.25 more than 40% shear capacity increment can be achieved due to strain-hardening of stainless steel.

D. M. M. P. Dissanayake (✉) · K. Pologanathan
Faculty of Engineering and Environment, University of Northumbria, Newcastle upon Tyne, UK
e-mail: madhushan.mudiyanselage@northumbria.ac.uk

S. Gunalan
School of Engineering and Built Environment, Griffith University, Queensland, Australia

K. D. Tsavdaridis
School of Civil Engineering, Faculty of Engineering and Physical Sciences, University of Leeds, Leeds, UK

N. Degtyareva
South Ural State University, Chelyabinsk, Russia

R. Dissanayake et al. (eds.), *ICSECM 2019*, Lecture Notes in Civil Engineering 94,
https://doi.org/10.1007/978-981-15-7222-7_19

Keywords Cold working · Corner strength enhancement · Stainless steel · Lipped channel sections · Shear capacity

1 Introduction

Stainless steel is becoming an attractive option for structural elements as it provides a range of benefits over the conventional carbon steel. Stainless steel exhibits non-linear stress–strain relationship with gradual yielding unlike carbon steel, which is characterised by a bi-linear stress–strain relationship with a sharp yield point. Therefore, stainless steel has beneficial strain-hardening effect under higher strains. As a result of this, strength enhancements can be seen in stainless steel sections during the forming process. These strength increments are considerably higher than the currently adopted material strengths in the design guidelines such as EN1993-1-4 [7]. Therefore, it is worth to study the effect of these strength enhancements on the structural behaviour of stainless steel sections in view of adopting those in the design process to utilise stainless steel more efficiently. On the other hand, many research has previously been conducted on shear behaviour of cold-formed channel sections. Shear behaviour of cold-formed lipped channel sections has been studied in a number of researches by Keerthan and Mahendran [13–16] while shear behaviour of LiteSteel beams has been investigated by Keerthan and Mahendran [12] and Mahendran and Keerthan [18]. Moreover, web crippling behaviour of cold-formed lipped channel sections has been studied by Sundararajah et al. [19, 20] However, limited attention has been given to stainless steel lipped channel sections. Therefore, this paper presents the details of finite element (FE) modelling undertaken to investigate the effect of corner strength enhancement and strain-hardening effect on the shear behaviour of press-braked stainless steel lipped channel sections.

There are two main cold-forming methods of manufacturing for thin-walled structural sections. Those are known as roll-forming and press-braking. Roll-forming is a mass production method where uncoiled sheet material is fed into a series of forming rollers to deform it into the desired cross section. A typical example for this method is hollow sections. On the other hand, press-braking is relatively simple and semi-manual method involving bending of flat material sheets into shapes such as angles and channels using a standard set of tools and dies. Both methods of manufacturing involve enhancement of material properties of sheets compared to its virgin properties. This is known as cold-working. In the roll-forming process, moderate strength enhancements can be seen in the flat parts of the final section while higher strength increments can be seen in the corner regions. In the press-braking these strength enhancements are confined to corner regions.

2 Predictive Models for Corner Strength Enhancement

The effect of cold-work of forming on corner strength enhancement of stainless steel sections has been investigated by a number of researches previously. Coetzee et al. [3] were the first to study the cold-working effect on the strength of stainless steel sections. Coupon tests and experimental studies on stainless steel lipped channel sections were conducted to study the effect of cold-working on the strength of stub columns. Van den Berg and Van der Merwe [21] proposed an equation to predict corner 0.2% proof strength using press-braked stainless steel corner coupon tests. Further studies have been conducted by Ashraf et al. [2] and Cruise and Gardner [4] on strength enhancements of corner regions of stainless steel sections induced during cold-forming.

In the study conducted by Cruise and Gardner [4], an existing model was modified using comprehensive data base of press-braked and cold-rolled sections for prediction of corner 0.2% proof strength. This proposed equation is based on a simple power model of internal corner radius (r_i) to material thickness (t) ratio, initially proposed for carbon steel by Karren [10]. Equation (1) gives the modified equation for corner 0.2% proof stress ($\sigma_{0.2,c}$) proposed by Cruise and Gardner [4] for press-braked sections.

$$\sigma_{0.2,c} = \frac{1.673\sigma_{0.2,v}}{\left(\frac{r_i}{t}\right)^{0.126}} \tag{1}$$

where $\sigma_{0.2,v}$ is the 0.2% proof stress of the virgin material.

Ashraf et al. [2] proposed an equation to predict corner ultimate strength ($\sigma_{u,c}$) using all available test results on stainless steel. This equation is given by Eq. (2) where $\sigma_{u,v}$ is the ultimate strength of the virgin sheet material.

$$\sigma_{u,c} = 0.75\sigma_{0.2,c}\left(\frac{\sigma_{u,v}}{\sigma_{0.2,v}}\right) \tag{2}$$

Further studies were conducted by Cruise and Gardner [4] to investigate the extent of corner strength enhancements in stainless steel cross-section. Based on this study it was found that corner strength enhancements extend to a distance of 2 × material thickness beyond the corner radius for roll-formed sections while that is confined to corner regions of press-braked sections.

3 Finite Element Modelling

3.1 Model Development

This section presents the details of FE modelling undertaken in this study to investigate the shear behaviour of stainless steel lipped channel beams (LCBs). Developed

FE models were validated against the experimental results and then utilise in the parametric study to investigate the corner strength enhancement and strain-hardening effects. Commercially available FE software package, ABAQUS CAE 2017 was used for the development of the FE models. Geometric and material properties, loading and boundary conditions were employed in the FE modelling to suitably simulate the experimental conditions. Details of experimental results can be found in Dissanayake et al. [5, 6] and Fareed et al. [8]. In the FE modelling single LCBs were employed instead of back-to-back setup used in the experimental programme. LCBs were simply supported at the two ends and loaded at the mid-span through shear centre using single web side plates to eliminate torsional effects. Tie constraints were introduced at the contact surface between the LCB web and web side plates. Similar FE models were previously employed by Keerthan and Mahendran [11] and Keerthan et al. [17].

S4R shell elements were assigned to the sections to simulate thin section behaviour under shear. Mesh sensitivity analysis results suggested that 5 mm × 5 mm mesh provided the convergence with good accuracy. However, for corner regions of LCBs, 1 mm × 5 mm mesh was introduced to define the corner curvature. Figure 1 illustrates the FE mesh assigned in the modelling.

To represent non-linear stress–strain behaviour of stainless steel modified two-stage Ramberg–Osgood material model proposed by Arrayago et al. [1] was used. Then using Eqs. (3) and (4), true stress (σ_{true}) and log plastic strain (ε_{ln}^{pl}) were calculated. When defining materials in Abaqus, sufficient number of data points were introduced using these two equations to accurately represent material behaviour. Corner material properties were calculated as described in Sect. 2. Since this study was on press-braked sections these enhancements were introduced only to corner regions as suggested in Cruise and Gardner [4].

$$\sigma_{true} = \sigma_{nom}(1 + \varepsilon_{nom}) \tag{3}$$

$$\varepsilon_{ln}^{pl} = \ln(1 + \varepsilon_{nom}) - \frac{\sigma_{true}}{E} \tag{4}$$

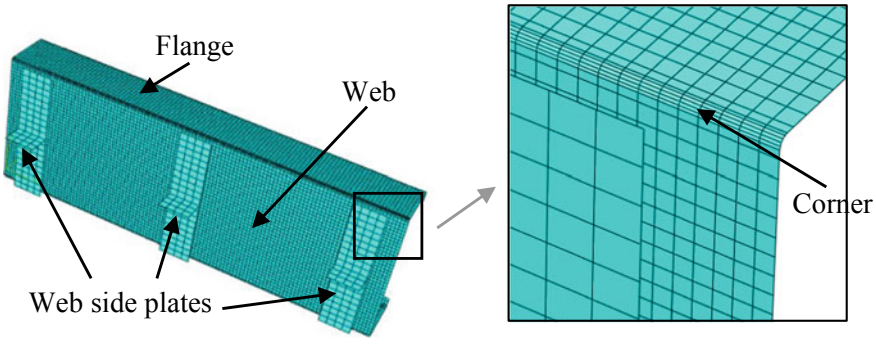

Fig. 1 FE mesh of LCB and web side plate

where σ_{nom} and ε_{nom} are engineering stress and strain, respectively and E is the Young's modulus.

To simulate the simply supported boundary conditions, a pin support and a roller support were assigned to the two ends of LCBs. Equal angle straps were attached to the LCB flanges to avoid distortional buckling and this was appropriately modelled. Figure 2 shows the boundary conditions assigned to the FE model. The details of boundary conditions used in the FE modelling are also summarised below where u_x, u_y and u_z are translations and θ_x, θ_y and θ_z are rotations in the x, y and z directions, respectively while 0 denotes free and 1 denotes restrained conditions.

- Left support: $u_x = 1\ u_y = 1\ u_z = 1\ \theta_x = 0\ \theta_y = 0\ \theta_z = 1$
- Right support: $u_x = 1\ u_y = 1\ u_z = 0\ \theta_x = 0\ \theta_y = 0\ \theta_z = 1$
- Mid span loading point: $u_x = 1\ u_y = 0\ u_z = 1\ \theta_x = 0\ \theta_y = 0\ \theta_z = 1$
- Strap locations: $u_x = 1\ u_y = 0\ u_z = 0\ \theta_x = 0\ \theta_y = 0\ \theta_z = 1$

Local geometric imperfection amplitude (ω_0) was calculated using modified Dawson and Walker model proposed by Gardner and Nethercot [9] and is given in Eq. (5). To identify local geometric imperfection mode shapes, an elastic buckling analysis was initially performed on each FE model. Then, using the modified Riks method, a geometrically and materially non-linear analysis was conducted up to failure to identify ultimate loads and failure modes.

$$\omega_0 = 0.023\left(\frac{\sigma_{0.2}}{\sigma_{cr}}\right)t \tag{5}$$

where σ_{cr} is the critical elastic buckling stress of the most slender element of the section.

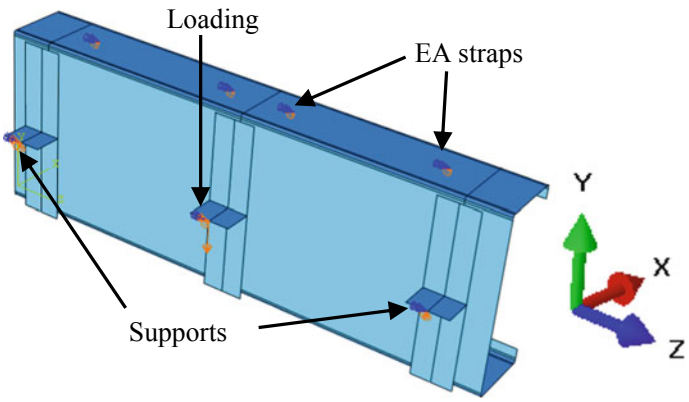

Fig. 2 Boundary conditions used in the FE modelling

3.2 Validation

Developed FE models were compared against the corresponding experimental results in terms of ultimate loads and failure modes to assess the performance. Table 1 compares the experimental and FE ultimate loads. Mean and coefficient of variance (COV) of experimental to predicted (FE) shear capacity ratio are 1.02 and 0.073, respectively. Therefore, it can be concluded that developed FE models are able to capture the ultimate shear capacities of stainless steel LCBs with reasonably good accuracy. Moreover, Fig. 3 shows the experimental and FE shear failure modes of LCB 200 × 75 × 15 × 1.2 section where the FE model agrees well with the experimental failure mode.

Table 1 Comparison of experimental and FE shear capacities

LCB section	$V_{Exp.}$(kN)	V_{FE} (kN)	$V_{Exp.}/V_{FE}$
LCB 100 × 50 × 15 × 1.2	18.49	16.86	1.10
LCB 100 × 50 × 15 × 1.5	24.44	23.90	1.02
LCB 100 × 50 × 15 × 2.0	36.00	32.72	1.10
LCB 150 × 65 × 15 × 1.2	21.60	20.09	1.08
LCB 150 × 65 × 15 × 1.5	26.26	28.40	0.92
LCB 150 × 65 × 15 × 2.0	43.55	42.60	1.02
LCB 200 × 75 × 15 × 1.2	22.98	22.97	1.00
LCB 200 × 75 × 15 × 2.0	47.05	52.11	0.90
Mean			1.02
COV			0.073

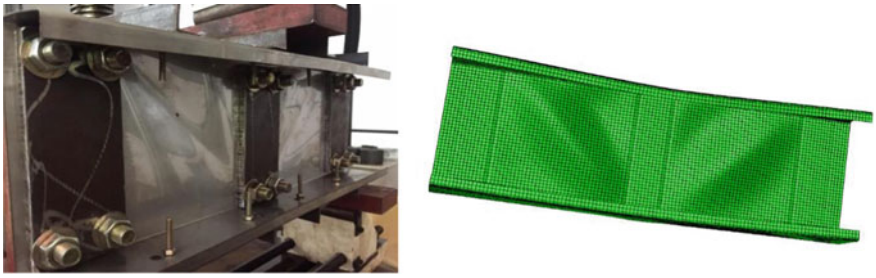

(a) Experiment (b) FE model

Fig. 3 Shear failure mode of LCB 200 × 75 × 15 × 1.2 section

4 Parametric Study

A detailed parametric study was conducted using the validated FE models to investigate the effect of corner strength enhancement and strain-hardening effect on the shear behaviour of press-braked stainless steel LCBs; the results are discussed in this section.

4.1 Effect of Corner Strength Enhancement

To study the effect of corner strength enhancement 120 FE models were developed. Table 2 summarises these results. r_i/t ratio was varied from 0.4 to 5 herein. Figure 4 compares the shear capacities with and without corner enhancement for LCBs with an internal radius of 5 mm. From the results, it can be concluded that corner strength enhancement has more effect on compact sections than slender sections. This can be explained by the fact that compact sections experience higher strains than slender sections at failure, therefore subjecting to more strain-hardening. Excluding unreliable FE results it was found that up to 9% shear capacity increment can be achieved from corner enhancement for press-braked LCBs. Similar findings were reported by Cruise and Gardner [4] for press-braked stub columns. Moreover, it showed that the effect of internal radius on the shear capacity is negligible for LCBs. This is illustrated in Fig. 5. In Figs. 4 and 5 V_u is the shear capacity, V_y is the shear yield capacity and λ_w is the web slenderness of the section.

4.2 Strain-Hardening Effect

Pronounced strain-hardening effect of stainless steel on the shear behaviour of LCBs were investigated in this section. Shear capacities of stainless steel LCBs were compared against the shear capacities of carbon steel LCBs in this context. In the FE modelling, stainless steel grade 1.4301 was used and for carbon steel FE models elastic-perfectly plastic material model with a yield stress equals to 0.2% proof stress of stainless steel grade 1.4301 was used. Four LCBs (LCB 100 × 50 × 15, LCB 150 × 65 × 15, LCB 200 × 75 × 15 and LCB 250 × 75 × 15) and five material thicknesses (1, 2, 3, 4 and 5 mm) were considered herein. Shear capacities are compared in Fig. 6. From the results it can be concluded that the effect of strain-hardening is more significant in compact sections where more than 40% shear capacity increment can be expected in stainless steel sections compared to carbon steel sections when web slenderness (λ_w) is less than 0.25 while that for slender sections are negligible. This capacity increment in compact sections is known as inelastic reserve capacity. However, a value of 1.2 has been introduced in EN1993-1-4 to include this additional capacity in the design process seems to be too conservative.

Table 2 Shear capacities and % increments due to the corner strength enhancement for stainless steel LCBs

Section	$r_i = 2$ mm		$r_i = 3$ mm		$r_i = 5$ mm	
	$V_{FE}^{*,a}$(kN)	$\%^{*,b}$	$V_{FE}^{*,a}$(kN)	$\%^{*,b}$	$V_{FE}^{*,a}$(kN)	$\%^{*,b}$
Grade 1.4301						
LCB 150 × 65 × 15 × 1	15.4	1.03	15.0	1.02	14.7	1.04
LCB 150 × 65 × 15 × 2	40.0	1.04	39.4	1.05	37.9	1.06
LCB 150 × 65 × 15 × 3	68.5	1.05	68.0	1.06	66.4	1.07
LCB 150 × 65 × 15 × 4	96.0	1.06	95.4	1.07	93. 3	1.08
LCB 150 × 65 × 15 × 5	131.8	1.07	130.1	1.08	128.2	1.09
LCB 200 × 75 × 15 × 1	17.2	1.03	18.6	1.13	16.5	1.04
LCB 200 × 75 × 15 × 2	47.3	1.03	47.1	1.05	44.7	1.05
LCB 200 × 75 × 15 × 3	82.5	1.05	81.0	1.05	79.3	1.06
LCB 200 × 75 × 15 × 4	114.6	1.05	113.9	1.06	111.7	1.07
LCB 200 × 75 × 15 × 5	171.2	1.18	151.7	1.06	150.2	1.08
Grade 1.4462						
LCB 150 × 65 × 15 × 1	26.0	1.04	25.6	1.06	26.0	1.04
LCB 150 × 65 × 15 × 2	76.0	1.04	73.4	1.04	68.9	1.05
LCB 150 × 65 × 15 × 3	128.6	1.04	127.7	1.04	124.3	1.06
LCB 150 × 65 × 15 × 4	175.6	1.05	174.2	1.06	170.5	1.06
LCB 150 × 65 × 15 × 5	229.9	1.05	228.0	1.06	225.0	1.06
LCB 200 × 75 × 15 × 1	27.7	1.04	30.3	1.05	26.4	1.08
LCB 200 × 75 × 15 × 2	86.4	1.02	84.9	1.04	79.4	1.04
LCB 200 × 75 × 15 × 3	158.9	1.05	157.1	1.06	150.2	1.05
LCB 200 × 75 × 15 × 4	218.7	1.05	216.6	1.06	211.0	1.06

(continued)

Table 2 (continued)

Section	$r_i = 2$ mm		$r_i = 3$ mm		$r_i = 5$ mm	
	$V_{FE}{}^{*,a}$(kN)	$\%^{*,b}$	$V_{FE}{}^{*,a}$(kN)	$\%^{*,b}$	$V_{FE}{}^{*,a}$(kN)	$\%^{*,b}$
LCB 200 × 75 × 15 × 5	283.3	1.05	281.4	1.06	276.9	1.06

Note a—including corner enhancement, b—increment due to corner enhancement

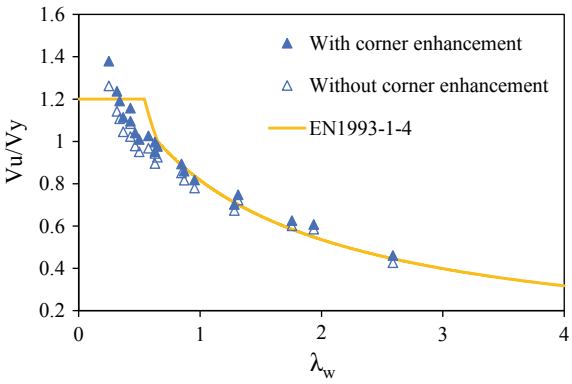

Fig. 4 Shear capacities of stainless steel LCBs with and without corner enhancement for $r_i = 5$ mm

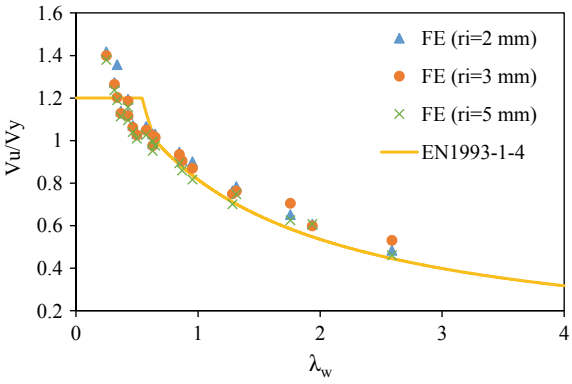

Fig. 5 Shear capacities of stainless steel LCBs for ri = 2 mm, 3 mm and 5 mm

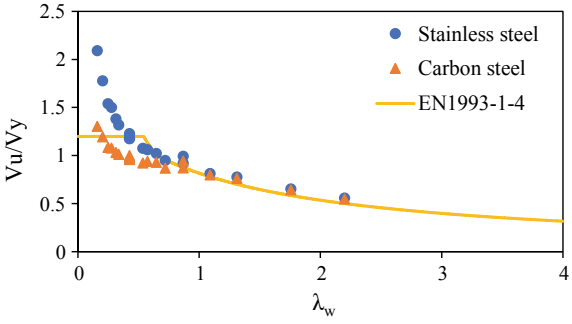

Fig. 6 Comparison of shear capacities for stainless steel and carbon steel LCBs

5 Concluding Remarks

Due to the cold-work of forming, stainless steel sections undergo strength enhancements during the manufacturing process. These are localised to corner regions in

press-braked sections. Previous research has been conducted to predict these strength enhancements in stainless steel sections. In this study, the effect of corner strength enhancement on shear capacity of LCBs was investigated. The r_i/t ratio of the sections covered in this study varied from 0.4 to 5. From the results, it can be concluded that corner strength enhancement is more pronounced on compact sections where up to 9% shear capacity increment can be observed from corner enhancement for press-braked LCBs. Further, it was demonstrated that the effect of internal radius on the shear capacity is negligible for LCBs. Another study was conducted to investigate the strain-hardening effect on shear behaviour of stainless steel LCBs. Due to the strain-hardening effect, more than 40% shear capacity increment can be observed for compact sections when web slenderness is less than 0.25 while that for slender sections is negligible.

References

1. Arrayago I, Real E, Gardner L (2015) Description of stress-strain curves for stainless steel alloys. Mater Des 87:540–552
2. Ashraf M, Gardner L, Nethercot DA (2005) Strength enhancement of the corner regions of stainless steel cross-sections. J Constr Steel Res 61(1):37–52
3. Coetzee JS, Van den Berg GJ, Van der Merwe P (1990) The effect of work hardening and residual stresses due to cold-work of forming on the strength of cold-formed stainless steel lipped channel section. In: Proceedings of the tenth international specialty conference on cold-formed steel structures, Missouri, USA, 23–24 October 1990, pp 143–62
4. Cruise RB, Gardner L (2008) Strength enhancements induced during cold forming of stainless steel sections. J Constr Steel Res 64(11):1310–1316
5. Dissanayake DMMP, Pologanathan K, Gunalan S, Tsavdaridis KD, Nagaratnam B, Wanniarachchi KS (2019) Numerical modelling and shear design rules of stainless steel lipped channel sections. J Constr Steel Res (in press)
6. Dissanayake M, Pologanathan K, Gunalan S, Tsavdaridis KD, Nagaratnam B (2019) Finite element analyses of cold-formed stainless steel beams subject to shear. Spec Issue Proc Nordic Steel 3(3–4):931–936
7. European Committee for Standardization (2015) EN 1993-1-4:2006+A1:2015. Eurocode 3. Design of steel structures. Part 1–4: general rules–supplementary rules for stainless steels. Brussels, CEN
8. Fareed I, Somadasa W, Pologanathan K, Gunalan S, Corradi M, Sivapalan S (2019) Finite element analyses of cold-formed stainless steel beam with web openings in shear. Spec Issue Proc Nordic Steel 3(3–4):907–912
9. Gardner L, Nethercot DA (2004) Numerical modelling of stainless steel structural components—a consistent approach. J Struct Eng 130(10):1586–1601
10. Karren KW (1967) Corner properties of cold-formed steel shapes. J Struct Div 93(ST1):401–432
11. Keerthan P, Mahendran M (2011) Numerical modeling of litesteel beams subject to shear. J Struct Eng 137(12):1428–1439
12. Keerthan P, Mahendran M (2012) Shear behaviour and strength of litesteel beams with web openings. Adv Struct Eng 15(2):171–184
13. Keerthan P, Mahendran M (2013) Experimental studies of the shear behaviour and strength of lipped channel beams with web openings. Thin-Wall Struct 73:131–144
14. Keerthan P, Mahendran M (2013) Shear buckling characteristics of cold-formed steel channel beams. Int J Steel Struct 13(3):385–399

15. Keerthan P, Mahendran M (2015) Experimental investigation and design of lipped channel beams in shear. Thin-Wall Struct 86:174–184
16. Keerthan P, Mahendran M (2015) Improved shear design rules of cold-formed steel beams. Eng Struct 99:603–615
17. Keerthan P, Mahendran M, Hughes D (2014) Numerical studies and design of hollow flange channel beams subject to combined bending and shear actions. Eng Struct 75:197–212
18. Mahendran M, Keerthan P (2013) Experimental studies of the shear behavior and strength of Litesteel beams with stiffened web openings. Eng Struct 49:840–854
19. Sundararajah L, Mahendran M, Keerthan P (2017) New design rules for lipped channel beams subject to web crippling under two-flange load cases. Thin-Wall Struct 119:421–437
20. Sundararajah L, Mahendran M, Keerthan P (2017) Web crippling experiments of high strength lipped channel beams under one-flange loading. J Constr Steel Res 138:851–866
21. Van den Berg GJ, Van der Merwe P (1992) Prediction of corner mechanical properties for stainless steels due to cold forming. In: Proceedings of the eleventh international specialty conference on cold-formed steel structures, Missouri, USA, 20–21 October 1992, pp 571–86

Shear Behaviour of Cold-Formed Stainless Steel Lipped Channels with Reduced Support Restraints

D. M. M. P. Dissanayake, K. Pologanathan, S. Gunalan, K. D. Tsavdaridis, and K. S. Wanniarachchi

Abstract Lipped channel beams are commonly used in buildings for load-bearing components such as floor joists and roof purlins. The typical practice is to use one-sided web side plates (WSPs) to attach beams from their webs to the supports at the connections, through bolts. In such realistic conditions, it is not practical to use WSPs over the full height of the webs, thus only a part of the web height is restrained at the supports. This controls the mobilising of diagonal tension field in the web and also provides less restraint to the lateral movement of the web. Therefore, realistic support conditions affect the shear capacity due to the lack of restraint of the web at the supports. On the other hand, the current shear design rules are based on ideal support conditions which do not represent the true scenario. Therefore, it is critical to investigate the effect of reduced support restraints on the shear capacity since it has been given less attention in the literature. This paper presents the effect of reduced support restraints on the shear capacity of stainless steel lipped channel beams. Finite element models were developed to study the effect with regard to various influential parameters. From the finite element results, it was found that the shorter the WSP—the higher the shear capacity reduction, where about 50% shear capacity reduction was observed for 60% reduction in WSP height. Furthermore, it was concluded that compact sections exhibit more significant capacity reduction than slender sections when reducing the WSP height. Therefore, a reduction factor was introduced to the current direct strength method shear design rules considering the effect of reduced support restraints on the shear capacity.

D. M. M. P. Dissanayake (✉) · K. Pologanathan
Faculty of Engineering and Environment, University of Northumbria, Newcastle upon Tyne, UK
e-mail: madhushan.mudiyanselage@northumbria.ac.uk

S. Gunalan
School of Engineering and Built Environment, Griffith University, Queensland, Australia

K. D. Tsavdaridis
School of Civil Engineering, Faculty of Engineering and Physical Sciences,
University of Leeds, Leeds, UK

K. S. Wanniarachchi
Faculty of Engineering, University of Ruhuna, Matara, Sri Lanka

R. Dissanayake et al. (eds.), *ICSECM 2019*, Lecture Notes in Civil Engineering 94,
https://doi.org/10.1007/978-981-15-7222-7_20

Keywords Reduced support restraints · Stainless steel · Lipped channel beams · Shear design rules · Direct strength method

1 Introduction

Lipped channel beams (LCBs) are commonly used as floor joists and roof purlins in steel structures. Figure 1 shows application of lipped channel sections as floor joists. They act as intermediate members to transfer loads from floors to columns. Different forms of simple connection types are used between these members which include double and single angle web cleats, header plates and fin plates. Due to the single symmetric nature of LCBs single angle web cleat connections, are the most common among lipped channel sections. At the connections these plates are bolted or screwed to the web. However, in the realistic conditions restraint provided by these connections is limited only to a part of the web height. Sufficient level of restraint provided by the supports is important in mobilising diagonal tension fields in spans, also known as tension field action (TFA). TFA for a lipped channel section is shown in Fig. 2. Mobilising of TFA is essential for a section to achieve its shear capacity. The effect of support conditions on TFA of cold-formed lipped channel sections subject to shear has been investigated by Pham and Hancock [17] while in a more recent study by Pham et al. [18], the effect of flange restraints on TFA has also been discussed. Moreover, Keerthan et al. [15] has investigated the effect of reduced support conditions on the shear behaviour of cold-formed hollow flange channel sections via experimental studies. In addition to these, shear behaviour of cold-formed lipped channel sections has been studied in a number of researches

Fig. 1 Lipped channel beams as floor joists [18]

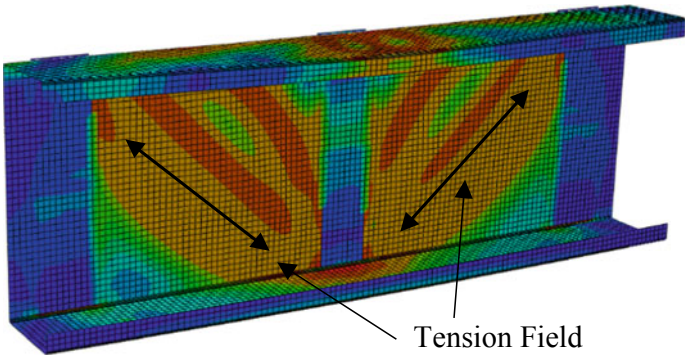

Fig. 2 Tension field action

by Keerthan and Mahendran [10, 12]. Moreover, Keerthan and Mahendran [9] and Mahendran and Keerthan [16] has investigated the shear behaviour of cold-formed LiteSteel beams. Further, studies have been conducted on the web crippling behaviour of cold-formed lipped channel sections by Sundararajah et al. [20, 21]. However, limited attention has been given to stainless steel lipped channel sections.

As a result of TFA, post-buckling strength can be observed particularly in slender sections subject to shear. This post-buckling strength available in cold-formed channel sections has been investigated in a number of studies conducted by Keerthan and Mahendran [11, 13]. Increased support restraints improve the post buckling strength, especially in sections subject to shear [18]. Reduced restraints at supports in realistic conditions affect the mobilising of TFA, thus reducing post-buckling strength and shear capacity of sections. On the other hand, current shear design provisions do not account for these capacity reductions, therefore relevant capacity reduction factors to those design rules should be introduced. Consequently, this paper presents the detailed finite element (FE) study conducted to investigate the effect of the reduced support restraints on the shear behaviour of cold-formed stainless steel lipped channel sections. FE results were utilised in determining the capacity reduction factors for the current direct strength method (DSM) shear design rules and all the details are also presented herein.

2 The DSM Shear Design Rules

The DSM was first introduced as an alternative to the conventional effective width method. It was adopted in both North American (AISI S100 [1]) and Australian (AS/NZS 4600 [19]) design standards for cold-formed steel. These DSM shear design rules with and without TFA are summarised below.

2.1 Without Tension Field Action

For section webs without holes and without any stiffeners, shear capacity (V_v) of the section without TFA is given by Eqs. (1)–(3). These equations do not account for the available post-buckling strength as well.

$$V_v = V_y \text{ for } \lambda \leq 0.815 \tag{1}$$

$$V_v = 0.815\sqrt{V_{cr}V_y} \text{ for } 0.815 < \lambda \leq 1.227 \tag{2}$$

$$V_v = V_{cr} \text{ for } \lambda > 1.227 \tag{3}$$

where V_y is the shear yield capacity and V_{cr} is the elastic shear buckling capacity. V_y and V_{cr} are defined by Eqs. (4) and (5), respectively. λ is the section slenderness and is expressed in Eq. (6).

$$V_y = 0.6\, f_y d_1 t_w \tag{4}$$

$$V_{cr} = \frac{k\pi^2 E t_w{}^3}{12(1-\upsilon^2)d_1} \tag{5}$$

$$\lambda = \sqrt{\frac{V_y}{V_{cr}}} \tag{6}$$

where f_y is the web yield stress, d_1 is the flat depth of the web, t_w is the web thickness, E is the Young's modulus and υ is the Poisson's ratio. Here, k is the shear buckling coefficient of the section. Keerthan and Mahendran [12, 13] proposed a set of equations to calculate the shear buckling coefficient (k) of LCBs considering the additional fixity available at the web-flange juncture of LCBs.

2.2 With Tension Field Action

Section shear capacity including TFA is given by Eqs. (7) and (8). These equations are in the form of the DSM section moment capacity equations and include post-buckling strength of the sections as well.

$$V_v = V_y \text{ for } \lambda \leq 0.776 \tag{7}$$

$$V_v = \left[1 - 0.15\left(\frac{V_{cr}}{V_y}\right)^{0.4}\right]\left(\frac{V_{cr}}{V_y}\right)^{0.4} V_y \text{ for } \lambda > 0.776 \tag{8}$$

2.3 Design Curve for Stainless Steel Sections

Based on the experimental and numerical studies current DSM shear design provisions were modified by Dissanayake et al. [3] to predict the shear capacity of stainless steel LCBs. Those proposals include both post-buckling strength of slender sections and inelastic reserve capacity of compact sections. Equations (9)–(11) give these modified rules for stainless steel.

$$V_v = 2V_y \text{ for } \lambda \leq 0.122 \tag{9}$$

$$V_v = 0.795\left(\frac{V_{cr}}{V_y}\right)^{0.439} V_y \text{ for } 0.122 < \lambda \leq 0.592 \tag{10}$$

$$V_v = \left[1 - 0.213\left(\frac{V_{cr}}{V_y}\right)^{0.35}\right]\left(\frac{V_{cr}}{V_y}\right)^{0.35} V_y \text{ for } \lambda > 0.592 \tag{11}$$

3 Numerical Modelling

3.1 FE Model Development

Details of FE modelling conducted to investigate the effect of shear behaviour of stainless steel lipped channel sections with different support heights is presented in this section. Developed FE models were first validated and then utilised in a detailed parametric study. Abaqus software package was used in this study for the FE modelling. FE modelling was based on the experiments carried out to study the shear behaviour of stainless steel LCBs. In the experiments, two LCBs were attached back-to-back using three T-stiffeners and full-height web side plates (WSPs). LCBs were simply supported from the two ends and loaded at the mid-span using displacement control. Equal angle straps were provided to the both top and bottom flanges at the supports and at the loading point to avoid distortional buckling. More details on the experimental results can be found in Dissanayake et al. [3, 4] and Fareed et al. [6].

In the FE modelling procedure, single LCBs were modelled considering the symmetry of the experimental setup. A pin and a roller support conditions were maintained at the two ends. Rotational degree of freedom around the longitudinal axis of the beam was restrained to avoid any torsional effects. Support conditions and loading were applied to the single WSPs where a single node of each WSP was restrained at the shear centre of the section. In the validation study, the full web height was restrained using WSPs to simulate experimental conditions while in the parametric study further FE models were developed restraining only a part of the web height. WSPs with reduced heights were attached symmetrically along the web

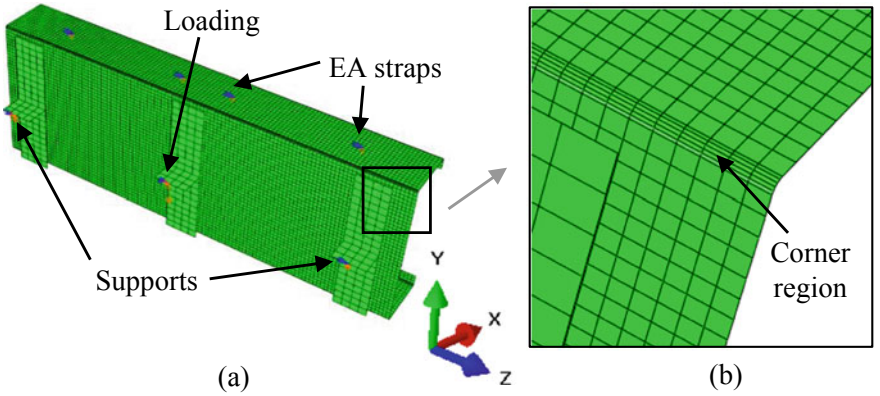

Fig. 3 **(a)** Boundary conditions and **(b)** FE mesh used in the modelling

height. A bolted connection between the section web and the WSPs was modelled using Tie constraints available in Abaqus software. Similar procedure has previously been followed for FE modelling of cold-formed sections by Keerthan and Mahendran [8] and Keerthan et al. [14].

S4R shell elements were employed to define the sections. Following a sensitivity study, it was concluded that a 5 mm × 5 mm mesh offers the convergence with a reasonable accuracy. However, for the corner regions, a relatively finer mesh of 1 mm × 5 mm was assigned. Figure 3 illustrates the boundary conditions and FE mesh used.

Modified two-stage Ramberg–Osgood material model proposed by Arrayago et al. [2] was used to represent the non-linear stress–strain behaviour of stainless steel. Corner strength enhancement was incorporated to the FE models as defined in Dissanayake et al. [5]. In order to introduce the effect of local geometric imperfections to the non-linear FE models an elastic buckling analysis was initially performed and critical buckling mode shapes were identified. Then those were superimposed to the non-linear FE models using a suitable imperfection amplitude. Modified Dawson and Walker model proposed by Gardner and Nethercot [7] was used in this study for the calculation of imperfection amplitude (ω_0) and is given by Eq. (12). Thereafter, a modified Riks analysis was performed on FE models.

$$\omega_0 = 0.023\left(\frac{\sigma_{0.2}}{\sigma_{cr}}\right)t_w \tag{12}$$

where $\sigma_{0.2}$ is the 0.2% proof stress and σ_{cr} is the critical elastic buckling stress of the slenderest element of the section.

3.2 Validation

Table 1 summarises the experimental ultimate shear capacities of 8 LCBs with FE predictions for full web height restrained support condition. From Table 1 it can be seen that mean and coefficient of variance (COV) of the experimental to FE shear capacity ratio are 1.02 and 0.073, respectively. Therefore, the elaborated FE models predict ultimate shear capacity of LCBs with reasonably good accuracy. Furthermore, Fig. 4 compares the experimental and FE shear failure modes for LCB 200 × 75 × 15 × 1.2 section. The FE model is able to capture diagonal shear failure of the web in both spans accurately.

Table 1 Comparison of experimental and FE shear capacities

LCB section	$V_{Exp.}$ (kN)	V_{FE} (kN)	$V_{Exp.}/V_{FE}$
LCB 100 × 50 × 15 × 1.2	18.49	16.86	1.10
LCB 100 × 50 × 15 × 1.5	24.44	23.90	1.02
LCB 100 × 50 × 15 × 2.0	36.00	32.72	1.10
LCB 150 × 65 × 15 × 1.2	21.60	20.09	1.08
LCB 150 × 65 × 15 × 1.5	26.26	28.40	0.92
LCB 150 × 65 × 15 × 2.0	43.55	42.60	1.02
LCB 200 × 75 × 15 × 1.2	22.98	22.97	1.00
LCB 200 × 75 × 15 × 2.0	47.05	52.11	0.90
Mean			1.02
COV			0.073

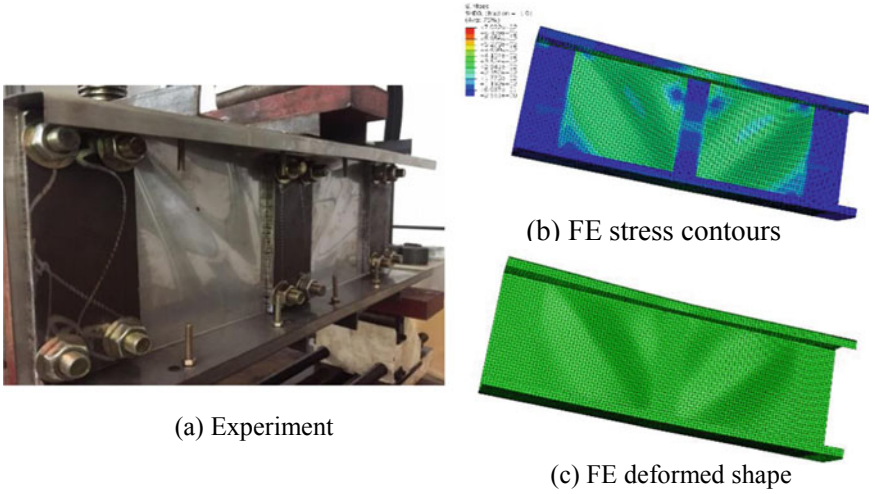

Fig. 4 Shear failure mode of LCB 200 × 75 × 15 × 1.2 section

3.3 Parametric Study

In order to study the level of restraints provided by the support on shear TFA of stainless steel LCBs 80 FE models were developed following the validation. Four WSP heights (h_{WSP}) were considered in this study and the details of FE results are summarised in Table 2.

Figure 5 plots the ultimate shear capacities of 80 FE models against the section slenderness (λ). It also includes the DSM shear design curve given by Eqs. (9)–(11). By analysing the results, it can be seen that the shorter the WSP—the higher the shear capacity reduction, where about 50% shear capacity reduction can be observed for 60% reduction in WSP height. When reducing the WSP height restraint provided by the support also reduces. Therefore, it can be concluded that insufficient level of restraint provided to fully mobilise TFA in webs causes this shear capacity reduction. Also, this capacity reduction is found to be higher in compact sections for the most cases considered.

4 Reduction Factor for DSM Shear Design Rules

Shear capacities of stainless steel LCBs with reduced WSP heights lie well below the current DSM shear design curve for stainless steel according to Fig. 5. Therefore, to fit these points closer to the current design curve, suitable reduction factor (RF) was proposed following a regression analysis. When proposing this reduction factor, FE data in the region A of Fig. 5 were not considered. The proposed reduction factor is given in Eq. (13) and can be used together with the current DSM shear design curve to predict shear capacity of stainless steel LCBs with reduced support restraints. The distribution of FE shear capacities after applying the proposed reduction factor is compared with the current DSM design curve and shown in Fig. 6. Actual-to-predicted shear capacity reduction ratio has a mean and COV of 1.00 and 0.097, respectively, therefore highlight the accuracy of the developed expression.

$$\mathrm{RF} = 0.195 + 0.479\left[\frac{h_{WSP}}{d_1}\right]^{6.424} + 0.117\left[\frac{f_u}{f_y}\right]^{0.852} + 0.175[\lambda]^{-0.183} \text{ for } \frac{h_{WSP}}{d_1} < 1 \tag{13}$$

where f_u is the ultimate tensile stress of the material.

Table 2 Summary of parametric study results

Section	Shear capacity (kN)			
	$h_{WSP} = d_1$	$h_{WSP} = 0.8 \times d_1$	$h_{WSP} = 0.6 \times d_1$	$h_{WSP} = 0.4 \times d_1$
Grade 1.4301				
LCB 150 × 65 × 15 × 1	15.6	14.5	14.5	14.3
LCB 150 × 65 × 15 × 2	41.2	33.8	31.9	32.6
LCB 150 × 65 × 15 × 3	72.0	54.2	49.2	48.5
LCB 150 × 65 × 15 × 4	106.2	82.7	68.6	68.0
LCB 150 × 65 × 15 × 5	148.7	118.9	105.2	100.5
LCB 200 × 75 × 15 × 1	17.3	15.9	15.9	14.8
LCB 200 × 75 × 15 × 2	48.1	34.7	32.3	33.1
LCB 200 × 75 × 15 × 3	85.4	57.3	50.8	50.1
LCB 200 × 75 × 15 × 4	124.6	88.7	72.2	70.6
LCB 200 × 75 × 15 × 5	171.2	123.1	103.2	95.1
Grade 1.4462				
LCB 150 × 65 × 15 × 1	26.5	25.5	24.0	22.8
LCB 150 × 65 × 15 × 2	76.6	50.0	44.8	46.1
LCB 150 × 65 × 15 × 3	134.3	87.9	76.6	73.0
LCB 150 × 65 × 15 × 4	190.9	142.1	110.5	104.2
LCB 150 × 65 × 15 × 5	255.3	205.4	174.6	157.7
LCB 200 × 75 × 15 × 1	28.4	24.8	23.9	22.5
LCB 200 × 75 × 15 × 2	88.2	51.1	46.0	47.4
LCB 200 × 75 × 15 × 3	162.7	92.7	80.1	76.7
LCB 200 × 75 × 15 × 4	235.1	150.9	117.8	110.6

(continued)

Table 2 (continued)

Section	Shear capacity (kN)			
	$h_{WSP} = d_1$	$h_{WSP} = 0.8 \times d_1$	$h_{WSP} = 0.6 \times d_1$	$h_{WSP} = 0.4 \times d_1$
LCB 200 × 75 × 15 × 5	310.3	215.5	174.4	152.5

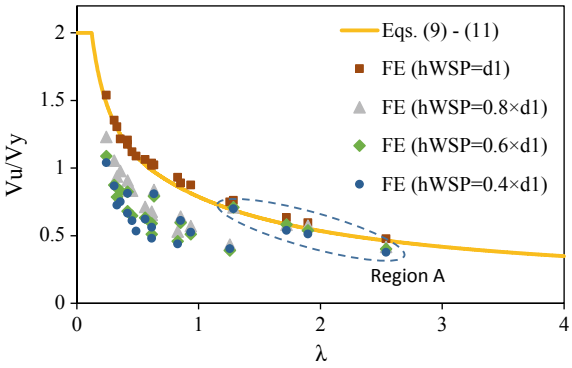

Fig. 5 FE shear capacities of LCBs with reduced WSP heights and DSM shear design curve

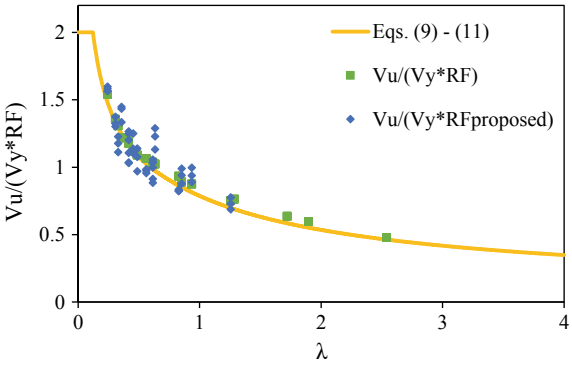

Fig. 6 Distribution of FE shear capacities of LCBs after applying the reduction factor and the current DSM shear design curve

5 Conclusions

In this paper the effect of reduced support restraints on the shear behaviour of stainless steel LCBs was investigated by means of FE modelling. Initially, FE models were validated with available full-height WSP test results from the literature and then parametric FE studies were conducted. Those results were then utilised to propose a reduction factor for DSM design rules to account for shear capacity loss due to the reduced support restraints. It can be concluded that shear capacity of stainless steel LCBs reduces with the reduction of the support height, where about 50% reduction in shear capacity can be observed for 60% reduction in WSP height while this capacity

reduction is higher in compact sections compared to slender sections. In order to account for these capacity reductions, a reduction factor for DSM shear design rules were proposed based on the FE results. Proposals found to be agree well with the FE results where actual-to-predicted shear capacity reduction ratio for the proposal has a mean and COV of 1.00 and 0.097, respectively. However, the applicability of this reduction factor is limited to compact sections. Therefore, further investigations are underway to address this limitation.

References

1. American Iron and Steel Institute (2007) AISI–S100–2007. North American specification for the design of cold-formed steel structural members, Washington (DC), AISI
2. Arrayago I, Real E, Gardner L (2015) Description of stress-strain curves for stainless steel alloys. Mater Des 87:540–552
3. Dissanayake DMMP, Pologanathan K, Gunalan S, Tsavdaridis KD, Nagaratnam B, Wanniarachchi KS (2019) Numerical modelling and shear design rules of stainless steel lipped channel sections. J Constr Steel Res (in press)
4. Dissanayake M, Pologanathan K, Gunalan S, Tsavdaridis KD, Nagaratnam B (2019) Finite element analyses of cold-formed stainless steel beams subject to shear. Spec Issue Proc Nordic Steel 3(3–4):931–936
5. Dissanayake DMMP, Pologanathan K, Gunalan S, Tsavdaridis KD, Degtyareva N (2019) Effect of corner strength enhancement on shear behaviour of stainless steel lipped channel sections. In: The 10th international conference on structural engineering and construction management, Kandy, Sri Lanka, 12–14 Dec 2019
6. Fareed I, Somadasa W, Pologanathan K, Gunalan S, Corradi M, Sivapalan S (2019) Finite element analyses of cold-formed stainless steel beam with web openings in shear. Spec Issue Proc Nordic Steel 3(3–4):907–912
7. Gardner L, Nethercot DA (2004) Numerical modelling of stainless steel structural components—a consistent approach. J Struct Eng 130(10):1586–1601
8. Keerthan P, Mahendran M (2011) Numerical modeling of litesteel beams subject to shear. J Struct Eng 137(12):1428–1439
9. Keerthan P, Mahendran M (2012) Shear behaviour and strength of LiteSteel beams with web openings. Adv Struct Eng 15(2):171–184
10. Keerthan P, Mahendran M (2013a) Experimental studies of the shear behaviour and strength of lipped channel beams with web openings. Thin-Wall Struct 73:131–144
11. Keerthan P, Mahendran M (2013b) Shear buckling characteristics of cold-formed steel channel beams. Int J Steel Struct 13(3):385–399
12. Keerthan P, Mahendran M (2015a) Experimental investigation and design of lipped channel beams in shear. Thin-Wall Struct 86:174–184
13. Keerthan P, Mahendran M (2015b) Improved shear design rules of cold-formed steel beams. Eng Struct 99:603–615
14. Keerthan P, Mahendran M, Hughes D (2014) Numerical studies and design of hollow flange channel beams subject to combined bending and shear actions. Eng Struct 75:197–212
15. Keerthan P, Mahendran M, Narsey A (2015) Shear tests of hollow flange channel beams with real support conditions. Structures 3:109–119
16. Mahendran M, Keerthan P (2013) Experimental studies of the shear behavior and strength of litesteel beams with stiffened web openings. Eng Struct 49:840–854
17. Pham CH, Hancock GJ (2012) Tension field action for cold-formed sections in shear. J Constr Steel Res 72:168–178

18. Pham CH, Zelenkin D, Hancock GJ (2017) Effect of flange restraints on shear tension field action in cold-formed C-sections. J Constr Steel Res 129:42–53
19. Standards Australia/Standards New Zealand (2005) AS/NZS 4600 cold-formed steel structures. Sydney, SA
20. Sundararajah L, Mahendran M, Keerthan P (2017a) New design rules for lipped channel beams subject to web crippling under two-flange load cases. Thin-Wall Struct 119:421–437
21. Sundararajah L, Mahendran M, Keerthan P (2017b) Web crippling experiments of high strength lipped channel beams under one-flange loading. J Constr Steel Res 138:851–866

Influence of Type of Interfaces on Railway Ballast Behavior

S. K. Navaratnarajah, K. R. C. M. Gunawardhana, and M. A. S. P. Gunawardhana

Abstract Railroads are one of the most popular modes of transportation in many countries including Sri Lanka. However, rapidly growing populations and increasing congestion in road transport have created severe challenges to the sustainability of rail transport infrastructure, which in turn elevate the demand for increased speed and higher capacity trains. Due to the increase of speed and load, excessive lateral stresses are induced in rail track foundations leads to lateral instability of the track. Ballast layer underneath and around the sleeper play significant role in resisting lateral movement and give stability to track structures. In addition to the ballast shear resistance, there are various interfaces in rail track such as ballast-sleeper (timber or concrete), ballast-resilient pads (under sleeper pads-USP or under ballast mats-UBM), and ballast-subgrade (or subballast) significantly influencing the overall shear behavior. It is important to understand the shear behavior of these interfaces. Therefore, this study is to evaluate the shear behavior under static loading condition of some of the commonly used interfaces found in ballasted rail track using large-scale direct shear apparatus considering full size ballast particles collected from nearby rail ballast quarry. The large-scale direct shear test has been carried out for fresh ballast and three different interfaces: (i) ballast–concrete sleeper, (ii) ballast–timber sleeper and (iii) ballast–USP under three different normal stress conditions (30, 60 and 90 kPa). Shear strength parameters of interfaces are evaluated and compared with that of the fresh ballast shear parameter. In addition to that, ballast degradation behaviour is also analyzed using the Ballast Breakage Index (BBI) method.

Keywords Ballast · USP · Direct shear test · Degradation · Friction angle

1 Introduction

Railway Ballast is the foundation material for rail track, and it is placed just below and around the sleepers. The loads from the wheels of trains come through rails

S. K. Navaratnarajah (✉) · K. R. C. M. Gunawardhana · M. A. S. P. Gunawardhana
Department of Civil Engineering, University of Peradeniya, Peradeniya, Sri Lanka
e-mail: navask@eng.pdn.ac.lk

R. Dissanayake et al. (eds.), *ICSECM 2019*, Lecture Notes in Civil Engineering 94,
https://doi.org/10.1007/978-981-15-7222-7_21

and sleepers is distributed by the ballast to the subgrade bed. The past studies have identified many functions of railway ballast. The main function of the ballast is to ensure fast drainage and reduce the magnitudes of vertical stress distributed to the underlying weak subgrade from heavy loading trains [6, 9, 12]. According to [2, 11], crushed, angular rock or hard stone ballast helps substructure to support against vertical, lateral and longitudinal forces from trains, provide firm and level bed for the sleepers to rest on; allow for maintaining correct track level without disturbing the rail roadbed, discourage the growth of vegetation, protect the surface of formation and to form an elastic bed, hold the sleepers in position during the passage of trains; transmit and distribute the loads from the sleepers to the subgrade and provide lateral stability to the track as a whole. Reference [1] has proposed that by using, (a) Finer ballast gradations, including the use of a layer of finer material beneath the sleeper (b) Using softer USPs (c) Using lower stiffness sleeper materials such as timber or plastic sleepers, an increase in the number and area of contacts can be achieved in the sleeper to ballast interface. Under Sleeper pads (USP) and Under Ballast Mat (UBM) both are resilient rubber materials that are used to enhance the ballast interface performances [8]. USP is installed between sleeper and ballast while UBM are installed between ballast and subgrade/subballast.

There are many different types of interfaces that can be identified in rail tracks such as (i) Rail-Sleeper, (ii) Sleeper–Ballast, (iii) Ballast–Subballast, (vi) Subballast–Subgrade. When resilient elements like Rail Pads (RP), Under Sleeper Pads (USP) and Under Ballast Mats (UBM) are inserted there are additional interfaces such as: (i) Rail-RP, (ii) RP-Sleeper, (iii) USP-Ballast, (iv) Ballast-UBM and (v) UBM-Subballast/Subgrade can be identified in rail track substructure. The type of sleeper material can be most commonly timber, concrete or steel. Therefore, the variation in material and interface types has a significant influence on rail track substructure behavior especially the shear resistance of the track.

This study is to evaluate the shear strength parameters of different types of interfaces and its influence on ballast breakage behavior under different static loading conditions and compare that of fresh ballast behavior. The ballast tested was based on Indian standard ballast gradation which is currently adopted in Sri Lankan rail tracks. Shear strength and degradation of fresh ballast were compared with that of three different interfaces: (i) Ballast-Concrete Sleeper, (ii) Ballast-Timber Sleeper and (iii) Ballast-USP on Concrete Sleeper under three different normal loads through a series of direct shear tests using large scale direct shear test apparatus design and built at the University of Peradeniya.

2 Materials and Methods

The tests were conducted on a biotite gneiss ballast sample obtained from a stockpile of the Gampola Railway Unit. The collected ballast sample was sieved and washed to remove any fine dust and clay adhering to them which can be contaminated at the storage site and then left to air dry [9]. The air dries sample then mixed in desired

proportions to obtain a standard Indian standard graded sample shown in Fig. 1. This Figure also shows the upper and lower limits of Indian standard gradation [7].

To simulate types of sleeper interface in the direct shear apparatus, a used timber sleeper was obtained from Gampola Railway Unit and was cut and made to circular in shapes of timber pieces to fit inside the direct shear test apparatus. Grade 60 concrete was used to make the circular concrete sleeper sample. A 10 mm thick USP was attached to a circular concrete sleeper to simulate the ballast-USP interface. Figure 2 shows prepared sleeper timber and concrete sleepers and a USP sample is attached on top of the concrete sleeper.

Large scale direct shear apparatus used in this study can accommodate an aggregate specimen of diameter 400 mm and height 300 mm, and at the execution of the test it could shear the sample into two halves. Based on ASTM standards, the maximum particle size for direct shear testing is limited to 0.1 of apparatus diameter. Reference [4] reported that for low normal stresses, this limit could be relaxed to 0.2 for cohesion-less materials with minimal increase in friction angle. In this test,

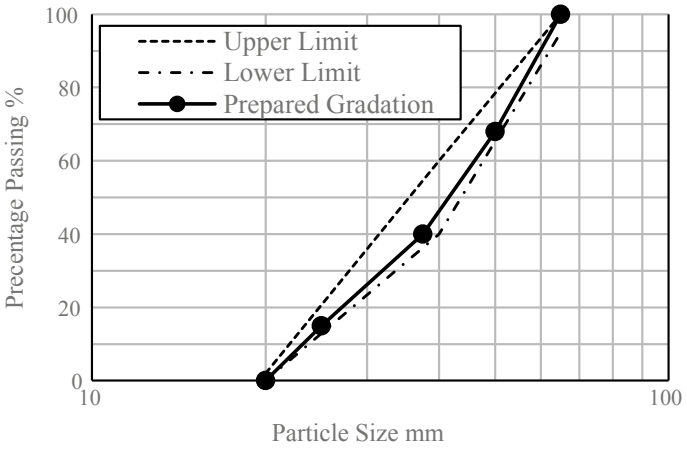

Fig. 1 Upper and lower limits of Indian standard gradation and prepared gradation

Fig. 2 Sleeper sample **a** Timber; **b** concrete; **c** USP

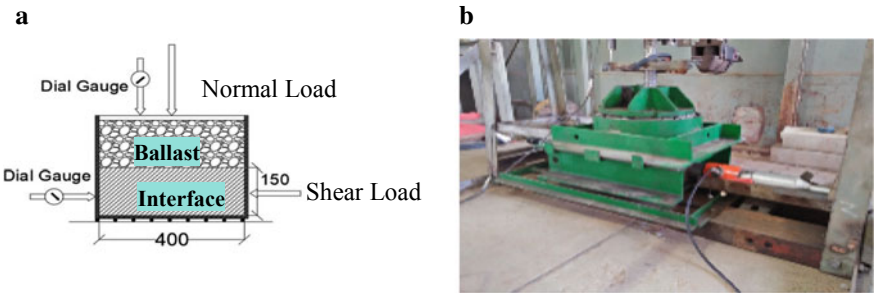

Fig. 3 Large scale direct shear apparatus **a** Schematic diagram; **b** actual apparatus

the maximum particle diameter of the aggregate mixture was 63 mm and the ratio of maximum particle size to the device diameter is 0.16 for the test sample.

The upper half of the direct shear apparatus is fixed to a frame and the lower half is free to move horizontally to make the test sample to shear with applied normal and lateral stresses. The top loading plate is free to move vertically to account for material dilation behavior. Shear and vertical displacements were measured using two displacement gauges fixed to top-loading plate and lover half cylinder of the apparatus. Shear force was applied using the hydraulic jack. Shearing rate of 4 mm/min was maintained throughout the experiment [3]. Applied shear force was measured using load cell fixed between hydraulic jack and lower half cylinder of the apparatus. Displacement gauges and a load cell were connected to a data logger to record data automatically. A schematic and photograph of the large-scale direct shear apparatus are shown in Fig. 3a, b, respectively. Normal loads were applied using lever technique through the top plates sitting on the top half cylinder of the apparatus. Tests were performed under three normal stresses of 30, 60 and 90 kPa. Specimens were sheared until a 60 mm maximum displacement corresponding to 15% shear strain is reached. At the end of each tests, the Ballast Breakage Index (BBI) was calculated according to the method proposed by [5].

3 Results and Discussion

Figure 4 illustrates the stress-strain relationships for fresh ballast and ballast with different interfaces under three normal loads. The shear area of the interface and the full height of the samples were considered for the stress-strain calculation. Based on the results, the fresh ballast exhibited higher shear resistance behavior showed at the strain of more than 10%. This was due to the higher interlocking nature of ballast aggregates. However, when the different interfaces are placed, the shear resistance gets decreased significantly as evident from Fig. 4. Surface friction of the interfaces is the main contributing factor for the shear resistance of the interfaces.

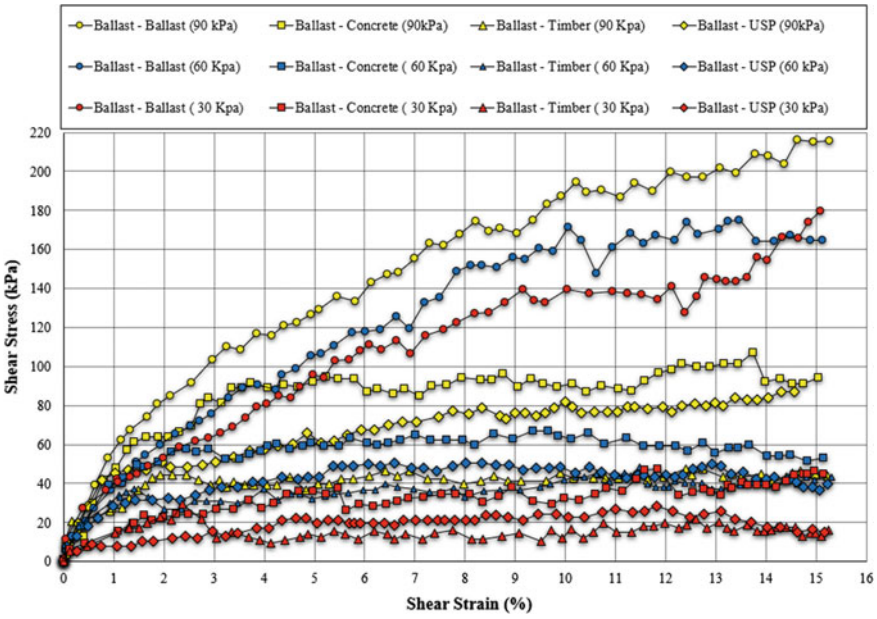

Fig. 4 Variation of shear stress with shear strain

Figure 5 illustrates the shear strain versus normal strain behavior of the specimens for each normal stress. Except for ballast-timber interfaces, fresh ballast and other

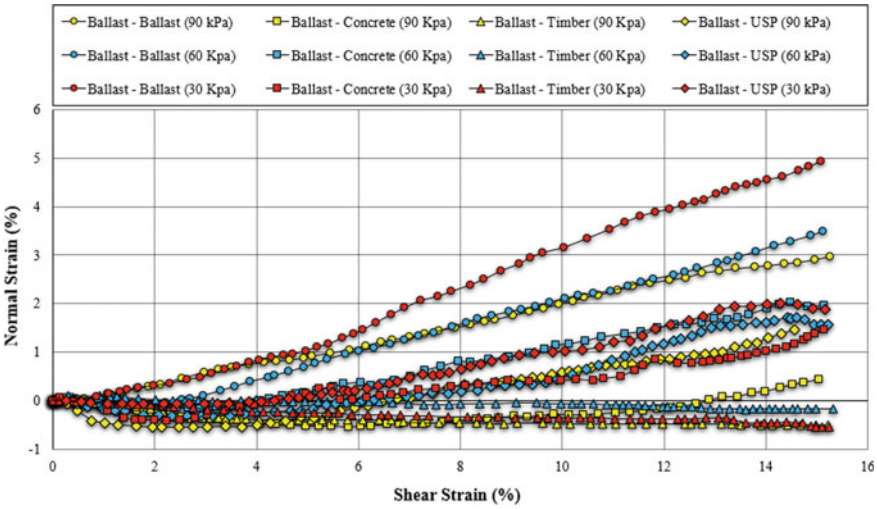

Fig. 5 Shear strain versus normal strain behavior

two interfaces exhibited the dilation behavior. Maximum dilation has occurred in fresh ballast and dilation has been increased with the decrease of normal load.

Dilation has not occurred in the Ballast-Timber interface because timber is relatively soft and smooth compared with concrete surface therefore the ballast particles tend to slide on the timber surface without particle rolling. It is evident from the visual observation of the timber sleeper before and after the test as shown in Fig. 6a, b where ballast slide scratch marks can be seen in the timber after the test.

The concrete sleeper before and after the test are shown in Fig. 7a, b. The concrete surface is hard and rough therefore, the ballast particles tend to roll on the concrete surface contributed to the dilation behavior. The concrete sleeper has not damaged much compared to timber sleeper.

Figure 8 shows shear stress to normal stress relationship at peak and the resulting Mohr-Coulomb (MC) failure surface with least-square fit assuming zero cohesion. The corresponding friction angle for fresh ballast and three other interfaces are shown in Table 1. Based on these results, fresh ballast exhibited higher shear resistance followed by Ballast-Concrete interface, Ballast-USP interface and then Ballast-Timber interface.

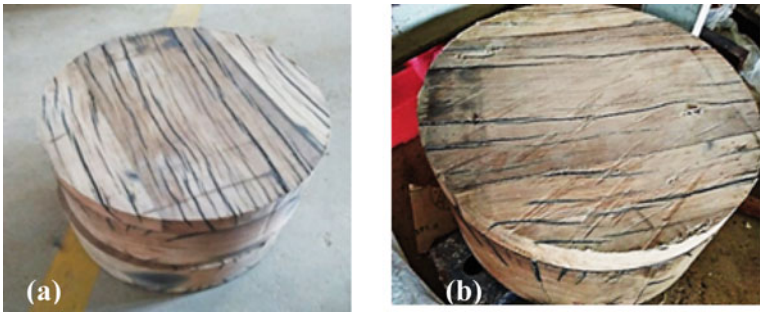

Fig. 6 Timber sleeper **a** before the test; **b** after the test

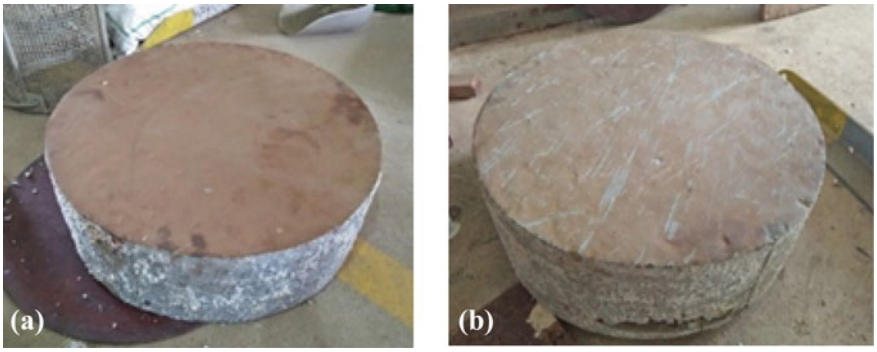

Fig. 7 Concrete sleeper **a** Before test; **b** after test

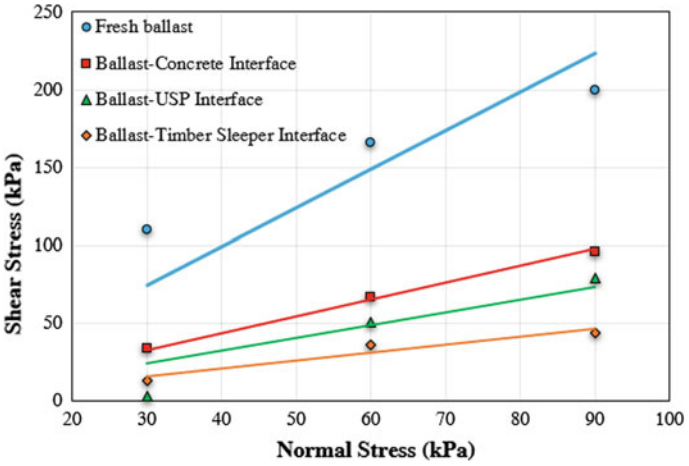

Fig. 8 Peak shear stress-normal stress relationship

Table 1 Friction angles of fresh ballast and three different interfaces

Interfaces	Friction angle (ϕ)
Fresh ballast	69°
Ballast-concrete interface	47°
Ballast-USP interface	39°
Ballast-timber interface	36°

At the end of each test, ballast samples were sieved again to obtain final PSD and subsequently, the corresponding BBI of each test was calculated as per [5]. The BBI calculated from this method is comparing the ballast gradation before and after the test with respect to an arbitrary boundary of maximum breakage as specified in [5]. Figure 9 shows the calculated ballast breakage index values. BBI has increased with the increase of normal load. The highest breakage has occurred in the fresh ballast and the lowest has occurred in the Ballast-USP interface. The highly angular interlocking ballast particles undergone significant breakage such as corner breakage, grinding and splitting during shearing [10]. USP is soft material therefore breakage is low in the ballast-USP interface. Ballast-Concrete interface has a comparatively higher breakage than the Ballast-Timber interface.

4 Conclusions

Ballast has the highest shear strength because of the particles are highly angular in nature and the strength of parent material is also high. Ballast–Concrete interface has relatively high shear strength due to the high hardness and high surface roughness.

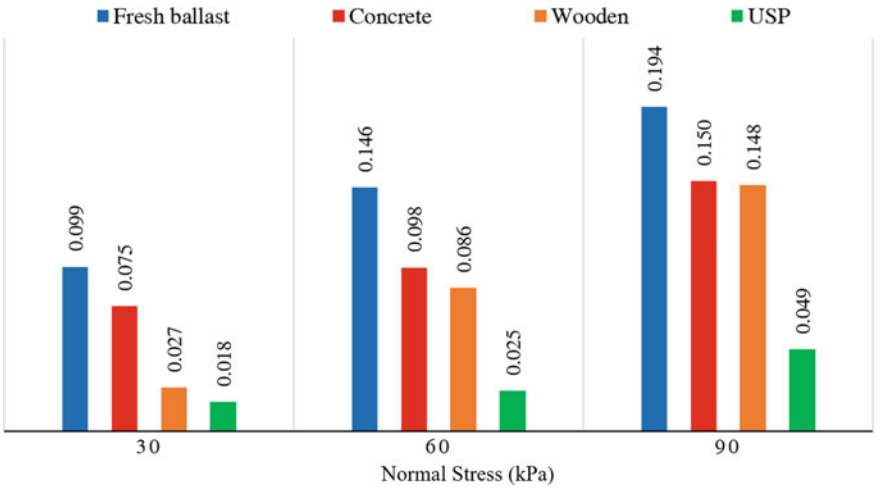

Fig. 9 Ballast breakage index (BBI)

Lowest shear strength has occurred in Ballast–Timber interface. Ballast–USP interface has high shear resistance than the Ballast–Timber interface. The highest breakage has occurred in the fresh ballast and the lowest has occurred in the Ballast-USP interface. The softer material of USP significantly lowered the breakage. Ballast-Concrete interface has a comparatively high breakage than the Ballast-Timber interface. Using a concrete sleeper will give high lateral resistance than using a wooden sleeper. However, ballast breakage is high in concrete sleepers. Introducing USP with the concrete sleeper significantly reduces the ballast breakages. Therefore, the life of ballast materials can be increased by introducing USPs to concrete sleepers.

Acknowledgements This research work is supported by the University of Peradeniya Research Grant (Grant No: URG-2017-29-E) and Accelerating Higher Education Expansion and Development (AHEAD) Operation of the Ministry of Higher Education funded by the World Bank (Grant No: AHEAD/RA3/DOR/STEM/No. 63) are acknowledged with the appreciation by the Authors. The authors sincerely appreciate the support provided by the Nanuoya Railway District Engineer, and staffs of the Gampola Railway units of Sri Lankan Railways for helping to collect the test materials.

References

1. Abadi T, Le Pen L, Zervos A, Powrie W (2015) Measuring the area and number of ballast particle contacts at sleeper/ballast and ballast/subgrade interfaces. Int J Railw Technol 4(2):45–72
2. Dahlberg T (2003) Railway track settlement—a literature review. Report for the EU project SUPERTRACK, Linköping University, SE-581 83 Linköping, Sweden
3. Dissanayake D, Kurukulasuriya L, Dissanayake P (2016) Evaluation of shear strength parameters of rail track ballast in Sri Lanka. J Natl Sci Found Sri Lanka 44(1):61–67

4. Fakhimi A, Hosseinpour H (2008) The role of oversize particles on the shear strength and deformational behavior of rock pile material. In: The 42nd US rock mechanics symposium (USRMS). American Rock Mechanics Association, pp 1–7
5. Indraratna B, Lackenby J, Christie D (2005) Effect of confining pressure on the degradation of ballast under cyclic loading. Géotechnique 55(4):325–328
6. Indraratna B, Salim W, Rujikiatkamjorn C (2011) Advanced rail geotechnology: ballasted track. CRC Press/Balkema, Rotterdam, Netherlands
7. IRS-GE-1 (2004) Specifications for track ballast. Indian Railway Specification
8. Navaratnarajah SK (2017) Application of rubber inclusions to enhance the stability of ballasted rail track under cyclic loading. Ph.D. Thesis University of Wollongong, Australia
9. Navaratnarajah SK, Indraratna B (2017) Use of rubber mats to improve the deformation and degradation behavior of rail ballast under cyclic loading. ASCE J Geotech Geoenviron Eng 143(6):04017015
10. Navaratnarajah SK, Indraratna B, Ngo NT (2018) Influence of under sleeper pads on ballast behavior under cyclic loading: experimental and numerical studies. ASCE J Geotech Geoenviron Eng 144(9):04018068
11. Profillidis VA (2014) Railway management and engineering. Ashgate Publishing, Ltd.
12. Suiker AS, Selig ET, Frenkel R (2005) Static and cyclic triaxial testing of ballast and subballast. J Geotech Geoenviron Eng 131(6):771–782

Effect of Loading Sequence in Fatigue Life Prediction of a 130 Years Old Railway Bridge

P. A. K. Karunananda, H. K. C. U. Herath, W. S. Madusanka, and W. M. A. D. Wijethunge

Abstract The Miner's rule is the simplest and the most commonly used fatigue life estimation technique for railway bridges [1]. One of its salient features is that life calculation is simpler and reliable when the detailed loading history is unknown. Further, it has been recognized for fatigue damage estimation in various codes of practices. However, in the case of existing railway bridges where the detailed loading history is known, Miner's rule might provide incorrect results because it does not not properly take account the loading sequence effect. In the light of this fundamental deficiency, a new damage indicator has been proposed to capture the load sequence effect more precisely by Mesmacque et al. (Int J Fatigue 27:461–467 [2]). The new damage indicator has successfully been applied by Siriwardane et al. in 2008 for fatigue damage estimation of a major bridge in Sri Lanka. From 2012 onwards, Sri Lankan Railways has introduced heavier class of locomotives and some of these new loco's have more than 40% heavier engine weights than previously used locomotives. The major objective of this study is to estimate the remaining fatigue life of above railway bridge using the sequential law under increased live loads. The bridge is one of the longest railway bridges in Sri Lanka, constructed in 1885, which is still in operation. A Finite Element model of the bridge was developed using SAP2000 V.14 general purpose software package and the fatigue damage estimation is performed by using a Mathlab code. The obtained fatigue lives are compared with commonly used Miner's estimations. The obtained results verify the effectiveness of the proposed model over commonly used Miner's rule for life prediction of steel bridges. Hence it could be concluded that it is advisable to apply the sequential law for assessment of remaining fatigue lives of riveted railway bridges, where the detailed stress histories are known. The results further strengthen the idea that necessity of sustainable asset management of civil infrastructures.

Keywords Railway bridges · Fatigue life · Miner's rule · Sequential law

P. A. K. Karunananda (✉) · H. K. C. U. Herath · W. S. Madusanka · W. M. A. D. Wijethunge
The Open University of Sri Lanka, Nawala, Nugegoda, Sri Lanka
e-mail: pakar@ou.ac.lk

R. Dissanayake et al. (eds.), *ICSECM 2019*, Lecture Notes in Civil Engineering 94,
https://doi.org/10.1007/978-981-15-7222-7_22

1 Introduction

Fatigue failure is a common phenomenon for metallic elements in structures when subjected to cyclic loading. It is generally recognized as one of the major failure mechanisms in structural and engineering components, accounting for about 90% of all mechanical failures. Most of the present day fatigue assessment approaches of railway bridges are generally based on combination of measured stress histories under actual traffic load, Miner's rule and fatigue curve which is also referred to as S–N or Wohler curve [3]. The Miner's rule is the simplest and the most commonly used fatigue life prediction technique. One of its interesting features is that life calculation is simple and reliable when the detailed loading history is unknown. However under many variable amplitude loading conditions, life predictions have been found to be unreliable since it did not properly take account the loading sequence effect [4]. As a result, real fatigue life due to same loading pattern is higher than the Miner's expectation for increasing of loads and it is lower than the Miner's expectation for decreasing of loads. Therefore, to overcome this problem recently a new damage indicator based on sequential law [2] was developed to capture the loading sequence effect of variable amplitude loads more precisely. The new damage indicator has successfully been applied by Siriwardane et al. in [4] for fatigue damage estimation of a major bridge in Sri Lanka. From 2012 onwards, Sri Lankan Railways has introduced heavier class of locomotives and some of these new loco's have more than 40% heavier engine weights than previously used locomotives. The aim of this study is to apply above method for fatigue life prediction of above railway bridge and identify the fatigue life difference of sequential based method with commonly used Miner's rule.

2 Kelani Railway Bridge

The selected bridge is one of the longest and busiest railway bridges in Sri Lanka spanning 160 m situated near Colombo (in marine environment) and carries the main railway line of the country. The bridge was constructed in 1885 and since then it has been in operation without any major structural alterations except some strengthening conducted in 1939. The bridge is semi-through having six double-system warren girders supported on cylindrical piers. The present service load varies from 30 to 120 tons.

The superstructure of the bridge consists of six riveted girders made of wrought iron. Each girder has an overall length of 85 ft 10 in., and the end girders are slightly different from central ones. Fish bellied cross girders, also of wrought iron, are supported on the lower booms of the main girders, and they have a span of 27 ft 2 in. The cross girders carry stringers, which in turn supports the two lines of the railway of gauge 5 ft 6 in. The bridge girders are supported on cylindrical piers, having cast-iron casings filled with concrete. The outer diameter of piers is 6 ft over

Fig. 1 Kelani railway bridge

the top 18 ft, and the diameter changes to 7 ft over a height of 4 ft, and remains at 7 ft over the bottom part. Diaphragms connect pairs of piers at the level of the taper. Reactions from the girders are transmitted to the piers through bed plates resting on pier fillings [5] (Fig. 1).

3 Methodology

Figure 2 shows the research flow chart. As shown below, there are seven main steps. At first the problem was identified. Then a literature survey was conducted to gather information related to the identified problem. After conducting a field visit some laboratory tests were carried out to identify the bridge component materials.

A model was developed using SAP2000 software and finally the life prediction of the bridge components were done using the Miner's rule and the sequential law.

4 Material Testing of Bridge Material

In order to ascertain the material properties of the wrought iron materials, following tests were carried out. The tests are tensile test, hardness test, Charpy test, microscopic examination and fatigue test. From these tests, following conclusions were made.

- The comparison of the mechanical properties shows that the Ultimate Tensile Strength values of wrought iron used in the bridge (i.e. 335–373 N/mm^2) falls within the range found in the literature (i.e. 234–373 N/mm^2). The lower value of

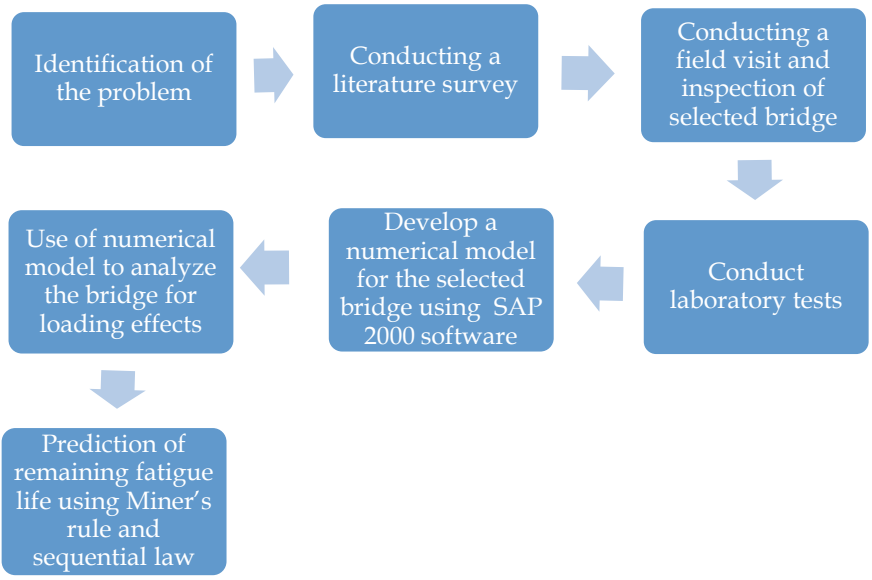

Fig. 2 Flowchart of the work flow

the range of Yield Strength of wrought iron used in bridge (i.e. 164–233 N/mm^2) also lies within the values given in the literature (159–221 N/mm^2).

- The tensile test carried out on the material shows that the Young's modulus of wrought iron is 193 GPa which is same as the experimental value for Young's modulus of wrought iron is found in the literature.
- Micro structural view of the sample is close enough with the micro structure of wrought iron which confirms that the sample is extracted from wrought iron material.
- Rockwell harndess number of 70.2 (approximately 70) also helps in the estimation of approximate tensile strength of material that is being tested and from the conversion charts, the approximate Tensile strength of Wrought Iron is about 61 ksi (420.5 N/mm^2).
- Impact test result indicates that the ductile to brittle transition temperature lies in the range in between 15 and 20 °C and the variation of impact energy vs temperature of wrought iron material exhibits a behaviour similar to low carbon steel.
- From fatigue test, possible S-N curve is obtained and fatigue limit is identified for the selected wrought iron specimen.

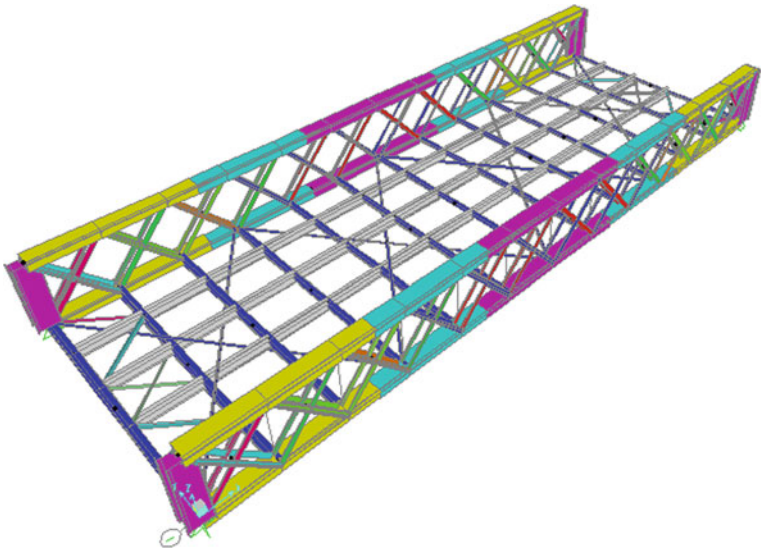

Fig. 3 Bridge model-3D extruded view

5 Modelling Details of Kelani Railway Bridge

The Kelani railway bridge consists of six spans of truss girders each simply supported on piers. Four middle spans are of similar trusses, while the two end spans have little variations at the ends. A 3D skeletal frame finite element model was developed for a complete span of the bridge incorporating the double trusses, cross girders, rail bearers and bracings. All these members are modeled with 3D frame elements. There were 19 different sets of member cross sections. Bridge dimensions and member dimensions were found from the structural drawings that were used in previous researches. Wrought iron material properties were used in the finite element modelling (Fig. 3).

6 Fatigue Life Prediction Using Sequential Law

The new damage indicator (present D_i value) was calculated from 2002 to the present by considering the sequence of stress ranges of each critical member. Assuming that future sequence of passage is similar to that of the present day, the time taken to reach the present day's D_i values to one (when $D_i = 1$ is considered as fatigue failure) was considered as the remaining fatigue life for each, critical member. The stress values were obtained under locomotives pass over the Kelani bridge for each type of bridge components separately. Then, the stress ranges and mean stresses were calculated according to the order of trains those are going through the bridge per day. The

Table 1 Damage fractions of bridge components using sequential law

Bridge component	Section	Damage fraction, D_i (per year)	Damage fraction, D_i (2002–2018)	Damage fraction, D_i (1885–2002)	$\sum_{1885}^{2018} D_i$
Main Girder	Set 2	0.0021203	0.0339248	0.38307	0.4169948
	Set 3	0.0013632	0.0218112	0.63255	0.6543612
	Set 4	0.0010738	0.0171808	0.54390	0.5610808
Cross Girders	Set 8	0.0199290	0.3188640	0.79454	1.1134040
Rail Bearers	Set 9	0.00070195	0.0112312	1.24476	1.2559912
Truss Diagonals	Set 6 out	0.0009488	0.0151800	0.50734	0.5225200
	Set 7 out	0.0027647	0.0442352	0.50327	0.5475052
	Set 8 out	0.0017890	0.0286240	0.22378	0.2524040
	Set 9 out	0.0028210	0.0451360	0.53167	0.5768060

Goodman equation that was mentioned above was used to do the correction of each stress range.

A mathematical code was written using a well-known numerical method, Newton Raphson in Mathlab software to obtain the damage for each component separately from 2002 to 2018. The results were obtained from the mathematical code are represented in Table 1.

Obtained Damage fraction, D_i for each member set were compared with the Miner's rule-based estimations as shown in Table 1. Even though the predicted damages from the two approaches illustrates some amount of deviation from each other, both approaches have highlighted that cross girders and rail bearers become the most vulnerable to fatigue failure. But actual load is not applied to the rail bearer and it transfer to the adjacent bearers and cross girders also. Further, it reveals that in case of main girder consisting of truss members, the sequential law-based damage fraction gives lower values than Miner's rule based values. But it is the opposite for bridge deck members (cross girders, rail bearers) (Table 2).

The remaining fatigue life of the critical bridge members was estimated using two approaches: (1) proposed model; which captures the loading sequence effect of variable amplitude loads (2) previous model (Miner's rule) and the obtained results are given in Table 3.

From the above, it can be concluded that, presently some member sets are safe since they have higher remaining fatigue lives. However, remaining fatigue lives of some members are relatively low compared to others. Therefore, these critical members should be carefully monitored and fatigue accumulation should continuously be checked. Once the remaining life reaches the target value, it is time to strengthen them.

Table 2 Damage fraction for critical members in member sets (2002–2018)

Bridge component	Member set	Damage fraction, D_i		Difference of D_i
		Miner rule	Sequential law	
Main Girder	Set 2	0.561523	0.4169948	0.144528
	Set 3	0.923874	0.6543612	0.269513
	Set 4	0.886072	0.5610808	0.324991
Cross Girders	Set 8	0.794759	1.1134040	−0.318650
Rail Bearers	Set 9	1.244854	1.2559912	−0.011140
Truss Diagonals	Set 6 out	0.755466	0.5225200	0.232946
	Set 7 out	1.119693	0.5475052	0.572188
	Set 8 out	0.597251	0.2524040	0.344847
	Set 9 out	1.140790	0.5768060	0.563984

Table 3 Summary of remaining fatigue lives of critical members in member sets

Bridge component	Member set	Remaining fatigue life (years)		Difference of remaining life
		Miner rule	Sequential law	
Main girder	Set 2	17.5774	+100	+100
	Set 3	1.5106	+100	+100
	Set 4	2.7762	+100	+100
Cross girders	Set 8	0.2583	0.690	0.432
Rail bearers	Set 9	−0.1967	0.762	0.959
Truss diagonals	Set 6 out	7.0688	+100	+100
	Set 7 out	−1.8963	+100	+100
	Set 8 out	10.3983	+100	+100
	Set 9 out	−2.2558	+100	+100

7 Conclusions

Comparison of Miner's estimation and sequential law's predictions illustrates + 100 year variation among the estimated remaining lives. Obviously the effect of members where the lives are very low (ex: Cross girders, rail bearers) becomes more significant in percentage terms. These observations and the phenomenological validity of the new damage indicator based sequential law tend to conclude that the application of sequential law based proposed approach is advisable for the evaluation of remaining fatigue life of riveted railway bridges where the detailed stress histories are known. Finally, these reasons conclude that it is of great importance to investigate accurately the condition of connections especially in old bridges for good judgment of fatigue life.

Acknowledgements Authors would like to highly acknowledge Dr. C. S. Bandara of the University of Peradeniya for his helps during material testing.

References

1. Imam B, Righiniotis TD, Chryssanthopoulos MK (2005) Fatigue assessment of riveted railway bridges. Int J Steel Struct 5(5):485–494
2. Mesmacque G, Garcia S, Nobile R, Panella FW (2005) Fatigue life prediction under variable loading based on a new non-linear continuum damage mechanics model. Int J Fatigue 27(4):461–467
3. Köröndi L, Szittner A, Kállóf L (1998) Determination of fatigue safety and remaining fatigue life on a riveted railway bridge by measurement. J Constr Steel Res 46(1–3)
4. Siriwardane S, Ohga M, Dissanayake R, Taniwaki K (2008) Application of new damage indicator—based sequential law for remaining fatigue life estimation of railway bridges. J Constr Steel Res 64(2):228–237
5. Ranaweera MP, Aberuwan H, Herath KRB, Maharoof ALM, Siriwardane SASC, Abesooriya AMND (2002) Assessment of Kelani railway bridge over Kelani river. Engineering Design Center, University of Peradeniya, Sri Lanka

Comparison of Rheology Measurement Techniques Used in 3D Concrete Printing Applications

Roshan Jayathilakage, Jay Sanjayan, and Pathmanathan Rajeev

Abstract 3D Concrete Printing (3DCP) is a novel and emerging construction technique to build using digital technologies and additive manufacturing concepts. Some main advantages of 3DCP are reduced formwork wastage, the capability of constructing complex geometric shapes, higher precision, shorter construction time and increased safety. In the particular method, the structure is built layer by layer by extruding the material through a nozzle. Initially, the material should be pumped and extruded with considerable fluidity and workability. Immediately after the extrusion, the extruded layers should have enough strength and stiffness to retain the desired shape. Therefore, controlling the rheology of the material is of high importance in 3DCP. Due to the higher stiffness, and higher time and rate-dependent material behavior (thixotropic behavior) compared to the conventional concrete, conventional rheology measurement techniques have many limitations when used for 3DCP material. Therefore, non-conventional (direct shear test, orifice extrusion, vane shear test), as well as conventional rheology measurement techniques (rotational rheometer and slump test), were conducted to compare the results and to characterize the rheological parameters. The rheological parameters (i.e. yield stress, viscosity, and thixotropic build rate) of concrete were measured for three different mixes. The achieved values were compared to decide the most suitable and reliable test method. The pros and cons of each test method also were discussed. The achieved yield stress values are different according to the test method used. However, a similar trend can be seen in all the testing methods. Rotational rheometer gives the lowest yield stress values, while an orifice extrusion test gives the highest yield stress values. Finally, it can be predicted that the extrusion-based testing methods such as orifice extrusion technique used in the current study give reliable results on yield stress and viscosity measurements due to the similarities between the measurement technique and the actual 3D printing extrusion process.

Keywords Rheology · Yield stress · Viscosity · Orifice extrusion · 3D concrete printing

R. Jayathilakage (✉) · J. Sanjayan · P. Rajeev
Department of Civil & Construction Engineering, Swinburne University of Technology, Melbourne, VIC, Australia
e-mail: rjayathilakage@swin.edu.au

R. Dissanayake et al. (eds.), *ICSECM 2019*, Lecture Notes in Civil Engineering 94,
https://doi.org/10.1007/978-981-15-7222-7_23

1 Introduction

1.1 3D Concrete Printing (3DCP)

3D concrete printing is a construction automation technology for manufacturing structural elements using a pre-defined 3D model. No formwork will be using in this particular method to support the structure. Also, geometrically complex shapes free from rectilinear shapes can be constructed easily and precisely in this method. The commonly used layer-based extrusion method is being implemented in different scales and types of 3D printers, where the material is extruded from a nozzle and print layer by layer to construct the required structure [16].

Initially, the material should be pumped and extruded with considerable fluidity and workability. Immediately after the extrusion, the extruded layers should have enough strength and stiffness to retain the desired shape [6]. Therefore, controlling the rheology of the material is of high importance in 3DCP [10].

Therefore, accurate measurements of rheological parameters are important to decide and optimize the mixes. In this paper, the vane shear test, direct shear test, and the orifice extrusion test were used for the rheology measurement of 3D printing concrete. Different mixes were tested for rheology measurements and the achieved values were compared to decide the most suitable and reliable test method.

1.2 Rheology of 3D Printing Concrete

Typically, concrete commonly being considered as a visco-plastic Bingham material. The flow of these type of material initiates if larger to critical shear stress, which is the yield stress (τ_y). The shear stress (τ) versus shear strain rate ($\dot{\boldsymbol{\gamma}}$) have a linear relationship while flowing. Plastic viscosity value (μ) will be the gradient of the shear stress versus shear rate line. Simply, the plastic viscosity can be defined as the resistance to flow. The Bingham model [4] is being commonly implemented for 3D printing concrete material as well.

Concrete and cementitious material also can be identified as thixotropic material. The material rheology may depend on the shear rate applied as well as the concrete age or resting time after mixing. With the concrete age after completion of the mixing, the yield stress can increase with time. As a result of the flocculation process of cement particles and internal structure build-up, this phenomenon can occur [13]. The model developed by Perrot et al. [11] explains the evolution of yield stress ($\tau_y(t)$) with concrete age (t) as in Eq. (1). The parameter A_{thix} is the structuration rate which can be assumed as a constant for a considered material. τ_{y0} is the initial yield stress at zero resting time. t_c defined as the characteristic time.

$$\tau_y(t) = A_{thix} t_c \left(e^{t/t_c} - 1\right) + \tau_{y0} \tag{1}$$

Measurement techniques used to assess the yield stress, viscosity and thixotropic build-up rate of 3D printing concrete will be discussed in the following sections. Some methods were reviewed in detail and were selected as suitable rheology measurement techniques for extrudable cement-based material by previous researchers [1, 9].

1.3 Rheology Measurement Techniques (Non-conventional)

1.3.1 Direct Shear Test

ASTM D3080/D3080M-11 standards were used for conducting the direct shear test. Refer previous work done by authors for more details on the test procedure [7].

1.3.2 Orifice Extrusion Test

The 3D printing concrete material can be filled inside an extruder barrel. Then, the material can be extruded through an orifice opening with different extrusion speeds to achieve the extrusion pressure variation with different velocities. Zhou et al. [17] developed the analytical model for orifice extrusion assuming that the extrudable cement-based material displays rigid-viscoplastic behavior due to the higher plastic strain compared with the elastic strain.

From previous studies done by Basterfield et al. [3] and Zhou et al. [17], it was found that the semi-solid fresh cement pastes and mortar in extrusion can be modeled using the uniaxial form of Hershel-Bulkley constitutive relationship. Using the uniaxial form of Hershel-Bulkley model and making the assumptions that the material is incompressible, the flow is sufficiently slow to neglect the inertia terms and the flow is not rotational, a closed-form relationship between the extrusion pressure and the material parameters was developed by Zhou et al. [17] as in Eq. (2):

$$P = 2\sigma_0 \ln\left(\frac{D_0}{D}\right) + Ak\left(\frac{2V}{D}\right)^n \left(1 - \left(\frac{D}{D_0}\right)^{3n}\right) \tag{2}$$

In Eq. (2), P, V, σ_0, k and n are extrusion pressure, extrusion velocity, uniaxial yield stress, uniaxial flow consistency, and uniaxial flow index respectively. D and D_0 are orifice diameter and barrel diameter respectively. A parameter is given in Eq. (3), where θ_{max} is the maximum convergent flow angle which can be taken as 45°. Basterfield et al. [3] found that the range of θ_{max} is around 40°–60°, assuming that the influence of the dead zones is such as to produce a slip plane of zero shear stress, which is roughly conical. Also, Basterfield et al. [3] found that the A parameter is a constant or not much sensitive for a particular value of n and θ_{max} of 40° and above.

$$A = \frac{2}{3n}[\sin\theta_{max}(1 + \cos\theta_{max})]^n \quad (3)$$

1.3.3 Vane Shear Test

Vane shear apparatus was used in the current study to evaluate the yield stress variation with the concrete age of the mixes. Vane shear test method was used by previous researchers to measure the yield stress of normal concrete [2] and 3D printing concrete [9]. In this study, an attempt was made to measure the thixotropic build-up rate of concrete using the vane shear apparatus in addition to the yield stress measurements.

1.4 Rheology Measurement Techniques (Conventional)

1.4.1 Rotational Rheometry

Usage of rotational rheometers is the most common and conventional testing method in order to measure the rheological parameters such as static yield stress, dynamic yield stress, viscosity, and thixotropy. The most commonly used rotational rheometers are co-axial type, parallel plate, and vane type rheometers [5]. However, coaxial and parallel plate geometries are only suitable for highly fluid concrete such as self-compacting concrete (SCC). 3D printing concrete mixes are of higher stiffness and usage of the parallel plate or coaxial type rheometers may result in wall slip effects. Therefore, for 3D printing concrete, the most effective and commonly used rheometer geometry is the vane geometry.

1.4.2 Slump Test

The slump test is a workability test, which commonly used to assess the workability of ready mixed concrete on-site. The slump height or the slump flow diameter (for SCC) gives a quick indication of the yield stress of a material. If the yield stress of a material is higher, lower the slump height and diameter or vice-versa. However, the viscosity may also have a considerable effect on slump height or flow diameter of highly fluid concrete [12]. Also, there are some analytical models available in the literature to assess the yield stress and viscosity of a mix, according to the slump height or flow diameter [12, 14].

Table 1 Mix proportions (weight proportions as ratios of the cement weight)

Mix	Cement	Silica fume	Coarse sand	Fine sand	Total sand	Water	Superplasticizer (ml/100 g of binder)	Retarders (ml/100 g of binder)
A	1	0.11	0.56	1.11	1.67	0.22	0.6	0.4
B	1	0.11	0.42	1.25	1.67	0.22	0.8	0.4
C	1	0.11	0.47	0.94	1.41	0.22	0.6	0.4

2 Experimental Work

2.1 Material and Mix

Three mixes were prepared using general-purpose cement according to AS3972 type I which is similar to ASTM C595/C595M. Graded sand with the coarse aggregate of 16/30 gradation (maximum particle size of 1.18 mm) and fine aggregate of 30/60 gradation (maximum particle size of 600 μm) was used for each mix with varying proportions. The mix proportions used are shown in Table 1.

2.2 Direct Shear Test

Shear Trac II was the testing setup used for the current experiment. A circular cross-section shear box with a diameter of 72.5 mm and a height of 42.7 mm was used. The shear box was filled with three layers of prepared mixes tamping each layer to minimize the void content. Lubricant oil was applied within the shearing surfaces of the shear box to reduce the friction of the surfaces.

The displacement rate and maximum applied normal stress are 8 mm per minute and 15 kPa respectively. Using the maximum shear stresses (after area correction) and the applied normal loads, Mohr-Coulomb failure envelops were developed to get the cohesion and friction angle values for each mix.

2.3 Orifice Extrusion Test

An in-house orifice extruder was used in the current study. The extruder barrel is 200 mm in diameter and 450 mm in height. The orifice used is of 40 mm diameter with zero thickness which gives a D/D_0 value of 0.2. According to Basterfield et al. [3], the selection of a larger barrel diameter is important in achieving more uniform packing and can accommodate more material. This means that the tests tend to be more consistent and more tests can be carried out for a single barrel load.

The material was filled up to half of the height of the barrel prior to testing. The testing was done using different piston driving velocities ranges from 0.1 to 4 mm s^{-1}. For each particular constant piston driving velocity, the constant extruding force (at steady state) was recorded. Three tests were performed for a considered piston driving velocity and the average extruding force considering the three trials can be calculated. Due to the assumption made that the material considered is incompressible, the material velocity at the orifice was not calculated experimentally but, calculated using mass conservation law.

Using the analytical model presented in Eq. (2), the best-fit curves for the experimental values were achieved to get the uniaxial yield stress, flow consistency and flow index values.

2.4 Vane Shear Test

Yield stress evolution was measured using a vane shear apparatus as done by Le et al. [8], according to the standard ASTM D4648/D4648M. The vane used had four blades with a height of 70 mm and a width of 90 mm. All the measurements were taken in order to comply with the standards and to prevent the slip effects of the material with the container wall. Shear strength or yield stress measurements were taken for 15 min time intervals from 0 to 60 min. The maximum angle measurements were taken and later converted to shear strength value according to the standards.

2.5 Rotational Rheometry

An ICAR rheometer with 4 blade vane geometry was used for the static yield stress, dynamic yield stress, and viscosity measurements. The blade used has a diameter and a height of 127 mm. For the static yield stress measurements, the slotted container (to prevent the wall slip effects) was filled with 20 L of concrete. Then, a low shear rate (1.5 rpm) was applied using the vane. The shear stress versus shear strain curve was used to find the maximum shear stress which can be considered as the static yield stress. For the dynamic yield stress and viscosity measurements, after filling the material inside the container, the rotational speed was increased from zero to 30 rpm within 50 s. The shear stress versus shear rate linear flow curves (Bingham model) were used to evaluate the dynamic yield stress (shear stress at zero shear rate) and the viscosity (slope of the flow curve) of the material.

2.6 Slump Test

In the current study, a slump test according to ASTM C143/C143M was done to achieve the slump value and the flow values of the 3 mixes. A standard slump cone with 200 mm bottom diameter, 100 mm top diameter and a 300 mm height was used for the tests. Initially, the slump cone was filled with material in 3 layers and each layer was compacted using a standard rod, according to the standards. Then, the top surface was trimmed by removing the excess material. The slump cone was then lifted vertically and the change in height (slump) and the bottom diameter (slump flow) was measured. Three trials were performed for each mix to get an average slump height and an average flow value.

3 Results and Discussion

The results achieved for each mix and in different experiments are as follows.

3.1 Direct Shear Test

Cohesion values (at zero normal stress) can be achieved from the Mohr-Coulomb failure envelops (Fig. 1). The cohesion value can be considered as the yield stress value of the mix considered due to the very low shear rates applied for shearing the sample (nearly 0.13 s^{-1} for 8 mm min^{-1} displacement rate) [7].

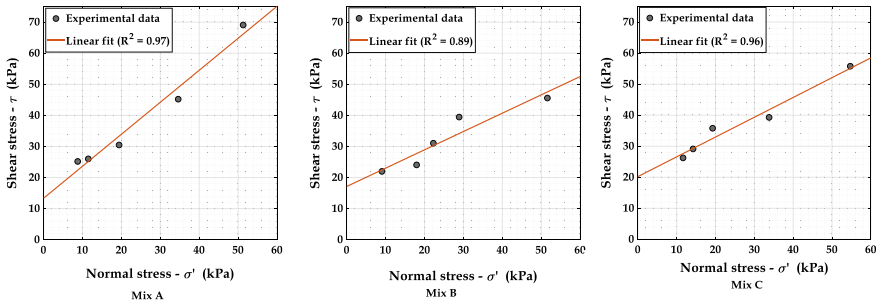

Fig. 1 Mohr-Coulomb failure envelops [7]

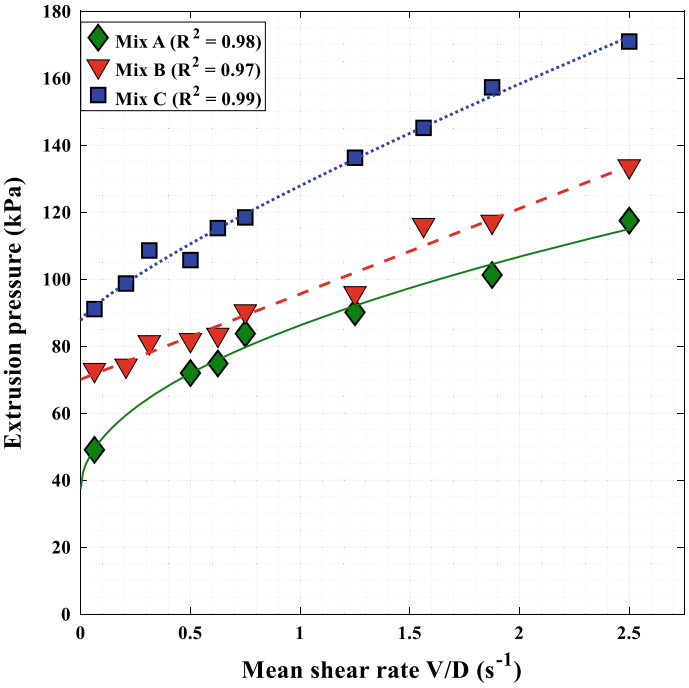

Fig. 2 Orifice extrusion pressure versus mean shear rate for different mixes and the curve fitting [8]

3.2 Orifice Extrusion

Figure 2 shows the extrusion pressure versus the mean shear rate values and the curve fitting using Eq. (2). Using the least square error regression analysis, the uniaxial yield stress, flow consistency and flow index values can be found for the three mixes.

3.3 Vane Shear Test

Vane shear test results are shown in Fig. 3. The yield stress evolution with time data can be fitted using Eq. (1).

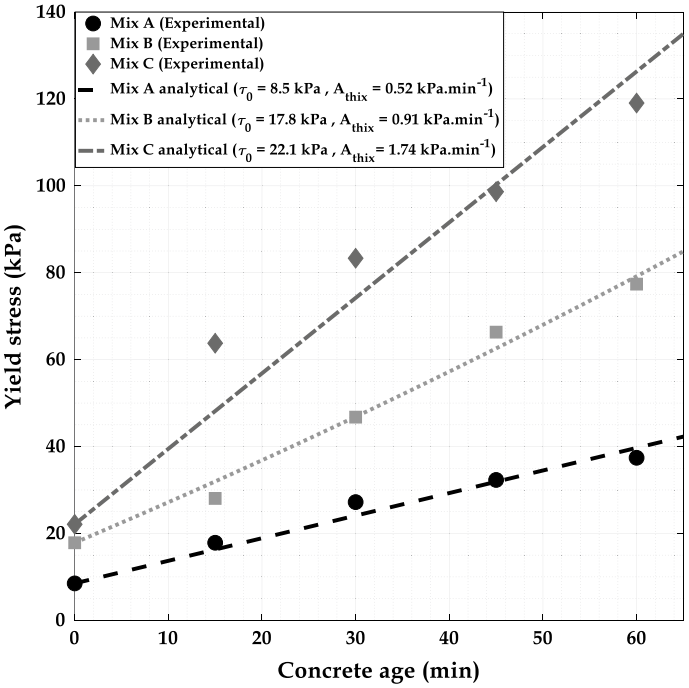

Fig. 3 Vane shear test experimental results and thixotropic model fitting

3.4 Rotational Rheometer

Torque versus rotational speed graphs for the three mixes are shown in Fig. 4. Later, the dynamic yield stress values and the viscosity of the mixes were achieved using the Bingham model fitting. The yield stress and shear rate conversion factors were used to convert the torque and rotational speed to shear stress and shear rate.

The achieved static yield stress for Mix A, Mix B, and Mix C are 2.4 kPa, 3.5 kPa, and 3.5 kPa respectively. The dynamic yield stress values for Mix A, Mix B, and Mix C are 1.2 kPa, 1.8 kPa, and 1.6 kPa respectively. Furthermore, the viscosity values achieved are 47.1 Pa s, 26.1 Pa s, and 24.2 Pa s respectively for Mix A, Mix B, and Mix C.

3.5 Slump Test

The achieved slump height for Mix A, Mix B, and Mix C are 35 mm, 32 mm and 27 mm respectively. The final slump diameter is 202 mm, 200 mm and 200 mm respectively for Mix A, Mix B, and Mix C. There were no specific changes in slump height or slump flow values in the mixes due to higher yield stresses.

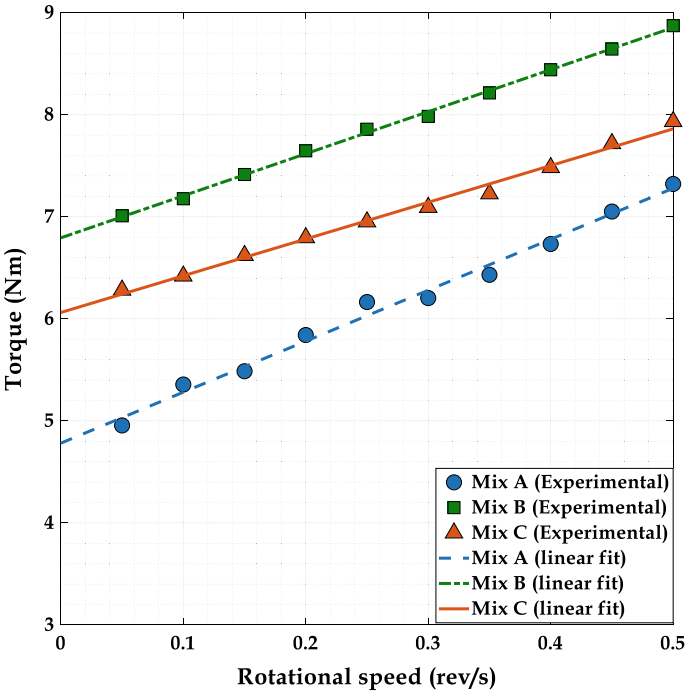

Fig. 4 Rheometer test results for torque versus rotational speed

Table 2 gives a summary of the results of each test.

From Table 2, it can be seen that the yield stress values achieved are varying according to the test method used. However, the similar increasing trend of yield stress from Mix A to Mix C can be seen in every test method. From the friction angles achieved from the direct shear test, it can be concluded that Mix A displays a higher frictional behavior compared to the other two mixes. This may be due to the higher coarse sand proportion and the higher aggregate proportion used comparatively to the other two mixes. A well-known issue in the direct shear test is, that due to the drained conditions of the test procedure, water drainage can happen while applying a normal load. This may result in high shear stress values [15].

Generally, the orifice extrusion test gives higher yield stress values compared to other testing methods. In orifice extrusion, the measured yield stresses are uniaxial yield stress values. All the other test methods provide a shear yield stress value. The material which does not exhibit flow anisotropy, the uniaxial yield stresses and flow consistencies are higher than the shear yield stress and flow consistency value [3]. Also, the shear rates used in orifice extrusion cover a wide range of shear rates (up to 3 s^{-1}), which are similar to the actual extrusion process [7]. Another advantage of the orifice extrusion method is that the viscosity of each mix can be achieved using the flow consistency and flow index values. Introducing a die, instead of an orifice at the outlet of the ram extruder may also give useful information on wall

Table 2 Summary of the rheological parameters achieved from different test methods

Mix	Direct shear test		Vane shear test	Orifice extrusion			Rheometer			Slump test
	Cohesion (kPa)	Friction angle (°)	τ_0 (kPa)	σ_0 (kPa)	k (kPa s^n)	n	Static yield stress (kPa)	Dynamic yield stress (kPa)	Viscosity (Pa · s)	Slump height (mm)
A	13.4	46	8.5	11.6	26.0	0.5	2.4	1.2	47.1	35
B	17.1	31	17.9	21.8	16.0	1.0	3.5	1.8	26.1	32
C	20.2	33	22.1	27.2	24.4	0.8	3.5	1.6	24.2	27

shear stress. This may be useful in quantifying "extrudability" term in concrete 3D printing applications and is of interest for future research.

The vane shear test also gives reasonably closer values to the cohesion values achieved from the direct shear test method. However, the values were expected to be closer to the static yield stress values achieved from the rheometer test due to the vane geometry used in the rheometer. The standard 20 L container (with 410 mm diameter) may not provide enough clearance between the vane and the rheometer wall while shearing the high yield stress material used here. Therefore, small slippage can be observed between the material surfaces near to the rheometer wall. This effect may result in low yield stress values compared to the vane shear test. Even though the non-conventional tests give different yield stress values for Mix B and Mix C, the rheometer static yield stresses are similar for Mix B and Mix C. If comparing the rheometer results with other test methods, a low resolution can be seen in the achieved static yield stress values.

The slump test gives the highest slump value (i.e. lowest yield stress) for Mix A and lowest slump value (i.e. highest yield stress) for Mix C. However, the slump height also has very low resolution and typically low values compared with the slump values for commonly used normal concrete in literature.

4 Conclusions

Three 3DCP mixes were tested for rheology using different methods, and the achieved values were compared to decide the most suitable and reliable test method. The following conclusions can be made from the study.

Each test method can be used to determine the yield stress values of each mix. However, different values for yield stress can be achieved from each test method with a similar trend (increasing trend from Mix A to Mix C).

The direct shear test may be overestimating the yield stress values for material due to the drained conditions used in the test method. Therefore, the direct shear test is not suitable for high w/c ratio mixes.

Vane shear test method is the easiest to conduct and most suitable to measure the thixotropic build-up of 3D printing concrete.

Orifice extrusion method may be the most appropriate test method to achieve uniaxial yield stress value, which is slightly higher than the shear yield stress value for material which does not display the flow anisotropy. Also, the similarity of the shear rates used for the testing method and the similarity between the orifice extrusion and the actual extrusion process may give the useful yield stress and flow consistency parameters for 3D printing concrete.

Rheometer test gives low static yield stress values for each mix with low resolution. 3D printing mixes have very low slump heights with very low resolution. Therefore, the slump test is not suitable for 3D printing mixes (used in the study) to compare the workability. Rheometers with vane geometry, which have appropriate yield stress measurement capacity and enough clearance space for shearing (to reduce the slip effects) should be selected.

References

1. Alfani R, Guerrini G (2005) Rheological test methods for the characterization of extrudable cement-based materials—a review. Mater Struct 38:239–247
2. Assaad JJ, Harb J, Maalouf Y (2014) Measurement of yield stress of cement pastes using the direct shear test. J Nonnewton Fluid Mech 214:18–27
3. Basterfield R, Lawrence C, Adams M (2005) On the interpretation of orifice extrusion data for viscoplastic materials. Chem Eng Sci 60:2599–2607
4. Bingham EC (1922) Fluidity and plasticity. McGraw-Hill
5. Feys D, Cepuritis R, Jacobsen S, Lesage K, Secrieru E, Yahia A (2018) Measuring rheological properties of cement pastes: most common techniques, procedures and challenges. RILEM Tech Lett 2:129–135
6. Jayathilakage R, Rajeev P, Sanjayan J (2020) Yield stress criteria to assess the buildability of 3D concrete printing. Constr Build Mater 240:117989
7. Jayathilakage R, Sanjayan J, Rajeev P (2019) Direct shear test for the assessment of rheological parameters of concrete for 3D printing applications. Mater Struct 52:12
8. Jayathilakage R, Sanjayan J, Rajeev P (2020) Characterizing extrudability for 3D concrete printing using discrete element simulations. In: Bos F, Lucas S, Wolfs R, Salet T (eds) Second RILEM International Conference on Concrete and Digital Fabrication. DC 2020. RILEM Bookseries, vol 28. Springer, Cham. https://doi.org/10.1007/978-3-030-49916-7_30
9. Le TT, Austin SA, Lim S, Buswell RA, Gibb AG, Thorpe T (2012) Mix design and fresh properties for high-performance printing concrete. Mater Struct 45:1221–1232
10. Lim S, Buswell RA, Le TT, Austin SA, Gibb AG, Thorpe T (2012) Developments in construction-scale additive manufacturing processes. Autom constr 21:262–268
11. Perrot A, Rangeard D, Pierre A (2016) Structural built-up of cement-based materials used for 3D-printing extrusion techniques. Mater Struct 49:1213–1220
12. Roussel N, Coussot P (2005) "Fifty-cent rheometer" for yield stress measurements: from slump to spreading flow. J Rheol 49:705–718
13. Roussel N, Ovarlez G, Garrault S, Brumaud C (2012) The origins of thixotropy of fresh cement pastes. Cem Concr Res 42:148–157
14. Shyshko S (2013) Numerical simulation of the rheological behavior of fresh concrete
15. Toutou Z, Roussel N, Lanos C (2005) The squeezing test: a tool to identify firm cement-based material's rheological behaviour and evaluate their extrusion ability. Cem Concr Res 35:1891–1899
16. Wolfs R, Salet T, Hendriks B (2015) 3D printing of sustainable concrete structures. In: Proceedings of IASS annual symposia, 2015. International Association for Shell and Spatial Structures (IASS), pp 1–8
17. Zhou X, Li Z, Fan M, Chen H (2013) Rheology of semi-solid fresh cement pastes and mortars in orifice extrusion. Cement Concr Compos 37:304–311

A Feasibility Study for Natural Disaster Simulations Using a Fully Explicit SPH Method in a GPU Environment

H. T. Senadheera, M. Asai, and D. S. Morikawa

Abstract Mesh-free particle methods are increasingly being used instead of grid based numerical methods in many engineering applications, including free-surface fluid flows. Smoothed Particle Hydrodynamics (SPH) method is one such meshless, Lagrangian particle method utilized for modeling large deformations or flows with free surfaces. In SPH, the problem domain is discretized into particles without any connectivity and physical quantities of the flow are obtained by tracing the motion of particles. SPH was originally developed for compressible flow and has later been improved to satisfy the incompressible condition by various authors. In typical incompressible smoothed particle hydrodynamics (ISPH) formulations, a semi-implicit integration scheme is applied to particle discretized equations to solve incompressible flow problems. This requires solving linear equations, which takes up a lot of device memory, thus limiting the possibility of carrying out large scale problems. This study explains the application of a fully-explicit time integration scheme for fluid simulations using the ISPH method. In addition, we used a GPU environment for the computer simulations through an authorial program written in CUDA Fortran. Thus, the purposes were to avoid the need of solving linear equations, therefore reducing memory usage and to utilize the parallel processing power of GPU to accelerate the code. On the other hand, GPU is more widely available compared to supercomputer CPUs, which is the generally used environment for ISPH calculations. Dam-break simulations and validation tests were conducted to validate the proposed SPH method. With the proposed method and computational environment, the calculation speed was increased and memory usage was decreased significantly and large fluid simulations could be carried out. Thus, the proposed method and improvements could pave way in simulating large-scale problems, such as tsunami run-up analyses and other natural disaster simulations.

Keywords Particle methods · Smoothed particle hydrodynamics · Incompressible smoothed particle hydrodynamics · Explicit time integration · GPU

H. T. Senadheera (✉) · M. Asai · D. S. Morikawa
Department of Civil Engineering, Faculty of Engineering, Kyushu University, Fukuoka, Japan
e-mail: harini-s@doc.kyushu-u.ac.jp

R. Dissanayake et al. (eds.), *ICSECM 2019*, Lecture Notes in Civil Engineering 94,
https://doi.org/10.1007/978-981-15-7222-7_24

1 Introduction

The Smoothed Particle Hydrodynamics (SPH) method was originally introduced by Lucy [1] and then developed by Gingold and Monaghan [2] for treating astrophysical problems. SPH is a Lagrangian and mesh-free numerical method that spatially discretizes the problem domain into a finite number of particles, and the physical quantities of the flow are obtained by tracing the motion of the particles. As one of the particle methods, SPH has been utilized for many engineering applications, mostly in the analysis of moving discontinuities and large deformation systems such as free-surface flows with breaking, splash and fragmentation, those which are difficult to predict using mesh-based Eulerian methods due to mesh distortion issues. SPH was originally developed for compressible flows and has later been improved to satisfy the incompressible condition (ISPH) by various authors [3, 4].

Currently, in parallel to the development of frameworks to increase the accuracy of ISPH simulations, researchers are carrying out a wide range of studies to increase the efficiency of simulations as well. For conventional ISPH calculations, CPU with parallel computing techniques has been the generally used environment [5] for a long time, given that particle methods require a large amount of memory and calculations. Recently, the use of parallel programming in General Purpose Graphic Processing Unit (GPGPU) has increased due to the added advantages it provides compared to CPU in terms of speed and accessibility. While a supercomputer CPU has around 8 cores, GPUs have cores on the order of thousand, which increases its computational power significantly. Following this trend, a GPU based SPH program was developed using the proposed method for this study.

However, due to the limitation of memory in GPU, in order to carry out finer resolution problems, there exists the need of choosing a method that uses limited memory. On the other hand, extending a study to simulate a large-scaled tsunami simulation requires using millions of particles. This is almost impossible due to the long time span history of tsunamis and restrictions in computational time even in supercomputer CPUs. In addition, in the original semi-implicit and fully-implicit time integration schemes for ISPH, pressure calculation requires solving linear equations which takes up a lot of memory to store the coefficient matrix. Therefore, using the implicit time integration schemes, it is difficult to carry out large-scale problems like tsunami run-up analyses. Thus, taking both accuracy and efficiency into account, an explicit time integration for ISPH has been proposed in this study, to speed up the calculations and save memory.

2 Projection-Based ISPH Formulations

In this section, the fundamental SPH methodology, ISPH formulations, Projection method and the semi-implicit time integration scheme will be explained briefly.

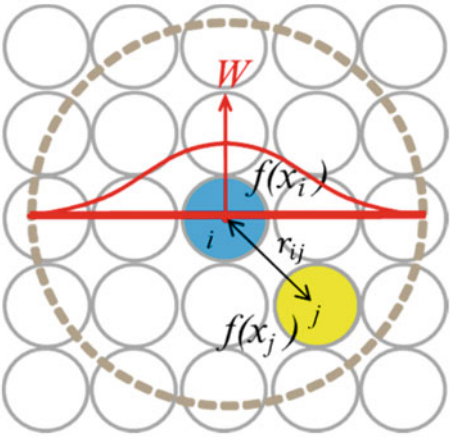

Fig. 1 Particle approximations in a support domain

2.1 SPH Methodology

SPH method in fluid dynamics simply works by dividing a fluid domain into a set of discrete elements, referred to as 'particles'. These particles have a spatial distance known as the 'smoothing length' that is typically represented as h, over which their properties are 'smoothed' by a kernel/weight function. In a general SPH analysis, the physical quantity of any particle i can be obtained by summing the relevant properties of all the particles that lie within the range of the kernel, called as the neighbor particles j of i. The contributions of each neighbor particle to a property of the main particle, are weighted according to their distance r_{ij} from the particle of interest i by a smoothing function W. The above explanation [6] can be represented by the following Eq. (1) and Fig. 1,

$$\phi(\boldsymbol{x_i}, t) = \int W(r_{ij}, h)\phi(\boldsymbol{x_j}, t)dV \tag{1}$$

where, $\phi(\boldsymbol{x_i}, t)$ is a physical scalar function at a sampling point $\boldsymbol{x_i}$, described according to SPH literature.

2.2 Governing Equations of Incompressible Flow

The following continuity equation and the Navier-Stokes equation are the two main equations of hydrodynamic problems of incompressible flow, which are solved numerically by the proposed ISPH method.

$$\nabla.\boldsymbol{v} = 0 \tag{2}$$

$$\frac{D\boldsymbol{v}}{Dt} = -\frac{\nabla P}{\rho} + \nu\nabla^2\boldsymbol{v} + \boldsymbol{g} \tag{3}$$

where $\boldsymbol{v}$ is the velocity vector, D/Dt the material derivative, P the pressure, ρ the density and ν the total kinematic viscosity, respectively. $\boldsymbol{g}$ and t indicate the gravitational acceleration and time.

2.3 Original Stabilized ISPH Semi-implicit Time Integration Scheme

This procedure uses the semi-implicit time integration scheme of the Moving-Particle Semi-Implicit method (MPS) adapted to the SPH method [7]. The semi-implicit time integration scheme is based on a projection method that updates the velocity in accordance with Eq. (3) in two steps, namely the predictor and corrector steps [7].

The contribution of viscous term and gravitational forces results in a predicted velocity (predictor) calculated explicitly as,

$$\boldsymbol{v}^* = \boldsymbol{v}^n + \Delta t\left(\nu\nabla^2\boldsymbol{v}^n + \boldsymbol{g}\right) \tag{4}$$

To illustrate the calculation procedure [8], the Laplacian of velocity of Eq. (3) is represented by the SPH approximation to discretize the equation with respect to target particle i,

$$\boldsymbol{v}_i^* = \boldsymbol{v}_i^n + \Delta t\boldsymbol{g} + \left(\Delta t\sum_j B_{ij}\right)\left(\boldsymbol{v}_j^n - \boldsymbol{v}_i^n\right) \tag{5}$$

where,

$$B_{ij} = m_j\frac{2\nu}{\rho_i}.\left(\frac{\boldsymbol{r_{ij}}.\nabla W\left(r_{ij},h\right)}{r_{ij}^2+\eta^2}\right) \tag{6}$$

Since the future velocity is expressed by the velocity at a known time step n, it is possible to calculate the particle velocity at the immediate step *, independently of the velocity of the neighbouring particle j at the same time. Therefore, unlike an implicit calculation, it is not necessary to prepare a large matrix (N × N), but preparing a vector (N) for storing the velocity at time step n would be sufficient.

Next, the pressure is calculated from the following Pressure Poisson Equation (PPE),

$$\left\langle\nabla^2 P_i^{n+1}\right\rangle = \frac{\rho_0}{\Delta t}\left\langle\nabla.\boldsymbol{v}_i^*\right\rangle + \alpha\frac{\rho_0 - \left\langle\rho_i^n\right\rangle}{\Delta t^2} \tag{7}$$

A stabilized ISPH method was proposed by Asai et al. [8] with the objective of introducing a relaxed density invariance condition in pressure calculation. The second source term on the right side is derived from the above stabilized method. This satisfy both the divergence-free and density-invariance conditions and ensures constant density and a smooth pressure distribution.

Finally, adding the contribution of the pressure field, the corrected velocity (corrector) is obtained implicitly as the following step,

$$\boldsymbol{v}^{n+1} = \boldsymbol{v}^{*} + \Delta \mathrm{t}\left(-\frac{1}{\rho_0}\nabla P^{n+1}\right) \tag{8}$$

In the above equations, Δt indicates the time increment, ρ_0 the initial density of the fluid, ρ_i^n a SPH approximation of the density, $\alpha (0 \leq \alpha \leq 1)$ the relaxation coefficient, n and $n+1$ the current and next iterations and * the intermediate state, respectively.

3 Fully-Explicit Time Integration Scheme (EISPH)

This section will explain the derivation of the fully-explicit time integration scheme for incompressible fluid simulations. A fully-explicit time integration scheme would eliminate the necessity of solving time-consuming linear equations.

The procedure in which the equations of the explicit time integration scheme were derived, is shown below.

3.1 Velocity Calculation (Predictor Step)

The calculation of velocity follows the same procedure as the above mentioned original stabilized ISPH semi-implicit time integration scheme. Velocity is explicitly updated using Eqs. (5) and (8).

3.2 Pressure Calculation

In the original stabilized ISPH semi-implicit time integration scheme, pressure is solved implicitly [8]. However, Ogasawara et al. [9] proposed a method (Stabilized EISPH method) to solve the Pressure Poisson Eq. (7) explicitly to save memory for large-scale problems. The differences in the calculation procedure of pressure between the two schemes are organized below.

Expressing the Laplacian of pressure by the SPH approximation with respect to Eq. (7), it can be rearranged as follows,

$$\sum_j A_{ij}\left(P_i^{n+1} - P_j^{n+1}\right) = B_i \tag{9}$$

By simplifying Eq. (9) the following Eq. (10) can be obtained to solve pressure,

$$P_i^{n+1} = \frac{B_i + \sum_j A_{ij} P_j^{n+1}}{\sum_j A_{ij}} \tag{10}$$

where,

$$A_{ij} = m_j \frac{2}{\rho_0}.\left(\frac{\boldsymbol{r_{ij}}.\nabla W\left(r_{ij}, h\right)}{r_{ij}^2 + \eta^2}\right) \tag{11}$$

$$B_i = \frac{\rho_0}{\Delta t}\left\langle \nabla.\boldsymbol{v_i^*}\right\rangle + \alpha \frac{\rho_0 - \left\langle \rho_i^n \right\rangle}{\Delta t^2} \tag{12}$$

As described above, to solve the Pressure Poisson Equation, solving simultaneous linear equations is generally required, using iterative solvers such as the conjugate gradient method. This presents a major downside as it implies high computational cost and the device memory is largely used to store the coefficient matrix. Therefore, the fully-explicit ISPH (EISPH) method is suggested to avoid the computational cost of solving the PPE.

In the explicit time integration scheme, it is assumed for a small time increment the change of pressure is so small that the pressure of the next time step for neighbour particles P_j^{n+1} can be regarded to be approximately equal to the previous pressure value P_j^n.

If the particle of interest is i and the surrounding particles are denoted by j, the above Eq. (10) can be transformed to Eq. (13) for the pressure to be solved explicitly,

$$P_i^{n+1} = \frac{B_i + \sum_j A_{ij} P_j^n}{\sum_j A_{ij}} \tag{13}$$

Since the pressure is approximated to be remained unchanged for neighbour particles, the calculated results might not guarantee sufficient accuracy. Therefore, numerical experiments and validation tests should be carried out to confirm the accuracy of pressure calculation.

4 Computational Environment

The numerical examples explained in Sect. 5 were performed using a program written in a Graphics Processor Unit (GPU) environment. Therefore, this section is aimed

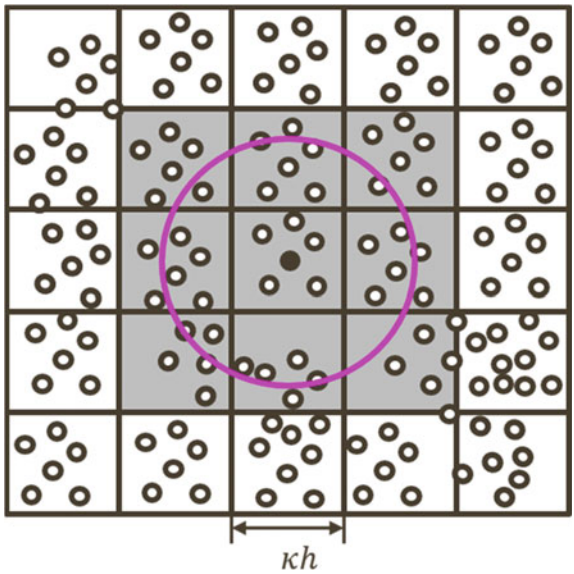

Fig. 2 Cell search approach for neighbour particle search in 2D

to provide an insight to the programing details specific to this study. The current version of the code uses one GPU card Tesla V100-DGXS.

4.1 Neighbouring Search

In the SPH method, only a finite number of particles in the support domain of dimension κh are used in the particle approximations. The process of finding the nearest particles is commonly known as nearest neighbouring particle searching (NNPS) [6].

In this study, a 'linked-list' search algorithm worked well for the NNPS process. It allows each particle to be assigned to a cell and for all the particles in the cell to be chained together for easy access. A temporary mesh is overlaid on the problem domain, with the mesh spacing set to κh. For a given particle i, the nearest neighbouring particles are on the same grid cell or the immediately adjoining cells (Fig. 2).

This approach is expected to reduce computational time substantially since the NNPS process is only necessary for a certain group of particles.

4.2 Programming Details of the Study

A GPU environment based on CUDA Fortran [10] is used to develop the computer program for this study. Figure 3 shows a flowchart of the single-device version of

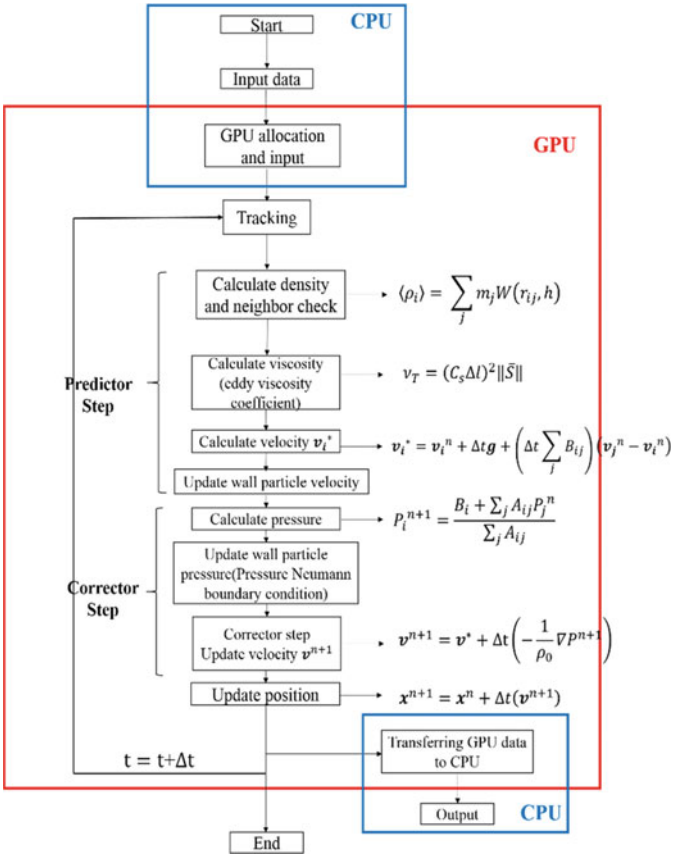

Fig. 3 Flowchart of the proposed EISPH method

the program. It can be noticed that, while most parts of the program, are performed using GPU, few parts are performed using CPU. This is because GPU variables in CUDA Fortran programs cannot retrieve input and output data directly. Thus, for input, it is needed to first transfer data from CPU to GPU and then from GPU to CPU for output. However, far greater degree of parallelism occurs within the GPU.

Subroutines that run on the GPU are executed by many threads in parallel. The equations mentioned above should be applied for each fluid particle 1, 2, …, N. The number of threads is fixed throughout the code and selected N/thr number of blocks, where thr is the fixed number of threads. Therefore, N will be the total number of threads used in the device, which means each particle can be designated to one thread. Figure 3 shows the step-by-step process of the SPH program utilized in this study.

5 Numerical Examples

In this section, several numerical examples are demonstrated to check the accuracy and efficiency of the proposed EISPH method. The two main objectives of carrying out the numerical examples for this study can be specified as below;

1. To carry out verification and validation (V&V) processes for the proposed method—Verification stands for the comparison of a numerical model with a theoretical solution of a simple case problem while Validation refers to the comparison with experimental results.
2. To check the performance of GPU computations i.e. efficiency and capacity of a single GPU.

Dam break problems were mainly used to carry out the above tasks. In all simulations of this section, the strain rate calculation derived by Violeau and Issa [11] was used.

5.1 Dam-Break Problem

A series of dam break simulations were performed to check the density, pressure and also to validate our proposed SPH method. Figure 4 shows a schematic cross section of the dam break problem to illustrate some geometrical parameters. Here, H indicates the original height of fluid column, a the base length of fluid column at initial state and z the distance of surge front from the starting axis/wall.

Figure 5 illustrates the motion of the water particles resulting from the dam collapse. The pressure values are shown in a color scale.

For 61,644 particles with 10^{-4} s time increment, the resulting computational time was 0.2 h to simulate the water movement for 1 s (10,000 iterations) since the dam collapse.

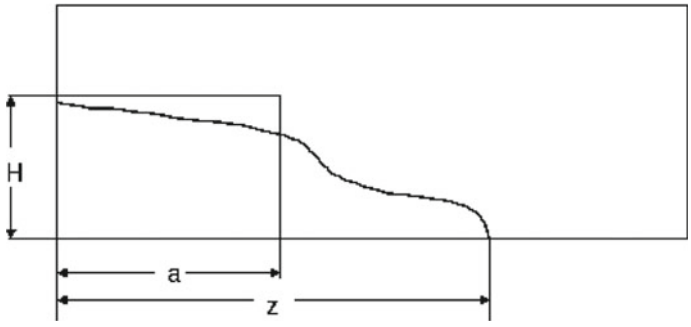

Fig. 4 Geometrical parameters of the dam break problem

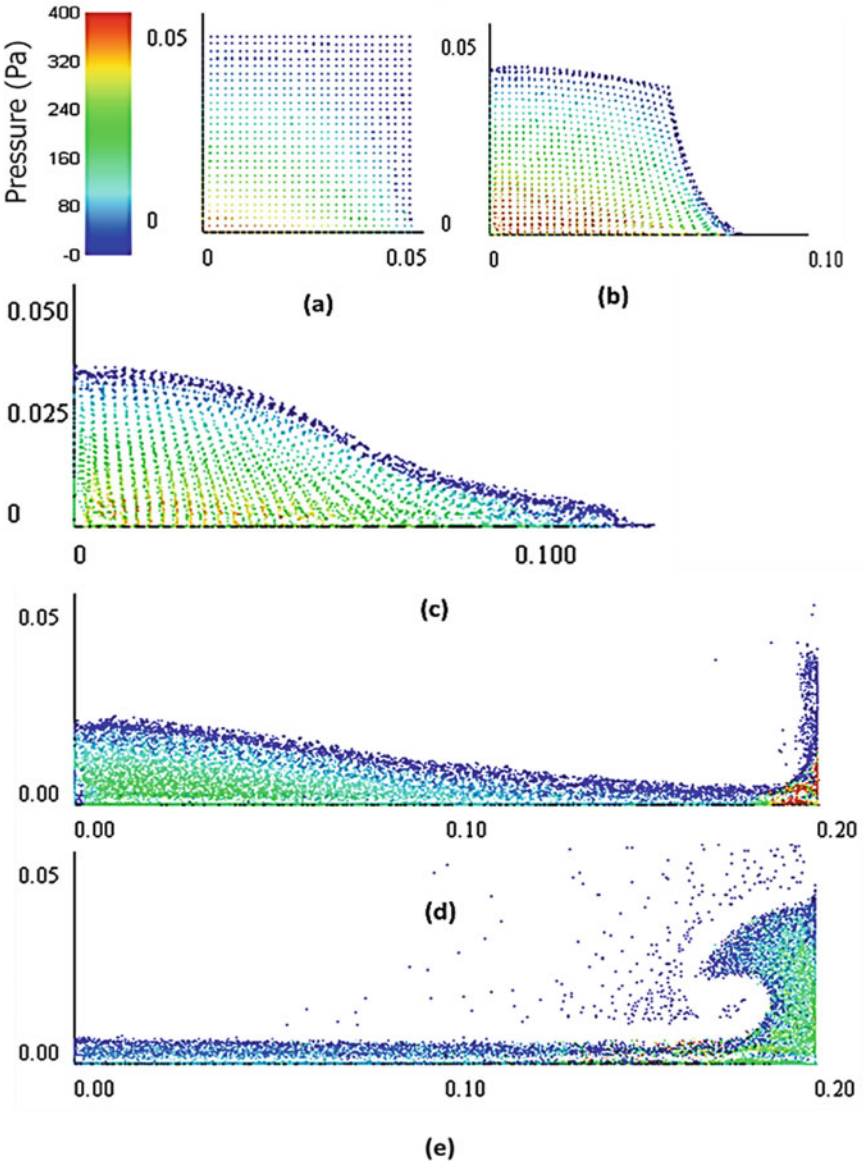

Fig. 5 Dam-break simulation proceeding sequentially from **a** to **e**

In Fig. 5, the snapshots a–e show the particle motion after 100, 500, 1000, 2000 and 4000 iterations respectively. In other words, since the time increment is 10^{-4} s, they respectively show the movement of the water column after 0.01, 0.05, 0.1, 0.2 and 0.4 s from the dam collapse.

5.1.1 Validation Tests for the Proposed EISPH Method

The pressure distribution obtained using the stabilized EISPH method was validated by a comparison with the original stabilized ISPH method. By measuring the pressure at a pressure sensor under same settings in the dam break problem, the following results (Fig. 6) could be obtained.

It can be seen that the pressure distribution of the proposed EISPH method shows good agreement with the original ISPH method.

Moreover, the renowned experimental study by Martin and Moyce [12] was also used to validate the proposed EISPH method. In the study, the results of the experiment were presented in non-dimensional quantities. Therefore, the quantities were defined using the same notation as below.

$$T = t\left(\frac{g}{a}\right)^{1/2} \tag{14}$$

$$Z = \frac{z}{a} \tag{15}$$

where, t is the time passed since the dam collapse and g is gravity.

The following parameters were used for the simulation: $H = a = 0.056$ m, particle diameter $(d) = 0.002$ m, $\rho_0 = 1000$ kg/m^3, $\nu_0 = 1.4\text{E}{-7}$ m^2/s and $\Delta t = 1\text{E}{-4}$ s.

The same dam break model was analysed using the fully-implicit integration scheme for SPH [13].

Figure 7 shows a graph of the simulation compared to the experimental results and numerical results from fully-implicit time integration scheme. Our proposed EISPH method exhibited closer results to both experimental and numerical results; however,

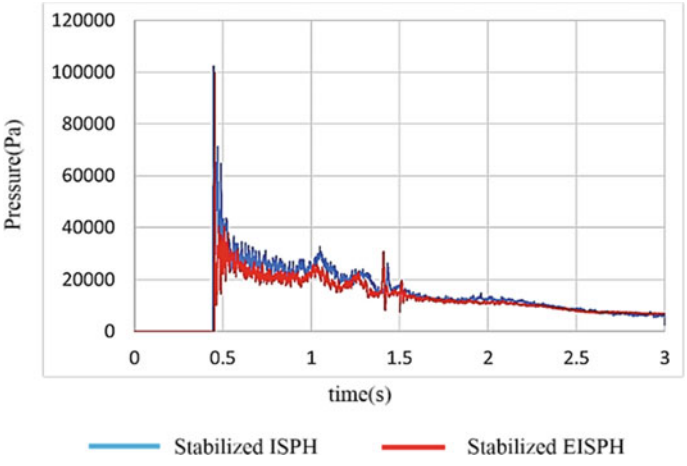

Fig. 6 Pressure Distribution comparison between EISPH and ISPH methods

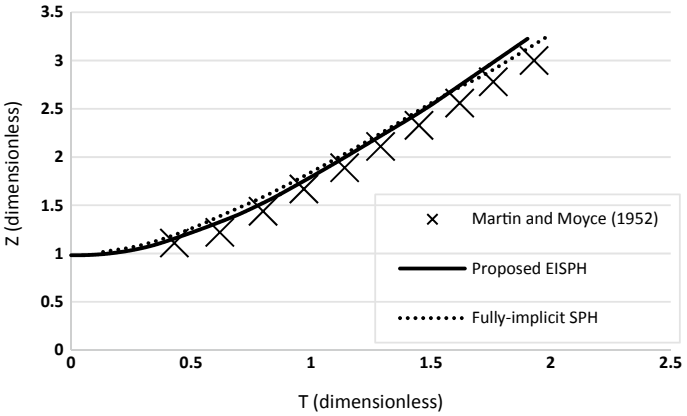

Fig. 7 Dam break simulation compared with validation tests

with slight variations due to uncertainties of the experiment and the selection of certain parameters in the simulation.

5.1.2 Dam Break Problems to Validate the Performance of GPU

A series of dam break simulations were carried out to investigate the performance of GPU computations for the proposed method as well. The dam break simulations were executed using different particle diameters, i.e. varying particle resolutions, ranging from coarse particle cases to finer particle cases. The intention was to examine the capacity, efficiency and cost performance of GPU with regard to EISPH calculations. Table 1 demonstrates the results of the dam break simulations that were carried out, all of which were obtained for 100,000 iterations.

Thus, it is evident that using the fully-explicit method much larger analyses could be carried out compared to the original semi-implicit time integration scheme, due

Table 1 Dam-break simulation results for different particle resolutions

Particle diameter (m)	No. of particles	Time increment (s)	Computational time (h)	Memory (GB)
0.002	68,239	1×10^{-6}	0.5	0.01
0.001	311,787	1×10^{-6}	2.5	0.05
0.001	997,101	1×10^{-6}	5	0.15
0.0005	1,930,003	1×10^{-6}	8	0.3
0.0005	5,107,147	1×10^{-5}	33	0.6
0.0005	7,468,995	1×10^{-5}	40	1.2

to the added advantage of memory saving. In addition, the use of GPU instead of CPU increased the efficiency of computations significantly.

5.2 A Dam Break Simulation with an Obstacle

After confirming the accuracy and performance of the program as mentioned above, the dam break simulation was extended with a complicated structure in front of the water block to examine the water motion. The arrangement and settings used for the simulation are explained below (Fig. 8 and Table 2).

The object used for the problem is a model of a Christian angel named 'Lucy' retrieved from *The Stanford 3D Scanning Repository,* 2011 [14]. After obtaining the polygon data of the object (Fig. 9a) particles were generated using the Meshman

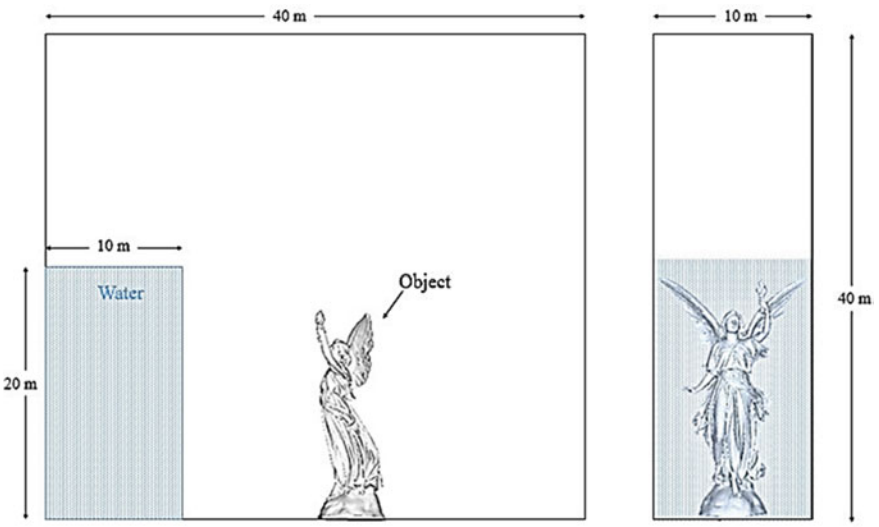

Fig. 8 Arrangement of the dam break simulation

Table 2 Settings for the dam break simulation

Parameter	Value
Particle diameter (cm)	10
No. of total particles	4,789,597
Time increment (dt)	1×10^{-4}
ν (cm^2/s)	1.4×10^{-2}
ρ (g/cm^3)	1
α	0.001

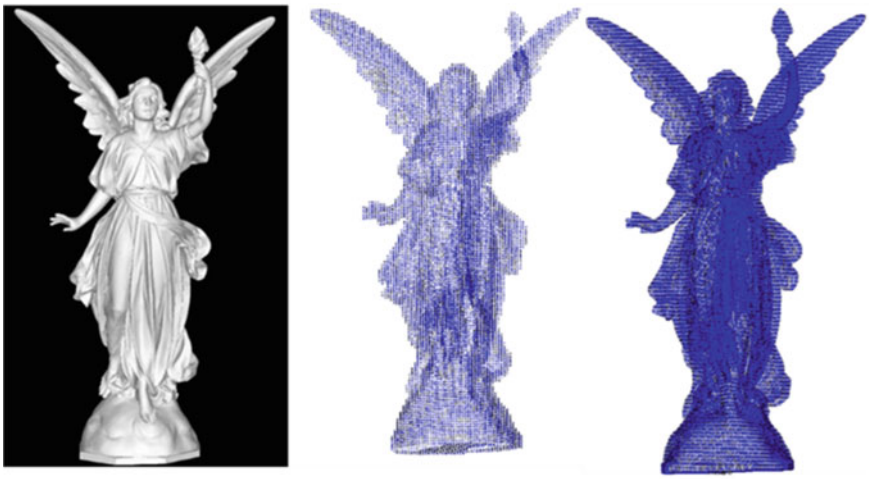

Fig. 9 The object 'Lucy' with polygon data (**a**) and particle data (**b**) particle diameter 10 cm and **c** particle diameter 4 cm

ParticleGen software developed by Insight Inc. [15] (Fig. 9b, c). From the figure it can be seen that the lower particle diameter i.e. higher particle number case can show a better representation of the object, which also assists in getting better simulation results and impose boundary treatment.

Figure 10 shows the motion of the water particles resulting from the dam collapse approaching the object and wall. For the following nearly 5 million particle problem, the computational time for 30,000 iterations was 6 h using only one GPU. It was found that for the original semi-implicit time integration scheme in CPU, it needs to use 8 nodes to achieve the above computational time for the same number of iterations.

A problem of 50 million particles could be solved using only about half of the memory available in a single GPU. Given that the memory of one GPU used was 16 GB, it was found that up to 100 million particle problems can be solved within one GPU. However, for the 50 million problem using a single GPU it takes around 5 days to solve the until 30,000 steps. Therefore, it is recommended to use a multi-GPU program for problems exceeding around 20 million particles to achieve less computational time.

6 Conclusions

With the stabilized explicit solution, the need for creating a matrix for the calculation of speed and pressure has been eliminated, and therefore, it is possible to significantly

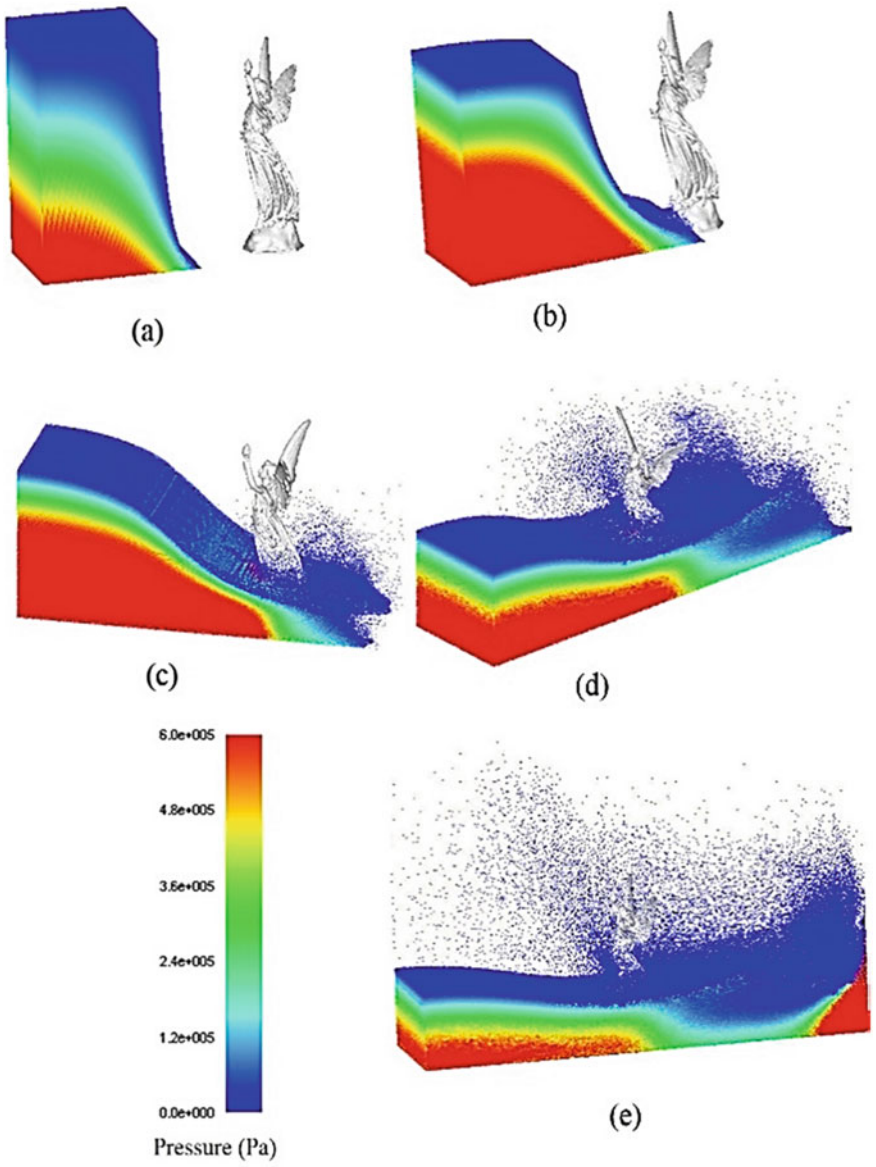

Fig. 10 Simulation Results of the dam break simulation at 5000, 10,000, 15,000, 20,000 and 25,000 steps

reduce the memory usage. This will enable to utilize the code to analyse some large-scale problems such as tsunami run-up analyses. With the current code, problems with a large number of particles can already be solved only using one GPU card. It can be noticed that by optimally manipulating the computational power of GPU, the current method can provide important results that would be beneficial for large-scale fluid simulations.

This study aims to maintain the program that can easily carry out calculations for up to tens of millions of particles using GPU. To date, a relatively simple configuration has been made to carry out tasks using a single GPU card. However, future operations should be aimed to achieve improved efficiency, boundary conditions and better communication between multiple GPUs.

Acknowledgements This work was supported by JSPS KAKENHI Grant Number JP17H02061. This work was also supported by "Joint Usage/Research Centre for Interdisciplinary Large-scale Information Infrastructures" in Japan (Project ID: jh180060-NAH, jh180065-NAH).

References

1. Lucy LB (1977) A numerical approach to the testing of the fusion process. Astron J 88:1013–1024
2. Gingold RA, Monaghan JJ (1977) Smoothed particle hydrodynamics: theory and application to non-spherical stars. Mon Not R Astron Soc 181:375–389
3. Morris JP, Fox PJ, Zhu Y (1997) Modeling low Reynolds number incompressible flows using SPH. J Comput Phys 136(01):214–226
4. Khayyer A, Gotoh H, Shao SD (2008) Corrected incompressible SPH method for accurate water-surface tracking in breaking waves. Coast Eng 55(03):236–250
5. Ihmsen M, Akinci N, Becker M, Teschner M (2011) A parallel SPH implementation on multi-core CPUs. Comput Graph Forum 30(01):99–112
6. Liu GR, Liu MB, Li S (2004) Smoothed particle hydrodynamics—a mesh free method. Comput Mech 33(06):491
7. Koshizuka S, Oka Y (1996) Moving-particle semi implicit method for fragmentation of incompressible fluid. Nucl Sci Eng 1233(03):421–434
8. Asai M, Aly AM, Sonoda Y, Sakai Y (2012) A stabilized incompressible SPH method by relaxing the density invariance condition. J Appl Math
9. Ogasawara K, Asai M, Furuichi M, Nishiura D (2017) Development of an explicit scheme of the stabilized ISPH for large scaled tsunami run-up simulation. J Jpn Soc Civ Eng Ser A2 (Appl Mech (AM)) 73 (in Japanese)
10. Fatica M, Ruetsch G (2011) CUDA Fortran for scientists and engineers. NVIDIA Corp., Santa Clara
11. Violeau D, Issa R (2007) Numerical modelling of complex turbulent free-surface flows with the SPH method: an overview. Int J Numer Meth Fluids 53(02):277–304
12. Martin J, Moyce W (1952) Part V. An experimental study of the collapse of liquid columns on a rigid horizontal plane. Philos Trans R Soc Lond Ser A Math Phys Sci 244(882):325–334
13. Morikawa D, Asai M, Idris NA, Imoto Y, Isshiki M (2019) Improvement in highly viscous fluid simulation using a fully implicit SPH method. J Comput Part Mech 1–16
14. The Stanford 3D Scanning Repository (2014) Available at: https://graphics.stanford.edu/data/3Dscanrep/#uses. Accessed 25 July 2019
15. Meshman (2017) https://www.meshman.jp/. Accessed 25 July 2019

Surfactant/Citrate Assisted Synthesis of Calcium Carbonate Nanostructures from Natural Calcite

M. R. Abeywardena, D. C. N. A. Wickramarathne, B. D. A. S. Fernando, D. G. G. P. Karunarathne, H. M. T. G. A. Pitawala, R. M. G. Rajapakse, A. Manipura, and M. M. M. G. P. G. Mantilaka

Abstract Synthesis of nanostructures from naturally available and easily accessible natural minerals is a growing area of research. It would be beneficial if nanotechnology is exploited for the value addition for inadequately utilized the aforementioned minerals. Calcium carbonate nanostructures can be employed in industrial products to improve their mechanical and other functional properties. In this study, citrate ion template-based method was employed for the synthesis of precipitated calcium carbonate nanostructures from naturally occurring calcite with different morphologies and sizes. For characterization of synthesized materials, X-ray Diffraction, Fourier Transform Infrared Spectroscopy, Thermal Gravimetric Analysis, and Scanning Electron Microscopic analysis were used. "Grain" like structure was observed from citrate template-based method while nanoparticles synthesized using surfactant-citrate method exhibited a surface morphology which is spherical in nature. The particle size of 70–80 nm was observed from nanoparticles using surfactant/citrate method and citrate template-based synthesized nanoparticles exhibited dimensions of 90 nm × 300 nm. Owing to the simplicity and cost-effectiveness, this novel method of synthesizing calcium carbonate nanoparticles would be industrial feasible approach.

Keywords Citrate template · Natural calcite · Industrially feasible · Surfactants

M. R. Abeywardena · D. C. N. A. Wickramarathne
Postgraduate Institute of Science, University of Peradeniya, Peradeniya, Sri Lanka

M. R. Abeywardena · D. C. N. A. Wickramarathne · B. D. A. S. Fernando · D. G. G. P. Karunarathne · A. Manipura (✉)
Department of Chemical and Process Engineering, University of Peradeniya, Peradeniya, Sri Lanka
e-mail: madupa543@gmai.com

H. M. T. G. A. Pitawala
Department of Chemistry, Faculty of Science, University of Peradeniya, Peradeniya, Sri Lanka

R. M. G. Rajapakse · M. M. M. G. P. G. Mantilaka (✉)
Sri Lanka Institute of Nanotechnology, Nanotechnology and Science Park, Mahenwatte, Pitipana, Homagama, Sri Lanka
e-mail: prasangaM@slintec.lk

R. Dissanayake et al. (eds.), *ICSECM 2019*, Lecture Notes in Civil Engineering 94,
https://doi.org/10.1007/978-981-15-7222-7_25

1 Introduction

Fabrication and manipulation of inorganic nanomaterials are currently attraction increasing for their variety of applications in various fields. As a result of smaller size, higher surface area, quantum confinement and other effects, they demonstrate properties that differ significantly from the respective bulk materials, as a result of small particle dimension, high surface area, quantum confinement, and other effects [6]. Calcium carbonate ($CaCO_3$) can be considered as one of the main concerned area in value addition to the natural and highly abundant minerals. Calcium carbonate crystallizes as calcite, aragonite, and vaterite. Most widespread $CaCO_3$ polymorphs are calcite and aragonite [4, 10]. Vaterite is the less stable $CaCO_3$ polymorph which transform into calcite via solvent intervened process. Natural calcite has become an ideal natural carbonate source due to its relatively high abundance. There is growing demand for high quality $CaCO_3$ for the paint, filler, paper [8] and adhesive/sealant based industries and in various medical and dietary applications and supplements [3]. By reason of the broad particle size distribution, different morphologies and different impurity levels applications of calcite are limited. Therefore, it is a big challenge for the aforementioned industries to sustain devoid of high quality precipitated calcium carbonate (PCC) [3].

Numerous methods have been extended for the production of $CaCO_3$ based nanomaterials, including sol-gel techniques [17], hydrothermal synthesis [9], solvothermal synthesis, ultrasonic assisted synthesis [2] and template assisted synthesis method [6]. In scaling up majority of these synthetic methods, industrially feasibility becomes less owing to their expensive chemical and instrumental usage. Template-assisted synthesis can be considered as an impressive approach to synthesize size/shape-controlled nanoparticles by comparatively low cost and feasible method [1]. On the other hand, complicated and time- consuming procedures are needed for the fabrication of most of the templates [7]. Hard template-assisted methods have been utilized for the preparation of nanomaterials especially with hollow structures [13, 14]. Nevertheless, the template removal process tend to be complicated which limits the practical applications [7, 15]. Fabrication of hollow PCC via surfactant/polymer templates is a successful approach utilized in number of studies [5, 16, 18]. It is reported that the synthesis of hollow bone-like $CaCO_3$ via surfactant/polymer template [5]. In another study, researchers had employed a precipitation method using urea polyphenols containing hydrated calcium salts and had found that the morphology and the size of the synthesized products are predominately controlled by the template used [12].

In this study, we have performed a novel and versatile method to synthesize $CaCO_3$ nanostructures from naturally occurring calcite using citrate template. By considering the chemical structure of citric acid, we reckoned the possibility of controlling the particle size by employing it as a soft template under certain conditions. Furthermore, since literature revealed the ability of Sodium Dodecyl Sulfate (SDS) in controlling the particle size and morphology, this manuscript focused on the effects of SDS on controlling the particle size and morphology [11].

2 Experimental

2.1 Materials

Freshly prepared distilled water was used for the preparation of all the solutions. Natural calcite (99%) was purchased from SCHAEFER KALK GmbH & Co. KG. Sodium carbonate (Na_2CO_3), hydrochloric acid (HCl), sodium hydroxide (NaOH), sodium lauryl/dodecyl sulfates (SDS), absolute alcohol of analytical grade were purchased from Aldrich.

2.2 Preparation of 0.5 M $CaCl_2$ Solution

At first, calcite was sieved through 400 μm mesh. Then, 0.55 g of calcite was taken into 1000 ml beaker. 6 M HCl was added to the flask while stirring until pH of the solution is decreased to 3. The resulting solution was filtered off and toped up with distilled water to obtain 1000 ml of the solution. The supernatant obtained was subjected to atomic absorption spectroscopic (AAS) analysis to determine the calcium concentration and it was found to be 0.48 M.

2.3 Preparation of Saturated $Ca(OH)_2$/Citrate and $Ca(OH)_2$/Citrate/SDS Templates

Ca^{2+} solution of 100 ml was taken into a 300 ml beaker followed by dissolving 1.44 g (15% molar ratio for Ca^{2+}) of citric acid. Then, 2 M NaOH solution was added while stirring until getting an opaque saturated solution. The solution filtered under suction to obtain saturated $Ca(OH)_2$/citrate template. In order to obtain the saturated $Ca(OH)_2$/citrate/SDS template, 0.5 g of anionic surfactant, SDS was added.

2.4 Synthesis of Products

Solution of aqueous 0.5 M Na_2CO_3 (50 ml) was added drop wise (3 ml per min) into both template solutions to gain products as shown in the Fig. 1. Suspension was aged for further 1 h after carbonation under constant stirring. Resulting materials were washed with distilled water two times and once with alcohol under centrifugation. The products were dried under vacuum for 6 h. All the experiments were performed under ambient conditions.

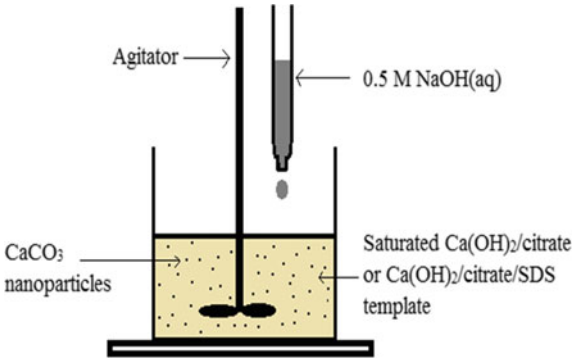

Fig. 1 Schematic illustration for synthesizing of materials

3 Results and Discussions

3.1 Effect of Citrate Template

The morphologies of the $CaCO_3$ samples were examined from SEM analysis. Images of PCC structures fabricated on saturated $Ca(OH)_2$/Citric template is shown in Fig. 2. SEM images reveal a "grain-like" morphology of PCC with average particle length of 300–400 nm and average particle width of 70–80 nm (Fig. 2a, b). As the shape of a particle with dimensions can clearly be observed in Fig. 2b with respect to Fig. 2a, it could be seen as an 'irregular grain-like" morphologies are formed with tiny particles of about 60–70 nm. Moreover, it is noticeable that that "grain-like" structure takes up as the majority of particles while some spherical and elongated particles could

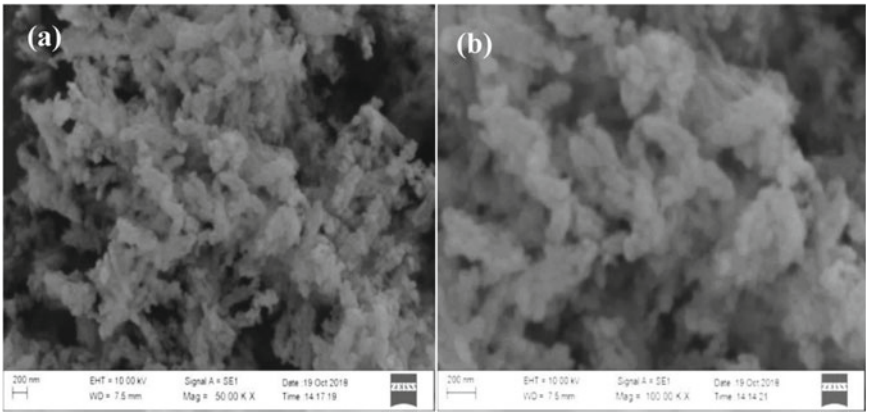

Fig. 2 SEM images of calcium carbonate fabricated with saturated $Ca(OH)_2$/citrate template

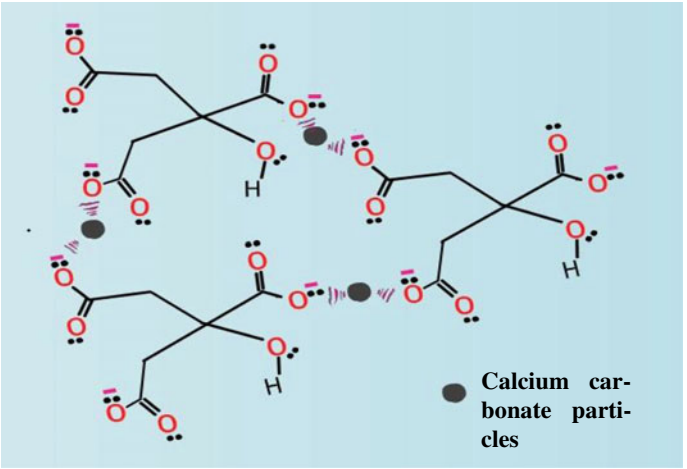

Fig. 3 Schematic diagram of interactions between citrate molecules and calcium carbonate particles

be observed randomly from Fig. 2b. The nature of the grain-like structure exhibiting irregularity is due to the amorphous nature on the surface of the resulted particles.

Citric acid is converted to its anionic form of citrate at higher pH values as shown in Eq. (1). The initial pH of the solution was observed to be about 10.5 as a result of addition of aqueous NaOH. Each citrate molecule contains three carboxylate groups which creates anionic environment. Those negatively charge groups can be influence the surface potential of the particles to restrict their growth. Moreover, particles show a tendency to agglomerate due to their higher surface energy.

The schematic representation of the proposed mechanism of interaction between citrate molecules and calcium carbonate particles are illustrated in Fig. 3. The nucleation and growth of the particles are strictly controlled by the anionic groups. This mechanism proposes the stabilization of the nanoparticles via electrostatic interactions and also by steric hindrance.

$$C_6H_8O_7 + 3NaOH \rightarrow C_6H_5O_7^{3-} + 3Na^+ + 3H_2O \quad (1)$$

3.2 *Influence of Addition of SDS on the Morphology of $CaCO_3$*

Scanning Electron Micrographs (Fig. 4), a and b show the morphology of in situ prepared calcium carbonate in the presence of SDS surfactant using the saturated calcium-citrate template. The surface of the nanoparticles is covered by SDS and

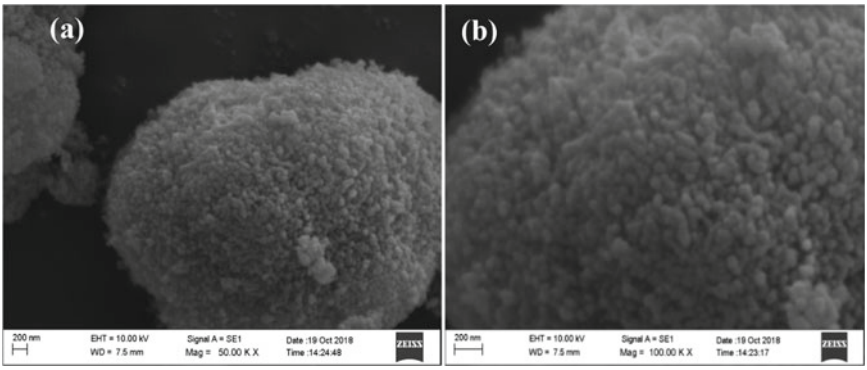

Fig. 4 SEM images of calcium carbonate fabricated with saturated $Ca(OH)_2$/citrate/SDS template

thereby they have grown separately into spherical nanoparticles. The particle size is about 70–80 nm while they are pooled to form 2–3 μm aggregates.

The (Fig. 5a, b) depicts how PCC are covered by SDS in order to restrict them in the nanoscale and the contact angles. The anionic head of SDS is adsorbed on to the positively charged PCC surface, while alkyl chains are arranged perpendicular to the surface forming micellular structure as shown in Fig. 5a. These structures interact with each other to result micro clusters as observed in SEM images. Furthermore, these structures exhibit hydrophobic nature (Fig. 5b) due to the monolayer arrangement of the alkyl chains and the contact angles were 120.8° and 119.5°.

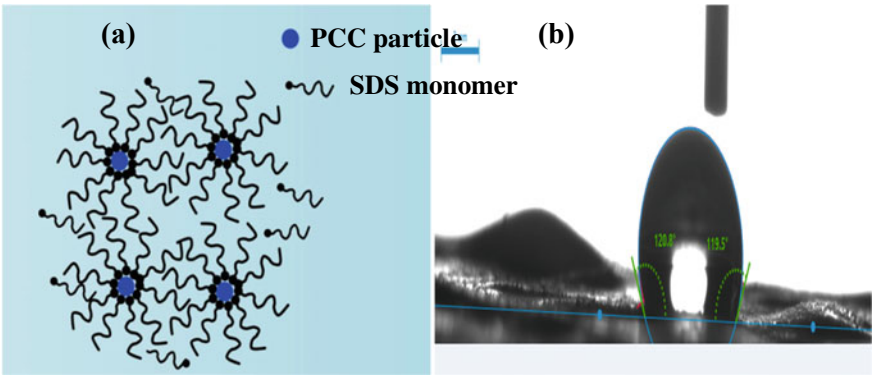

Fig. 5 **a** Schematic diagram for stabilization of PCC in the presence of SDS, **b** contact angle for synthesized PCC presence of SDS

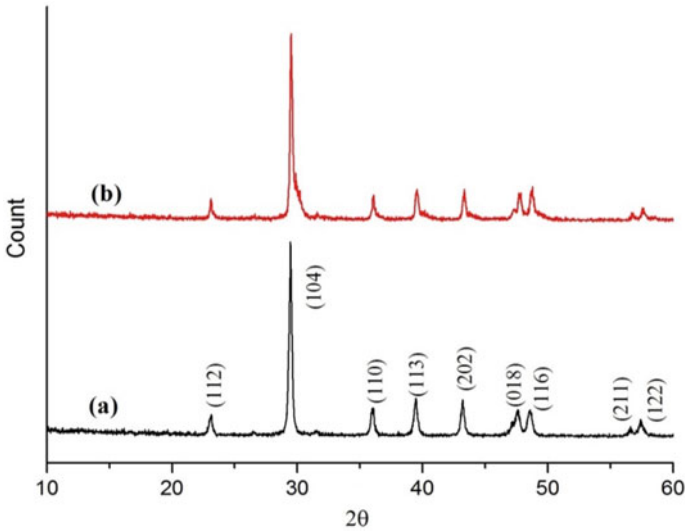

Fig. 6 XRD spectra of PCC: **a** saturated $Ca(OH)_2$/citrate, **b** saturated $Ca(OH)_2$/citrate/SDS templates

3.3 XRD Analysis of the Products

The X-ray Diffraction spectra of synthesized products are illustrated in Fig. 6. XRD patterns of PCC products fabricated on $Ca(OH)_2$/Citrate and $Ca(OH)_2$/Citrate/SDS templates are shown in Fig. 6. Both XRD patterns are comprised of peaks at 2θ values of 23.0, 29.4, 36.0, 39.3, 43.1, 47.6, 48.5, 56.7 and 57.4 with corresponding basal planes of (112), (104), (110), (113), (202), (018), (116), (211) and (122). All these peaks can be assigned to calcite crystalline form of $CaCO_3$ (JCPDS card no. 83-1762). There are two extraneous peaks at 26.5° and 31.5° with very low intensity which may attribute to impurities. No other crystalline forms of PCC are found in both these XRD patterns. Therefore, from XRD studies, it is confirmed that the PCC products are composed of calcite as the only crystalline form of $CaCO_3$.

3.4 FTIR Analysis of the Products

The Fourier Transform Infra-red spectrum of synthesized products via aforementioned two methods and citric acid is illustrated in Fig. 7. The bands of FTIR positioned at 1070 cm^{-1} (υ_1, Symmetric stretching of CO_3^{2-}), 712 cm^{-1} (υ_2, Out of plane bending of CO_3^{2-}), 1428 cm^{-1} (υ_3, Doubly degenerate asymmetric stretching of CO_3^{2-}), 875 cm^{-1} (υ_4, Doubly degenerate in plane bending of CO_3^{2-}), 1795 cm^{-1}

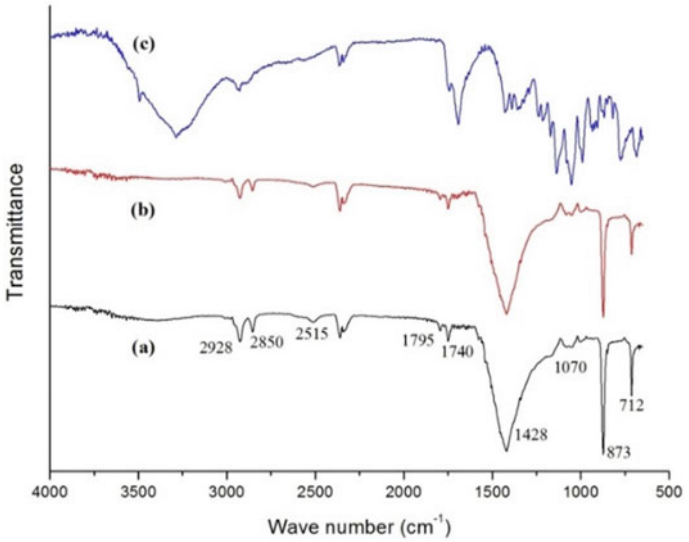

Fig. 7 FTIR spectrum of PCC: **a** $Ca(OH)_2$/citrate template, **b** $Ca(OH)_2$/citrate/SDS template, **c** citric acid

($\upsilon_1 + \upsilon_4$, combination band) and 2515 cm^{-1} ($2\upsilon_2 + \upsilon_4$, combination band) reveal the presence of calcite (Table 1).

The presence of two relatively low intensity bands at 2920 and 2850 cm^{-1} which are attributed to 'C–H' stretching and a single band at 1740 cm^{-1} reveal the adsorption of citrate on to the surface of PCC. The appearance of the peak at 1070 cm^{-1} might be due to the amorphous nature of the synthesized products.

Table 1 Vibrational modes of calcium carbonate with their respective wavenumbers

Mode		Wave number (cm^{-1})
υ_1	Symmetric stretching of CO_3^{2-}	1070
υ_2	Out of plane bending of CO_3^{2-}	712
υ_3	Doubly degenerate asymmetric stretching of CO_3^{2-}	1428
υ_4	Doubly degenerate in plane bending of CO_3^{2-}	873
$\upsilon_1 + \upsilon_4$	Combination bands	1795
$2\upsilon_2 + \upsilon_4$	Combination bands	2515

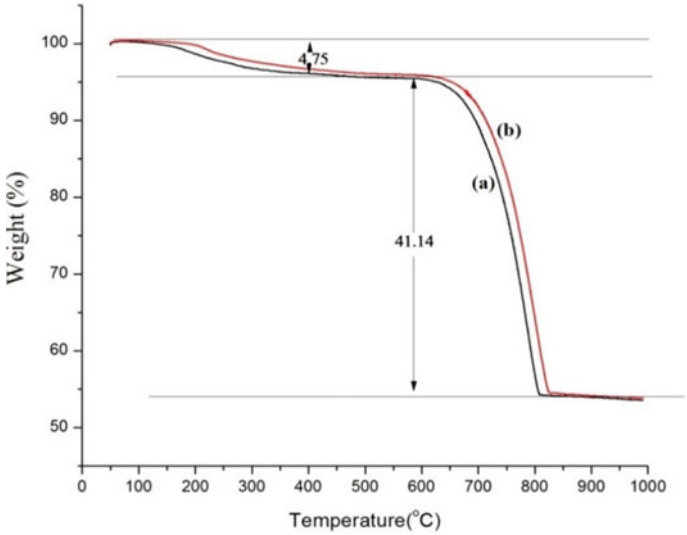

Fig. 8 TGA curve of the synthesized PCC: **a** saturated $Ca(OH)_2$/citrate, **b** saturated $Ca(OH)_2$/citrate/SDS template

3.5 Thermal Gravimetric Analysis of the Products

The TGA curves for samples treated under normal air atmosphere show a similar pattern with only two characteristic weight losses (Fig. 8). The first weight loss appears at about 160 °C, and it becomes constant at 420 °C, resulting in 4.75% weight loss. The second weight loss appears at about 600 °C, and it becomes constant at 825 °C, giving 41.14% weight loss. The first weight loss may be attributed to the decomposition of organic molecules adsorbed on to the particular surface while the second weight loss is attributed to the decomposition of $CaCO_3$ to form CaO.

4 Conclusion

Grain-like structures of PCC have been synthesized on a saturated $Ca(OH)_2$/citrate template and $Ca(OH)_2$/citrate/SDS templates starting from naturally occurring calcite. The synthesized grains were having average length of 300–400 nm and average particle width of 70–80 nm. It is supposed that anionic surfactant SDS adsorbed on to PCC surface to form micelles in order to restrict the material in spherical shape with size of 70–80 nm. In addition, SDS had introduced a hydrophobic nature on to the particle surface. It was investigated that the chemical nature of citric acid is suitable to employ it as a soft template. The crystallinity of the synthesized product showed the formation of calcite and also no other crystal form was

observed. Therefore, it revealed about the feasibility of using citrate as a soft template in synthesizing variety of nanomaterials with different sizes and morphologies.

Acknowledgements The authors thank National Scientific Foundation of Sri Lanka (Grant No. TG/2016/Tech-D/02) for their financial support. All technical support from various laboratories at Faculty of Engineering and Faculty of Science, University of Peradeniya, Sri Lanka and National Institute of Fundamental Studies, Sri Lanka (NIFS) are acknowledged.

References

1. Gong L, Jiang H, Zhu F (2010) A facile and green approach for the fabrication of ZnO nanorods using bamboo charcoal as the template. Mater Lett 64(23):2582–2584. https://doi.org/10.1016/j.matlet.2010.08.073
2. He M et al (2005) Ultrasonication-assisted synthesis of calcium carbonate nanoparticles. Chem Eng Commun 192(10–12):1468–1481. https://doi.org/10.1080/009864490896025
3. Jimoh OA et al (2018) Synthesis of precipitated calcium carbonate: a review. Carbonates Evaporites 33(2):331–346. https://doi.org/10.1007/s13146-017-0341-x
4. López-Macipe A, Gómez-Morales J, Rodríguez-Clemente R (1996) Calcium carbonate precipitation from aqueous solutions containing Aerosol OT. J Cryst Growth 166(1–4):1015–1019. https://doi.org/10.1016/0022-0248(96)00101-7
5. Mantilaka MMMGPG et al (2014) Formation of hollow bone-like morphology of calcium carbonate on surfactant/polymer templates. J Cryst Growth 392:52–59. https://doi.org/10.1016/j.jcrysgro.2014.02.007
6. Matalkah BF (2017) Mechanochemical synthesis of, pp 53–59
7. Norek M et al (2011) A comparative study on the hydrogen absorption of thin films at room temperature deposited on non-porous glass substrate and nano-porous anodic aluminum oxide (AAO) template. Int J Hydrogen Energy 36(18):11777–11784. https://doi.org/10.1016/j.ijhydene.2011.06.046
8. Onimisi JA et al (2016) A novel rapid mist spray technique for synthesis of single phase precipitated calcium carbonate using solid-liquid-gas process. Korean J Chem Eng 33(9):2756–2760. https://doi.org/10.1007/s11814-016-0093-7
9. Qi C, Zhu YJ, Chen F (2014) Microwave hydrothermal transformation of amorphous calcium carbonate nanospheres and application in protein adsorption. ACS Appl Mater Interfaces 6(6):4310–4320. https://doi.org/10.1021/am4060645
10. Qi RJ, Zhu YJ (2006) Microwave-assisted synthesis of calcium carbonate (vaterite) of various morphologies in water—ethylene glycol mixed solvents. J Phys Chem B 110(16):8302–8306. https://doi.org/10.1021/jp060939s
11. Sibilio S et al (2016) A review of electrochromic windows for residential applications. Int J Heat Technol 34(Special Issue 2):S481–S488. https://doi.org/10.18280/ijht.34s241
12. Škapin SD, Sondi I (2010) Synthesis and characterization of calcite and aragonite in polyol liquids: control over structure and morphology. J Colloid Interface Sci 347(2):221–226. https://doi.org/10.1016/j.jcis.2010.03.070
13. Sun X, Liu J, Li Y (2006) Use of carbonaceous polysaccharide microspheres as templates for fabricating metal oxide hollow spheres. Chem Eur J 12(7):2039–2047. https://doi.org/10.1002/chem.200500660
14. Yin Y et al (2001) Template-assisted self-assembly: a practical route to complex aggregates of monodispersed colloids with well-defined sizes, shapes, and structures. J Am Chem Soc 25(6):8718–8729
15. Yu H et al (2007) 'Template-free hydrothermal synthesis of CuO/Cu_2O composite hollow microspheres. Chem Mater 16:4327–4334

16. Yu J et al (2005) Controlled synthesis of calcium carbonate in a mixed aqueous solution of PSMA and CTAB. J Solid State Chem 178(3):861–867. https://doi.org/10.1016/j.jssc.2005.01.002
17. Zhao H et al (2008) Synthesis method for silica needle-shaped nano-hollow structure. Mater Lett 62(19):3401–3403. https://doi.org/10.1016/j.matlet.2008.03.020
18. Zhao L, Wang J (2012) Biomimetic synthesis of hollow microspheres of calcium carbonate crystals in the presence of polymer and surfactant. Colloids Surfaces A: Physicochem Eng Asp 393:139–143. https://doi.org/10.1016/j.colsurfa.2011.11.012

Fully-Modular Buildings Through a Proposed Inter-module Connection

S. Srisangeerthanan, M. J. Hashemi, P. Rajeev, E. Gad, and S. Fernando

Abstract Modular buildings are built using factory manufactured building units or modules that are transported and assembled on-site. Among the many different types used, modules of volumetric form analogous to intermodal freight containers have the greatest potential to achieve complete building systems or fully-modular building systems where on-site work could be reduced to foundation, module assembly and the finishing of module-to-module interfaces as required. However, despite the many reported benefits, volumetric module use has some technical, logistical and regulatory issues that have constrained its widespread application. Two of such issues that have been widely reported are the lack of efficient structural systems for lateral load transfer and the lack of high-performance inter-module connections that can not only meet structural demands but can also fulfil certain constructional and manufacturing needs as well. Therefore, this paper focuses specifically on the latter of the two identified issues and briefly summarises the work conducted into its resolution.

Keywords Prefabrication · Modular buildings · Steel · Connections

1 Introduction

Prefabrication technology deals with the factory manufacture of building units which are subsequently transported to site for building construction. These building units differ in fundamental forms based on the degree of modularisation adopted for the construction of a building. Since inception, most modularisations were done to the elemental level of a structure. Linear and planar forms such as beams, columns, trusses, slabs, wall panels, etc. were the most widely used due to their relative ease in manufacture, transport and handling. However, with advancements in science, engineering and technology, spatial modularisation has become an emergent practice.

Spatial modularisation results in the formation of volumetric units that are analogous to intermodal freight containers. These units can either be of bare structural

S. Srisangeerthanan (✉) · M. J. Hashemi · P. Rajeev · E. Gad · S. Fernando
Department of Civil and Construction Engineering, Swinburne University of Technology, Melbourne, Australia
e-mail: ssrisangeerthanan@swin.edu.au

R. Dissanayake et al. (eds.), *ICSECM 2019*, Lecture Notes in Civil Engineering 94,
https://doi.org/10.1007/978-981-15-7222-7_26

framing or be fully-finished. Buildings built using volumetric units are widely recognised as modular buildings, and such units as modules. The advantages of modular buildings are widely documented [11, 21, 25, 28] and a few examples for such buildings are the 44 storey LaTrobe tower in Melbourne, Australia [18], the 32 storey 461 Dean Street building in New York, America [17] and the 28 storey Apex House Building in London, United Kingdom [27].

Though such systems are at the forefront of revolutionising the construction industry, they are still largely dependent on tedious conventional methods for module inter-connectivity and additional structural systems for meeting structural demands such as conventionally built lateral force resisting systems (LFRS) and on-site concreting to achieve diaphragm rigidity. This results to such systems being classified as hybrid-modular building construction systems. However, current trends are towards achieving fully-modular building construction, where on-site work could be reduced to foundation, module assembly and module-to-module interface finishing as required (see Fig. 1). Fully-modular building construction systems have the greatest potential to maximise off-site work that can make use of automated assembly line mass manufacturing techniques and thereby increase the degree of automation associable to a construction project. Moreover, simple easy to engage connectivity between modules can tremendously reduce the need for specialised on-site work and further increase the potential for automating such highly repetitive tasks.

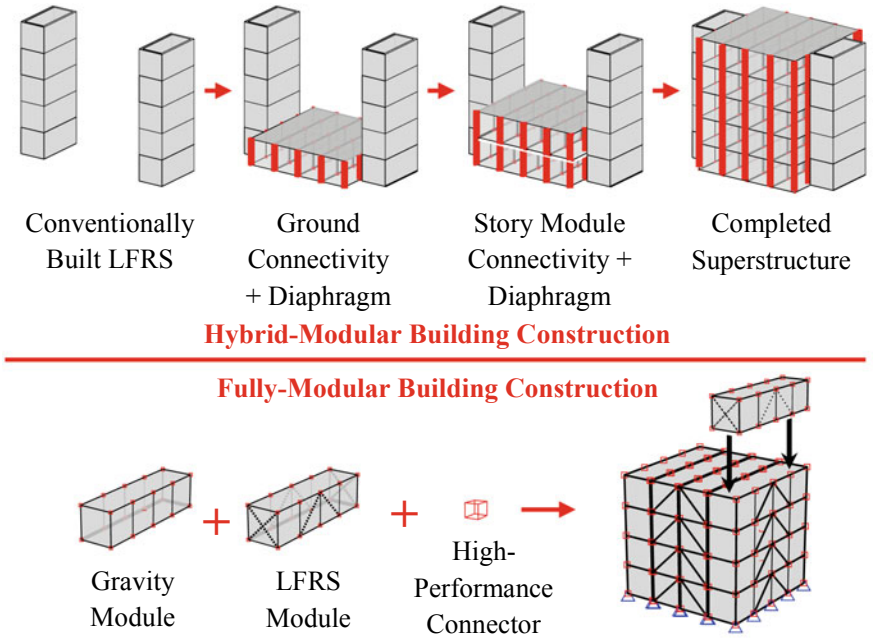

Fig. 1 A general comparison between hybrid-modular building construction and fully-modular building construction where a building is simply assembled requiring minor finishing

Therefore with the aim to realise fully-modular building construction, this overall research attempts to resolve two identified structural limitations, which are namely, (1) the lack of efficient structural systems for lateral load resistance and (2) the lack of simple high-performance connections for module interconnectivity, and this paper focuses particularly on the latter issue. Furthermore, it should be noted that logistical (such as transportable mass and size limits including on-site handling) and regulation related issues are of equal concern, but are beyond the scope of this research.

2 Connections in Fully-Modular Buildings

As mentioned in the introduction, modular buildings are built using factory manufactured volumetric building units termed modules. These modules are typically an assembly of structural elements such as beams, columns, slabs and panels, and are held together by the connections between those elements which are defined as intra-module connections. These connections can be of any conventional standardised form of beam-beam, beam-column and bracing connections. Intra-module connections and module elements affect the overall stiffness and strength of a module and their various arrangements can enable modules to function as either gravity-modules or lateral-force-resisting-modules. Lateral-force-resisting-modules would typically form the LFRS of a modular building and the remaining regions would be formed by gravity-modules provided that efficient diaphragm action can be established.

Achieving efficient diaphragm action and efficient lateral force resistance via the LFRS of a fully-modular building requires robust high-performance connections between modules. These connections predominantly govern overall building behaviour and are defined as inter-module connections. Inter-module connections can also be of any conventional standardised form of beam-beam or column-column connections, however the achievement of fully-modular building construction inevitably requires such connections to fulfil certain structural, constructional and manufacturing performance requirements.

Structural performance requirements constitutes the ability of an inter-module connection to resist (S1) vertical plane axial and shear forces to function within an LFRS and (S2) horizontal plane axial and shear forces to function within a diaphragm.

Constructional performance requirements constitutes the ability of an inter-module connection to simplify on-site work and maximise the degree of off-site manufacturing for modules by having (C1) self-aligning capability (does not require manual adjustments), (C2) remote operability (does not require direct or access through modules), (C3) simple functionality for assembly (does not require tedious on-site bolting, welding or concreting), (C4) less operations to establish on-site connectivity (does not require any complex sequence of on-site operations to achieve interconnectivity), (C5) less tools, (C6) ease in disassembly, (C7) minimises non-usable space between modules (does not require space to provide accessibility and facilitate design requirements for the connecting elements such as fastener end spacing), (C8) scalable to varying sections and thereby loads (does not require

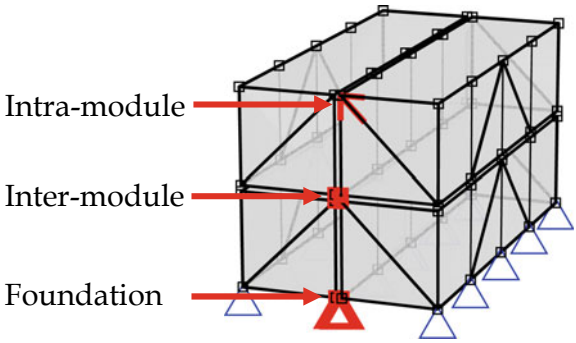

Fig. 2 The general key connection types in a modular building

complex calculations to determine suitable geometric forms), and (C9) capable of handling large construction tolerances.

Manufacturing performance requirements constitutes the complexities of manufacturing by assessing (M1) the number of unique components, (M2) required manufacturing processes, (M3) the complexity of post manufacturing integration of manufactured components, (M4) the number of finalised off-the-shelf components and (M5) the complexity of integration on to modules. An inter-module connection that can convincingly satisfy these performance requirements is considered to be suitable for fully-modular building construction.

A third category of connections apart from intra-module and inter-module connections, are foundation connections which are essentially for grounding modules to foundation or transfer frames. Other connections such as those for facades, though important, may be deemed non-critical for the overall structural performance of fully-modular buildings. Figure 2 details these connection varieties in a simple stack of modules.

3 Proposed Inter-Module Connection

It is inferred from the many inter-module connection concepts available in the public domain [1–10, 12–16, 18–24, 26, 29, 30] that the current state-of-the-art for inter-module connectivity is commonly achieved through the use of bolted or welded assemblies that have several un-integrated components and require comparatively laborious on-site work for module assembly. Although these systems can be made to fulfil structural demands, it may be challenging for most to satisfy manufacturing and constructional performance requirements.

Therefore, on this note, three basic directions for concept development were identified keeping in mind the need to satisfy the identified performance requirements, and were, (1) connections incorporated with a driven mechanism, (2) connections incorporated with a gravity assisted mechanism, and (3) connections that utilise pre-tensioning. Of those three, the driven mechanism type connection was favoured for

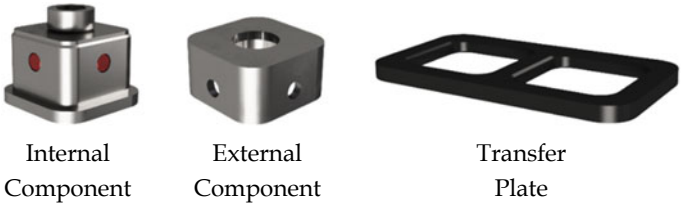

Fig. 3 Key components of the proposed connection

further development. The proposed connection features a connector comprising of an internal unit that houses a mechanism which relates an applied torque to linearly translate a set of pins that would engage with an external unit once lowered in place (see Fig. 3).

The engagement between the internal and external units via the pins provides for vertical load transfer in tension, whereas in compression, the bearing of the external unit onto the internal unit is relied upon. Vertical plane shear forces are transferred through the bearing of internal and external unit surfaces and/or via the pins. The capability of the proposed connection in transferring vertical plane axial and shear forces affirms its viability for use within the LFRS of fully-modular buildings. The horizontal plane load transferring system is however decoupled from the vertical plane load transferring system, where the required levels of axial tension and compression, and shear resistance is provided through a transfer plate held in position by adjacent internal units when considering an assembly of modules. Therefore the proposed connection meets both structural performance requirements (Fig. 4 details the different load transfer paths described).

The connector failure mode in vertical plane tension, is governed by the interaction of the pin with relevant connector surfaces, where wall thickness, pin diameter and end distances are easily manipulated for any desired tension performance for the connector. When under compression and/or shear, the bearing of internal and external unit surfaces provides for sufficiently rigid elastic behaviours where, as before, wall thickness and the height of the connector which is based on the end distances are also

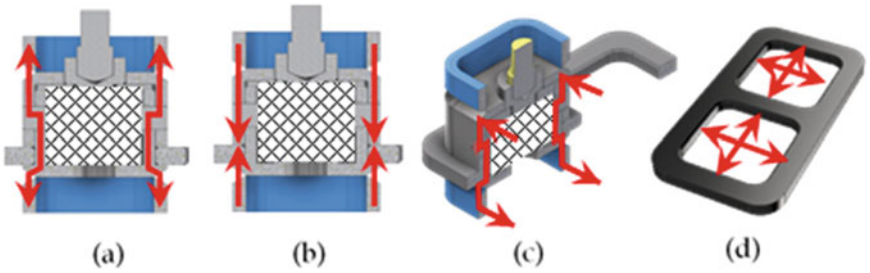

Fig. 4 Load transfer paths, vertical plane (**a**) tension, (**b**) compression, (**c**) shear (through pins or bearing of relevant surfaces) and horizontal plane, (**d**) axial and shear

easily adjusted to meet any such required demands. Moreover, considering a specific design for the connector for use with a grade 350 structural steel 100 × 100 × 9 square hollow section, it is capable of achieving 112% of the designed column member's section capacity in compression, 139% in shear and ~40% in tension, where for tension it was experimentally verified to be ~23% at mechanism yielding, ~40% at connection yielding and ~50% at connection ultimate, whereas for shear it was verified to be ~149%. On the other hand, the transfer plate's structural performance is principally governed by the thickness of the plate, where secondary concerns were the considered cross-section profile, other than rectangular, and the allowed clearance between relevant connector surfaces, which are evaluated numerically. Figure 5 depicts the experimental setup, where (a) was for the axial and (b) for shear tests.

In consideration of the proposed connection in meeting manufacturing performance requirements, though it has only three final off-the-shelf integrated components, the manufacturing stage requires the casting of internal and external units, forming of plates, forging of pins and the machining of components that would make up the mechanism. The variety of processes used suggests complexity in the manufacturing stage and thereby increased manufacturing costs, however assembly line mass manufacturing techniques are worth exploring and are applicable for reducing the unit cost if deemed excessively high. Post- manufacture component integration requires the mechanism components to be assembled within the internal unit and both units are required to be welded on to the respective ends of module framing columns or beams (see Fig. 6). Therefore, in overall the proposed connection can modestly satisfy manufacturing needs.

With regard to the constructional needs fulfilment, the proposed connection seems superior to most other inter-module connections surveyed. The incorporation of a mechanism enables easy assembly and disassembly, where the connector device can

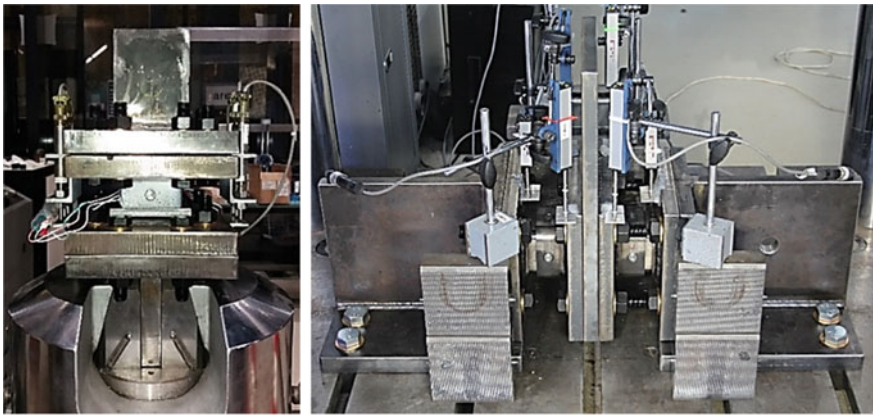

Fig. 5 Experimental setup for (**a**) axial and (**b**) shear tests

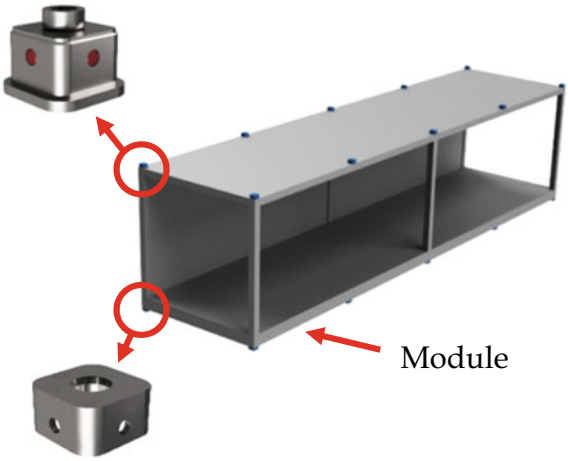

Fig. 6 Key components attached to a module

be operated remotely without requiring direct access and without much effort as it requires only the application of a torque through a single drive-tool (see Fig. 7, where remote operability was verified from a height >4.0 m). Geometric detailing at the edges of both the internal and external units enables self-location within a tolerance of 2 mm. On-site assembly essentially requires the placement of the transfer plate, lowering of modules, lowering of the drive tool and the application of a torque to engage connectivity. Moreover, the overall external design of the connector is based on the standard dimensions of square hollow sections, since such sections are superior

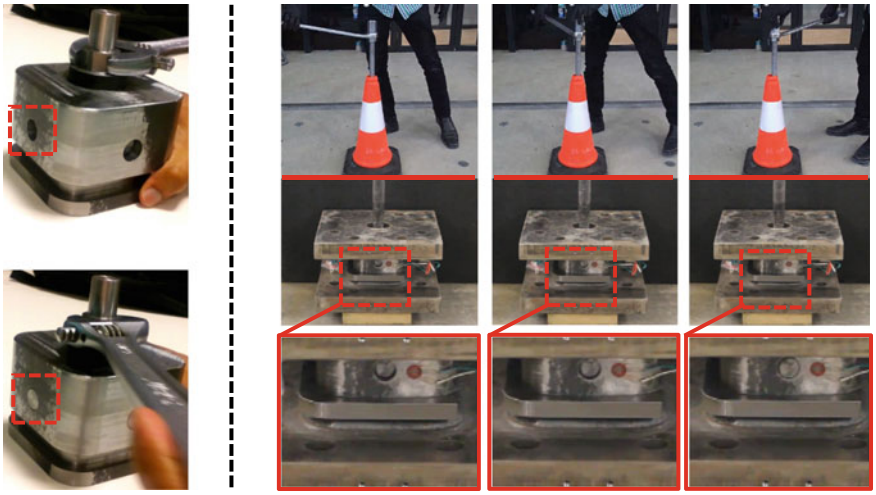

Fig. 7 Demonstrating (**a**) functionality and (**b**) remote operability

in structural characteristics especially with regard to torsional and lateral buckling resistance and are the generally preferred sections for use as module columns, and, as a result, it is expected that the external surfaces of both the connector and columns will be flushed for architectural gains.

Also, since horizontal connectivity is via the insertion of a transfer plate, the connection is independent from the use of any bolts, and is thereby free from having to have to meet specific end distances or bolt spacing requirements which may consume considerable on-plan space and avoids the need for additional detailing or other relevant allowances to provide for adequate access during assembly, especially when in consideration of internal connection locations which require the connectivity of up to eight module nodes. The proposed connection further avoids the need for any specialised access holes to be placed on framing elements or the need for any specific framing element modifications which may result to the need for additional localised strengthening and subsequently increased costs. The connector, though being capable of specialised tweaking, is easily scaled, volumetrically, from its current designed form to meet the requirements of a variety of square hollow section sizes, such as 100×100, 150×150 and/or 200×200.

Nevertheless, despite such constructional advantages, the greatest limitation for the proposed connection is the need for precise manufacturing and therefore it may not be capable of handling large construction related tolerances. Moreover, though module manufacture may achieve the required complimentary levels of precision, as it would be completed in a factory environment, on-site construction activities, on the other hand, at present, may not be capable of achieving such levels of required precision. Manipulation of module framing elements to overcome any misalignments may be inevitable, but, it maybe arguably so that if the receiving points at the foundation level are precisely located, module placement and assembly may likely be achieved with relative ease. However, tolerance tolerant variations of the connector are worth exploring.

Therefore, though applicability for use within fully-modular structural framing assemblies made of partially finished or unfinished modules is guaranteed, fully-modular building construction using fully-finished modules is likely achievable through appropriate foundation design or precise positioning of a conventionally built strong/transfer frame or through the manipulation of partially finished or unfinished ground level modules.

4 Conclusion

This paper presents a proposed connection for inter-module connectivity in modular buildings. The proposed connection comprises of an internal unit which houses a mechanism, an external unit and a transfer plate. An engaged internal and external unit contributes towards vertical plane axial and shear resistance, whereas the transfer plate achieves horizontal plane axial and shear resistance. For the connection variant designed for use with a typical module column of size $100 \times 100 \times 9$, the structural

performance of the connector unit was verified to be satisfactory. The connector's functionality and remote operability were verified to be sufficiently simple and easy, and this semi-automatic nature of the proposed connector enables it to satisfy other key constructional performance requirements as well. However it requires modifications or alternative solutions to accommodate large construction tolerances. Moreover, though the connector satisfies manufacturing performance requirements, reduction in unit costs can further be achieved through assembly line mass manufacturing techniques resulting in economies of scale, and could potentially replace a conventional bolted or welded assembly to achieve simple yet robust high-performance inter-module connectivity. Fully-modular building construction is likely realised including the increased potential for automating on-site activities.

Acknowledgements The authors would like to acknowledge the Cooperative Research Centres programme for Low Carbon Living (CRC-LCL) and associated partners for supporting this research (RP1031).

References

1. Annan CD (2009) Applicability of traditional design procedures to modular steel buildings. Doctor of Philosophy, Ph.D. thesis, University of Western Ontario
2. Chen Z, Li H, Chen A, Yu Y, Wang H (2017) Research on pretensioned modular frame test and simulations. Eng Struct 151:774–787
3. Chen Z, Liu J, Yu Y (2017) Experimental study on interior connections in modular steel buildings. Eng Struct 147:625–638
4. Chen Z, Liu Y, Zhong X, Liu J (2019) Rotational stiffness of inter-module connection in mid-rise modular steel buildings. Eng Struct 196:109273
5. Choi K-S, Lee H-C, Kim H-J (2016) Influence of Analytical Models on the Seismic Response of Modular Structures. J Korea Inst Struct Maint Insp 20:74–85
6. Dai X-M, Zong L, Ding Y, Li Z-X (2019) Experimental study on seismic behavior of a novel plug-in self-lock joint for modular steel construction. Eng Struct 181:143–164
7. Deng E-F, Yan J-B, Ding Y, Zong L, Li Z-X, Dai X-M (2017) Analytical and numerical studies on steel columns with novel connections in modular construction. Int J Steel Struct 17:1613–1626
8. Deng E-F, Zong L, Ding Y, Dai X-M, Lou N, Chen Y (2018) Monotonic and cyclic response of bolted connections with welded cover plate for modular steel construction. Eng Struct 167:407–419
9. Dhanapal J, Ghaednia H, Das S, Velocci J (2019) Structural performance of state-of-the-art VectorBloc modular connector under axial loads. Eng Struct 183:496–509
10. Farnsworth D (2016) Modular building unit connection system. 14072063, 22 Apr 2014
11. Gibb AGF (1999) Part one context. In: Off-site fabrication: prefabrication, pre-assembly and modularization. Whittles Publishing
12. Gunawardena T (2016) Behaviour of prefabricated modular buildings subjected to lateral loads. Doctor of Philosophy, Ph.D. thesis, The University of Melbourne.
13. Heather D (2008) Building including a connector system for building modules and method of constructing a building. Great Britain patent application
14. Heather D, Harding CE, Harding RH, Macdonald R, Ogden RC (2007) Building modules. United States patent application 10/575925

15. Hwan Doh J, Ho NM, Miller D, Peters T, Carlson D, Lai P (2017) Steel bracket connection on modular buildings. J Steel Struct Constr 02
16. International Organization for Standardization (2016) ISO 1161. Series 1 freight containers, Corner and intermediate fittings Specifications. The International Organization for Standardization, Switzerland
17. Krulak R (2017) Modular high-rise: the next chapter. CTBUH J 4
18. Kumar S (2016) Hickory building system (HBS) innovation and successful application in a 44 storey building in Melbourne. Australian Structural Engineering Conference. Australia
19. Lacey AW, Chen W, Hao H, Bi K (2019) New interlocking inter-module connection for modular steel buildings: experimental and numerical studies. Eng Struct 198:109465
20. Lacey AW, Chen W, Hao H, Bi K, Tallowin FJ (2019) Shear behaviour of post-tensioned inter-module connection for modular steel buildings. J Constr Steel Res 162:105707
21. Lawson M, Ogden R, Goodier C (2014) Design in modular construction. CRC Press
22. Lee S, Park J, Kwak E, Shon S, Kang C, Choi H (2017) Verification of the seismic performance of a rigidly connected modular system depending on the shape and size of the ceiling bracket. Materials (Basel), 10
23. Sanches R, Mercan O, Roberts B (2018) Experimental investigations of vertical post-tensioned connection for modular steel structures. Eng Struct 175:776–789
24. Sharafi P, Mortazavi M, Samali B, Ronagh H (2018) Interlocking system for enhancing the integrity of multi-storey modular buildings. Autom Constr 85:263–272
25. Smith RE (2010) Prefab architecture. In: A guide to modular design and construction. Wiley, New York
26. Styles AJ, Luo FJ, Bai Y, Murray-Parkes JB (2016) Effects of joint rotational stiffness on structural responses of multi-story modular buildings. In: The international conference on smart infrastructure and construction (ICSIC). ICE
27. The Chartered Institute of Building (CIOB) (2017) Up, up and away: on site at Europe's tallest modular tower in Wembly, which will take just a year to complete. In: Construction manager. Atom Publishing, London
28. Torre MLDL, Sause R, Slaughter S, Hendricks RH (1994) Review and analysis of modular construction practices. ATLSS reports. Lehigh University
29. Viscomi BV, Michalerya WD, Lu LW (1994) Automated construction in the ATLSS integrated building systems. Autom Constr 3:35–43
30. Yu Y, Chen Z (2018) Rigidity of corrugated plate sidewalls and its effect on the modular structural design. Eng Struct 175:191–200

Determining Roundabout Capacity by Modifying HCM Model Under Mixed Traffic Conditions

M. A. K. Sandaruwan, H. K. D. T. Karunarathne, and W. M. V. S. K. Wickramasinghe

Abstract Roundabouts are commonly implemented as transportation infrastructure facilities due to their improved performance. Capacity is a key performance measure of a roundabout which is considered at its design stage. Highway Capacity Manual (HCM) 2010 provides an exponential regression model for determining capacity at entry for a roundabout. However its applicability in heterogeneous traffic conditions has not yet been thoroughly researched. In Sri Lanka the island nation in the Indian Ocean, the percentage of contribution to the vehicle mix by motorcycles and three-wheelers are 45–55%. Thus, in this study HCM 2010 roundabout capacity model was modified to determine the capacity of a selected four legged roundabout in Kandy, Sri Lanka. Data acquisition was carried out by a turning movement count survey and video recording. Circulatory traffic volume, composition of each vehicle class, critical gap and follow-up headway were determined. A method incorporating the mixed traffic conditions was adopted to determine critical gap value. Stream equivalent follow up headway of 2.97 s and critical gap value of 5.07 s were used to determine the entry capacity. The graph plotted for variation between circulatory flow and entry flow at the roundabout was in negative exponential behaviour. The graph showed that entry capacity reduced exponentially when the circulatory flow increased. The study was further extended to determine adjustment factors for capacity estimation from the HCM 2010 roundabout capacity model directly. The results of this study could be useful in sustainable design of roundabouts in countries that experience mixed traffic conditions like Sri Lanka.

Keywords Vehicle mix · Roundabout capacity · Heterogeneous traffic · Critical gap · Follow-up headway

M. A. K. Sandaruwan (✉) · H. K. D. T. Karunarathne · W. M. V. S. K. Wickramasinghe
Faculty of Engineering, University of Peradeniya, Peradeniya 20400, Sri Lanka
e-mail: amilakanchana65@gmail.com

R. Dissanayake et al. (eds.), *ICSECM 2019*, Lecture Notes in Civil Engineering 94,
https://doi.org/10.1007/978-981-15-7222-7_27

1 Introduction

Roundabout is defined as "intersections with a generally circular shape characterized by yield on entry and circulation around a central island" by the Highway Capacity Manual (HCM) 2010. The circulatory flow is either clockwise as in Sri Lanka or counter-clockwise. Roundabout elements ensure flow with weaving, merging and diverging in acute angles. Roundabouts ensure reduced speeds and number of conflicts compared with other types of intersections (Fig. 1). Roundabouts improve the safety at a particular intersection hence preferred to be implemented at various types of intersections.

Feasibility study of a roundabout for an intersection is conducted through the operational performance analysis by road infra-structure planners and designers. Operational performance of a roundabout is carried out using capacity estimation models considering its design. This capacity prediction assists in vital decision

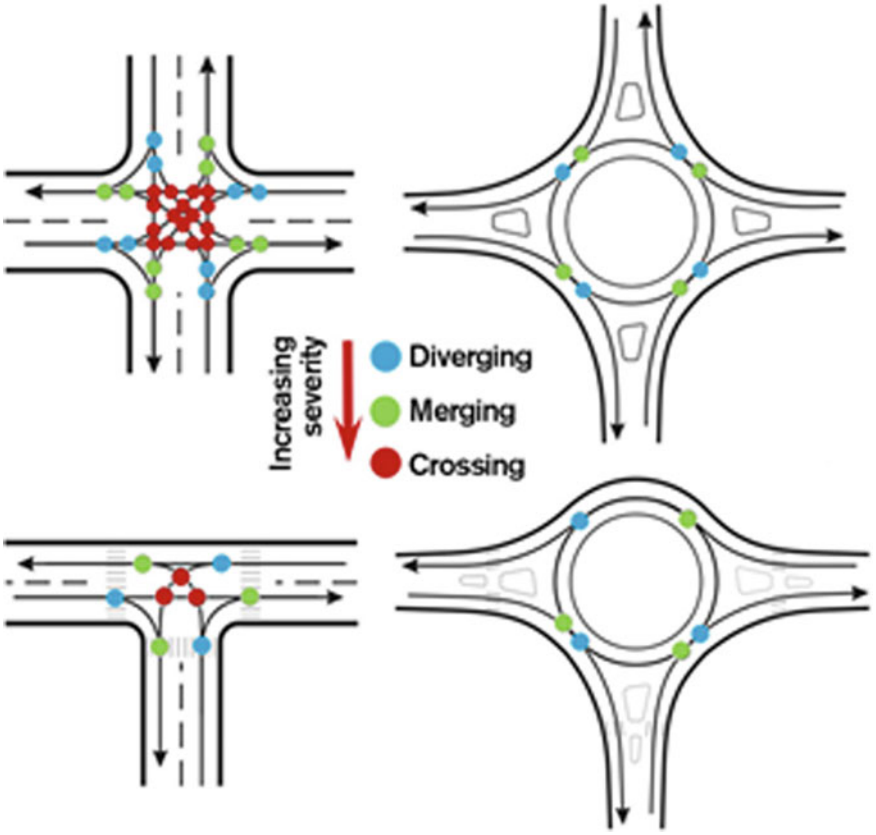

Fig. 1 Conflict points at intersection and roundabout

making process of geometric parameters and number of lanes. This should ensure sustainable design parameters for optimizing costs, land use and benefits.

Although there are several methods for capacity estimation, most of them are based on homogeneous traffic and cannot be directly used in mixed traffic condition. HCM 2010 presents a roundabout capacity model that can be used for performance analysis of roundabouts. It is an exponential model based on gap acceptance theory. Critical gap and follow up headway are governing factors in this model. This research is focused on analysing the performance of a four legged roundabout in Kandy, Sri Lanka modifying HCM 2010 roundabout capacity model for mixed traffic condition according to vehicle categories.

2 Literature Review

Several models have been introduced to estimate the capacity at a roundabout. These methods for estimation of entry capacity of a roundabout can be classified in to two main categories namely empirical models and analytical models.

Capacity models for roundabouts such as U.K model, Swiss method and Indian model (IRC-65, 1976) are empirical models which are based on direct field data. The U.K. roundabout capacity model is based on the equation proposed by Transport and Road Research Laboratory (TRRL) which uses geometric parameters of the roundabout such as entry width, flared length, sharpness of flare, radius and angle of entry, inscribed circle diameter and etc. [8]. The Swiss method is similar to the U.K. method but considers the effect of exiting traffic in the direction opposite to the entering traffic [4]. The Indian formula for estimation of capacity of a rotary is based on Wardrop's equation which is empirical in nature and takes into account the geometric elements like entry or exit width, length and width of weaving section, and the proportion of weaving traffic with respect to the total traffic in weaving section. The entire roundabout is divided into separate weaving sections and the practical capacity of the roundabout is synonymous with the weaving section having the least capacity [11].

German, Australian and HCM roundabout capacity models can be identified as analytical models and they are based on the gap acceptance behavior of drivers. The German roundabout capacity model uses circulatory flow, number of circulating lanes, number of lanes at the entry, minimum headway between circulating vehicles, critical gap and follow up headway. The minimum headway between circulatory vehicles, critical gap and follow up head way has been found out as 2.1, 4.12 and 2.88 s for German conditions [6]. Lane by lane capacity at the roundabout can be obtained from the Australian formula. Entry lane which has the largest entry flow is referred to as the dominant entry lane while the entry lane which has the smallest entry flow is referred to as the subdominant entry lane [2]. An exponential model for roundabout capacity has been introduced in HCM 2010 as an analytical approach based on gap acceptance behavior. Critical gap and follow-up headway are the major parameters in this model. The recommended values of critical gap and follow-up

time are 4.1–4.6 s and 2.6–3.1 s respectively. The method is modified for different number of circulatory and entry lanes. Critical gap and follow-up headway have to be verified for important locations which are different for those in U.S.A. [11]. Hence it is necessary to modify the HCM 2010 roundabout capacity model for mixed traffic condition in the locality.

2.1 Traffic Flow Conditions

A homogeneous traffic mix is expected to have no variations in operating speeds, size and driving characteristics of the vehicle. Therefore, calculations for the analysis of homogeneous traffic is made much simpler as size, speed and following distances of vehicles' can be held constant [1]. Heterogeneous traffic or mixed traffic condition is suggested to be the opposite of homogeneous traffic. Vehicles of different types operate at different characteristics and varying speeds. Heterogeneous traffic condition (mixed traffic) is referred to traffic flow when the percentage of dominant travel mode is less than 80% of the total vehicular mix [3, 7].

2.2 Critical Gap

Critical gap (t_c) is expressed as the smallest gap an entering driver in to a roundabout would find acceptable in order to merge with the circulatory flow around the central island. This is determined by the gap acceptance behavior of the entering drivers and cannot be directly observed at site. Only accepted gap and rejected gap can be observed at site and these define upper and lower values for critical gap but not the exact value. Critical gap depends among other factors, vehicle type and the target lane [9]. Accepted gap and rejected gap are determined using Fig. 2 to estimate critical gap.

Vehicles B, C and D are circulating in the roundabout in front of an entry leg where vehicle A is about to enter. Say;

- Vehicle A arrives at the roundabout and stops at line "1" at t = 0 s
- Vehicle B is circulating the roundabout and arrives and crosses the line "S" at t = 1 s; $B_s = 1$ s
- Vehicle C is circulating in the round-about and crosses the line "S" at t = 3 s; $C_s = 3$ s
- Vehicle A enters the roundabout and crosses line "2" at t = 6 s
- Vehicle D is circulating in the round-about and crosses the line "S" at t = 8 s; $D_s = 8$ s

Between Vehicles B and C

$$\text{Rejected gap} = C_s - B_s$$

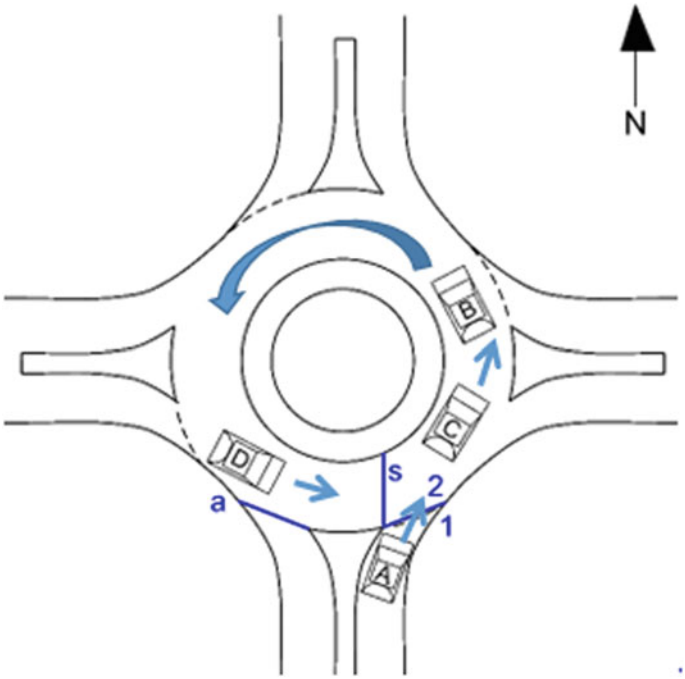

Fig. 2 Diagram for rejected gap and accepted gap calculation by NCHRP method

$$= 3s - 1s$$
$$= \underline{2s}$$

Between Vehicles D and C

$$\text{Accepted gap} = D_s - C_s$$
$$= 8s - 3s$$
$$= \underline{5s}$$

There are several critical gap estimation procedures. Previous methods for estimating critical gap have been compared and it has been found out that the best results could be obtained by the Maximum likelihood method [5, 12]. Further it has been found that maximum likelihood method provides superior results over Wu's method when drivers were inconsistent (Troutbeck 2014). The method of minimizing sum of absolute differences has been compared with Ashworth, Harders, Maximum likelihood, Wu's and modified Raff's method and concluded that minimizing sum of absolute differences method provides superior results over others [1]. New method called square root of squared differences method has been introduced and compared with the minimizing sum of absolute differences method. Comparing average percentage

of violators, the square root of squared differences method is recommended for determining critical gap under mixed traffic conditions [13]. The equation recommended for estimation of critical gap is presented in the following equations (Eqs. 1 and 2).

$$f = \sqrt{(T_c - R_i)^2 + (T_c - A_i)^2} \tag{1}$$

$$F = Min\Sigma\sqrt{(T_c - R_i)^2 + (T_c - A_i)^2} \tag{2}$$

where;

T_c Critical gap
A_i Accepted gap
R_i Highest rejected gap.

Corresponding f value is determined for each vehicle of the considered vehicle category. Summation of corresponding f value is determined. Summation of "f" values for the considered vehicle class is carried out iteratively to obtain a minimum value. Optimization of the "F" function results in critical gap value. Stream equivalent critical gap is determined by weighted average method [13].

$$t_{c,mix} = \Sigma(t_i \times P_i) \tag{3}$$

where;

$t_{c,mix}$ Stream equivalent critical gap
t_i Critical gap of each class
P_i Percentage composition of vehicles of each class.

2.3 Follow-Up Headway

Follow-up headway (t_f) is the gap in seconds between departure times of the first (previous) vehicle and second (next) vehicle from roundabout entry which utilizes the same headway in circulatory flow under queuing condition at entry leg. If the headway in circulatory flow allows further vehicles from entry in to the roundabout in queuing condition, they are passing the edge of the roundabout in follow-up headway one after the other. Calculation is carried out by averaging the difference between passage times of entering vehicles.

HCM 2010 recommends an average follow-up headway value of 3.20 s for U.S. roundabouts. However follow-up headway values which depend on vehicle behavior for mixed traffic conditions have to be adopted for Sri Lanka. The following equation can be used for estimation of follow-up headway.

$$t_f = t_f^{next} - t_f^{previous} \tag{3}$$

where;

t_f follow-up headway in seconds (s)
t_f^{next} passing time of roundabout edge by next vehicle
$t_f^{previous}$ passing time of roundabout edge by previous vehicle.

2.4 HCM 2010 Roundabout Capacity Model

HCM 2010 roundabout capacity model is a combination of single lane based regression and gap acceptance parameters. A general form is also presented in HCM 2010 allowing for calibration for specific conditions in a city, region or country. The model to be calibrated is presented in the following equations.

$$C = A \times e^{-B \times Q_{nwl}} \text{ (pcu/h)} \tag{4}$$

$$A = \frac{3600}{t_f} \tag{5}$$

$$B = \frac{t_c - \frac{t_f}{2}}{3600} \tag{6}$$

where;

C Capacity
A and B Model Parameters
t_f Follow-up headway
t_c Critical gap
Q_{nwl} Circulatory flow (pcu/h).

This form of the gap acceptance model depends mainly on behaviours of traffic users, expressed in this case through such parameters as critical headway (tc), follow-up headway (tf) and local habits. Therefore, according to the form of the model contained in the HCM 2010, model validity and accuracy of traffic capacity calculations are determine these two parameters, i.e. tc and tf [10].

3 Methodology

A suitable and easily accessible roundabout was selected for the study after carrying out an inventory survey. A four legged roundabout at Gatambe in Kandy, Sri Lanka (Fig. 3) was selected after concerning the mutually perpendicularity of the four entry legs, availability of uncontrolled flow durations, zero gradient at entry, negligible interference with pedestrians and cyclists and having no signalized control at close range. Roundabout selected for the study lay on A1 Colombo-Kandy Road

Fig. 3 Selected roundabout at Getambe, Kandy, Sri Lanka

and connects to Gannoruwa Road, William Gopallawa Mawatha (AB 42), Sirimawo Bandaranayake Mawatha and Peradeniya leg (Fig. 2). Inscribed circle diameter is 40 m. Entry from each lane faces single lane circulatory flow. Entry widths for Peradeniya leg, Sirimawo Bandaranayake Leg, Gannoruwa Leg and Willian Gopallawa Leg were 4.2 m, 3.41 m, 4.6 m and 7.65 m respectively.

A turning movement count survey and video recording of the roundabout was carried out simultaneously on Thursday, 27th September 2018. The survey was carried out at the roundabout for fourteen consecutive hours from 6.00 a.m. to 8.00 p.m. The survey considered the vehicle classes of motorcycles, three-wheelers, car/jeep category, passenger van, medium buses, large buses, light goods vehicles and lorries. Turning movement count survey was used to determine entry flow, circulatory flow rate and vehicle composition of each vehicle category.

Four cameras were set up to have an undisturbed clear view of entry on each leg. Data extraction from video recording was done with a least count of 0.04 s using Wondershare Filmora 8.7.4 video editing software. Data extracted from video recording was used to determine the gap acceptance parameters; critical gap and follow-up headway. Critical gap and follow-up headway was determined considering each vehicle category. Microsoft Excel 2010 with solver add-in was used for the optimization. Weighted average method was adopted in determining the stream equivalent critical gap and follow-up headway incorporating the percentages shared by vehicle categories from the total vehicle mix. HCM 2010 roundabout capacity model expressed by Eq. 4 was used for performance analysis of the roundabout. Circulatory flow in pcu/h, stream equivalent critical gap and follow-up headway in seconds were used. Obtained results are presented in the following section.

4 Results and Discussion

Table 1 presents a sample of highest rejected gaps and accepted gaps used to determine critical gap by optimization for one vehicle class.

This procedure was carried out for each vehicle class and critical gap value for each category has been determined. The lowest critical gap value was 4.22 s for motorcycles while the highest was 7.91 s for the large bus category. Each category of motor cycles, three-wheelers and car/jeep shares up to 25% of the total vehicle mix hence more than 75% of the vehicle mix is occupied by those classes. Follow-up headway was calculated considering the leader and follower at the entry for each vehicle class. Average follow-up headway value for each vehicle class was used in determining follow-up headway for the total stream. Table 2 presents the obtained parameters. Critical gap and follow-up headway values for the total traffic stream were determined as 5.07 s and 2.97 s respectively from the weighted average method. And the ratio of tf/tc was 0.59. These values were used to calibrate the HCM 2010 roundabout capacity model for the locality. HCM 2010 default parameters are: B = 0.000875 for single lane (corresponding to $t_f = 2.7$ s and $t_c = 4.5$ s). The variation of entry flow and circulatory flow at each entry has been plotted for HCM 2010 model using both calibrated and default gap acceptance parameters.

Table 1 Table for critical gap (t_c) calculation by optimizing the function

Vehicle No.	Highest rejected gap (s)	Accepted gap (s)	f (s)
1	3.08	4.76	1.53
2	4.32	4.8	0.34
…	…	…	…
…	…	…	…
59	1.92	8.04	4.36
60	1.40	6.68	3.81
Minimum summation			240.72
t_c (s)			4.60

Table 2 Critical gap (t_c) and follow-up headway (t_f) values

Vehicle type	Vehicle flow (total)	Vehicle (%)	t_c (s)	t_f (s)
Motor cycles	188	25.41	4.22	2.31
Three-wheelers	194	26.22	4.60	2.52
Car/jeep	181	24.46	5.08	3.05
Passenger van	43	5.81	4.71	3.22
Medium bus	3	0.41	4.40	3.92
Large bus	94	12.7	7.91	4.85
Light goods vehicles	28	3.78	5.09	3.14
Lorry	9	1.22	4.83	3.51

Figures 4, 5, 6 and 7 represent the variation of entry flow with circulation flow for both HCM 2010 default method and HCM 2010 calibrated method at the Getambe roundabout, Kandy.

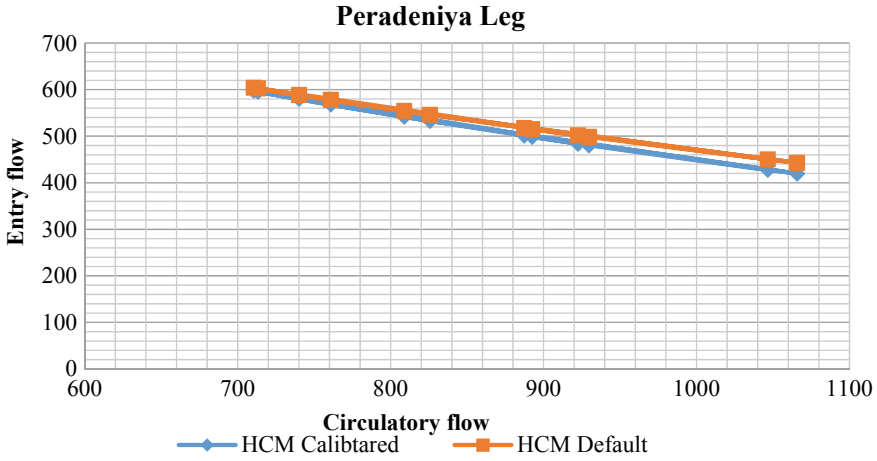

Fig. 4 Variation of entry flow with circulation flow in Peradeniya Leg

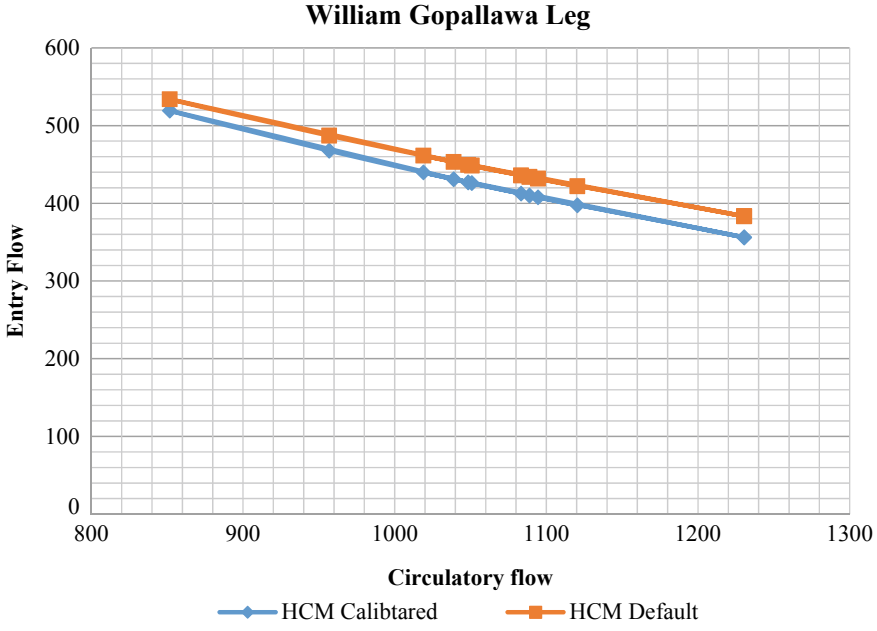

Fig. 5 Variation of entry flow with circulation flow in William Gopallawa Leg

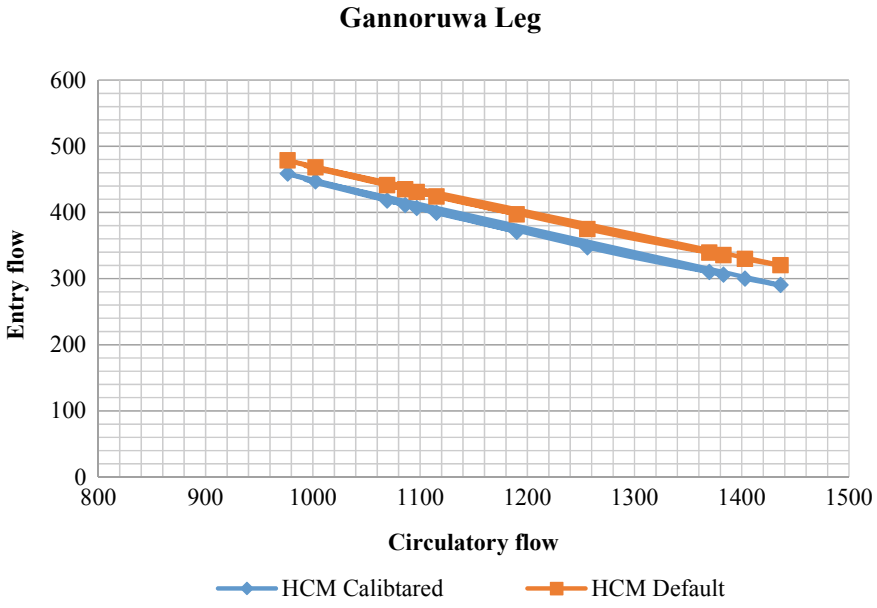

Fig. 6 Variation of entry flow with circulation flow at Gannoruwa Leg

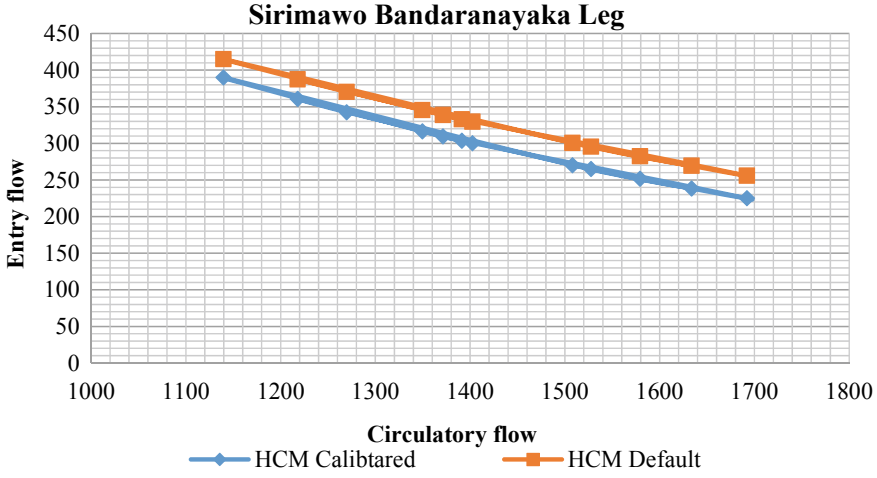

Fig. 7 Variation of entry flow with circulation flow at Sirimawo Bandaranayake Leg

The highest entry flow can be observed at the Peradeniya entry while the highest circulatory flow can be observed at Sirimawo Bandaranayake Leg for the selected time period at the roundabout. Figure 8 shows the variation of the calibrated method and default method with varying circulatory flow from 0 to 2600 pcu/h. HCM 2010

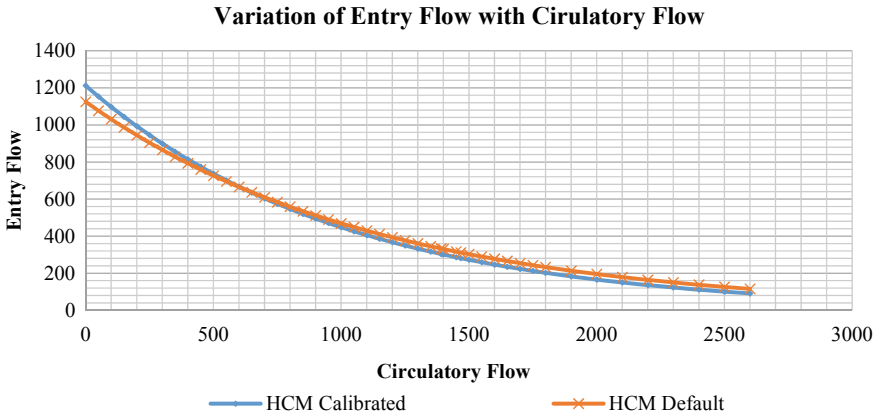

Fig. 8 Variation of entry flow with circulation flow for both HCM 2010 default and calibrated methods

calibrated method allows higher entry flow than the default method in low circulatory flow. When the circulatory flow is higher HCM 2010 default method allows higher entry flow. The differences between these two methods have been considered for determining percentage adjustment as shown in Fig. 9.

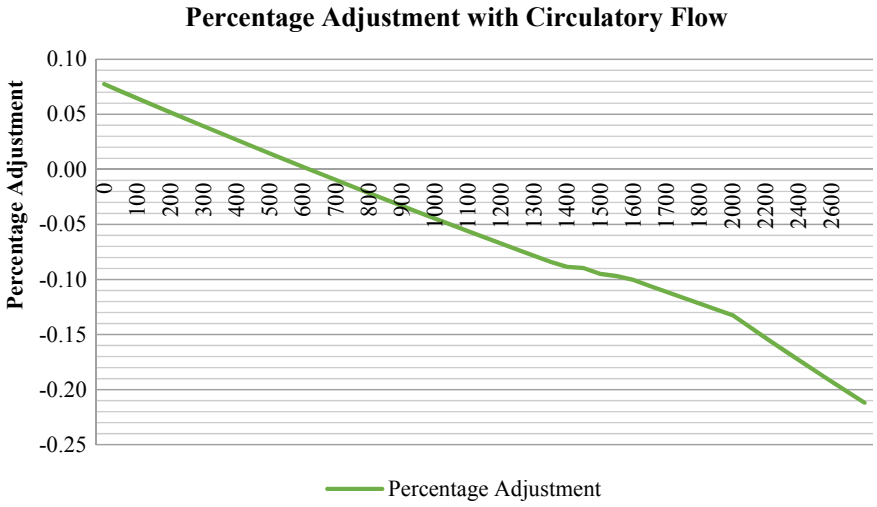

Fig. 9 Variation of percentage adjustment with circulation flow

5 Conclusion

Mixed traffic flow at the selected roundabout consists 25% of motorcycles 26% of three-wheelers and 24% from the car/jeep category. The stream equivalent critical gap and the stream equivalent follow-up headway were 5.07 s and 2.97 s respectively. These gap acceptance parameters were used to calibrate the HCM 2010 roundabout capacity model for mixed traffic condition in the locality. Default equation and calibrated equation were used to determine the entry flow. Both methods derived the same entry flow when circulation flow was 620 pcu/h. Calibrated method derived higher entry flow values than the default method when the circulatory flow was lower than 620 pcu/h. Calibrated method derived lower entry flow values than the default method when the circulatory flow was higher than 620 pcu/h. The adjustment percentages vary from 8 to −21% when the circulatory flow ranges from 0 to 2600 pcu/h. These adjustment factors can be directly used to calculate entry flows from HCM 2010 default method.

References

1. Ahmad A, Rastogi R, Chandra S (2015) Estimation of critical gap on a roundabout by minimizing the sum of absolute difference in accepted gap data. Can J Civ Eng. www.nrcresearchpress.com/cjce
2. Akcelik R, Chung E, Besley M (1998) Roundabouts: capacity and performance analysis. Research Report No. 321, ARRB Transport Research Ltd., Australia
3. Arasan VT, Krishnamurthy K (2008) Effect of traffic volume on PCU of vehicles under heterogeneous traffic conditions. Road Transp Res 32–49
4. Bovy H, Dietrich K, Harmann A (1991) Guide Suisse des Giratoires. Lausanne, Switzerland
5. Brilon W, Koenig R, Troutbeck R (1999) Useful estimation procedures for critical gaps. Transp Res Part A 33:161–186
6. Brilon W, Wu N, Bondzio L (1997) Unsignalized intersections in Germany—a state of the art. In: Proceedings of the third international symposium on intersections without traffic signals, Portland, Oregon, USA, 21–23 July, pp 61–70
7. Fazio J, Hoque M, Tiwari G (1999) Fatalities of heterogeneous street traffic. Transp Res Rec: J Transp Res Board 55–60. https://doi.org/10.3141/1695-10
8. Kimber RM (1980) The traffic capacity of roundabouts. TRRL Laboratory, Report 942, Crowthorne, Berkshire, UK
9. Kususma A, Haris NK (2011) Critical gap analysis of dual lane roundabouts. Procedia Soc Behav Sci 16:709–717. https://doi.org/10.1016/j.sbspro.2011.04.490
10. Macioszek E (2016) The application of HCM 2010 in the determination of capacity of traffic lanes at turbo roundabout entries. Transp Problems 11(3). https://doi.org/10.20858/tp.2016.11.3.8
11. Mahesh S, Ahamad A, Rastogi R (2016) An approach for the estimation of entry flows on roundabouts. Transp Res Procedia 17:52–62
12. Miller A (1974) Nine estimators of gap-acceptance parameters. In: 5th international symposium on the theory of traffic flow and transportation. Newell G.F. New York: American Elsevier Publishing Co., Inc.

13. Sandaruwan A, Karunarathne T, Wickramasinghe V (2019) Estimating critical gap at roundabout under mixed traffic conditions in Sri Lanka. In: Proceedings of the eastern Asia society for transportation studies, vol 12
14. Troutbeck, RJ (2014) Estimating the mean critical gap. Transp Res Rec: J Transp Res Board. Washington D.C 2461(1):76–84

Capacity Analysis for Urban Roundabouts in Sri Lanka Using Modified SIDRA Model

H. K. D. T. Karunarathne, M. A. K. Sandaruwan, U. K. A. H. Madushani, and W. M. V. S. K. Wickramasinghe

Abstract Traffic performance of an intersection can be more effectively controlled by roundabouts than other methods due to increased safety and efficiency. Vehicle flows merge and diverge at small angles with low speeds in one circulatory direction within the roundabout. Designing a roundabout requires thorough analysis of its capacity and other performance parameters. There are many methods to estimate the capacity of roundabout entry. However these methods are developed in countries with homogeneous traffic conditions which consist of higher percentage of passenger cars. Traffic flows in Sri Lanka consists of 45–55% of light vehicles such as motor bikes and three wheelers. Therefore, most available roundabout capacity estimation methods cannot be directly applied to the traffic condition in Sri Lanka. An adjustment should be done to the mixed traffic condition before applying the existing estimation methods. This research aims to introduce an adjustment method to estimate the capacity of urban roundabouts in Sri Lanka by modifying the SIDRA roundabout analysis method. Statistical analyses were done to identify the significance of the adjustment methods. The results show that the existing SIDRA model can be used when the traffic flow is adjusted using passenger car equivalency factors. It can be concluded that the adjustment method gives more sustainable estimations to the roundabout entry capacity for local traffic flow conditions.

Keywords Mixed traffic condition · Roundabout entry capacity · SIDRA capacity model · Statistical analysis

1 Introduction

Roundabouts are considered as an effective intersection control methods for low to medium traffic flows. Vehicle flows merge and diverge within the circulatory area of a

H. K. D. T. Karunarathne (✉) · M. A. K. Sandaruwan · W. M. V. S. K. Wickramasinghe
Faculty of Engineering, University of Peradeniya, Peradeniya 20400, Sri Lanka
e-mail: tharukaakarunarathna@gmail.com

U. K. A. H. Madushani
Faculty of Science, University of Peradeniya, Peradeniya 20400, Sri Lanka

R. Dissanayake et al. (eds.), *ICSECM 2019*, Lecture Notes in Civil Engineering 94,
https://doi.org/10.1007/978-981-15-7222-7_28

roundabout in small angles. Furthermore, the speed is reduced within the roundabout. Therefore, the safety is increased.

Entry capacity of a roundabout is an important performance measure in planning and analysis stages. There are two basic methods to estimate roundabout entry capacity. One of these methods is empirical models based on the geometry of roundabout including entry width, entry angle, the number of lanes in entry and circulatory area. Gap acceptance based models depend on gap acceptance parameters such as critical gap and follow on headway.

Capacity models used in most countries are developed for homogeneous traffic flow which usually consists of passenger cars. Traffic flow in most of the developing countries including Sri Lanka is identified as heterogeneous or mixed traffic. Due to variations of the size and the speeds of these different types of vehicles, the existing capacity estimation models must be modified to use for the local traffic flows.

This research aims to develop a more economical and sustainable method to estimate roundabout entry capacity.

2 Literature Review

Highway Capacity Manual [3] states that even though the empirical models are generally better in capacity estimation, they require a number of congested roundabouts for calibration. The advantage of gap acceptance models is that they can be developed from uncongested roundabouts. HCM 2000 has presented a gap acceptance based capacity model. The capacity at a roundabout can be estimated using gap acceptance techniques with two major parameters; critical gap and follow-up time. HCM 2000 assumes that the capacity for each entry leg of a roundabout can be determined independently of the other legs. HCM 2000 defines the critical gap as the minimum time gap, in seconds, between successive circulating stream vehicles, in which an entry flow vehicle is accepted to enter into the roundabout. Follow-up time has been defined in HCM 2000 as the time in seconds, between the departure of one vehicle of entry flow and the departure of next vehicle using the same gap in circulatory flow under a condition of continuous queuing. The capacity estimation model of HCM 2000 is given below in Eq. 1.

$$C_a = \frac{V_c e^{-V_c t_c/3600}}{1 - e^{-V_c t_f/3600}} \tag{1}$$

where, C_a is approach capacity in veh/h, V_c is conflicting circulating traffic (veh/h), t_c is critical gap (s), and t_f is follow-up time (s).

HCM 2000 has tabulated the ranges of critical gap and follow-up time as shown in Table 1. However HCM 2000 states that drivers at some countries have been found to accept smaller gaps. The relationship between approach capacity and circulating flow for these upper and lower bound critical gap and follow-up time show negative exponential variations.

Table 1 Critical gap and follow-up time for roundabouts (HCM, 2000)

	Critical gap (s)	Follow-up time (s)
Upper bound	4.1	2.6
Lower bound	4.6	3.1

HCM 2010 entry capacity estimation model considers that vehicle mix composition consists only of passenger cars, heavy vehicles and bicycles. The mixed traffic adjustment is addressed by applying passenger car equivalency factors [6]. According to NCHRP report, the flow rate for each movement must be adjusted for vehicle stream characteristics using passenger car equivalency factors given in the report. The capacity equations given in the report incorporate these factors. Using the given equivalencies, the heavy vehicle adjustment factor is calculated using Eqs. 2 and 3 given below.

$$v_{i,pce} = \frac{v_i}{f_{HV}} \tag{2}$$

$$f_{HV} = \frac{1}{1 + P_T(E_T - 1)} \tag{3}$$

where, $v_{i,pce}$ = demand flow rate for movement i (pc/h), v_i = demand volume for movement i (veh/h), f_{HV} = heavy vehicle adjustment factor, P_T = proportion of demand volume that consists of heavy vehicles, and E_T = passenger car equivalent for heavy vehicles.

NCHRP report presents an entry capacity estimation model based on HCM 2010. The capacity of an entry lane opposed by one circulating lane is based on the conflicting flow. The equation for estimating the capacity is given as Eq. 4 below.

$$c_{e,pce} = 1130e^{(-1.0\times10^{-3})v_{c,pce}} \tag{4}$$

where, $c_{e,pce}$ = lane capacity, adjusted for heavy vehicles (pc/h) and $v_{c,pce}$ = conflicting flow (pc/h). This relationship also gives a negative exponential variation of entry capacity with the conflicting flow rate.

Akcelick et al. [2] developed a roundabout analysis model known as SIDRA based on the roundabout analysis method of Special Report 45 (SR 45) of Australian Road Research Board. This is a gap acceptance based model in AUSTROADS method. The gap acceptance parameters used in SIDRA are related to roundabout geometry as well as circulation and entry flows. They are entry stream minimum departure headway which is also known as follow-on headway and the mean critical gap. Follow on time and critical gap are the parameters related to the opposed (entry) flow, and intra bunch headway and the proportion of free vehicles are the parameters related to the opposing (circulating) flow.

In SIDRA, the effect of heavy vehicles on the capacity of the entry traffic stream has been predicted using passenger car equivalency. For roundabouts, SIDRA method recommends that flow in unit pcu/h to be used instead of veh/h when heavy vehicle

flow exceeds 5% with heavy vehicle equivalents of 2 for single unit trucks and 3 for articulated vehicles. If the percentage of heavy vehicles is lower than five percent, equivalent is $e_{HV} = e_{LV} = 1.0$, and when heavy vehicle percentage is higher than five percent, $e_{HV} > 1$. Heavy vehicle adjustment factor used in SIDRA method is given in Eq. 5 [1].

$$f_{HV} = \frac{1.0}{1.0 + (e_{HV} - 1.0)(P_{HV} - 0.05)} \tag{5}$$

for $P_{HV} > 0.05$

$f_{HV} = 1.0$ for $p_{HV} \leq 0.05$

where, P_{HV} = percentage of heavy vehicles and e_{HV} = passenger car equivalent of heavy vehicles.

The circulating flow rate should be adjusted for heavy vehicle effect using Eq. 6 [1].

$$q_{ca} = q_c / f_{HV} \tag{6}$$

where, q_{ca} is the adjusted circulating flow rate in pcu/h.

The entry lane capacity model of SIDRA based on SR 45 is shown in Eqs. 7 and 8 [1].

$$Q_e = \frac{3600^{\varphi} q_c e^{-\lambda(\alpha - \Delta)}}{1 - e^{-\lambda\beta}} \tag{7}$$

$$\lambda = \frac{^{\varphi} q_c}{1 - \Delta q_c} \tag{8}$$

where, Q_e = capacity of the roundabout entry (veh/h), q_c = total flow rate (adjusted) for the circulating stream (veh/s), β = follow-up time, α = mean critical gap, $^{\varphi}$ = proportion of free vehicles, Δ = intra-bunch headway.

Karunarathne et al. [4] has discussed the SIDRA model used for determine the critical gap and follow-on headway for this study in depth. According to this method the entry capacity determined from Eq. 7 should be multiplied by the adjustment factors found for the entry flow to adjust the entry lane capacity for mixed traffic effect. Equation 9 shows the adjusted entry capacity for mixed traffic in entry lane [1].

$$Q_{ea} = f_{HV} * Q_e \tag{9}$$

Kumarage [5] has done a study on PCE standards for Sri Lankan highway design. The PCE factors have been obtained for four different roundabouts in Sri Lanka and the average values are presented to be used in urban roundabouts. Table 2 shows the PCE factors estimated for roundabouts in Sri Lanka.

Table 2 PCE factors for Sri Lankan roundabouts

Vehicle type	PCE
Cart	3.8
Bicycle	1.0
Motor bike	0.7
Three wheel	0.9
Car	1.0
Van	1.2
Mini bus	1.6
Bus	2.2
LGV	1.5
MGV	2.0
HGV	4.4

3 Methodology

3.1 Data Collection

A roundabout located in Kandy city, Sri Lanka was selected for the data collection. "Gatambe roundabout" selected for this study is a four approach intersection with perpendicular entries. An inventory survey, manual traffic movement survey and a video survey was done on Thursday, 27th September 2018 for 14 h. The inventory survey was done to collect geometric data required for the capacity estimation. Video survey and the traffic movement volume count were done from 6.00 am to 8.00 pm. Traffic flow data for four hours were selected for the data analysis considering the gap acceptance behavior of the flow.

Figure 1 shows the Gatambe roundabout and the four entries. Geometric data used for the analysis is tabulated in Table 3.

3.2 Data Analysis

Tables SIDRA roundabout analysis method was used to determine the entry capacity of the four approaches separately. Original SIDRA capacity estimation model facilitates adjustment of circulating and entry traffic flows for passenger cars and heavy vehicles only by an adjustment factor shown in Eqs. 5 and 6.

However the traffic movement survey data indicates that the traffic flow of this selected location consists of 50–60% of motor bikes and three wheelers, 25% - 30% of passenger cars and 10–15% of heavy vehicles. Therefore, an adjustment should be done for the flow rates before using in capacity estimation models. Karunarathne

Fig. 1 Gatambe roundabout

Table 3 Geometric parameters of the Gatambe roundabout

Geometric Element	Approach leg (entry)			
	P	S	G	W
Inscribed circle diameter (m)	40	40	40	40
No. of circulating lanes	1	1	1	1
Entry lane width (m)	4.2	3.41	4.6	7.65
No. of entry lanes	1	1	2	2

et al. [4] proposed two adjustment methods to modify the flow rates for the mixed traffic condition. The two methods are discussed below.

3.2.1 Mixed Traffic Adjustment Method 1

In this method Eq. 5 was used to find the adjustment factors separately for each vehicle category only when the percentages exceeded five percent. The adjustment factors for motor bikes, three wheelers and busses were denoted as f_{MB}, f_{TW}, f_B respectively. When the percentage was lower than five percent, the adjustment factor was considered as 1. Finally the circulation flow was divided by the adjustment factors to determine the adjusted circulation flow q_{ca}.

3.2.2 Mixed Traffic Adjustment Method 2

In this method the adjustment factor was determined using Eq. 10 given below. Then the circulation flow was divided by the adjustment factor to determine the adjusted circulation flow q_{ca}. When the percentage of the vehicle type is less than five percent it was not considered in adjustment factor calculation.

$$\text{Adjustment factor} = \frac{1.0}{1.0 + \Sigma(e_x - 1.0)(p_x - 0.05)} \tag{10}$$

where, e_x denotes PCE factors for each vehicle type and p_x is the percentages the vehicle type considered, respectively.

The circulating flow for 15 min period was first calculated for each entry lane without considering the vehicle type. Then it was adjusted using the adjustment factors. PCE equivalencies used in adjustment factor calculation are tabulated in Table 2.

In order to check whether there exists any significant difference between the entry capacity obtained by original SIDRA method and the two adjustment methods, statistical tests were performed using R studio statistical software. This analysis was done for the four roundabout entries separately.

Traffic flow data for four hours with gap acceptance traffic flow behavior at the roundabout was selected from the video recordings for data analysis. Classified circulating flow rate was found for 15 min periods for vehicle types motor bikes, three wheelers, passenger cars, medium busses, large busses, Light Good Vehicles (LGV), Medium Good Vehicles (MGV), and Heavy Good Vehicles (HGV). Circulating flow rates opposing each entry was determined with the percentages of each type of vehicles. Then the adjustment for mixed traffic was done considering the percentages. Using the adjusted circulating flow values, the gap acceptance parameters α and β were determined for both adjustment methods. Then, the entry capacity was found for each entry using the entry width, opposing circulatory flow and inscribed circle diameter as inputs. Finally, the entry capacity was adjusted for the entry lane mixed traffic composition.

Then the circulatory flow rate was determined using the original SIDRA method. In this step motor bikes, three wheelers, passenger cars and passenger vans were considered as light vehicles and no adjustment was done for these vehicle type. Busses and other heavy vehicle types having PCEs higher than 2 were considered as heavy vehicles and the flow rates were adjusted for heavy vehicles only.

4 Results and Discussion

The results for original SIDRA method and the adjustment methods were then compared and the results are shown in Figs. 2, 3, 4 and 5.

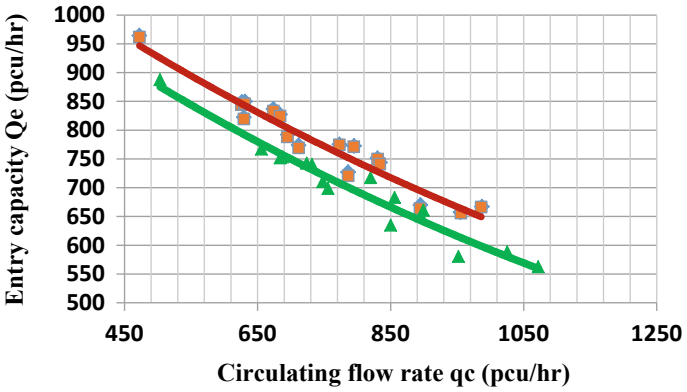

Fig. 2 Comparison of capacity at Peradeniya entry

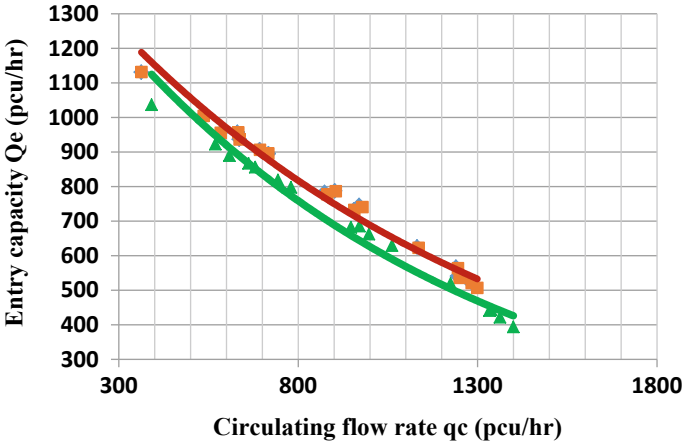

Fig. 3 Comparison of capacity at Gannoruwa entry

According to the results it can be identified that relationship between the entry capacity and the circulation flow rate in negative exponential variation. Methods 1 and 2 show nearly same negative exponential variation for entry capacity with circulating flow rate. Highest entry capacity can be observed at the William Gopallawa entry due to the larger entry lane width. The lowest entry capacity can be seen in the Sirimavo Bandaranayke entry. The results showed that adjustment of traffic flow for mixed traffic results an increase in entry capacity. This is mainly due to the low PCE factors assigned for motor bikes and three wheelers. The increment of entry capacity due to adjustment for mixed traffic is highest for William Gopallawa entry. This is also due to the higher percentage of light vehicles in the entry flow.

For the statistical tests for each approach leg, the sample of entry capacity obtained by the original SIDRA method (Q0), the sample entry capacity obtained by mixed

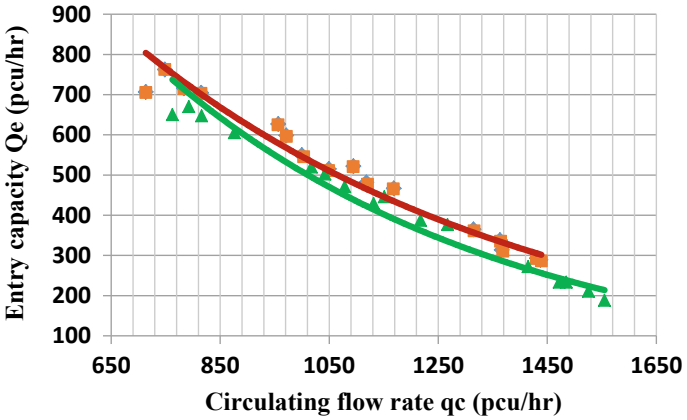

Fig. 4 Comparison of capacity at Sirimavo Bandaranayke Road entry

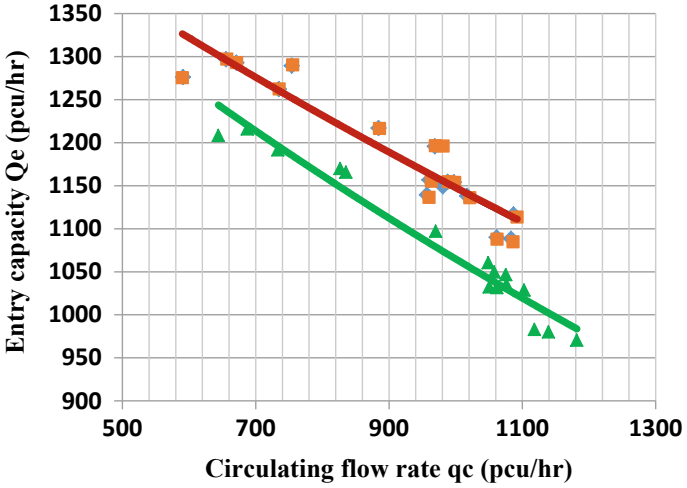

Fig. 5 Comparison of capacity at William Gopallawa Road entry

traffic adjustment method 1 (Q1) and the sample of entry capacity obtained by mixed traffic adjustment method 2 (Q2) were considered as three samples. The two samples Q1 and Q2 depend on the original sample (Q0) because the adjusted capacity samples were obtained by applying factors to the original data sample. Therefore, paired tests were used to check the difference between Q0 and Q1. Similarly paired tests were used to check the difference between Q0 and Q2. Since the two samples Q1 and Q2 are completely independent, unpaired tests were used to check the mean difference between Q1 and Q2.

Following hypothesis was used to check the mean difference of the samples Q0 and Q1. To check the mean difference of the samples Q0 and Q2 the same hypothesis were used.

H_0: $\mu_{Q0} - \mu_{Qi} = 0$ (There is no any significant difference between the means of Q0 and Qi)

Versus

H1: $\mu_{Q0} - \mu_{Qi} \neq 0$ (There is a significant difference between the means of Q0 and Qi)

where, i = 1, 2.

The mean difference of the two samples Q1 and Q2 was checked using the following hypothesis.

H_0: $\mu_{Q1} - \mu_{Q2} = 0$ (There is no any significant difference between the means of Q1 and Q2)

Versus

H1: $\mu_{Q1} - \mu_{Q2} \neq 0$ (There is a significant difference between the means of Q1 and Q2)

However, the two samples should be checked first for normality for selecting the suitable test to be applied to check the mean difference. Anderson Darling test was used to check the normality of the three samples of each entry. Accordingly, following hypothesis was developed to check the normality.

H_0 = Data are normally distributed

Versus

H_1 = Data are not normally distributed

Then the normality and the mean difference were checked for the three samples of each approach separately.

Peradeniya Entry

According to the Anderson Darling Test,

P value for Q0, Q1 and Q2 > 0.05 and thus H_0 was not rejected. Therefore data are normally distributed for all three samples.

Since Q0 and Q1 are normally distributed and Q1 depend on Q0, paired t-test was used to check the mean difference between Q0 and Q1. Similarly, since Q0 and Q2 are normally distributed and Q2 depend on Q0, paired t-test was used to check the mean difference between Q0 and Q2. According to the t-test, P value< 0.05 for both sets, and thus, H_0 was rejected. Therefore, it can be concluded that there is a significant mean difference between Q0 and Q1 and between Q0 and Q2.

Since Q1 and Q2 are normally distributed and do not depend on each other unpaired t-test was used to check the mean difference between Q1 and Q2. According

to the un-paired t-test, P value > 0.05, and thus, H_0 cannot be rejected. Therefore, it was concluded that, there is no significant difference between Q1 and Q2.

Gannoruwa Entry

According to the Anderson Darling Test,

P value for Q0, Q1 and Q2 > 0.05, and thus reject H_0 was not rejected. Therefore data are normally distributed.

Since Q0 and Q1 are normally distributed and Q1 depend on Q0, paired t-test was used to check the mean difference between Q0 and Q1. Similarly, since Q0 and Q2 are normally distributed and Q2 depend on Q0, paired t-test was used to check the mean difference between Q0 and Q2. According to the t-test, P value < 0.05 for both sets, and thus, H_0 was rejected. Therefore, it can be concluded that there is a significant mean difference between Q0 and Q1 and between Q0 and Q2.

Since Q1 and Q2 are normally distributed and do not depend on each other, unpaired t-test was used to check the mean difference between Q1 and Q2. According to unpaired t-test, P value > 0.05, and thus, H_0 was not rejected. Therefore, it can be concluded that there is no significant difference between Q1 and Q2.

Sirimavo Bandaranayke Entry

According to the Anderson Darling Test, all P value > 0.05, and thus H_0 was not rejected. Therefore all three data samples are normally distributed.

Since Q0 and Q1 are normally distributed and Q1 depend on Q0, paired t-test was used to check the mean difference between Q0 and Q1. Similarly, since Q0 and Q2 are normally distributed and Q2 depend on Q0, paired t-test was used to check the mean difference between Q0 and Q2. According to the t-test, P value < 0.05 for both sets, and thus, H_0 was rejected. Therefore, it can be concluded that there is a significant mean difference between Q0 and Q1 and between Q0 and Q2.

Since Q1 and Q2 are normally distributed and do not depend on each other, unpaired t-test was used to check the mean difference between Q1 and Q2. According to unpaired t-test, P value > 0.05, and thus, H_0 was not rejected. Therefore, it can be concluded that there is no significant difference between Q1 and Q2.

William Gopallawa Entry

According to Anderson Darling Test, P values for Q1 and Q2 > 0.05, and thus, H_0 was not rejected. Therefore, data samples are normally distributed.

P value for Q0 < 0.05, thus, H_0 was rejected. Therefore data are not normally distributed.

Since Q0 is not normally distributed and Q1 depends on Q0, Wilcoxon Rank sum test was used to check the mean difference between Q0 and Q1. Similarly, since Q0 is not normally distributed and Q2 depends on Q0, Wilcoxon Rank sum test was used to check the mean difference between Q0 and Q2. According to the Wilcoxon Rank sum test, P values > 0.05 for both sets, and thus H_0 was rejected. Therefore, it can be concluded that there is a significant mean difference between Q0 and Q1 and between Q0 and Q2.

Since Q1 and Q2 are normally distributed un-paired t-test was used to check the mean difference between Q1 and Q2. According to the un-paired t-test, P value > 0.05, and thus H_0 cannot be rejected. Therefore there is no significant difference between Q1 and Q2.

According to the statistical analysis, it can be concluded that, for all four entries there is a significant difference between Q0 and Q1, and Q0 and Q2. Furthermore, there is no any significant difference between Q1 and Q2 for all four entries. Therefore, both adjustments can be used to estimate the capacity at a roundabout entry. Also, it can be identified that the adjustment methods give more reliable output.

A summary of the statistical analysis is shown in Table 4.

Table 4 Summary of the statistical analysis

Entry	Samples	P-value	Behavior comparison between two Samples
Peradeniya	Original method and adjustment method 1	3.577×10^{-14}	Significant difference exists
	Original method and adjustment method 2	5.249×10^{-14}	Significant difference exists
	Adjustment method 1 and adjustment method 2	0.9167	Significant difference does not exist
Gannoruwa	Original method and adjustment method 1	3.291×10^{-13}	Significant difference exists
	Original method and adjustment method 2	1.307×10^{-13}	Significant difference exists
	Adjustment method 1 and adjustment method 2	0.9767	Significant difference does not exist
Sirimavo Bandaranayaka	Original method and adjustment method 1	6.94×10^{-14}	Significant difference exists
	Original method and adjustment method 2	8.368×10^{-14}	Significant difference exists
	Adjustment method 1 and adjustment method 2	0.9735	Significant difference does not exist
William Gopallawa	Original method and adjustment method 1	3.052×10^{-5}	Significant difference exists
	Original method and adjustment method 2	3.052×10^{-5}	Significant difference exists
	Adjustment method 1 and adjustment method 2	0.9362	Significant difference does not exist

5 Conclusion

Vehicle flow at the selected location consists of 20–25% of motor bikes, 20–30% of three wheelers, 25–30% of passenger cars and 10–15% of heavy vehicles in the circulating flow during the selected four hours.

Two adjustment methods were proposed to adjust the circulation flow rate to be used in the entry capacity model for the mixed traffic. The capacity was estimated by these two methods and the original SIDRA method. The two developed methods show the same negative exponential variation of entry capacity. Statistical tests also have proven that there is no any difference between the two adjustment methods. When the gap acceptance governs the traffic flow at the roundabout and the flow is heterogeneous, it can be concluded that the modified entry capacity is significantly higher than that of the original SIDRA method. Therefore the modified capacity estimation methods give reliable values than the original SIDRA method for the mixed traffic flow.

References

1. Akcelick R, Troutbeck R (1991) Implementation of Australian roundabout analysis method in SIDRA. In: Proceedings of international symposium of highway capacity. Karlsruhe, Germany, 24–27 July 1991, pp 7–37
2. Akçelick R, Chung E, Besley M (1997) Analysis of roundabout performance by modeling approach flow interactions. In: Third international symposium on intersections without traffic signals, Portland, Oregon, USA, 2l–23 July 1997
3. Highway Capacity Manual (2000) Transport Research Board, National Research Council, pp 571–575
4. Karunarathne T, Sandaruwan M, Wickramasinghe V (2019) Modification of SIDRA model for capacity estimation of urban roundabouts under mixed traffic condition in Sri Lanka. J Eastern Asia Soc Transp Stud
5. Kumarage AS (1996) PCU standards for Sri Lanka highway design. Paper Presented at the annual sessions, Institute of Engineers Sri Lanka, Oct 1996
6. NCHRP report 672 (2010) Roundabouts: an informational guide, 2nd edn. Transportation Research Board, Washington, DC, pp 111–113

Investigation of the Institutions Formed and Empowered from Disaster Risk Governance Policies: Case Studies from Sri Lanka, Myanmar and Maldives

W. K. D. Rathnayake, C. S. A. Siriwardana, C. S. Bandara, and P. B. R. Dissanayake

Abstract Regardless of the country, communities are highly vulnerable and exposed to disasters induced by natural hazards. There is a number of disaster risk management mechanisms in place to mitigate and address disasters. A question unanswered regarding the disaster risk management mechanisms is why the damage and destruction due to disasters are not getting decreased and why are the same errors getting repeated. Hence, it is required to evaluate the effectiveness of these disaster risk management mechanisms to better tackle disasters. When understanding the disaster risk management mechanisms there are policies, which govern the mechanisms, and there are institutions, which operate, empowered and defined from these policies. Institutions that govern, plan, address and response to disasters are different and have different mechanisms of work. Networking, coordination, and dependencies of the institutions are a critical factor in disaster risk management. This research paper analyses the empowerment of institutions and identifies the placement of institutions in risk management mechanisms comparatively. The research study is based on case studies from Sri Lanka, Myanmar, and the Maldives. A number of community visits and institutional visits were conducted in three countries for the data collection of the research work. It was observed that in the above-mentioned countries, different approaches, techniques, and processes are used for disaster risk management. Hence, initially, this research study attempts to holistically understand the overall scenario of policies in place for disaster risk governance. As the next step, all the institutions were mapped and summarized for analysing. The outputs from the research work can be used to understand the interdependencies of an institution in the disaster management mechanisms and to evaluate the involvement of each institution in disaster risk management.

Keywords Risk analysis · Disaster management · Disaster risk reduction

W. K. D. Rathnayake (✉) · C. S. Bandara · P. B. R. Dissanayake
University of Peradeniya, Peradeniya, Sri Lanka
e-mail: kusaldanidu@gmail.com

C. S. A. Siriwardana
University of Moratuwa, Moratuwa, Sri Lanka

R. Dissanayake et al. (eds.), *ICSECM 2019*, Lecture Notes in Civil Engineering 94,
https://doi.org/10.1007/978-981-15-7222-7_29

1 Introduction

Disasters induced form natural hazards are a critical risk of the entire world. According to the world economic forum global risks perception survey for the year 2019 "Extreme Weather Events", "Failure of climate-change mitigation and adaptation" and "Natural disasters (Disasters induced from natural hazards) are the top three likelihood risks. Also in terms of impact top three risks consists with "Weapons of mass destruction", Failure of climate-change mitigation and adaptation" and "Extreme weather events". Whereas "Natural disaster (Disasters induced from natural hazards" is in the 5th position among top 10 risks in terms of impact [13].

This indicates the exceptionally outstanding nature of the natural hazard induced disaster risk in terms of likelihood and impact. The question attached to this identification of the prime risks is "who is going to affect most?" Jochen Hinkel in 2018 published that the coastal communities are the most dynamic environments on earth. Hinkel further evaluates that the coastal societies do have a long history in facing and adapting to environmental changes. To further illustrate this fact, the total population of the world is above 7 billion. Whereas the highest population concentration is in low elevation coastal zones (defined as less that 10 m elevation) [2].

With these two facts on natural hazard induced disaster risk magnitude and the areas which are going to affect most, this paper is written to evaluate the risk mitigation and addressing methods/mechanisms available as disaster risk management mechanisms. The disaster risk management mechanisms available and in use are unique to the area of exposure (Country, Region) yet has the drives form global frameworks such as the Sendai framework for Disaster Risk Reduction 2015 etc. Hence the approaches taken by each country in managing disaster risk in identifying disaster risk, assessing disaster risk, evaluating disaster risk and monitoring of disaster risk are diverse.

The disaster risk management mechanisms are composed from number of policies and frameworks which turns into action from various institution and stakeholders. There similarities as well as differences in policies in place, stakeholders involved, collaboration mechanisms in place when comparing disaster management mechanisms. This paper identifies three disaster management mechanisms and compares the attributes of each mechanism. The disaster management mechanism of Sri Lanka, Myanmar and Maldives were compared for the above mentioned. The countries do carry identical disaster profiles and also carries same profiles in cultural, political and vulnerability status. A detailed reasoning of election of the disaster mechanisms are presented in a following section of this paper.

2 Methodology

A questionnaire survey was build up in assessing the disaster management mechanisms [9]. The survey was carried out in two segments, an institutional survey and a community survey. Institutional survey was conducted with key stakeholder institutions in each country with the objective of identifying the disaster management mechanism and understanding the role of each stakeholder. Whereas Community survey was conducted to understand the reality of practice in policies and framework in the grass root level and to identify the gaps in the mechanism.

In Sri Lanka Disaster Management Center, Department of Meteorology were visited for the institutional survey. The National Disaster Management Authority of Maldives, the Meteorology Department of Maldives, Department of Meteorology and Hydrology of Myanmar, Department of Disaster Management of Myanmar were other institutions visited for the survey. Matara in Sri Lanka, Bu Gwe Gyi and Thazin Villages in Myanmar, and Maamigili in Maldives are the community areas visited for the community survey.

The paper is flowed with the identification of disaster management policies in each country. With that understanding on the policies available, which defines and empowers the institutions, the institutions involved are summarized for each country. The organizations which are in the disaster management system in the undisturbed situation were recognized as internal organizations and they were only considered for the research purposes.

3 Context of Sri Lanka, Myanmar and Maldives

The research work is focused on three case studies from Sri Lanka, Myanmar and Maldives. The three Asian countries were chosen as two island countries and one continental country.

The coast line length, total population, and coastal population of Sri Lanka, Myanmar and Maldives are as in Table 1.

When looking at the cultural similarities, these countries do have collectivists culture, a high power distance, and same level of masculinity [4]. Also floods, abrasion, cyclones are similar hazard profiles with 2004 Tsunami as a break through disaster in policy changes [8].

Table 1 Context of Sri Lanka, Myanmar and Maldives

Attribute	Sri Lanka	Maldives	Myanmar
Coast line length (km)	1340	1129	1930
Total population	21,336,833	532,668	59,094,870
Coastal population	4,355,000	532,668	1,554,000

Sources [3, 8, 12]

With these similar attributes the research work is focused to identify the policy implementation in each country.

4 Disaster Management Policies

After a thorough literature review on the policy documents available on each country and also by refereeing to the institutional survey data the policies of Sri Lanka, Myanmar and Maldives were summarized and identified as follows.

4.1 Disaster Management Policies of Sri Lanka

The institutions and legislations related to Disaster Management Mechanism of Sri Lanka have undergone several changes since 1977, where in 1977 it was the responsibility of Ministry of Social Services. A dedicated body to manage disasters was first recognized through the establishment of a National Disaster Management Centre (NDMC) under the Ministry of Health, Highways and Social Services during 1996. Then until the establishment of the Disaster Management Act in 2005 National Council for Disaster Management led the preparedness activities while the Department of Social services led the relief assistance [6, 10].

Following are the formations of acts and policies in a timely order.

- Reconstruction and Rehabilitation Fund Act, No. 48 of 1993: Used to provide relief to persons affected, reconstruct of property and for rehabilitation.
- Disaster Management Act No. 13 of 2005: provides the institutional structure and governs the disaster management structure. And also defines the National Council for Disaster Management (NCDM) and Disaster Management Centre (DMC).

The Disaster Management Act of 2005, provided institutional structure to be adopted to facilitate the disaster risk management. The act assigns three broad functions to the NCDM. Policy formulation/planning, Monitoring and Ensuring disaster preparedness are the three functions. In addition the act authorise the relevant authorities to act upon the requirement such as empowering the president to declare a state of disaster.

After the act of 2005 there were number of policies, plans compiled with accordance to the international frameworks available and as per the timely needs. Following are the compiles of such nature.

- National Disaster Management Policy: prepared in 2010 according to the Hyogo framework for action.
- Ministry of Finance and Planning—Budget Circulars No. 152 (I) (II) and (III): Issued in 2013 and 2014: to mitigate the duplication of funding.

- National Disaster Management Plan: prepared for 2013–2015. Provides guidance to the formulation of the disaster management plans in all levels of administration.
- National Emergency Operations Plan: Provides guidelines for emergency preparedness (2015).
- Sri Lanka Comprehensive Disaster Management Programme: The action plan for 2014–2018.
- National Adaptation Plan for Climate Change Impacts of Sri Lanka: is prepared for 2018–2025 in line with United Nations Framework on Climate Change.
- Sri Lanka Disaster Management Plan: prepared in accordance with Sendai Framework for the years 2018–2030.

4.2 Disaster Management Policies of Myanmar

Myanmar Disaster Management Mechanism (Herein after DMM) complied from;

- Disaster Management Law, 2013 (The pyidaun gsu Hluttaw Law No. 21, 1013).
- Disaster Management Rules, 2015 (Notification No. 22/2015 from the Ministry of Welfare, Relief and Resettlement).

2013 dated disaster management law of Myanmar empowered number of institutions in disaster risk management. Ministry of Welfare, Relief and Resettlement is an institution empowered to carry out the office task. With the given powers the Ministry compiled the 2015 dated Disaster Management Rules for Myanmar. In following two sections the Disaster Management Law and Rules were comprehensively identified.

4.2.1 Disaster Management Law, 2013

Disaster Management Law compromised with 9 Chapters as described below.

Chapter 1 and 2 compromised with "Title and Definition" and "Objectives" respectively. The chapter one embarks the name of law and then defines the terms of State, Disaster, Disaster Management, Disaster Risk Reduction, Resource, National Committee, Local Body, International Organizations, Foreign regional organizations and Victims.

There are 5 objectives identified in the chapter two. Implementation and formation of programs and bodies. Coordination of different stakeholders, conserving the environment, and provisions management are specified as objectives.

Formation of National Disaster Management Committee and defining its Duties and Powers is done in the chapter 3. The union government is empowered to form and reform the National Disaster Management Committee (Herein after NDMC) from the clause No. 4 of the chapter 3. The clause No. 5 identifies 31 duties and powers of the NDMC. Laying down policies, forming supporting bodies, delegating duties to the relevant stakeholders, coordination with stakeholders, reporting, guiding and supervising are some of the key duties and powers mentioned. The clause No. 6

empowers The Ministry of Welfare, Relief and Resettlement to undertake the related office work.

Formation of Disaster Management Bodies and defining its Duties and Powers was done in the chapter 4. The Union government and the region or state government is empowered for formation of the disaster management bodies from clauses No. 7 and No. 8. The clause No. 9 defines the duties and powers of the National disaster management bodies. The actions and duties falls accordingly to implement the disaster management under the guidance of NDMC.

Chapter 5 defines the process of declaration of being a disaster affected area and authorize the president of the country to carry out the task. Clauses No. 11 and No. 12 empowers the President in declaring area as a disaster affected area.

The chapter 6 includes 6 clauses from No. 13 to No. 18 which defines the functions on disaster management as follows.

- Clause No. 13: Defines the acts and powers of stakeholders in disaster management.
- Clause No. 14: Preparatory measures for disaster risk reduction before disaster.
- Clause No. 15: Preparatory measures to be organized before disaster in the area where is likely to strike the disaster.
- Clause No. 16: Preventive measures to be carried out in the area where is likely to strike disaster before the disaster.
- Clause No. 17: Actions when the disaster strikes, emergency responses including search and rescue.
- Clause No. 18: Rehabilitation and reconstruction activities to be carried out after the disaster.

The Disaster Management Fund is established form the chapter 7. NCDM and Region or State bodies are empowered and defined the actions on establishing, reporting, budgeting, allocating, and auditing the funds under the clauses No. 19 to No. 24.

A separate chapter (Chapter 7) is compiled with “Offenses and Penalties” regard to disaster management. Which includes clauses No. 25 to No. 31. They defines the types of offenses and the repercussions of each act.

Exemption of tax for provisions, use of uniforms, compensation entitlement, issuing of notifications are some of the entitlements listed under the final chapter 9, miscellaneous.

4.2.2 Disaster Management Rules, 2015

Disaster Management Rules include 12 chapters. Where Chapter 1 is on the Title and Definition of the rules.

Chapters 2, 3 and 4 identifies functions and duties the Ministry of social welfare, relief and resettlement, other relevant ministries, government departments, government agencies and also department.

Chapter 5 includes the Disaster management plans whereas chapter 6 describes the declaring a state of disaster affected area and its duration. Disaster preparedness and prevention for disaster risk reduction at the pre-disaster phase is rules under the chapter 7.

Emergency response activities including search and rescue during the disaster stage is ruled under the chapter 8. Final four chapters respectively ruled, Rehabilitation and reconstruction during the post disaster phase, Communication and collaboration with the assisting international actors Maintenance, expenditure and disposal of the national disaster management fund.

4.3 Disaster Management Policies of Maldives

The Disaster Management Act, 2015 of Maldives enables and empowers the disaster management mechanism of Maldives. Even though the act is legalized in the year 2015, there were number of guidelines prepared before that. The guidelines act as drivers of the disaster management mechanism. The delay of legalizing the act made the guidelines coming to action only after 2015.

The act is composed with the purposes as follows. (The following summary of the Disaster Management Act of Maldives is compiled from a translation obtained from the gazette issued in Thaana script.)

- To protect the people from natural hazards and man-made disasters.
- To incorporate guidelines on disaster risk mitigation and preparedness.
- To reduce disaster risk and to adapt a preparatory national strategy, to identify responsible parties to manage disaster risk, and to identify their responsibilities.
- To provide assistance at emergency situations and to provide assistance on the relief efforts, to incorporate such guidelines to coordinate such assistance.
- To state the roles and responsibilities of the City Councils, Atoll Councils, and Island Councils in reducing disaster risk and mitigation in emergency situations.
- To create awareness among the people in reducing disaster risk and mitigation in emergency situations, and to incorporate guidelines to protect the people from such dangers and enhance coping capacity.
- To incorporate disaster risk reduction guidelines and policies within the sustainable National development projects.
- To make the people responsible and accountable towards disaster risk reduction and mitigation.

Other than to the act there are three guidelines in place to drive the disaster management mechanism of Maldives. The three guidelines are;

1. Community Based Disaster Management (CBDRM) Framework
2. National Internally Displaced People (IDP) Framework
3. Mainstreaming Disaster Risk Reduction into local development (Country report and action plan)

1. Community based disaster management framework

The framework is developed by the lead of Maldives National Disaster Management Center (herein after NDMC) on 2014. The (CBDRM) is of two parts. First part of it is the analysis of country assessment and a comparison assessment on institutional arrangement, human capacity, technical capacity, partnerships, and financial resources. Part two introduce the CBDRR strategy and implementation, monitoring and evaluation mechanisms.

2. National Internally Displaced People (IDP) Framework

This framework defines actions to be followed by local, national and international agencies to assist displaced people during a disaster situation.

3. Mainstreaming Disaster Risk Reduction into local development (Country report and action plan)

This guideline was prepared in 2014 with 6 modules. Concepts, use of tools, planning, developing, linking with local development planning and measuring are the aspects in detail described in the modules.

With this understanding on policies of disaster management from each country the research work is now directed in identifying the institutions involved in the disaster management mechanism. Most of these organizations were established and empowered from the policies implemented. Whereas some of the institutions due to the nature of work they carry out.

5 Summary of Institutional Involvement

Table 2 was prepared to compare the institutional arrangement from disaster management policies. The institutional involvement was categorized under three divisions namely; planning for disaster risk, Disaster risk monitoring and disaster treatment.

Planning for disaster risk involves the establishment of risk context (disaster management policy planning), risk identification (disaster and hazard mapping), risk pre-treatment (disaster risk reduction) activities. The institutions listed under that category are empowered and established institutions in each country to carry out and conduct such work.

Disaster risk monitoring activities involve the early warning related institutions of each country. Similarly the disaster treatment related institutions are whom responsible and empowered to carry out emergency response and recovery of a disaster.

Table 2 Overall internal organizational identification of Sri Lanka and Maldives

Disaster/risk stage	Sri Lanka	Myanmar	Maldives
Planning for disaster risk	National Council for Disaster Management	National natural Disaster Management Central Committee	National Steering Committee
	Ministry of Disaster Management	State Working Committees	National Disaster Management Authority
	Disaster Management Center	Ministry of Home Affairs	DRR Unit
	Ministry of Defense	Ministry of Social Welfare, Relief and Resettlement Department	Cooperate affairs unit
	Ministry of Health	Ministry of Health	
	Other line ministries	Ministry of Foreign Affairs	
		Department of Disaster Management	
		Asian Disaster Reduction Center	
		ASEAN Committee on Disaster Management	
Disaster risk monitoring	Department of Meteorology	Department of Meteorology and Hydrology	Meteorology Department
	Department of Irrigation		
	National Building Research Organization		
	National Aquatic Resources Research and Development Agency		
	Marine Environment Protection Authority		
	Geological Survey and Mines Bureau		
Disaster treatment	National Disaster Relief Services Center	Relief and Resettlement Department	National Emergency Operations Center
	Provincial Councils	Emergency Operation Centre	National Emergency Response forces
	District Secretariat Offices	District Working Committees	Maldives National Defense Forces

(continued)

Table 2 (continued)

Disaster/risk stage	Sri Lanka	Myanmar	Maldives
	Divisional Secretariat Offices	Township Working Committees	Atoll DM units
		Village Working Committees	City DM units
		Armed forces of Myanmar	Island DM units

Sources [1, 5, 7, 11]

6 Conclusion

In Sri Lanka, Myanmar and Maldives the upstream of the disaster management mechanism has the highest level of involvement from power hierarchy. It was essential and evident that well attained in three countries. The head of the state chairs the top most committee/council established for disaster management. Also from the policy identification it was evident that these institutions and personals were given adequate empowerment to effectively manage a disaster event.

The mechanism under these top bodies are different in contrast. Whereas in Sri Lanka the top body act as a platform to generate the collaboration of all the other parties. In Myanmar the 12 working committee mechanism is downscaled in four steps. Whereas in Maldives it has the similar structure as Sri Lanka.

In Maldives and Myanmar it was only being able to identify Meteorology department and Department of Meteorology and Hydrology respectively as the sole bodies responsible for the hazard monitoring and early warning generation. The early warning dissemination processes are different in each country. In Sri Lanka certain other bodies were identified as responsible for hazard monitoring from the system.

In disaster treatment (Emergency response stage and recovery stage) the Sri Lankan and Maldives has an identical system with direct government involvement. Whereas in Myanmar the system is community based. The structure at Myanmar empowers the community to own the disaster management and building back phases.

The prepared summary of elements only include the internal institutions. There are external institutions as well. Analysing and comparing their involvement is an extension of this research work. Also other than to these institutional work there exists a people hierarchy which affects the overall effectiveness of disaster management mechanisms.

The effectiveness of each system in managing an identical disaster (2004 Tsunami) is an extension of this research work. Such analysis will enable an evaluation of each stakeholder and will critically identify the most effective mechanism.

Acknowledgements This study was conducted with the financial aid from CABARET (Capacity Building in Asia for Resilience Education), a project of the European Union's Erasmus+ Programme– Key action 2– Capacity building in the field of higher education.

References

1. Center for Excellence in Disaster Management & Humanitarian Assistance (2017) Myanmar (Burma) Disaster Management Reference Handbook, Myanmar
2. Center for International Earth Science Information Network (2018) Percentage of total population living in coastal areas, USA
3. Coastline Lengths/Countries of the World [WWW Document] (2019) http://world.bymap.org/Coastlines.html. Accessed 8.20.19
4. Hofstede G, Hofstede GJ, Minkov M (2010) Cultures and organizations: software of the mind, 3rd edn. McGraw-Hill
5. Government of Maldives (2015) The Disaster Management Act, 2015
6. Jayasiri GP (2018a) Disaster management frameworks in Sri Lanka and its compliance with global standards
7. Jayasiri GP (2018) Disaster management frameworks in Sri Lanka and its compliance with global standards. Department of Civil Engineering, University of Moratuwa, Sri Lanka
8. Mondae (2010) Understanding Maldivian culture: Hofstede Cultural Dimensions. hamblogs. https://hamblogs.wordpress.com/2010/05/29/understanding-maldivian-culture-hofstede-cultural-dimensions/. Accessed 8.20.19
9. Rathnayake WKD, Randil OPC, Siriwardana CSA (2018) Development of an evaluation framework to assess the efficiency of the disaster management framework of Sri Lanka. In: Presented at the international conference on sustainable built environment (ICSBE), Kandy, Sri Lanka
10. Siriwardana CS, Jayasiri GP, Hettiarachchi SSL (2018) Investigation of efficiency and effectiveness of the existing disaster management frameworks in Sri Lanka. Procedia Eng 212:1091–1098
11. The Ministry of Social Welfare, Relief and Resettlement (2015) Disaster Management Law, 2013 and Disaster Management Rules, 2015. Yangon, Myanmar
12. Total Population by Country 2019 [WWW Document] (2019) http://worldpopulationreview.com/countries/. Accessed 8.20.19
13. World Economic Forum (2019) The Global Risks Report 2019 (No. 14th Edition), Geneva

Piled Raft Foundation System for Tall Buildings

B. G. S. T. Gamage, B. Kiriparan, B. Waduge, W. J. B. S. Fenrnado, and P. Mendis

Abstract Design of a safe and economical foundation system is an important task in tall build-ing design. Deep foundations such as piled foundations are generally adopted to transfer heavy loads from superstructure to the bearing stratum. Providing adequate geotechnical capacity and limiting the deferential settlement are two important design considerations in the design of piled foundations. The foundation design becomes economical when both the criteria of bearing capacity and settlement are satisfied in an optimum way. A piled raft foundation is an advanced concept in which the total load coming from the superstructure is partly shared by the raft through bearing from soil and the remaining load is shared by piles through skin friction and end bearing. Consequently, piled raft system is generally adopted when pile foundations for tall buildings become uneconomical or unsatisfactory. Due to the three dimensional nature of the load transfer, piled raft foundations are regarded as very complex systems involving many interaction factors such as pile-to-raft, raft-to-soil, and pile-to-soil. This paper intended to present a detailed discussion on the analysis of piled raft system addressing available analytical methods to analysis piled raft system. Considering of deferent factors influencing the pile raft behaviour are summarized in this paper. A detailed numerical analysis approach for the analysis of piled raft foundation is discussed. Further, a case study investigating the performance of piled raft system for an eighty-one storied tall building is presented.

Keywords Piled raft foundation · Soil-Structure interaction · Finite element analysis (FEA) · Settlement

B. G. S. T. Gamage · B. Kiriparan (✉) · B. Waduge · W. J. B. S. Fenrnado
Civil and Structural Engineering Consultants (Pvt) Ltd., Colombo, Sri Lanka
e-mail: kiriparan@csec.com.lk

P. Mendis
University of Melbourne, Melbourne, Australia

R. Dissanayake et al. (eds.), *ICSECM 2019*, Lecture Notes in Civil Engineering 94,
https://doi.org/10.1007/978-981-15-7222-7_30

1 Introduction

As the inevitable results of rising population and growing land scarcity, high-rise buildings have become more predominant in many capitals in recent years. This phenomenon has forced the designers to design a suitable foundation system to satisfy the safety and economy for any kind of ground condition. The aspect of balancing the performance and cost of the foundation system is a challenge for the geotechnical and structural engineers. Also, geotechnical capacity and the settlement are the most key consideration during the designing of tall buildings. Due to the difficulty involved in the soil-structure interaction, proper foundation with systematic design guidelines, specified by both geotechnical and structural designers, is needed to predict the performance of the foundation system accurately.

Raft, pile and the piled raft foundations are the three major types of foundations commonly used in tall buildings. Generally, shallow foundations can be the most economical option for buildings loaded on subsoil with good load-bearing capacity. But the challenge in tall buildings is, due to heavy load from the super-structure, the thickness of the raft should be increased. It results excessive settlement and expensive. Further, due to the relatively low thickness-to-width ratio, the raft foundations exhibit flexible characteristics to some extent even under stiff ground environments. Uneven loading and varying ground conditions may increase the flexible features and result the differential settlement. These effects made up the building foundation design as crucial. Due to these limitations in the raft foundation systems, the idea of using piles as settlement-reducers was started in the seventies.

The other option of traditional pile foundation system are limiting the settlement and also satisfy the safety and the serviceability requirements in an effective manner. Under pile foundation all the loads from the superstructure is directly transferred to bedrock or underlying hard soil layer. This is the most common method currently used around the world. However, it is an uneconomic solution for both perspective of cost and time due to the requirement of higher number and larger length of piles required for tall buildings. Following that the concept of piled raft foundation system had been brought out by the re-searchers Randolph, Davis and Poulos [6].

This paper discusses background of piled raft foundation system and its analysis and design approach through a case study in Sri Lanka.

2 Pile Raft Foundation

The piled raft foundation is a combined system of piles and raft where both are partly shared loads of the superstructure. The Superstructure loads are shared between the piles using shaft friction and end bearing, while the raft supported on direct soil bearing. In this system the pile group typically carrying about 80% of the total load directly into the deeper strata. This system can be categorized into two major forms such as the raft-enhanced pile group and the pile-enhanced raft.

The piled raft foundation system transfers the loads by involving complicated three-dimensional interaction among the fundamental elements of pile, raft and the soil. In the traditional pile group, the interaction is acting only between piles and the soil. In case of piled raft foundation system, four interactions are trendy namely,

1. Pile-Soil Interaction.
2. Pile-Pile interaction.
3. Raft-Soil Interaction.
4. Pile-Raft Interaction.

In addition, the safety of the system depends on the combined system of raft, pile and the soil instead of only in the pile group as in the pile foundation. Therefore, design and the analyses of the piled raft system seems as complicated. Additionally, several issues needed to be addressed when designing the piled raft foundation. Such as, ultimate load capacity for vertical, lateral loadings, maximum settlement, differential settlement, raft moments and shears for the structural design of the raft and pile loads and moments for the structural and geotechnical design of the piles [6].

Pile raft shall be favourable when the soil underneath the raft has a profile with relatively stiff clay or relatively dense sand. But in the cases where soil profile beneath raft with soft cays, loose sand, soft and compressible layers at shallow depths risk of having consolidation settlement considering the pile raft action is unfavourable. These kinds of soils can lead to long term settlement and reduce the contribution to load sharing. Consolidation settlement could lead to losing the contact between the soil and the raft and finally, all the loads shall be shared by the Piles [6].

The design process of the pile raft foundation can be categorized as three stages, starting with the preliminary stage to evaluate feasibility, followed by assessing the number of piles required and locations finally end up with gaining the detailed design information including optimum number, location, and layout of the piles. In the preliminary stage, it is important to evaluate the performance of a pile and raft foundations individually if the raft or piles unable to satisfy the design criteria such as geotechnical capacity, settlement in an optimum manner a combined system is adopted.

In the piled raft design, several approaches are adopted to find the bearing capacity and the settlement. Such as:

1. Poulos and Davis [7].
2. Randolph [8].
3. Strip on springs analysis, using the program GASP (Poulos 1991).
4. Plate on springs approach, using the program GARP [5]

Poulos Davis method describes method of calculating the stiffness of the pile group and raft separately to find the amount of load sharing among them [7]. Flow Chart 1 describes the process of the analysis.

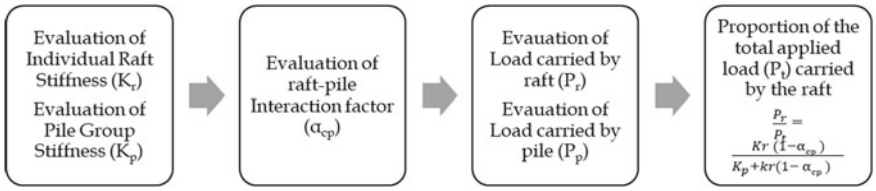

Flow Chart 1 The process of analysis for settlement

2.1 Finite Element Analysis of Pile Raft System

Real problems encountered in the application of piled raft systems for tall buildings are more complex. In solving such complex cases in practice with irregular pile layout and loading arrangements most accurate results cannot be obtained using those conventional analysis methods. Almost all the designs of tall buildings nowadays carried out by three-dimensional (3D) finite element model (FEM) analysis. With the aid of FEM analysis technics complex non-leaner behavioural pattern of materials and interactions as discussed above can be easily and more precisely accounted.

Under FEM analysis firstly it is important to select a software that capable to handle the designer's requirement. The Software should be included with good element library, array of material behaviour models and provisions for mesh refinement [1]. In the FE model that used for pile raft should be able to consider three-dimensional behaviour of a pile raft foundation and simulate the behaviour of a single pile to check its reliability and adjust the applied parameters depending on the chosen pile type. The 3D model should be able to take account of non-linear behaviour of pile and soil at pile and the pile shaft and stress-strain behaviour of the soil according to the applied stresses and strain to the soil. Finally, this model should able to consider the interactions mentioned above that govern the functionality of the pile raft System.

The processes of 3D FEM pile raft analysis can be summarized as below Flow Chart 2. According to the Flow Chart 2, 3D FEM model and the parameters shall be validated by a test pile results and recalibrate the model parameters.

In modelling piled raft system piles can be modelled using three finite elements such as;

1. Solid element model.
2. Beam solid connectivity model.
3. Line to solid interface model (Embedded pile).

In solid element modelling all the piles and the soil are modelled as 3D solid elements and an inter-face element is used for allow relative moment within the pile and the soil. This type of models, consumes much time on model definition, messing and computation. Pile Forces and moments cannot be directly taken in these types of models. In beam solid connectivity models, piles are modelled as line elements and

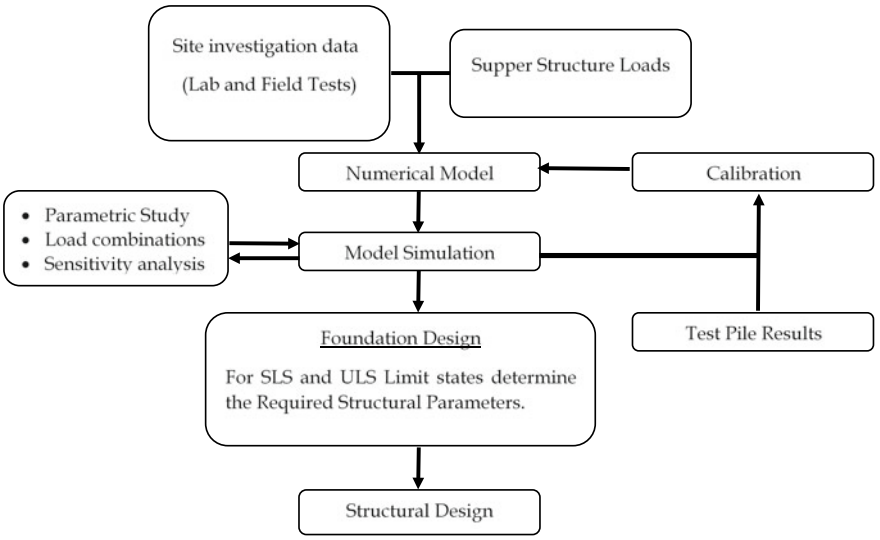

Flow Chart 2 Steps of pile raft FEM analysis

surrounding soil is modelled as solid elements. In this approach relative moments between pile and the soil is not allowed.

The line to solid interface modelling approach is the most ideal approach for modelling the pile in FEM model. In this method pile and soil meshing can be done independently as the interface element connects them. Nonlinear friction slip properties between pile and soil can be assigned to the interface element. The refinement of mesh is a minimum than previous two approaches which reduce computational time. A most suitable modelling approach shall be selected by the designers based on the objective of the analysis.

2.2 Piled Raft Foundation-Case Histories

There are many case histories available for piled raft foundations worldwide. Among those, some projects are summarized in Table 1. Other than the above-mentioned project the world tallest building Burj Khalifa was also supported on a pile raft system.

Table 1 Piled Raft foundation-case histories [4]

Tower	Structure (height/stories)		Load share (%)		Instrumentation	Settlement S_{max}
	Height (m)	Storey	Piles	Raft		
Messe-Torhaus, Frankfurt	130	30	75	25	Yes	NA
Messeturn, Frankfurt	256	60	57	43	Yes	144
Westend1, Frankfurt	208		49	51	Yes	120
Petonas, Kuala Lampur	450	88	85	15	Yes	40
QVI, Perth, West Australia.		42	70	30	NA	40
Treptower, Berlin	121		55	45	Yes	73
ICC, Honhg Kong	490	118	70	30	NA	NA
Commerzbank, Frankfurt	300		96	4	Yes	19
Skyper, Frankfurt	153		63	27	Yes	55

3 Case Study

3.1 Description of the Building

A detailed conceptual study carried out for the foundation system of an 81 storied tall building proposed in Colombo, the capital city of Sri Lanka is discussed in this section, which consists of 81 stories residential tower integrated with a 5 story podium for car parks and amenity at Level 6. Column loads extracted from the 3D finite element analysis carried out by the structural engineer are present in Fig. 1.

3.2 Sub-soil Condition

A detailed site investigation was carried out exploring 31 number of boreholes. A residual soil layer was found up to completely weathered rock (Biotite Gneiss) which was found at a depth of about 12–24.2 m. Basement rock level was encountered in between 18.00 and 36.00 m depth from the existing ground.

In general, the top layer consists of a 1 m filling layer overlaying 9 m of sandy soil. Below the sandy soil layer 6 m thick sandy clay layer overlaying 10 m thick highly weathered rock was identified. Below the highly weathered rock grade III moderately weathered rock was observed at 24 m below the ground level. Groundwater level was established at a range of 0.00–4.15 m depth.

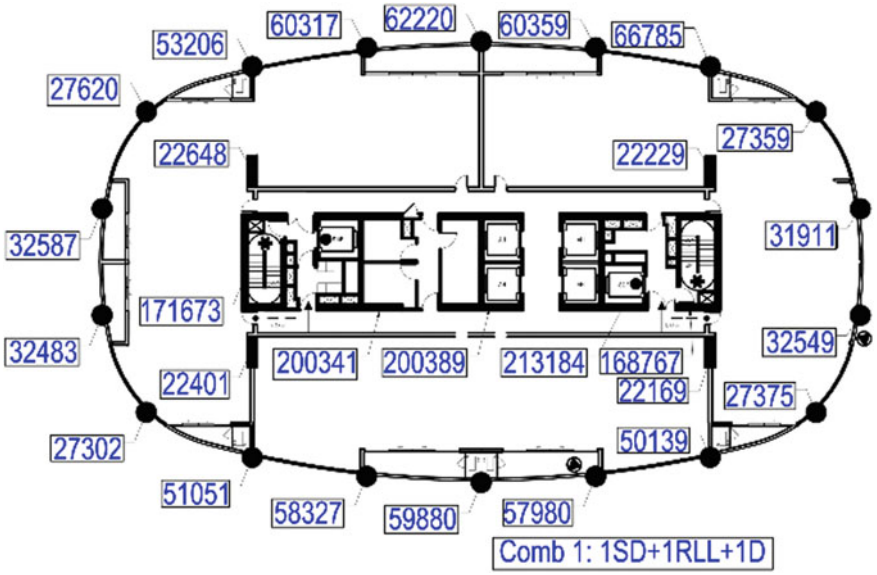

Fig. 1 Column load map at foundation level obtained with the aid of ETABS model (Gravity load case-kN)

Geological characteristics of the project area were analyzed from the review of the borehole investigation data, field observations, published and unpublished literature, and existing geology maps. Soil and rock characteristics, soil type and chemical and organic contents in groundwater and soils were determined during the field investigations.

Generalized borehole log data for tower area and geotechnical parameters recommended by the geotechnical consultant for different sub-soil conditions and rock categories are presented in Table 2.

3.3 Pile Foundation Design for Proposed Tower Foundation

Initially, a traditional pile foundation system was considered for the proposed building according to the above geological information. 138 of Bored and cast-in situ piles of diameter 1500 mm have been used based on the loading intended from the super-structure. Figure 2 shows the layout of the proposed piled foundation system. Symmetrical arrangement with the same spacing between piles was used.

A 4000 mm thick pile cap has been proposed to connect all the piles at 4 m below the ground level. The formation level of the pile cap at lift core is 3800–5200 mm below the ground Level.

Table 2 Sample borehole details

Depth (m)	State	SPT value	Ultimate skin friction (kN/m^2)	Allowable end bearing (kN/m^2)	CR (%)	RQD[a] (%)	UCS (MPa)
3.30	Very dense sand with clay	50	65	–			
6.30	Medium dense SAND with clay	13	15	–			
13.80	Medium dense to dense sand with clay	19	25	–			
21.30	Very dense sand with clay and mica	>50	70	–			
25.70	Completely weathered rock (Hornblend biotite gneiss)		150	–	100	57	12.04
29.50	Moderately weathered rock (Garnet biotite gneiss)		200	3000	97	60	10.51
31.50	Moderately weathered rock (Garnet biotite gneiss)		200	3000	46	–	–
34.70	Moderately weathered rock (Biotite gneiss)		200	3000	77	15	26.12
39.70	Slightly weathered rock (Biotite gneiss)		200	4000	100	44	24.13

[a]*RQD* Rock quality designation *CR* Rock Recovery Ratio

According to the geotechnical data and geotechnical engineer's recommendation, the calculated pile capacity with minimum 4.5 × pile diameter rock socketing is presented in Table 3.

A three-dimensional finite element model of tower with a proposed pile arrangement was developed with the aid of a commercially available computer software CSI ETABS as shown in Fig. 3.

Pile colour	Diameter	No. Piles
	1500	138

Fig. 2 Proposed piles layout

Table 3 Summary of the pile foundation design

Pile diameter (mm)	Pile geotechnical capacities (kN)	No of piles
1500	15,450	138

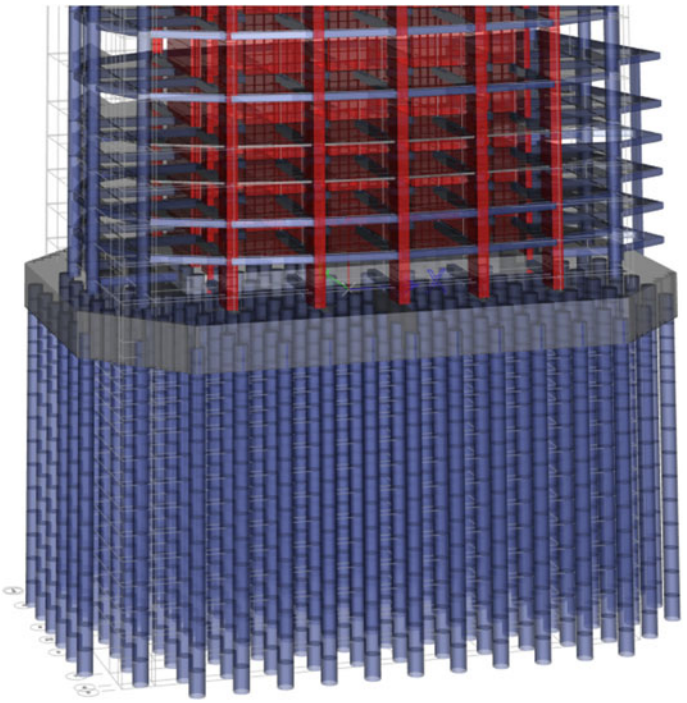

Fig. 3 Etab Model with Piles

Lateral support from soil was modeled as springs and lateral soil subgrade modulus used in the piled supported analysis model is calculated based on the geotechnical parameters given in the site investigation report and the approach presented by Glick [3] and Bowles [2].

$$k_s' = \frac{22.4E_s(1-\mu)}{(1+\mu)(3-4\mu)\left[2\ln\left(\frac{2L_p}{B}\right)-0.433\right]} \tag{1}$$

$$k_s = \frac{k_s'}{B} \tag{2}$$

E_s Stress Strain Modulus.
μ Poissons's Ratio.
L_p Pile Length.
B Pile Width
k_s Lateral Spring Constant

For the soil, lateral spring constants between 25,000 and 45,000 kN/mm and for the rock between 80,000 and 550,000 kN/mm were used. Figure 4 shows the final pile loads from the analysis. The raft action from the pile cap was neglected in the analysis and raft is only utilized to transfer load within the piles.

From, the analysis result it can be observed that piles under the center core wall are heavily-loaded whereas at the boundary piles are lightly-loaded. According to the analysis loads from the tower were not properly distributed among the pile was due to ignoring soil-structure interaction of piles (pile settlement behaviour).

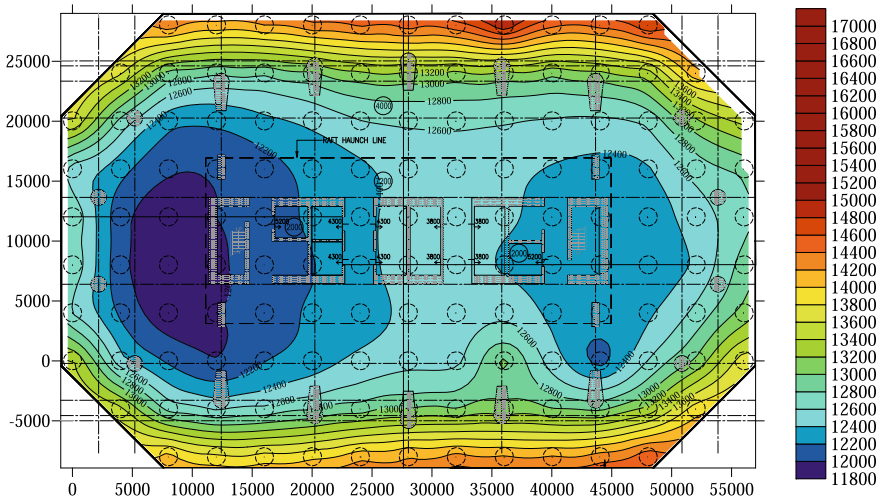

Fig. 4 Pile load contour for pile foundation option

Finally, a comprehensive soil-structure interaction analysis was carried out to find the pile loads. In order to satisfy the geotechnical capacity for pile option minimum 10 m rock socketing was needed. This leads to an increase in foundation costs and reduces construction efficiency. In order to address this problem a piled raft system with treating the piles in combination with raft founded 4 m below ground level was considered. Detailed soil-structure interaction analysis was performed using a 3D finite element model developed in Midas GTS NX.

3.4 Pile-Raft Analysis for the Proposed Tower Foundation

A 3D finite element model was developed for the proposed pile raft system using Midas GTS NX commercially available software as shown in Fig. 5. The line to solid interface model (embedded pile) was utilized in the modeling of piled raft system. The material properties used for FEM modeling are presented in Table 4.

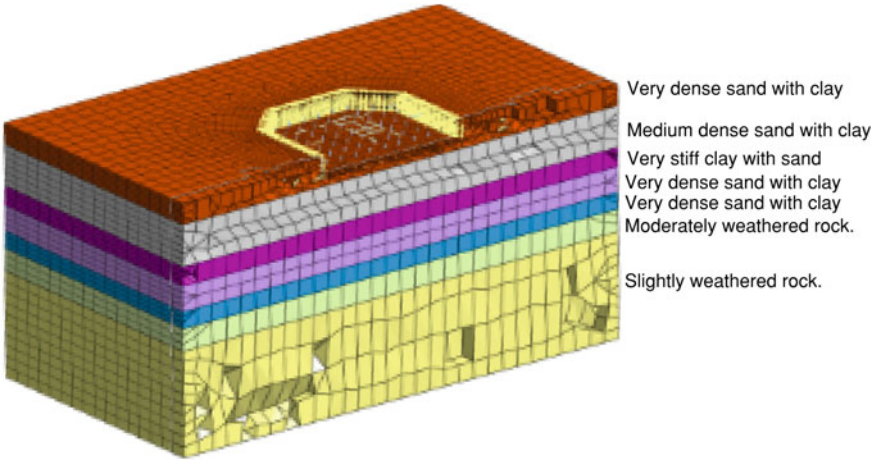

Fig. 5 Midas GTX pile raft model

Table 4 Material models used in FE modeling

Element	Material	Element type	Material behaviour type
Piles	Concrete	2D beam	Isotropic material with elastic behavior
Walls	Concrete	2D shell	Isotropic material with elastic behavior
RAFT	Concrete	3D solid	Isotropic material with elastic behavior
Soil strata	Soil	3D solid	Isotropic material with Mohr-Coulomb behavior
Rock strata	Rock	3D solid	Isotropic material with Hoek Brown behavior

More often in 3D finite element analysis soil is modeled in Mohr-Coulomb behavior. As the rock is more hard and rigid than soil, behaviour cannot be predicted by deriving the stiffness changes due to applied stress. Therefore, Hoek and Brown proposed a concept of equivalent continuum to define the reduction of stress phenomenon in jointed rock masses. This method accommodates to consider unconfined compressive strength of rock which is not considered in Mohr-Coulomb behaviour which leads to simple and accurate representation of rock behaviour.

Raft, soil and the rock were modeled using solid elements while the pile was modeled by a line element as described in an embedded pile approach. The interface between piles and soil was modelled by interface element available in the software which accommodates to simulate the boundary behaviour between same or different materials. Interface parameters are given in Table 6.

The material properties used in the analysis according to the geotechnical report used are summarized below in Table 5.

When modeling the soil boundary, a minimum length equal to the pile cap width was maintained from the edge of the Pile cap to the X-Y plane boundary. The boundary of the rock layer was kept one pile length from the pile base level.

The hybrid meshing method in the programmed was adopted in the analysis. These hybrid elements are formed by combining pyramid and tetrahedron on a hexahedron base which leads to more accurate results that were used for the meshing of elements. The size of the mesh was reduced near pile cap and pile surface. Control points were added in locations of the columns and walls to apply the loads from the supper structure as shown in Fig. 6. At the boundary of soil and rock element points were pinned.

The analysis was carried out under four construction stages. Pile loads for the analysis are given in Fig. 7 and the expected settlement contours are in Fig. 8.

According to Figs. 7 and 8 it was observed pile loads have distributed between all the piles due to the settlement of heavily loaded piles under the core of the building. Table 7 illustrate the final loads share by piles group and raft for each analysis method.

Based on this detailed soil-structure interaction analysis it was observed approximately 11% of the total load is shared by the raft. Further, a nearly uniform distribution of pile loads was observed due to the stiffness contribution of the raft. The effective raft area is 2051 m^2 and average bearing pressure was 110 kN/m^2. Consequently, results from this analysis assisted to minimize the pile loads and rock socketing required. A more economical, safe and constructible foundation design using the piled raft system was obtained.

Around 25% of the total load from the superstructure was shared by the raft in most of the pile rafts designs around the world where the piles are friction piles. In this case study piles were end-bearing piles, and this leads to a higher stiffness ratio of pile group. Therefore only 11% of the total load was shared by the raft.

Table 5 Material properties used for FE modeling

Category	Depth of Layer (m)	Depth from Ground (m)	Elastic Modulus (MPa)	Poisson Ratio	C′ (KPa)	Cu (KPa)	Friction Angel (φ)	Ultimate Skin Friction (kPa)	UCS (MPa)
Very dense sand with clay	6.3	6.3	2	0.3	10		38	15	–
Medium dense sand with clay	7.5	13.8	25	0.28	–	–	32	25	–
Very stiff clay with sand	4.5	18.3	14	0.3	–	190	–	50	–
Very dense sand with clay and mica	6	24.3	40	0.25	40	–	10	70	–
Moderately weathered rock	9.2	33.5	350	0.25	–	–	–	200	12.00
Slightly weathered rock	5.5	39	600	0.2	–	–	–	200	26.00
Concrete	–	–	25,000	0.2					

Table 6 Interface properties used for FE modeling

Category	Ultimate shear force (kN/m^2)	Normal stiffness modulus (kN/mm)
Pile to soil interface	50	30,000
Pile rock interface	200	500,000

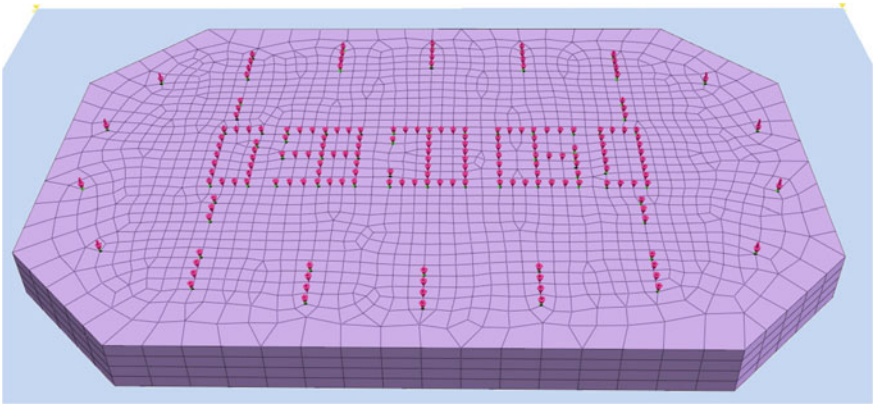

Fig. 6 Loads applied at the controlled points

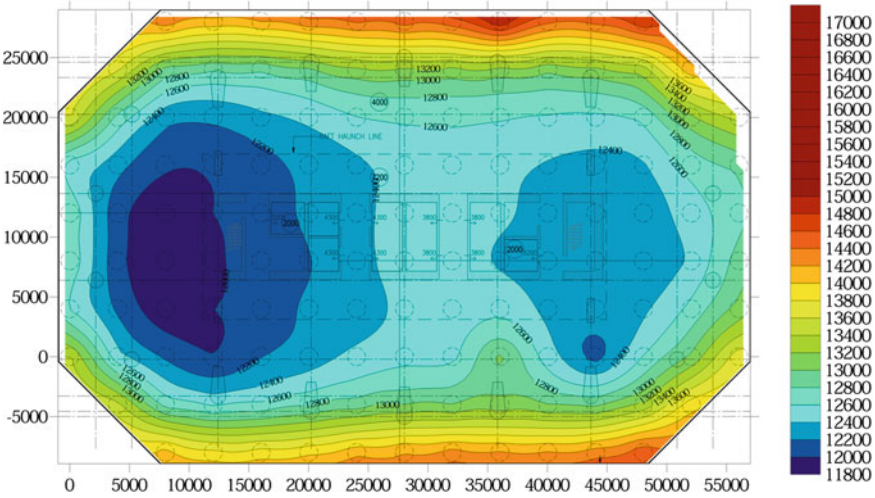

Fig. 7 Pile load contour from pile raft analysis

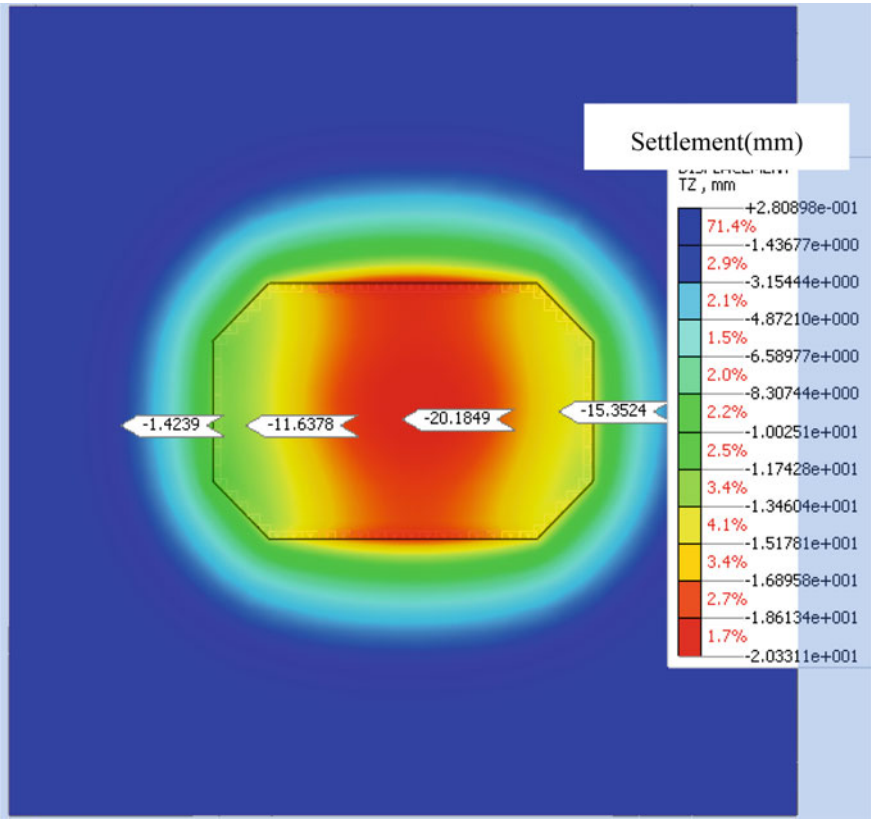

Fig. 8 Settlement contour from pile raft analysis

Table 7 Load carried by pile and raft for different models

	Load carried by pile (MN)	Load carried by raft (MN)
Etabs model	1994.63	–
Midas GTS NX model	1771.27	223.36

4 Conclusion

The concept of the piled raft foundation system and its advantages for tall buildings is discussed in this paper. Background of the piled raft foundation system, behaviour and various analysis methods including finite element methods were outlined. Important considerations to be made in the Finite element modeling and analysis of piled raft foundation were discussed. Significance of adopting piled raft foundation for tall buildings located in fractured rock sites over conventional pile foundation was

explained through a case study. Obtaining a sustainable foundation design for a tall building considering geotechnical pile capacities, pile settlements, cost, and constructability, etc. were highlighted.

References

1. Balakumar V, Huang M, Oh E, Balasubramaniam AS (2017) A critical and comparative study on 2D and 3D analyses of raft and piled raft foundations. s.l., s.n
2. Bowles JE (1996) Foundation analysis and design. McGraw-Hill
3. Glick GW (1948) Influence of softground on the design of long piles. In: Proceedings of 2nd International Conference on Soil Mechanics and Foundation Engineering, vol 4. Institution of Civil Engineers, London, pp 84–88
4. Long PD (2010) Piled Raft—a cost-effective foundation method for high-rises. Geotech Eng J SEAGS & AGSSEA 41(03)
5. Poulos HG (1994a) An approximate numerical analysis of pile-raft interaction. Int J Numer and Analytical Methods Geomech London 18(2):73–92
6. Poulos HG (2001) Piled raft foundation: design and applications. Geotechnique 2:95–113
7. Poulos HG, Davis EH (1980) Pile foundation analysis and design. Wiley
8. Randolph MF (1994) Design methods for pile groups and piled rafts. In: Proceeding of 13th International Conference on Soil Mechanics and Foundation Engineering, vol 5. New Delhi, pp 61–82

Stakeholder Preference for Ongoing Green Urban Planning in Kandy

E. G. I. Sevwandi

Abstract Urban planning has become a mind stimulating concept in the twenty-first century which has been successfully adapted by many countries in the world in order to achieve a sustainable urban development. Stakeholders as the ultimate beneficiaries, plays a vital role in urban development platform whose opinions must be critically considered in the decision making process of urban planning. This research attempts to question and assess the preference of three stakeholder groups regarding the planning interventions that have been applied recently in the Kandy urban development platform. Its objective is to contribute insights to the planning and design of urban greening in Kandy in order to support user needs and preferences. The study is conducted through mixed methods via a visual preference survey and a semi-structured questionnaire survey. Samples were selected by judgmental sampling method including professionals, permanent residents and daily travelers within the Kandy Municipal Council area. This study reveals that the three stakeholder groups have different preferences towards the ongoing urban planning interventions based on their daily interactions with the city. In a nutshell, it can be stated that the stakeholder preference is well inclined towards manageable urban green spaces. They prefer the ongoing projects implemented beneath strategic cities development programme where the green features are incorporated and sometimes their preference pervades over strategic interventions and embrace the existing natural. Stakeholders emphasize the drastic need of green infrastructure planning into Kandy as a futuristic strategy in order to bridge the gap between compact urban constructions and natural ecosystems. Hence, it's essentially important to promote a social discourse on best green planning practices raising awareness and academic stimuli. Moreover, the research evidences can be utilized to indicate the potential strengths and weaknesses of ongoing planning endeavors and broader researches must be conducted to execute further visually preferred plans in Kandy.

Keywords Stakeholder preference · Green urban planning · Kandy

E. G. I. Sevwandi (✉)
Department of Geography, University of Peradeniya, Kandy, Sri Lanka
e-mail: isurika327@gmail.com

R. Dissanayake et al. (eds.), *ICSECM 2019*, Lecture Notes in Civil Engineering 94,
https://doi.org/10.1007/978-981-15-7222-7_31

1 Introduction

Urban planning has become a mind stimulating planning concept in the twenty-first century which is renowned as the "Urban Century" due to the fact that Urban Century initiative brings together scholars, policymakers, and practitioners to look at innovative approaches and successful models that may help to alleviate some of the pressures that necessarily accompany rapid expansion of population and land area covered by cities. Hence, green urban planning is gaining much significance as a productive path of rediscovering the hidden potentials lie in the city to adapt into the successive urban changes both morphological and urbanism related in its way to sustainable development.

Kandy, the last capital of Sri Lankan ancient dynasties and the royal residence, is a testimony for the process of urban transformation from Sri Lankan ancient to contemporary periods [3]. Kandy has been renowned for its ancient history of utilizing the geographic location tactfully in order to defend its prestigious kingdom and residents. Being the last kingdom in Sri Lanka (1469–1815 AD), it still has a stimulating reputation to maintain as both a sacred city where the Temple of the Tooth Relic is situated and as an economic and administrative capital to the Central Province. Being the second largest city in Sri Lanka, Kandy houses a multi religious—multi ethnic population of 1, 30,000 within a land extent of 26.45 km^2. Estimated transient population occupying in Kandy per day is 500,000 whereas employment per day is 90,000 and education per day is 60,000. City profile is further consisted of local and foreign tourists and pilgrims (per day) of 6000 and vehicle arrival (per day) of 56,085 [2].

A city with such unique backdrop necessitates an eco-friendly strategy of urban planning to preserve its idiomatic urban character. Thus, that mechanism should be multidimensional and the city community should be predominantly availed from that. This fundamental rational of urban planning has not been academically assessed to examine the progress of previous planning initiatives. Consequently, this research attempts at focusing on one aspect of aforementioned research gap, which is the 'stakeholder preference' towards ongoing green planning in Kandy.

1.1 Research Problem and Objective

This scenario emphasizes the pressing need of urban planning into Kandy as a crucial element of development since it entails choice making in pursuit of goals such as improving living conditions for individuals and societies in the context of urban development. It is obvious that planning process is changing over time to address the rapid changing nature of problems associated with city structure. Ergo, the recent urban planning initiatives which took place in Kandy also concerned on incorporating green features into the city. Yet, there have never been any intellectual dialogue on the preference of stakeholders regarding these concurrent planning initiatives.

Somarathne [1] claim that the absence of the proper studied urban development plan is one of the core factors for the urban development disparity of the country. Hence, the engagement of stakeholders in the planning process can be identified as one of the critical strategy in the creation of a habitable urban environment. This precisely indicates the planning gap created by the absence of the stakeholder involvement since they play a dominant role in any urban planning platform. Their preference and inclination is very much important in the orientation of an urban vision. Hence, exploring stakeholder preference will assist in re invigorating the urban vision of Kandy with regard to urban planning.

The need of a knowledge base on stakeholder preference regarding Kandy urban planning becomes a pressing requirement whereas to ensure the targeted urban objectives meet with city community desires. Accordingly, exploring the stakeholder visual preference can catalyze the planning mechanism to yield livable green heritage city as expected by the ultimate beneficiaries of the city. As derived through the literature review, there is a considerable research gap regarding stakeholder visual preference in Kandy urban scenario where academics have not paid adequate attention. Accordingly, I have convinced that it's very important to approach this gap which will clear the path for many more futuristic researches. So the objective of this study is inquiring the stakeholder preference towards green urban planning in Kandy.

2 Methodology

The methodology followed here adapted a constructivist worldview that adopts a mixed method approach. Therefore, my study incorporates both qualitative and quantitative data from primary as well as secondary data sources.

Primary data sample size was determined by the researcher as 50 including 10 samples of professionals engaged in Kandy urban planning, 30 samples of permanent residents settled in KMC area and 10 samples of daily travelers within the KMC area. Permanent residents were selected from three specific areas covering the Lake Side, Aniwaththa and Watapuluwa assuming the full coverage of Kandy Municipal Council area. These purposive samples were utilized for the visual preference survey and questionnaire survey depending on the convenience and the accessibility to the most representative and productive sample who will reveal the reality by responding to the questions with much enthusiasm.

The semi-structured questionnaire survey was conducted in order to explore stakeholder perception on the development initiatives in Kandy. The visual preference survey was conducted with the intention to provide this study with a body of information on whether the city dwellers actually prefer the ongoing urban planning initiatives and to investigate whether they really prefer/call for urban greening. Their perceptions and preferences is essential in parallel with discussing green strategies

because if the city community does not request or demand green concerns, it is meaningless to apply green interventions to Kandy urban planning further.

Visual preference survey sheet contained 10 photographs of Kandy city. 5 photographs in the left side were excerpted from the Strategic Cities Development Programme—Kandy, which demonstrates how Kandy will look like after the completion of each separate mini project. Photographs in the right side show the existing conditions of the same five locations. Each photograph contains various levels of greenery so that the preference of the city dwellers towards both existing and futuristic improvements could be assessed through ranking.

Conveniently selected sample of permanent residents, travelers and professionals were given the opportunity to rank these 10 photographs from 1–5 rating scale based on their preference as how much they would like to perceive Kandy as depicted in the photographs. Moreover, four open ended questions were asked along with in order to find out the relationship between the photo preference and amount of greenery.

As it is essential to apply needful interventions to protect and conserve the existing green cover and to promote environmental friendly infrastructure planning, landscape photo preference methodology was used to elicit preferences for visual spatial form that includes strategic urban planning interventions with a range of density and greening. The images were chosen with the intent to explore whether people prefer urban greenery and proposed strategic planning interventions. Photographs were obtained both from actual setting in the study area and proposed 3D representations of the Strategic City Development Programme which can be relate to the life experiences of the local participants. Survey participants indicated preference for each image in response for the prompt: "Please circle the choice that describes how much you would like to perceive Kandy such as those shown in the pictures" on a 1–5 Likert scale: 1—not at all 2—a little 3—somewhat 4—quite a bit 5—very much.

Participants included both male and female (50%) covering permanent residents in the KMC area, daily travelers and professionals engaged in Kandy city urban planning. The participant's ages in years (excluding professionals sample) ranges from 0–20, 21–40, 41–60 and 60> representing 25% each from the sample. Participants were self-selected by the researcher based on their convenience and preference to attend the visual preference survey.

Major source of secondary data was documentary data. The documentary data could be classified into three types such as development project reports, development panning maps and newspaper/journal articles.

Eventually, the retrieved data from the secondary sources and the primary data revealed through questionnaire and visual preference survey together was integrated to investigate the green planning interventions in Kandy. The overall study follows a descriptive content analysis as it is the best method to reveal the grass root level findings. Further, this study contains limitations on the basis of sample selection because the sample does not reveal the opinion of the huge population. Hence, I attempt to reveal the general idea of the sample and to link it with what is observable in the reality.

3 Stakeholder Preference

The results will be presented in two ways. First section will deal with overall stakeholder preference. Second section will focus on group based stakeholder preference. Further, a discussion would be done on whether the amount of greenery really matters regarding the stakeholder preference of ongoing green interventions.

First section reveals that the highest overall stakeholder preference was obtained by Kandy Lakeside Walkability Improvement project. Second section highlights that each stakeholder group has specific preferences among ongoing green strategic planning interventions. The results, therefore, provides a motive regarding the development and translation of user preference strategic interventions into policy and delivery programmes. Moreover, by providing urban planners, architects, and developers with a greater level of understanding regarding stakeholder preferences, a number of avenues will be provided to improve more sustainable, functional, and user-friendly spaces in the city of Kandy.

3.1 Overall Stakeholder Preference

The results of the stakeholder visual preference survey has discovered three mostly preferred photographs that provide insights of the stakeholders' ideas and prospects of how desirable they are to see Kandy in future. The below mentioned photographs depict two strategic interventions and one existing city condition. A number of ecological elements are reported as being important in discussions of those strategic planning preferences. Different types and shapes of trees, the presence of water, the level of perceived management at a site, and whether or not people can be seen in an image have all been noted as affecting preferences of the most preferred urban interventions. This survey results assesses the extent to which these elements are deemed important and contextualizes the responses, with the broader thinking on strategic planning interventions and how much greenery incorporated into those corresponding interventions.

3.1.1 Kandy Lake Walkability Improvement Project

According to the overall stakeholder preference, the most preferred photograph (p#9 in Fig. 1) presents the Kandy Lake Walkability Improvement project. Reasons underlying the preference included abundance of green cover, broad trailed walkways, water and proper drainage system, shade, open space and ventilation.

These responses highlighted the complexity in the reasoning that supports different strategic intervention preferences. Although stakeholders emphasized strongly the physical elements of the image, respondents also described the images in motive terms such as relaxation, serenity and power as the reasons why they liked

Fig. 1 Most visually preferred photograph

the photograph. Respondents therefore took the physical elements of the images and discussed them in the social and emotional context which they daily interact with. Consequently, it can be proposed that experience, knowledge and perception were all used in the decision-making propose of respondent comments.

It can be stated that almost all the stakeholders prefer walkability improvement as a means of easy and fast access to places and opportunities within the city of Kandy. Development related to walkable urbanism is preferred by professionals as it enhances accessibility status of city community while residents prefer it as stimuli towards healthy and active life style. Travelers also prefer walkability improvement intervention because it saves time wasted on the non walkable streets.

3.1.2 Rehabilitation of the George E. de Silva Park

Second highest preferred photograph (p#7 in Fig. 2) indicates Rehabilitation of the George E De Silva Park. Reasons for preference included abundance of trees, floral diversity, scenic beauty, recreation space, open space, eco-friendly urban landscaping and ventilation.

Stakeholders who did not prefer this photograph much stated that the place seemed to highly manipulated/altered by the concrete constructions so that they do not like it. Some argued that the place is more open which would directly impact on the privacy of their life if they rest in such a place at a crowded town like Kandy. Further, they stressed that gardening in a small land plot will add only a glamour to the city in appearance but the cooling breeze and the green scenes around the Kandy lake is much more sensitive during their busy days. Moreover, they stated the scene of fins

Fig. 2 Modest visually preferred photograph

and marine animals, bird chirps and lake waves together with the picturesque view of Sacred Tooth Relic brings them mental satisfaction into their exhausted city life.

However, stakeholders had preferred this strategic intervention because it enhances the scenic beauty of the city center area which is frequently visited by people. It adds a little green effect which would enhance the cooling effect in the dusty and heated area of Torrington square.

3.1.3 Existing Kandy Lake Walk Around

Third highest preferred photograph was (p#10 in Fig. 3) depicting Existing Kandy Lake walk around. Reasons behind the preference included abundance of trees, recreation and open space, ventilation, cooling breeze and the scenery of the Temple of the Tooth Relic.

This photograph portrays an existing condition in the city of Kandy. What was most interesting regarding this photograph was that it has been scored the third highest ranking of overall stakeholder visual preference survey over three other proposed strategic interventions. This remarkably states that the stakeholders sometimes prefer existing green spaces in Kandy rather than new strategic interventions. It was discovered that the pilgrims who visit Kandy prefer the existing Lake walk around which is inherently bounded to their cultural and religious values. This implies an exceptional issue in the urban dimension of Kandy as any urban intervention cannot exceed its heritage image maintenance rather than uplifting it. It is evident that even the stakeholders prefer to see Kandy with less manipulation towards its scared impression.

Fig. 3 Third highest visually preferred photograph

Each of these responses showed, although the stakeholders value the strategic urban planning ventures, they additionally care whether there are any green concerns included into those interventions to make their life more easy and comfortable. Some have stated that the existing landscape in Kandy is more powerful even without the planning interventions. They further elucidated that it has been attracted both local and foreign tourists as well as investment opportunities even without huge master plans when compared to cities like Colombo. Less preference towards the photographs depicting high rise buildings, skyscraper city looks and dense compact development implies that the stakeholder preference is inclined towards natural greenery which can be identified as green infrastructure.

3.2 Preference by Stakeholder Group

Group based stakeholder visual preference (Fig. 4) implies that each stakeholder group separately has different preferences regarding the ongoing strategic interventions and existing conditions in the city of Kandy. There is a clear deviation of the choices and preferences of each stakeholder group depending on their involvement and perspective towards city planning. It also encompasses their real expectations and prospects of Kandy city planning based on their individual interpretation and the power relations of their involvement in the city planning. Even though all three stakeholder groups are going to be facilitated by any strategic urban intervention (vice versa), their preference seemed to be an expression of what they really hope from a well-planned city. Hence, the different preference rankings indicated distinctive juxtapositions of each stakeholder groups regarding Kandy urban planning.

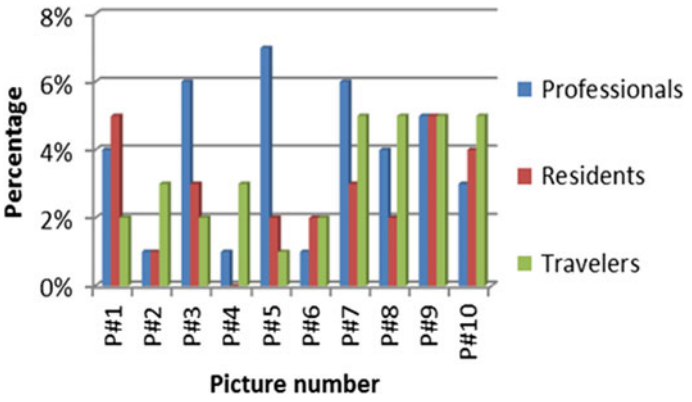

Fig. 4 Visual preference by stakeholder group

3.2.1 Professionals Preference Towards Traffic Alleviation Strategies

Kandy Multi Modal Transport Terminal has become the highest preferred photograph by the professionals who have been engaged in the Kandy urban planning. It was found that this intervention would sort out the traffic jam in the city and open up business and recreational space for the city community. Hence, their preference is inclining towards the interventions that try to unclose investment opportunities into the city, such as the construction of Kandy Multi Modal Transport Terminal, construction of the Tomlin Park and the rehabilitation of the George E. De Silva Park. Their desire is to introduce new physical planning interventions rather than protecting the existing situation or natural resources.

3.2.2 Residents' Demand for New Parking Lots

Resident stakeholder group comprised of people who have the longest experiences regarding the evolution of Kandy city planning and the ongoing planning interventions. They are the ones who spent much time in the city as dwellers as well as dependents on the city operations. So their preference regarding the city planning has been placed in another position as they prefer KMC Car Park Rooftop improvement intervention as the highest preferred one. This inculcates how different stakeholder groups prefer the urban interventions depending on their hierarchical positions in the city mechanism. Since the resident sample came from the highly recruited family backgrounds who owns extremely expensive lands in the KMC area, their urbanism related behavior and attitudes are quite different from the ordinary city dwellers. These people usually travel outskirts for their daily routine and come back home at the evenings. The only time they spent at the city may be the weekends enjoying their family. What really crews up them is the parking lots and recreational space when considering their involvement with the city. Therefore, the luxurious residents

in the city center prefer high class amenities and lifestyle features in the city planning which can boost and refresh their ongoing life style. Yet, these residents further prefer the Kandy Lake and surrounding nature. It was highlighted that they believe it is a privilege to live in Kandy and desirable to see urban interventions that go parallel with the architectural and scenic elegance of the city. They also demand that the remaining urban green spaces need to be preserved amidst these interventions.

3.2.3 Travelers' Preference for Open Spaces

The third stakeholder group incorporated into this study included travelers who come to the city of Kandy. They usually represent the floating population of the city who can give and receive a big influence towards the city planning operations. These travelers were selected randomly so their preferences are diverse based on numerous factors, basically on why and how often they come to the city. However, travelers' preferences were inclined towards recreation spaces and their proposed developments. Whereas most of the people who visit Kandy do not have a proper place to rest and dine, travelers urged proper planning towards improving recreational spaces with good food and sanitary facilities under one roof. They preferred even existing George E. De Silva Park over other strategic interventions because they are quiet familiar to them than the far away Tomlin Park. This denotes that the traveler preference of ongoing development interventions have a connection between their relevance and familiarity to those places. They prefer to see urban planning interventions targeted in the most crucial places which are frequently utilized by travelers, for examples public toilets and washrooms.

3.3 Does Amount of Green Really Matters Regarding Urban Planning Preference?

After exploring the overall preference rankings, the study looked at the results of the content analysis of the visual preference survey which further explains the stakeholder preference of the ongoing strategic interventions and urban greening in the KMC area.

Question one was asked with the intention to understand what qualities characterize the images ranked most and least preference. 86% of the respondents answered that the green features such as tree avenues, water and open space influenced them to rank the corresponding photographs with highest preference. 8% of people suggested that green mixed modern structures were favored by them as they prefer to see the city with high rise buildings as a more engineered city. 6% of participants had a neutral idea towards the preference as they had no clear reason for their preference and indicated they just ranked the photographs according to their personal interest on the photo.

Open ended question two sought to tease apart does density and amount of green predict the preference. More than 90% of the participants agreed that the amount of greenery pursued their preference and the remaining 10% suggested that they prefer dense development over the open space and green surrounding as an indication that the city of Kandy is being planned well. Third question raised by the visual preference survey concerned on what is the relationship between amount of green planning and the preference towards the ongoing planning interventions. Participants have been answered through numerous dimensions on this regard. This suggests that while more greening and lower density may be highly preferred, their lack does not necessarily mean that a development initiative will be least preferred. Rather, it may be that a strategic use of greening; and the dynamic relationship between greening, density and development design, can help buffer the perceived consequences of more dense living environments. However 91% of the participants concluded that amount of green planning matters most for their preference. They even highlighted that green concerns must be enhanced as a solution for the urban heat effect in Kandy which is increasing rapidly. Most importantly, those 91% stated their dislike towards the diminishing of natural vegetation for new building constructions specially in the hilly area.

The study participants spanned a range of ages and backgrounds, prompting the fourth research question; what themes emerged with your photo preferences. The age group of 0–20 indicated that the environment, trees, open spaces were the themes that emerged through their preference. Moreover, they indicated that Kandy city needs to improve more natural areas such as open parks, kiddies' gardens where children can spend time. Further, they stressed its essential to maintain their quality not only physically but environmentally too. This denotes that even the school children prefer to see Kandy as a natural beauty. The age group of 21–40 prefers more compact development since they tend to compare Kandy with Colombo and other developed cities in overseas. The emergent themes yielded from their answers demonstrated privacy, crowding, safety, housing characteristics, pavement, intangibles and capacity to provide amenities that were important to the participants. Age 41–60 group indicates that they prefer more cooling and ventilation above all amenities. They prefer to see Kandy as natural heritage as well as scenic city with natural beauty. Themes such like heritage value, nature and protection emerges from them. The last age group over 60 years denotes that they prefer Kandy as a unique religious capital. Themes such as peaceful surrounding, calm and quietness is preferred by them over the constructions.

Stakeholder suggestions towards improving the green planning interventions included vegetated setback from the street to help provide a buffer between public and residential spaces and provide multiple ecological benefits. Development structures that abut the street consistently received lower preference ratings from all respondents. Privacy was important to people. While many appreciated the amenities of urban life, there was a strong preference for settings that afforded a sense of a safe and protected haven with greening or spatial form. Further, people preferred open spaces over concrete constructions due to the cooling effect they can feel as the city of Kandy is getting more congested with the new development activities. Multi-units in larger

complexes were less preferred. For instance, even the Kandy multi-modal transport hub was not preferred over the urban parks and Kandy Lake walk around, though it serves many amenities. Most importantly, existing Kandy Lake walk around was preferred over the rehabilitation of the George E. De Silva Park. This highly emphasized that the stakeholders in Kandy prefer natural environment over the manipulated green settings.

A robust body of this study suggests that urban greening which supports connection with nature contributes positively to personal wellbeing. However, efforts to garner support for urban greening are not always successful and urban greening is inequitably distributed along the urban socio-economic gradient. Even the ongoing planning interventions have targeted only the city center though there are many natural habitats are in Kandy (for instance, Udawaththa Kele and Dunumadalawa Forest) which needs to be strategically preserved and incorporated into urban upgrading.

The results of the visual preference survey points to the importance of street trees and residential greening to provide localized, incidental access to nature. It was urged by all the age groups that they prefer natural greenery in the city of Kandy. Though their personal perceptions quite vary with the maturation and life experiences regarding Kandy town, more natural green mixed modern landscape is preferred by each of them. The short answer portion of the survey did provide insight into the personal values underlying the ratings, and the amount of greenery was a theme among reasons that an image was more or less preferred. This further supports the consent that city dwellers and travelers still prefer urban greenery specially in a well-organized and attractive way even though professionals pay much weight on constructional physical planning. Hence, ongoing urban planning interventions that enable more natural environment upgrading are embraced by the stakeholders, which is a stimulating motivation to encourage greener infrastructure initiatives further.

Planning for a sustainable urban future requires understanding the types of residential settings that local residents imagine as ideal or preferable. Often times, certain segments of the population, specially children and adolescents, are left out of public participation and visioning processes. Therefore, this study explored the use of their idea also that would become a strength in order to initiate the most essential green urban planning interventions, with special focus on ‘green infrastructure’ as a cost effective strategy in making Kandy a more desirable city.

4 Conclusion

All three stakeholder groups incorporating professionals, residents and travelers prefer existing urban green spaces over the strategic interventions and seek more green surroundings amongst strategic urban interventions. It further stressed that there is still a considerable request of greenery from urban dwellers and planning

professionals that should be concerned by the planners and essentially incorporated into urban planning. There is a common discourse that urban greening helps to ameliorate negative perceptions of density in a residential setting. Hence there is all time preference towards greenery in urban area.

Further, urban green canopy was preferred as it was seen as providing nearby nature, beauty, a buffer from crowding and cooling shade for all stakeholders. Almost all the stakeholder justifications of their visual preference included their like towards greenery and attempted to identify greenery as a means to rank those strategic interventions. Positive preferences towards strategic interventions always followed some kind of aesthetic interpretations of ecological greenery. Hence, it can be summed up as any kind of strategic planning intervention in Kandy must meet with green concerns since the stakeholder groups thoroughly demand it.

Different preference stances took by each of the stakeholder groups implied their specific desires regarding urban planning in Kandy. While professionals try to address essential issues in Kandy, residents try to uplift their city life through those interventions. Travelers demand more open spaces and related amenities to facilitate their travelling experience. As we take all these things into account, professionals' point of view seemed to be more powerful with their intellectual base and regulatory power as they are quiet familiar with the most feasible interventions. Yet, residents are the most concerned people regarding the planning interventions in the city because they are experiencing the city life and more to experience in the future. Hence, their preferences are more responsible as citizens and development oriented. However the preference of travelers cannot be neglected due to the fact that they comprise the largest part of the city that can have a big influence on the city mechanism. Therefore, all of their preference should be carefully concerned to initiate the best strategic planning interventions incorporating green concerns. Accordingly, green infrastructure planning interventions emerge as a futuristic strategy for Kandy urban planning.

In a nutshell, it can be concluded that the stakeholder preference is well inclined towards manageable urban green spaces. They prefer the ongoing strategic interventions where the green features are incorporated and sometimes their preference pervades over strategic interventions and embrace the existing natural settings for example the Kandy Lake.

Ergo, appropriate green infrastructure planning solutions should be enclosed to the Kandy urban planning platform and broader researches must be conducted on how they can be utilized in the urban policy planning. Hence, it's essentially important to promote a social discourse on best green planning practices. Both academic and empirical avenues must be cleared towards introducing environmental friendly planning practices and techniques into the city of Kandy since the green light is really dim at the moment.

References

1. Somarathne HW (2018) Urban planning process—special reference to Kandy city development plan 2018–2030. Urban Landscape Ecological Planning: Case Study on Kandy. University of Peradeniya: PGIHS
2. Urban Development Authority (2018) Available at: http://www.uda.gov.lk/project-kandy.html. Accessed 23 Feb 2018
3. Wijesundara J (2015) Re-invigorating the spirit of place of Kandy: Urban Design and City planning strategies. Built-environment: Sri Lanka, vol 11 Issue 2. Available at: https://besl.sljol.info/articles/abstract/10.4038/besl.v11i2.7606/. Accessed 05 May 2018

Prediction of Across Wind Response of Tall Buildings: An Overview

B. Kiriparan, J. A. S. C. Jayasinghe, and U. I. Dissanayake

Abstract Wind induced lateral loading is one of the vital factors governing the design of tall buildings. Along wind, across wind and torsional responses are three important considerations in wind design of tall buildings. A well-established gust factor approach is adopted in most of the wind design codes to predict the dynamic response of tall buildings in the along wind direction. Along wind predictions using this approach is found to be with reasonable accuracy when the wind flow is not significantly affected by neighbouring buildings. However, the applicability of most of the wind design codes are restricted to regular shaped structures with limitation on height or natural frequency. Dynamic motion of tall and slender structures perpendicular to the direction of the wind is known as across wind excitation. This phenomenon can be resulted from three mechanisms and their higher time derivatives such as vortex shedding, incident turbulence mechanism and higher derivatives of cross-wind displacement (i.e., galloping, flutter and lock-in). Due to the complex nature of the wind, characteristics of vortices and its interaction with the structure, significant limitations are found among the provisions set out in different international standards for the prediction of across wind responses. Though most of the existing codes are capable of predicting the along wind loading to reasonable accuracy, only a few international standards provide provisions for across wind effects. Unlike the along wind responses significant discrepancies are found among the across wind responses estimated by different standards. This paper presents an overview of capabilities and limitations of design provisions available in seven international codes/standards such as BS 6399-2:1997, BS EN 1991-1-4:2005, AS/NZS1170.2:2011, AIJ: 2004, CNS: 2012, ASCE 7-10 and NBCC: 2005 for the prediction of across wind responses. Comparisons of predicted across wind induced response for different building configurations (range of plan aspect ratio form 1–2, height aspect ratio from 4 to 8 and height from 120 to 240 m) are used to explain the influence of methods adopted in each of those wind codes.

Keywords Tall buildings · Across wind responses · Vortex shedding · Wind design codes

B. Kiriparan (✉) · J. A. S. C. Jayasinghe · U. I. Dissanayake
Faculty of Engineering, University of Peradeniya, Peradeniya, Sri Lanka
e-mail: Kiriparan@gmail.com

R. Dissanayake et al. (eds.), *ICSECM 2019*, Lecture Notes in Civil Engineering 94,
https://doi.org/10.1007/978-981-15-7222-7_32

1 Introduction

Modern tall buildings are becoming more slender, flexible, light weight and low damping due to urbanization and advancement of technologies such as high strength concrete, light weight partitions etc. This makes modern tall buildings more vulnerable under wind induced dynamic excitations. Along wind, across wind and torsional responses (as shown in Fig. 1) are three important considerations in wind design of tall buildings. Wind design codes and standards are utilized in prediction of wind effect on tall buildings in the preliminary design stages.

Along wind predictions from the existing standards are found to be with reasonable accuracy when the wind flow is not significantly affected by neighbouring buildings. However, the applicability of most of the wind design codes are restricted to regular shaped structures with limitation on height or natural frequency. Dynamic motion of tall and slender structures perpendicular to the direction of the wind is known as across wind excitation. Due to the complex nature of the wind, characteristics of vortices and its interaction with the structure, significant limitations are found among the provisions set out in different international standards for the prediction of across wind responses. Though most of the existing codes are capable of predicting the along wind loading to reasonable accuracy, only a few international standards provide provisions for across wind effects. Unlike the along wind responses significant discrepancies are found among the across wind responses estimated by different standards [1].

This paper presents an overview of capabilities and limitations of design provisions available in seven international codes/standards such as BS 6399-2:1997, BS EN 1991-1-4:2005, AS/NZS1170.2:2011, AIJ: 2004, CNS: 2012, ASCE7-10 and NBCC: 2005 for the prediction of across wind responses. Comparisons of predicted across wind induced response for different building configurations (range of plan aspect ratio form 1–2, height aspect ratio from 4–8 and height from 120 to 240 m) are used to explain the influence of methods adopted in each of those wind codes.

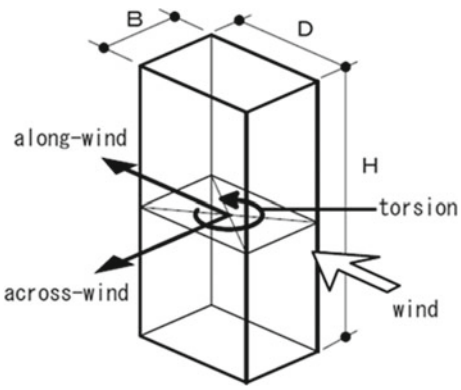

Fig. 1 Wind effects on tall buildings

Based on the comparison of predicted responses on selected building configurations; consistency of each wind codes in estimation of wind loading and accelerations are discussed. Capability of different wind codes and their limitations in across wind response estimation is outlined.

2 Background of Across Wind Loading

Wind is a very complicated phenomenon as the movement of air particles are turbulent due its low viscosity. Fluctuation of the wind speed shown in Figs. 2 and 3 illustrate the random nature of wind with both time and along building height respectively.

Due to this fluctuation in wind speed flexible structures like tall buildings are subjected to dynamic excitation under the wind loading. Generally, a structure is considered to be dynamically sensitive under wind loading if first natural frequency is less than 1 Hz (ASCE-7-10). Dynamic interaction of wind with structural system of a flexible structure leads amplification of wind induced responses. Aerodynamic loads acting on flexible tall buildings are magnified based on their dynamic characteristics. A well-defined peak factor method originally established by Davenport [2] used widely to predict dynamic amplification of along wind loading caused by the pressure fluctuation between wind ward and leeward faces. Predicted along wind buffeting

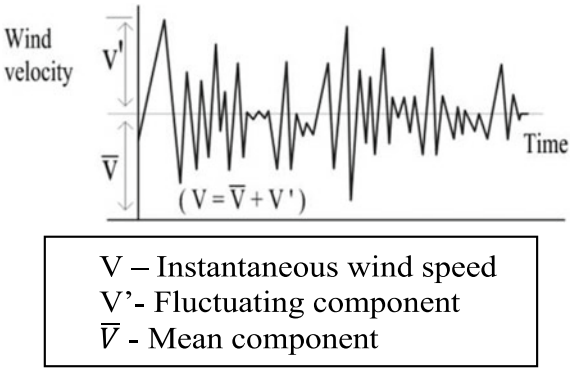

Fig. 2 Wind speed variation with time

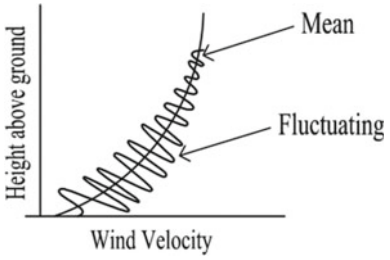

Fig. 3 Wind speed variation along height

loads using this theoretical method employed in most of the international wind codes are found to be within reasonable accuracy [3].

In dynamically sensitive tall buildings wind induced motion in the across wind direction caused by alternative shedding of vortices is an important phenomena to be considered in the design. A dimensionless parameter called 'Strouhal number' is used to identify the potential of particular structure, to the influence of vortices shedding. Figure 4 illustrates different factors associated with the across wind loading.

If the natural frequency of the structure coincides with the shedding frequency of the vortices, large amplitude displacement response may occur due to the resonance. This condition is referred as lock-in phenominon which can generally occurs within 10% range of building's natural frequency. Based on the geometry of the building Strouhal number is determined from wind tunnel testing.

A measured spectra of along-wind and across-wind load components of a flexible tall building reported in [4] reproduced in Fig. 5 to demonstrate the vortex shedding.

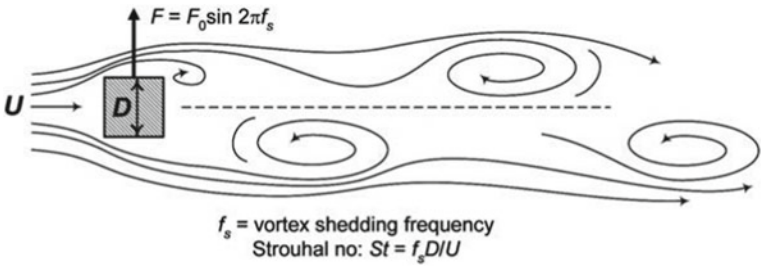

Fig. 4 Vortex shedding

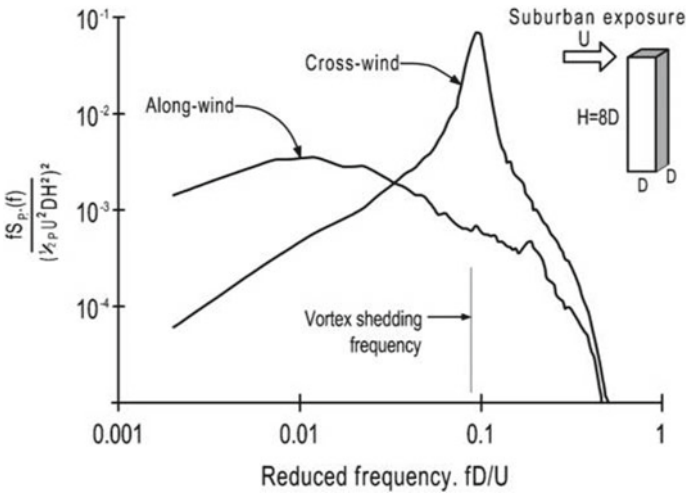

Fig. 5 Comparison of along and across wind spectra measured on a wind tunnel model [4]

Along wind dynamic response decrease when frequency increase whereas across-wind spectra has an intermediate peak resulted from vortex shedding, that highly affect the resonant response.

The magnitude of across wind response resulted from vortex shedding highly depends on building geometry. Buildings with regular geometries and sharp corners highly susceptible for cross wind effects. Aerodynamic shaping of buildings to minimize the across wind loading is a well-established exercise performed during the conceptual design stage to optimize the structural scheme against across wind effects.

Unlike along wind buffeting forces induced by the pressure fluctuations, strip and quasi-steady theories are not capable of predicting across wind excitation due to the complex nature of vortex shedding. Wake dynamics theories are used to explain the across wind excitation [5].

3 Overview of Codal Provisions for Prediction of Across Wind Effects

Many international design standards/guidelines are available for the prediction of wind response of tall buildings. Scope of most of the wind design codes are limited to regular shaped structures and due to the governance of dynamic responses again the limitations are imposed either based on building height or natural period. Still, for the buildings falls in the scope of the design codes inconsistences are found in the results obtained from different design codes [1]. Capabilities and limitations of seven major intentional codes: British Standard (BS 6399-2:1997), Australian Standard (AS/NZS1170.2:2011), Euro Code (EN1991-1-4:2005), Japanese Code (AIJ 2004), National Building Code of Canada (NBCC 2005), ASCE Minimum Design Loads for Buildings and Other Structures (ASCE 7:10) and China National Standard (CNS: 2012) are summarized in Table 1.

All seven standards considered set out provisions for the prediction of along wind loading. Provisions for calculation of across wind loading is provided in only five standards namely AS/NZS1170.2:2011, AIJ 2004, NBCC 2005, ASCE 7-10, and CNS: 2012. Further, across wind effects are only introduced very recently in many of those codes (e.g. included in CNS: 2012 while upgrading from CNS: 2006). In addition, BS 6399-2:1997 does not provide any guidelines for the calculation of wind induced accelerations whereas only along wind acceleration calculations are presented in EN1991-1-4:2005 and ASCE 7-10. In most of the cases across wind vibrations induced due to the vortex shedding is more critical than the along wind vibration. AS/NZS 1170.2:2011, AIJ 2004, NBCC 2005 and CNS 2012 provides guidelines for the calculation of both along wind and across wind accelerations. Procedures given for the across wind loading and accelerations are only discussed in this paper. A detailed comparison of expressions provided in those international standards for across wind load calculation are summarized in Table 2.

Table 1 Applicability of different international wind codes

Criteria	Code						
	BS 6399	EN1991-1-4:2005	AS/NZS 1170.2:2011	AIJ2004	ASCE 7-10	CNS:2012	NBCC:2005
Height	No provisions for h > 300 m	No provisions for h > 200 m	No provisions for h > 200 m	No explicit limit specified		No provisions for h > 550 m	No explicit limit specified
Frequency		No provisions for f < 0.2 s	No provisions for f < 0.2 s	No explicit limit specified			
Geometry	No provisions for buildings with complicated shapes						
Along wind loading	Geometrical and height restrictions in along wind load calculations Geometrical						
Across wind loading	No provision for given	Geometrical and height restrictions in across wind load calculations			No provisions	Geometrical and height restrictions in across wind load calculations	
Torsional loading	No provision for given	Nominal eccentricities specified		Detailed provision	Nominal eccentricities specified		
Along wind accelerations	No provision for given	Provision are given					
Cross wind accelerations	No provision for given	No provision for given	Provision are given		No provision for given	Provision are given	
Torsional accelerations	No provision for given			Provision given	No provision for given		

Table 2 Comparison of across wind prediction by international wind codes

Standard	Formula for across wind loading
AS/NZS1170.2:2011	$W_{eq}(z) = 0.5\rho_{air} V_{des,\theta}^2 dC_{fig} C_{dyn}$ $V_{des,\theta} =$ design velocity at building height d = horizontal depth of the building parallel to the wind stream C_{fig} = aerodynamic shape factor C_{dyn} = dynamic response factor $C_{fig}C_{dyn} = 1.5g_R\left(\frac{b}{d}\right)\frac{K_m}{(1+g_v I_h)^2}\left(\frac{z}{h}\right)^k\sqrt{\frac{\pi C_{fs}}{f}}$ b = width of the building normal to the wind direction h = building height z = height of interest K_m = mode shape correction factor I_h = turbulence intensity factor C_{fs} = across wind spectrum generalized for linear mode ϵ = critical damping ratio
AIJ-RLB-2004	$W_L(z) = 3q_h C_L^{'} A\frac{z}{h}\sqrt{1+\emptyset_L^2} R_L$ $C_L^{'} = 0.0082\left(\frac{d}{b}\right)^3 - 0.071\left(\frac{d}{b}\right)^2 + 0.22\left(\frac{d}{b}\right)$ q_h =velocity pressure at roof level A = projected area z = height of interest h = building height $\emptyset_L$ = correction coefficient for vibration mode R_L = resonance factor

(continued)

Table 2 (continued)

Standard	Formula for across wind loading
NBCC (2005)	$M_c = f_c^2 g_R (BD)^2 \left(\frac{78.5\times 10^{-3}}{g\sqrt{\varepsilon}}\right)\left[\frac{V_H}{f_c\sqrt{BD}}\right]^{3.3}\frac{H^3}{3}$ H = average height to the roof top B = Breadth of the structure normal to the wind D = Depth of the structure parallel to the wind V_H = Mean wind speed, in $\frac{m}{s}$ at the building height, H f_c = First mode natural frequency of vibration of a structure in across wind direction (in Hz) g_R = Peak factor for across wind, taken as 3.75 ε = Critical damping ratio in across wind direction
GB5009-2012	$M_c = g_R w_0 \mu_z (2+2\alpha)\gamma_{CM}\sqrt{1+R_L^2}B_z d_z$, $\gamma_{CM} = C_R - 0.019\left(\frac{D}{B}\right)^{-2.54}$ $R_L = \frac{1.4}{(\alpha+0.95)}\left(\frac{z}{H}\right)^{-2\alpha+0.9}\sqrt{\frac{\pi S_{FL}}{4\varepsilon\gamma_{CM}^2}}$ w_0 = Reference wind pressure g_R = Peak factor for across wind, taken as 3.0 μ_z = Exposure factor of a 10 -minute mean wind pressure profile $\mu_z = C_E\left(\frac{z}{H}\right)^{-2\alpha}$, $C_E$is terrain roughness α = Wind speed profile index $S_{FL} = f S_{ML}(f)/qHBH^2$ =Power spectrum of non -dimensional across wind generalised force

Table 3 Building configurations used for comparison of wind response predictions

Building ID	B × D × H	D/B	H/B	f_0
$M_{3030120}$	30 × 30 × 120	1.0	4	0.30
$M_{3030183}$	30 × 30 × 183	1.0	6	0.20
$M_{3046183}$	30 × 46 × 183	1.5	6	0.20
$M_{3060183}$	30 × 60 × 183	2.0	6	0.20
$M_{3030240}$	30 × 30 × 240	1.0	8	0.15

Table 4 Design wind speeds (m/s)

Averaging time	Ultimate limit states	Serviceability limit state
3-s	59	35
10-min	41	25
1-h	37	22

4 Numerical Example

Wind induced response of five building configurations as tabulated in Table 3, (including a benchmark building called CAARC) were determined using the seven wind design codes discussed.

All the buildings were assumed to be with uniform mass of 160 kg/m^3 throughout the height. Natural frequency of the building in along wind and across wind direction was considered as 36/H. This relationship is selected based on structural engineer's data provided for several wind tunnels including the benchmark building considered [6].

Calculations to predict along wind force, across wind force, along wind and across wind accelerations were carried out using different wind loading codes. Wind speeds shown in Table 4 were considered for the calculations [7].

5 Results and Discussion

Along wind and across wind base shears calculated based on different standards are presented in Tables 5 and 6. The Coefficient of Variation (CoV) are calculated to represent the discrepancies between predicted wind responses by different design standards. Along wind forces predicted using seven international standards are found to be consistent with a Coefficient of variation less than 15%. However, when the building height and natural period of the building increases, coefficient of variations are increasing due to the significance of dynamic responses. Variation of along wind base shear with height aspect ratio is shown in Fig. 6. The prediction of CNS: 2012 is

Table 5 Comparison of along wind base shear (kN)

	$M_{3030120}$	$M_{3030183}$	$M_{3046183}$	$M_{3060183}$	$M_{3030240}$
BS	11,525	17,292	17,292	17,292	21,868
EC	14,256	21,866	21,866	21,866	29,425
AS	13,967	20,979	20,979	17,525	28,925
AIJ	13,852	21,548	23,837	23,837	29,838
ASCE	11,318	17,053	17,053	17,053	24,585
CNS	10,895	16,580	16,580	16,580	21,015
NBCC	10,928	16,855	16,568	16,568	21,456
CoV (%)	12	13	14	15	16

Table 6 Comparison of across wind base shear (kN)

	$M_{3030120}$	$M_{3030183}$	$M_{3046183}$	$M_{3060183}$	$M_{3030240}$
BS	–	–	–	–	–
EC	–	–	–	–	–
AS	12,515	18,927	28,805	36,007	33,650
AIJ	17,013	24,936	40,862	58,796	49,196
ASCE	–	–	–	–	–
CNS	13,855	23,680	32,645	54,620	38,967
NBCC	11,800	17,424	26,253	39,568	27,950
CoV (&)	17	17	20	24	24

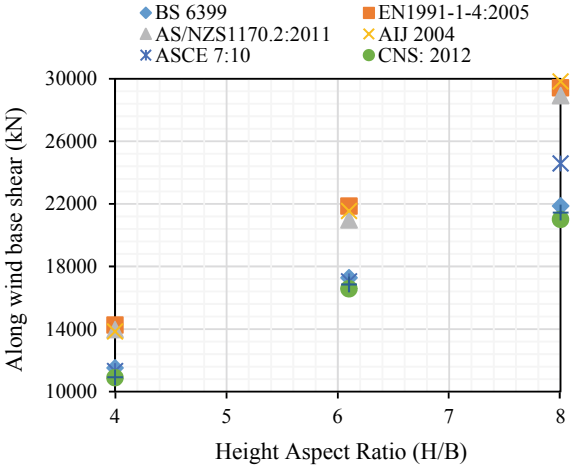

Fig. 6 Variation of along wind response with height aspect ratio

observed to be as lower bound for all the cases considered. EN1991-1-4:2005 estimations give higher value for lower height aspect ratios whereas AIJ: 2004 prediction for more slender and flexible buildings are found to be higher than all other standards. Different velocity profiles adopted by each codes and variations in the calculations of peak factors cause such inconsistences in the along wind predictions.

Coefficient of variation for across wind loading predictions are found to be significantly high (>15%). Unlike along wind loadings, crosswind spectra-based methods set out in the design standards for across wind loadings are derived from different wind tunnel sources. This may be the important reason for such higher discrepancies. With the increment of height and plan aspect ratios the deviations are further increasing as presented in Figs. 7 and 8 respectively. Prediction of NBCC and

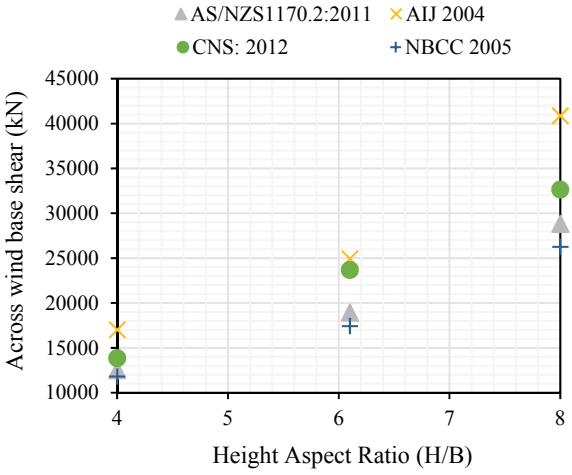

Fig. 7 Variation of across wind response with height aspect ratio

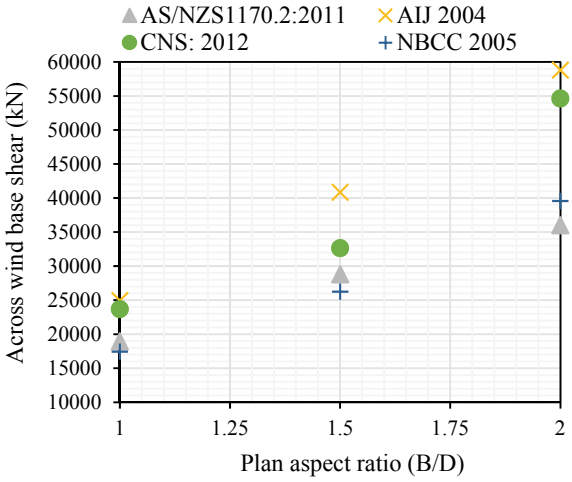

Fig. 8 Variation of across wind response with plan ratio

Table 7 Comparison of along wind accelerations (milli-g)

	$M_{3030120}$	$M_{3030183}$	$M_{3046183}$	$M_{3060183}$	$M_{3030240}$
BS	–	–	–	–	–
EC	10	14	11	8	15
AS	13	16	13	11	18
AIJ	11	15	10	10	16
ASCE	8	10	8	7	11
CNS	9	11	10	8	12
NBCC	12	14	13	10	17
CoV (%)	18	18	18	17	19

Table 8 Comparison of across wind accelerations (milli-g)

	$M_{3030120}$	$M_{3030183}$	$M_{3046183}$	$M_{3060183}$	$M_{3030240}$
BS	–	–	–	–	–
EC	–	–	–	–	–
AS	44	51	36	28	61
AIJ	36	42	28	24	51
ASCE	–	–	–	–	–
CNS	40	44	30	27	53
NBCC	41	48	33	26	56
CoV (%)	8	9	11	7	8

AS/NZS are laying at the lower side, on the other hand AIJ estimations provides relatively higher crosswind loading compare to all other standards.

Along wind and across wind peak accelerations calculated based on each standard are presented in Tables 7 and 8. Inconsistencies in the along wind acceleration predictions are increasing with building height and height aspect ratios. The influence of mass to minimize the building motion can be clearly seen from this results. Only four standards considered are capable of predicting the across wind accelerations. Coefficient of variation among those few available provisions are found less than along wind cases. Variation of along wind and across wind accelerations are with height aspect ratio are shown in Figs. 9 and 10.

Dynamic wind effect is one of the governing factor in the design of tall buildings. Thus, it is important to predict the wind effects precisely during the preliminary design in order to arrive at an optimum and safe structural scheme. Capabilities and limitations of different wind codes and consistency of their predictions were discussed in this study.

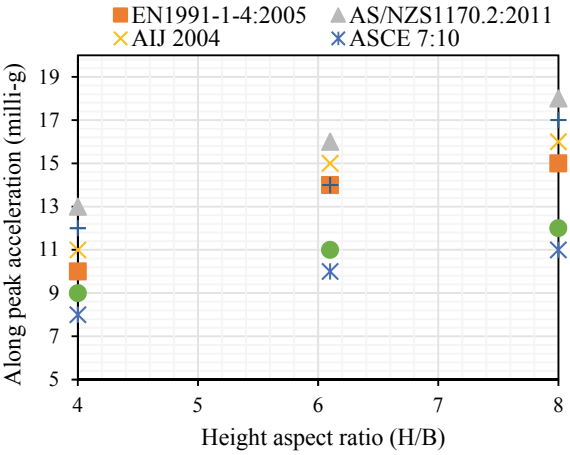

Fig. 9 Variation of along accelerations with height aspect ratio

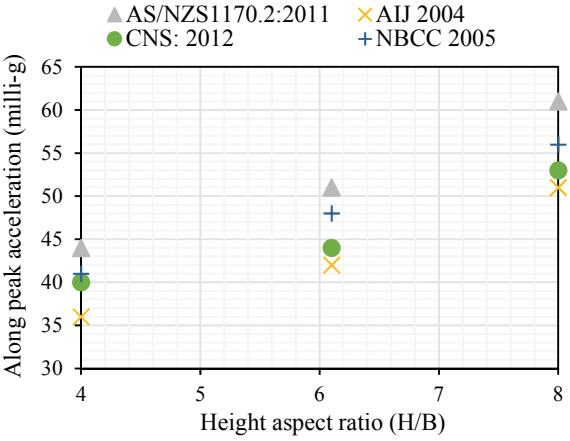

Fig. 10 Variation of across wind acceleration with height aspect ratio

6 Conclusion

This study presents an overview and importance of across wind loading in tall building design. The fundamentals associated with the across wind loadings and available provisions in seven international standards were discussed. Finally, a numerical comparison of predicted wind induced base shear and peak accelerations using those wind codes was carried out. The study shows consideration of across wind loadings is equally important as along wind loading in the design of tall buildings. Further, following observations were made from this study.

- When the plan aspect ratio is higher than unity across wind loading is increasing even beyond the along wind loading for few cases considered. Thus, for the

buildings with rectangular geometry across wind loading effect is higher than square geometries.

- Along wind loading predictions by all seven codes are within reasonable accuracy (CoV < 15%) for buildings up to 200 m and natural period not greater than 5 s. For building configurations considered beyond this limit variations are found to be increasing. CNS: 2012 provide lower bound along wind load among all seven standards, EN1991-1-4:2005 estimations gives higher value for lower height aspect ratios whereas AIJ: 2004 prediction for more slender and flexible buildings are found to be higher than all other standards.
- Significant discrepancies (CoV > 15%) in across wind loads estimated by different international standards are noticed. Prediction of NBCC and AS/NZS are laying at the lower side, whereas AIJ estimations provides relatively higher acrosswind loading compare to all other standards.
- Also, significant discrepancies (CoV > 15%) are observed in along wind acceleration predictions for more slender and flexible buildings.
- Only four international standards considered provide provisions for across wind accelerations predictions and their predictions are found to be consistent for the cases considered in this study. Similar source of limited aeroelasticity test results used to develop the across wind acceleration predictions by different wind codes may provide this consistency.

7 Recommendation for Further Work

Although similar comparative studies were conducted previously only few studies are available for the comparison of all these seven standards together. Further across wind predictions are very recently introduced in few of those standards such as CNS 2012. Significant inconsistencies are found in prediction of across wind loading estimations. Since across wind response is leading the along wind response for rectangular geometries an extensive parametric study may be performed to investigate this further. In addition, there are several models proposed by the researchers for the prediction of across wind responses a comparison with such predictions and existing wind tunnel test results will give more insight.

References

1. Kwon DK, Kareem A (2013) Comparative study of major international wind codes and standards for wind effects on tall buildings. Eng Struct 51:23–35
2. Davenport AG (1967) The treatment of wind loading on tall buildings. J Struct Div, ASCE Pergamon Press Ltd 93:11–34
3. Kijewski T, Kareem A (1998) Dynamic wind effects: a comparative study of provisions in codes and standards with wind tunnel data. Wind Struct Int J 1(1):77–109
4. Boggs D, Dragovich J (2006) The nature of wind loads and dynamic response. Aci Sp240, SP 240, pp 15–44

5. Mendis P, Mohotti D, Ngo T (2014) Wind design of tall buildings, problems, mistakes and solutions. In: 1st international conference on infrastructure failures and consequences
6. Melbourne WH (1980) Comparison of measurements on the CAARC standard tall building model in simulated model wind flows. J Wind Eng Ind Aerodyn 6(1–2):73–88
7. Holmes J, Tamura Y, Krishna P (2009) Comparison of wind loads calculated by fifteen different codes and standards, for low, medium and high-rise buildings. In: 11th Americas conference on wind engineering
8. American Society of Civil Engineers (ASCE) (2010) Minimum design loads for buildings and other structures. ASCE, Reston (VA)
9. Architectural Institute of Japan (AIJ) (2004) RLB recommendations for loads on buildings. Structural Standards Committee, Architectural Institute of Japan, Tokyo (Japan)
10. Bureau of Indian Standards (1987) Indian standard code of practice for design loads (other than earthquake) for buildings and structures. Part 3—Wind loads. IS: 875 (Part 3)—1987
11. European Committee for Standardization (CEN) (2010) Eurocode 1: actions on structures—Part 1–4: General actions—wind actions. EN 1991-1-4:2005/ AC: 2010 (E). Europe: European Standard (Eurocode), European Committee for Standardization (CEN)
12. Aiswaria GR, Jisha SV (2018) Along and across wind loads acting on tall buildings, pp 91–96
13. Joint Technical Committee (2011) AS/NZS 1170.2:2011 structural design actions—part 2: Wind actions. Australian/New Zealand Standard (AS/NZS): Joint Technical Committee BD-006, Australia/ New Zealand
14. Kareem A (1984) Model for predicting the across wind response of buildings. Eng Struct 6:136–141
15. Kwok KCS (1982) Cross-wind response of tall buildings. Eng Struct 4:256–262
16. National Research Council (1995) National building code of Canada. Canadian Commission on Building and Fire Codes, Canada
17. China National Standard (2006) Load code for the design of building structure. GB 50009-2001 (revised): China Architecture and Building Press
18. Patidar B, Patil AR, Thiele K, Mandal S (2014) Across-wind loading for structures: an overview
19. Saunders JW, Melbourne WH (1977) Cross-wind moment spectra on rectangular buildings and the prediction of dynamic response, pp 17–20
20. Vyavahare AY, Godbole PN, Nikose T (2012) Analysis of tall building for across wind response. Int J Civil and Strcut Eng 2(3):979–986
21. Xie ZN, Gu M (2009) Across-wind dynamic response of high-rise building under wind action with interference effects from one and two tall buildings. Struct Des Tall and Spec Build 18:37–57

Enablers for Effective Multi-hazard Early Warning System: A Literature Review

K. Hemachandra, R. Haigh, and D. Amaratunga

Abstract The intensity and frequency of natural hazards have increased unprecedentedly, resulting in devastating impacts on lives and economies. The present challenge for practitioners and policymakers is to reduce such impacts and related risks with innovative measures. A multi-hazard early warning system has been recognized as a crucial element in most disaster risk reduction measures. However, recent hazard incidents revealed that existing early warning systems are not completely able to save lives and reduce economic losses due to many reasons. Hence, this paper is conducted to provide a comprehensive understanding of the enablers to be considered when developing a fully comprehensive multi-hazard early warning system. Further, the study presents the benefits of establishing an effective multi-hazard early warning over single early warning systems. The paper is based on a narrative review applying a systematic basis for selecting research papers for the study. According to study results, three aspects to be considered when developing and operating an effective multi-hazard early warning system. Policy, legislative and institutional arrangements; social and cultural considerations and technological and scientific arrangements are the three categories. Policy, legislative and institutional arrangements contain governance, political recognition, mainstreaming early warning into development planning, stakeholder partnerships, periodic feedback, empowerment of local authorities and provision of resources/infrastructure. Social and cultural consideration includes training and capacity building, awareness and education, planning and preparedness, community engagement and empowerment and consideration of gender perspective and cultural diversity. Finally, integration of technological and scientific knowledge, risk information, hazard warning dissemination and communication, and monitoring and forecasting are the technological and scientific arrangements to be assured for an effective multi-hazard early warning for disaster risk reduction and enhancing resilience.

Keywords Multi-hazard early warning · Natural hazards · Disaster risk reduction · Enablers · Early warning systems

K. Hemachandra (✉) · R. Haigh · D. Amaratunga
University of Huddersfield, GDRC, School of Applied Sciences, Queensgate, Huddersfield HD1 3DH, UK
e-mail: K.Hemachandra2@hud.ac.uk

R. Dissanayake et al. (eds.), *ICSECM 2019*, Lecture Notes in Civil Engineering 94,
https://doi.org/10.1007/978-981-15-7222-7_33

1 Introduction

Natural hazards have been reported increasingly in the twenty-first century across the world. This includes several mega-disasters [14]. The recoded number of natural hazards between 2001 and 2019 is 7428 when compared to the period of 1981–2000 as 5181 [17]. 2004 Indian Ocean Tsunami, 2008 Cyclone Nargis in Myanmar and the 2010 Haitian earthquake are some of the unforgettable mega-disasters happened within the twenty-first century. Among these hazards, major impacts were reported due to geological hazards and climate-related hazards [14].

More than 1.35 million deaths were reported during 1996–2015 due to natural hazards [14]. Their impact was exacerbated by multiple causes, for example, poverty, lack of early warning systems, poor risk governance and absence of civil protection mechanisms, especially among low and middle-income countries [14, 22, 45].

This situation demands policymakers and practitioners to design and develop innovative and efficient methods/strategies to reduce the risk of future disasters [62]. Among these innovative strategies, multi-hazard early warnings (MHEW) has been recognized as a strategy to address disaster risks among disaster-prone countries [27, 45, 55, 58, 62].

However, recent incidents show that some countries have not paid adequate attention and do not have the capacities for establishing and operating effective MHEW [10, 58] due to lack of interest or lack of political will or due to many other reasons [32]. Hence, this paper is written to emphasise the role of MHEW in addressing disaster risks and then to present the enablers that comprise an effective MHEW system based on a literature review.

2 Methods

Literature reviews are important in many different ways of conducting researches. Primarily, literature reviews present and assess what has been published around a field of study [19, 25]. Even though it does not generate new data, it provides information on primary research studies and hence it is known as secondary research [19].

A literature review can be conducted in two ways: systematic reviews and non-systematic reviews which are also known as narrative reviews [19, 25]. Narrative reviews identify and summarize what is already published and identify the areas not yet studied. In contrast, systematic reviews are conducted to formulate a question and analyse evidence either qualitatively or quantitatively [19]. Neither of these methods is superior to each other since each of the methods has its strengths and limitations [19, 25].

In this study, a narrative review was conducted to achieve study objectives. One reason for selecting a narrative review is because of study objectives. The narrative review has the ability to address more than one question in a study [19]. Furthermore, it saves time by presenting several studies in a few pages in a study by summarising

and presenting studies around a topic. It also helps to understand easily the present status and its evolution of a particular topic even to a naïve to the field [25]. Narrative reviews further generate more information and develop new scientific principles and concepts are other benefits [19].

A narrative review can be presented in chronological order as a summary of the research area. This can easily identify the trends in a particular topic as well as helps to develop a conceptual framework [19]. A narrative review can also be presented either as a summary of each article used in the study or as a critique of others written around a topic [25].

There is no standard method for conducting a narrative study. However, to avoid possible limitations when conducting a narrative review, researchers can apply some strategies applicable to a systematic review. For example, giving a complete explanation of the method of sample selection is not necessary for a narrative review. Because some researchers argue that this may lead to a selection bias of articles that are included in a narrative review [19].

Therefore, this study applied a clear method in the selection of articles and documents for the review. Further, to maintain the quality of this narrative review, the authors follow the contents that are considered as the contents of a quality narrative review [25]. Hence, the paper begins with the title, followed by an abstract, introduction, methods, discussion, conclusions, acknowledgment, references and tables and figures if applicable.

The study used two electronic databases; Science Direct and Scopus and a search engine Google Scholar. The keywords used to search literature were "multi-hazard early warning", "multi-hazard early warning systems", natural hazards and multi-hazard early warning" and "natural hazards and multi-hazard early warning systems". The study used inclusion criteria as full- text availability, published between 2000 and 2019, reviewed articles. The exclusion criteria were: articles that were not published in English and articles in the press. Selected articles were checked manually for duplication and removed from the list. The remaining articles were used in this narrative review.

In Sect. 3.1, the paper presents the importance of MHEW along with an introduction to its origin. Section 3.2 presents the enablers of an effective MHEW that were identified and analysed based on the literature review.

3 Methods

3.1 Multi-hazard Early Warning Systems

Early warning systems have been recognised as a life-saving tool for many hazards due to its ability to effective monitoring and forecasting of future hazards and hence make necessary preparedness measures [2, 16, 18, 24, 26, 37, 41, 42, 49, 68, 4]. The Hyogo Framework for Disaster Reduction which was the global framework for

disaster risk reduction during 2005–2015 too emphasised the role of early warning in 2005 [61].

However, due to increasing hazards and its complexities for example multi-hazard nature of hazards, many researchers, practitioners and policymakers proposed to replace early warning systems with multi-hazard early warning systems at local, national, regional and global level [5, 6, 24, 27, 29, 55, 58, 62, 65, 66]. For example, post-Hyogo Framework, the Sendai Framework for Disaster Risk Reduction introduced in 2015 mentioned in its seventh global target as to substantially increase the availability of and access to multi-hazard early warning systems and disaster risk information and assessments to people by 2030 [62]. Further, the Sustainable Development Goals (SDGs) too acknowledge the importance of MHEW in its 13th goal to strengthen resilience and adaptive capacities to climate-related hazards and disasters in all countries by integrating climate change measures into national policies, strategies, and planning [57]. It highlights the necessity of MHEW along with climate change mitigation, adaptation, impact reduction methods [2]. Besides, the Paris Agreement furthermore stipulates early warning systems as strategies to enhance adaptive capacity and resilience as well as reducing vulnerabilities and losses due to climate change [60].

In parallel to these global initiatives, many international, regional and national levels initiatives have been taken place specifically on multi-hazard forecasting and early warnings. For example, French Rainfall Flood Vigilance System in France. There, Meteo-France provides meteorological vigilance maps twice a day regarding different types of extreme weather conditions including coastal hazards [2].

There are benefits of introducing an effective MHEW towards disaster risk reduction. The role of MHEW as a system addressing several hazards and/or impacts of a similar or different type in contexts where hazardous events may occur alone, simultaneously, cascadingly or cumulatively over time, and considering the potential interrelated effects [5, 24, 63]. Its special feature is that the system is able to warn of one or more hazards increases the efficiency and consistency of warnings through coordinated and compatible mechanisms and capacities [24]. Another benefit of MHEW is its ability for updating and accurate hazards identification and monitoring for multiple hazards [5, 63]. Researchers identify MHEW as an effective strategy for disaster risk reduction, ability to achieve economies of scale, sustainability and efficiency of EW [27, 50, 55] and for the sustainability of existing systems [5]. Effective MHEW also ensures the optimum advantage of the collective capacities of all stakeholders involved in different components of EWS for different hazards [24].

Having understood the benefits and importance of effective MHEW, the concept of MHEW was initiated at the Third Early Warning Conference held in 2006 as a result of the request made by participants for an integrated and holistic approach to early warnings for multiple hazards and risks [24, 67].

As a result, the first MHEW conference was held in Cancun, Mexico 2017 [66]. At the conference, key elements of an End-to-End, people-centered early warning system were presented along with a checklist. They were classified into 4 categories:

- Disaster risk knowledge: systematic collection and analysis of data along with hazard dynamics and vulnerabilities.
- Detection, monitoring, analysis, and forecasting of hazards and possible consequences: continuous monitoring of hazard parameters for issuing an accurate and timely warning.
- Warning dissemination and communication: use of standards and protocols when issuing warnings to target groups.
- Preparedness and response capabilities: through proper education and awareness programmes for people to inform on options for safe behaviour to reduce disaster risks [67].

In parallel, World Meteorological Organization coordinated and documented ten principles for developing MHEW irrespective of economic, social and institutional settings based on seven good practices revealed by a study consists of seven case studies [24].

However, based on the literature review this study identifies more enablers are categorised into three distinct categories based on the stakeholder belongings and within a broad social, economic, and institutional context. The new enablers and new classification help the users to identify the areas in which every variable should be established and in which context the variables have emerged. This also helps to easily identify the stakeholders responsibly, and measures can be implemented to assure such enablers. The identified 16 enablers are presented in Fig. 1.

3.2 Enablers of Effective MHEW

Based on the narrative review, the study presents a conceptual framework with identified variables/enablers for an effective MHEW.

1. **Policy, legislative and institutional arrangements**

- **Governance**

Governance is a key element of an effective disaster risk reduction strategy [21]. Because it has the capacity to enhance effectiveness, accountability, and transparency of any decisions taken for uncertain situations [31, 48, 50]. Since disasters are another type of uncertain event, governance can be applied to minimize any possible adverse effects. Hence, developing effective MHEW, governance can be introduced as a key criterion for its successful implementation. This can be achieved by the participation of multi-stakeholders in designing MHEW. Establishment of governance is significantly appropriate for developing countries that face difficulties or capacity gaps within administrative, organizational, financial and political boundaries when dealing with disaster risk reduction [35]. Through governance, the state can provide necessary resources for the functioning of disaster risk reduction measures [44] and facilitates better coordination between science and policy [4, 44]. Researchers found

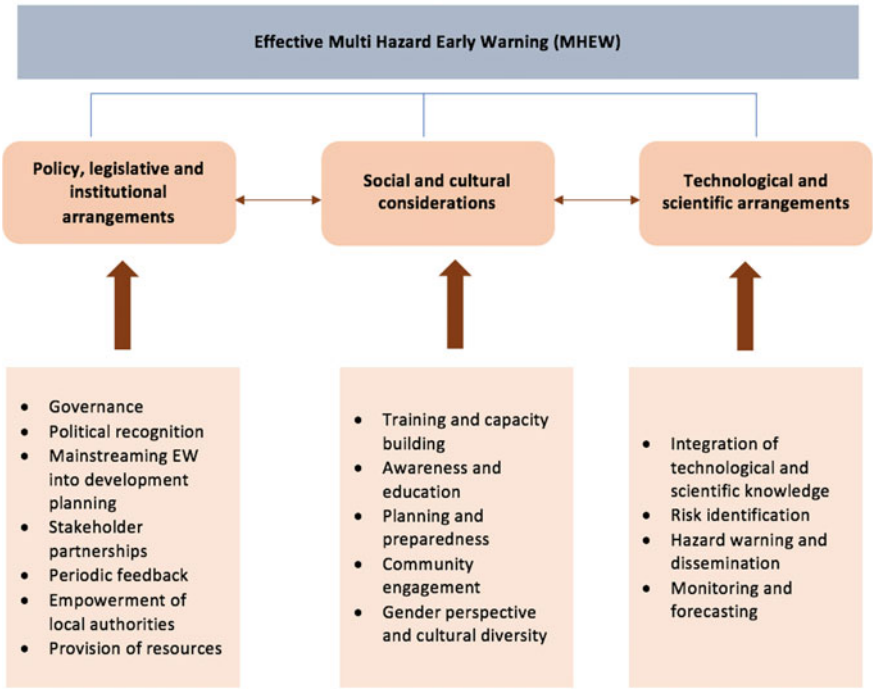

Fig. 1 Enablers of an effective multi-hazard early warning system

that well-developed governance structures along with robust legal and regulatory frameworks, political commitment and effective institutional arrangements help the development and sustainability of sound early warning systems [28, 50, 52].

- **Political recognition**

Political recognition or political support affects the success of any DRR strategy. Sound political recognition has the ability to determine priorities, has the power to introduce new legal provisions as well as to influence resource allocation [50]. Strong political recognition about the benefits of EWS is reflected in harmonized national to local disaster risk management policies, planning, legislation and budgeting [24]. Most EW systems are established and run by state governments. This shows the importance of political sponsorship for implementing and operating EW systems. However, when an EW system delivers results that are against government policies and agendas, the level of political support may reduce [39].

A case of the Philippines explains how the political support and acceptance saved lives during Typhoon Koppu in 2015. The Government of the Philippines introduced a Zero Casualty policy after following the Typhoon Haiyan in 2013. This new policy lead towards a substantial reduction in terms of loss of lives and the number of affected people from Typhoon Koppu [58].

Another example is found in Bangladesh. After the super cyclone hit Bangladesh in 1970, the Government and the Red Cross together established Cyclone Preparedness Programme. Besides, the government has introduced several legal provisions to support its DRR strategy. As a result, they were able to reduce the impact of their next disasters [26]. Hence, strong political and policy support is identified as another critical factor for effective MHEW.

- **Mainstreaming EW into development planning**

State-of-the-art technological and scientific knowledge do not ensure effective early warnings as risk reduction strategies [58]. Early warnings should be incorporated into development planning for its successful implementation and sustainability [62, 13]. Many researchers claim that properly integrated early warnings to institutional mechanisms have the ability to reduce disaster risks and enhance resilience [2, 68]. This has been recognised by the Sendai Framework for Disaster Risk Reduction as the leading global initiative towards disaster risk reduction. The framework emphasises the necessity of integration of MHEW into the development planning process across developed and developing nations [16, 62, 68].

For successful integration of early warnings into development planning, resource allocation and changes to the governance structure are further recommended. For example, in the African region, early warnings on meteorological changes have been incorporated to land-use planning and food planning policies in Africa to address the food security issue in the region [9]. This can be facilitated by establishing key institutions at the national and local levels [2].

- **Stakeholder partnerships**

Another important element for an effective MHEW is stakeholder partnerships. No single institute can provide a fully comprehensive solution towards DRR [62]. Hence, stakeholder partnerships are helpful for the successful implementation of EW and other DRR strategies [37, 50].

Jubach and Tokar [37] outlined the role of stakeholder partnerships at national and regional level disaster risk reduction strategies when addressing transboundary hazards. These partnerships provide opportunities to share expertise from a broader field of knowledge, better use of limited financial resources at the national level and sharing expensive early warning systems regionally, with lessons learned. These partnerships collaborate with experts from a wide range of disciplines and provide consistent messages from multiple sources [37, 50]. Because the development and operation of MHEW are costly and need more technical expertise. Hence these partnerships could benefit for success.

Stakeholder partnerships can be developed among government agencies, media, non-government organizations, academic institutions and schools, emergency relief and humanitarian agencies meteorological societies, private sectors and utility service providers [50] using legislation, directives, Memorandums of Understanding (MoUs)

and institutional arrangements. This will help in determining clear roles and responsibilities among different organizations as well as facilitate their existence and operation [24, 50]. Further, stakeholder partnerships can be identified based on many methods. Shehara et al. [53], used Emergency Operation Procedures assigned for different institutions in Sri Lanka to identify relevant stakeholders.

- **Periodic feedback**

Effective feedback mechanisms are considered essential for the improvement of any systems. Similarly, for effective MHEW, feedback will help identify their strengths and weaknesses [26]. Further, periodic feedback could provide inputs for planning, coordination, operational and technical aspects of the EWS [24]. User feedback also helps to identify weaknesses or limitations in the existing system and accordingly, make recommendations [37].

For example, the Government of Japan has established a Technical Investigation Group on Inheritance of Lessons from Disasters (TIGLD) to review their early warning system to identify problems and challenges experienced in disasters and drawing suggestions for further improvements [29]. The United States, another example, has implemented National Weather Services as a strategy of collecting feedback (NWS). Local NWS offices are responsible to evaluate and review operations after a disaster event to identify best practices as well as lessons learned. Their objective is to further improve existing EW. They use local emergency management feedback and media as a source of feedback. They further conduct formal assessments through emergency management communities and NWS peers [7].

The Government of Bangladesh similarly provides feedback on their existing EWS as a part of the Standing Order on Disasters (SOD). They collect feedback from the government, media, volunteers, and the general public. Their SOD assigns responsibility to each person to record any weaknesses in the system as well as make recommendations [26]. Hence, effective feedback and improvement mechanisms are recommended to be placed at all levels of EW to provide systematic evaluation and ensure system improvement over time [24].

- **Empowerment of local authorities**

Most hazards are local by nature. Hence, any disaster risk reduction strategies are advised to be initiated and implemented at local level institutions [3]. Local governments or local authorities are aware of local hazards, their significance, local communities and their capacities [23, 51]. Local authorities are very important in early warning dissemination and acting on early warning alerts [13]. Early warnings received from national agencies need to be communicated to communities at risk through local governments in time and a reliable manner [26]. There, local authorities can play a significant role in this effort as the lower-level state representation in many countries. They are considered as the closest government unit to citizens.

A public opinion survey conducted by the Pew Research Center for the People and the Press [47] revealed that communities are more favourable for local government than the federal government in the United States. Hence, they believe disaster

information given by local governments than other government agencies. A similar finding is revealed by the study of Collins [11], local government's EW radio alert system can play a major role by communicating EW through radio system for alerts on hazards. He further explains that the local government can also give feedback to the warning providers regarding warning messages to identify weaknesses or challenges. Hence, developing effective MHEW, the empowerment of local authorities should be considered for better dissemination of early warnings.

- **Provision of resources/infrastructure**

The success of any risk reduction programme depends on the availability of resources and infrastructure [26]. The provision of adequate human, financial and other resources are necessary for their successful operation and sustainability [24]. Most early warning systems are funded and maintained by governments [65] whose funding availability is limited to their budgetary capacities.

For example, the Government of Japan finances early warning and other disaster risk reduction programmes through national and local governments' budgets. Their allocations have been further increased after a disaster to restore and future disaster prevention efforts [29]. In addition, governments allocate resources such as airplanes, boats and other assets of armed forces and coast guards as precautionary efforts [58]. For example, in Hong Kong, early warnings are supported by other infrastructure facilities such as transportation and communication network during a disaster to help communities affected in hazards [50]. However, the budgetary share allocated for preparedness measures including early warning systems is comparatively low to post-disaster recovery and relief efforts [30, 52]. Researchers explained this is due to the inability to estimate the benefits of the prevention of disasters [50]. Further, MHEW is complexed and expensive to operate. Hence limited national budgets can be overcome by directing resources from regional initiatives [33].

In addition to the above-mentioned policy, legislative and institutional factors, social and cultural factors have been identified as enablers for effective MHEW.

Social and cultural considerations

- **Training and capacity building**

Training and capacity building is central for the effective functioning of early warnings since it provides necessary education and awareness for the operation of early warnings according to the predetermined plan [2]. Community training can enhance community disaster preparedness culture to act upon EW alerts [8]. Similarly, training for institutional members can enhance the integration of EW into planning and policymaking at all levels of governments [2].

For example, the Government of Tamil Nadu with the assistance of the UNDP undertakes a project to strengthen and institutionalize EW within coastal districts affected by tsunamis in Tamil Nadu. The programme trained more than 1500 people and gave a training manual published in both English and Tamil languages. That

training focussed on raising awareness and building capacities among communities in coastal risks in Tamil Nadu in India [8].

Training can be incorporated into formal and informal educational programmes. Informal training is provided through talks, conferences, radio and TV channels whereas formal training is provided through short courses, school curricular, and producing training manuals [24, 65]. Besides, regular drills and tests can also be conducted among stakeholders who engage in emergency procedures [2]. Training on EW systems covers many aspects. For example, raising awareness, identifying potential risks, recognizing warning signals during an event and accordingly to take necessary actions [50].

- **Awareness/education**

Public awareness is another vital enabler for designing an effective EW system and its implementation [2, 46, 50]. The importance of community awareness of natural hazards has suddenly raised after the 2004 Indian Ocean Tsunami incident [4]. Better educated communities are considered as more resilient than others in society [20].

For example, the Government of Bangladesh has created awareness among coastal communities to act on early warning messages before Cyclone Sidr. As a result, they were able to reduce the number of deaths from the disaster [46]. A similar finding is reported by Frankenberg et al. [20] from the Indonesian context. They found that better informed and educated Indonesian males survived during the 2004 Indian Ocean Tsunami when compared to women. Similarly, educated communities were found to be doing well in the evacuation centers compared to others. The study further highlighted that educated communities reported better health conditions after disasters.

Hence, communities should be aware of the threats generated by different hazards, their potential impacts, threat levels indicated by warning messages and recommended actions [24]. Ongoing education and awareness can be implemented via schools and universities within their curricular system in addition to the use of mass media. Further, it has to be tailored to meet the different needs of different communities [50]. Awareness can be introduced through formal and informal education at different levels in society. Formal education can be introduced through the introduction of modules and courses to school and university curricular whereas informal education and awareness can be introduced through training, drills, through mass media and social media.

According to Tang et al. [55], in China, education and awareness on MHEW to local communities were given through the internet, media, brochures on MHEW, posters, training, and exercise. Another special feature of Shanghai MHEW is that public awareness is carried out through special channels that broadcast weather-related programmes. Besides, the image education programme was conducted among 60 primary schools with more than 50,000 students in Shanghai. This programme was aimed to raise awareness of meteorological hazards among students. For further improvement, existing education and awareness programmes are evaluated to identify its weaknesses [50].

- **Planning and preparedness**

Disaster preparedness and response planning are other key factors for reducing disaster effects in any society [2]. There are many evidences suggest that well planned DRR strategies have reduced the loss of lives and economic losses in global disaster history.

For example, preparedness programme on evacuation routes, shelters and EW communication methods in Bangladesh abled to reduce all types of losses from Cyclone Sidr when compared to Cyclone Gorky [46]. They also reduce post-disaster response and recovery efforts [62].

Furthermore, it is accepted to support preparedness and response planning with scientific and technical information. For example, the Japanese Basic Disaster Management Plan is supported with scientific information for assessing disaster risks for tsunamis, earthquakes and other types of disasters [29]. Another example of different types of preparedness measures can be identified from Shanghai's MGHEW system. Further, these plans can be integrated with governments' development plans [2]. These plans and preparedness measures should not be ad hoc, fragmented and lacking proper coordination with other development plans. Emergency response plans are developed with consideration for hazard/risk levels and characteristics and needs of exposed communities as well as other stakeholders such as emergency respondents, hospitals, schools, and campgrounds [24].

- **Community engagement and empowerment**

One of the key stakeholders of people-centered EW is the community [50]. The community has been recognized as the target group of any last-mile warning system [62]. Thomalla and Larsen [56] emphasise that community representation in EW design as considered as a bottom-up approach. Their absence may hinder the capacity of hazard responses [51].

According to [12] well informed and alerted community enhances the effectiveness of the EW system. When communities are aware of risk priorities, they are motivated to respond to early warning systems without waiting for warnings from outsiders [56]. Similarly, raising community awareness helps in creating a preparedness culture in the community [38]. Community awareness can be given on available safe options, escape routes, and mechanisms to avoid and minimize life and property damages [50].

According to Rogers and Tsirkunov [50], traditional and indigenous knowledge can be introduced to enhance the effectiveness of EW. One such successful community engagement programme was conducted by the Government of Bangladesh when disseminating EW messages to communities at risk. More than 42,000 community members were engaged in disseminating EW messages using hand sirens and megaphones. They disseminated warning messages released by the Bangladesh Meteorological Department through Cyclone Preparedness Program [26].

One of the weaknesses among communities is that their poor level of responses to most hazard warnings due to many reasons. For example, Paul [46] mentioned that during the Cyclone Sidhr, some community members did not follow evacuation

orders and either stayed at their homes or returned to their homes from safe locations. Lack of adequate evacuation shelters in their area, inadequate spaces in those shelters and the distance from their homes to evacuation centres were highlighted as reasons for not following EW orders. According to Paul, reported fatalities and losses can be further minimized if communities follow these orders. Hence, furthermore, actions to be taken to enhance community participation in MHEEW development.

- **Gender perspective and cultural diversity**

Different hazards have different levels of impacts on diverse communities [15, 36]. Hence, identification of their problems and needs during an event is essential in developing a successful EW. Especially, cultural differences and gender are important to be considered since these factors can influence their preparedness and response capacities greatly [50]. Especially, men and women have different roles in society. Hence, the communication of warnings could be different for different target groups during a disaster. Especially, women have limited access to EW information [12]. For example, most women stay at home during the daytime whereas men have gone outside for work. Accordingly, these gender perspectives should be considered since men and women engage in different social roles and are bound with different social and cultural norms [50].

In addition, socio-economically vulnerable groups such as the elderly, disabled communities are similarly considered when developing MHEW. According to Mayhorn and McLaughlin [43], technological aspects of warning communication have been considered whereas cultural diversity and community characteristics have not been considered in most situations. Hence, they propose to utilize a more systematic approach when designing warning messages considering end-users' cultural and personal values and believes.

Technological arrangements

- **Integration of technical and scientific knowledge**

Technical and scientific information is considered as the third pillar of enablers of MHEW. They provide a basis for risk identification and risk assessment in an effective EW system [40, 65]. Sound knowledge of meteorological or hydrological phenomenon provides a basis for predictions, preparedness and response planning measures [50]. Hence, their findings are necessary to be incorporated into institutions' operating systems [68].

For example, the state of Virginia used Coastal GeoFIRM for the development of the Digital Flood Insurance Rate Map at the Federal Emergency Management Agency of the United States to assess flood risk and making flood recovery maps. The maps are furthermore tailored to match each state-specific spatial considerations [64]. Similarly, Indonesia uses the Tsunami Early Warning System to identify tsunami risks in the Indian Ocean after the 2004 Indian Ocean Tsunami incident. They need the most accurate scientific information to identify and assess tsunami risks than other countries since they have a very limited time of issuing EW and taking actions.

Hence, the Government of Germany also provides further technical and scientific support for the development of the Tsunami Early Warning System in Indonesia for a more reliable and accurate tsunami EW system [40, 54].

- **Risk information**

Another vital element of effective MHEW is risk information. Hydrometeorological data, climatological data and some socio-economic and demographic data are considered as risk information. They are widely used for vulnerability assessments [66]. Risk information provides hazard, exposure, and vulnerability information to communities as well as officials. They are useful when designing emergency planning, drawing risk maps and developing warning messages to communities and authorities [24, 54].

Risk information is also used for the sustainability of EW systems [4, 56]. The daily briefing, bulletins, special reports, websites, and workstations are used in the process of formulation and dissemination of risk data. For example, Japan JMA provides risk information to public and municipal authorities through their websites and publications to deliver risk information in a timely and precisely to interested groups [29]. According to [50], risk information should be tailored to the specific needs of users.

Besides, sharing risk information within a region helps to maintain cost-effective early warning systems [58]. For example, Indian Ocean Tsunami Early Warning Systems (IOTWMS) shares risk information and dealt with issuing warning messages to its member countries [59]. These benefits member countries accessing reliable data through regional databases. This makes possible to issue timely warning messages to people at risk efficiently [50].

- **Hazard warning dissemination and communication**

Hazard warnings dissemination and communication is another essential aspect in people-centered, end-to-end early warning system [65]. Warnings are expected to be disseminated and communicated to people who are at risk in a timely, clear and reliable manner to take required actions [12, 24]. Warnings are mostly issued by state agencies, for example, meteorological offices, disaster management centres and ministries [58, 65]. They use different modes of communication to issue hazard warning: faxes, SMS, emails, telephones, the internet, radio, coloured flags and so on [65].

It is also important to assure that hazard warnings are issued with more specific information. According to Alfieri et al. [2] location, hazard type expected onset and its duration, possible damages and communities are affected are some of the specific information to be included in warning messages. This will enhance the reliability of hazard warnings among communities.

Similarly, hazard warnings should be clear. Clear hazard warnings can be issued using pre-determined warning mechanisms. Simple, useful and usable messages can be used when disseminating and communicating hazard warnings. Many countries

use colour codes, numbers or hazard levels when communicating and disseminating warning messages [24].

Vertical and horizontal communication of EW among stakeholders is also essential for effective EW [49, 50]. Further, it is necessary to ensure that communication of information to emergency management authorities should provide adequate lead time for initiating preparedness actions [49, 50]. Even though vertical and horizontal communication is an important element in a well-functioning EWS, there is a lack of attention from operational contexts [56]. Researchers emphasize that warning should be communicated with reliability. There are many instances where communities do not believe warnings and did not take action accordingly. For example, according to [1], disbelief of hazard warning had greatly affected their evacuation decision during the Bangladesh cyclone in 1991.

Also, communication gaps between the scientific community and policymakers [34] and language barriers are some other issues identified when communicating hazard warnings. For example, language differences among diverse communities have become a challenge to convey warning messages in Asia [58]. Another important consideration when disseminating hazard warnings is to ensure that dissemination methods can survive in any conditions like lack of electricity, wind speed, etc. According to Paul [46], wind speed and wind direction affected when issuing warnings during Bangladesh Cyclone in 1991. A similar incident is reported from Indonesia in 2018. Before the recent two tsunami incidents, hazard warnings were not disseminated to communities due to electricity failure [10].

- **Monitoring and forecasting**

Hazard monitoring and forecasting are some of the key elements in people-cantered and end-to-end EW systems [49, 50, 66]. This helps in identifying future risks through hydro-meteorological parameters and thus provisioning of archived and real-time data, conducting hazard mapping and analysis and forecasting their patterns.

For Example, in the UK, United Kingdom Coastal Monitoring and Forecasting (UKCMF) network has been set up to monitor and forecast coastal hazards. This initiative works with forecasters, coastal authorities, academics, government, emergency respondents, industry, and public. They provide a prediction for tide levels and real-time observations of waves and tide data. They also forecast coastal flooding and accordingly advise relevant authorities for taking necessary actions using their archived data and information. The network work with European partners to share knowledge, data, research and forecasting techniques. Their main aim is to provide coastal flood risk forecasts and provide long term evidence for developing long term forecasts models.

4 Conclusions

Disaster risk reduction has become a major challenge in the twenty-first century when responding to increasing natural hazards across the globe. Among many disaster risk reduction strategies, MHEW has been identified as a lifesaving instrument or mechanism by researchers, practitioners, and policymakers. However, many countries struggle to operate a comprehensive MHEW due to many reasons. This has been evident with the recent incidents of natural hazards and their impacts irrespective of the economic and social status of countries.

Hence, this study aimed to presents a literature review in the form of a narrative review to present the importance of MHEW and also to present the enablers of an effective MHEW. Accordingly, the study presents 16 enablers under broad categories as institutional, policy and legislative measures, social and cultural considerations and technological and scientific measures.

Acknowledgements The European Commission support for the production of this publication as a product of CABARET project and the Commission does not constitute an endorsement of the contents which reflects the views only of the authors, and the Commission cannot be held responsible for any use which may be made of the information contained therein.

References

1. Alam K, Rahman MH (2014) Women in natural disasters: a case study from the southern coastal region of Bangladesh. Int J Disaster Risk Reduct 8:68–82
2. Alfieri L, Salamon P, Pappenberger F, Wetterhall F, Thielen J (2012) Operational early warning systems for water-related hazards in Europe. Environ Sci Policy 21:35–49
3. Bang HN (2013) Governance of disaster risk reduction in Cameroon: The need to empower local government. JAMBA-J Disaster Risk Studies 5
4. Basher R (2006) Global early warning systems for natural hazards: systematic and people-centered. Philos Trans Royal Soc London A: Math Phys and Eng Sci 364:2167–2182
5. Bildan L (2006) Eleven-country cooperation in establishing a regional multi-hazard early warning system in the Indian Ocean and Southeast Asia. In: Centre ADP (ed) Multi-hazards early warning systems: asian disaster management news. ADPC, Pathumthani, Thailand
6. Boxberger T, Fleming K, Pittore M, Parolai S, Pilz M, Mikulla S (2017) The multi-parameter wireless sensing system (MPwise): its description and application to earthquake risk mitigation. Sensors 17:2400
7. Buan S, Diamond L (2012) Multi-hazard early warning system of the United States National Weather Service. Institutional Partnerships in Multi-Hazard Early Warning Systems. Springer
8. Chaimanee N (2006) The role of geoscience in hazard mitigation. Asian disaster management news—Newsletter 12:6–6
9. Challinor A, Wheeler T, Garforth C, Craufurd P, Kassam A (2007) Assessing the vulnerability of food crop systems in Africa to climate change. Clim Change 83:381–399
10. CNN (2018) Indonesia tsunami: grim search for survivors continues as death toll reaches 430 [Online]. Available: https://edition.cnn.com/2018/12/25/asia/indonesia-tsunami-intl/index.html. Accessed
11. Collins AE (2009a) Disaster and development. Routledge

12. Collins AE (2009b) Early warning: a people-centered approach to early warning systems and the 'last mile'
13. Collins ML, Kapucu N (2008) Early warning systems and disaster preparedness and response in local government. Disaster Prev Manage: An Int J 17:587–600
14. CRED–UNISDR (2016) Poverty & death: disaster mortality mortality trends from major disasters from 1996 to 2015
15. De Silva K, Amaratunga D, Haigh R (2015) Gender equity in disaster early warning systems. In: Proceedings of the 8th international conference of faculty of architecture
16. Dutta R, Basnayake S (2018) Gap assessment towards strengthening early warning systems. Int J Disaster Resilience Built Environ 9:198–215
17. EM-DAT (2019) EMDAT -database [Online]. Available: https://www.emdat.be/emdat_db/. Accessed 15th Oct 2019
18. Fathani TF, Karnawati D, Wilopo W (2016) An integrated methodology to develop a standard for landslide early warning systems. Nat Hazards Earth Syst Sci 16:2123–2135
19. Ferrari R (2015) Writing narrative style literature reviews. Med Writing 24:230–235
20. Frankenberg E, Sikoki B, Sumantri C, Suriastini W, Thomas D (2013) Education, vulnerability, and resilience after a natural disaster. Ecology and society: A J Integr Sci Res Sustain 18:16
21. Gall M, Cutter SL, Nguyen K (2014) Governance in disaster risk management IRDR AIRDR Publication No 03. Int Res Disaster Risk, Beijing
22. Gault B, Hartmann H, Jones-Deweever A, Werschkul M, Williams E (2005) The women of new orleans and the gulf coast: multiple disadvantages and key assets for recovery: part I. Poverty, race, gender and class, institute for women's policy research (IWPR)
23. Gerber BJ, Robinson SE (2009) Local government performance and the challenges of regional preparedness for disasters. Public Perform Manage Rev 32:345–371
24. Golnaraghi M (2012) Institutional partnerships in multi-hazard early warning systems: a compilation of seven national good practices and guiding principles. Springer Science & Business Media
25. Green BN, Johnson CD, Adams A (2006) Writing narrative literature reviews for peer-reviewed journals: secrets of the trade. J Chiropractic Med 5:101–117
26. Habib A, Shahidullah M, Ahmed D (2012) The Bangladesh cyclone preparedness program. A vital component of the nation's multi-hazard early warning system. Institutional Partnerships in Multi-Hazard Early Warning Systems. Springer
27. Haigh R, Amartunga D, Hemachandra K (2018) A capacity analysis framework for multi-hazard early warning in coastal communities. Procedia Eng 212:1139–1146
28. Harley MD, Valentini A, Armaroli C, Perini L, Calabrese L, Ciavola P (2016) Can an early-warning system help minimize the impacts of coastal storms? A case study of the 2012 Halloween storm, northern Italy. Nat Hazards and Earth Syst Sci 16:209–222
29. Hasegawa N, Harada S., Tanaka S, Ogawa S, Goto A, Sasagawa Y, Washitake N (2012) Multi-hazard early warning system in Japan. In: Institutional partnerships in multi-hazard early warning systems. Springer
30. Healy A, Malhotra N (2009) Myopic voters and natural disaster policy. Am Polit Sci Rev 103:387–406
31. Hemachandra K, Amaratunga D, Haigh R (2018) Role of women in disaster risk governance. Procedia Eng 212:1187–1194
32. Hemachandra K, Haigh R, Amaratunga D (2019a) A regional analysis of the role of multi-hazard early warnings for coastal community resilience in Asia. In: The 9th international conference on sustainable built environment: transforming our built environment through innovation and integration. Springer, Singapore, pp 62–70
33. Hemachandra K, Haigh R, Amaratunga D (2019) Regional cooperation towards effective multi-hazard early warnings in Asia. Int J Adv Sci Eng Inf Technol 9:287–292
34. IFRC (2009) World disasters report: focus on early warning, early actions. Int Federation of Red Cross, Satigny/Vernier, Switzerland
35. Ishiwatari M (2012) Government roles in community based disaster risk reduction. In: Shaw R (ed) Community-based disaster risk reduction. Emerald Group Publishing

36. Islam MR, Ingham V, Hicks J, Manock I (2014) The changing role of women in resilience, recovery and economic development at the intersection of recurrent disaster: a case study from Sirajgang, Bangladesh. J Asian Afr Stud
37. Jubach R, Tokar A (2016) International severe weather and flash flood hazard early warning systems—Leveraging coordination, cooperation, and partnerships through a hydrometeorological project in Southern Africa. Water 8:258
38. Kadel M (2011) Community participation in disaster preparedness planning: a comparative study of nepal and Japan
39. Kelman I, Glantz MH (2014) Early warning systems defined. Early warning systems for climate change. Springer, Reducing disaster
40. Lauterjung J, Münch U, Rudloff A (2010) The challenge of installing a tsunami early warning system in the vicinity of the Sunda Arc, Indonesia. Nat Hazards Earth Syst Sci 10:641
41. Lumbroso D, Brown E, Ranger N (2016) Stakeholders' perceptions of the overall effectiveness of early warning systems and risk assessments for weather-related hazards in Africa, the Caribbean, and South Asia. Nat Hazards 84:2121–2144
42. Macherera M, Chimbari MJ (2016) A review of studies on community-based early warning systems. Jàmbá: J Disaster Risk Stud 8
43. Mayhorn CB, McLaughlin AC (2014) Warning the world of extreme events: a global perspective on risk communication for natural and technological disaster. Saf Sci 61:43–50
44. Meerpoël M (n.d.) Disaster risk governance: the essential linkage between DRR and SDGs. France: Catholic University of Lille
45. Mukhtar R (2018). Review of national multi-hazard early warning system plan of Pakistan in context with sendai framework for disaster risk reduction. Procedia Eng 212:206–213
46. Paul BK (2009) Why relatively fewer people died? The case of Bangladesh's Cyclone Sidr. Natural Hazards, 50:289–304
47. Pew Research Center For The People And The Press (2013) Trust in government nears record low, but most federal agencies are viewed favorably. [Online]. Available: http://www.people-press.org/2013/10/18/trust-in-governmentnears-record-low-but-most-federal-agencies-are-viewed-favorably/. Accessed 15 Sep 2016
48. Renn O (2012) Inclusive risk governance. 2011–2012 Distinguish lecture series, environmental science and policy programme. Michigen State University
49. Rogers D, Tsirkunov V (2011a) Costs and benefits of early warning systems. Global Assess Rep
50. Rogers D, Tsirkunov V (2011b) Implementing hazard early warning systems. Global facility for disaster reduction and recovery
51. Scott Z, FEW R (2016) Strengthening capacities for disaster risk management: Insights from existing research and practice. Int J Disaster Risk Reduction, In Press
52. Seng DSC (2013) Tsunami resilience: multi-level institutional arrangements, architectures and system of governance for disaster risk preparedness in Indonesia. Environ Sci Policy 29:57–70
53. Shehara PLAI, Siriwardana CSA, Haigh R (2019) Application of social network analysis (SNA) to identify communication network associated with multi-hazard early warning (MHEW) in Sri Lanka. In: 2019 Moratuwa engineering research conference (MERCon), IEEE, pp 141–146
54. Strunz G, Post J, Zosseder K, Wegscheider S, Mück M, Riedlinger T, Mehl H, Dech S, Birkmann J, Gebert N (2011) Tsunami risk assessment in Indonesia. Nat Hazards and Earth Syst Sci 11:67–82
55. Tang X, Feng L, Zou Y, Mu H (2012) The Shanghai multi-hazard early warning system: addressing the challenge of disaster risk reduction in an urban megalopolis. In: Institutional partnerships in multi-hazard early warning systems. Springer
56. Thomalla F, Larsen RK (2010) Resilience in the context of tsunami early warning systems and community disaster preparedness in the Indian Ocean region. Environ Hazards 9:249–265
57. UN (2015) Sustainable Development Goals [Online]. UN- Sustainable Development Group. Available: https://sustainabledevelopment.un.org/?menu=1300 Accessed
58. UN-ESCAP (2015) Strengthening regional multi-hazard early warning systems economic and social commission for Asia and the Pacific committee on disaster risk reduction fourth session Bangkok: economic and social commission for Asia and the Pacific

59. UNESCO-ICO; UN/ISDR/PPEW; WMO (2005) Assessment of capacity building requirements for an effective and durable tsunami warning and mitigation system in the Indian Ocean: consolidated report for 16 countries affected by the 26 December 2004 Tsunami Paris
60. UNFCCC (2015) Paris agreement
61. UNISDR (2005) Hyogo framework for action 2005–2015: building the resilience of nations and communities to disasters. In UNISDR (ed) Hyogo, Japan
62. UNISDR (2015) Sendai framework for disaster risk reduction 2015–2030. United Nations, Geneva Switzerland
63. UNISDR (2017) UNISDR terminology on disaster risk reduction. Switzerland, Geneva
64. Valenzuela M, Gangai J (2008) 2008. Coastal Geofirm Tools for Coastal Risk Identification, Solutions to Coastal Disasters
65. WMO (2016) Multi-hazard early warning systems (MHEWS) [Online]. Available: http://www.wmo.int/pages/prog/drr/projects/Thematic/MHEWS/MHEWS_en.html-presentations. Accessed
66. WMO (2017) Good practices for multi-hazard early warning systems (EWS) [Online]. Available: https://public.wmo.int/en/resources/meteoworld/good-practices-multi-hazard-early-warning-systems-ews. Accessed 17 Feb 2017
67. WMO (2018) Multi-hazard early warning systems: a checklist. World Meteorological Organization, Geneva, Switzerland
68. Zia A, Wagner CH (2015) Mainstreaming early warning systems in development and planning processes: Multilevel implementation of Sendai framework in Indus and Sahel. Int J Disaster Risk Sci 6:189–199

Deterioration Modelling of Timber Utility Poles

S. Bandara, P. Rajeev, and E. Gad

Abstract Timber utility poles are extensively used in power distribution and telecommunication sectors to support the overhead cables and other attachments. These utility poles are designed to have sufficient inherent capacity to withstand the imposed actions. However, timber poles deteriorate with time losing the strength and toughness mainly due to weathering, decay and termite attacks. Therefore, pole failures occur when the imposed stresses on the pole exceed the remaining strength of the pole. It is essential to avoid pole failures which will have severe safety concerns and significant economic impacts. This paper presents a brief review of the currently available timber deterioration models and proposes a framework for evaluating the residual strength of the in-service timber utility poles. The developed framework permits the asset managers to evaluate the structural reliability of these assets and to determine the optimum pole replacement rates. The residual strength of an in-service pole is directly related to the remaining section modulus of the pole at its critical section which is the ground line region of the pole. Hence, this paper presents the evaluation of the remaining section modulus for sectioned pole specimens which were condemned from service due to pole replacements. Further, the variation of section modulus with the service life is illustrated for the analysed Australian pole specimens and compared with the predictions of the current deterioration models.

Keywords Timber poles · Section modulus · Service life · Deterioration models

1 Introduction

Timber utility poles represent a significant part of the infrastructure in Australian power distribution and telecommunication sectors. There is an estimated amount of 5.3 million timber utility poles in Australia with an estimated value over $12 billion [8]. Timber poles contribute to about 80% of the total Australian utility pole population and about 90% of the pole population in Queensland and New south

S. Bandara (✉) · P. Rajeev · E. Gad
Department of Civil and Construction Engineering, Swinburne University of Technology, Melbourne, VIC 3122, Australia
e-mail: snarayanamudiyansela@swin.edu.au

R. Dissanayake et al. (eds.), *ICSECM 2019*, Lecture Notes in Civil Engineering 94,
https://doi.org/10.1007/978-981-15-7222-7_34

Fig. 1 Deterioration of timber poles. **(a)** Fungal attack **(b)** and **(c)** termite attacks

wales are timber [3]. Timber poles have relative advantages when compared with the alternative pole types such as concrete, steel and composite poles. Higher strength to weight ratio, durability, heat and electrical insulation of wood are some of the key factors for timber poles to be used predominantly. Moreover, the simplicity in handling and erection of timber poles seem to increase its use. Nevertheless, strength of timber poles degrades with time due to various factors including the soil and climatic conditions. Decay induced by fungus and termite attacks are dominant types of defects observed in timber poles. Figure 1 illustrates these typical defects in uprooted and sectioned timber poles.

Deterioration process potentially reduce the service life of poles and can eventually result in pole failures if serious damages are overlooked. Pole failures have severe safety concerns and economic impacts. Moreover, failures of timber poles and supported equipment have been associated with previous bush fires in Victoria [2]. Therefore, routine pole inspections are conducted by asset managers to monitor the structural integrity of timber poles and to avoid the pole failures while extracting the maximum use of these assets. Currently practiced timber pole inspection techniques include visual inspection, sounding and drilling. Figure 2 shows the practice of these techniques. Visual inspection is conducted to check the availability of decay pockets, splits and excessive cracks in the pole. Sounding inspection is performed by striking the pole using a handheld hammer to observe the generated sound and the rebounding effect of the hammer. Drilling is an internal inspection where the inspectors check the feel of the resistance of the drill and the texture of wood shavings to decide on the available sound timber in the pole. Reliability of the estimate of the pole condition based on the observations of these techniques are questionable due to the involved subjective nature. Moreover, multiple drillings can reduce the cross-sectional area of the pole at its critical section close to the ground level of the pole, potentially reducing the load carrying capacity of the pole. Alternative non-destructive testing techniques like stress wave propagation are adopted by researchers for the condition assessment of timber poles (e.g. [1, 7]).

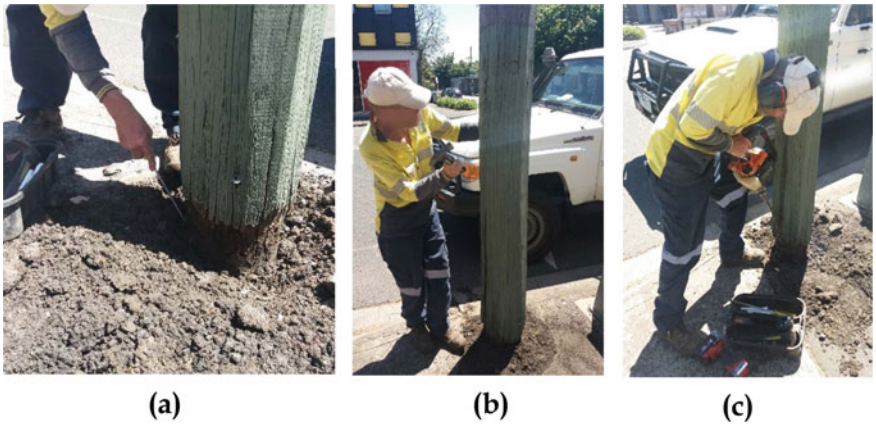

Fig. 2 Current inspection techniques for timber utility poles **(a)** visual inspection **(b)** sounding **(c)** drilling

Typical service life of a timber pole is estimated to be 40 to 60 years [4]. Nevertheless, service life a pole may exhibit a large variability depending on the species of wood, location of instalment, pertaining soil and climatic conditions, type of preservative treatment and the level of maintenance. Further, the initiation and progression of the damages determine the residual strength and the remaining service life of the pole.

In order to accurately access deterioration of timber poles, it is essential to account for the uncertainty involved in the above-mentioned factors. This paper presents a brief review of the currently available timber deterioration models and proposes a framework for evaluating the residual strength of the in-service timber utility poles. Residual strength of an in-service pole is directly related to the remaining section modulus of the pole at its critical section which is the ground line region of the pole. Hence, this paper presents the evaluation of remaining section modulus for sectioned pole specimens which were condemned from service due to pole replacements. Further, the variation of section modulus with service life is illustrated for the analysed Australian pole specimens.

2 Timber Deterioration Models

Different techniques are adopted by researchers to estimate the strength of in-service timber poles. Non-destructive field static bending approaches are proposed by some researchers to estimate the breaking strength of poles by correlating the slope of load-deflection curves (e.g. [5]). However, timber deterioration models are the widely used techniques to monitor the condition of poles with time. Rate of deterioration of a timber pole relies on the species of wood, type of preservative treatment,

pertaining climatic conditions (i.e., rainfall, temperature and humidity) and the nature of the induced defects. Due to the uncertainty associated with some of the above-mentioned factors, most of the deterioration models are approximations about the actual condition in the field.

Li et al. [6] proposed a degradation-path model for wood utility poles considering the degradation data of 13,940 poles ranging in age up to 79 years with a mean age of 30 years. Wang et al. [12] proposed a timber deterioration model for the inground decay based on a comprehensive study involving decay patterns of 77 Australian timber species over a 35-year period. In this model, decay depth, d_t at a given time, t is idealised to follow a bi-linear relationship characterised by a decay lag time, $t_{lag}(years)$ and a decay rate, $r(mm/yr)$.

$$d_t = \begin{cases} ct^2 & if \quad t \leq t_{d0} \\ (t - t_{lag})r & if \quad t > t_{d0} \end{cases} \tag{1}$$

$$r = k_{wood} k_{climate} \tag{2}$$

$$t_{lag} = 5.5 r^{-0.95} \tag{3}$$

where t_{do} is the time in which decay reaches its threshold depth (do), which is assumed to be 5 mm if there is experimental evidence. k_{wood} is a wood parameter for heartwood, sapwood and core based on the durability class and, $k_{climate}$ is a climate parameter. Once the decay depth is estimated, bending resistance of the pole at a given time, $R_{b(t)}$ can be determined using the bending theory.

$$R_{b(t)} = f_b \pi (D - 2d_t)^3 / 32 \tag{4}$$

where f_b is the bending strength of timber and D is the initial diameter. This deterioration model is for a homogeneous cross-section. However, timber poles cannot be assumed as homogeneous and thus, this model is developed later to account for the different decay rates in sapwood, heartwood and core wood.

Shafieezadeh et al. [11] proposed a framework for the development of age-dependant fragility curves of utility wood poles which relies on the age-dependant probabilistic capacity models. In this work, expected time-dependant capacity of the wood poles, $E[R(t)]$ was derived using linear regression models as;

$$E[R(t)] = E[R_o][1 - (a_1 t - a_2)(b_1 t - b_2)] \tag{5}$$

where R_o is the initial capacity of the pole, a_1, a_2, b_1 and b_2 are calibrated regression constants.

These different deterioration models adopt different approaches. Hence, a significant variability of the predicted strength of the poles are observed [9]. The selected deterioration model will dominate the predictions and consequently, accuracy and

reliability of the deterioration model will have a significant impact on the decisions regarding pole management.

3 Capacity of the Poles Based on the Section Modulus

Pole ground line diameter to be used for a particular scenario is based on the applied design moment calculated at the pole ground line based on the considered loadings. Calculated design moment can be used to obtain the required pole ground line diameter in accordance with AS/NZS 7000:2000.

$$\emptyset M = \emptyset k_1 k_{20} k_{21} k_{22} k_d \left[f_b' Z \right] \tag{6}$$

where $\emptyset M$ is the design bending capacity of the pole, $\emptyset$ is the capacity reduction factor, k_1 is the duration of load factor, k_{20} is the immaturity factor, k_{21} is the shaving factor,k_{22} is the processing factor, k_d is the pole degradation factor, f_b' is the characteristic bending strength and Z is the section modulus of the pole.

It can be noticed that the bending capacity of a pole can be determined if the remaining section modulus of the pole can be accurately estimated. Bending strength of poles and the variation of bending strength with in one timber species can be obtained from experimental results of full-scale pole bending tests. Details of pole bending tests for typical Australian timber species can be found in the published studies (e.g. [10]). This bending fibre strength is the highest bending stress parallel to the grains in the timber pole that the timber can sustain before breaking.

In this study, section analysis is carried out to estimate the remaining section modulus of condemned poles from service due to pole replacements. Sectional cuts are made in the uprooted poles close to the ground level. Then the measurements are taken. Moreover, digitised images of the sections are obtained to analyse the sectional properties. Figure 3 shows a sectioned timber specimen close to the ground

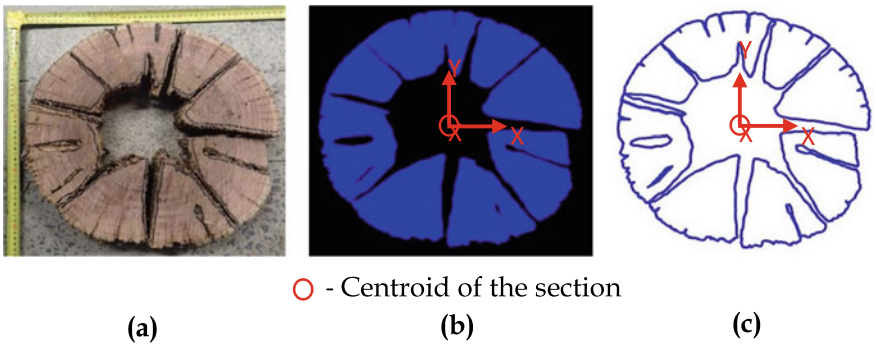

Fig. 3 **(a)** Sectioned timber pole specimens **(b)** and **(c)** digitised images to calculate the section modulus

level of the pole and its corresponding digitised images. Sectioned pole specimens are initially checked for the availability of decay induced deterioration, splits and cracks. These deteriorated regions are marked in the specimen and the corresponding area is removed in the digitised images. Then a ratio between the initial and the existing section modulus is obtained. Initial study contains the analysis of 27 Victorian pole specimens installed in different years. Analysed poles belonged to Western Stringybark, Yellow Stringybark and Messmate timber species.

Figure 4 illustrates the variation of the section modulus ratio with service-life for the analysed specimens. Significant variability can be observed in the section modulus ratio for timber poles installed even in the same year due the influence of the inherent soil conditions, climatic conditions and progression of deterioration. It is important to note that some of the analysed sections showed a significant reduction in cross-sectional area due to multiple drilling inspections over the service life of the poles. Figure 5 shows some sectioned timber pole specimens where number of drilling operations have caused reductions in the cross-sectional area. Therefore, it is evident that the influence of the drill holes has to be accounted for the deterioration models of timber utility poles. Pole failure-rate curves need to be developed based on the existing failure data to determine the section modulus ratio at which the pole replacements need to be done.

Figure 6 shows a comparison of box and whisker plots for the section modulus ratio considering actual scenario and corresponding same area poles. Same area pole is based on a solid circular section having the same estimated solid timber cross sectional area as the deteriorate section. On each box, the central mark indicates

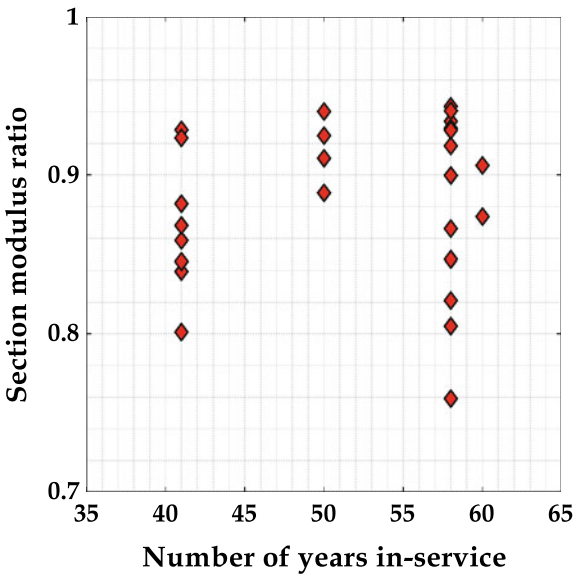

Fig. 4 Variation of the section modulus ratio with service-life

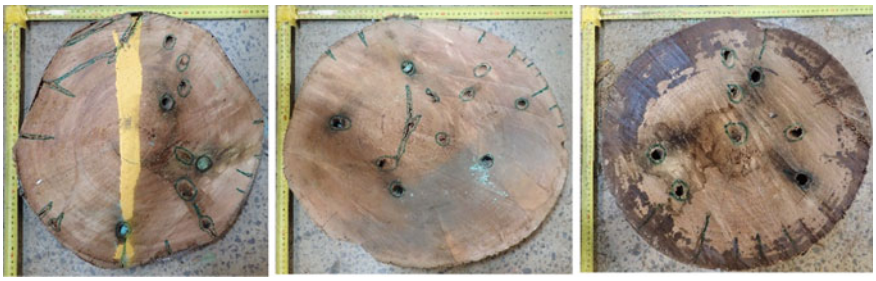

Fig. 5 Reduction in cross-sectional area due to multiple drill holes in sectioned timber pole specimens

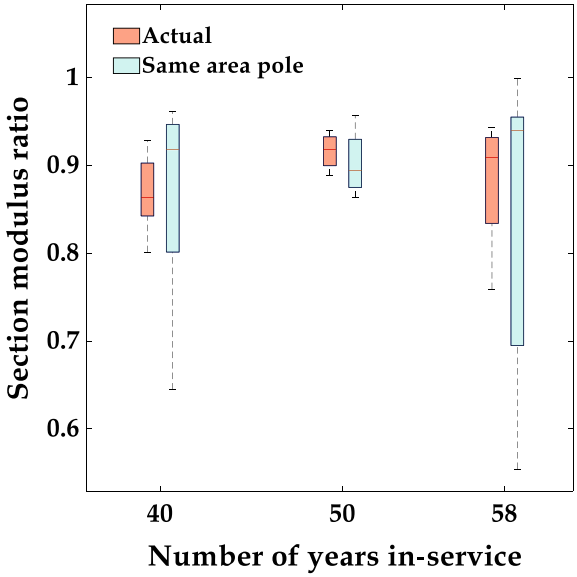

Fig. 6 Variation of section modulus ratio with service-life considering a same area pole and the actual scenario

the median, and the bottom and top edges of the box indicate the 25th and 75th percentiles, respectively. The whiskers extend to the most extreme data points. For the existing deterioration models for round timber poles, it should be assumed that the defect either initiate from the perimeter progressing inwards or from the pith zone progressing outwards. However, from Fig. 6, it can be noticed that there is a significant difference in section modulus ratio between the actual scenario and these assumptions.

In most of the sectioned pole specimens, internal deterioration was observed. Thus, the decay depth was calculated using the initial diameter and the diameter of the same area pole is based on a solid circular section having the same estimated solid

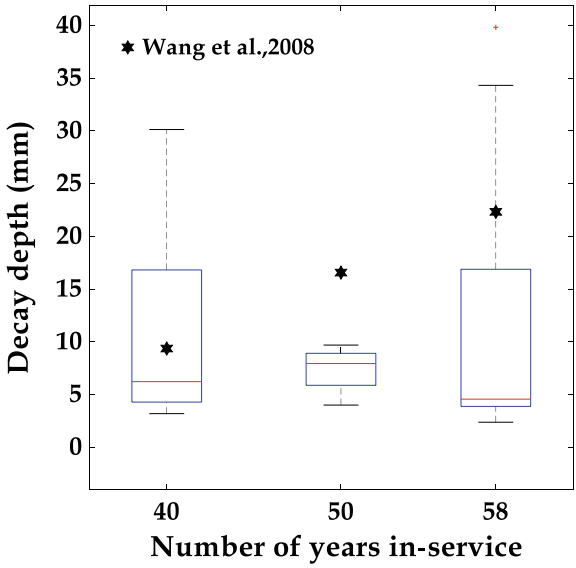

Fig. 7 Comparison of the variation of calculated decay depth with decay model of [12]

timber cross sectional area as the deteriorate section. Figure 7 shows the comparison of this calculated decay depth with the predictions of the deterioration model of [12]. Durability class of wood, pertaining climatic factors, CCA (Copper Chromium Arsenate) preservative treatment and the extent of core wood are considered in estimating the decay depth using the model of [12]. For the decay model, it is assumed that decay initiated from the core wood and progressed outwards. It can be noticed that there is a significant difference between median of the actual decay depth and the estimations of the model.

Selected deterioration model will dominate the predictions and consequently, accuracy and reliability of the deterioration model will have a significant impact on the decisions regarding pole management. Based on the observations of the preliminary analysis, a framework is proposed to evaluate the residual strength of in-service timber poles as follows.

Step 1: Develop a database to evaluate the bending capacity of timber poles. Previous experimental works of full-scale bending test results can be incorporated to this database. This database should cover poles belonging to all the strength classes and the timber species used in the distribution network. Suitable number of pole samples should be tested from each species to obtain a representative value for the bending strength and the variability of the estimated bending strength needs to be determined.

Step 2: Develop a deterioration model to estimate the section modulus of in-service timber poles. For this, section analysis needs to be done for a large data set of poles at the stage of replacement. For the deterioration model, pertaining soil and climatic conditions of the pole, type of preservative treatment used and species of wood needs to be incorporated. Pole installation year, species and the length of the pole can be

read from the attached pole discs to identify the pole. Further, these can be verified with the records of the asset managers. As noticed in the section analysis results, influence of drill holes needs to be accounted for the model.

Step 3: Representative sample of the uprooted poles need to be subjected to full scale bending tests to determine the actual residual capacity. Results of the bending tests can be compared with the determined strength with the use of deterioration model to evaluate the performance of the proposed method

Step 4: Asset management decisions can be taken regarding renewal and replacement of poles based on the developed framework to maintain the structural integrity of the distribution network.

4 Conclusion

This paper provides a brief review of the existing timber deterioration models and proposes a framework to evaluate the residual strength of in-service timber poles. This framework can facilitate the asset managers in deciding the optimum pole replacement rates avoiding premature pole replacements and pole failures. Proposed residual capacity estimation is based on determination of the remaining section modulus of the timber poles. Influence of different factors for timber deterioration is accounted in the model. Initial section analysis results have shown that, there is a significant effect of the drill holes for the remaining section capacity. A database can be developed to evaluate the bending capacity of intact poles including the previous experimental works of full-scale bending test results. Performance of the proposed method to estimate the residual strength can be evaluated by conducting bending tests on condemned poles to compare the actual remaining capacity.

References

1. Bandara S, Rajeev P, Gad E, Sriskantharajah B, Flatley I (2019) Damage detection of in-service timber poles using Hilbert-Huang transform. NDT and E Int 107:102141
2. Bushfire Royal Commission (2010) Final report summary—2009 victorian bushfires royal commission, Parliament of Victoria, Australia
3. Francis L, Norton J (2006) Australian timber pole resources for energy networks. A review
4. Han Sen E, Morrell J (2002) Wood pole purchasing, inspection, and maintenance: A survey of utility practices. Forest products J 52:43
5. Hron J, Yazdani N (2010) Nondestructive strength assessment of in-place wood utility poles. J Perform Constructed Facil 25:121–129
6. Li Y, Yeddanapudi S, Mccalley JD, Chowdhury AA, Moorehead M (2005) Degradation-path model for wood pole asset management. In: Proceedings of the 37th annual north american power symposium, IEEE, pp 275–280
7. Mudiyanselage S, Rajeev P, Gad E, Sriskantharajah B, Flatley I (2019) Application of stress wave propagation technique for condition assessment of timber poles. Struct Infrastruct Eng 15(9):1234–1246

8. Rahman A, Chattopadhyay G (2007) Soil factors behind inground decay of timber poles: testing and interpretation of results. IEEE Trans Power Delivery 22:1897–1903
9. Rajeev P, Gad E, Sriskantharajah B (2015) Probabilistic condition assessment technique for timber power poles. In: 8th structural engineering and construction conference, ISEC
10. Ryan PC, Stewart MG, Spencer N, Li Y (2014) Reliability assessment of power pole infrastructure incorporating deterioration and network maintenance. Reliab Eng Syst Safety
11. Shafieezadeh A, Onyewuchi UP, Begovic MM, Desroches R (2013) Age-dependent fragility models of utility wood poles in power distribution networks against extreme wind hazards. IEEE Trans Power Delivery 29:131–139
12. Wang C-H, Leicester RH, Nguyen M (2008) Probabilistic procedure for design of untreated timber poles in-ground under attack of decay fungi. Reliab Eng Syst Safety 93:476–481

Effect of Polypropylene Fibres on the Workability Parameters of Extrudable Cementitious Materials

T. Suntharalingam, B. Nagaratnam, K. Poologanathan, P. Hackney, and J. Ramli

Abstract Additive manufacturing in construction industry has been introduced as an aspiration for a more sustainable built environment and currently evolving with high demand amongst researches. This study is an investigation of the influence of polypropylene (PP) fibre addition on the workability parameters of a new extrudable concrete mixture. As the quality of final printed structure prominently depends on the fresh state properties of concrete, this investigation mainly focused on the rheological properties such as workability (flow), setting time, extrudability and buildability. These parameters were systematically investigated through a small scale experimental process with time after mixing. The selected control mix with Ground granulated blast furnace slag (GGBS) and Silica Fume (SF) was used in this analysis. The Control cementitious specimens without fibre inclusion and with fibre addition in different volume fraction of binder, ranging from 0.5 to 3% were printed. The results showed that the fibre addition of 0, 0.5 and 1.0% have the better flowability and extrudability compared to 1.5, 2 and 3%. Also, reduction in the print quality was assessed visually with increasing fibre percentage. However, results indicated that the initial setting time is comparatively low for those mixes with higher fibre inclusion which is required for better bond strength between layers. Moreover, higher fibre content caused better buildability and shape retention in the extruded samples.

Keywords Additive manufacturing · Extrusion-based 3D concrete printing · Polypropylene (PP) fibres · Fresh properties · Workability

1 Introduction

Three dimensional printing (3DP), also known as Additive Manufacturing (AM) is an automated process which builds three-dimensional physical objects by laying down consecutive layers according to the computer controlled model [1]. The potential of 3D printing has been clearly recognized in a wide range of applications, varying

T. Suntharalingam (✉) · B. Nagaratnam · K. Poologanathan · P. Hackney · J. Ramli
Northumbria University, Newcastle upon Tyne NE1 8ST, UK
e-mail: thadshajini.suntharalingam@northumbria.ac.uk

R. Dissanayake et al. (eds.), *ICSECM 2019*, Lecture Notes in Civil Engineering 94,
https://doi.org/10.1007/978-981-15-7222-7_35

from the household needs to aerospace engineering. Unsurprisingly, the building construction industry has adopted this technique with the aim of turning the complex building design into reality and developing environmentally friendly structures in large scale.

The positive characteristics of concrete such as flexibility, durability and non-combustibility directly contribute it to be the most extensively used construction material. Despite the fact, the conventional formwork concrete technology is restricted geometrically and has obvious sustainability issues towards the environment. Hence 3D concrete printing has been introduced as an aspiration for a more sustainable built environment. There are excellent advantages of 3D concrete printing technique over the conventional formwork concreting method such as labour efficiency, time and cost savings, environmental and economic impacts, and design complexity [7].

Material is the prime limiting factor in 3D concrete printing. A particular composite and concrete mixture which is denser than the typical concrete has to be used, while ensuring the mix design of concrete meets the performance requirements of both fresh and hardened state properties of concrete [3]. The main challenge in the development of a printable mix is to have no-slump and self-compaction concrete, which are two conflicting aims. In principle, materials (thixotropic) with high (static) yield stress and low viscosity are suitable for concrete printing application [12]. The material must be extrudable through a nozzle smoothly and able to maintain its shape, once deposited over the printing bed. Secondly, the deposited layers should not collapse under the load of subsequent layers and thirdly, good bond strength between the layers to achieve required hardened strengths must be ensured. Further limitation is the crucial fluctuation of material properties with unique setup and specifications of 3D concrete printer. Therefore, the major challenge is to develop a suitable printable material for corresponding printing machine [6]. Hence [9] has defined four critical parameters of the fresh printable concrete as pumpability, printability or extrudability, buildability and open time which are controlled by the rheology and hydration properties of the printable material.

Based on previous literatures [8, 13], the requisitions for a printable concrete are; high powder content, no coarse aggregate, improved paste fraction, and use of viscosity modifying accelerator. Hambach and Volkmer [5] were the first to endeavour adding short different types of fibres (carbon, glass and basalt fibres) into 3D printed composite of Portland cement paste. Feng et al. [4] also used fibres in powder based concrete printing and observed significant strength reduction between layers due to formation of air bubbles. Recently [10] investigated the effect of polypropylene (PP) fibres on the hardened properties of 3D-printed fibre-reinforced geopolymer mortars [11] investigated the effect of type of fibre on inter-layer bond and flexural strengths of extrusion-based 3D printed geopolymer and Bos et al. [2] studied the effect of adding short straight steel fibres on the failure behaviour of print mortar through several tests on cast and printed concrete, on different scales. However, a detailed analysis on the effect of fibre in the fresh properties and workability loss with time has not been investigated.

Hence, this paper is concerned about the influence of polypropylene (PP) fibre on the workability parameters of a novel extrudable concrete mixture. The purpose of current study is to present and examine an outline for experimental based laboratory testing and evaluation of extrudable mixture. Moreover, it has to be noted that only fresh properties of a mixture are considered in this study, while further examination is desired to examine the mechanical performance for hardened mixture.

2 Experimental Investigation

2.1 Materials and Mix Design

Type I Ordinary Portland Cement and tap water were used for all the mixtures. Midas Sand and Limestone Fines were used as fine aggregates. Ground Granulated Blast furnace Slag (GGBS) and Silica Fume (SF) were used as a partial cement substitute and SF based 3D printing concrete mixture showed better adhesiveness. A high range water reducing admixture (HRWRA) was added with water in order to reduce the water consumption while improving the workability and strength. In addition, to increase the plastic viscosity and cohesion of printing mixtures, a viscosity modifying admixture (VMA) was used. Polypropylene fibre was also used as a shrinkage reinforcement for a printing mixture. Addition of this fibre inhibits and controls the formation of plastic and drying shrinkage cracking in concrete.

Initially, eight control mixes were selected and tested for the fresh properties such as flowability, extrudability, initial setting time, buildability and print quality. Hence, according to the results three mix designs those were satisfying all the aforementioned criteria were selected for further printing and experimental analysis. Printing quality and dimensions of printed layers are the criteria used to decide whether it could be an extrudable material or not.

Afterwards, one of the selected three control mixes was printed with fibre addition in different volume fraction of binder in order to examine the effect on fresh properties. Fibre was added in different mass fraction of binder in 0.5, 1.0, 1.5, 2.0 and 3%. The material compositions investigated in this study are given in Table 1. All proportions were kept constant in the control mixes, except the fibre and the amount of water. The water/binder ratio was maintained in a range of 0.31–0.33 with the intention of satisfying the smooth extrudability criteria. The fibres and water content variation is given in Table 2.

2.2 Mixing of Extrudable Concrete

The mixtures were prepared in a free fall Hobart mixer with tilting drum and two rotating blades. The Midas sand and other dry components were dry mixed for about

Table 1 Material composition of the control mix (kg/m^3)

Binder	Cement	350
	GGBS	185
	SF	100
Fine aggregate	Midas sand	500
	Limestone fines	250
Admixture	HRWRA	8
	VMA	4
	Block	10

Table 2 Fibre and water content variation (kg/m^3)

Mix ID	Water	W/B	Fibre
Control mix	195	0.31	0
PP 0.5%	195	0.31	3.18
PP 1.0%	200	0.31	6.35
PP 1.5%	210	0.33	9.53
PP 2.0%	210	0.33	12.70
PP 3.0%	212	0.33	19.05

a minute. Then the solution of admixtures with water was gradually added to the dry mix and the mixing was continued for about 5 min. After the mixture ingredients were thoroughly mixed, the fibres with different volume fractions were gradually added and mixed. The mixing was continued for about 3–4 min to achieve the appropriate rheology for the extrusion. Sufficient amount of water was added to avoid the loss of material while mixing. The mix was decided to be extrudable by visual assessment. The total mixing time was maintained for all the mixes approximately for 10 min.

2.3 Concrete Printing

The samples were manually extruded using a custom made small scale cement mortar pointing gun fitted with a rectangular nozzle of 25 mm × 25 mm cross section. This was used to simulate the extrusion based 3D concrete printing in the laboratory scale. The samples were printed as blocks with approximate size of 300 mm length, 220 mm wide and 50 mm depth. The block size was decided as above in order to extract minimum 6 samples for the flexural tests from each mixture. The sample preparation is shown in Figs. 1. The printed specimens consisted of two extruded layers and the print time interval between subsequent layers was maintained as 15 min.

Fig. 1 Material extrusion

2.4 Fresh State Tests on Concrete

2.4.1 Flow Table Test

Flowability is a rheological parameter of the mixture consistency with time. There are several Standards dedicated to determination of this characteristic. The flowability of the concrete was tested using the flow table test according to ASTM C1437 (2007). The control mix was printed with different volume fraction of fibre and the flowability of each batch was tested at 0, 15, 30, 45, 60 min interval after mixing in order to determine the rate of workability loss. The mixture was placed inside a mini conical brass mould. During the test, the mortar was flowed to form a circular mass by the vibration of 1.67 Hz as the flow table rose and dropped 25 times in 15 s and the diameter of the mass was measured and compared to the initial size.

2.4.2 Initial Setting Time

Setting time is another essential parameter, which determines the working time of printable concrete. Vicat needle apparatus was used to measure the initial setting time according to EN 196-3 (2005). This test was performed measuring the penetration of a steel needle into the mortar over the course of several minutes. When the penetration of the needle into the material was less than 5 mm from the bottom in mortar, the material is assumed to be achieved its initial setting time.

2.4.3 Extrudability and Buildability

The extrudability of concrete is interconnected with rheological characteristics of the fresh mix. The print quality of the extruded layers was evaluated using classification presented by [6] such as defect free surface, squared edges, dimension conformity

and dimension consistency. The chosen criteria for a mixture to be extrudable through the nozzle smoothly and continuously to produce the layers without being blocked in the path.

Buildability defines the feasibility of fresh mix for layer by layer deposition and its resistance to deformation under the stress caused by the subsequent layers. The parameter is extensively associated with workability and extrudability of the mix.

In this study, the constant open time of 15 min was retained for the considered mix. Specimens of two extruded layers were printed in time interval of 15 min to examine the buildability. The print quality and buildability were examined solely through visual assessment on the two extruded layers.

2.5 Results and Discussion

2.5.1 Flow Table Test

It is known from the preliminary examination that the increasing quantity of fibre inversely affect the workability. The workability loss of all mixes is described in Fig. 2. It is clearly identified that the mixtures lost its workability with increasing time. But some of the mixtures behave differently. This phenomenon should be examined further. PP 0.5% shows higher flow compared to the control mix in 15 and 30 min after mixing. However, a reducing tendency after 45 and 60 min could be noticed. PP 1.0% mix exhibited the maximum spread diameter compared to all other mix. For the mixtures with increasing fibre percentage more than 1.5% indicated a reducing flowability. It appeared to be too rigid and formation of fibre lumps was also witnessed.

As seen in Fig. 2, the change of flow value of the fresh extrudable concrete declined gradually with time but there is still 116–142 mm spread value was achieved

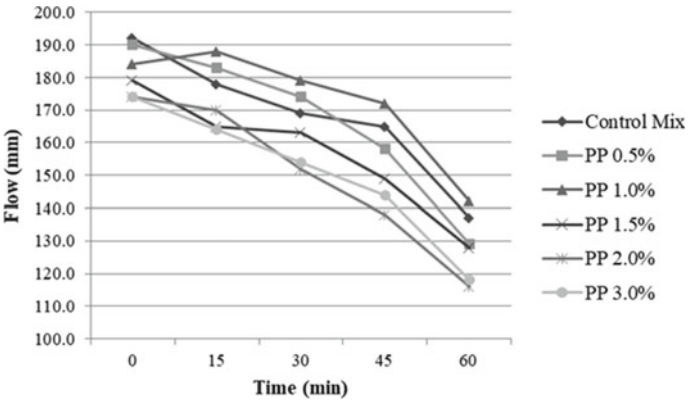

Fig. 2 Loss of workability with time of the mix

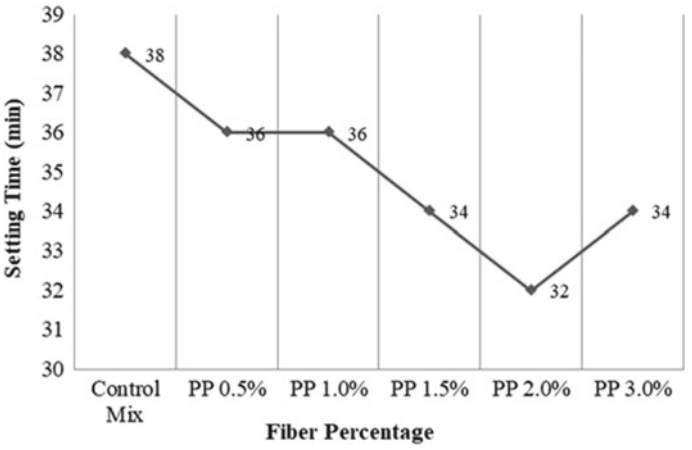

Fig. 3 Initial setting time variation

according to flow table test in 60 min. It makes a realistic situation to pump and extrude the 3D printing concrete mix due to fluidity. Moreover, it must be noted that all mixes did not reveal high flow when lifting the mini conical brass mould, before shocks were applied to the flow table. Therefore, the assumption of all the fresh mixtures had approximately zero-slump can be justified, which is an important material aspect for the extrusion process.

2.5.2 Initial Setting Time

The variation of initial setting time of each mix is illustrated in the following graph (Fig. 3). These results specify that the initial setting time is progressively decreasing with increasing fibre addition which is required for better bond strength between layers. Since there is no significant deviation within the setting time, the PP fibres had insignificant influence on the initial setting time.

2.5.3 Extrudability and Buildability

The extrusion of material through the nozzle became difficult with increasing volume fraction of fibre content. Moreover, imperfections in the print quality were assessed visually with both very low and very high fibre percentage. Only PP 1.0% and PP 1.5% mixes satisfied the print quality criteria mentioned above.

The top surface was achieved to be level and smooth with 25 mm width, almost close to the nozzle diameter with the mixtures PP 1.0% and above. Though the higher fibre content caused better buildability and shape retention in the extruded samples, the simultaneous discontinuity in the extrusion was identified with increasing fibre

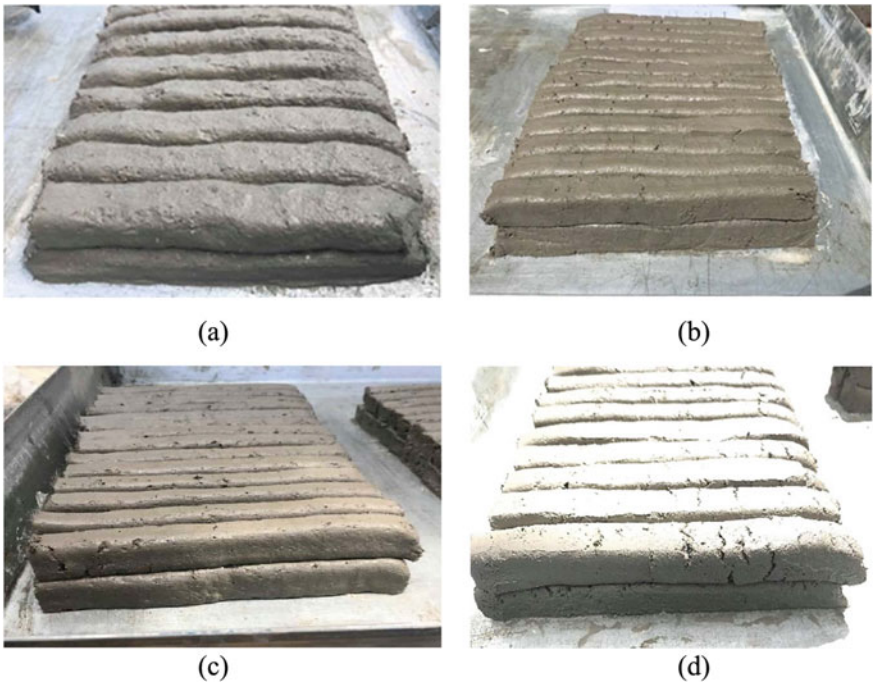

Fig. 4 **a** Extruded specimen of PP 0.5%, **b** Extruded specimen of PP 1.0%, **c** Extruded specimen of PP 1.5%, **d** Extruded specimen of PP 2.0%

inclusion. Figure 4a–d illustrates the extruded samples with different fibre content. Hence, PP 1.0% and PP 1.5% fulfilled the extrudability and buildability measures compared to other mixtures.

3 Conclusion and Recommendations

A novel concrete that has extrudability and buildability was developed for the custom made extruder. The crucial properties of this printing concrete mix were the flowability and buildability which have contradict mutual relationship were analysed for the selected mixture. In allusion to the experimental study and results analysis the following summary were concluded.

1. All mixes developed in this study, with and without fibres are showing sufficient workability in terms of flowability and setting time. However, the mixes PP 0.5% and PP 1.0% showed the better flowability with time and further investigation between the fibre percentages 0.5 and 1.0 is preferred to have a clear conclusion in the variation with increasing time.

2. There is no major variation was identified in the setting time for selected mixtures. Therefore, the effect of PP fibres on the initial setting time is negotiable.
3. Buildability and shape retention ability have been increased with increasing fibre content. Moreover, PP 1.0% and PP 1.5% achieved the extrudability and buildability criteria compared to other mixtures.
4. As per the overall investigation, the incorporation of 1 and 1.5% fibre considerably satisfies all the fresh property criteria to be accepted as the optimized extrudable mixture for the customized extruder used in this experiment series.
5. The anomalous behaviour of the flow with fibre addition for the mixes requires further investigation to identify the causes behind the fluctuating behaviour.
6. Study has indicated that the open time is one of the most significant aspects in 3D printing of concrete.

References

1. Beyhan F, Arslan Selçuk S (2018) 3D printing in architecture: one step closer to sustainable built environment. In: Proceedings of 3rd international sustainable buildings symposium (ISBS 2017) lecture notes in civil engineering, pp 253–268
2. Bos FP, Bosco E, Salet TAM (2019) Ductility of 3D printed concrete reinforced with short straight steel fibers. Virtual Phys Prototyping 14(2):160–174
3. De Schutter G, Lesage K, Mechtcherine V, Nerella VN, Habert G, Agusti-Juan I (2018) Vision of 3D printing with concrete—technical, economic and environmental potentials. Cem Concr Res 112:25–36
4. Feng P, Meng X, Chen J-F, Ye L (2015) Mechanical properties of structures 3D printed with cementitious powders. Constr Build Mater 93:486–497
5. Hambach M, Volkmer D (2017) Properties of 3D-printed fibre-reinforced Portland cement paste. Cement Concr Compos 79:62–70
6. Kazemian A, Yuan X, Cochran E, Khoshnevis B (2017) Cementitious materials for construction-scale 3D printing: Laboratory testing of fresh printing mixture. Constr Build Mater 145:639–647
7. Kidwell J (2017) Best practices and applications of 3D printing in the construction industry
8. Le TT, Austin SA, Lim S, Buswell RA, Gibb AGF, Thorpe T (2012) Mix design and fresh properties for high-performance printing concrete. Mater Struct 45(8):1221–1232
9. Lim S, Buswell RA, Le TT, Austin SA, Gibb AGF, Thorpe T (2012) Developments in construction-scale additive manufacturing processes. Autom Constr 21:262–268
10. Nematollahi B, Vijay P, Sanjayan J, Nazari A, Xia M, Naidu Nerella V, Mechtcherine V (2018a) Effect of polypropylene fibre addition on properties of geopolymer made by 3D printing for digital construction. Materials (Basel), 11(12)
11. Nematollahi B, Xia M, Sanjayan J, Vijay P (2018b) Effect of type of fibre on inter-layer bond and flexural strengths of extrusion-based 3D printed geopolymer. Materials science forum, vol 939 Trans Tech Publications, pp 155–162
12. Panda B, Tan MJ (2018) Experimental study on mix proportion and fresh properties of fly ash based geopolymer for 3D concrete printing. Ceram Int 44(9):10258–10265
13. Perrot A, Rangeard D, Pierre A (2015) Structural built-up of cement-based materials used for 3D-printing extrusion techniques. Mater Struct 49(4):1213–1220

Synthesis of Carbon and Silica Nanospheres for Removal of Heavy Metals in Wastewater

H. M. R. S. Herath, W. M. M. C. Welagedara, and C. A. Gunathilake

Abstract Treatment of heavy metals containing industrial effluent becomes quite necessary before being discharged to the environment. In this study, potential of carbon nanospheres (CS) and silica nanospheres (SS) for the adsorption of heavy metals were tested. SS were synthesized by the Stöber process and CS were synthesized by a slightly modified Stöber process. Products obtained were tested with Scanning Electron Microscope to identify their spherical shape. N_2 adsorption-desorption analysis was conducted to measure the specific surface area and porosity. SS showed higher total pore volume compared to that of CS and CS showed higher specific surface area compared to SS. Adsorption capacities of both particles were tested for lead ions (Pb^{2+}) through equilibrium and kinetic studies. SS showed a better adsorption capacity than CS. Results show no substantial difference. So, both can be used as effective adsorbents to remove heavy metals in wastewater. This study can be extended to obtain the best material which has a greater adsorption capacity by adjusting synthesis conditions.

Keywords Heavy metals · Adsorption · Carbon nanospheres · Silica nanospheres · Equilibrium study · Kinetic study

1 Introduction

Heavy metals, such as mercury (Hg), cadmium (Cd), arsenic (As), chromium (Cr), thallium (Tl), zinc (Zn), nickel (Ni), copper (Cu) and lead (Pb) are naturally occurring elements that have a high atomic weight and a density relative to water. They are considered to be one of the most hazardous pollutants in water because of their toxic effect on human and the environment. Although heavy metals are naturally occurring

H. M. R. S. Herath (✉) · W. M. M. C. Welagedara (✉) · C. A. Gunathilake
Department of Chemical and Process Engineering, Faculty of Engineering, University of Peradeniya, Peradeniya, Sri Lanka
e-mail: randiherath0@gmail.com

W. M. M. C. Welagedara
e-mail: markswelagedra@gmail.com

R. Dissanayake et al. (eds.), *ICSECM 2019*, Lecture Notes in Civil Engineering 94,
https://doi.org/10.1007/978-981-15-7222-7_36

elements, most environmental contamination result from anthropogenic activities such as mining, mineral processing and metallurgical operations [10]. Heavy metals present in the wastewater are persistent and non-degradable in nature. They can get bioaccumulated and biomagnified by entering into food chains. If they get absorbed above the permissible levels, it could lead to serious health disorders. So, treatment of heavy metals containing industrial effluent becomes quite necessary before being discharged into the environment. The conventional methods for heavy metal removal are chemical precipitation, chemical oxidation, ion exchange, membrane separation, reverse osmosis, electrodialysis etc. Those methods are not very effective, are costly and require high energy input [4]. It is also found that adsorption methods are very effective for removal of heavy metals in water [10]. Silica and carbon nano particles are considered to be very effective adsorbents due to their high adsorption capacity, high specific surface area, and high porosity [1, 2, 7, 8] .

This study is aimed to test the ability of silica nanospheres and carbon nanospheres in the removal of heavy metals in polluted water. Silica nanospheres are synthesized by the Stöber method where TEOS (tetraethylorthosilicate) is hydrolyzed and condensed in ethanol, in presence of ammonia as a catalyst [9]. Carbon nanospheres are synthesized by mixing resorcinol with ethanol and formaldehyde, in the presence of ammonia as a catalyst [11]. Objective of this study is to synthesize the two types of adsorbents, characterize their properties such as specific surface area and porosity, and measure the adsorption capacity through equilibrium and kinetic studies.

2 Method

In this study, adsorption capacities of silica nanospheres and carbon nanospheres were tested for an artificially prepared lead (Pb^{2+}) solution through equilibrium and kinetic studies. Silica and carbon nanospheres act as the adsorbent and lead ions act as the adsorbate. Lead solution was prepared by Lead Nitrate ($Pb(NO_3)_2$) solid.

2.1 Synthesis of Silica Nano Spheres: Stöber Method

Tetraethylorthosilicate (TEOS), Aqueous solution of NH_3 (25%), Ethanol and water are needed to synthesize silica nano particles. 0.011 mol (2.4 cm^3) of TEOS was added to 20 cm^3 of absolute ethanol and stirred for 1 h. 2.2 mol (127.6 cm^3) of ethanol was added to 17.8 mol (316 cm^3) of water and stirred for 1 h. Above prepared two mixtures were mixed and 7 ml of 25% w/w ammonium hydroxide was added and stirred for 4 h. Then, the solution was kept in the oven at 100 °C for 24 h for the hydrothermal treatment [3, 9].

2.2 Synthesis of Carbon Nano Spheres

Resorcinol (2.4 g), 37% w/w formaldehyde (3.4 ml), Ethanol (9.6 ml), 25% w/w ammonium hydroxide (1.2 ml) and distilled water (240 ml) are needed for the synthesis of carbon nanospheres. All the chemicals were mixed and stirred for 24 h. Hydrothermal treatment was done for 24 h at 100 °C and then dried for 24 h at 100 °C and resorcinol-formaldehyde polymer was produced [11].

Then the calcination process was done for the prepared polymer spheres by heating in a muffle furnace using heating rate of 5 °C/min up to 180 °C, dwelled for 1 h, and resuming heating rate of 5 °C/min up to 400 °C and dwelled for 2 h as shown in Fig. 1. Carbon spheres obtained were activated by mixing solid KOH at a Carbon to KOH ratio of 1:2.5 by mass followed by a thermal treatment in muffle furnace using heating rate of 5 °C/min up to 350 °C, dwelled for 1 h, and resuming heating rate of 5 °C/min up to 600 °C and dwelled for 2 h as shown in Fig. 2. The obtained product was washed with distilled water and dried at 100 °C.

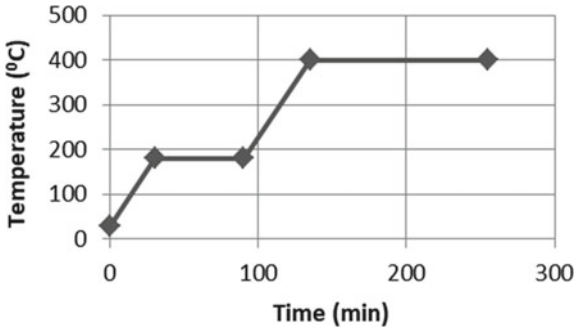

Fig. 1 Temperature profile for calcination

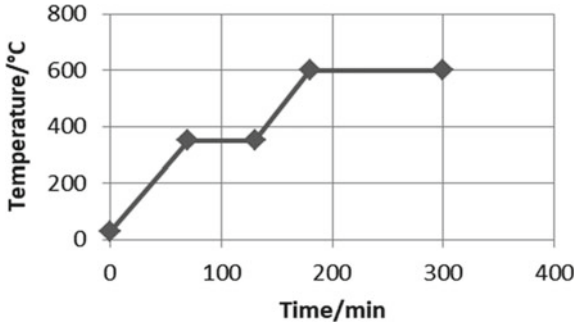

Fig. 2 Temperature profile for activation

2.3 Characterization of Synthesized Adsorbents

The sharpness, size, and distributions of the dried colloidal particles were observed by the image taken by the scanning electron microscope (SEM).

The specific surface area and porosity of the particles were examined by using the nitrogen gas adsorption-desorption analyzer. The commonly used method for the calculation of the specific surface area from adsorption isotherms is that based on the Brunauer-Emmet-Teller (BET) model. The number of gas molecules adsorbed on the entire surface in a monolayer called the monolayer capacity (n_m) is obtained by fitting the experimental data into the linear form of the BET equation. Other than the BET surface area, single point pore volume (V_{sp}), volume of fine pores (V_{mi}), pore width (W_{max}) and total pore volume (V_t) is measured using nitrogen adsorption analyzer. Nitrogen adsorption isotherms were measured at −196 °C on an ASAP 2010 volumetric analyzer (Micromeritics, Inc., Norcross, GA). Prior to adsorption measurements, all samples were outgassed under vacuum at 110 °C for 2 h.

2.4 Measuring Adsorption Capacity

Adsorption capacities of synthesized carbon and silica nano particles were measured for artificially prepared wastewater solution containing lead ions. Equilibrium and kinetic studies were conducted for both silica and carbon nano particles.

2.4.1 Equilibrium Adsorption Measurements for Lead Ions

Equilibrium study was done using 50 ml samples of lead ion solutions with concentrations ranging from 50 to 300 ppm, stirring (150 rpm) for a period of 6 h by placing a 50 mg dose of adsorbent in each.

The adsorption isotherms under the Langmuir model and Freundlich model are developed and the most suitable model for each adsorbent is evaluated by comparing the coefficient of determination and the model constants are also calculated [5].

Langmuir equation,

$$q_e = \frac{K_L C_e q_m}{(1 + K_L C_e)} \tag{1}$$

In the linear form,

$$\frac{1}{q_e} = \frac{1}{q_m} + \frac{1}{K_L q_m C_e} \tag{2}$$

where, K_L is the Langmuir constant, C_e is the equilibrium concentration in mg/l, q_m and q_e are the maximum and equilibrium adsorbed quantities in mg/g.

Freundlich equation,

$$q_e = KC_e^{1/n} \tag{3}$$

The linear model is expressed as,

$$\log q_e = \log K + \frac{1}{n} \times \log C_e \tag{4}$$

where q_e is the equilibrium concentration of adsorbate in the solid phase in mg/g, C_e is the equilibrium concentration of adsorbate in the liquid phase in mg/l, K is the adsorption capacity and 1/n is the Adsorption Intencity.

The amount of adsorbed Pb^{2+} ions per unit mass of the solid at equilibrium (q_e) was determined as follows

$$q_e = \frac{(C_o - C_e) \times V}{m} \tag{5}$$

where, C_0 (mg/L) is the initial concentration of lead ions, V (L) is the volume of lead ion solution, and m (mg) is the mass of the adsorbent. C_e (mg/L) is the equilibrium concentration of Pb^{2+} determined by atomic absorption spectroscopy.

2.4.2 Kinetic Adsorption Measurements for Lead Ions

Kinetic study was done for a lead solution of 100 ppm which was kept under stirring (150 rpm) with 50 mg dose of the adsorbent. 0.2 ml samples were collected at 10 min time intervals for 2 h.

The amount of adsorbed lead ions per unit mass of the adsorbent at time t, (q_t) was determined using the following equation:

$$q_t = \frac{(C_o - C_t) \times V}{m} \tag{6}$$

where, C_t (mg/L) is the concentration of lead ions at a given time, C_0 (mg/L) is the initial concentration of lead ions, V (L) is the volume of lead ion solution, and m(g) is the mass of the adsorbent.

Analysis of adsorption kinetics data was performed by using the two models [5].

The first order adsorption kinetics model:

$$\frac{dq_t}{dt} = K_1(q_e - q_t) \tag{7}$$

In the linear form,

$$\log(q_e - q_t) = \log q_e - \frac{K_1 t}{2.303} \tag{8}$$

where q_e (mg/g) and q_t (mg/g) are the amounts of adsorbed metal ions at the equilibrium and time t (min), respectively. K_1 (min^{-1}) is the rate constant of the first order adsorption reaction. The Pseudo-second-order kinetic model:

$$\frac{dq_t}{dt} = K_2(q_e - q_t)^2 \tag{9}$$

In the linear form,

$$\frac{t}{q_t} = \frac{1}{K_2 q_e^2} + \frac{t}{q_e} \tag{10}$$

where, K_2 is the Pseudo-second order rate constant (g mg^{-1} min^{-1}).

3 Results and Discussion

3.1 Characterization

Hydrolysis and Condensation steps involving in Stober process of producing silica particles are as follows [6].

$$Si(OEt)_4 + H_2O \rightarrow Si(OEt)_3OH + EtOH$$

$$Si(OEt)_4 + 2H_2O \rightarrow Si(OEt)_2(OH)_2 + 2EtOH$$

$$2Si(OEt)_3OH \rightarrow (EtO)_3Si\text{-}O\text{-}Si(OEt)_3 + H_2O$$

$$Si(OEt)_3OH + Si(OEt)_4 \rightarrow (EtO)_3Si\text{-}O\text{-}Si(OEt)_3 + EtOH$$

$$Si(OEt)_3OH + Si(OEt)_2(OH)_2 \rightarrow (EtO)_3Si\text{-}O\text{-}Si(OEt)_2OH + H_2O$$

Figure 3 shows the image obtained by Scanning Electron Microscope for silica particles. SEM image reveals that synthesized particles are spherical and are in the nano range.

The N_2 adsorption isotherms measured at −196 °C for Silica Spheres (SS) and Carbon Spheres (CS) are shown in Fig. 4.

The pore size distribution for silica and carbon nanospheres is shown in Fig. 5.

The structural parameters of silica and carbon particles calculated based on the nitrogen adsorption data are shown in Table 1.

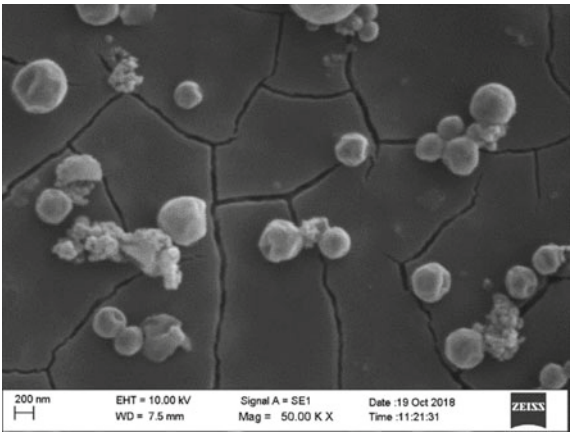

Fig. 3 SEM image obtained for silica particles

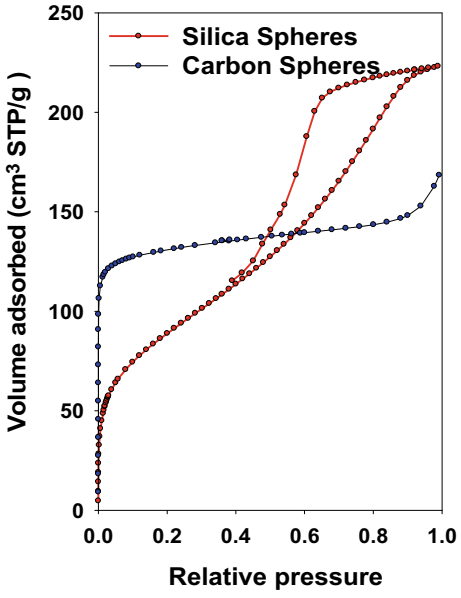

Fig. 4 N_2 adsorption isotherms for silica and carbon nanospheres

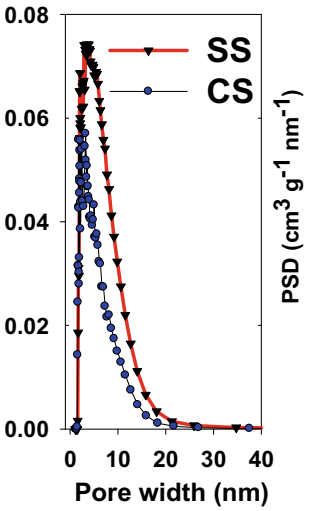

Fig. 5 Pore size distribution obtained for silica and carbon nanospheres

Table 1 Adsorption parameters for silica and carbon particles

Content	S_{BET} (m^2/g)	V_{mi} (cm^3/g)	V_{sp} (cm^3/g)	W_{max} (nm)	V_{tot} (cm^3/g)
Silica spheres (SS)	324	0.08	0.35	4.0	0.37
Carbon spheres (CS)	452	0.15	0.25	2.7	0.26

V_{sp}—single point pore volume calculated at the relative pressure of 0.98; V_{mi}—volume of fine pores (micropores below 2 nm) calculated by integration of the PSD curve up to 2 nm; S_{BET}—specific surface area calculated from adsorption data in relative pressure range 0.05–0.20; W_{max}—pore width calculated at the maximum of PSD obtained by using the improved KJS method; V_{tot}—calculated by integration of the PSD curve up to 5 nm

Nitrogen adsorption isotherm for the SS sample shows a type IV isotherm with an H2 type hysteresis loop characteristic for mesoporous materials. This sample exhibits broad capillary condensation-evaporation step starting at relative pressure of ~0.75–0.90. SS sample exhibits the total pore volume and surface area of ~0.37 cm^3/g and 324 m^2/g, respectively. W_{max} (maximum pore size) obtained from PSD curve is 4.0 nm for SS sample (Fig. 5).

Nitrogen adsorption isotherm for the CS sample shows a type I isotherm and no hysteresis loop is shown. CS sample exhibits the total pore volume and surface area of ~0.26 cm^3/g and 452 m^2/g, respectively. W_{max} (maximum pore size) obtained for CS sample is 2.7 nm (Fig. 5).

Micropore volume value obtained of SS sample is higher than that of CS sample while CS shows a higher specific surface area than that of SS.

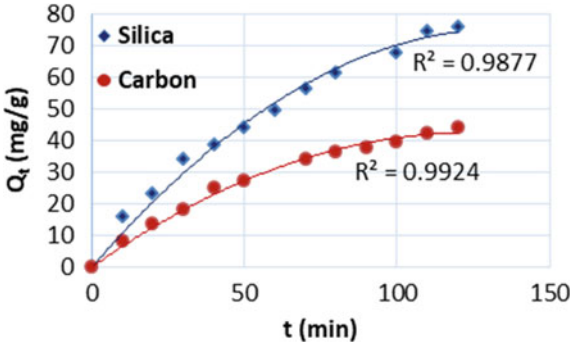

Fig. 6 Experimental adsorption kinetics of silica and carbon nanospheres for Pb^{2+} ions

3.2 *Kinetic Studies for Pb^{2+} Ion Adsorption*

Kinetic studies of metal ion adsorption process revealed the rate of Pb^{2+} ion uptake by the synthesized silica and carbon nanospheres. The time dependence of the adsorption of Pb^{2+} ions by the silica and carbon nanospheres is shown in Fig. 6.

The linear form of Pseudo-first order and Pseudo-second-order kinetic models were applied to obtain the rate of ion adsorption. These forms of linear equations were used to model the adsorption process and the validity of each equation was checked using correlation coefficient (R^2) for each brick type in each ion solution. The experimental data for both the adsorbents fitted well with the second-order kinetic model with coefficients of determination 95.96% and 98.7% for silica and carbon respectively. Data fitting for linearized Pseudo second-order kinetic model is shown in Fig. 7.

The resulted Pseudo-second-order rate constants and adsorbed quantities at equilibrium are shown in Table 2. Both the adsorbents show somewhat similar kinetics. But, SS shows slightly higher values.

3.3 *Equilibrium Studies for Pb^{2+} Ion Adsorption*

Equilibrium studies were investigated based on two models which are Langmuir isotherm and Freundlich isotherm, for the uptake of Pb^{2+} ions. Figure 8 shows that adsorption of Pb^{2+} ions initially increases with increasing metal concentration and then levels off which might be due to the availability of more vacant sites at the beginning.

The experimental data fitted well with the Langmuir model for both the adsorbents with higher coefficients of determination. Data fitting for the linearized Langmuir model is shown in Fig. 9.

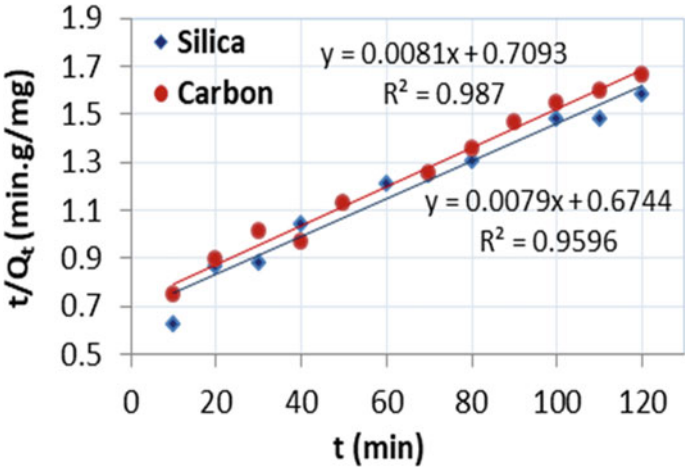

Fig. 7 Linearized Pseudo-second order model for silica and carbon nanospheres

Table 2 Resulted parameters for Pseudo-second-order model

Particle	K_2 (g/mg min)	Q_e (mg/g)	R^2 (%)
Silica	9.25×10^5	126.58	95.96
Carbon	9.24×10^5	123.46	98.70

Fig. 8 Pb^{2+} ion adsorption into silica and carbon nanospheres

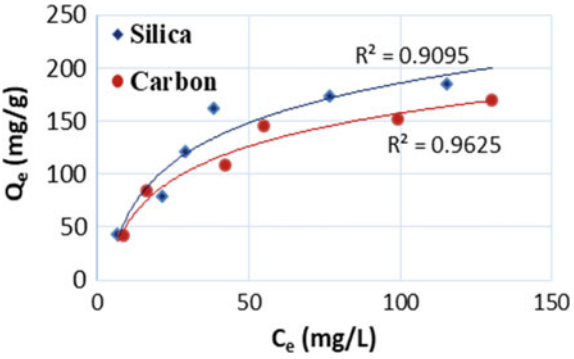

Resulted Langmuir constants and maximum adsorbed quantities are shown in Table 3. Higher Q_m and K_L are resulted by silica nanospheres which reveal that silica has a higher adsorption capacity than that of carbon.

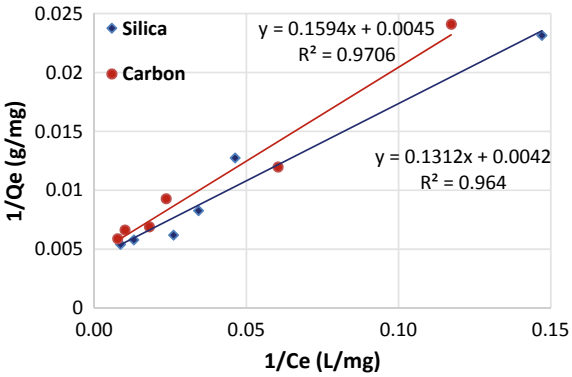

Fig. 9 Linearized Langmuir model for silica and carbon nanospheres

Table 3 Resulted parameters for Langmuir model

Particle	Q_m (mg/g)	K_L (L/mg)	R^2 (%)
Silica	238.1	0.032	96.40
Carbon	222.2	0.028	97.06

4 Conclusions

Stöber process of synthesizing silica particles can be used to yield nano size spherical silica particles. And a slightly modified Stöber process followed by calcination and activation can be used to synthesize nano size spherical active carbon particles. As revealed by the SEM image, spherical nature and small size of the particles have led to high specific surface area enhancing the adsorption capacity. The synthesis process of SS is less time and resource-consuming process compared to that of CS.

Characterization of synthesized particles revealed that SS have a higher pore volume compared to that of CS and CS have higher specific surface area compared to SS. These properties can be adjusted by controlling synthesis conditions.

According to kinetic and equilibrium studies, SS shows a better adsorption capacity than CS which might due to the high total pore volume of SS. But, the difference between adsorption capacities of SS and CS is very small. So, both can be used as effective adsorbents to remove heavy metals in wastewater.

These results were obtained for carbonized CS which have not been activated. As the activation leads to obtain a higher amount of pores with small size, higher adsorption capacity can be expected for active carbon spheres which might be very much greater than that of SS and CS.

This study can be extended to obtain silica and carbon nanospheres with better adsorption capacities by changing the synthesis conditions. Adsorption of Pb^{2+} ions is considered in the current study. We expect to extend the study to measure the adsorption of few other heavy metal ions by silica and carbon nanospheres.

Acknowledgements The authors sincerely acknowledge the encouragement and guidance provided by Dr. Chamila Gunathilake, project supervisor, Dr. Achala Pallegedara, course coordinator, Dr. C. S. Kalpage, Head, Department of Chemical and Process Engineering, University of Peradeniya, and all the members of the academic and non-academic staff members of Department of Chemical & Process Engineering, University of Peradeniya, Environmental Laboratory of Department of Civil Engineering, University of Peradeniya, and Dr. Aman Singe from Department of Chemistry, California State University.

References

1. Ahmed A, Clowes R, Willneff E, Myers P, Zhang H (2010) Porous silica spheres in macroporous structures and on nanofibres. Philos Trans R Soc A: Math, Phys Eng Sci. Royal Society, pp 4351–4370. https://doi.org/10.1098/rsta.2010.0136
2. Basu H, Singhal R, Pimple M, Reddy A (2015) Synthesis and characterization of silica microsphere and their application in removal of uranium and thorium from water. Int J Environ Sci Technol 12(6):1899–1906. https://doi.org/10.1007/s13762-014-0550-y. Center for Environmental and Energy Research and Studies
3. Chou KS, Chen CC (2006) Preparation of monodispersed silica colloids using sol-gel method. In: Innovative processing and synthesis of ceramics, glasses and composites, vol VIII, p 166
4. Gautam R, Sharma S, Mahiya S, Chattopadhyaya M (2014) Chapter 1. Contamination of heavy metals in aquatic media: transport, toxicity and technologies for remediation. In: Heavy Metals In Water. Royal Society of Chemistry, pp 1–24. https://doi.org/10.1039/9781782620174-00001
5. Gunathilake C, Kadanapitiye M, Dudarko O, Huang S, Jaroniec M (2015) Adsorption of lead ions from aqueous phase on mesoporous silica with P-containing pendant groups. ACS Appl Mater Interfaces 7(41):23144–23152. https://doi.org/10.1021/acsami.5b06951. American Chemical Society
6. Ibrahim I, Zikry A, Sharaf M, Zikry A (2010) Preparation of spherical silica nanoparticles: Stober silica. J Am Sci. Available at: http://www.americanscience.org
7. Mubarak N, Sahu J, Abdullah E, Jayakumar N (2014) Removal of heavy metals from wastewater using carbon nanotubes. Sep Purif Rev 43(4):311–338. https://doi.org/10.1080/15422119.2013.821996
8. Ruparelia J, Duttagupta S, Chatterjee A, Mukherji S (2008) Potential of carbon nanomaterials for removal of heavy metals from water. Desalination 232(1–3):145–156. https://doi.org/10.1016/j.desal.2007.08.023
9. Stober W, Fink A, Ernst Bohn D (1968) Controlled growth of monodisperse silica spheres in the micron size range 1. J Colloid Interface Sci
10. Tripathi A, Rawat Ranjan M (2015) Heavy metal removal from wastewater using low cost adsorbents. J Bioremediat Biodegrad 06(06). https://doi.org/10.4172/2155-6199.1000315. OMICS Publishing Group
11. Wickramaratne N, Jaroniec M (2013) Activated carbon spheres for CO2 adsorption. ACS Appl Mater Interfaces 5(5):1849–1855. https://doi.org/10.1021/am400112m

Integration of the Concept of Disaster Resilience for Sustainable Construction—An Analysis on the Competency Requirements of the Built Environment Professionals

N. Dias, D. Amaratunga, R. Haigh, C. Malalgoda, and S. Nissanka

Abstract Sustainable construction involves a commitment to: Economic sustainability, Environmental sustainability and Social sustainability. However, the notion of 'resilience' has not been mainly integrated to the sustainable construction. Within this context, researchers have emphasised the need to bring these two notions 'sustainability' and 'resilience' into one framework as both these notions are interrelated. However, in order to integrate disaster resilience to the sustainability agenda, it is extremely important to identify the competency requirements of the built environment professionals. As a part of a key research project entitled CADRE, an analytical framework was developed to identify various built environment professionals, different resilience aspects and stages of the construction project cycle. Accordingly, based on this analytical framework, an extensive literature review was conducted to identify the competency requirements of the built environment professionals under different resilience aspects in the construction stage of the project cycle. Findings reveal, that the built environment professionals should have a variety of competencies to enhance resilience in the built environment projects and through that contribute to integrate the notion of resilience to the sustainability agenda.

Keywords Resilience · Sustainability · Built environment stakeholders · Competency requirements

1 Introduction

1.1 Research Need and Background

Sustainability in the built environment is becoming a strong force in the construction industry to achieve social and environmental benefits and to lower negative environment impacts [1]. The first international conference on sustainable construction which held in Tampa, Florida, USA, in 1994, defined sustainable construction as

N. Dias (✉) · D. Amaratunga · R. Haigh · C. Malalgoda · S. Nissanka
Global Disaster Resilience Centre, University of Huddersfield, Huddersfield, UK
e-mail: n.dias@hud.ac.uk

R. Dissanayake et al. (eds.), *ICSECM 2019*, Lecture Notes in Civil Engineering 94,
https://doi.org/10.1007/978-981-15-7222-7_37

"Creating a healthy built environment using resource-efficient, ecologically-based principles". Sustainable construction involves a commitment to: Economic sustainability, Environmental sustainability and Social sustainability [9]. Even though, sustainable construction has a detailed definition which entails the social, economic and environmental aspects, the notion of 'resilience' has not been mainly integrated to the sustainable construction. UNISDR [18] describes resilience as the ability of a system, community or society exposed to hazards to resist, absorb, accommodate, adapt to, transform and recover from the effects of a hazard in a timely and efficient manner, including through the preservation and restoration of its essential basic structures and functions through risk management. Within this context researchers such as Marchese et al. [13], Zhang and Li [20] have emphasised the need to bring these two notions 'sustainability' and 'resilience' into one framework as both these notions are interrelated. Zhang and Li [20] describes urban development should be rational and not irrational. And Rational urban development can be achieved only when it is both resilient and sustainable. These arguments set the background to identify the need of integrating the notion of resilience into sustainable construction. Accordingly, the aim of this paper is to provide a guideline to the policy makers in the construction industry to achieve sustainability by integrating the notion of resilience to the current triple bottom line (social, economic and environmental) of the sustainability agenda. Section 1.2 briefly explains the CADRE research project which is the basis to develop this research paper.

1.2 About the CADRE Project

There are wide-ranging origins and causes to the many disasters that have affected communities across Europe and globally with ever-greater frequency. If construction researchers and practitioners are to be able to contribute to reduce risk through resilient buildings, spaces and places, it is important that capacity is developed for modern design, planning, construction and maintenance that are inclusive, interdisciplinary, and integrative. In order to address this challenge, the CADRE project was initiated to mainstream disaster resilience in the construction process through development of an innovative professional doctorate programme that addresses the requirements for lifelong learning and actively promotes collaboration between European Higher Education Industries, and the community. This novel programme will address the career needs, and upgrade the knowledge and skills, of practising professionals working to make communities more resilient to disasters, and particularly those in, or who aspire to, senior positions within their profession [2].

Accordingly, based on the findings of the CADRE project, this paper was developed to provide a guideline to the policymakers in the construction industry to incorporate disaster resilience to the construction process.

2 Methodology

Malalgoda et al. [11] developed an analytical framework (Fig. 1) to analyse the competency requirements of the Built Environment Professionals as a part of the research project, CADRE. The framework was developed through an extensive consultation process with project partners and was refined with the emerging literature findings and the opinion of stakeholders who had been interviewed [11].

Accordingly, the analytical framework defines built environment stakeholders, dimensions of resilience and stages of the property cycle. The details are as follows.

2.1 Property Cycle

The first axis of the framework consists of different stages of the property cycle. The property cycle represents a sequence of recurrent activities associated with a construction project from its inception to the end of use. The aim of the framework is to understand gaps in the knowledgebase of construction professionals to contribute to the development of a more disaster resilient society. Accordingly, the property cycle was acknowledged as the first axis to reflect the construction perspective in the analysis framework. Having the property cycle as the first axis provided a sound basis to understand the needs and skills associated with a construction professional in contributing to the development of a more disaster resilient society throughout the property lifecycle. Across the construction industry, various terminologies are used

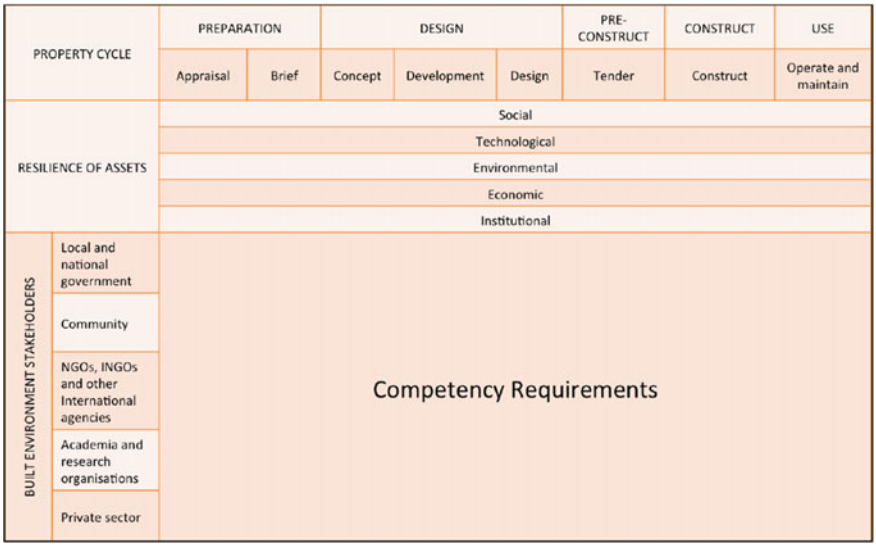

Fig. 1 Analytical framework Malalgoda et al. [11]

to identify different stages of the property cycle. Some of the established forms of property cycles include: RIBA Plan of Work, 2013, BIM digital plan of work 2013, BS 6079-1:2010, ISO 21500:2012 and OGC gateways. RIBA Plan of Work, 2013 is the definitive UK model for the building design and construction process, and therefore, it was used as a basis in defining key stages of the property cycle [3].

Accordingly, the defined stages of property cycle are as follows,

Stages of property lifecycle: Preparation Stage (PS); Design Stage (DS); Pre-Construction Stage (PCS); Construction Stage (CS) and Use Stage (US).

2.2 Dimensions of Resilience

The dimensions of resilience were acknowledged as the second axis to reflect the disaster resilience perspective in the analytical framework. Having dimensions of resilience as the second axis provided a sound basis to understand the disaster resilience needs and skills associated with a construction professional in contributing to the development of a more disaster resilient society [3]. Within the scope of disaster risk, the concept of resilience can be applied in a range of contexts for example, to individuals, households and communities and to their knowledge, assets and livelihoods, to cities or specific sectors within city economies and to national economies [16]. This research aims to mainstream disaster resilience within the construction process, and therefore, resilience is defined within the context of the built environment. However, the research classified resilience into five dimensions to ensure all aspects of resilience are considered [3]. Accordingly, defined five resilience aspects are as follows,

Dimensions of resilience: Economic Resilience; Environmental Resilience; Institutional Resilience; Social Resilience and Technological Resilience.

2.3 Built Environment Stakeholders

Disaster resilience and management is a complex task which requires numerous efforts by various stakeholders such as local government decision makers, city officials and departments, central and provincial governments, the private sector, civil society, nongovernmental organisations, community-based organisations, research institutions and institutions of higher learning [19]. Accordingly, all these stakeholders engage with built environment practice in increasing societal resilience to disasters. The third axis of the framework consists of built environment stakeholders. The aim of the framework is to understand gaps in the knowledgebase of construction professionals to contribute to the development of a more disaster resilient society. Construction professionals provide their services to a number of built environment stakeholders and as such, built environment stakeholders were acknowledged as the third axis. Accordingly, based on extensive consultations with the CADRE project

partners and based on Ginige et al. [8], all stakeholders were grouped into following five categories:

National and local government organisations; the community; non-governmental organisations (NGOs), international nongovernmental organisation (INGOs) and other international agencies; academia and research organisations; and the private sector. All private sector organisations, including construction service providers, contractors, clients, professional bodies, insurance providers and small- and medium-sized enterprises, were considered under private sector.

Accordingly, based on the defined aspects of the analytical framework an extensive literature review was conducted to identify the competency requirements of the built environment stakeholders under defined resilience aspects for the whole property cycle. However, the focus of this paper is only on investigating the competency requirements of key stakeholders under above mentioned resilience aspects for the construction stage of the project cycle.

3 Results and Discussions

3.1 Competency Requirements of Local and National Governments

The competency requirements in relation to the local and national governments could be mainly discussed under the main resilience aspects of Social, Technological, Environmental, Economic and Institutional resilience. In order to improve social resilience during the construction stage, the local governments should enhance their competencies to engage local decision makers. This provides an ownership to the community by promoting community driven and locally managed processes during the construction stage [7]. In respect of enhancing the technological resilience of the built environment the local and National governments could contribute in numerous ways. As National Disaster Management Authority India [14] highlights national and local governments should have competencies to provide special skills training on disaster resistant technologies to construction workers. For example, National Society for Earthquake Technology (NSET) in association with the Lutheran World Federation (LWF), Nepal under the LWF-DIPECHO-CPDRR component, implemented the Earthquake Safety Construction Skill Training for Masons and Construction Technicians in Bhadrapur, Gaur, Bhaktapur, Madhyapur Thimi, Kirtipur Municipality and Kathmandu Metropolitan. A total of 635 Masons/Construction Technicians and technicians have been trained on earthquake-resistant construction technology; under different training programs conducted in Bhadrapur Municipality of Jhapa, Gaur Municiplity of Rautahat and Kathmandu Valley. Further, apart from the Masons/Construction Technicians, a total of 104 Self Builders have been trained in Kathmandu Valley [6]. Furthermore, they should have competencies to conduct regular inspections and safety audits, and should have the ability to avoid construction

of reduced quality buildings. Enforcement of strict building regulations are important in achieving the technological resilience specially during the construction stage [12]. From the environmental resilience perspective, protection of natural resources such as coastal barriers and zones, floodplains, wetlands and other natural resources becomes vital in disaster risk reduction [7]. National and local government bodies are the main authorities to initiate theses action and they should always have the competencies to ensure that the construction procedures align with the sustainable principles. In enhancing the economic resilience of the built environment, the local governments should encourage the utilization of local materials and skills, and low-tech, low-cost technologies which are embedded in the indigenous knowledge and skills of the communities. This will positively contribute in upgrading the economic resilience of the local communities (National Disaster Management Authority—Government of India [14]. Finally, in establishing the institutional resilience of the built environment Local and National governments have a responsibility in establishing and implementing, suitable systems and instruments monitor the effectiveness and the efficiency of the available laws and regulations.

3.2 Competency Requirements of Community

National Disaster Management Authority—Government of India [14] emphasizes that in order to enhance the social resilience of the community's adoption of community-inclusive risk reduction and building practices is important. Such practices will positively contribute to rebuild the healing process after a hazardous event. In additional to this social aspect this will uplift the economic resilience of the local communities as well. Mannakkara and Wilkinson [12] further contributes to this point from the technological perspective whereas these local labour forces utilized must be given the due supervision and support from trained personnel would give more confidence and enhance the quality and productivity of the output. Furthermore, the structural changes necessary to embed disaster resilient aspects into the construction will be more successful if the community and other relevant stakeholders are made aware of the implications and trained on how to adopt them. From an environmental perspective taking environmental protective measures during the construction process will reduce the risk of future disasters and allows the environment to maintain the natural capacity to withstand disasters. Furthermore, these contributes to achieve the other sustainability aspects such as wildlife and open life preservation. After a hazardous situation normally the reconstruction works will mainly focus in withstanding the specific disaster that was experienced which will could increase the vulnerabilities to other disasters. Commonly adopting these practices reduce this risk as well [10]. In upgrading the economic resilience of communities during the construction stage of a project other than providing employment opportunities for the local communities allowing them loans and grants to build disaster resilient

homes, businesses and public facilities is also necessary [7]. In terms of the institutional resilience providing proper training and education is a key in encouraging solid resilience measures such as structural changes.

3.3 Competency Requirements of NGOs, INGOs and Other International Agencies

NGOs, INGOs and other International agencies are known to import construction work force specially for the post disaster reconstruction works. In terms of the technological resilience Mannakkara and Wilkinson [12] argues that while some of these parties maintain high standards of work quality some fail in achieving the expected standards in the structures due to the lack of awareness about local guidelines and regulations. One such incident was the poor quality of the reconstructions after the tsunami reconstruction in Sri Lanka (GoSL and UN, 2005 cited [12]. However, by providing the disaster training and the required skills to the construction workers NGOs, INGOs and other International agencies can play a major role to uplift the technological resilience of the built environment (National Disaster Management Authority—Government of India [14]. In terms of the economic perspective, the wellbeing of the local companies and businesses also should be looked after by NGOs, INGOs and other International agencies in the reconstruction projects led by them. Therefore, with the local materials and labour the involvement of the companies are also important for these local businesses to sustain. In the projects funded by NGOs, INGOs and other International agencies they should ensure that disaster resistant features are incorporated in the actual construction. This could be done through regular supervision of construction process as well as providing training and education to owners/contractors. Conducting awareness campaigns on safe construction has also been stressed by National Disaster Management Authority—Government of India [14].

3.4 Competency Requirements of the Academic Sector

Academia and research organisations have a role to play in terms of the empowering the built environment with the new findings and knowledge relating to early warning systems, temporary retrofitting to buildings and awareness to disaster and preparedness. The research organisations which tend to be government based create the foundation for this knowledge transfer by supplementing academic research of universities. The academia needs to transfer this knowledge to the construction professionals and the built environment stakeholders and also facilitate the development of regulations and standards through the constant evolution of construction techniques and innovation.

3.5 Competency Requirements of the Private Sector

The private sector is a major player in the construction industry globally. Especially in funding the disaster resilient aspects the private sector has a major role to play in the absence of sufficient funding from the public authorities. Establishing the new technologies related to early warning systems, temporary retrofitting to buildings and awareness to disaster and preparedness is a main necessity that needs to be initiated with the contribution from the private sector. In enhancing the technological resilience of the built environment, a reference Manual is published by the United Nations development program regarding the disaster resistant construction practices. This indicate alterations and good practices to be conducted during construction of a building to holdup against disasters like Tsunami and earthquakes [17]. Regarding the economic resilience aspect, the necessity is to obtain value for money. In reducing the cost of construction, the quality of the structures could be compromised leading to heavy risk of unanticipated failures during a natural disaster. Therefore, the private sector has a role in identifying the optimal designs that provide value for money with the required quality within the funding constraints. The construction works heavily contribute to the environmental pollution and according to the data is responsible for about 4% particulate emissions, more water pollution incidents than any other industry [5] Therefore, the environmentally friendly practices should be followed in the construction practices so that the risk of potential future disasters could be reduced. In ensuring the institutional resilience the communication channels between key construction and emergency management personnel need to be established well. In the circumstances of an emergency situations the emergency service access options are considered and that up to date and secure building schematics must be made available to the emergency services as projects progress [4].

4 Conclusions

Integration of the notion of 'resilience' to the sustainability agenda is vital to achieve long last sustainability. However, in achieving these, the built environment stakeholders should have particular competencies under different resilience aspects (social resilience, technological resilience, economic resilience, environmental resilience and institutional resilience). There are key different built environment stakeholders and it is vital to identify the competency requirements of these key stakeholders under the above-mentioned resilience aspects. For example, a built environment professional who got adequate competencies on resilient aspects will ensure to build with robust Materials: Some of the qualities of robust building materials include versatility, strength, wind and water resistance, tsunami resistance, fire resistance, energy efficiency and durability [15]. Accordingly, identifying these competency requirements will enable built environment professionals to improve themselves and

it will support the built environment stakeholders to achieve resilience in construction projects and through that ensure construction projects are sustainable not only in the triple bottom line of social, economic and environment, but, sustainable in terms of the 'resilient' aspect as well.

Acknowledgements "This project has been funded with support from the European Commission. This publication [communication] reflects the views only of the author, and the Commission cannot be held responsible for any use which may be made of the information contained therein".

References

1. Ahn YH, Pearce AR, Wang Y, Wang G (2013) Drivers and barriers of sustainable design and construction: the perception of green building experience. Int J Sustain Build Technol Urban Dev 4(1):35–45
2. Amaratunga D, Haigh R, Malalgoda C, Keraminiyage K (2017) Mainstreaming disaster resilience in the construction process: professional education for a resilient built environment: a report of the CADRE project: Collaborative Action towards Disaster Resilience Education
3. Amaratunga D, Malalgoda CI, Keraminiyage K (2018) Contextualising mainstreaming of disaster resilience concepts in the construction process. Int J Disaster Resil Built Environ 9(4/5):348–367
4. Bosher L (2014) Built-in resilience through disaster risk reduction: operational issues. Build Res Inf 42(2):240–254
5. Dietz T, York R, Rosa EA (2001) Ecological democracy and sustainable development. Paper presented at the open meeting of the human dimensions of global environmental change research community, Rio de Janeiro, Brazil
6. Earthquake Safe Communities in Nepal (2019) Disaster News on Nepali Media NSET On Social Media Facebook Youtube Feeling the Risks : A Video Do
7. FEMA (2011) National disaster recovery framework: strengthening disaster recovery for the nation. http://www.fema.gov/pdf/recoveryframework/ndrf.pdf
8. Ginige K, Amaratunga D, Haigh R (2010) Developing capacities for disaster risk reduction in the built environment: capacity analysis in Sri Lanka. Int J Strateg Prop Manag 14(4):287–303
9. Hussin JM, Rahman IA, Memon AH (2013) The way forward in sustainable construction: issues and challenges. Int J Adv Appl Sci 2(1):15–24
10. Kennedy J (2009) Disaster mitigation lessons from build back better following the, 26 December 2004 Tsunamis. In: Ashmore J, Babister E, Kelman I and Zarins J (eds) Water and urban Development paradigms, Taylor and Francis Group, London, pp 297–302
11. Malalgoda C, Amaratunga D, Keraminiyage K, Haigh R (2016) Knowledge gaps in the construction industry to increase societal resilience: a local and national government perspective: Tampere University of Technology. Department of Civil Engineering
12. Mannakkara S, Wilkinson S (2013) 'Build back better' principles for land-use planning. Proc Inst Civ Eng-Urban Des Plan 166(5):288–295
13. Marchese D, Reynolds E, Bates ME, Morgan H, Clark SS, Linkov I (2018) Resilience and sustainability: similarities and differences in environmental management applications. Sci Total Environ 613:1275–1283
14. National Disaster Management Authority India (2010) National and local governments roles and responsibilities. https://ndma.gov.in/en/
15. Peng T, Lemay L (2014) Concrete building systems: disaster resilient solutions for safer communities. Homel Secur Rev 8:41
16. Satterthwaite D (2013) The political underpinnings of cities' accumulated resilience to climate change. Environ Urban 25(2):381–391

17. UNDP (2006) Disaster resistant construction practices: a reference manual. Retrieved from
18. UNISDR (2017) Terminology. https://www.unisdr.org/we/inform/terminology-letter-r
19. Waldt G, Khalo T, Nealer E, Phutiagae K, van der Walt C, van Niekerk D, Venter A (2007) Municipal management: serving the people. Juta and Company Ltd., Cape Town
20. Zhang X, Li H (2018) Urban resilience and urban sustainability: what we know and what do not know? Cities 72:141–148

Review on Geosynthetic Inclusions for the Enhancement of Ballasted Rail Tracks

S. Venuja, S. K. Navaratnarajah, C. S. Bandara, and J. A. S. C. Jayasinghe

Abstract Currently, there is an increasing demand for rail transport from a growing and urbanizing population worldwide as it is a resource-efficient transport system. Moreover, its popularity among people is due to safety, reliability and economic profit. The rail track system consists of rails, fastening systems, sleepers, ballast, sub-ballast and subgrade. Ballast is a highly angular coarse granular material which is the major load-bearing component as it transmits the stresses exerted by moving trains from sleepers to the subballast and subgrade at a reduced level. Ballast degradation is a major problem caused by the high dynamic and cyclic loads from faster and heavier trains as well as the impact loads due to wheel and rail irregularities and tracks at stiffness transition zones. It affects the track longevity together with the track geometry thereby a necessity of regular monitoring and maintenance. Ballast fouling is accompanied by ballast degradation as the broken ballast particles intrude into the voids of the ballast layer and obstruct the drainage. The popular method to reduce the excessive ballast deformation and degradation is the inclusion of geosynthetics such as geogrids, geotextiles, geocomposites, and geocells to the track foundation. This paper provides an extensive review of past studies on geosynthetics to reinforce the track foundation. In conclusion, this review presents the limitations of existing studies and provides recommendations for further studies.

Keywords Rail track · Ballast · Degradation · Ballast fouling · Geosynthetics

1 Introduction

The rail track system is divided into two parts: (i) Superstructure consisting of rail, fastening systems, ties or sleepers; (ii) Substructure consisting of ballast, sub-ballast or capping and compacted subgrade base or a concrete base. Ballast is divided into four subdivisions as crib, shoulder, top ballast, and bottom ballast. Short-term and

S. Venuja (✉) · S. K. Navaratnarajah · C. S. Bandara · J. A. S. C. Jayasinghe
Department of Civil Engineering, Faculty of Engineering, University of Peradeniya, Peradeniya 20400, Sri Lanka
e-mail: venujas@eng.pdn.ac.lk

R. Dissanayake et al. (eds.), *ICSECM 2019*, Lecture Notes in Civil Engineering 94,
https://doi.org/10.1007/978-981-15-7222-7_38

long-term deformations of the ballasted rail tracks depend on the substructure components' characteristics. Ballast degradation is high under stiff subgrade conditions and heavy cyclic loads which affects the track stability and longevity [11, 15]. It also leads to increased maintenance costs, speed restrictions, track and vehicle component failures, stoppage and delays [4, 14].

One of the most widely used techniques in reducing ballast degradation is the inclusion of geosynthetic material to the track foundation. There are planar (geogrids, geotextiles, and geocomposites) and cellular layers (geocells) that are extensively adopted in the improvement of ballast performance. In this review paper, many past studies on geosynthetic enhancement of ballasted rail tracks were comprehensively reviewed.

2 Ballasted Rail Tracks

Conventional ballasted tracks and slab tracks are the two types of tracks extensively used nowadays as illustrated in Fig. 1. Even though the slab tracks have a longer lifespan compared to ballasted tracks, their initial construction and repair costs are much higher. Therefore the ballasted tracks are the most preferred [1]. In ballasted tracks, the ballast layer is the largest component in the substructure and it includes

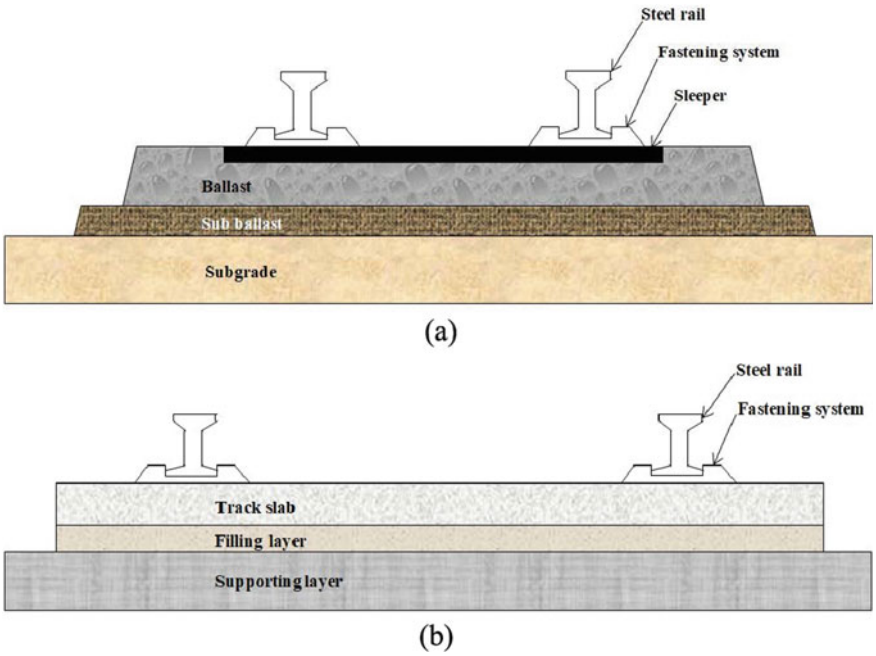

Fig. 1 Schematic diagram of **a** Ballasted rail track; **b** slab rail track

dolomite, rheolite, gneiss, basalt, granite, limestones, recycled slag and quartzite [4, 9]. Key functions of the ballast layer are but not limited serving as a bed to the rail tracks, maintains the gauge between sleepers thus alignment of the rails, providing track and substructure stability, drain out water quickly and barrier the growth of vegetation [2, 14]. Performance of the ballast depends on the strength and type of the parent rock, aggregate shape and size distribution, hardness and toughness, specific gravity and load cycles [9, 13, 19]. Anbazhagan et al. [2] critically analyzed the optimum ballast gradation which takes high shear strength (well-graded) and high permeability (uniformly graded) into consideration.

Ballast degradation is normally caused by particle breakage, abrasion, finer particles intrusion and contamination and, it reduces the shear strength and stiffness thereby high compressibility [15, 20]. The higher rate of ballast degradation and lateral spreading of the ballast occur due to repeated heavier and faster trains [16, 21]. The degradation of ballast depends on the load cycles, aggregate gradation, angularity and fracture strength of each particle and track confining pressure [9]. Ballast settlement can be either elastic which is an initial settlement due to the compaction of ballast or plastic where settlement is due to the densification and breakage of ballast particles.

Consequences of ballast degradation are track settlement and instability, poor track geometry, reduction in track longevity, poor drainage, necessity of regular monitoring and maintenance, involving cost and time consuming remedial actions such as stone blowing and ballast renewal [4, 11, 18]. Therefore, it affects safety, comfort, reliability, availability, speed and overall railway performance.

3 Geosynthetic Reinforcement

Generally, the major portion of the track maintenance cost is due to ballast degradation, poor drainage, track settlement and misalignment [17]. For nearly 30 years, geosynthetics are used for the improvement of railway tracks. Typically, geosynthetics are used as a separation layer between ballast and sub-ballast or subgrade layers in order to prevent ballast contamination through the intrusion of finer particles from the bottom layer. As shown in Fig. 2, there are various types of two dimensional or planar and three dimensional or cellular geosynthetics that are accessible based on the applications.

3.1 Past Experimental Studies

Railway tracks reinforced with geosynthetics were experimentally analyzed by many researchers (Biabani et al. [3], Fattah et al. [5], Horníček et al. [6], Indraratna et al. [8], Indraratna and Nimbalkar [10], Ngo et al. [18], Ngo and Indraratna [17] and Sweta and Hussaini [22]). The conventional design of railroad tracks concentrates more on

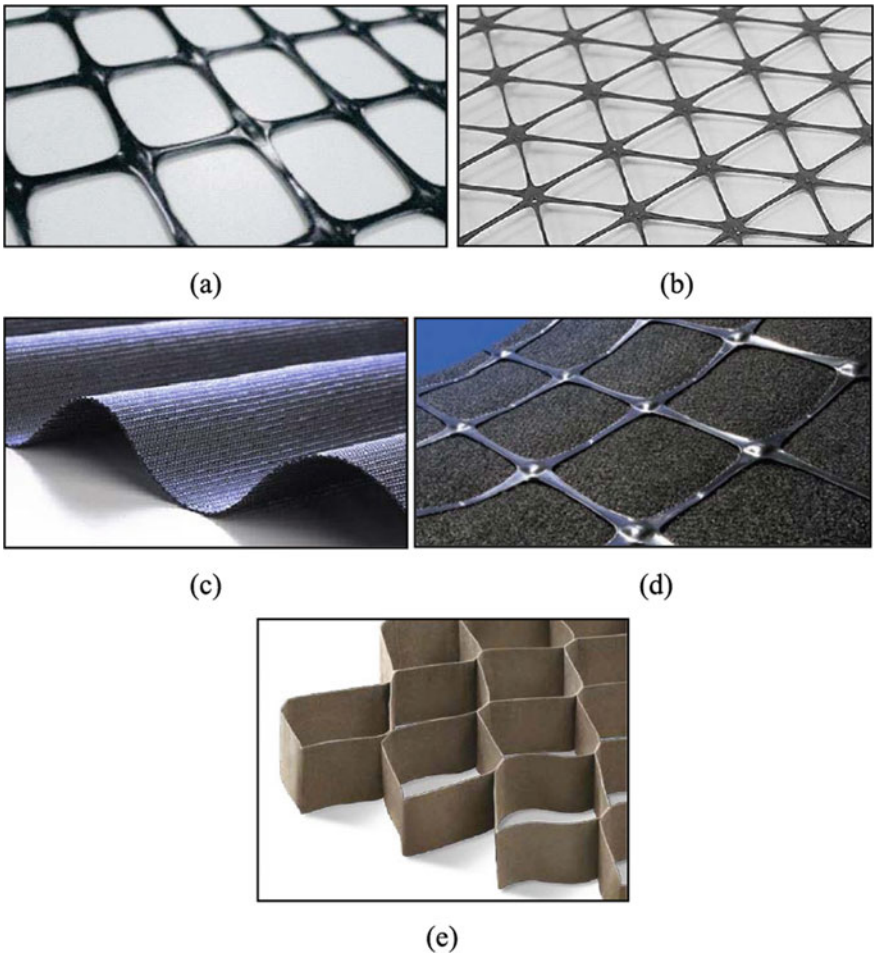

Fig. 2 Types of geosynthetics **a** Biaxial Geogrid; **b** triaxial Geogrid; **c** geotextile; **d** geocomposite; **e** geocell

the design of track superstructure while that pays little attention to the design of track substructure. It also considers quasi-static loading and too uniform particle sizes thus neglecting cyclic, impact loadings and particle sizes, shapes and subsequent particle breakage, respectively [10].

Large scale direct shear test is adaptable to analyze the behavior of ballast and geosynthetic [8, 17, 18] or sub-ballast and geosynthetic [3, 10, 22] or subgrade and geosynthetic interfaces [6] according to the location of the geosynthetic as indicated in Fig. 3. Ngo et al. [18] analyzed the interface behavior of ballast and geogrid using biaxial and triaxial geogrids with different aperture sizes where the geogrid was placed at the interface between the upper and lower shear boxes which are filled

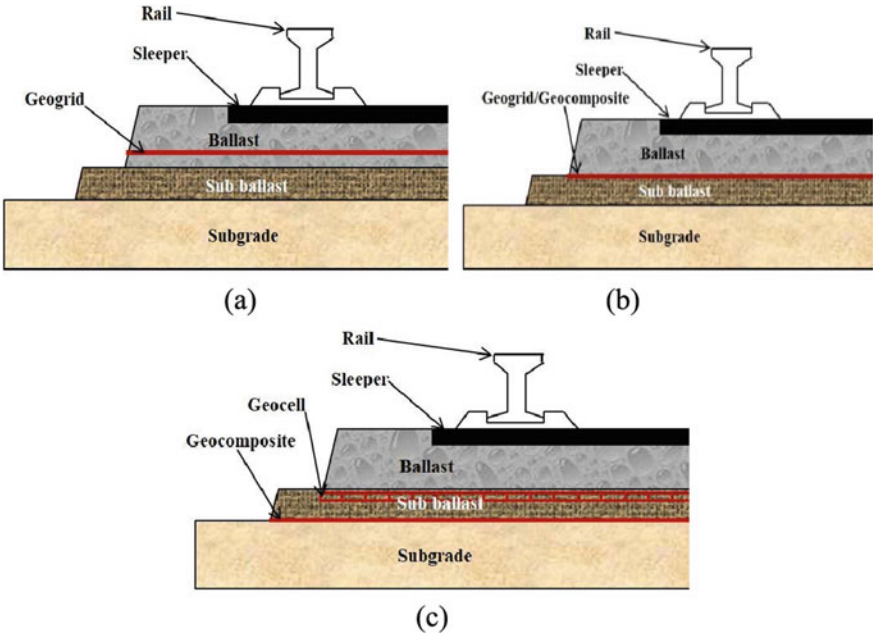

Fig. 3 Geosynthetic inclusion **a** Inside the ballast layer; **b** between ballast and sub-ballast layers; **c** combination

with ballast, along the shearing direction. This research came up with the conclusions of (i) Triaxial geogrids (Fig. 2b) that are not that much efficient compared to biaxial geogrids (Fig. 2a) in enhancing the performance of granular ballast particles through mechanical interlocking. It is because of the smaller triangular apertures where ballast particles not get complete interlocking and get a slippery plane, (ii) Geogrids prevent the free movement of ballast particles through mechanical interlocking as illustrated in Fig. 4. On the other hand, Sweta and Hussaini [22] studied the effect of normal stress and shearing rate on the interface shear behavior of the ballast and sub-ballast interface with and without the inclusions of biaxial and triaxial geogrids with various aperture sizes and shapes. The equivalent aperture sizes of rectangular geogrids are the square root of the aperture area where for triangular geogrid is the diameter of the largest inscribed circle inside the aperture. The outcomes of this study are (i) geogrid inclusion at the ballast and sub-ballast interface that reduces the extent of dilation for different normal stresses and shearing rates, (ii) the increase in the normal stress as well as in the shearing rate that reduces the shear strength, the friction, and dilation angle at the ballast and sub-ballast interfaces for both geogrid-reinforced and unreinforced conditions. This is because of the ballast breakage and quicker sliding of the ballast particles, respectively. Further, Biabani et al. [3] investigated the effect of normal stress, rate of shearing, relative density and open area on the interface behavior of sub-ballast reinforced with different types of geocells and geogrids. This study encountered the following closures: The aperture shape and size

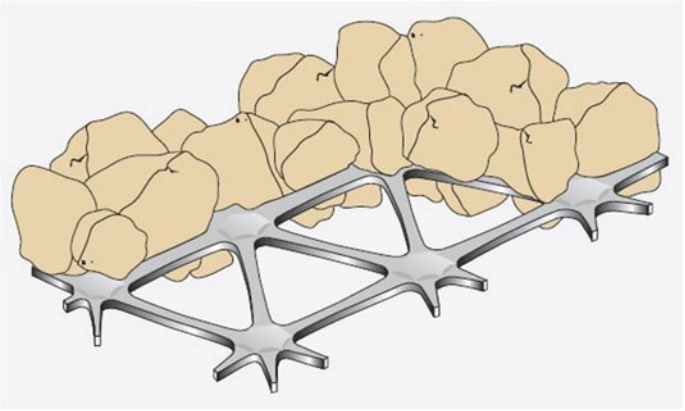

Fig. 4 Mechanical interlocking of ballast particles into apertures of triaxial geogrid

affect the performance of the granular material. Higher shearing rate leads to faster particle rearrangement and densification thereby decreases the interface coefficient. Frictional resistance reduces with the increase in the open area of the reinforcement. The triaxial geogrids provide more passive resistance than biaxial geogrids due to the effectiveness of transverse ribs thus maximum performance improvement was obtained for sub-ballast reinforced with triaxial geogrid. Geocells give much better lateral confinement than planar geo-inclusions as it provides maximum interface shear resistance.

Cyclic loading tests are used to analyze the degradation behavior of ballast under cyclic loads. Ngo et al. [18] studied vertical and lateral deformation of geogrid-reinforced and unreinforced ballast under 420 kPa cyclic stress and 15 Hz frequency up to 500,000 load cycles. There was a rapid settlement in the ballast observed at the initial load cycles due to the particle rearrangement and densification, and the settlement became marginal after a certain number of cycles.

Geogrids resist the lateral movement of ballast thus it can be used as a non-horizontal boundary. Geogrids reduce the ballast breakage through reducing the pressure at the ballast layer by interlocking the particles into the apertures. Further, the highest efficiency of geogrid reinforcement was obtained when the geogrid was placed at a 1/3 height of ballast layer thickness, from the interface of ballast and capping layers. But there are practical issues when the maintenance activities are taking place. Geogrids interfere with the removal of used ballast and placing of fresh ballast using machinery. Thus, it is advisable to place the geogrids at the ballast and capping layer interface considering the convenience during the track maintenance. Indraratna and Nimbalkar [10] investigated the degradation behavior of granular layers and their developments using planar and cellular geo-inclusions. The planar geosynthetic (geogrid, geotextile, and geocomposite) was placed at the ballast and sub-ballast interface. Ballast stabilized with geocomposite resulted in low vertical strain followed by geogrid and geotextile stabilization as well as more effective

in reducing the ballast breakage. Cyclic loading test was also conducted for the sub-ballast reinforced with geocell. Geocell can be more effective at low confining pressures and at high frequencies by confining the infill soil into its pockets.

Indraratna et al. [8] examined the performance of a fully instrumented field track with various types and aperture sizes of geosynthetics and various subgrade conditions. Track sections constructed with both fresh and recycled (used) ballast were tested in this study. Outcomes of this research are: (i) geocomposite inclusion for fresh as well as recycled ballast reduced the vertical and lateral deformations of the track through interlocking the ballast particles into the apertures, (ii) lateral deformation of ballast was higher at the crest and it always occurs spreading the particles outwards, and (iii) geogrids were more effective for the soft subgrade condition in comparison with hard rock base. Horníček et al. [6] also conducted field tests such as static plate load tests and impact plate load tests for the period of 2.5 years on the real rail track reinforced with geocomposite between ballast and subgrade. It was observed that the rail seat level at reinforced track section has a higher load-bearing capacity than the unreinforced section and there was a reduction in rail deflection, therefore, improved riding comfort and lower wear of the track components. Further, the optimum aperture of the geogrid when inserted into the ballast is 1.2 times d_{50} [7, 12, 18]. Geocomposite acts as both reinforcement and separation layer when installing at the ballast and the sub-ballast interface. It prevents the movements of fines from sub-ballast layer into the voids in the ballast layer, such that it reduces the ballast fouling as well.

3.2 Past Numerical Studies

Discrete type elements are used in modeling the ballast layer as ballast is a coarse granular particle as shown in Fig. 5. Discrete Element Modeling (DEM) was introduced by Cundall and Strack in 1979. Ngo et al. [18] discussed some previously generated *DEM*s and their outcomes in detail. They simulated *DEM* with large scale direct shear test results to study the interface mechanism between geogrid and ballast using a micromechanical analysis. They validated their model in capturing the shear stress-strain behavior of both unreinforced and reinforced ballast by comparing the stress-strain curves obtained from laboratory tests and model analysis. They mentioned that the strain behavior of geogrids could be studied using *DEM* analysis, which could not be measured from experimental analysis due to the complexity of strain gauge installation. They also analyzed the significance of the coordination

Fig. 5 Ballast particles modeled using DEM

number and the contact force orientations on the shear strength behavior of granular materials.

Fattah et al. [5] used *PLAXIS 3D* software to conduct the numerical analysis of geogrid reinforced ballast. The previously available numerical analysis methods such as Composite Element Test, the *ABAQUS* model, ballast track settlement prediction model and aggregate imaging-based *DEM* were also discussed individually. Hardening soil, Mohr-Coulomb, Linear elastic and Elastic material models were used for clay, ballast, timber sleeper also steel rail and geogrid, respectively. This research concluded that the settlement behavior is depended on the aggregate shape, gradation, thickness and the initial density of the ballast layer.

4 Conclusions and Recommendations

Geosynthetic reinforcements are more beneficial for tracks on soft subgrades as it provides a marginal improvement in the ballast performance on hard base condition. The behavior of geosynthetic-stabilized ballast depends on normal stress, rate of shearing, type of geosynthetic (also aperture shape and size) and relative density. Recycled ballast could be used in the rail tracks with geosynthetic reinforcement thus reduce the necessity for the new ballast. Geocells provide more confinement than planar geo-inclusions and perform well at low confining and high-frequency conditions. Geocomposite provides ballast confinement and barrier the fine particles intrusion from the subgrade to the ballast layer. Optimum location of geogrid derived as 2/3 of the ballast thickness, depth from the bottom of the sleeper and the optimum aperture size of geogrid is 1.2 times of d_{50}.

There are many journal publications that examined the effect of geo-inclusions for only a few ballast gradations. It is not readily applicable to other countries that are using different ballast gradations. Therefore, it is recommended to analyze the effectiveness of geosynthetic enhancement with different ballast gradations as well as installing these geo inclusions at different positions of track foundation. Blasting of rock to obtain ballast material is a big concern nowadays due to the air and noise pollution, also a scarcity of parent rocks because of frequent quarrying. Therefore, studies could be conducted in analyzing the reuse of used ballast materials with geosynthetic reinforcements into the railway applications. It also leads to a reduction in land use of ballast disposal sites. Moreover, it is suggested to examine the benefits of a few layers of geosynthetic inclusions (more than one layer, also different types of geosynthetics) into the track substructure. Most of the past numerical studies considered only the elastic behavior of ballast. Thus a numerical model could be developed incorporating elasto-plastic behavior of ballast in *ABAQUS* software to validate using experimental outcomes. This will help to perform a parametric study to understand the rail track behavior by varying different gradations of ballast and different types of geosynthetics.

Acknowledgements This research is supported by the Accelerating Higher Education Expansion and Development (AHEAD) Operation of the Ministry of Higher Education funded by the World Bank (Grant No: AHEAD/RA3/DOR/STEM/No. 63).

References

1. Al-Douri YK, Tretten P, Karim R (2016) Improvement of railway performance: a study of Swedish railway infrastructure. J Mod Transp 24(1):22–37
2. Anbazhagan P, Bharatha TP, Amarajeevi G (2012) Study of ballast fouling in railway track formations. Indian Geotech J 42(2):87–99
3. Biabani MM, Indraratna B, Nimbalkar S (2016) Assessment of interface shear behaviour of sub-ballast with geosynthetics by large-scale direct shear test. Procedia Eng 143:1007–1015
4. Chan CM, Johan SFSM (2016) Performance enhancement of railtrack ballast with rubber inclusions: a laboratory simulation. Japan Geotech Soc Spec Publ 2(47):1640–1643
5. Fattah MY, Mahmood MR, Aswad MF (2018) Experimental and numerical behavior of railway track over geogrid reinforced ballast underlain by soft clay. International Congress and Exhibition "Sustainable civil infrastructures: innovative infrastructure geotechnology", pp 1–26
6. Horníček L, Břešťovský P, Jasanský P (2017) Application of geocomposite placed beneath ballast bed to improve ballast quality and track stability. IOP Conference Series: Materials Science and Engineering. IOP Publishing, pp 1–8
7. Indraratna B, Hussaini SKK, Vinod JS (2011) On the shear behavior of ballast-geosynthetic interfaces. Geotech Test J 35(2):305–312
8. Indraratna B, Navaratnarajah SK, Nimbalkar S, Rujikiatkamjorn C, Neville T (2015) Performance monitoring—case studies of tracks stabilised by geosynthetic grids and prefabricated vertical drains. In: FMGM 2015. Sydney, pp 233–246
9. Indraratna B, Ngo N, Nimbalkar S, Rujikiatkamjorn C (2018) Two decades of advancement in process simulation testing of ballast strength, deformation, and degradation. In: Railroad Ballast Testing and Properties. ASTM International, pp 11–38
10. Indraratna B, Nimbalkar S (2016) Improved behaviour of railway track substructure using 2D (planar) and 3D (cellular) geo-inclusions. In: CORE 2016: Maintaining the Momentum, pp 522–531
11. Indraratna B, Nimbalkar S, Navaratnarajah SK, Rujikiatkamjorn C, Neville T (2014) Use of shock mats for mitigating degradation of railroad ballast. Geotech J 6:32–41
12. Indraratna B, Nimbalkar S, Neville T (2014b) Performance assessment of reinforced ballasted rail track. In: Proceedings of the ICE: Ground Improvement, pp 24–34
13. Koohmishi M, Palassi M (2020) Degradation of railway ballast under compressive loads considering particles rearrangement. Int J Pavement Eng 21(2):1–13
14. Navaratnarajah SK, Indraratna B (2017) Use of rubber mats to improve the deformation and degradation behavior of rail ballast under cyclic loading. J Geotech Geoenviron Eng 143(6):1–15
15. Navaratnarajah SK, Indraratna B (2018) Application of under sleeper pads to enhance the sleeper-ballast interface behaviours. IGC. Bengaluru, pp 1–8
16. Navaratnarajah SK, Indraratna B, Nimbalkar S (2015) Performance of rail ballast stabilized with resilient rubber pads under cyclic and impact loading. In: ICGE. Colombo, pp 617–620
17. Ngo NT, Indraratna B (2016) Improved performance of rail track substructure using synthetic inclusions: experimental and numerical investigations. Int J Geosynthetics Ground Eng 2(3):1–16
18. Ngo NT, Indraratna B, Bessa Ferreira F, Rujikiatkamjorn C (2018) Improved performance of geosynthetics enhanced ballast: laboratory and numerical studies. Proceedings of the Institution of Civil Engineers - Ground Improvement 171(4):202–222

19. Sadeghi J, Emad Motieyan M, Ali Zakeri J (2019) Development of integrated railway ballast quality index. Int J Pavement Eng 1–9
20. Stark TD, Swan RH, Yuan Z (2014) Ballast direct shear testing. In: Joint Rail Conference. USA, pp 1–10
21. Sun Q, Indraratna B, Nimbalkar S (2016) An elasto-plastic method for analysing the deformation of the railway ballast. Procedia Eng 143:954–960
22. Sweta K, Hussaini SKK (2019) Behavior evaluation of geogrid-reinforced ballast-subballast interface under shear condition. Geotext Geomembr 47(1):23–31

Finite Element Modelling of Wall Panels Under Standard and Hydrocarbon Fire Conditions

I. R. Upasiri, K. M. C. Konthesingha, K. Poologanathan, S. M. A. Nanayakkara, and B. Nagaratnam

Abstract Fire is one of the severe conditions in which structures may be exposed during their life span. When considering the structural elements, wall panels play a vital role during a fire scenario, since the spreading of the fire could be either controlled or accelerated due to the type of the wall partition. Standard fire tests are generally used to evaluate the fire performance of structural elements. However, the fire tests are expensive and time consuming to carry out. Therefore, numerical methods have been developed to evaluate the fire performance of these structural elements. In this study ABAQUS, finite element software was used to model the fire performance of lightweight foamed concrete and normal weight concrete wall panels. Experimental results of the previous studies were used to validate the models. Parametric studies were conducted using the developed models to evaluate the fire performance of two different types of wall panels under standard and hydrocarbon fire conditions. Lightweight foamed concrete wall panels exhibited better fire performance compared with the normal weight concrete wall panels. Three to five times of fire performance enhancement under insulation criteria could be obtained for wall panels of different thicknesses, by replacing normal weight concrete wall panels with lightweight foam concrete wall panels.

Keywords Fire · Finite element method · Wall panels · Normal weight concrete · Light-weight concrete · ABAQUS

I. R. Upasiri (✉) · K. M. C. Konthesingha
University of Sri Jayewardenepura, 41 Lumbini Ave, Dehiwala-Mount Lavinia, Sri Lanka
e-mail: irinduupasiri@gmail.com

K. Poologanathan · B. Nagaratnam
Northumbria University Newcastle, Northumbria University, Ellison Building ELB117, Newcastle upon Tyne NE18ST, UK

S. M. A. Nanayakkara
University of Moratuwa, Katubedda, Moratuwa, Sri Lanka

R. Dissanayake et al. (eds.), *ICSECM 2019*, Lecture Notes in Civil Engineering 94,
https://doi.org/10.1007/978-981-15-7222-7_39

1 Introduction

Statistical data on fire loss states that thousands of lives and millions of property are lost each year due to structural fire damages [1]. Shanghai Fire (2010), Grenfell Tower Fire (2017), Brazil National Museum Fire (2018) and Paris Notre-Dame Fire (2019) are few of the structural fires that shaken the world humanity in the recent past. Structures undergo higher temperature variation in a fire situation where the stability of the structural elements tend to weaken [2]. Therefore fire safety of the structure is important in the designing process to withstand the destructive effects of fire [3]. According to the cause of fire generating, the structural fire could be categorized as accidental fires, arson fires, terrorist attack fires, and natural disaster fires. Generally, accidental fire is considered in designing a structure to a fire situation [4]. Fire safety of a structural member is rated according to the insulation, integrity, and load-bearing criteria [5]. Insulation criteria measure the temperature rise in the unexposed surface and integrity criteria checks the ability to prevent the fire spreading to adjacent compartments while load-bearing criteria assess the ability of the structural element to bear the loading without collapsing during a fire [4]. According to the International Organization for Standardization's guidelines [6], standard fire test insulation criteria are limited to an average temperature rise of 140 K in the unexposed surface. Integrity criteria are measured as per the ignition of the cotton pad held close to an opening for 10 s. Load bearing criteria are assessed limiting the downward deformation of the flexural member to $L/30$ where L is the span of the member [7].

When a fire situation occurs in a high rise building, rapid evacuation of occupants is difficult. Therefore the spreading of fire should be controlled as much as possible. Wall panels play a vital role when it comes to the spreading of a structural fire. For instance, fire generated in one room could easily spread to the adjacent rooms through walls. Therefore fire rating of the wall panel material in a building is important. Many research has been carried out in fire safety of LSF wall system [8]; Dias et al. [7, 9–16], however, limited research has been carried out for fire performance of lightweight concrete. In this research study fire performance of non-load bearing normal weight concrete wall panels and foamed lightweight concrete wall panels were studied.

Concrete is a chemically inert particulate material consists of aggregate, cement and water [17]. Concrete is one of the most consuming construction materials due to its strength, durability, ease of fabrication and non-combustible properties. Moreover, concrete can be identified as a good fire resisting material. Low thermal conductivity, high heat capacity and slower strength degradation with temperature brands concrete as a good fire performing material [5]. Sustainability issues have caused a rise in demand for concrete with varying characteristics with regard to the nature of the application [18]. Foamed lightweight concrete is a novel type of concrete that is produced by introducing foam into cement mortar. Foam is created using a foaming agent which makes the structure cellular and therefore reduces the density [7]. Foam concrete exhibits high flowability, low self-weight, minimal consumption of aggregate, low strength and excellent thermal insulation properties [19]. While normal

weight concrete has a density of 2500 kg/m^3 foamed concrete could be produced in the density range of 400–1600 kg/m^3 [20, 21].

The simplest way of representing fire loading is a time-temperature curve. ASTM E119 and ISO 834 are the most widely used standard fire curves. Standard fire curves are important when comparing the fire performance of different materials. Apart from standard fire curves [22], considering the environmental condition, fuel availability, ventilation effects, material composition, and boundary conditions, natural and parametric fire curves are also defined [23]. In industrial facilities such as oil refineries and fuel sheds, certain units are subjected to hydrocarbon fire. Due to the high flammability of hydrocarbon gas, hydrocarbon fire is more aggressive compared to standard fire [24]. The time-temperature relationship between standard and hydrocarbon fire is given in Eqs. (1) and (2) respectively [25]. The temperature increment rate of the hydrocarbon curve is higher in the early stage. After 5 min, hydrocarbon fire achieves 940 °C while standard fire achieves only 300 °C. However, in the latter part of the fire curve, hydrocarbon fire temperature is limited to 1100 °C after 81 min, while the standard fire curve keeps increasing the temperature with time as shown in Fig. 1. Therefore materials might behave differently in these two different fire situations.

$$\theta_g = 20 + 345 \log_{10}(8t + 1) \tag{1}$$

$$\theta_g = 1080\left(1 - 0.325e^{-0.167t} - 0.675e^{-2.5t}\right) + 20 \tag{2}$$

where $\boldsymbol{\theta_g}$ is the gas temperature in the fire in Celsius and t is the time in minutes.

Conventional practice to evaluate the fire performance of a structural element is the fire tests. Due to its high cost and time-consuming drawbacks, numerical methods were developed to evaluate the fire performance of structural elements [5]. These

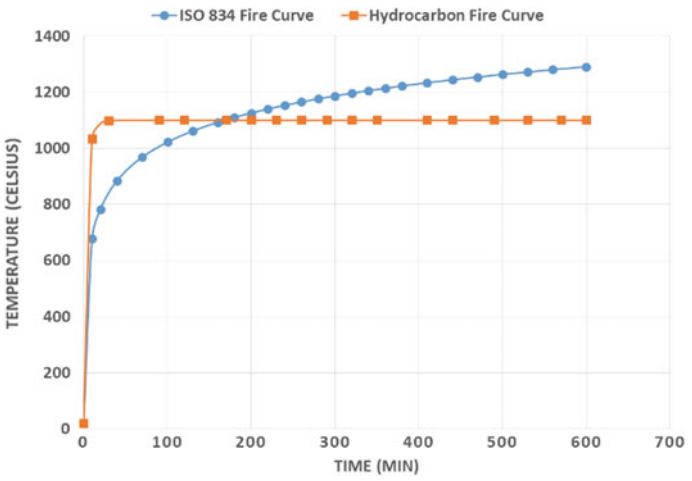

Fig. 1 Time-temperature variation of standard and hydrocarbon fire

numerical models are developed considering the variation of the material properties at elevated temperatures [7]. In this research study, thermal finite element model was developed to evaluate the fire performance of non-load bearing normal weight concrete and foamed lightweight concrete using ABAQUS finite element software based on material properties at elevated temperatures given in Euro code [26] and previous studies [27]. The model was validated with the fire test results of wall panels given in previous studies.

Then a parametric study was conducted with the validated FEM model to evaluate the fire rating of normal weight concrete and foamed lightweight concrete wall panels under standard and hydrocarbon fire situations.

2 Finite Element Modelling (FEM)

Finite element method is a powerful tool used to analyse the behaviour of structures in different loading conditions [28]. The analysis of structures in a fire situation consists of two calculation stages. In the first stage, a nonlinear thermal analysis is carried out to determine the temperature distribution. In the second stage, the variations in the deformation and stress due to changes in the material properties of the structure are calculated accordingly, and a static analysis is performed in a number of time-steps until failure [29]. The availability of material properties at elevated temperatures permits the finite element method to determine the fire resistance of the structure [5]. Since this research study focused on non-load bearing walls only, the nonlinear thermal analysis was considered to determine the temperature distribution of the wall panels during a particular time period exposed to fire.

Three-dimensional heat transfer finite element model was developed using ABAQUS finite element software package. Properties of the materials at elevated temperatures such as thermal conductivity, specific heat, and mass density were used for the material model. Fire loading was defined as the time-temperature variation and assigned as the boundary condition for the exposed surface. Unexposed surface heat loss due to convection and radiation was defined as the interaction properties of the wall. Mesh size of 0.01 m (see Fig. 2) was used to get the converged results for the analysis. The temperature distribution of the panel in each time step was obtained as the results of the analysis (see Fig. 3).

3 Elevated Temperature Material Properties

Thermal conductivity, specific heat, density, and mass loss influences the temperature rise and distribution in the structural member during a fire exposure [5]. Therefore thermal conductivity, specific heat, and density of normal weight concrete and lightweight foamed concrete at elevated temperature were used to develop the finite element model.

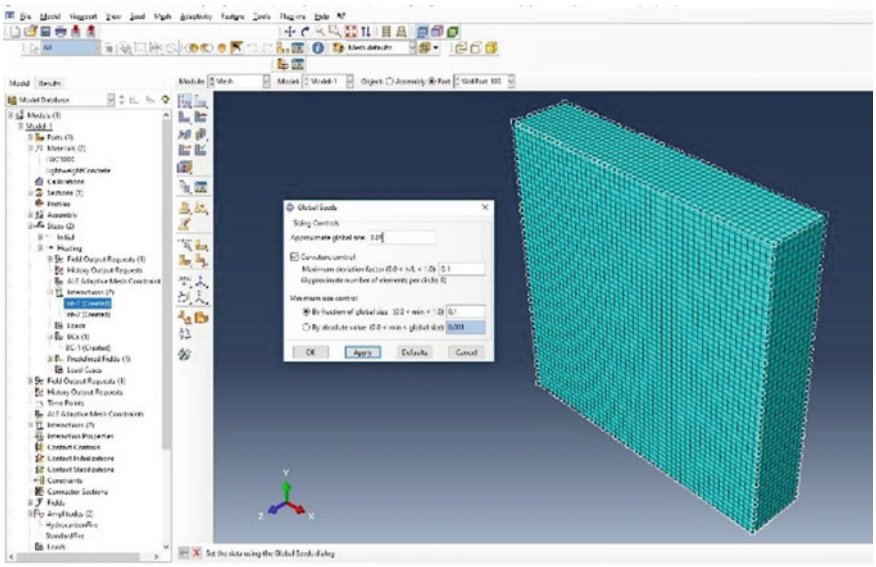

Fig. 2 Mesh (size 0.01 m) of the wall

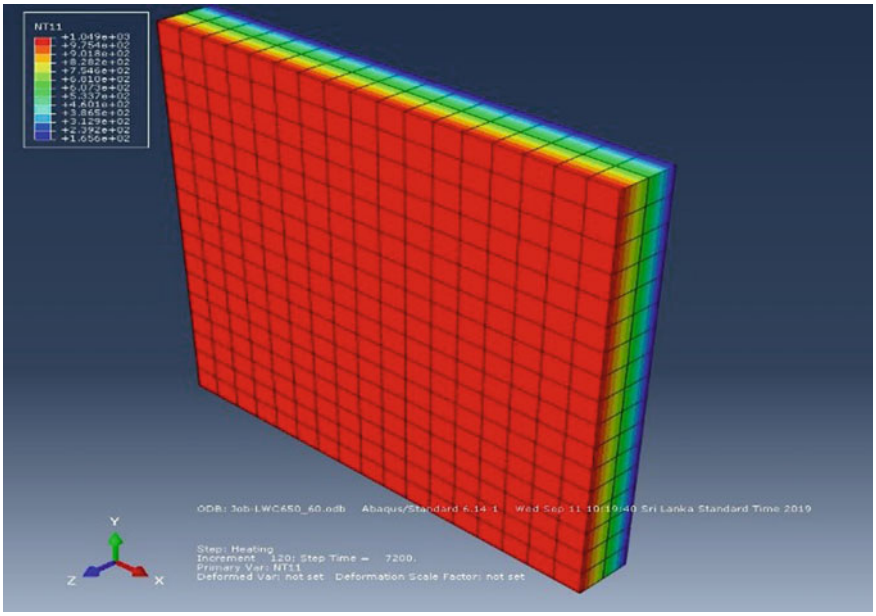

Fig. 3 Temperature distribution result of the thermal analysis

3.1 Properties of Normal Weight Concrete at Elevated Temperature

Many research studies have been carried out to measure the elevated temperature properties of concrete with different types of aggregates. In this research study, elevated temperature properties of normal weight concrete containing siliceous or calcareous aggregate were considered. Properties are given in [26]: Eurocode 2: Design of concrete structures-Structural fire design were used as given in Eqs. (3)–(11).

$$\lambda(\theta) = 2{-}0.2451\left(\frac{\theta}{100}\right) + 0.0107\left(\frac{\theta}{100}\right)^2 \text{W/m K}$$
$$for\ 20\,^{\circ}\text{C} < \theta < 1200\,^{\circ}C \tag{3}$$

$$Cp(\theta) = 900\left(\frac{\text{J}}{\text{kg}}\,\text{K}\right)$$
$$for\ 20\,^{\text{o}}\text{C} \le \theta \le 100\,^{\text{o}}\text{C} \tag{4}$$

$$Cp(\theta) = 900 + (\theta - 100)(\text{J/kg K})$$
$$for\ 100\,^{\circ}\text{C} < \theta \le 200\,^{\circ}\text{C} \tag{5}$$

$$Cp(\theta) = 1100 + \frac{\theta - 200}{2}\left(\frac{\text{J}}{\text{kg}}\,\text{K}\right)$$
$$for\ 200\,^{\circ}\text{C} < \theta \le 400\,^{\circ}\text{C} \tag{6}$$

$$\text{Cp}(\theta) = 1100(\text{J/kg K})$$
$$for\ 400\,^{\circ}\text{C} < \theta \le 1200\,^{\circ}\text{C} \tag{7}$$

$$\rho(\theta) = \rho(20\,^{\circ}\text{C})\text{kg/m}^3$$
$$for\ 20\,^{\circ}\text{C} < \theta \le 115\,^{\circ}\text{C} \tag{8}$$

$$\rho(\theta) = \rho(20\,^{\circ}\text{C}).\left(1 - \frac{0.02(\theta - 115)}{85}\right)\text{kg/m}^3$$
$$for\ 115\,^{\circ}\text{C} < \theta \le 200\,^{\circ}\text{C} \tag{9}$$

$$\rho(\theta) = \rho(20\,^{\circ}\text{C}).\left(0.98 - \frac{0.03(\theta - 200)}{200}\right)\text{kg/m}^3$$
$$for\ 200\,^{\circ}\text{C} < \theta \le 400\,^{\circ}\text{C} \tag{10}$$

$$\rho(\theta) = \rho(20\,^{\circ}\mathrm{C}).\left(0.95 - \frac{0.07(\theta - 400)}{800}\right)\mathrm{kg/m^3}$$
$$for\ 400\,^{\circ}\mathrm{C} < \theta \leq 1200\,^{\circ}\mathrm{C} \tag{11}$$

where $\boldsymbol{\lambda}$ is the thermal conductivity, $\boldsymbol{Cp(\theta)}$ is the specific heat, $\boldsymbol{\rho(\theta)}$ is the mass density and $\boldsymbol{\theta}$ is the temperature in Celsius.

3.2 *Properties of Foamed Lightweight Concrete at Elevated Temperature*

Othuman and Wang [27] in their study on properties of lightweight foamed concrete at elevated temperature, have proposed analytical models for thermal conductivity, specific heat, and density at elevated temperatures for 650 and 1000 kg/m^3 density foamed concrete. They have measured the properties up to 250 °C and considering lightweight foamed concrete as a two-phase material with solid cement and air pores thermal properties were predicted up to 1000 °C with analytical models. Further, they have done fire tests to validate their material model. In this research study, elevated temperature properties proposed by Othuman and Wang [27] were considered along with fire test results to validate the foamed light-weight concrete wall panel model in ABAQUS. Variation of thermal conductivity, specific heat, and density with temperature for normal weight concrete and lightweight foamed concrete are shown in Figs. 4, 5 and 6.

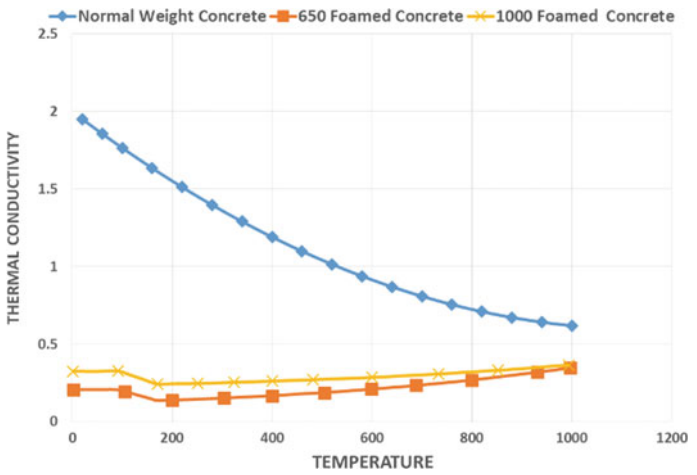

Fig. 4 Thermal conductivity variation with temperature

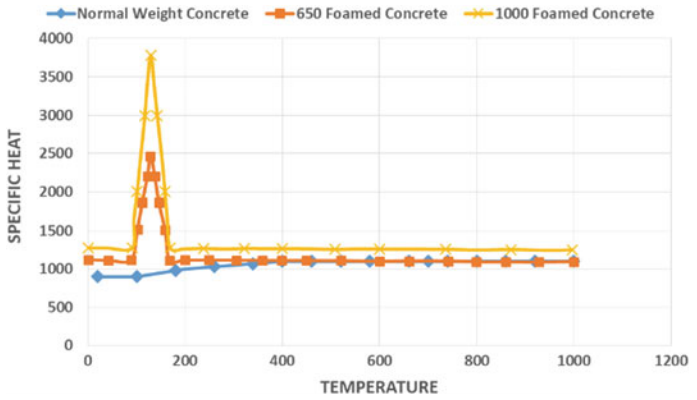

Fig. 5 Specific heat variation with temperature

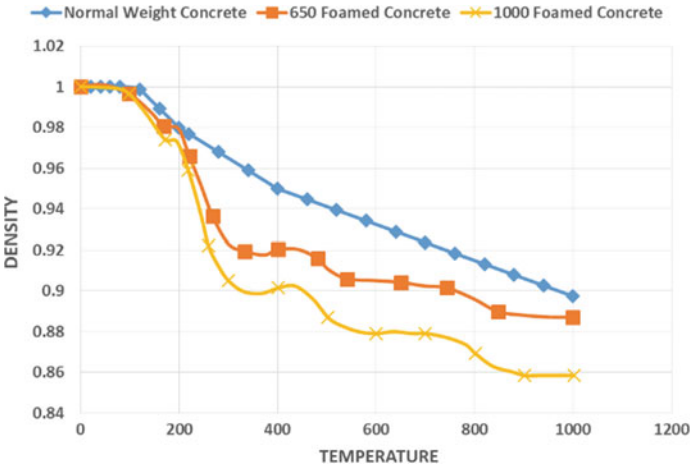

Fig. 6 Relative density variation with temperature

4 Validation of Result

ISO 834 standard fire curve was used as the fire loading in modelling of the fire performance of wall panel. Material models for thermal conductivity, specific heat and density at elevated temperature described in Sect. 3 were used in thermal analysis of wall panels under fire loading. For normal-weight concrete, unexposed surface heat loss due to convection and radiation was considered as given in the [26]. Convection coefficient 25 W/m^{2}K and emissivity factor 0.7 were used for normal-weight concrete. Foamed lightweight concrete, unexposed surface convection coefficient 10 W/m^{2}K and emissivity factor 0.92 were used as given in Othuman and Wang [27].

4.1 Normal Weight Concrete

According to the [26] fire rating of non-load bearing concrete walls of thickness 100, 120 and 150 mm were given as 90 min, 120 min, and 180 min. respectively. Normal weight concrete wall panels of thickness 100, 120 and 150 mm were analyzed using the FEM model under standard fire and obtained the unexposed surface temperature variation of each wall considered as shown in Fig. 7. According to the ISO 834 standard, the insulation fire rating was limited to the temperature rise of 140 K. Considering ambient temperature as 20 °C, the time taken to reach 160 °C temperature in the unexposed surface was calculated using the FE model developed to rate the walls under standard fire. It was found to be 90, 130 and 190 min for 100, 120 and 150 mm walls of normal weight concrete respectively. Table 1 shows the comparison of fire rating obtained from the FE model and values given in [26]. It can be seen that model predictions are very close to the values specified for the fire rating of normal weight concrete panels under the insulation criteria given in [26].

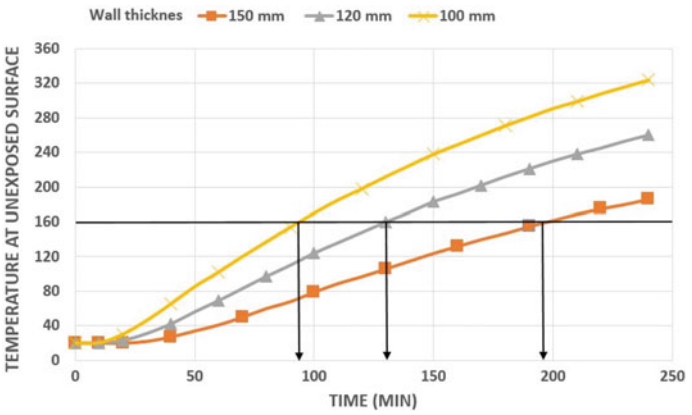

Fig. 7 Variation of temperature at the unexposed surface of a concrete wall panel under standard fire loading

Table 1 Comparison of normal weight concrete fire rating with the FE model and Euro code values

Thickness of wall panel (mm)	Fire rating	
	EN 1992-1-2 (min)	ABAQUS (min)
100	90	90
120	120	130
150	180	190

4.2 Lightweight Foamed Concrete

In the experimental investigation by Otuman et al. [27], a wall panel of 430 mm × 415 mm having thickness of 150 mm has been used for the fire testing under ISO 834 standard fire. Two-hour temperature variation across the thickness of the panel at 37.5, 75, 112.5 and 150 mm (unexposed surface) has been measured using thermocouples. A panel with similar dimensions was analyzed using the developed FE model incorporating elevated temperature material properties proposed by Othuman and Wang [27] and obtained the temperature variation across the thickness at 75, 112.5 and 150 mm (unexposed surface). Results obtained from the FE model were very close with the experimental data for the both densities of foamed lightweight concrete as shown in Figs. 8 and 9.

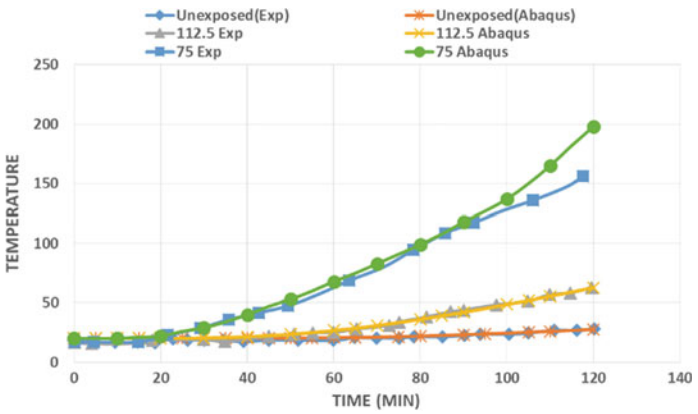

Fig. 8 650 kg/m^3 foamed lightweight concrete fire test results validation with ABAQUS

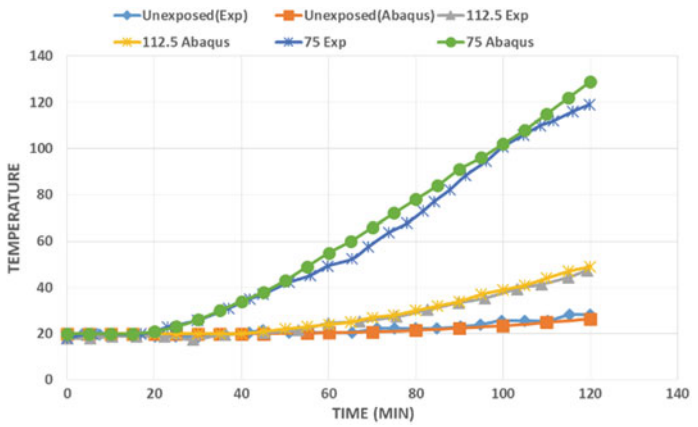

Fig. 9 1000 kg/m^3 foamed lightweight concrete fire test results validation with ABAQUS

5 Parametric Study

Different wall thicknesses of normal weight concrete and lightweight foamed concrete were analyzed under standard fire and hydrocarbon fire using the validated FE models.

5.1 Standard Fire Ratings

ISO 834 standard fire condition was used to rate the walls with different thicknesses. Since the walls are non-load bearing, only the insulation and integrity criteria need to be checked to rate the walls. According to the ISO 834 standard, an average temperature rise of the unexposed surface should be limited to 140 K. Therefore, considering the ambient temperature as 20 °C, time taken the unexposed surface temperature to rise to 160 °C was considered as the fire rating of the wall under insulation criteria.

Normal weight concrete walls, 650 kg/m^3 density and 1000 kg/m^3 density Lightweight foamed concrete walls with 30, 60, 75 and 100 mm thicknesses were modeled using ABAQUS finite element software to determine the unexposed surface temperature variation under standard fire condition. Considering the limiting temperature as 160 °C it was observed that 30, 60, 75 and 100 mm walls had a fire rating of 6 min, 30 min, 45 min, and 90 min respectively for normal weight concrete (see Fig. 10). For similar wall thicknesses with 650 kg/m^3 Lightweight foamed concrete walls, the predicted fire rating is 25, 110, 210, and over 300 min while fire rating of

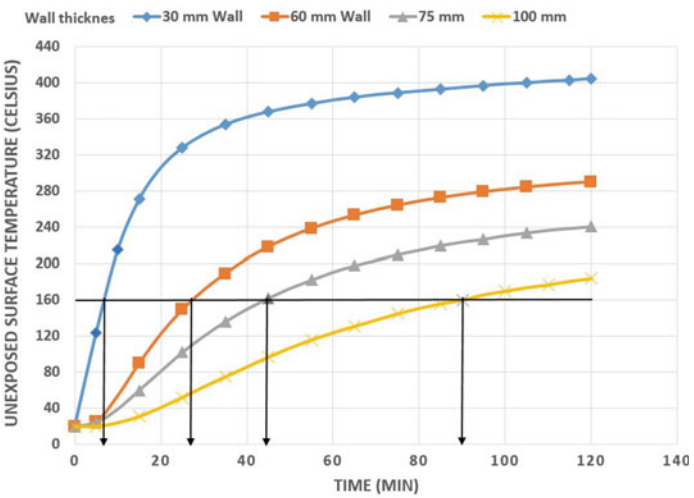

Fig. 10 Normal weight concrete—standard fire rating

25, 105, 170, and over 300 min was observed for 1000 kg/m^3 density Lightweight foamed concrete walls (see Figs. 11 and 12). A comparison of the fire rating of wall types under standard fire is given in Table 3.

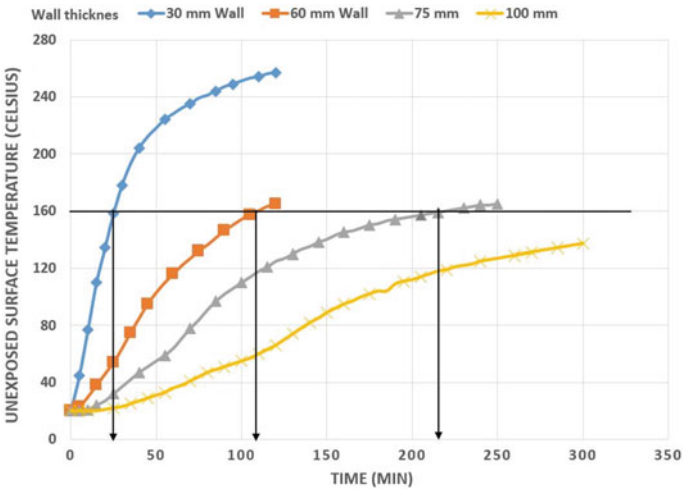

Fig. 11 650 kg/m^3 density foamed lightweight concrete—standard fire rating

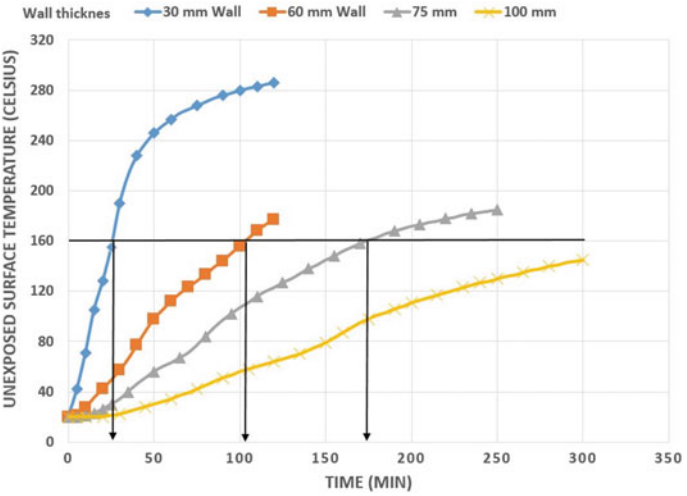

Fig. 12 1000 kg/m^3 density foamed lightweight concrete—standard fire rating

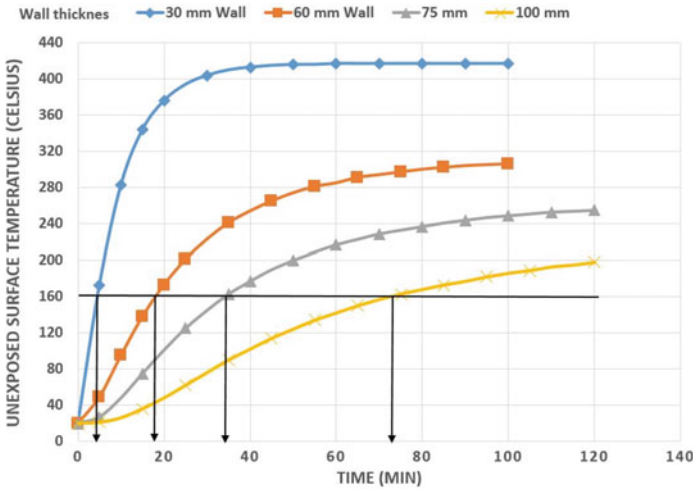

Fig. 13 Normal weight concrete-hydrocarbon fire rating

5.2 Hydrocarbon Fire Ratings

Normal weight concrete walls, 650 and 1000 kg/m^3 density Lightweight foamed concrete walls with 30, 60, 75 and 100 mm thicknesses were modeled using ABAQUS finite element software to determine the unexposed surface temperature variation under hydrocarbon fire condition. Considering the limiting temperature as 160 °C it was observed that 30, 60, 75 and 100 mm normal weight concrete walls had a fire rating of 4 min, 16 min, 35 min, and 75 min respectively (see Fig. 13). For 650 kg/m^3 Lightweight foamed concrete walls 12, 65, 180, and over 300 min fire ratings were observed while, fire rating of 15, 75, 135, and over 300 min were exhibited for 1000 kg/m^3 density Lightweight foamed concrete walls (see Figs. 14 and 15). A comparison of the fire rating of different wall types under standard and hydrocarbon fire is given in Tables 2 and 3 respectively.

5.3 Unexposed Surface Temperature Variation of Wall Panels

Unexposed surface temperature variation of normal weight concrete, 650 and 1000 kg/m^3 density lightweight foamed concrete wall panels with different thicknesses (30, 60, 75 and 100 mm) were studied under standard and hydrocarbon fire conditions (see Fig. 16, 17, 18, 19, 20, 21, 22 and 23).

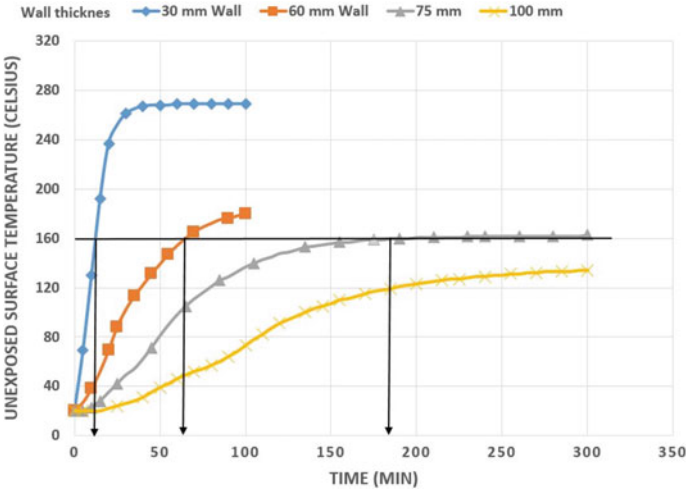

Fig. 14 650 kg/m^3 density foamed lightweight concrete—hydrocarbon fire rating

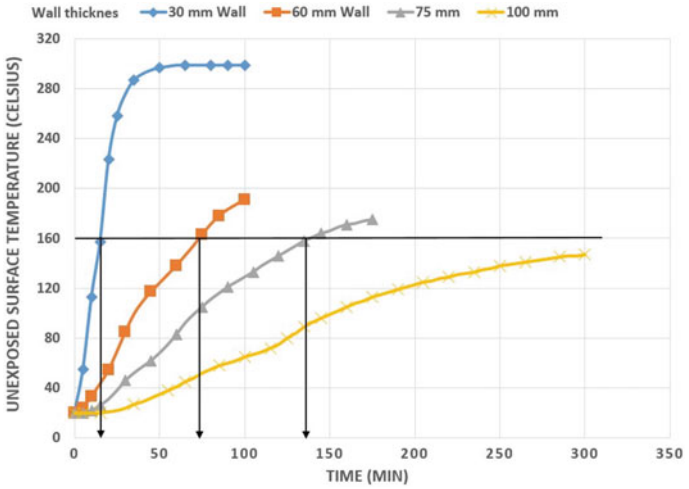

Fig. 15 1000 kg/m^3 density foamed lightweight concrete—hydrocarbon fire rating

Table 2 Fire rating comparison of different wall panels under standard fire

Fire rating (min)				
Type of concrete	Wall thickness			
	30 mm	60 mm	75 mm	100 mm
Normal weight concrete	6	30	45	90
650 kg/m^3 lightweight foamed concrete	25	110	210	>300
1000 kg/m^3 lightweight foamed concrete	25	105	170	>300

Table 3 Fire rating comparison of different wall panels under hydrocarbon fire

Fire rating (min)				
Type of concrete	Wall thickness			
	30 mm	60 mm	75 mm	100 mm
Normal weight concrete	4	16	35	75
650 kg/m^3 lightweight foamed concrete	12	65	180	>300
1000 kg/m^3 lightweight foamed concrete	15	75	135	>300

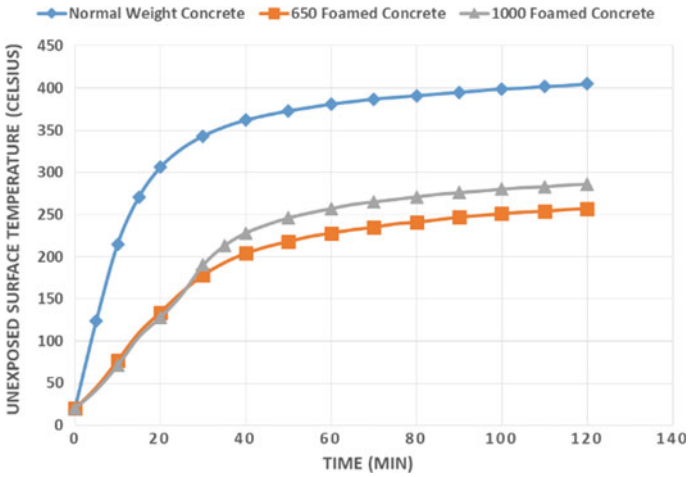

Fig. 16 Unexposed surface temperature variation under standard fire—30 mm wall panels

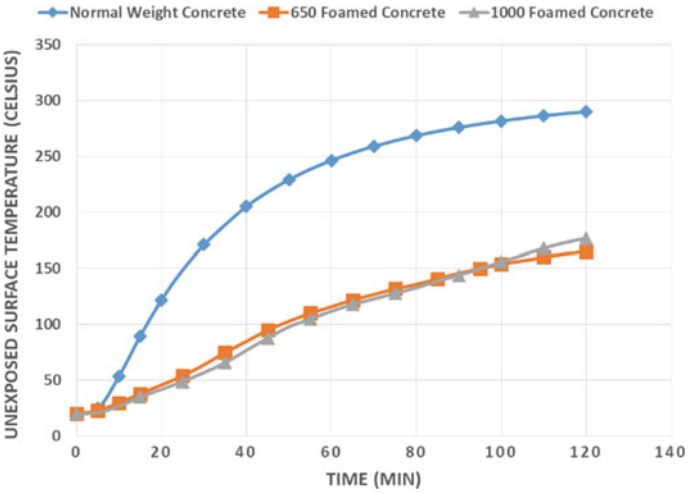

Fig. 17 Unexposed surface temperature variation under standard fire—60 mm wall panels

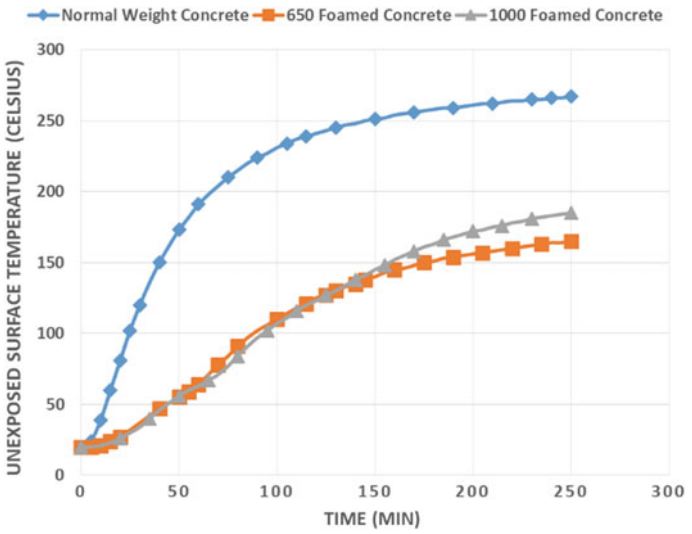

Fig. 18 Unexposed surface temperature variation under standard fire—75 mm wall panels

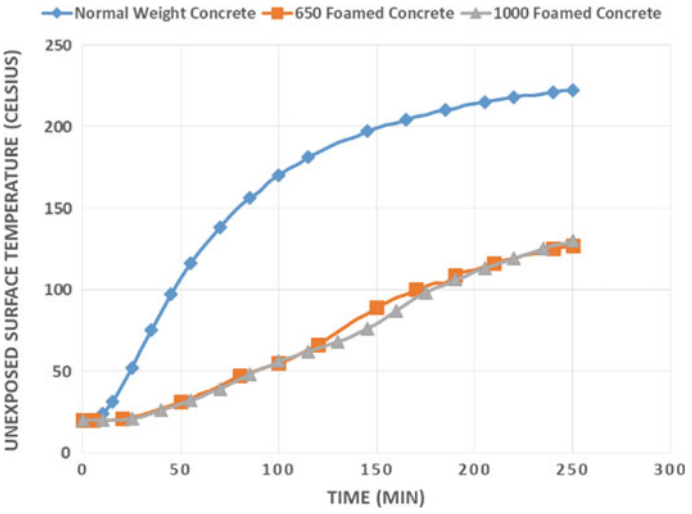

Fig. 19 Unexposed surface temperature variation under standard fire—100 mm wall panels

6 Results and Discussion

Under standard fire conditions, 650 kg/m^3 density foamed lightweight concrete walls exhibited better fire performance compared with the walling materials considered. When normal weight concrete wall panels were replaced with foamed lightweight

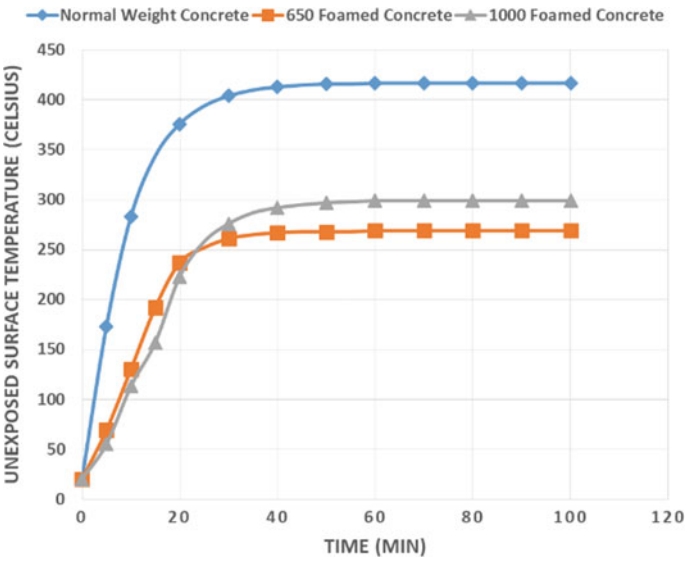

Fig. 20 Unexposed surface temperature variation under hydrocarbon fire—30 mm wall panels

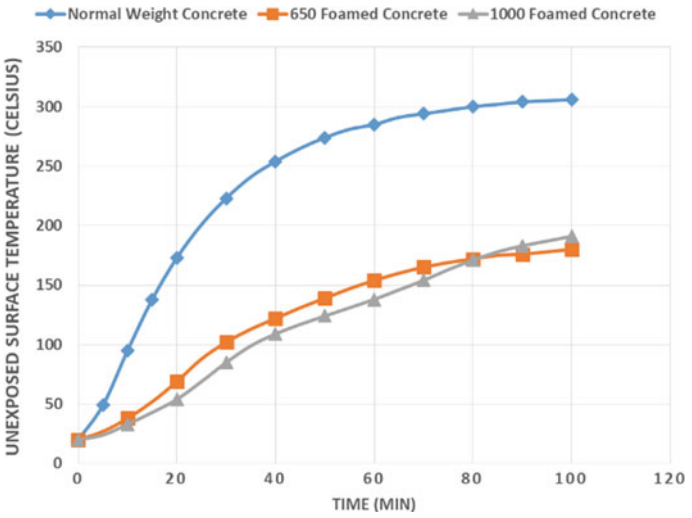

Fig. 21 Unexposed surface temperature variation under hydrocarbon fire—60 mm wall panels

concrete wall panels 3–4 times fire performance enhancement could be obtained for different thicknesses under insulation criteria.

Under hydrocarbon fire condition 650 kg/m^3 density lightweight foamed concrete walls exhibited better fire performance under insulation criteria for 30, 75 and 100 mm wall thickness while, 1000 kg/m^3 density lightweight foamed concrete

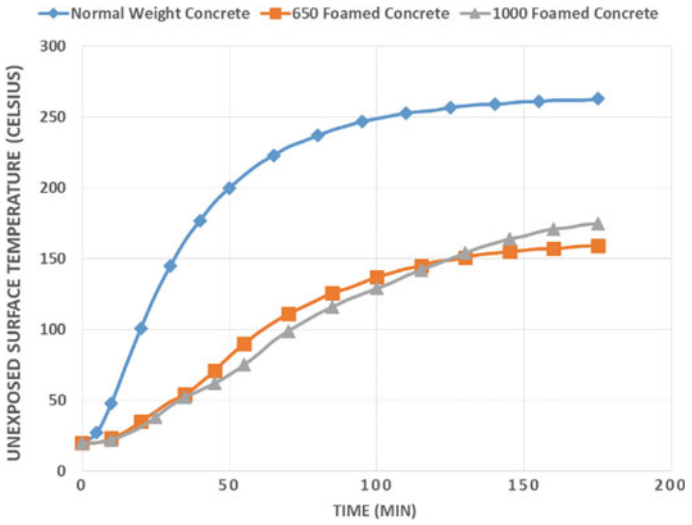

Fig. 22 Unexposed surface temperature variation under hydrocarbon fire—75 mm wall panels

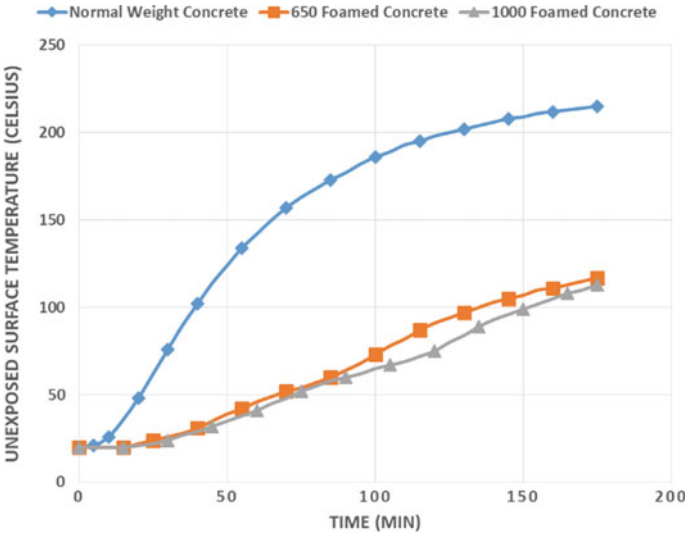

Fig. 23 Unexposed surface temperature variation under hydrocarbon fire—100 mm wall panels

exhibited better fire performance for 60 mm wall. By replacing normal weight concrete walls with lightweight foamed concrete fire performance under insulation could be improved by 3–5 times for different wall thicknesses respectively.

Considering the fire performance of wall panels under standard fire conditions and hydrocarbon fire condition foamed lightweight concrete exhibited better performance. When comparing the unexposed temperature rise of the wall panels 30, 60, 75 and 100 mm lightweight foamed concrete, temperature increment is only half of the temperature increment in normal-weight concrete. When comparing the 650 and 1000 kg/m^3 foamed concrete, lighter density concrete performed well in the early stage of both standard and hydrocarbon fire conditions. After the unexposed temperature exceeeds150 °C, 1000 kg/m^3 foamed lightweight concrete panels behave better compared to the 650 kg/m^3 density panels.

References

1. Brushlinsky NN, Ahrens M, Sokolov SV, Wagner P (2017) World fire statistics. International Association of Fire and Recue services. Center for Fire Statistics, checked on 10/8/2019
2. Tan X, Chen W, Wang J, Yang D, Qi X, Ma Y et al (2017) Influence of high temperature on the residual physical and mechanical properties of foamed concrete. Constr Build Mater 135:203–211. https://doi.org/10.1016/j.conbuildmat.2016.12.223
3. Dwaikat MB, Kodur VKR (2009) Hydrothermal model for predicting fire-induced spalling in concrete structural systems. Fire Saf J 44(3):425–434. https://doi.org/10.1016/j.firesaf.2008.09.001
4. Hung WY, Chow WK (2002) Review on the requirements on fire resisting construction. Int J Eng Perform-Based Fire Codes 4:68–83
5. Kodur Venkatesh (2014) Properties of concrete at elevated temperatures. ISRN Civ Eng 2014(2):1–15. https://doi.org/10.1155/2014/468510
6. ISO 834-1: 1999 (E) Fire-resistance tests-Elements of building construction-Part 1: General Requirements
7. Upasiri I, Konthesingha K, Poologanathan K, Nanayakkara S, Nagaratnam B (2019) Review of fire performance of cellular lightweight concrete. In: International conference on sustainable built environment, pp 470–478
8. Dias Y, Keerthan P, Mahendran M (2018) Predicting the fire performance of LSF walls made of web stiffened channel sections. Eng Struct 168:320–332
9. Dias Y, Keerthan P, Mahendran M (2019) Fire performance of steel and plasterboard sheathed non-load bearing LSF walls. Fire Saf J 103:1–18
10. Dias Y, Mahendran M, Poologanathan K (2019) Axial compression strength of gypsum plasterboard and steel sheathed web-stiffened stud walls. Thin-Walled Struct 134:203–219
11. Dias Y, Mahendran M, Poologanathan K (2019) Full-scale fire resistance tests of steel and plasterboard sheathed web-stiffened stud walls. Thin-Walled Struct 137:81–93
12. Imran M, Mahendran M, Keerthan P (2018) Mechanical properties of cold-formed steel tubular sections at elevated temperatures. J Constructional Steel Res 143:131–147
13. Keerthan P, Mahendran M (2012) Numerical modelling of non-load-bearing light gauge cold-formed steel frame walls under fire conditions. J Fire Sci 30(5):375–403
14. Keerthan P, Mahendran M (2012) Numerical studies of gypsum plasterboard panels under standard fire conditions. Fire Saf J 53:105–119
15. Keerthan P, Mahendran M (2014) Thermal performance of load bearing cold-formed steel walls under fire conditions using numerical studies. J Struct Fire Eng 5(3):261–290
16. Dodangoda M, Mahendran M, Keerthan P, Frost R (2019) Developing a performance factor for fire-rated boards used in LSF wall systems. Fire Saf J 109:102872
17. Awana M, Kumar C (2017) Cellular lightweight concrete. Int J Innov Res Sci Eng 3(4):673–678

18. Nagaratnam BH, Mannan MA, Rahman ME, Mirasa AK, Richardson A, Nabinejad O (2019) Strength and microstructural characteristics of palm oil fuel ash and fly ash as binary and ternary blends in self-compacting concrete. Constr Build Mater 202:103–120
19. Ramamurthy K, Kunhanandan Nambiar EK, Indu Siva Ranjani G (2009) A classification of studies on properties of foam concrete. In Cem Concr Compos 31(6):388–396. https://doi.org/10.1016/j.cemconcomp.2009.04.006
20. Mydin MAO, Wang YC (2012) Mechanical prop-erties of foamed concrete exposed to high temperatures. Constr Build Mater 26(1):638–654. https://doi.org/10.1016/j.conbuildmat.2011.06.067
21. Mydin MAO (2010) Lightweight foamed cocrete (Lfc) thermal Ad mechaical properties at elevated temperatures Ad its application to composite Walling system. Doctor of Philosophy. University of Manchester
22. "Standard test methods for fire tests of building construction and materials," (2008) ASTM E119-08b, ASTM International, West Conshohocken, PA, USA
23. Ariyanayagam A, Mahendran M (2014) Development of realistic design fire time-temperature curves for the testing of cold-formed steel wall systems. Frontiers of Structural and Civil Engineering 8(4):427–447
24. Mahamid M, Taghipour Anvari A (2019) Comparison of fire resistance of damaged fireproofed steel beams under hydrocarbon pool fire and ASTM E119 fire exposure. J Struct Fire Eng 10(2):193–232. https://doi.org/10.1108/JSFE-02-2018-0004
25. EN 1991-1-2: Eurocode 1: actions on Structures—part 1-2: general actions—actions on structures exposed to fire
26. EN 1992-1-2: Eurocode 2: Design of concrete structures—Part 1-2: General rules—Structural fire design
27. Othuman MA, Wang YC (2011) Elevated-temperature thermal properties of lightweight foamed concrete. Constr Build Mater 25(2):705–716. https://doi.org/10.1016/j.conbuildmat.2010.07.016
28. Chaudhari SV, Chakrabarti MA (2012) Modeling of concrete for nonlinear analysis using finite element code ABAQUS. Int J Comput Appl 44
29. Terro MJ (1998) Numerical modelling of the behaviour of concrete structures in fire. Aci Struct J 95:183–193

Low Fidelity Numerical Models for Evaluation of Subgrade Reaction: A Review

R. M. D. L. Rathnayake, S. K. Navaratnarajah, C. S. Bandara, and J. A. S. C. Jayasinghe

Abstract In soil-structure interaction problems, both the superstructure and the subgrade must be analyzed together in order to determine the overall behaviour accurately. In geotechnical engineering problems, software with advanced soil models is often used to represent the complex soil characteristics. However, merging such a model with the superstructure modelled in detail will demand unrealistic large computational cost. In this context, adopting low fidelity numerical models to represent soil-structure interaction is more effective. These models are both relatively easy to implement using commercially available software as well as represent the soil characteristics sufficiently correct. Two basic classical approaches namely the Mechanical approach and Continuum approach are identified in literature when it comes to modelling of subgrade. Later, using the features of both approaches, hybrid models have been developed. Numerous modified subgrade models that use mechanical, continuum and hybrid approaches have been proposed in the literature. This paper investigates and describes the possible soil-structure interaction models available in the literature and presents a classification based on the theory behind their evolution. Strengths and limitations of various types of models are discussed in brief in order to choose the most suitable model for a particular problem.

Keywords Continuum soil model · Low fidelity numerical models · Soil-structure interaction · Subgrade reaction

1 Introduction

The behaviour of the structures, their foundations and soil medium below the foundations is always interdependent. They alter each other's actual behaviour. Therefore, conducting an accurate analysis when it comes to soil-structure interaction (SSI) is essential. Although modelling a certain SSI problem using a full Finite Element (FE) analysis of soil considering complex soil characteristics give precise results, the

R. M. D. L. Rathnayake (✉) · S. K. Navaratnarajah · C. S. Bandara · J. A. S. C. Jayasinghe
Department of Civil Engineering, University of Peradeniya, Peradeniya, Sri Lanka
e-mail: dimalir@eng.pdn.ac.lk

R. Dissanayake et al. (eds.), *ICSECM 2019*, Lecture Notes in Civil Engineering 94,
https://doi.org/10.1007/978-981-15-7222-7_40

computational cost required is unrealistically large. Also, it requires a deep understanding of both structural and geotechnical aspects [6, 16]. Due to these obstacles when applying such sophisticated models, the use of low fidelity SSI models are continued to be used widely to the present.

According to the literature, there are two completely different theoretical approaches for developing subgrade models namely the Mechanical approach and Simplified Continuum approach. The Mechanical approach which is originated from the Winklerian approach is more commonly used. The mechanical approach assembles mechanical elements such as axial springs, tensioned membranes, shear layers, and flexural layers [11]. Simplified-continuum approach starts with complex sets of differential equations with partial derivatives governing the behavior of the soil as a semi-infinite continuum, and then introduce simplifying assumptions with respect to displacements and stresses in order to solve the equations [21]. Hybrid models have been developed by combining features of both approaches in addition to mechanical models and continuum models. According to the literature published by Horvath [8, 9] and Horvath and Colasanti [10], equation governing the relationship between subgrade reaction, p (vertical normal stress applied at the subgrade), and surface displacement, w (Settlement of the surface to which p is applied) will have the same basic form as given in Eq. 1.

$$p + \nabla^2 p + \nabla^4 p + \cdots = w + \nabla^2 w + \nabla^4 w + \cdots \tag{1}$$

Here, the coefficients multiplying the p and w terms have been excluded here for clarity. Those terms will vary in accordance with the model. Also, the appearing of the higher-derivative terms too will depend on the specific subgrade model. ∇^2 is the Laplace operator.

In this paper, the possible low fidelity SSI models available in the literature up to date are briefly discussed in the order of their advancement. Theory and the equations which yield the models are mentioned. The evolution of fundamental models in order to eliminate their limitations is also explained. Table 1 represents a summary of the approaches and models discussed in this paper together with their governing equations. Finally, few models which are developed in order to capture some complex behaviour of soil are discussed.

2 Mechanical Approaches

2.1 Winkler's Hypothesis

"Winkler's idealization represents the soil medium as a system of identical but mutually independent, closely spaced, discrete, linearly elastic springs" (Winkler, cited in Dutta and Roy [6]). Winkler model which was firstly introduced by Winkler, in 1867 is the oldest and the simplest mechanical representation of a foundation subgrade

Table 1 Subgrade models and their governing equations

Subgrade model		References	Yielding equations
Mechanical approach	Winkler's Hypothesis	Worku [23]	$p(x, y) = kw(x, y)$ p = vertical contact pressure, w = vertical displacement, k = coefficient of subgrade reaction
	Filonenko-Borodich foundation	Dutta and Roy [6]	$p = kw - T\nabla^2 w$ $p = kw - T\frac{d^2w}{dx^2}$ p = vertical contact pressure, w = vertical displacement, k = coefficient of subgrade reaction, T = tensile force
	Pasternak's Hypothesis	Pasternak [18]	$p = kw - G\nabla^2 w$ p = vertical contact pressure, w = vertical displacement, k = coefficient of subgrade reaction, G = shear modulus of shear layer
	Modified Kerr/Pasternak model	Kerr [15]	$p - \frac{G_K}{(k_{Ku}+k_{Ki})}\nabla^2 p = \frac{k_{Ku}k_{Ki}}{(k_{Ku}+k_{Ki})}w_0 - \frac{G_K k_{Ki}}{(k_{Ku}+k_{Ki})}\nabla^2 w_0$ p = vertical contact pressure, w_0 = vertical displacement, k_{Ku} = stiffness coefficient of upper spring, k_{Ki} = stiffness coefficient of lower spring, G_K = shear modulus of the shear layer

(continued)

Table 1 (continued)

Subgrade model		References	Yielding equations
Simplified Continuum approach	Reissner Simplified Continuum	Reissner [19]	$p - \left(\frac{GH^2}{12E}\right)\nabla^2 p = \left(\frac{E}{H}\right)w - \left(\frac{GH}{3}\right)\nabla^2 w$ p = vertical contact pressure, w = vertical displacement, E = Young's modulus, G = shear modulus, H = thickness of soil layer
	Vlasov foundation model	Vlasov and Lenot'ev (1960)	$p = kw - 2t\frac{d^2 w}{dx^2}$ p = vertical contact pressure, w = vertical displacement, k = coefficient of subgrade reaction, t = coefficient depending on shearing strain of foundation
Hybrid models	Modified Kerr-Reissner model (MK-R)	Horvath and Colasanti [10]	$p - \frac{T}{k_u + k_i}\nabla^2 p = \frac{k_u k_i}{k_u + k_i}w - \frac{Tk_u}{k_u + k_i}\nabla^2 w$ p = vertical contact pressure, w = vertical displacement, ku = stiffness coefficient of upper spring, ki = stiffness coefficient of lower spring, T = tensile stress of membrane

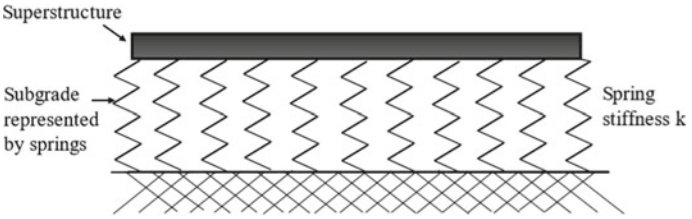

Fig. 1 Visualization of Winkler model

and the most well-known and used foundation model for SSI analysis by structural engineers [11, 21, 23].

As discussed in Kerr [14], Worku [23] and Dutta and Roy [6], mathematically Winkler's model translates into,

$$p(x, y) = kw(x, y) \tag{2}$$

where, p is the vertical contact pressure at an arbitrary point (x, y) in the foundation-soil interface area; w is the corresponding vertical displacement, and k is a proportionality constant of the springs representing contact pressure per unit deformation. This is commonly referred to as the coefficient of subgrade reaction or as the subgrade modulus. Note that k is the only quantity characterizing the subgrade material. Also, Eq. 2 can be identified as a representation of the simplest form of Eq. 1 which was described by Horvath et al. [12]. A visualization of a structural Winkler model is represented in Fig. 1.

A primary deficiency of the Winklerian model is the displacement discontinuity which appears at the edges of the loaded area. This is due to neglecting the shear capacity of the soil. Displacement has no spread in the transverse direction in the absence of shear stresses [2, 21]. Also, in the Winkler model, points undergo vertical deformation independently because the springs act independently of each other. But, the soil is a continuous medium and transfers shear stresses [2, 23].

Another major problem with the use of this model is to evaluate the stiffness of elastic springs used to replace the soil below the foundation. This is complicated as the coefficient of subgrade reaction depends on both nature of the subgrade and dimensions of the loaded area [6]. Determining the subgrade stiffness accurately will lead to a more realistic outcome since the subgrade stiffness is the only parameter in the Winkler model to idealize the physical behaviour of the subgrade as represented in Eq. 2.

In order to eliminate the deficiency of the Winkler model, improved theories have been introduced on the refinement of Winkler's model, by visualizing various types of interconnections such as shear layers and beams along with the Winkler springs [14]. While Winkler's model is having the zero-order derivative relationship between p and w that is shown by Eq. 1, the improved models influenced by Winkler's hypothesis appears with higher derivative terms. Table 2 has summarized the most

Table 2 Subgrade models and physical elements used

Subgrade model	Physical elements used to visualize model
Winkler's hypothesis	Springs (Fig. 1)
Filonenko-Borodich foundation	Pre-tensioned membrane + springs (Fig. 2a)
Pasternak's hypothesis	Shear layer + springs (Fig. 2b)
Modified Kerr/Pasternak model	Springs + shear layer + springs (Fig. 2c)

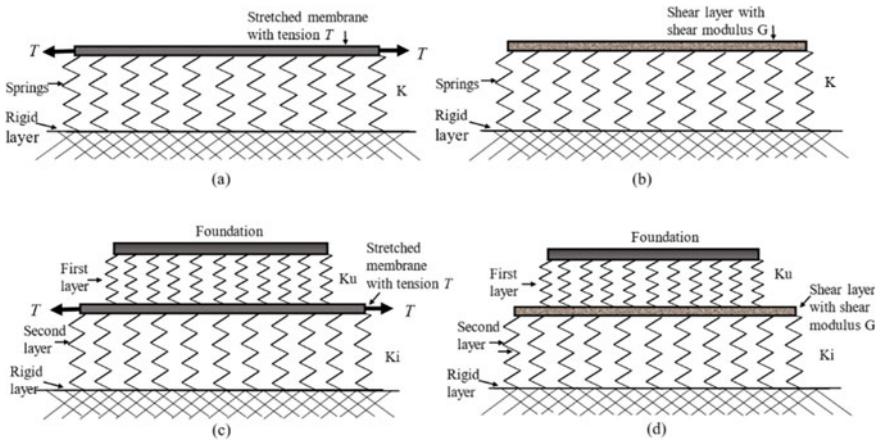

Fig. 2 Mechanical models **a** Filonenko-Borodich model; **b** Pasternak's model; **c** modified Filonenko-Borodich model and **d** Modified Kerr/Pasternak model

common subgrade models discussed in the literature with the physical elements used to visualize the model. Figure 2 represents the visualizations of the discussed models.

2.2 Filonenko-Borodich Foundation

Filonenko-Borodich model was introduced in around 1940s. this model assumed that the top ends of the spring elements were connected to a thin membrane under uniform tension which could sustain tensile stresses. This membrane is attached at the top ends of the springs to achieve some degree of interaction between the spring elements [13, 14, 25]. The mathematical representation of the Filonenko-Borodich model for rectangular/circular foundation and strip foundation is shown by Eqs. 3 and 4 respectively [6]. T is the tensile force. Figure 2a is a visualization of the FilonenkoBorodich model.

$$p = kw - T\nabla^2 w \tag{3}$$

$$p = kw - T\frac{d^2w}{dx^2} \tag{4}$$

2.3 Pasternak's Hypothesis

Pasternak's model is much similar to the Filnenko-Boroditch model except that it uses a pure-shear layer with shear stiffness G to connect the springs at their heads instead of the thin membrane under uniform tension T [16, 18, 25]. Figure 2a represents the Pasternak's model. The existence of shear interaction among spring elements is assumed to be accomplished by connecting the ends of the springs to a shear layer that only undergoes transverse shear deformation. This shear layer can be a beam or a plate [6].

The relationship between the load and deflection can be represented mathematically as,

$$p = kw - G\nabla^2 w \tag{5}$$

It should be noted that the uniform tension of the thin membrane discussed in the Filnenko-Boroditch model is replaced by the shear modulus of the shear layer, *G*. Pasternak model is a good representative of improved Winkler model for homogeneous subgrade [14]. Modelling a shear only layer in commercial software being somewhat challenging is a major drawback of Pasternak's model.

2.4 Modified Kerr/Pasternak Model

Kerr [15], modified Pasternak's model to improve the shear interaction among the springs by introducing a second bed of springs on the top of the shear layer as shown in Fig. 2d. The mathematical relationship that describes the model is shown by Eq. 6.

$$p - \frac{G_K}{(k_{Ku} + k_{Ki})}\nabla^2 p = \frac{k_{Ku}k_{Ki}}{(k_{Ku} + k_{Ki})}w_0 - \frac{G_K k_{Ki}}{(k_{Ku} + k_{Ki})}\nabla^2 w_0 \tag{6}$$

Here, k_{Ku} and k_{Ki} are stiffness coefficients of upper and lower spring beds respectively. G_K is the coefficient of the shear layer. Later, this shear layer was replaced by a perfectly flexible membrane under constant tension T, inheriting the work of Filonenko-Borodich (Fig. 2c). This model is called the Modified Kerr/HorvathColasanti model or modified Filonenko-Borodich [11].

3 Elastic Continuum Approach

A continuum is defined as a continuously distributed matter through space and the simplest elastic continuum inherent the linear elastic isotropic behaviour given by Hook's law. When modelling the subgrade using continuum approach, the subgrade is idealized as a layer overlying a rigid base and involve three parameters consisting of the elastic modulus, the Poisson's ratio and the layer thickness [7, 14, 19, 24].

One of the major attractions of this approach is that the coefficients of the equation, defining the load-displacement response of the simplified elastic layer are always well defined in terms of problem parameters. But, there is difficulty in implementing the models in commercially available structural analysis software [12]. Also, the elastic continuum is assumed to have infinite capacity, which in reality can be questioned for soil [2].

3.1 Reissner Simplified Continuum Model (RSC)

Reissner Simplified Continuum (RSC) model consists of an isotropic, homogeneous layer of linear elastic material underlain by a rigid base. Reissner [19] developed a solution to the problem represented in Fig. 3 which represents an elastic medium representing the subgrade with height H, Young's modulus, E, and shear modulus, G with a distributed load p. The load-displacement behaviour of this model is given in Eq. 7 [2, 12]. Also, this equation agrees with the general form of all subgrade model equations represented in Eq. 1.

$$p - \left(\frac{GH^2}{12E}\right)\nabla^2 p = \left(\frac{E}{H}\right)w - \left(\frac{GH}{3}\right)\nabla^2 w \tag{7}$$

The physical parameters which appear in this equation can be clearly evaluated on-site. Although this model has been available since 1950, the use is constrained in practice due to the difficulty of implementing in commercial software [12].

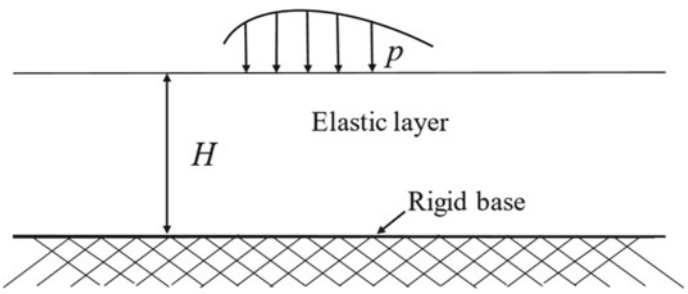

Fig. 3 Reissner simplified continuum

All continuum models make certain assumptions to ease the mathematical work involved. The performance of a given model depends on the nature of simplifying assumptions it makes. Reissner's model assumes in-plane stresses throughout the foundation layer and horizontal displacements at the upper and lower surfaces of the foundation layer as zero [6]. Also, the elastic medium is assumed to be weightless. Due to these assumptions, Reissner's equation is much suitable to be applied only for the near-surface. It is not recommended to be used to study stresses inside the medium [5, 21].

3.2 The Vlasov Foundation Model

Another SSI model that uses the continuum approach is the Vlasov foundation model. This model has been developed using the variational principle [22]. The Vlasov model assumes that the horizontal displacements are negligible when compared with the vertical displacements as there are no horizontal loadings. The vertical deformation is expressed as,

$$w(x, y) = w(x).h(z) \tag{8}$$

Hence, function $h(z)$ describes the variation of displacement in the vertical direction and is chosen in accordance with the nature of the problem. Depending on experimental evidence $h(z)$ is expressed as,

$$h(z) = \sinh[\gamma(H - z)]/\sinh(\gamma H) \tag{9}$$

where, γ is unknown constant determining the rate of decrease of displacement with depth, depending on the elastic properties of the foundation [13, 22]. This model has both the advantages of continuum approaches and the simplicity of mechanical approaches. When the correct choice of the vertical deformation profile is used the model can be reduced to a model identical to the KerrReissner model which is also discussed in this paper briefly.

This model strongly depends on the assumed vertical deformation profile. Jones and Xenophontos [13] has used a similar approach based on a different variational principle which provides a more precise theoretical basis for the form of the vertical deformation profile.

4 Hybrid Models

It is noticed that although mechanical type models are easy to model, the difficulty of estimating the realistic parameters increase when they are improved with multi parameters. Continuum models can estimate the required parameters more accurately

but can be difficult to implement in today's existing structural design software. Hybrid models are developed by combining the features of both approaches in order to create advanced models having all the advantages of two approaches and reduce the shortcomings of each approach. One of the best representations of hybrid models is the Modified Kerr-Reissner (MK-R) model.

Modified Kerr and RSC models are combined to form the MK-R model and, in order to eliminate the negative aspects of each model if considered independently. The concept of developing subgrade models based on a simplified elastic continuum was first suggested by Reissner [19]. The model yields the formula presented in Eq. 7. Kerr studied Reissner's equation and identified that it has the same order of accuracy and the same form of partial differential equations as the equations yield by modified Kerr models [10]. The equation of the MK-R model is given by,

$$p - \frac{T}{k_u + k_i}\nabla^2 p = \frac{k_u k_i}{k_u + k_i} w - \frac{T k_u}{k_u + k_i}\nabla^2 w \tag{10}$$

5 Modelling Complex Characteristics of Soil

Soil characteristics depend on various factors such as soil texture, density, water content, degree of void saturation, loading rate, confining pressure and stress history. Due to this behavior of soils are very complicated [1].

When an incrementing load is applied to the soil mass, strain imparted to the soil mass is elastic at the beginning. Then it may enter the plastic range depending on the magnitude of the applied load. This can be well represented when an elastic element (Hookean Spring) is connected with a plastic element in series. A new schematic system is formed when these two elements are connected in series. It is known as St. Venant's unit. The use of a number of these elements helps to simulate the gradual transition of soil strain from elastic to plastic zone [6]. Figure 4 represents the St. Venant elastoplastic unit.

Another complicated soil property is time-dependent stress-strain behaviour under an applied load. This is called as the viscoelastic behaviour of soil. In mechanical

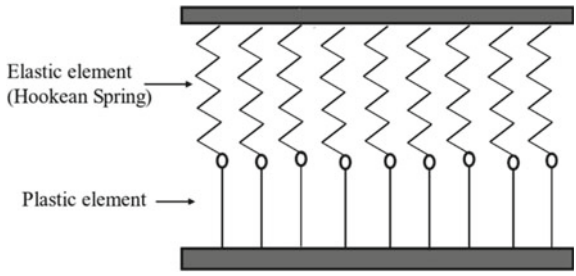

Fig. 4 St. Venant elasto-plastic unit

models, this property is represented by using a combination of spring and dashpot in series. Maxwell model and Kelvin model are the basic models representing the stress-strain state of soil media over time. A visualization of those models is shown in Fig. 5a, b respectively [17, 20].

Also, spring and dashpot models are used to represent the response of soil under dynamic and cyclic behaviour. Choudhury et al. [3] has introduced a two degrees of freedom (2-DOF) mass-spring-dashpot (MSD) model to calculate the dynamic earth pressure on a retaining wall. Later, inheriting that, an MSD model was developed to capture the vertical dynamic behaviour of both ballast and subgrade layers of underneath a rail track [3]. Figure 6 shows a visualization of the 2-DOF MSD model (Fig. 6).

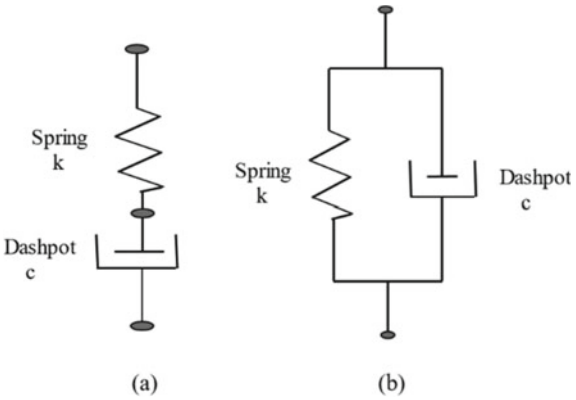

Fig. 5 **a** Maxwell model and **b** Kelvin model

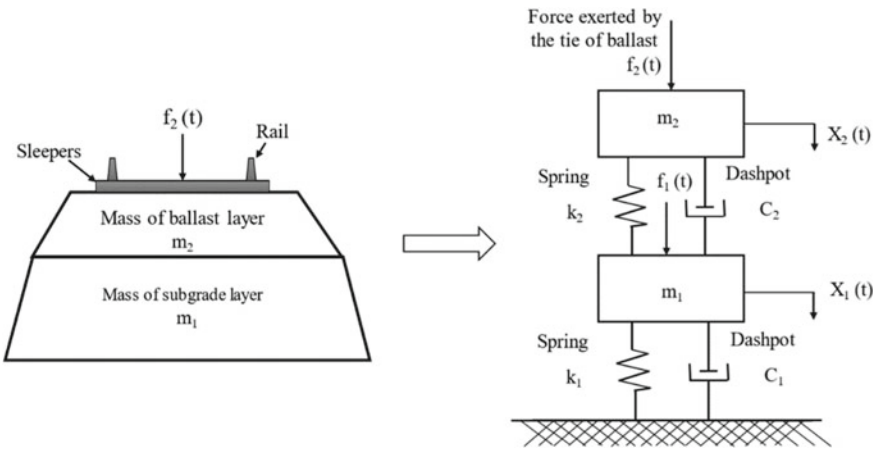

Fig. 6 Representation of railway substructure as a 2-DOF MSD model

6 Conclusion

Low fidelity subgrade models are developed following two approaches namely, Mechanical and Continuum. Both approaches are based on certain types of assumptions to ease the mathematical work involved. The accuracy and appropriateness of a subgrade model, to be used in a particular problem depends on the nature of simplifying assumptions it makes. Winkler model as the most fundamental model of all has major flows such as neglecting shear capacity of soil and difficulty of estimating spring stiffness. Also, it is less satisfactory when applied to the loaded surface area.

Higher-order mechanical models such as the Filonenko-Borodich model and Pasternak's models are using additional elements to represent shear interaction. Pasternak-type models neglect horizontal deformations. Also, modelling the shear layer presented in this model in commercial software is challenging. Modified Kerr models are improved versions of the above two models by introducing a second bed of springs on the top of the shear layer/elastic membrane. This model develops the shear interactions among the springs.

Elastic continuum approaches, unlike mechanical models, have means of estimating model parameters. This approach also uses assumptions. Reissner's model is based on neglecting the in-plane stresses. Due to this, Reissner's equation is more suitable to be applied only for the near-surface and not recommended to be used to study stresses inside the medium. The Vlasov model assumes that the horizontal displacements are negligible when compared with the vertical displacements as there are no horizontal loadings. Also, this model strongly depends on the assumed vertical deformation profile. Improved versions of the Vlasov model which has a more solid theoretical base for the form of vertical displacement profile is available in the literature.

The frequently used model for a more detailed SSI problem is hybrid models. These models when combined together has advantages of both approaches and eliminate shortcomings of both approaches.

Evidence of mechanical type models developed to represent complex soil characteristics such as elastoplastic behaviour and viscoelastic behaviour are available in the literature. Using a model with visco-elastic idealization is more suitable in modelling low permeable soil such as clay. Conceptually, these models imitate the soil structures more accurately but they are not widely used in SSI problems due to difficulties that occur in arranging such models at the base of the structure. The 2-DOF MSD model can simulate both features of the soil layer and the ballast layer together. Such models can be used to represent the effect of soil layering conveniently.

The extent of the accuracy of a model depends on the extent of accuracy of the results expected from the analysis. Therefore, a suitable model can be chosen depending on the accuracy required and computational facility available. The major focus must be on the main parameters which govern the problem. The model must have the ability to evaluate those parameters in a reliable manner.

Acknowledgements This research was supported by the Accelerating Higher Education Expansion and Development (AHEAD) Operation of the Ministry of Higher Education funded by the World Bank (Grant No: AHEAD/RA3/DOR/STEM/No. 63).

References

1. Bezgin O (2010) An insight into the theoretical background of: soil structure interaction analysis of deep foundations. İstanbul. http://www.ymprefab.com.tr/download/
2. Caselunghe A, Eriksson J (2012) Structural element approaches for soil-structure interaction. Master of Science Thesis. Chalmers University of Technology
3. Choudhury D, Bharti RK, Chauhan S, Indraratna B (2008) Response of multilayer foundation system beneath railway track under cyclic loading. J Geotech Geoenviron Eng 134(10):1558–1563
4. Choudhury D, Chatterjee S (2006) Dynamic active earth pressure on retaining structures. Sadhana 31(6):721–730
5. Colasanti RJ, Horvath JS (2010) Practical subgrade model for improved soil-structure interaction analysis: software implementation. Pract Period Struct Des Constr 15(4):278–286
6. Dutta SC, Roy R (2002) A critical review on idealization and modeling for interaction among soil–foundation–structure system. Comput Struct 80(20–21):1579–1594
7. Horvath J (2002) Basic SSI concepts and applications overview. Research Rep. CGT-2002-2, Manhattan College School of Engineering, New York
8. Horvath JS (1983) Modulus of subgrade reaction: new perspective. J Geotech Eng 109(12):1591–1596
9. Horvath JS (1989) Subgrade models for soil-structure interaction analysis. Foundation engineering: current principles and practices. ASCE
10. Horvath JS, Colasanti RJ (2011a) New hybrid subgrade model for soil-structure interaction analysis: foundation and geosynthetics applications. Geo-Front 2011: Adv Geotech Eng 4359–4368
11. Horvath JS, Colasanti RJ (2011) Practical subgrade model for improved soil-structure interaction analysis: model development. Int J Geomech 11(1):59–64
12. Horvath JS, Colasanti RJ, Energy U (2011) A practical subgrade modell for improved soil-structure interaction analysis: parameter assessment. Bronx, New York, USA
13. Jones R, Xenophontos J (1977) The Vlasov foundation model. Int J Mech Sci 19(6):317–323
14. Kerr AD (1964) Elastic and viscoelastic foundation models. J Appl Mech 31(3):491498
15. Kerr AD (1965) A study of a new foundation model. Acta Mech 1(2):135–147
16. Lager E, Karlsson P (2019) Methods for numerical analysis of soil-structure interaction. M.Sc. Master's Dissertation. Lund University
17. Noda T, Fernando G, Asaoka A (2000) Delayed failure in soft clay foundations. Soils Found 40(1):85–97
18. Pasternak P (1954) On a new method of an elastic foundation by means of two foundation constants. Gosudarstvennoe Izdatelstvo Literaturi po Stroitelstuve i Arkhitekture
19. Reissner E (1958) A note on deflections of plates on a viscoelastic foundation. J Appl Mech, ASME 25:144–145
20. Swain A, Ghosh P (2019) Determination of viscoelastic properties of soil and prediction of static and dynamic response. Int J Geomech 19(7):04019072
21. Teodoru I-B (2009) Beams on elastic foundation the simplified continuum approach. Buletinul Institutului Politehnic din lasi. Sectia Constructii, Arhitectura 55(4):37
22. Vlasov V, Leont'ev N (1960) Beams, plates, and shells on an elastic base. Phys Math Liter Publ, Moscow (in Russian)
23. Worku A (2009) Winkler's single-parameter subgrade model from the perspective of an improved approach of continuum-based subgrade modeling. Zede J 26:11–22

24. Worku A (2010) Part I: a generalized formulation of continuum models for elastic foundations. In: GeoFlorida 2010: advances in analysis, modeling & design, pp 1641–1650
25. Worku A (2012) Calibrated analytical formulas for foundation model parameters. Int J Geomech 13(4):340–347

Assessment of Groundwater Quality for Drinking Water from Deep Confined Aquifer in Wanathawilluwa

A. C. Galhenage, E. G. S. S. Kumari, A. M. L. U. Kumara, T. W. L. R. Thalgaspitiya, V. Edirisinghe, M. Vithanage, and B. C. L. Athapattu

Abstract Potable water draws attention of human being due to scarcity of clean water. Contamination of surface, subsurface and groundwater has thus become a serious problem in nationwide. Hence, the assessment of water quality is utmost important to preserve and restore the surface, subsurface and deep-water sources. The main intent of this paper is to present of the groundwater quality status for future planning and management of Wanathawilluwa aquifer in Puttalam district. The assessment of the water quality was carried out in the different locations at Wanathawilluwa. Physiochemical analysis was carried out for surface, subsurface and deep aquifer water samples to provide a single number for Water Quality Index (WQI) that expresses the overall water quality of corresponding water at certain location. WQI was calculated using the weighted arithmetic index based on several water quality parameters such as pH, Total Dissolved Solids, Phosphate, Nitrate, Turbidity, Electrical Conductivity, Dissolved Oxygen and Chemical Oxygen Demand. By representing the whole Wanathawilluwa aquifer, 21 deep and subsurface water samples from different locations were tested and results were compared with stipulated Sri Lanka Standards for potable water. The estimated WQI of Wanathawilluwa aquifer reveals that the overall water quality class is 'good' and water is acceptable for domestic use.

Keywords WQI · Groundwater · Wanathawilluwa aquifer · Physiochemical parameters

A. C. Galhenage · E. G. S. S. Kumari · A. M. L. U. Kumara · B. C. L. Athapattu (✉)
Department of Civil Engineering, Faculty of Engineering, The Open University of Sri Lanka, Nugegoda, Sri Lanka
e-mail: bcliy@ou.ac.lk

T. W. L. R. Thalgaspitiya
National Water Supply and Drainage Board, Ratmalana, Sri Lanka

V. Edirisinghe
Isotope Hydrology Section, Atomic Energy Board, Wellampitiya, Sri Lanka

M. Vithanage
Faculty of Applied Sciences, University of Sri Jayewardenepura, Nugegoda, Sri Lanka

R. Dissanayake et al. (eds.), *ICSECM 2019*, Lecture Notes in Civil Engineering 94,
https://doi.org/10.1007/978-981-15-7222-7_41

1 Introduction

Water is an important requirement of human life and activities related with industry, agriculture, and etc. Water considers as one of the most precious parts of the environment. Among the main types of water, groundwater is a vital source of drinking water and it is a valuable resource. Groundwater is the water that exists underground in saturated zones beneath the land surface and it is contained in aquifers which are geological formations of permeable material capable to store water which consists of different materials such as unconsolidated sands and gravels, permeable sedimentary rocks such as sandstones or limestone, fractured volcanic and crystalline rocks. The speed at which groundwater flows, depends on the size of the spaces in the soil or rock [1]. Groundwater can be found almost everywhere and it is used for domestic and industrial water supply and irrigation all over the world. Groundwater resources are affected by excessive use of fertilizers and pesticides in agricultural areas, untreated/partially treated wastewater to the environment and excessive pumping and improper management of aquifers [2]. If groundwater becomes polluted, it will no longer be safe to drink. Safe drinking water is a basic requirement for good health, and it is also a basic right of human. According to WHO organization, about 80% of all the diseases in human beings are caused by water. Once the groundwater is contaminated, its quality cannot be restored by stopping the pollutants from the source. Therefore it becomes imperative to regularly monitor the quality of groundwater and to device ways and means to protect it. The quality of water is defined in terms of its physical, chemical and biological parameters [3]. Development and management of water quality plays a vital role in agriculture production, poverty reduction, environmental sustenance and sustainable economic development. In Sri Lanka, about 70% of rural and 25% of urban households satisfy their daily water requirements with groundwater by means of dug wells or tube wells. In Puttalam district, most of the population dependent on groundwater as the only source of drinking water supply. Wanathawilluwa area, which is considered in this study, is located in the dry zone of Puttalam district where groundwater is used for everyday activities of the residents and for agricultural activities. Among the identified six types of aquifers in Sri Lanka, at the Wanathawilluwa area there is a deep confined aquifer which is found within the sedimentary limestone and sandstone formations of the north-western and northern coastal plains [3, 4]. Recent drill boreholes in this area indicate that this aquifer is over 60 m thick, and in the deeper parts the sedimentary succession is over 500 m thick [5]. Since groundwater in Wanathawilluwa deep confined aquifer is used for daily need as consumption and irrigation it is vital to analyze the quality of the groundwater in order to ensure whether it is safe for consumption. Water quality index is one of the most effective tools to communicate information on the quality of water to the concerned citizens. It, thus, becomes an important parameter for the assessment and management of groundwater [3]. WQI is defined as a rating reflecting the composite influence of different water quality parameters and it is calculated from the point of view of the suitability of groundwater for human consumption [6]. Therefore the objective of this study is to discuss

the suitability of groundwater for human consumption based on computed water quality index values.

1.1 Study Area

The study was carried out in the deep confined aquifer in Wanathawilluwa which was located in the west coastal region of Sri Lanka and belongs to the Puttalam district in North Western Province of Sri Lanka. According to the Koppen's climate classification [3] Wanathawilluwa belongs to tropical savanna climate where both wet and dry seasons were visible during the year. The short dry season is from June to September and another dry season is from January to March. Wet season is mainly falls on October to December time period. Also this area gets rain during inter monsoon period with the prominent rainfall type being convectional rain and there is no significant fluctuation in average temperature during the year. Compared to the wet zone temperature of this area is a high. In Wanathawilluwa area twenty-one numbers of sample locations were selected as shown in the Fig. 1. The Description of each location is given in Table 1.

Pre-existing tube wells—8 sampling locations (T1, T2, T3, T4, T5, T6, T7 and T16)
Dug wells—4 sampling locations (D1, D5, D9 and D15)
Surface water bodies—9 sampling locations (S3, S5, S8, S9, S10, S11, S12, S13 and S15).

Fig. 1 Sampling locations in Wanathawilluwa

Table 1 Details of sampling locations

Sample ID No.	Sampling location	GPS location (N)	GPS location (E)
Deep water			
T1	Mylankualam (EAP land)—total depth 70 m	08° 06.871′	079° 52.321′
T2	Samagipura—total depth 50 m	08° 07.823′	079° 50.843′
T3	9th Mile post Malwila—total depth 65 m	08° 08.968′	079° 52.753′
T4	Morapathawa Temple—total depth 70 m	08° 11.167′	079° 54.292′
T5	12th Mile Post Wanathawilluwa town—total depth 62 m	08° 12.181′	079° 51.543′
T6	Aruwakkaru—total depth 100 m	08° 15.609′	079° 51.322′
T7	Hafis Land Serakkuli—total depth 100 m	08° 13.991′	079° 48.558′
T16	Insee Lime Quarry Site—total depth 172 m	08° 14.623′	079° 49.473′
Shallow water			
D1	Mylankualam	08° 06.559′	079° 51.973′
D5	12th Mile Post Wanathawilluwa town	08° 11.196′	079° 51.636′
D8	Eriikanawilluwa, Karatiwu Road	08° 12.219′	079° 50.351′
D14	Balagollagama, Ihalapuliyankulama	08° 09.354′	080° 02.267′
Surface water			
S3	9th Mile post Malwila	08° 08.886′	079° 52.023′
S5	12th Mile Post Wanathawilluwa town	08° 11.196′	079° 51.636′
S8	Eriikanawilluwa, Karatiwu Road	08° 12.219′	079° 50.351′
S9	Achchimale tank	08° 16.420′	079° 52.947′
S10	Eluwankulama	08° 11.211′	079° 51.673′
S11	Maha wewa	08° 09.364′	080° 02.279′
S12	Pahalapuliyankulama wewa	08° 11.476′	080° 01.253′
S13	Kuda ottupallama wewa	08° 13.396′	079° 59.374′
S15	Neelabemma	08° 12.924′	080° 04.943′

2 Methodology

A total number of 21 different locations were selected from the study area to determine the water quality parameters during the dry season. The coordinates of the sampling locations in terms of latitudes and longitudes were taken with the GPS. The water samples were collected from various sources such as private hand pumps,

government hand pumps, dug wells and surface water during July 2019. The depth of less than 30 m was considered as shallow aquifer while the depth greater than 30 m was considered as deep aquifer. Each of the groundwater samples was analyzed for parameters such as pH, electrical conductivity, Total Dissolved Solids, Total Phosphate, Nitrate, Dissolved Oxygen, Turbidity and Chemical Oxygen Demand using standard procedures recommended by APHA [7]. The pH, Conductivity, Salinity, Total Dissolved Solids (TDS), Dissolved Oxygen (DO) and temperature were measured by HQ40D Portable Multi Parameter. The Nitrate, Phosphate and Chemical Oxygen Demand (COD) were measured by colorimetric method.

2.1 Water Quality Index

One of the most effective tool for monitoring the surface as well as ground water pollution is WQI. Eight parameters have been selected for developing the Water Quality Index [8]. In the present study the WQI has been calculated in three steps.

In the first step, each of the 08 parameters (pH, TDS, $PO_4{}^{3-}$, $NO_3{}^{-}$, DO, Temperature, Turbidity and COD) has been assigned a weight (*wi*) according to its relative importance in the overall quality of water for drinking purposes as shown in Table 2.

In the second step, the relative weight (*Wi*) is computed from Eq. 1.

$$W_i = \frac{w_i}{\sum_{i=1}^{n} w_i} \tag{1}$$

Wi and *wi* is the relative weight and weight of each parameter, respectively, and *n* is the number of parameters.

In the third step, *Qi* which is defined as a quality rating scale for each parameter is assigned by dividing its concentration *Ci,* in each water sample by its respective standard *Si* according to the guidelines laid down in the

Sri Lankan Standards (Eq. 2)

Table 2 Details of chemical parameters with their relative weight and assigned weight with drinking water standard [6]

Parameter	Unit	Drinking water standard
pH	–	6.5–8.5
Conductivity	mS/m	50
Nitrates	mg/l	50
Total phosphate	mg/l	2
COD	mg/l	10
Turbidity	NTU	2
TDS	mg/l	500
DO	mg/l	5

Table 3 Range of WQI specified for drinking water [9]

S. No.	WQI range	Water quality
1	<50	Excellent
2	50–100	Good
3	100–200	Fair
4	200–300	Poor
5	>300	Very poor

$$Q_i = \frac{C_i \times 100}{S_i} \tag{2}$$

WQI can be determined by using the SI which considered as the first determination for each chemical parameter (Eqs. 3 and 4)

$$SI_i = W_i \times Q_i \tag{3}$$

$$WQI = \sum_{i=1}^{n} SI_i \tag{4}$$

The computed WQI values were categorized into five types as in Table 3.

3 Results and Discussion

3.1 pH

pH takes an important place in clarification process and disinfection of drinking water. Sri Lanka Standards (2013) has prescribed permissible limit of pH to be 6.5–8.5. When the pH of water is less than 7, such water is more likely to be corrosive and it adversely affect on taste and appearance of water. The pH value of groundwater samples in the present study has been analyzed and it lies in the range 5.68–8.66 (Fig. 2).

3.2 Turbidity

The turbidity of the collected samples has been observed in the range 1.6–16.4 NTU (Fig. 3). Standard value for the turbidity in drinking water is 2 NTU. In the present study, none of the samples w Kottek ere well within the acceptable limit (Table 2).

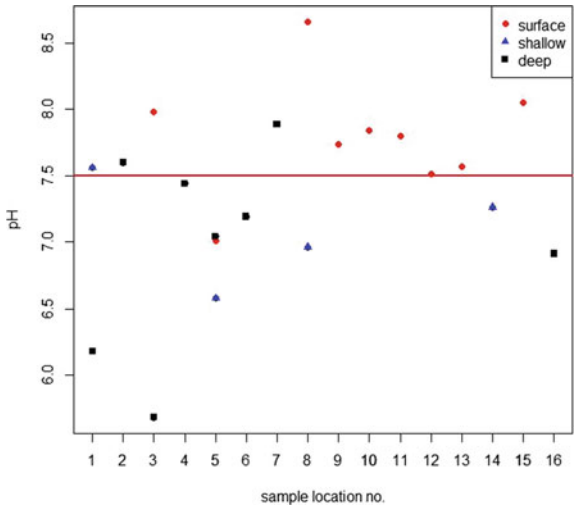

Fig. 2 Variation of pH in sample locations

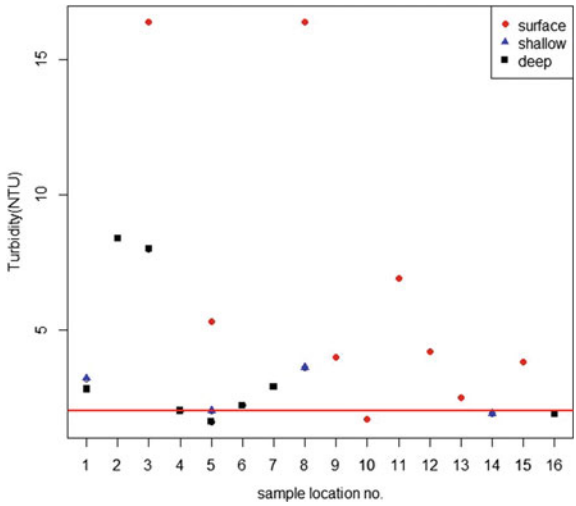

Fig. 3 Variation of turbidity in sample locations

3.3 Chemical Oxygen Demand (COD)

The quantity of COD determines the quantities of organic matter found in water. Chemical Oxygen Demand (COD) content of water samples in studied area was between the ranged from 0–500 mg/L (Fig. 4). The lowest COD value was recorded in tube well water sample at 12th Mile Post Wanathawilluwa town water sampling area and the highest COD values recorded in surface water samples at 9th Mile post Malwila and Eriikanawilluwa sampling areas. According to WHO (2012), almost all

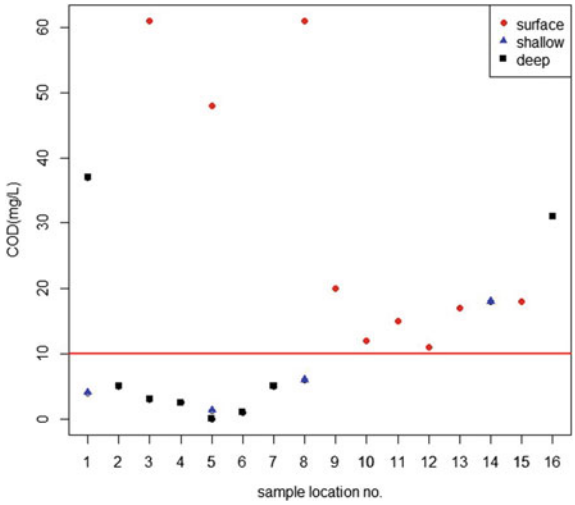

Fig. 4 Variation of COD in sample locations

the surface water samples were not within the recommended permissible limit for drinking purpose. The maximum allowable COD value for drinking water is 10 mg/L.

3.4 Dissolved Oxygen (DO)

Dissolved oxygen (DO) refers to the level of free, non-compound oxygen present in water. It is an important parameter in assessing water quality because of its influence on the organisms living within a body of water. A dissolved oxygen level that is too high or too low can affect water quality. DO of collected samples vary in the range of 1.86–9.86 mg/L (Fig. 5). According to the results DO in collected samples, most of sample locations are above the standard value 5 mg/L.

3.5 Conductivity

Conductivity is a parameter which measures the capability of water to pass an electrical flow due to the presence of dissolved ions. Organic compounds do not conduct electric current very well and hence their contribution to conductivity is very low. So the conductivity could be an indicator to identify the dissolved solids in water. Conductivity of collected samples varies in the range of 241–5460 μS/cm (Fig. 6).

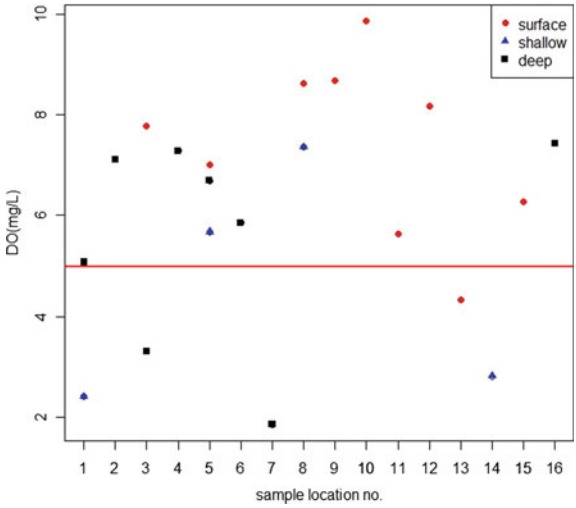

Fig. 5 Variation of DO in sample locations

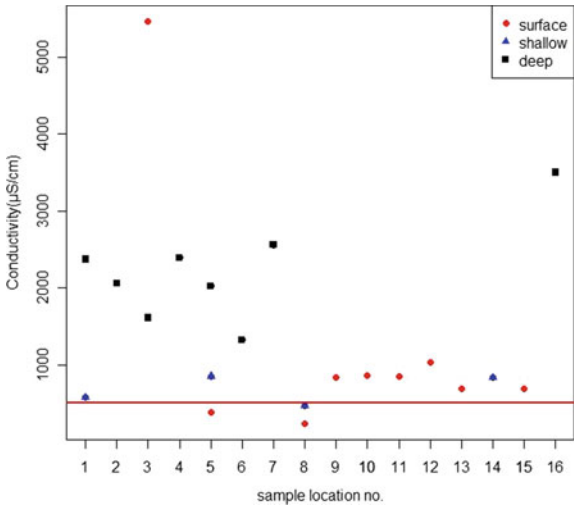

Fig. 6 Variation of conductivity in sample locations

3.6 Total Dissolved Solids (TDS)

TDS comprise inorganic salts principally such as calcium, magnesium, potassium, sodium, bicarbonates, chlorides, and sulphates and some small amounts of organic matter that are dissolved in water. The presence of dissolved solids in water may affect its taste. Acceptable limit for TDS is 500 mg/L (Table 2).the samples in the present study lies in the range of 117.0–2650.5 mg/L (Fig. 7).

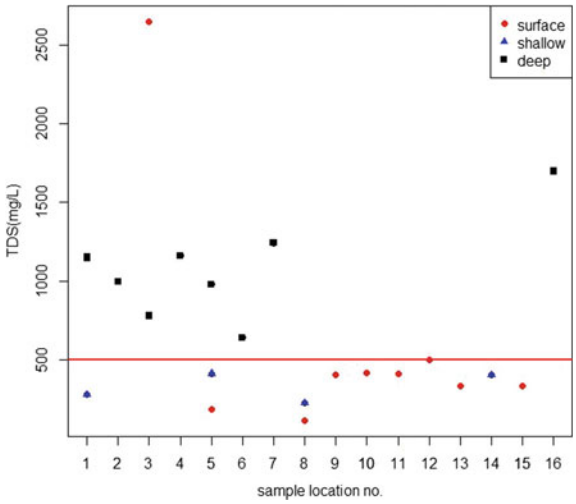

Fig. 7 Variation of TDS in sample locations

3.7 Nitrate

Groundwater may have a Nitrate (NO_3) contamination as a consequence of leaching from natural vegetation. The presence of large quantities of nitrate in drinking water is a potential health hazard because if nitrates combined with amines, amides, or other nitrogenous compounds through the action of bacteria in the digestive tract it may results in the formation of nitrosamines, which are potentially carcinogenic. The maximum allowable nitrate concentration for drinking water is 50 mg/L as NO_3. The concentration of nitrate in water samples of the study area ranges between 0.1 and 8.1 mg/l (Fig. 8) and it is within the desirable limit (Table 2).

3.8 Phosphate

The contamination of water bodies with phosphate has resulted in widespread via fertilizers, wastewater, and washing detergents. The maximum allowable phosphate concentration for drinking water is 2 mg/L (Table 2). The concentration of phosphate in water samples of the study area ranges between 0.13 and 2.04 mg/l (Fig. 9).

The summary of WQI variation of 21 samples is given in Table 4. It is observed that minimum and maximum value of WQI has been found to be 54 and 342 delineated 'Good' and 'Very poor' category, according to range of WQI specified for drinking water as shown in Table 3. The maximum WQI value is found in surface water and minimum WQI value is in shallow well water. In the present study, in Wanathawilluwa deep confined aquifer it is observed that majority of groundwater samples i.e., 58% qualify in the 'Good water quality' category which is suitable for all purposes. The variation of the WQI based on the sampling locations are given in Fig. 10.

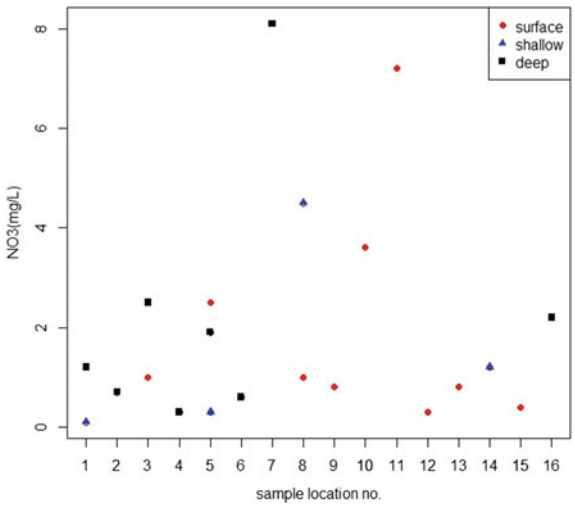

Fig. 8 Variation of NO_3 in sample locations

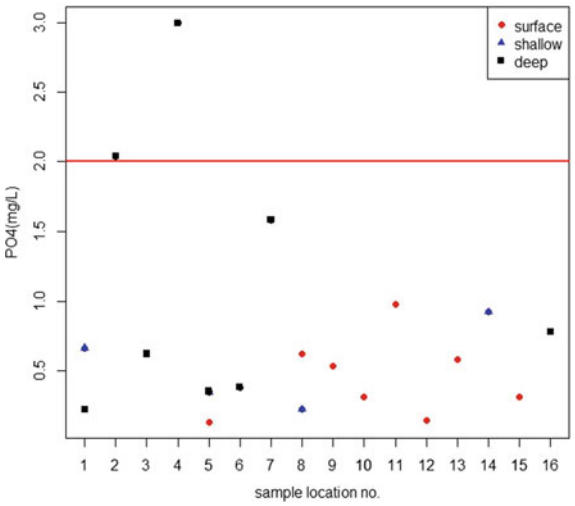

Fig. 9 Variation of PO_4 in sample locations

4 Conclusion

The WQI for 21 samples ranges from 54 to 342. The high value of WQI at these stations has been found to be mainly from the higher values of iron, nitrate, total dissolved solids, hardness, fluorides, bicarbonate, chloride and manganese in the groundwater. In this part, the groundwater quality may decrease due to no inflow of good quality fresh water during dry season. 58% of the samples are within the WQI range of 50–100, which is considered as the good quality for drinking. Also 38% of samples are within the range 100–200, which is considered as fair

Table 4 Details of WQI and water quality of samples

Sample No.	Sample location	WQI	Water quality
Deep water			
T1	Mylankualam (EAP land)—total depth 70 m	155	Fair
T2	Samagipura—total depth 50 m	133	Fair
T3	9th Mile post Malwila—total depth 65 m	100	Good
T4	Morapathawa Temple—total depth 70 m	118	Fair
T5	12th Mile Post Wanathawilluwa town—total depth 62 m	85	Good
T6	Aruwakkaru—total depth 100 m	69	Good
T7	Hafis Land Serakkuli—total depth 100 m	119	Fair
T16	Insee Lime Quarry Site—total depth 172 m	180	Fair
Shallow water			
D1	Mylankualam	56	Good
D5	12th Mile Post Wanathawilluwa town	54	Good
D9	Eriikanawilluwa, Karatiwu Road	60	Good
D14	Balagollagama, Ihalapuliyankulama	82	Good
Surface water			
S3	9th Mile post Malwila	342	Very poor
S5	12th Mile Post Wanathawilluwa town	130	Fair
S8	Eriikanawilluwa, Karatiwu Road	199	Fair
S9	Achchimale tank	98	Good
S10	Eluwankulama	77	Good
S11	Maha wewa	103	Fair
S12	Pahalapuliyankulama wewa	86	Good
S13	Kuda ottupallama wewa	79	Good
S15	Neelabemma	86	Good

quality of drinking water. Analysis of results reveals the fact that WQI pertaining to the groundwater of Wanathawilluwa area needs some degree of treatment before consumption.

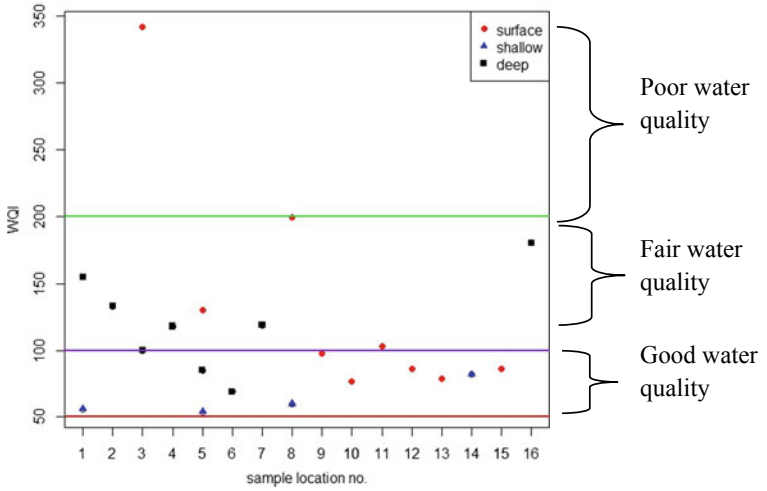

Fig. 10 Variation of WQI in sampling locations

Acknowledgements The authors are thankful to the Department of Civil Engineering, Open University of Sri Lanka; Faculty of Applied Sciences, University of Jayewardenepura; Sri Lanka Atomic Energy Board, and National Institute of Fundamental Studies for providing research facilities.

References

1. Arasaretnam S, Prasadini H, Venujah K (2018) Assessment of open well water quality around Puttalam District, Sri Lanka. Int J Adv Sci Res Eng 4(12):225–232
2. Gunawardena E, Pabasara PKD (2016) Groundwater availability and use in the dry zone of Sri Lanka A framework for groundwater policy for Sri Lanka. Kandy
3. Rubel F, Brugger K, Haslinger K, Auer I (2017) The climate of the European Alps: shift of very high resolution Köppen-Geiger climate zones 1800–2100. Meteorol Z 26:115–125
4. Girija TR, Mahanta C, Chandramouli V (2007) Water quality assessment of an untreated effluent impacted urban stream: the Bharalu Tributary of the Brahmaputra River, India. Environ Monit Assess 130:221–236
5. Harshan S, Thushyanthy M, Gunatilake J, Srivaratharasan T, Gunaalan K (2016) Assessment of water quality index. Ving J Sci 13(1&2)
6. Herath G (2014) Water Quality Management in Sri Lanka; current situation and issues. s.l.: Department of Civil Engineering; University of Peradeniya
7. Standard APHA Methods for the examination of water, 22nd edn (2012)
8. Srinivas K, Srinivas P (2011). Studies on water quality index of ground water of Aland. Int J Appl Biol Pharm Technol 2(4):252–256
9. Singh S, Hussian A (2016) Water quality index development for groundwater quality assessment of Greater Noida sub-basin, Uttar Pradesh, India. Cogent Eng 3-1. SLS (2013). Sri Lanka standard 614:(part 1):5–10
10. Palanisamy P, Kavitha S (2010) An assessment of the quality of groundwater in a textile dyeing industrial area in Erode City, Tamilnadu, India. J Chem 7

11. Srinivasamoorthy K, Chidambaram S, Prasanna MV, Vasanthavihar M, John peter A, Anandhan P (2008) Identification of major sources controlling groundwater chemistry from a hard rock terrain—a case study from Mettur taluk, Salem district, Tamil Nadu, India. J Earth Syst Sci 117:49–58

Finite Element Modeling and Simulation of Rubber Based Products: Application to Solid Resilient Tire

N. M. L. W. Arachchi, C. D. Abegunasekara, W. A. A. S. Premarathna, J. A. S. C. Jayasinghe, C. S. Bandara, and R. R. M. S. K. Ranathunga

Abstract This paper explores the procedure of selecting the best-fitted hyper-elastic material model to describe the mechanical behavior of filled vulcanized rubber-based products, by using nonlinear 3D numerical simulation. Constitutive relationships of these hyper-elastic material models are represented by the strain-energy density functions with the form of polynomial equations. These models utilize to capture the non-linear elasticity and incompressible behavior of elastomers, such as rubber-like materials. In this study, the curve fitting approach and three statistical indexes (**MAPE**, **MAD**, and **MSD**) are proposed to find the best fit hyper-elastic material model and coefficients for a given set of test data of a filled vulcanized rubber sample. Moreover, it highlights the contradictories of each material model by considering the available test data. A three-layered solid resilient tire is used as the numerical example for this study. In this numerical study, the minimum values of the three statistical indexes and coefficients which are obtained from the best-fitted material model with the given experimental data are conformed. The results show that the Yeoh model has a good agreement with the stress-strain curve, which obtained from the experimental data. Further, a static analysis is conducted on the target industrial solid tire, by introducing the selected material model and reasonable displacement and stress results are obtained.

Keywords Non-linear finite element simulation · Rubber-like material · Hyper-elastic material models · Strain-energy density function

N. M. L. W. Arachchi (✉) · C. D. Abegunasekara · W. A. A. S. Premarathna · J. A. S. C. Jayasinghe · C. S. Bandara
Faculty of Engineering, University of Peradeniya, Peradeniya, Sri Lanka
e-mail: nadeeshawa@eng.pdn.ac.lk

R. R. M. S. K. Ranathunga
Elastomeric Engineering (Co) LTD., Horana, Sri Lanka

R. Dissanayake et al. (eds.), *ICSECM 2019*, Lecture Notes in Civil Engineering 94,
https://doi.org/10.1007/978-981-15-7222-7_42

1 Introduction

Rubber products manufacturing in Sri Lanka began with the establishment of a tire retreading facility. Today Sri Lanka is renowned to be the worlds' largest producer of industrial solid tires, together with the production of pneumatic tires, molded and extruded products such as auto mobile rubber parts, tubes, foot ware, rubber hoses, examination, and surgical gloves, a wide variety of automotive components, agricultural and other rubber-based products, industrial flooring, etc. Furthermore, rubber has become a little important substance to one of the world's most important raw materials with the process of vulcanization, by the adding of a certain percentage of sulfur followed by heating to a suitable temperature. In addition, several chemicals such as carbon black, have been incorporated to optimize the consistency and the performance of the product. Being a major product of carbon black filled vulcanized rubber, it is momentous to research on industrial solid tires, with the growing technical specificities of the industry.

Moreover, due to numerous applications of rubber, products, and prediction of the behavior of rubber-like material and its products have become a very active field of research at present. The emerging field of numerical techniques with the advancement of the finite element method (FEM), enables researchers to design and analyze complex large deformations and behaviors of three-dimensional elastomeric components.

Conversely, the study focuses on the conceptual and mathematical expressions of constitutive relationships of filled vulcanized rubber and their contradictories. Further, it illustrates the approach for the selection of the best fit constitutive relationship to a given carbon black filled-rubber compound, which is widely used in the industrial solid tire industry. Finally, it focuses on developing and simulating a 3D static finite element model on an industrial solid resilient tire to illuminate the application of the selected hyper-elastic material model. Considering the above factors, the main aim of this study is to investigate the best fitted hyper-elastic material model which can be used to describe the behavior of filled vulcanized rubber-based products by using nonlinear 3D numerical simulations.

2 Constitutive Relations for Rubber

According to ASTM Standard D 1566-98, "elastomer" is a term used for rubber and polymers that have properties similar to those of vulcanized rubber. Elastomers are composed of long, randomly coiled, and loosely cross-linked molecular chains that can be stretched easily but can return to their original shapes when the force or stress is removed [12]. This study conducted to evaluate the behavior of filled vulcanized rubber as it is the most used practical engineering elastomer. A large number of cross-links formed by vulcanization would make the material rigid, hard, and closer in properties to a thermoplastic from thermoset [23]. In 1904 Stern added

carbon black to rubber and a significant improvement of its mechanical properties was observed [23]. The cross-linking of rubber with sulphur restricts the movement of the molecular chains and imparts strength, improve elasticity during stretching and recoiling, while carbon black resists for UV radiation, sensitivity to ozone cracking due to the presence in double bond in each and every repeat unit, wear and aging [23].

Green-elastic or hyper-elastic materials are the elastic materials that own a strain-energy function [17]. In the mathematical analysis, they assumed elastomers are elastic, isotropic and incompressible having a Poisson's ratio very close to 0.5 [17]. In order to evaluate the properties of elastomers that respond elastically when subjected to large deformations, hyper-elastic material models are used.

To identify the basic response of the hyper-elastic material which exhibits viscoelastic properties, basic mechanical models of viscoelasticity, rheological models or mechanical models were introduced. The Maxwell and Kelvin models have been introduced to form, the linear viscoelastic models, with the combinations of the linear elastic spring and the linear viscous dash-pot as shown in Fig. 1 [11].

In order to capture the complete behavior of elastomers rather than mechanical models, hyper-elastic material models were developed. During the past few years, researchers have tried to develop strain-energy functions to compatible with rubber-like materials using statistical, phenomenological, and response functions to evaluate and compare the ability of hyper-elastic models to reflect the complete behavior of elastomers [13, 17].

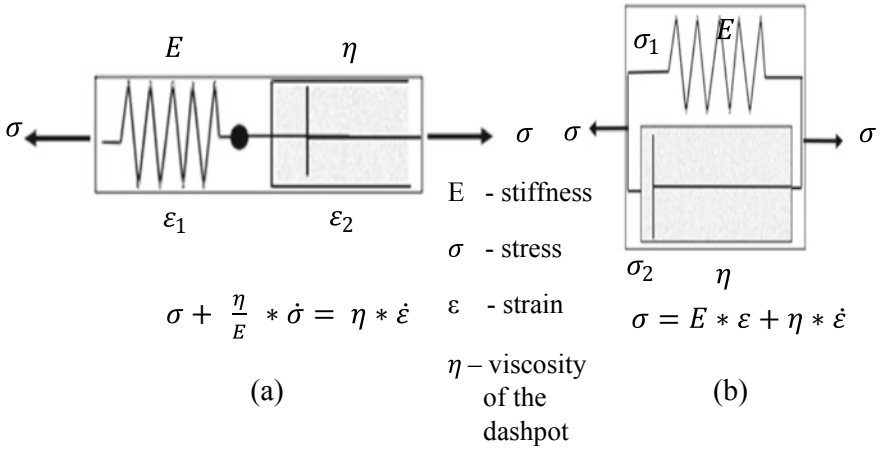

Fig. 1 Rheological models; **a** Maxwel model and **b** Kelvin [5]

2.1 Hyper-Elastic Material Models

There are two main types of hyper-elastic material models and they are shown in Fig. 3. They are phenomenological models, with reference to continuum mechanics where material constants are generated by curve fitting approach. The other type is micro-mechanical models, with reference to microstructure where material constants are generated by specific material tests [20, 22]. At the same time, material models can be classified according to the deformation as shown in Fig. 2.

Some researchers have published their own strain-energy density functions especially for large strain [1, 15, 17, 25]. Some researchers have compared those models with experimental validations [6, 8, 13, 19, 20].

Though many constitutive models have been proposed to describe the elastic response of elastomers, only a few describe the complete behavior of the material satisfactorily, for different loading conditions under uniaxial, biaxial tension and compression and planar tests [13]. It is considered that the most accurate models are those which describe the complete behavior of rubber-like material with the minimal

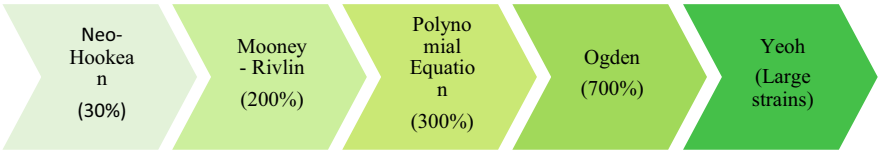

Fig. 2 A material model classification based on deformation

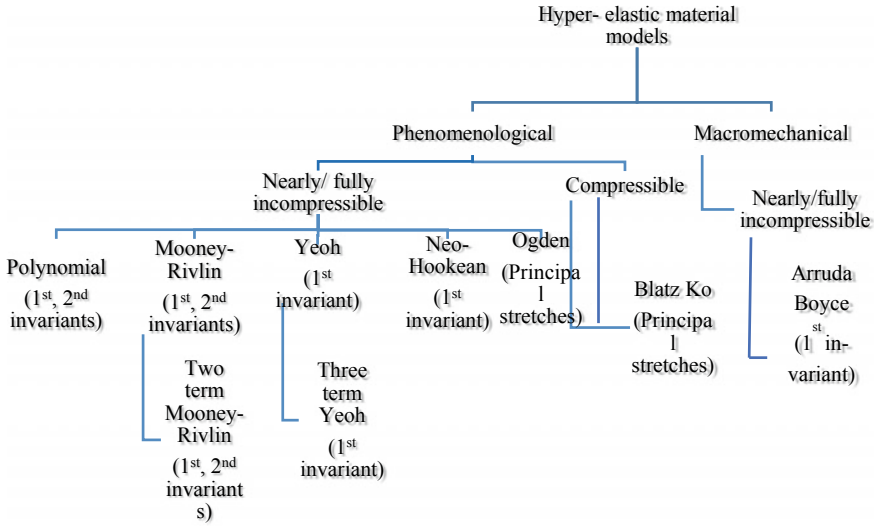

Fig. 3 Material model classification

number of experimentally determined material parameters [13]. With the consideration of the above, Mooney had implemented a general strain-energy function based on the main three assumptions [15]. They are, (1) material is isotropic, (2) volume change and hysteresis are negligible, (3) shear is proportional to the traction in order to interpret the stress-strain behavior by statistical mechanics of rubbery elasticity as well as by invariant based or stretch based continuum mechanics theories [1].

The stress-strain relationship for a hyperelastic, isotropic elastic solid rubber-like material is derived from the strain-energy density function which represents the strain energy stored in the material per unit of a reference volume, W, can be expressed simply with the use of Hooke's law approach;

$$S_{ij} = \frac{\partial W}{\partial E_{ij}},$$

where S_{ij} is the component of the seconPiola-Kirchhoff stress tensor, E_{ij} is the components of the Lagrangian strain tensor. Mathematically strain-energy density function (W) can be interpreted in terms of finite deformation quantities, in terms of Green's strain, invariants of the Cauchy-Green deformation tensor, or principal stretch ratios as frame-invariant strain measures [18]. Further,$W = f(I_1, I_2, I_3)$, and also it can be expanded into a deviatoric (W_d), and volumetric term (W_b) as $W = W_d(I_1, I_2) + W_b(\text{Jel})$.

In the continuum mechanics, approach strain-energy density depends on stretch via, I_1, I_2 and I_3, the first, second and third invariants where, $I_1 = \lambda_1^2 + \lambda_2^2 + \lambda_3^2$, $I_2 = \lambda_1^2 * \lambda_2^2 + \lambda_2^2 * \lambda_3^2 + \lambda_1^2 * \lambda_3^2$, $I_3 = \lambda_1^2 * \lambda_2^2 * \lambda_3^2$ of the stretch tensor [1]. The stretch tensor depends on the strain through the principal stretches λ_1, λ_2 and λ_3 by which completely specified relative to a given reference configuration the state of strain at each material element [7]. For the incompressible case, $\lambda_1 * \lambda_2 * \lambda_3 = 1$. For rubber-like material Poisson's ratio (v) is very close to 0.5 [2], in Eq. 1 where, K_0: initial bulk modulus and μ_0: initial shear modulus.

$$v = \frac{3K_0}{\mu_0} - 2 \Big/ \frac{6K_0}{\mu_0} + 2 \tag{1}$$

The polynomial model equation is formulated with deviatoric and volumetric terms as in Eq. 2 [19].

$$W = \sum_{i=0}^{n} C_{ij} (\overline{I_1} - 3)^i (\overline{I_2} - 3)^j + \sum_{i=1}^{N} \frac{1}{D_i} (J_{el} - 1) \tag{2}$$

where C_{ij}—material constant, which controls the shear behavior and can be determined from uniaxial, biaxial and planar tests, D_i—the material constant controls bulk compressibility where initial bulk modulus—$K_0 = \frac{2}{D_1}$ and set to zero for fully incompressible rubber and estimated from the volumetric test, J_{el}—elastic volume ratio.

There are few facts, the static preload which leads to a compressive permanent set of a segment and the periodic deformation which leads to hysteresis behavior and heat generation, which may affect to properties of elastomers [14]. Elastomer's stress-strain behavior exhibits the Mullins effect, which only dependents on the maximum deformation previously reached in the history of the material, the Payne effect, creep, relaxation, and losses due to a sinusoidal input [4, 23]. This nature results in stress-strain behavior leading to configurationally entropy changes in stretching and recoiling [1]. The entropy change at the stretching of rubber is calculated by statistical methods, neglecting intermolecular attractions and deformation of bonds and bond angles [24]. The stress softening induced by the first loading cycle is known as the Mullins effect. It has been included in constitutive equations for strain-energy density function by adding damage, with the use of D_i [3]. At affixed temperature, elastomers can be taken as very nearly elastic for quite large quasi-static deformations from the undistorted state where hysteresis effect is very small [17].

There are several forms of strain energy potentials available to model approximately incompressible isotropic elastomers; Mooney-Rivlin form, Neo-Hookean form, Yeoh form, Ogden form, Arruda-Boyce form, Marlow form, Polynomial form, Reduced polynomial form, Van der Waals form. Based on the literature most popular five models are selected considering the applicability and they are briefed in Table 1.

3 Numerical Simulation of Solid Tire

The Finite Element Analysis is used as an approach that uses a mathematical approximation to simulate geometry, load conditions, interactions, and boundary conditions. For this study, the advanced finite element analysis and computer-aided engineering software, *ABAQUS* is used. Further, the main three stages of the finite element simulation, pre-processing, analysis and post-processing has followed [16]. To get a clear idea about the above all descriptions, as an example an industrial solid tire is taken into consideration.

Basically, a solid tire consisted of three main layers, tread, cushion, and base as shown in Fig. 4, which are comprised of three different rubber compounds with different properties. The base layer which is harder and consists of embedded with suitable standard-length bead reinforcements. The hardness is achieved by the use of a special rubber compound which is non-thermoplastic, to eliminate softening during service. The steel bead wires provide the strength while maintaining the flexibility of rubber. The inner layer of the base is specially designed to prevent rotations of the tire on the rim. The tire cushion layer is designed to uphold the balance. The middle (cushion) layer's resilience and hardness ensure low heat build-up and better comfort. The total confinement of the tread compound prevents sidewall tears and ensures low abrasion and hard-wearing. It is specially designed to perform on rough terrain in different environmental conditions. It has high tensile and tear resistance properties to minimize the chipping and fragmenting as well.

Table 1 Selected constitutive models

Model	Remarks	Governing equation
Mooney-Rivlin [21, 22, 25]	• Two parameters phenomenological model • Fits well for moderately large strains about 100%, to 200% • Uses for the bodies of ideal highly elastic materials which are incompressible and isotropic in their undeformed state • This model does not obey the filled rubber • The most used form is the two-term Mooney Rivlin model	$W = C_{10}(\overline{I_1} - 3) + C_{01}(\overline{I_2} - 3) + \frac{1}{D_1}(J_{el} - 1)^2$ $\overline{I}_1, \overline{I}_2$—The principal invariants of the deviatoric Cauchy-Green deformation tensor C_{ij}, D_i—Temperature dependent material constants J_{el}—Elastic volume ratio
Neo-Hookean [2, 10, 26]	• A reduced form of Mooney Rivlin form with $C_{01} = 0$ • Can be used when material data is insufficient • Make good approximation at relatively small strains (30%) at the initial linear range	$W = C_{10}(\overline{I_1} - 3) + \frac{1}{D_1}(J_{el} - 1)^2$ $\overline{I}_1$—The principal invariants of the deviatoric Cauchy-Green deformation tensor C_{ij}, D_i—Temperature dependent material constants J_{el}—Elastic volume ratio
Yeoh [25, 26]	• A reduced form of polynomial model based on first invariant only • Fits well for large strains for filled rubber • Can simulate various modes of deformation with limited data	$W = \sum_{i=0}^{3} C_{10}(\overline{I_1} - 3)^i +$ $\sum_{i=1}^{3} \frac{1}{D_i}(J_{el} - 1)^{2i}$ $\overline{I}_1$—The principal invariants of the deviatoric Cauchy-Green deformation tensor C_{ij}, D_i—Temperature dependent material constants J_{el}—Elastic volume ratio
Ogden [9, 26]	• This is based on principal stretch ratios • This is a power series with added extra terms for additional degrees of freedom which allows the regression analysis in fitting stress-strain data • Fits for large deformations up to 700% • A good agreement in experimental data for unfilled rubber	$W =$ $\sum_{i=1}^{N} \frac{2\mu_i}{\alpha_i^2}\left(\overline{\lambda_1}^{\alpha_i} + \overline{\lambda_2}^{\alpha_i} + \overline{\lambda_3}^{\alpha_i} - 3\right) +$ $\sum_{i=1}^{N} \frac{1}{D_i}(J_{el} - 1)^2 \overline{\lambda_i}$—Deviatoric principal stretch μ_1, α_1, D_i—Temperature dependent material coefficients

(continued)

Table 1 (continued)

Model	Remarks	Governing equation
Arruda-Boyce [1]	• Statical mechanical model • It is based on the molecular 8-chain network, based on the representative volume (hexahedron) element from the center to the corners • Two-parameter shear model fits well with limited test data	$W = \mu \sum_{i=1}^{5} \frac{C_i}{\lambda_m^{2i-2}} \left(\overline{\lambda_1}^{i} - 3^i \right) + \frac{1}{D_i} \left(\frac{J_{el}^2 - 1}{2} - \ln(J_{el}) \right)$ $\overline{i}$—Deviatoric principal stretches C_{ij}, D_i—Temperature dependent material constants $\mu = 2(C_{10} + C_{01})$—Initial shear modulus

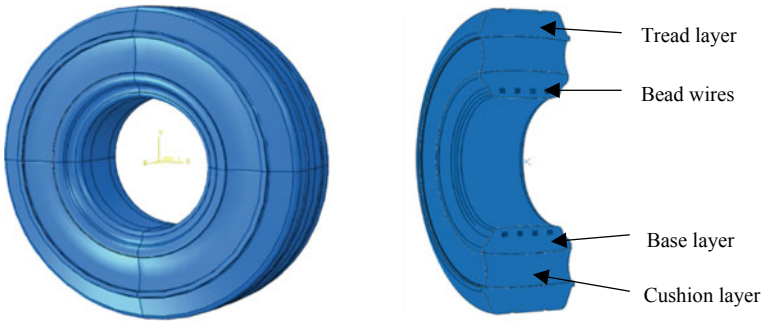

Fig. 4 Layers of the solid tire

3.1 Selection of an Appropriate Material Model for FE Simulation

Hyper-elastic material models represent mechanical behavior with large deformations of filled/unfilled rubber with finite element analysis (FEA). From the mentioned material models, at first, find the best-fitting constitutive material model to evaluate the hyper-elastic behavior of the rubber compounds. Curve fitting is the procedure which use to fit the parameters of a model function in such a way that the fitted curve is as close to the measured curve as possible. Accurate material test data is necessary when performing curve fitting the large strain response of rubber and elastomer materials. At least two material tests from the uniaxial tension or uniaxial compression, biaxial tension or biaxial compression, planar shear and volumetric tests are needed to get a good evaluation between test and constitutive models [4, 13]. Curve fitting for hyper-elastic material models follows four steps. First, the stress-strain curves need to be revised and adapted by test data and the least-squares method or R^2 is used to find out the quality of the curve fitness for the data points. Second, a constitutive equation (material model) has to be chosen by plotting the curves for the

above mentioned five material models selected based on literature., Thirdly, an error calculation with respect to test data is done to compare the above curves by using three selected statistical indexes; Mean Absolute Percentage Error (MAPE), Mean Absolute Deviation (MAD), Mean Squared Deviation (MSD) as shown in Eqs. 3, 4 and 5 respectively where, the test data values (y_t) and obtained stress values ($\hat{y}$) using each constitutive equation is included in Table 1. The final step is to conduct a qualitative and quantitative comparison of the resulting curve of the selected material model with the test data.

$$MAPE = \frac{\sum_{t=1}^{n} \left| \frac{y_t - \hat{y}}{y_t} \right|}{n} * 100\% \tag{3}$$

$$MAD = \frac{\sum_{t=1}^{n} |y_t - \hat{y}|}{n} \tag{4}$$

$$MSD = \frac{\sum_{t=1}^{n} |y_t - \hat{y}|^2}{n} \tag{5}$$

In this study, the uniaxial tensile test data and planar shear data are used for investigations. The strain-energy density values (W) of the material can be obtained with the use of the equation formulations for each model is done with the determination of optimal material parameters for each model using the test data provided. Though Mooney-Rivlin, Yeoh, and Neo-Hookean material models are available within the polynomial form of the strain energy potential, the Mooney-Rivlin model is not taken into consideration as it is not appropriate for filled rubber [14, 25]. Yeoh model has been used by most researchers when limited test data is available [8, 22]. All the hyper-elastic models depend on fitted coefficients. The ability of a model to predict material behavior depends strongly on the choice of these coefficients. With the obtained hyper-elastic curves Ogden model shows an instability for the available test data while Arruda-Boyce, Neo-Hookean and Yeoh model are stable. Among those three material models, to find out the best-fitted material curve the following procedure is followed (Table 2).

Table 2 Statistical index values of the layers of the solid tire

Layers of the tire	Base			Cushion			Tread		
Index	Model								
	Arruda	Neo	*Yeoh*	Arruda	Neo	*Yeoh*	Arruda	Neo	*Yeoh*
MAPE	22.26	22.26	*4.84*	100	32.92	*4.61*	17.6	34.99	*7.55*
MAD	0.96	0.96	*0.28*	9.34	3.47	*0.17*	1.53	3.74	*0.36*
MSD	1.2	1.2	*0.11*	129.54	22.61	*0.04*	4.41	26.95	*0.19*

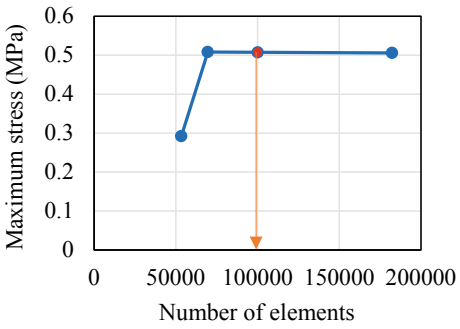

Fig. 5 Mesh convergence analysis—variation of maximum rubber stress with number of elements

The validity of the models is then quantified by calculating the errors by using the selected three statistical indexes (MAPE, MAD, and MSD). It is clear from the error measurements, Yeoh material model obtains minimum values for the statistical indexes and it is taken as the best-fitted material model for further analysis in this study.

3.2 Mesh Sensitivity Analysis of the Numerical Model

The static model developed with three solid layers called the base, cushion, and tread. The tire is numerically modeled in order to analyze the behavior of the solid tire to illuminate the quality of the selected material model. Material properties are assigned respectively with the test data obtained from laboratory experiments. Yeoh model and its coefficients are applied as the hyper-elastic model to describe the behavior of the rubber components of the tire. Moreover, to assign a rim the inner layer of the base layer is defined as a rigid surface whose control point is assigned as the center

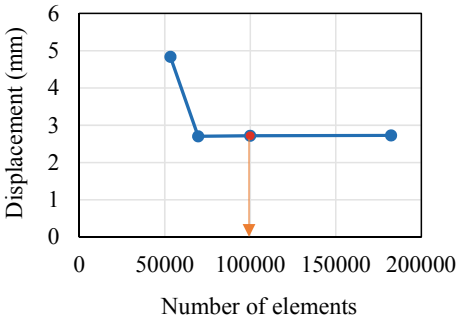

Fig. 6 Mesh convergence analysis—variation of maximum displacement in vertical direction with number of elements

and a static load is applied. A road surface is created as an analytical rigid surface as a contact surface for the tire.

The mesh is assigned as the standard element library a family of 3D Stress. The eight nodes brick elements (C3D8RH) are used for modeling rubber layers and C3D8R elements are used for steel rings. The most appropriate mesh size is generated by the mesh convergence study. Mesh convergence is done by changing the mesh sizes of the layers to increase the mesh density of the model. The third model is selected as the converged numerical model for displacement and stress where the number of elements in the model is 100,000 as shown in Figs. 5 and 6.

4 Results

The developed 3D FE model for static loading analysis of solid tire, in this study, delivers reasonable prediction of load-deflection behavior of a real solid tire. The deduced analysis parameters such as strain energy density, Von Mises stress, the variation of vertical direction displacement, horizontal direction displacement and maximum stress on the solid tire with the applied load is taken by the FE analysis are acceptable, reasonable and can be used to improve the design of solid tires. Von Mises Stress and displacement on vertical (U2) direction variation on the tire is shown in Figs. 7 and 8 for the load condition of 2800 N.

Variation of maximum stress on rubber is shown in Fig. 9, maximum stress on bead wires is shown in Fig. 10, maximum displacement in the vertical direction is shown in Figs. 11 and 12 shows the maximum displacement in the horizontal direction. As an extension of this study next it is going to evaluate of properties of the tire using the selected model along with the validation.

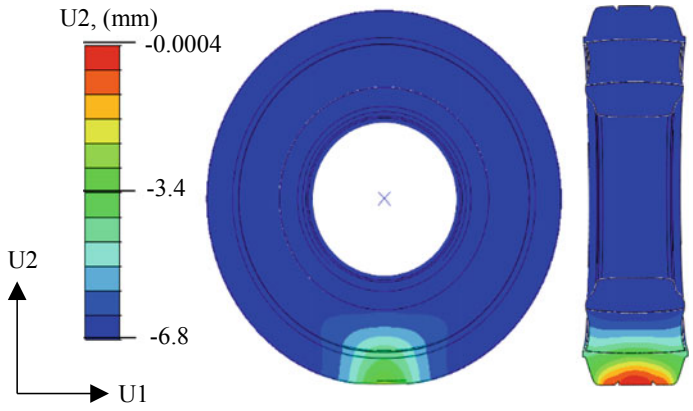

Fig. 7 Von misses stress distribution of rubber at 2800 N

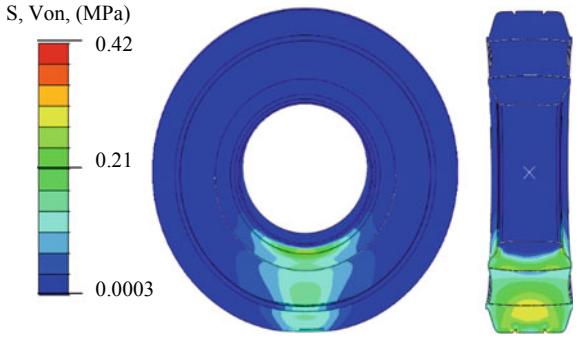

Fig. 8 Displacement distribution on vertical direction (U2) at 2800 N

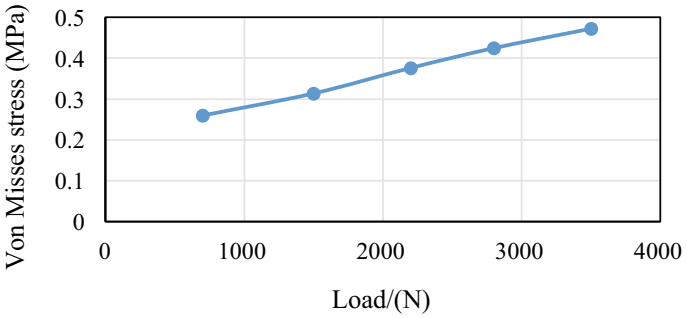

Fig. 9 Variation of maximum von misses stress of rubber with load

Fig. 10 Variation of maximum von misses stress of bead wires with load

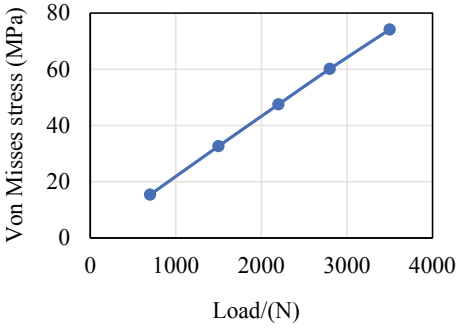

5 Conclusion

The study presents the approach of selecting an appropriate hyper-elastic material model for rubber-like material and its application with non-linear numerical simulation. Based on the literature, the most popular five hyper-elastic material models

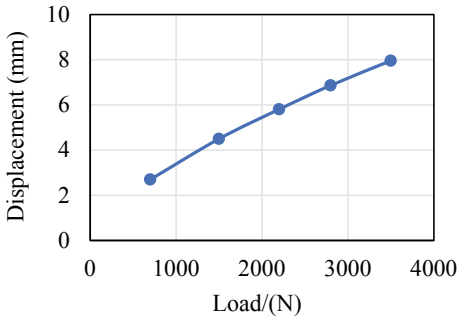

Fig. 11 Variation of maximum vertical displacement (U2) with load

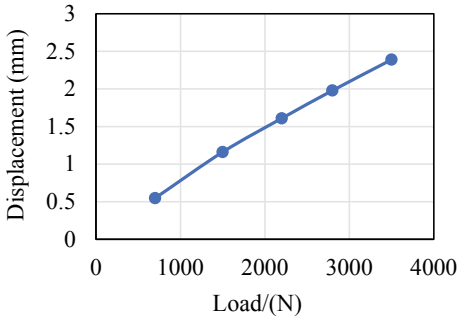

Fig. 12 Variation of maximum horizontal displacement (U1) with load

with uniaxial and planar shear tests are accounted for the study. Moreover, the curve fitting approach and three statistical indexes (MAPE, MAD, and MSD) are used to select the best fitted constitutive model for carbon black- filled rubber. The results show that the Yeoh hyper-elastic material model has good agreement with the experiment data. Further, a static numerical model of the industrial solid resilient tire is implemented to illuminate the use of a best-fitted material model which is the best constitutive model for reproducing the mechanical behavior of carbon black filled vulcanized rubber. The developed model is aided to investigate the vertical deformation, horizontal deformation, and stress distribution through the real solid tire reasonably. Further, the quality of the selected material model can be improved and more sensible comparison of material models can be conducted by introducing more test data at the stage of selection of the appropriate material model.

Acknowledgments The authors would like to give their acknowledgment for licensed applications of the *ABAQUS* package facilitated by the Finite Element Simulation Centre, Rubber Research Institute of Sri Lanka, Rathmalana.

References

1. Arruda E, Boyce M (2000) Constitutive models of rubber elasticity: a review. Rubber Chem Technol 73(3):504–523
2. Crocker LE, Duncan BC, Urquhart JM, Hughes RG, Olusanya A (2011) The application of rubber material models to analyze flexible adhesive joints, National Physical Laboratory, Teddington, UK, TW11 OLW Now with Loctite, Dublin
3. Diani J, Brieu M, Gilormini P (2006) Observation and modeling of the anisotropic visco-hyperelastic behavior of a rubberlike material. Int J Solids Struct 43(10):3044–3056
4. Gornet L et al (2012) A new isotropic hyperelastic strain energy function in terms of invariants and its derivation into a pseudo-elastic model for Mullins effect: application to finite element analysis. In: Constitutive models for rubber VII—Proceedings of the 7th European conference on constitutive models for rubber, ECCMR, pp 265–271
5. Harwood S (1999) Thermo mechanical analysis of non-pneumatic rubber tyres, 1st edn. Curtin University of Technology, Perth
6. Hossain M, Denzer R, Possart G, Steinmann P (2007) On phenomenological and micro-mechanical models in finite elasticity and viscoelasticity for rubber-like materials. PAMM 7(1):4060051–4060052
7. Hossain M, Steinmann P (2013) More hyperelastic models for rubber-like materials: consistent tangent operators and comparative study. J Mech Behav Mater 22(1–2). https://doi.org/10.1515/jmbm-2012-0007
8. Huri D, Mankovits T (2018) Comparison of the material models in rubber finite element analysis. IOP Conf Ser Mater Sci Eng 393:012018
9. Jones DF, Treloar LRG (1975) The properties of rubber in a pure homogeneous strain. J Phys D Appl Phys 8(11):1285–1304. https://doi.org/10.1088/0022-3727/8/11/007
10. Kim B, Lee S, Lee J, Cho S, Park H, Yeom S, Park S (2012) A comparison among the Neo-Hookean model, Mooney-Rivlin model, and Ogden model for chloroprene rubber. Int J Precis Eng Manuf 13(5):759–764
11. Kelly R (1960) Solid-liquid reactions: Part I. The determination of solid-liquid reaction mechanism. Canad J Chem 38(7):1209–1217
12. Lu B (2008) Emergent physics at the vulcanization transition Introduction: the percolation picture, pp 1–13
13. Marckmann G, Verron E (2006) Comparison of hyperelastic models for rubber-like materials. Rubber Chem Technol 79(5):835–858
14. Marvalova B (2008) Viscoelastic properties of filled rubber. Experimental observations and material modeling. In: Proceedings of the 5th European conference on constitutive models for rubber, ECCMR 2007, vol 14, no 1, pp 79–84
15. Mooney M (1940) A theory of large elastic deformation. J Appl Phys 11(9):582–592
16. Nicholson D, Nelson N, Lin B, Farinella A (1998) Finite element analysis of hyperelastic components. Appl Mech Rev 51(5):303–320
17. Ogden R (1973) Large deformation isotropic elasticity—on the correlation of theory and experiment for incompressible rubberlike solids. Rubber Chem Technol 46(2):398–416
18. Olley P (2006) A Cauchy-stress based solution for a necking elastic constitutive model under large deformation. Int J Numer Meth Eng 65(7):1068–1087
19. Phromjan J, Suvanjumrat C (2018) A suitable constitutive model for solid tire analysis under quasi-static loads using finite element method. Eng J 22(2):141–155. https://doi.org/10.4186/ej.2018.22.2.141
20. Rackl M (2015) Material testing and hyperelastic material model curve fitting for Ogden, polynomial and Yeoh models. In: ScilabTEC (7th International Scilab Users Conference), May, pp 1–18
21. Rivlin R, Saunders D (1951) Large elastic deformations of Isotropic materials. VII. Experiments on the deformation of rubber. Philos Trans R Soc A: Math Phys Eng Sci 243(865):251–288
22. Shahzad M et al (2015) Mechanical characterization and FE modeling of a hyperelastic material. Mater Res 18(5):918–924. https://doi.org/10.1590/1516-1439.320414

23. Vijayaram TR (2009) A technical review on rubber. Int J Des Manuf Technol 3(1):25–37
24. Wall FT (1942) Statistical thermodynamics of rubber. J Chem Phys 10(2):132–134. https://doi.org/10.1063/1.1723668
25. Yeoh O (1990) Characterization of elastic properties of carbon-black-filled rubber vulcanizates. Rubber Chem Technol 63(5):792–805
26. Yeoh OH (1997) Hyperelastic material models for finite element analysis of rubber. J Nat Rubber Res 12(3):142–153

A Review on Thermo-mechanical Behaviour of CFRP-Concrete Composites at Elevated Temperature and Available Insulation Systems

A. Selvaratnam and J. C. P. H. Gamage

Abstract The use of Carbon Fibre Reinforced Polymer (CFRP) composites have become a prominent solution for retrofitting the concrete structures. Though CFRP composites have superior mechanical properties, resistance of CFRP/Concrete composites to fire remains unsolved. The degradation of the epoxy resin at elevated temperature makes the FRP composites weaker due to the low glass transition temperature of epoxy resin. A review on CFRP-concrete composites at elevated temperature and available insulation systems are presented in this paper. The paper summarises the results obtained from experimental and numerical studies on the fire performance of CFRP-concrete composites. Hence, it was concluded that by providing appropriate insulation system, the CFRP-concrete members can be protected from fire. However, there are several drawbacks with available insulation systems, such as high cost, addition of dead load, and less aesthetic appearance which are also discussed in this paper.

Keywords CFRP/Concrete composites · Insulation system · Fire resistance · Elevated temperature

1 Introduction

Investigation on application of Fibre Reinforced Polymer (FRP) materials was started in 1980s due to its rapid use in the Construction industry [10]. FRP composites are produced by embedding high strength fibres into the polymer matrix and hence, they achieve excellent properties such as high strength to weight ratio, low conductivity, and flexibility [3]. Generally, the fibres have high strength and the matrix helps to protect the fibres from degradation and to transfer the stresses between fibres [22]. Though FRP composites have excellent mechanical and thermal behaviour at service temperature, it's properties get drastically affected at elevated temperature due to the low glass transition temperature (T_g) of epoxy resin [13].

A. Selvaratnam (✉) · J. C. P. H. Gamage
Department of Civil Engineering, University of Moratuwa, Moratuwa, Sri Lanka
e-mail: aaruga93@gmail.com

R. Dissanayake et al. (eds.), *ICSECM 2019*, Lecture Notes in Civil Engineering 94,
https://doi.org/10.1007/978-981-15-7222-7_43

When the FRP composites are heated to high temperature, the consistency of the resin will change from brittle to viscous [11, 17]. This process is called as "Glass transitioning" and glass transition temperature for epoxy resin varies from 50 °C to 100 °C [5, 6]. Beyond the T_g, all polymer resins will soften and eventually ignite and makes the resin matrix weaker. Therefore, the mechanical properties such as bond strength, tensile strength, and elastic modulus of the FRP composites drastically reduces [7, 11, 13, 17].

Fire resistance is a key property for construction materials and typically varies from 30 to 240 minutes depending on the requirements [9]. Several researches have been focused on the behaviour of FRP strengthened concrete members subjected to fire and it was found that the epoxy layer reaches the T_g within 5–6 min under exposure to the standard fire [13]. Therefore, it is required to provide adequate fire resistance for CFRP strengthened members to ensure the integrity between FRP and concrete at elevated temperature. The suitability of several insulation systems for CFRP-concrete members such as calcium silicate board, ultra-thin coating, Vermiculate, Vermitex, and perlite have been investigated in recent times [12, 16, 21].

2 The Behaviour of FRP-Concrete Members Under Elevated Temperatures

Strengthening the concrete structures using FRP composites was found as a successive solution over the last two decades. The two widely used techniques are the Externally bonded reinforcement (EBR) technique and Near-surface mounted (NSM) technique where NSM technique has many advantages such as larger bond surface, high resistance to peeling-off, and less installation time [1]. Szabo et al. have shown that using the same amount of laminate, a higher flexural performance can be achieved in the NSM technique compared to EBR technique [23].

Many researchers have investigated the bond performance of CFRP strengthened concrete members at elevated temperature. Blontrock et al. conducted a double-lap shear test on concrete member strengthened with CFRP laminates using EBR technique and the noted bond strength percentages were 141%, 124%, and 82% at 40 °C, 55 °C, and 70 °C, respectively [4]. And a concrete cohesive failure was observed at ambient temperature and concrete-adhesive interface failure was observed at elevated temperature. Gamage et al. performed a single-lap shear test on CFRP sheet bonded concrete blocks and they have also observed strength reduction with increasing temperature. A combination of bond failure and concrete rupture was noted in low temperatures less than 50 °C. And peeling-off of the CFRP sheet was the recorded failure pattern for the samples tested at high temperatures greater than 60 °C [14]. The proposed relative strength variation of CFRP-epoxy-concrete bond obtained by Gamage et al. is shown in Fig. 1.

Palmieri et al. have investigated the concrete members strengthened with CFRP strips and rods using NSM technique at a temperature between 20 °C and 100 °C.

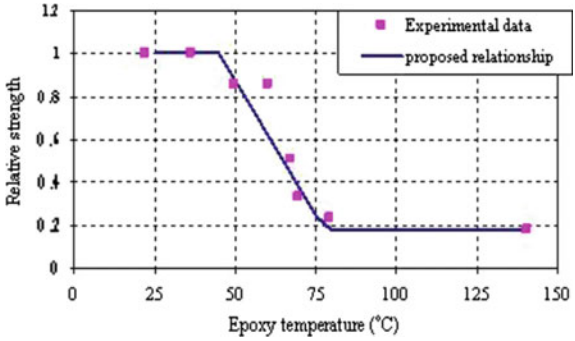

Fig. 1 Proposed relative strength variation of CFRP/epoxy/concrete bond [14]

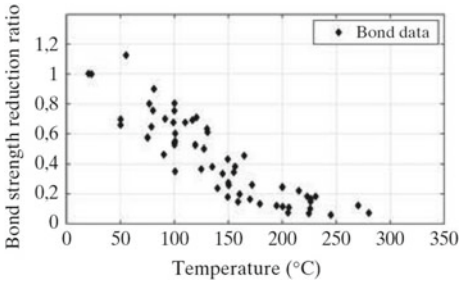

Fig. 2 Variation of bond strength with temperature [17]

They also noted that the bond strength increases below the adhesive Tg and decreases above T_g. The failure mode changed from a combined failure of debonding and splitting of resin to combined failure of debonding at CFRP-epoxy interface and pull-out of the CFRP strips/bars [18]. Maraveas et al. have reviewed the CFRP-Concrete structures exposed to fire and suggested that the temperature can compromise the bond between the concrete and FRP [17]. The variation in the bond strength obtained by Maraveas et al. is shown in Fig. 2.

The tensile strength of FRP composites plays also an important role when determining the load carrying capacity of FRP strengthened concrete members. The effect of temperature on the tensile strength and elastic modulus have investigated by several researchers [11, 17]. It was noted that the tensile strength of FRP materials reduces similarly with increasing temperature. However, the tensile strength of epoxy reduces suddenly when the temperature reaches the T_g. Similar behaviour was observed in the tensile modulus also, with increasing temperature.

3 Thermal Insulation Materials

The major parameters affecting the performance of thermal insulation materials are thermal conductivity, temperature, specific heat, thermal resistance, density, open joints, convection, moisture, ageing, and permeability [19, 24]. However, thermal

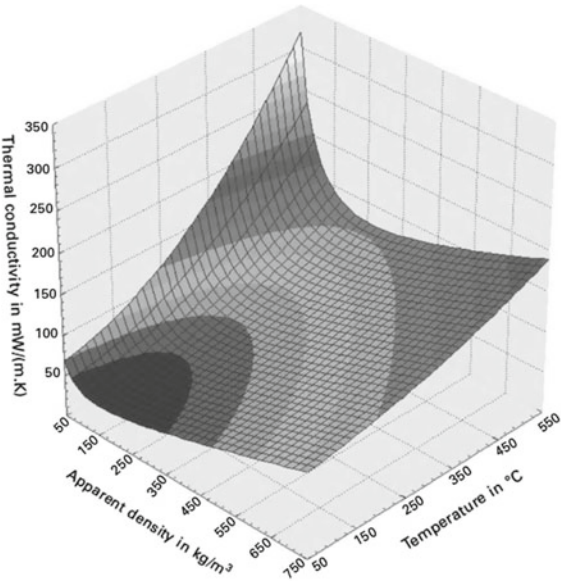

Fig. 3 Themal conductivity of insulation materials depending on apparent desnity and temperature [24]

conductivity is the key property of thermal insulation materials in the general strategy [20]. The thermal conductivity of a material is depended on the temperature and the apparent density [20]. The interdependence of the conductivity on temperature and apparent density is shown in Fig. 3. It was noted that the effect of thickness on thermal conductivity is small compared to the effect of temperature [24].

Most widely used thermal insulation materials for building constructions are Mineral fibre (0.03–0.04 W/m K), Cellulose (0.04–0.05 W/m K), Expanded polystyrene (EPS) (0.036 W/m K), Polyurethene (0.03–0.04 W/m/K), Vermiculite (0.06-0.12 W/m K), Aerogel (0.013 W/m K) [15, 20]. Among various thermal insulation materials, the appropriate material should be selected depending on the cost, durability, strength, fire resistance, airtightness, availability, environmental impact, and ease of application [2].

4 Thermal Insulation Systems for FRP-Concrete Members

Many researchers have investigated the insulation systems to provide protection for the CFRP-concrete composites during the fire. Dong et al. have investigated the fire behaviour of CFRP-bonded reinforced concrete beams with various insulation systems [8]. Four similar CFRP strengthened reinforced beams were cast and insulated completely using 50 mm thick coating (L1), partially using 50 mm thick coating (L2), completely using 40 mm thick calcium silicate board (L3), and completely using 1.5 mm thick ultrathin coating (L4). The anchorage zone of the beams was in the fire

except the beams insulated using the thick coating. In this study, the main intention of fire protection materials was to delay the adhesive failure and hence reduce the degradation of CFRP-concrete beams. The cross sections of CFRP-strengthened beams with the insulation scheme are shown in Fig. 4.

Gamage et al. have studied the bond characteristics of CFRP plated concrete members during the fire [13]. A three-dimensional numerical model has been simulated to investigate the heat effects and validated using experimental results. Concrete with compressive strength 55 MPa was used to this study. 0.176 mm thickness CFRP laminates were bonded to the surface of the concrete member with the use of epoxy adhesive. After revealing the need of insulation, Vermitex-TX was used as an insulation material for fire protection, which thermal conductivity is 0.127 W/m K. The finite element model of CFRP-concrete specimen with insulation is shown in Fig. 5. It was noted that the thermal conductivity and the thickness of the insulation layer affect the fire resistance of the CFRP-concrete specimen significantly. It was also observed that the bond length does not have considerable effects on the fire resistance [12]. Fire resistance of 1.76 h was able to achieve using a 50 mm thick Vermitex layer.

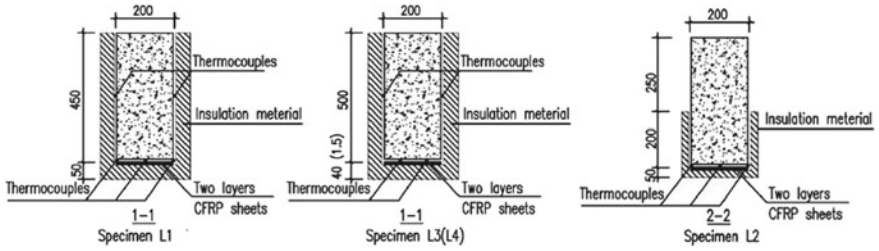

Fig. 4 Insulation and thermocouple details for specimens [8]

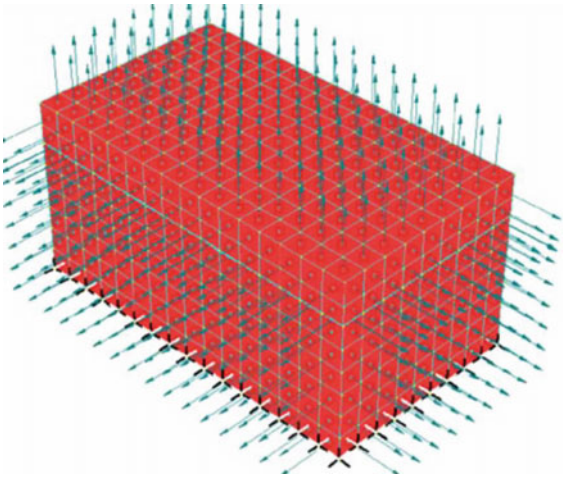

Fig. 5 Finite element model of insulated CFRP-concrete specimen [13]

Salama et al. investigated the behaviour of CFRP strengthened RC beams subjected to the duel effect of elevated temperature [21]. Six distinct cement-based mixes using Perlite and Vermiculite were developed to obtain the most appropriate mix which gives both, low thermal conductivity, and adequate strength. The thermal conductivities were tested according to ASTM C177-07 and the obtained thermal conductivities for Perlite, and Vermiculite mortar were in the range of 0.158–0.277 W/m K, and 0.329–0.396 W/m K, respectively. The developed mixes were applied on reinforced concrete beams as cement rendering up to 5 cm thickness. All the beams covered by thermal insulation layer showed no loss in the capacity up to 500 °C temperature.

Firmo and Correira also investigated the performance of flexural strengthened reinforced concrete beams with EBR CFRP strips and NSM CFRP strips [10]. The focus of this study was understanding the structural effectiveness of CFRP retrofitting systems during the fire and evaluating the efficiency of fire protection. Calcium silicate (CS) boards were used as the insulation material at the bottom surface of the beam. The EBR-CFRP and NSM-CFRP strengthened beams insulated with CS boards are shown in Fig. 6a, b, respectively.

The thickness of the insulation layer ranged from 0 to 50 mm. A numerical model was simulated to analyse the fire performance using an advanced finite element software. A two-point loading was applied to investigate the structural performance of the beams subjected to ISO 834 fire. The results confirmed that the NSM technique has a better fire resistance compared to EBR technique irrespective from the insulation thickness. It was also noted that the higher the thickness of the insulation layer, higher the fire resistance. The comparison of fire resistance of NSM and EBR strengthening system with different thickness insulation layer is shown in Fig. 7.

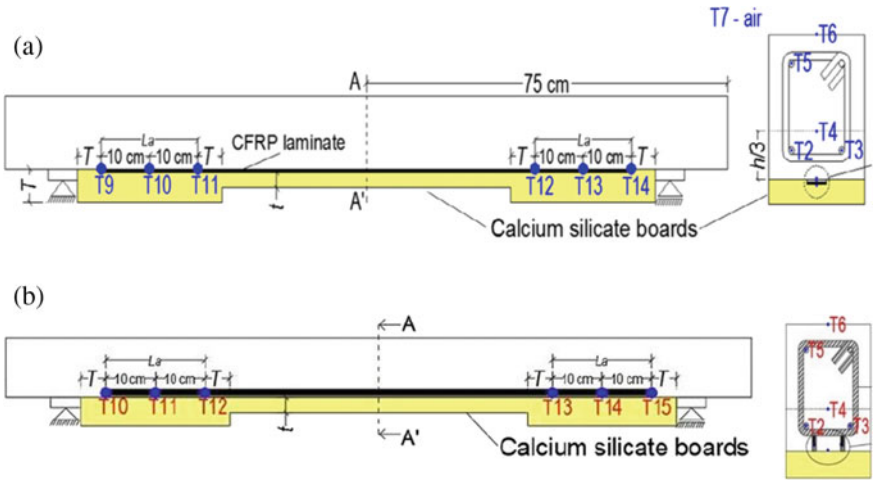

Fig. 6 **a** EBR-CFRP-strengthened RC beams with CS boards [10]. **b** NSM-CFRP-strengthened RC beams with CS boards [10]

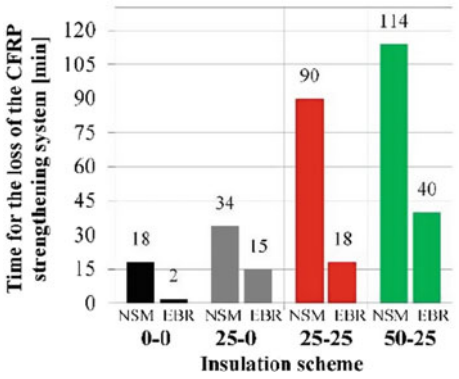

Fig. 7 Comparison between the fire performance of EBR and NSM strengthening systems [10]

5 Conclusions

This paper discussed the behaviour of CFRP-strengthened beams during the fire and the effect of available insulation systems. In order to predict the thermo-mechanical behaviour of CFRP-concrete members at elevated temperature, bond tests and flexural tests could be conducted. Generally, the single-lap shear tests, double-lap shear test, and pull-out tests were the most widely used bond tests to predict the bond performance between CFRP-epoxy-concrete. Many researchers have concluded that by using appropriate insulation to CFRP-concrete member, the required fire resistance can be achieved. The adhesive temperature, insulation thickness, thermal conductivity, rate of heating, and CFRP amount were noted as the key factors affecting the thermal resistance of the insulation system. And the bond length, insulation density, and the specific heat capacity of insulation material were found as less susceptible parameters.

Further, several investigations have concluded that the NSM-CFRP concrete members have relatively high fire resistance compared to the EBR-CFRP concrete members. However, majority of the researchers have shown that, in order to achieve a fire resistance of 2 h, more than 50 mm thickness of insulation is required if the thermal conductivity of insulation is greater than 0.12 W/mK result in high cost. This will cause for additional dead load transfer to the structural members. Therefore, further investigations are required to overcome such problems in the fire performance of CFRP-strengthened members.

Acknowledgements The authors would like to express their sincere gratitude to all the staff in Building materials Laboratory of Department of Civil Engineering, University of Moratuwa. The financial support provided by National Reachearch Council, Sri Lanka; grant number PPP 18-01 is greatly appreciated.

References

1. Aaruga S (2019) Finite element modelling on flexural performance of CFRP strengthened reinforced concrete curved beams. In: Moratuwa engineering research conference (MERCon). IEEE, pp 662–667. Available at: https://doi.org/10.1109/MERCon.2019.8818797
2. Al-homoud MS (2005) Performance characteristics and practical applications of common building thermal insulation materials. Build Environ 40:353–366. https://doi.org/10.1016/j.buildenv.2004.05.013
3. Arunothayan R, Gamage JCPH (2016) Modelling of CFRP strengthened concrete beam to quantify the effects of bond parameters in flexure. In: 7th international conference on sustainable built environment, p 8
4. Blontrock H (2003) Analysis and modeling of the fire resistance of concrete elements with externally bonded FRP reinforcement. Ghent University, Ghent, Belgium
5. Blontrock H, Taerwe L, Vandevelde P (2017) Fire testing of concrete slabs strengthened with fibre composite laminates, thermal and external effects
6. Chandrathilaka ERK, Gamage JCPH, Fawzia S (2018) Mechanical characterization of CFRP/Steel bond cured and tested at elevated temperature. Compos Struct. https://doi.org/10.1016/j.compstruct.2018.09.048
7. Chowdhury EU, Bisby LA, Green M (2011) Mechanical characterization of fibre reinforced polymers materials at high NRCC-50851 (May 2014). https://doi.org/10.1007/s10694-009-0116-6
8. Dong K, Hu K, Gao W (2018) Fire Behavior of full-scale CFRP-strengthened RC beams protected with different insulation systems. J Asian Archit Build Eng 7581:9. https://doi.org/10.3130/jaabe.15.581
9. EN 1992-1-2 (2004): Eurocode 2: Design of concrete structures—Part 1-2 (2004)
10. Firmo JP, Correia JR (2015) 'Fire behaviour of thermally insulated RC beams strengthened with NSM-CFRP strips: experimental study. Compos B Eng 76:112–121. https://doi.org/10.1016/j.compositesb.2015.02.018
11. Firmo P, Correia R, Bisby LA (2015) Fire behaviour of FRP-strengthened reinforced concrete structural elements: a state-of-the-art review. Compos B 80:198–216. https://doi.org/10.1016/j.compositesb.2015.05.045
12. Gamage JCP, Al-mahaidi R, Wong B (2005) Effect of insulation on the bond behaviour of CFRP-plated concrete elements. In: Proceedings of the international symposium on bond behaviour of FRP in structures, pp 119–123
13. Gamage JCPH, Wong MB, Al-mahaidi R (2006) Bond characteristics of CFRP plated concrete members under elevated temperatures. Compos struct 75:199–205. https://doi.org/10.1016/j.compstruct.2006.04.068
14. Gamage J, Wong B, Al-mahaidi R (2005) Performance of CFRP strengthened concrete members under elevated temperatures. In: Proceedings of the International Symposium on Bond behaviour of FRP in Structures, pp 113–118
15. Hawileh RA (2014) Heat transfer analysis of reinforced concrete beams reinforced with GFRP bars (October 2011), pp 299–314. https://doi.org/10.5772/22236
16. Hu K, He G, Lu F (2007) Experimental study on fire protection methods of reinforced concrete beams strengthened with carbon fiber reinforced polymer. Front Archit Civil Eng China 1(4):399–404. https://doi.org/10.1007/s11709-007-0054-7
17. Maraveas C et al (2012) Fiber-reinforced polymer-strengthened/reinforced concrete structures exposed to fire: a review. Struct Eng Int 4(November 2012):500–513. https://doi.org/10.2749/101686612X13363929517613
18. Palmieri A, Matthys S, Taerwe L (2011) Bond behavior of NSM FRP bars at elevated temperatures. In: First Middle East conference on smart monitoring assessment and rehabilitation of civil structures, Dubai, p 8
19. Papadopoulos AM (2005) State of the art in thermal insulation materials and aims for future developments. Energy Build 37:77–86. https://doi.org/10.1016/j.enbuild.2004.05.006

20. Petter B (2011) Traditional, state-of-the-art and future thermal building insulation materials and solutions—properties, requirements and possibilities. Energy Build J 43(7465):2549–2563. https://doi.org/10.1016/j.enbuild.2011.05.015
21. Salama AE et al (2012) Behavior of thermally protected RC beams strengthened with CFRP under dual effect of elevated temperature and loading. HBRC J 8(1):26–35. https://doi.org/10.1016/j.hbrcj.2012.08.005
22. Stoner JG (2015) Finite element modelling of GFRP reinforced concrete beams
23. Szabo Z, Balazs G (2007) Near surface mounted FRP reinforcement for strengthening of concrete structures. Periodica polytechnica; Civil Eng 51(1):33–38. Available at: https://doi.org/10.3311/pp.ci.2007-1.05
24. Zeitler M, Munchen F (2010) Thermal insulation material for building equipment, pp 274–304. https://doi.org/10.1033/9781845699277.2.274

Utilization of Textile Waste in Development of Interlocking Paving Blocks for Foot Paths

G. K. B. M. Gannoruwa, S. M. A. Nanayakkara, and S. S. K. Muthurathna

Abstract Unrecyclable fabric waste generates a major environmental problem in Sri Lankan textile industry. Embedding polyester spandex fabric waste into cement matrix for manufacturing of paving blocks was investigated in this study. In the initial stage of investigation, effect of shredded form of polyester spandex pieces in cement paste was investigated to find the optimum fabric content which can incorporate into cement paste-fabric mix. Admixtures were used to prevent segregation of fabric pieces from cement paste and to improve the workability of mixture. There were improvements of compressive strength of cement paste with shredded fabric and the optimum strength was achieved at 26% of fabric content by volume. Interlocking paving blocks were cast with the use of manufactured sand, shredded form of fabric and cement which were tested for compressive strength, splitting tensile strength and water permeability. Two distinct mix proportions yielded high compressive strength and splitting tensile strength, which were 17.42 MPa and 3.64 MPa, respectively. Hence, depending on the strength requirement, the user can select the suitable mix proportion for a particular application. Failure pattern of fabric incorporated paving blocks gives an indication on its energy absorption capability which can provides better foot comfort by using these paving blocks in foot paths, jogging paths and surfaces for sports areas. Water permeability of fabric embedded paving blocks are 100 times greater than that of conventional cement paving blocks which helps to reduce surface runoff during a heavy rain.

Keywords Polyester spandex fabric · Paving blocks · Walking comfort · Permeable

G. K. B. M. Gannoruwa (✉) · S. S. K. Muthurathna
National Building Research Organisation, 99/1, Jawatte Road, Colombo 00500, Sri Lanka
e-mail: 178074G@uom.lk

S. M. A. Nanayakkara
Department of Civil Engineering, University of Moratuwa, Katubedda, Sri Lanka

R. Dissanayake et al. (eds.), *ICSECM 2019*, Lecture Notes in Civil Engineering 94,
https://doi.org/10.1007/978-981-15-7222-7_44

1 Introduction

In Sri Lanka apparel industry is one of the most significant and dynamic contributor for the economy and it generates 44,100 tons of fabric offcuts per year [1]. Use of synthetic blended fabric is approximately 40% of total fabric usage and those offcuts create a significant waste disposal problem. Polyester spandex is a synthetic fiber blended fabric which is difficult to recycle due to its spandex blend and disposed as a waste. Currently synthetic blended offcuts are incinerated in the cement kiln by cement manufacturers or ends up being illegally dumped or burned in the landfills [1]. Fabric waste burning in the cement kiln is not economical due to high transportation cost and burning cost. Burning of spandex blended fabrics increase the tendency of environmental pollution due to CO_2 emission. The better way to manage waste is the using of waste as a raw material for another industry. The use of waste materials for the creation of raw materials for the construction area is a topical issue, with a promising future and primarily aimed at environmental preservation.

Polyester is a type of polymer which consist of ester functional groups in the main chain. Spandex is a synthetic polymer which is chemically made up of a long-chain polyglycol combined with a short diisocyanate, and contains at least 85% polyurethane [2]. Its elastic recovery ability is a direct result of the material's chemical composition. Polyester fibers are blended with spandex fibers to improve the stretching ability of fabric. Polyester spandex consist of 60–95% polyester and 40–5% spandex.

The reinforcement of cement matrices by means of textile fibers, leads to change the nature of cement matrix from brittle to ductile during failure. The quantity and length of fibers are significant parameters which determine the extent of ductility [3]. Furthermore, these textile fibers would lead to form three dimensional geometrical interlock within the matrix yielding the better mechanical strength [4]. The textile fibers are used for low-cost lightweight construction commodities in conjunction with Portland cement binder as a potential substitute for particular concrete products [5]. Consequently, spandex fibers can be suggested as a possible candidate for reinforcing the cement based products.

The present study discovered the suitability of polyester spandex fabric waste in manufacturing of paving blocks while focusing on environmental preservation through waste management.

2 Experimental Investigation

2.1 Materials

Shredded form of polyester spandex samples collected from one apparel manufacturer were used for this study. Commercially available manufactured sand, Ordinary Portland Cement and chemical admixtures (i.e. viscosity modifying agent—type C

and polycarboxylate (PCE) superplasticizer—type H) were used in making paving blocks with polyester spandex.

2.2 Material Properties

Material properties were tested prior to casting test specimens. Particle density of shredded spandex and Ordinary Portland Cement were measured according to SLS 1144 Part 2 [6]. Size distribution of shredded spandex pieces was measured by mechanical sieving according to BS 812: Part 103.1 [7]. Surface area of shredded spandex pieces was analysed through image analysis with the use of ArcGIS 10.6 software. Fiber composition of polyester spandex was analysed according to ISO 1833 [8]. Grams per Square Meter (GSM) value of polyester spandex fabric was measured according to BS EN 12127 [9]. Water absorption, particle size distribution and fines content of manufactured sand were tested according to BS 812: Part 2 [10].

2.3 Preparation of Cement Paste Samples

Cement paste prism samples (160 mm × 40 mm × 40 mm) were cast with shredded fabric, cement, admixtures and water for different mix proportions. Mix proportions were altered by changing fabric content and admixture type.

2.4 Measurement of Mechanical Properties of Cement Paste Specimens

Cement paste prism samples were tested for flexural strength and compressive strength at 7 days and 28 days as per BS EN 196-1 [11]. Surface finish and cross sections were visually inspected to observe dispersion of fabric pieces.

2.5 Casting and Testing of Paving Blocks

Paving block samples were cast with optimized shredded polyester spandex percentage obtained by testing of cement paste prism samples. Required workability of the mixture was achieved by adjusting water content while using admixtures and the workability was measured with the use of cone penetrometer. Penetration depth was maintained in the range of 7–11 mm by means of the weight of 150 g. The depth

was measured after the completion of 30 s time period since the weight was fallen on to the surface.

Paving blocks were cast by manual compaction of the mortar mix with shredded fabric into a mould of 200 mm × 100 mm × 60 mm and further compaction was achieved through vibration [12].

Paving blocks were tested for compressive strength as per SLS 1425 [12] and splitting tensile strength as per BS EN 1338 [13] standards.

Water permeability of blocks were tested using cylindrical shape specimens with 75 mm cross sectional diameter and 60 mm height [14].

3 Results and Discussion

3.1 Material Properties

Density of shredded polyester spandex fabric was found to be 1386 kg/m^3 and that of ordinary portland cement was 3276 kg/m^3. Accordingly reduced density of fabric leads to show light weight attributes in the fabric embedded cement based products. Specific gravity of manufactured sand on oven-dried basis was 2.70 and water absorption of that was 0.37 as a percentage of oven dry mass.

Polyester spandex fabric sample used for this study consist of 90.8% polyester fibers and 9.2% spandex fibers. GSM value gives an idea about thickness of the fabric and it is 141 g/m^2 for the polyester spandex fabric used in the investigation.

Test results obtained for mechanical sieving of shredded fabric pieces were shown in Table 1. According to the sieve analysis results, majority (66%) of fabric pieces were lies in the 2.36–5 mm range. Sieve analysis of fabric pieces does not facilitate clear picture on sizes of fabric pieces due to its deformability. Therefore image analysis was used to get clear idea on sizes of shredded fabric pieces.

Figure 1 shows the image of shredded fabric sample and it was analysed for calculating surface area of shredded polyester spandex fabric pieces. Number of fabric pieces used for area analysis was 577. Area analysis results were summarized in Table 2. According to the results of area analysis, 93.4% of fabric pieces were smaller than 150 mm^2.

Manufactured sand used for sample preparation is complied with the specified requirements for medium graded fine aggregate given in BS 882 standard [15] as shown in Table 3.

Table 1 Size distribution of shredded polyester spandex fabric pieces through mechanical sieving

Test Sieve (mm)	10.0	5.0	4.75	4.00	2.36	1.18	0.600	0.300	0.150
Passing %	100	76	49	30	10	3	2	1	1

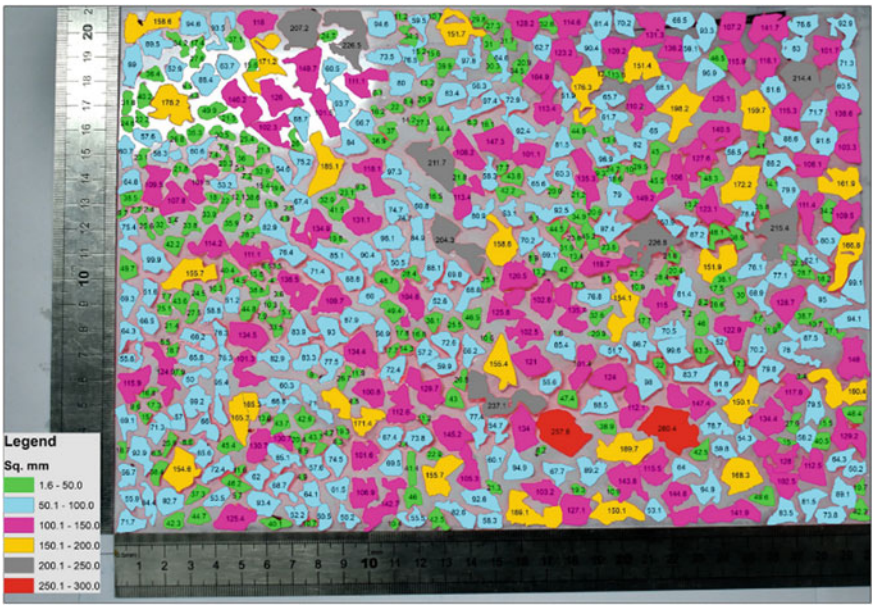

Fig. 1 Surface area analysis of fabric pieces

Table 2 Results of surface area analysis

Range of area in mm^2	Num. of fabric pieces	Percentage of fabric pieces
0–50	247	42.8
51–100	199	34.5
101–150	93	16.1
151–200	28	4.9
201–250	8	1.4
251–300	2	0.3

Table 3 Particle size distribution of manufactured sand

Test Sieve (mm)	10.0	5.0	2.36	1.18	0.600	0.300	0.150	0.075
Passing %	100	100	76	53	40	27	16	10
Specified limits for medium graded fine aggregate according to BS 882: 1992	100	89–100	65–100	45–100	25–80	5–48		0–16

3.2 *Mechanical Properties of Cement Paste Specimens*

Cement paste prism samples were cast by changing fabric content from 5 to 35% by volume while maintaining water/cement ratio, type of admixture and its dosage as constant. Three numbers of prism specimens were cast for each mix proportion to flexural strength test. Flexural strength tested specimens were test for compressive strength and it is amounts to six numbers for each mix proportion. Cast specimens were de-moulded after 24 h and then cured under water at 27 °C until perform the test. Figure 2 illustrates the variation of flexural strength of cement paste specimens at 7 days and 28 days with the increment of fabric content. Figure 3 illustrates the variation of compressive strength of cement paste specimens at 7 days and 28 days with the increment of fabric content.

Compressive and flexural strength values were increased up to 26% of fabric content and thereafter it was gradually decreased due to further increment of fabric content. This strength changing behaviour indicates that fabric pieces act as fibers reinforcing the cement matrix and contributing to strength increase but when the amount of fabric percentage is larger (in this particular case it about 26%) it reduces the composite action of hydrated cement paste and fabric pieces as a result of reduction of cohesiveness in the matrix.

Fabrics provide anchorage and bond development properties to the cement-fabric matrix. According to literature it is found that flexural strength of cement based composite products incorporating with low modulus polymeric fabric is very high. It results due to increased bonding between fabric and cement matrix [4]. In this

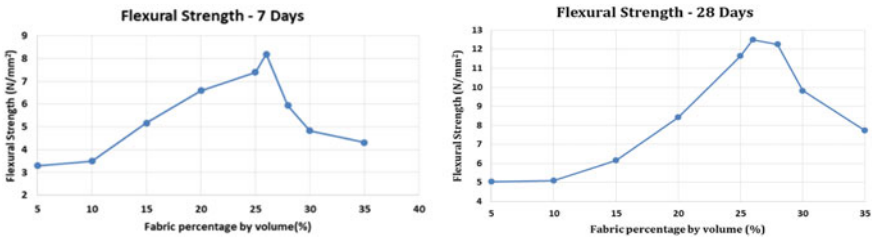

Fig. 2 Flexural strength of cement paste specimens

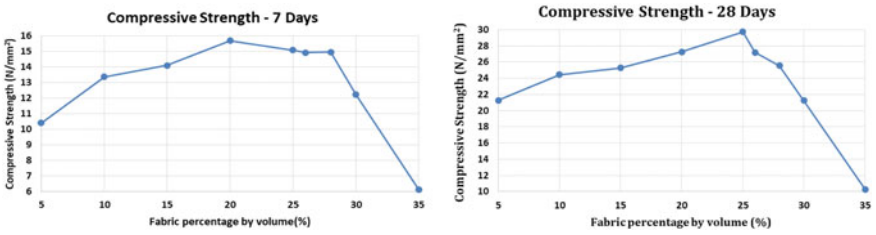

Fig. 3 Compressive strength of cement paste specimens

research also it can be predicted that individual yarns within the spandex fabric structure can incorporate with cement matrix cause to high flexural strength of fabric-cement composite. A microstructural analysis of composite using a scanning electron microscope (SEM) can be used to examine the interfacial bond characteristics between spandex fabrics and cement matrix.

Furthermore, cement paste prism samples were cast using different sizes of fabric pieces and strength was tested to observe the variation of strength with respect to size of fabric pieces. As shown in Fig. 4 considerable strength variations were not observed for the specimens cast with 4–10 mm sizes of fabrics. Therefore, considering the less amount of small fabric pieces in the mix, difficulties in removing small fabric pieces from the mix and cost incurred for that, it was decided to use mixed sizes of fabric pieces (less than 10 mm) for making paving blocks.

Suitable admixture types were selected for fabric cement matrix by casting prism samples and observing dispersion of fabric pieces in cement matrix as shown in Fig. 5.

H type admixture was used to improve the workability of mixture at low W/C ratios. Admixture type C helps to prevent segregation of fabric pieces from cement paste. Therefore admixture type C improves the homogeneity of mixture. Accordingly it was decided to use both admixture type H and type C to achieve homogeneous mixture with good workability.

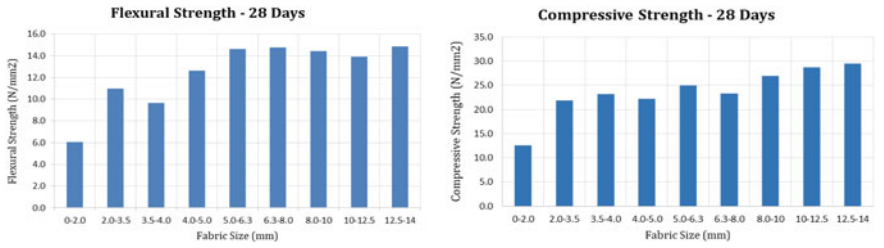

Fig. 4 Variation of strength with respect to size of fabric pieces

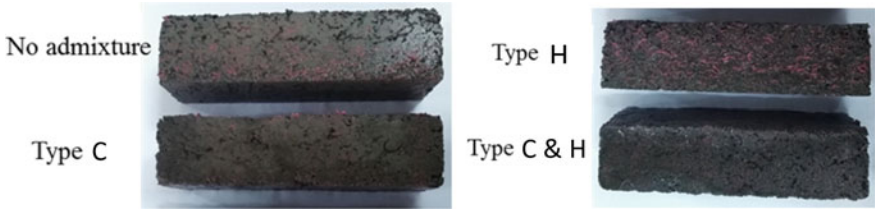

Fig. 5 Surface appearance of prism samples with different admixtures

3.3 Properties of Paving Blocks

Paving blocks were cast using 26% of fabric content by volume, cement, manufactured sand (content was changed from 5% to 60% by volume), selected admixtures and water. Mix proportions used to cast paving blocks are given in Table 4. Cast paving blocks were cured under water at 27 °C after de-moulding, until perform the test. Figure 6 shows the surface appearance of paving blocks at different mix proportions. It illustrates the reduction of smoothness with the increment of sand content in the mixture due to reduction of binder content.

Four numbers of paving blocks were tested for compressive strength and splitting tensile test for each mix proportion. Typical load deformation variation under compression testing of paving blocks is shown in Fig. 7. It can be seen that there is no clear failure point of the load deformation pattern. Therefore failure point is identified as change in linear portion of the load deformation pattern to non-linear portion. Accordingly compressive strength was calculated based on the load changing point from elastic to plastic behaviour as shown in Fig. 7.

From Table 4 it can be noted that compressive strength and tensile strength values of paving blocks were reduced with the increase of sand content, due to reduced binder content. The F26/MS20/0.6/C,H mix satisfies the strength requirement for strength class 4 paving blocks (i.e. 15 N/mm^2) as per SLS 1425 which can apply for pedestrian use. The F26/MS30/0.6/C,H mix satisfies the tensile strength requirement for paving blocks (i.e. 3.6 MPa) as per BS EN 1338. As per the failure pattern under the compressive load shown in Fig. 8 the sharpness of edges and block thickness was reduced due to compaction. Figure 9 illustrates the deformation of paving block under splitting tensile test. Splitting tensile strength of fabric embedded paving block is higher than that of commercially available paving blocks.

Ductile failure pattern of these blocks indicate its ability to absorb impact energy which facilitates better foot comfort. Failure pattern of fabric embedded paving block is ductile which is totally different from that of commercially available cement based paving blocks and it can provides better foot comfort in footpaths, jogging paths and surfaces for sports areas.

Water infiltration capability of paving blocks were measured by performing constant head permeability test and the permeability was measured in terms of volume of water permeate through the sample at constant time intervals [14]. Permeable water content was measured by applying 1.1 bar constant pressure head to the cylindrical shape test specimen. According to the results shown in Table 5 fabric embedded paving blocks leads to reduce surface runoff during heavy rain due to improved water infiltration capability by 100 times when compared with commercially available conventional cement based paving blocks.

Permeability nature of paving blocks cause to increase the durability of the product as well. It allows deteriorate agents such as UV light, Chemicals to go through capillary pores inside the cement—fabric matrix. Manufacturing cost is highly depend on the manufacturing scale. The material cost for mixes F26/MS25/0.6/C,H and F26/MS30/0.6/C,H are Rs. 29.50 and Rs. 27.00 respectively per block.

Table 4 Mix proportions and test results of paving blocks

Mix id	Constituents percentage by volume %			W/C	Compressive strength (MPa)	Failure strain under compression (%)	Splitting Tensile strength (MPa)	Failure strain under splitting (%)
	Fabric	Cement	Manufactured sand					
Fv26/ms05/0.5/C,H	26	69	5	0.5	25.21	4.67	5.56	16.69
Fv26/ms10/0.5/C,H	26	64	10	0.5	22.22	5.33	5.38	17.65
Fv26/ms15/0.6/C,H	26	59	15	0.6	17.87	5.50	4.75	16.68
Fv26/ms20/0.6/C,H	26	54	20	0.6	17.42	5.17	4.18	19.56
Fv26/ms25/0.6/C,H	26	49	25	0.6	13.52	5.17	4.21	17.3
Fv26/ms30/0.6/C,H	26	44	30	0.6	7.62	5.50	3.64	44.06
Fv26/ms35/0.7/C,H	26	39	35	0.7	6.00	7.00	2.9	46.98
Fv26/ms40/0.8/C,H	26	34	40	0.8	2.63	6.67	2.95	47.62
Fv26/ms45/0.8/C,H	26	29	45	0.8	1.92	5.00	1.42	48.29
Fv26/ms50/1.0/C,H	26	24	50	1	1.42	5.83	1.08	52.06
Fv26/ms55/1.3/C,H	26	19	55	1.3	0.74	5.50	0.72	47.17
Fv26/ms60/1.6/C,H	26	14	60	1.6	0.12	0.33	–	–

Fig. 6 Surface appearance of paving blocks

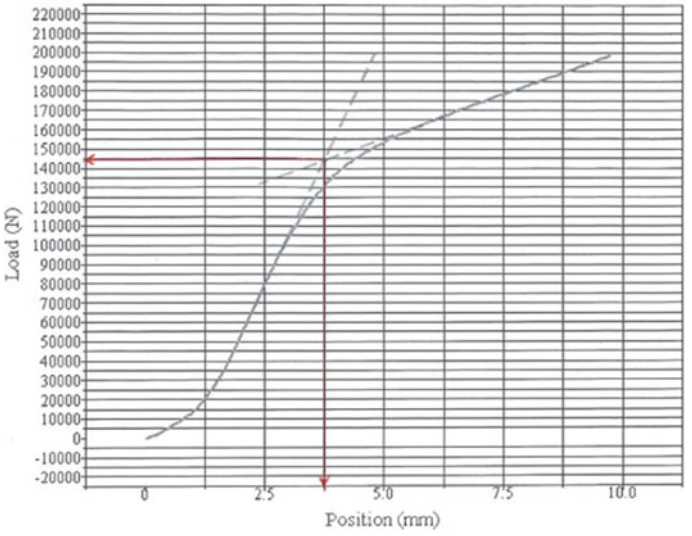

Fig. 7 Load deformation variation of compressed paving blocks

Fig. 8 Failure pattern of paving blocks under compressive load

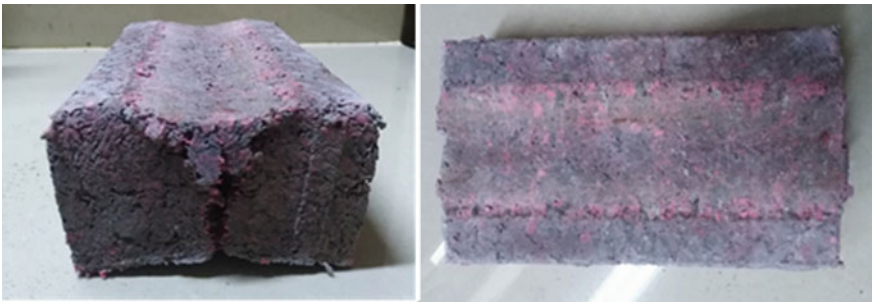

Fig. 9 Failure pattern of paving blocks under splitting tensile test

Table 5 Results of permeability test

Sample ID	Permeable Water (liters per square meter)			
	30 min	60 min	90 min	120 min
F26/MS25/0.6/C,H	99.6	205.9	321.3	440.1
F26/MS30/0.6/C,H	88.2	176.5	270.4	363.2
Conventional paving block	1.1	2.0	2.7	3.2

4 Conclusion

Shredded form of polyester spandex can be effectively utilized to produce paving blocks which shows impact energy absorption characteristics. Shredded fabric pieces showed the effect similar to fiber reinforcement in the cement matrix which resulted in strength improvement. Incorporation of fabric pieces into the cement matrix leads to improve water infiltration capability of the final product while satisfying strength requirements. On the other hand, this study has been alluded a viable solution for the major issue of waste fabric.

Acknowledgements The authors wish to express their gratitude to National Building Research Organisation research fund for the financial support and laboratory staff at Building Materials Research and Testing Division of NBRO and the Department of Civil Engineering of University of Moratuwa for the support given to carry out this research project.

References

1. Steve Evans CP (2017) Transtextile project report. Center for Industrial Sustainability, Cambridge
2. Singha K (2012) Analysis of spandex/cotton elastomeric properties: spinning and applications. Int J Compos Mater 2:11–16
3. Saverio Spadea IFACFF (2015) Recycled nylon fibers as cement mortar reinforcement. Constr and Build Mater, 200–209
4. Alva Peled SSBM (2006) Bonding in fabric-cement systems; effects of fabrication methods. Cem Concr Res 36(9):1661–1671
5. Aspiras FF (1995) Utilization of textile waste cuttings as building material. Mater Process Technol 48(4):379–384
6. SLS1144-Part:2 (1996) Specification for ready-mixed concrete, Part 2: Test methods, s.l.: Sri Lanka Standards Institution
7. BS812-Part103.1 (1985) Testing aggregates, Section 103.1 Sieve tests, s.l.: British Standards Institution
8. ISO1833 (2006) Textiles—quantitative chemical analysis, s.l.: International Standards Organization
9. BSEN:12127 (1998) Textiles, Fabrics, Determination of mass per unit area using small samples, s.l.: British Standards Institution
10. BS812-Part:2 (1975) Sampling and testing of mineral aggregates, sands and fillers, Part 2 Physical properties, s.l. British Standards Institution
11. BSEN:196-1 (2005) Methods for testing cement, Part 1: Determination of strength, s.l.: British Standards Institution
12. SLS1425 (2011) Specification for concrete paving blocks, Part 1: Requirements, Part 2: Test methods, s.l.: Sri Lanka Standards Institution
13. BSEN1338 (2003) Concrete paving blocks—requirements and test methods, s.l.: British Standards Institution
14. Halim NHA (2018) Permeability and strength of porous concrete paving blocks at different. J Phys, Issue Series 1049
15. BS882 (1992) Specification for aggregates from natural sources forconcrete, s.l.: British Standards Institute

Fires and Building Safety

R. Purasinghe, J. Chavez De Rosas, G. Mejia, M. Thomas, and X. Chen

Abstract Fires are widespread during the recent past and wildland fires and building fires have been reported. A building is computer modeled using Zone Modeling concept to study the temperature and smoke distribution of a one-story building due to a fire based on conservation of mass and energy. The results documented have smoke distribution as well as oxygen and carbon dioxide levels at different targets of the building and correlate to the levels of human exposure to the products of combustion.

Keywords Building fires · Zone models · Human comfort · Heat flux distribution · CFAST

1 Introduction

Fires are widely reported in recent times, in buildings and away from buildings. For flame propagation to occur, oxygen, heat, fuel, and the chemical chain reaction (known as fire tetrahedron) must be present. Several factors affect the behaviour of **wildland fires**, including terrain, weather, wind, fuels, and season. In the Western United States, lightning, industrial operations such as logging, and sparks and heat from trains traversing the wooded areas were known to start fires. However, some of the latest and most devastating fires have been attributed to careless human acts, including campfires, discarded smoking materials, and arson. According to US Fire service, more than 700 wildfires occur annually, destroying over 25,000 buildings and burning about 7 million acres of land. The economic cost is estimated to be about $5 billion each year. **Building Fires** are subject to internal causes, which bring together the ingredients of the fire tetrahedron—and grow in a self-staining manner. It is of interest to study how fire propagates in a building once started and how the temperature distribution of a building increases due to fire. The power output of a fire is usually described as a heat release rate (HRR), and for example a trashcan fire is

R. Purasinghe (✉) · J. C. De Rosas · G. Mejia · M. Thomas · X. Chen
California State University, Los Angeles, USA
e-mail: rpurasi@calstatela.edu

R. Dissanayake et al. (eds.), *ICSECM 2019*, Lecture Notes in Civil Engineering 94,
https://doi.org/10.1007/978-981-15-7222-7_45

known to be about 100 KW. There are computer fire models that are used to evaluate heat transfer occurring in a building. Two such models are Zone models and Field models.

In Zone Models, the compartment is divided into two layers and by solving equations of conservation of mass and conservation of energy for each zone determines the conditions in a room. The Consolidated Model of Fire and Smoke Transport (CFAST) computer program is a popular program for such studies. In Field models, many control volumes in a compartment are modeled, and the conservation equation in each such a volume is solved to determine the condition in a room. A popular computer program used to model Field Models is Fire Dynamic Simulator (FDS). An example of computer modeling of a building using CFAST with Smoke View (SMV) is presented in this study.

2 Methods and Analysis

A concrete building comprised of ten compartments was studied using CFAST computer simulation, with fire being placed in compartment B2. A scenario was created in which all windows and some doors were closed. Refer to Fig. 1 and Table 1 for the locations and dimensions of the compartments, respectively.

In looking at this example and further scenarios, the goal is to find the point in time in which humans in separate compartments start to feel the pain from the heat radiated.

To find these values, targets were set in the same compartment as the fire, as well as in a further room to compare the rates and time it takes for the heat from the fire to transfer from room to room. These targets were set to simulate actual

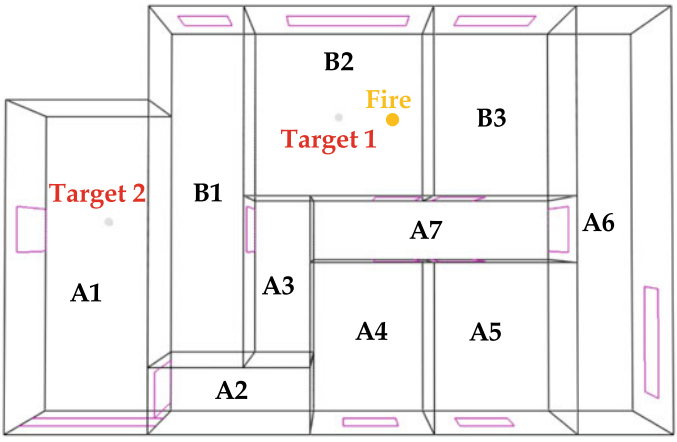

Fig. 1 3D plan view of single-story building layout in Smokeview

Table 1 Building compartment dimensions

Compartment	Width (m)	Length (m)	Height (m)
A1	3	7	3
A2	3.4	1.4	3
A3	2.6	3.6	3
A4	3	3.6	3
A5	2	9	3
A6	1.4	3.6	3
A7	5.6	1.4	3
B1	2	7.6	3
B2	4	4	3
B3	3	4	3

human occupants by assigning average human properties found in Table 2, created using work from Bauer et al. [2], Holmes (n.d.), Farris (n.d.), Herman [1], and Thermo-Works (n.d.).

Within the program, a wood fire was modelled (Fig. 2) based on the available pre-set options that have the fire grow as a function of the time squared. The peak heat release rate reached is about 1055 kW with a fire area of 0.09 m^2 that burns for a total time of 900 s.

The fire growth and decay rate is derived using the following equation:

Table 2 Average human target properties

Target properties	Average value
Density [2]	985 kg/m^3
Epidermis thermal conductivity (Holmes n.d.)	0.209 kW/(m °C)
Epidermis thickness (Farris n.d.)	0.0001 m
Specific heat [1]	3.5 kJ/(kg °C)
Emissivity (ThermoWorks n.d.)	0.98

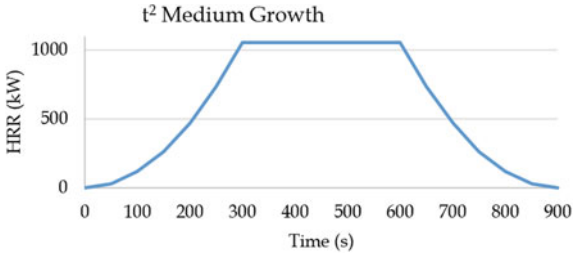

Fig. 2 Compartment B2 Fire HRR from CFAST

$$\dot{Q}(t) = \dot{Q}_{peak}\left(\frac{t}{t_{peak}}\right)^2, \quad (1)$$

where $\dot{Q}$ is the heat release rate and t_{peak} is 300 s, the time it takes for the HRR to reach 1055 kW, seen in Fig. 2.

3 Results

Following the analysis in CFAST, Smokeview (SMV) is used to visualize the compartments along with the smoke and temperature. While looking at the heat flux in the two targets, carbon dioxide, and oxygen levels are also paramount to safety to the people within the building.

For the scenario where all the windows are closed, but some doors are open, there is an enormous build-up of smoke as seen in Fig. 3. Values important to note can be found in Tables 3, 4 and 5 for compartments B2 and A1, respectively, which can be compared with Table 3 for reference, compiled using an online article by Malesky (n.d.).

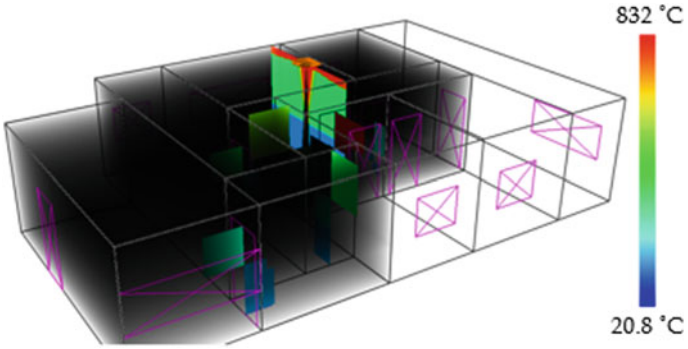

Fig. 3 B2 fire Smokeview simulation

Table 3 Dangerous O_2 and heat flux levels

Dangerous O_2 levels (Malesky n.d.)	Impairment
16%	Cells fail to function properly w/physical activity
14%	Impaired mental functions and intermittent respiration
6%	Death
Heat flux pain threshold for average human	1.7 kW/m^2

Table 4 B2—O_2, CO_2 levels, and heat flux

Upper O_2 (%)	Upper CO_2 (%)	Time (s)	Lower O_2 (%)	Lower CO_2 (%)	Time (s)
15.87	2.07	240	15.9	2.03	405
13.99	2.91	285	13.9	2.96	480
5.99	4.05	615	12.8	3.43	915
Target 1 heat flux			1.702 kW/m^2		
Time			225 s		
Target 1 max heat flux			3.133 kW/m^2		
Time			600 s		
Target 1 heat flux No longer painful			1.640 kW/m^2		
Time			690 s		

Table 5 A1—O_2, CO_2 levels, and heat flux

Upper O_2 (%)	Upper CO_2 (%)	Time (s)	Lower O_2 (%)	Lower CO_2 (%)	Time (s)
15.8	2.09	420	14.7	1.5×10^{-3}	855
14.0	2.93	495	13.1	1.4×10^{-3}	870
12.8	3.41	2535	5.8	6.3×10^{-4}	975
Target 2 max heat flux			0.0143 kW/m^2		
Time			615		

4 Conclusions

In the room where the fire is occurring, the point at which humans can feel pain from the fire comes a mere 15 s before the oxygen level starts affecting the occupants. Although the oxygen levels in the lower layer do not affect occupants until 405 s after the fire has started, they would still have to start getting low to be able to breathe by the 240 s mark.

In the separate compartment of A1, the heat flux never reaches the point that it starts to hurt the average human. It is important to note, however, that the oxygen levels in the upper layer of the compartment become dangerously low after 420 s of the fire ignition.

This is a work in progress research, as we are to study many different scenarios to represent real-world experiences. Cases with sprinklers, stairways, and multiple stories are underway, but could not be completed in time for this current publication.

Acknowledgements Partial financial support to the two student authors from the Nabib Youssef fund at the California State University, Los Angeles, is greatly appreciated.

References

1. Herman IP (2016) Physics of the human body, 2nd edn. Springer International Publishing, New York
2. Bauer W, Westfall GD (2010) University physics volume one. McGraw-Hill
3. CFAST. https://www.nist.gov/el/fire-research-division-73300/product-services/consolidated-fire-and-smoke-transport-model-cfast. Accessed: November 2019
4. Farris PK (n.d.) Nu skin. [Online] Available at: https://www.nuskin.com/en_ZA/corporate/company/science/skin_care_science/skin_anatomy_andphysiology.html. Accessed: November 2019
5. Holmes KR (n.d.) Thermal properties
6. Malesky M (n.d.) Minimum oxygen concentration for human breathing. sciencing.com
7. FDS, SMV. https://www.nist.gov/services-resources/software/fds-and-smokeview
8. ThermoWorks (n.d.) Thermoworks [Online]. Available at: https://www.thermoworks.com/emissivity-table. Accessed: November 2019

Ultra-Low Cycle Fatigue Failure Analysis of Steel Concentrically Braced Frames Using Non-Linear Fiber Beam Column Elements

E. M. S. D. Jayasooriya, C. S. Bandara, J. A. S. C. Jayasinghe, and K. K. Wijesundara

Abstract Earthquake induced steel structural failures are prevalent due to the high lateral forces applied to the structures resulting in excessive sway and more importantly ultra-low cycle fatigue of structural members. Even though lateral load resisting systems such as concentrically braced frames are installed to the moment resisting frames, ultra-low cycle fatigue induced brace failures play a dominant role in the context of local buckling of the members due to the amplified strains at the vicinity of the brace mid length followed by high strain concentrations. However, the concentric braced frames are designed and detailed deliberately to buckle out of plane in order dissipate the input seismic energy given to the structure by an earthquake. This global buckling of the braces is favorable to a structure in terms of the hysteretic response where the local buckling of the braces drives instant failure of the brace due to ultra-low cycle fatigue fracture. Cyclic void growth models are used to predict this fracture initiation due to ultra-low cycle fatigue in small scale steel components where the method requires a detailed stress and strain history obtained from a meticulous finite element model. If these models are to apply to a case where a multi storey building with braced frames in which an earthquake is applied, analysis of the finite element model to obtained the stress and strain histories until the failure, is quite impossible due to the high computational expense. In this regard, the present study first proposes a new method to model the structural behavior of concentric braces under cyclic loading using fiber beam column elements used in the OpenSees framework and then a new modified cyclic void growth model is proposed. To do that, experimental tests of concentric braces were modeled using OpenSees to observe the applicability and the limitations of fiber beam column element in terms of hysteretic response and strain variation in predicting the ultra-low cycle fatigue fracture. These tests were modeled using OpenSees in such a way, the numerical models fail at the same circumstances as the experimental test and thus validated the hysteretic response asserting the good prediction of global behavior by the numerical model. Penultimately, the resultant stress, strain histories having very low values due to fiber beam column element's inability of predicting local buckling were used to calibrate a cyclic void growth parameter called modified damageability index. Finally, all the

E. M. S. D. Jayasooriya (✉) · C. S. Bandara · J. A. S. C. Jayasinghe · K. K. Wijesundara
Faculty of Engineering, University of Peradeniya, Peradeniya, Sri Lanka
e-mail: darshana.jayasooriya@eng.pdn.ac.lk

R. Dissanayake et al. (eds.), *ICSECM 2019*, Lecture Notes in Civil Engineering 94,
https://doi.org/10.1007/978-981-15-7222-7_46

calibrated modified damageability values (λ') for several experiments were initially found and in future studies, a regression analysis to build a relationship for λ' in terms of brace geometric parameters such as slenderness ratio and width to thickness ratio to come up with a virgin equation in supporting the new simplified cyclic void growth model will be formulated.

Keywords Concentrically braced frame steel structures · Ultra-low cycle fatigue · Cyclic void growth models · Fiber beam column element models

1 Introduction

Earthquake induced structural failures were very dominant in the past where most of the steel moment resisting frames (SMRF) subjected to heavy cyclic loads experienced huge damages. The Northridge and Kobe earthquakes occurred in 1994 and 1995 are examples to prove the catastrophic damages to the structures. One major drawback in early structures was, people believed and had esteemed expectations that MRFs can withstand against large plastic rotations such as 2% or more. After these severe failures, engineers and researchers persistently worked for the development of these steel structures in terms of making new guidelines and techniques for modulation and modernizing [1]. As a result of these new steps, concentrically braced frame (CBF) steel structures came in to the picture and now has experienced a huge development in its structural response gradually and continuously. However, it was evident that CBFs alone can not perform efficiently and effectively without proper detailing and designing of the connections and structural components associated with the braces. Not only that, researchers found out that there is a special phenomenon called ultra-low cycle fatigue failure occurred in these braces when subjected to extreme seismic loads. Occurrence of local buckling which is resulted from the strain concentrations at the middle of the braces due to cyclic loads and degradation of the compressive strength with the cycling progressed also brought suffers. In the past, large number of experimental studies have been performed in order to identify and predict this brace fracture and various researchers have come up with empirical formulations to recognize how these failures can anticipate in terms of geometric and material properties. Lack of reliability and accuracy of theses predictions due to high empiricism in the findings led the researchers in to finding out more sophisticated methods and techniques to evaluate this fracture phenomenon. Strain-stress based failure predictions in which the failure was predicted using stress-strain histories obtained from a detailed finite element model (FEM) were then prevalent due to its accuracy and easiness. Cyclic void growth model (CVGM) developed by Kanvinde and Deierlein [2] is a fine instance for aforementioned context. Even though, they have implemented these fracture criteria for small scale structural models and components, it is very difficult and rigorous to implement within a multi storey building because that sort of a model developed in current finite element packages like ABAQUS, ANSYS, MIDAS etc. using shell or solid elements demands a huge computational

power and time to analyse together with much sophisticated modelling as well. It exemplifies the difficulty in obtaining a resultant stress-strain history for that sort of a model under extreme cyclic loads. As a result, it makes complicated to apply CVGM in predicting brace failure when it comes to a multi storey building. It is very useful if a less computationally expensive model can implement to analyse these multi storey building and can apply CVGM using the resultant stress-strain histories. Force-based fibre beam column element model formulated by Spacone et al. [5] and used within the OpenSees computer framework is such a numerical tool that we can use in this context. The use and limitations of fibre beam column element in this certain problem will be discussed hereafter.

2 Comparison of the Local and Global Performance of Different Steel Brace Models

Force based fibre beam column element utilized within the OpenSees framework is able to capture the effect of moment and axial force interaction, since, the inelastic beam-column element accounts for the interaction along the brace by integrating the uniaxial hysteretic steel material model over the cross section of the brace. Manegotto-Pinto model developed for steel material is used as the material model and it accounts for the kinematic and isotropic hardening along with the consideration of Bauschinger effect as well. Uriz et al. [6] noted that number of elements to create the brace, number of integration points within the element, initial camber and the nature of the fibre discretization govern the inelastic response of the brace element. Two elements were used to model a brace and an initial crookedness of 0.5% of the total length of the brace was allowed as an imperfection to initiate Bucklin. In addition to that, five integration points were decided to assign for each element followed by a sensitivity analysis. To analyse the accuracy of the brace models developed by fibre beam column elements, an experimental text called 1B performed by Shaback [4] was modelled in Opensees and MIDAS FEA software using shell elements. The Young's modulus and yield stress were taken as 191000 Mpa and 421 Mpa respectively for all the models. The specimen is a steel hollow tubular brace with a width and height of 127 mm and thickness of 8 mm. The brace is fixed at the ends. Figure 1

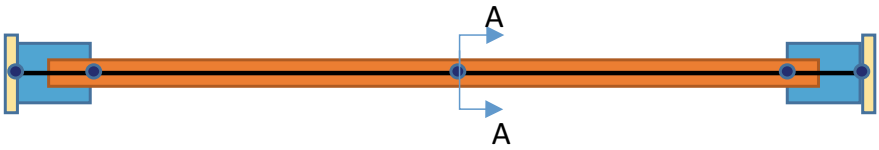

Fig. 1 Brace model with 2 inelastic elements

demonstrates a schematic of the brace model with two inelastic elements in which gusset plates are attached at both ends of the brace by another two elements while Fig. 2 illustrates the three-dimensional shell model developed for the brace.

A cyclic displacement history was applied to both the models according to the actual experiment as shown in Fig. 3 and observed the global and local hysteretic responses of the models. Axial forces versus axial displacement (Fig. 4), axial force versus lateral displacement (Fig. 5) were compared in terms of the global response

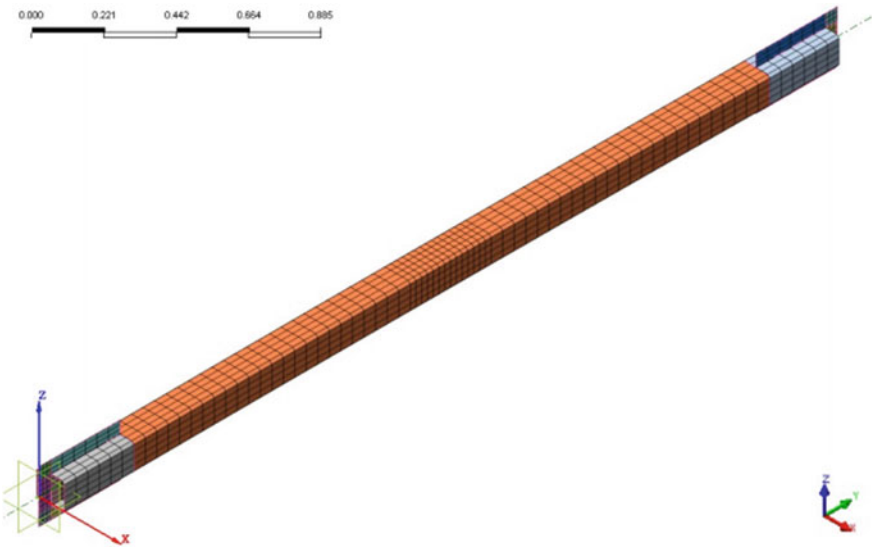

Fig. 2 Three-dimensional model developed with shell elements in MIDAS FEA (Mesh size: 12.5 mm × 12.5 mm)

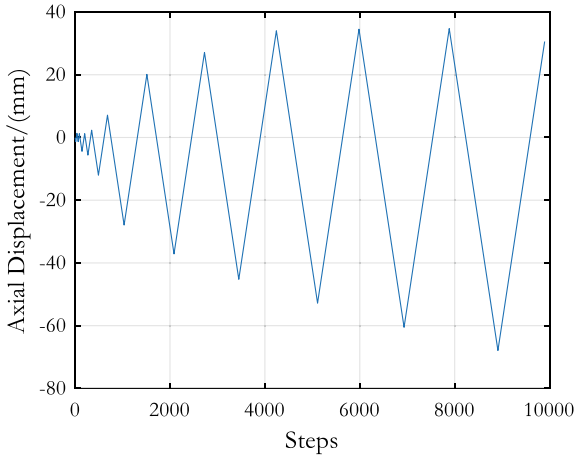

Fig. 3 Displacement history of specimen 1B

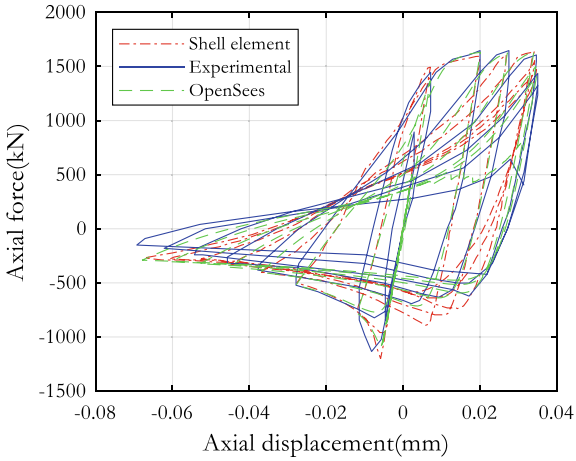

Fig. 4 Comparison between the axial force-axial displacement of shell and fiber models with experimental data

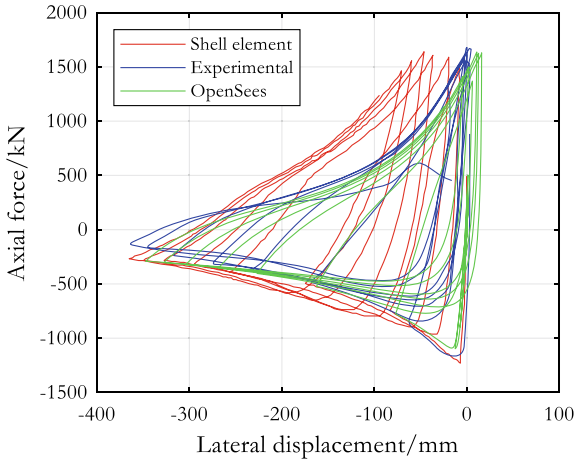

Fig. 5 Comparison between the axial force-lateral displacement of shell and fiber models with experimental data

of the brace while strain versus axial displacement (Fig. 6) and axial force versus strain (Fig. 7) were compared in terms of the local structural response.

When the global response is compared, it is clear that OpenSees can predict the structural response very accurately. Shell element prediction postulates that OpenSees also is capable of predicting the global behaviour as it does.

When the local structural behaviour predicted by numerical analysis is compared, a significant deviation between two models are seen. This is because of the fibre beam column elements inability to cater local buckling and resultant high stress concentrations. It is evident that strain values obtained from the OpenSees analysis are very low. Even though, the global response is predicted accurately by OpenSees with a substantial reduction in computational cost compared to shell element models, it lacks in predicting the strain variation accurately which will directly limit the

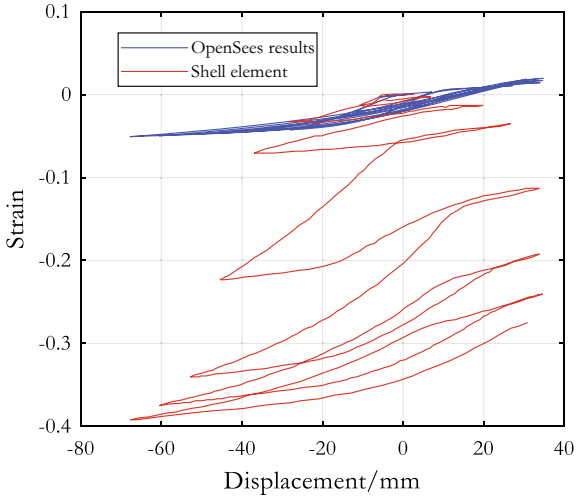

Fig. 6 Comparison between the strain-displacement behaviour of shell and fiber models

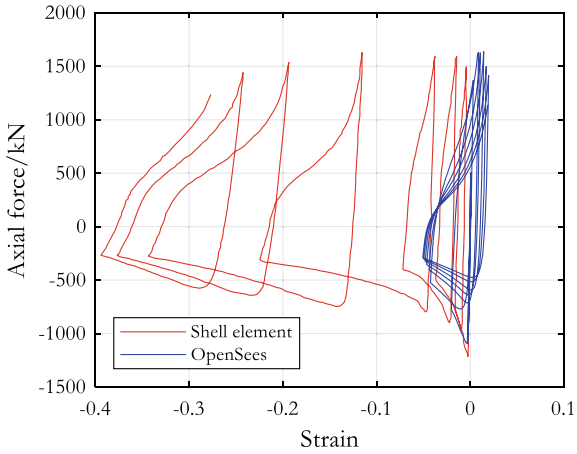

Fig. 7 Comparison between the strain-force behaviour of shell and fiber models

use of stress-strain histories generated from OpenSees in implementing with Cyclic void growth model (CVGM) proposed by Kanvinde and Deierlein [2]. Hence, the CVGM should be modified with its parameters in order to properly apply it within the Opensees analysis results.

3 Cyclic Void Growth Model

Cyclic void growth model is used to predict the ductile fracture initiation of steel structures subjected cyclic loads. In this model, ductile fracture initiation is assumed

to be actuated by void nucleation, void growth and coalescence followed by the combine action of stress and strain. In addition to that, when the cycling progressed voids start to shrink and swell due to the alternate tension and compression where the material structure gets damaged itself due to this. This predicts the number of voids at a certain plastic state and the material fails when a particular number of voids reach its material void capacity. The CVGM developed by Kanvinde and Deierlein [2] is given below.

$$\frac{dR}{R} = sign(T) \cdot C \cdot \exp(|1.5T|) \cdot d\varepsilon_p \tag{1}$$

where, $\frac{dR}{R}$ is the rate of change of void radius (considering R is void radius) and T is stress triaxiality defined by σ_e/σ_m where σ_e and σ_m stand for the effective stress and mean stress respectively. Here, sign (T) indicates the alternate tension and compression cycles while it is considered that when sign (T) is positive, voids grow and when the sign (T) is negative, voids shrink which is the dominant mechanism attributed to CVGM that leads to material damageability [3]. The above equation simplifies to,

$$\ln\left(\frac{R}{R_0}\right)_{cyclic} = \sum_{Tensile\ \ Cycles} C1 \int_{\varepsilon_1}^{\varepsilon_2} \exp(|1.5T|) \cdot d\varepsilon_t^p - \sum_{Compressive\ Cycles} C2 \int_{\varepsilon_1}^{\varepsilon_2} \exp(|1.5T|) \cdot d\varepsilon_c^p \tag{2}$$

$$VGI_{cyclic} = \frac{\ln\left(\frac{R}{R_0}\right)_{cyclic}}{C} = \sum_{Tensile\ \ Cycles} \int_{\varepsilon_1}^{\varepsilon_2} \exp(|1.5T|) \cdot d\varepsilon_t^p - \sum_{Compressive\ Cycles} \int_{\varepsilon_1}^{\varepsilon_2} \exp(|1.5T|) \cdot d\varepsilon_c^p \tag{3}$$

where, R, R_0, $C1$, $C2$, C, ε_t^p, ε_c^p, ε_1, ε_2 and VGI_{cyclic} are void radius at a particular state, initial void radius, Constant, constant, constant, plastic strain in tension, plastic strain in compression, initial strain value, next strain value at a particular strain state and finally the void growth index (void demand) respectively.

$$\text{Cyclic void growth model failure criterion; } VGI_{cyclic} \geq VGI_{cyclic}^{critical} \tag{4}$$

here, $VGI_{cyclic}^{critical}$ stands for the maximum void amount that the material can sustain without a fracture. This can be found by,

$$VGI_{cyclic}^{critical} = VGI_{monotonic}^{critical} \exp\left(-\lambda \varepsilon_p^{accumulated}\right) \tag{5}$$

where, $VGI_{monotonic}^{critical}$, the void capacity under monotonic loading condition, which is mostly a material dependent parameter can be calculated by a notched bar test along with the stress strain histories taken from a detailed finite element model using Eq. 6. λ is damageability index where the coefficient dominates the effect of stress alteration for a particular material. Here, $\varepsilon_p^{accumulated}$ is the plastic strain that has been accumulated at the beginning of each tensile excursion.

$$VGI_{monotonic}^{critical} = \exp(1.5T)\left(\varepsilon_p^{monotonic}\right)_{critical} \tag{6}$$

$\left(\varepsilon_p^{monotonic}\right)_{critical}$ is the maximum plastic strain that the material can sustain during monotonic loading.

4 Simplification of the Cyclic Void Growth Model

The inability of the force based fibre beam column element to predict the local response accurately limits the application of CVGM in its general format when it needed to be executed with the strain-stress results generated from OpenSees for a particular structural model. This section proposes a method to reconcile this issue and modify the parameters in the CVGM to use within the OpenSees results. This simplified CVGM is characterized by uniaxial stress (σ_{11}) and modified damageability index λ′ where the stress triaxiality (T) is replaced with the normalized stress T' (σ_{11}/σ_y) and damageability index λ is replaced by modified damageability index λ′. Here, σ_y refers to the yield stress of the material. Here, ε_t^p, ε_c^p, ε_1, ε_2 were taken as the plastic strains generated by fibre beam column element brace model but with the same definition mentioned before. By replacing those in the above equations finalizes the modified void growth index as follows.

$$VGI'_{cyclic} = \frac{\ln\left(\frac{R}{R_0}\right)_{cyclic}}{C} = \sum_{Tensile\ Cycles} \int_{\varepsilon_1}^{\varepsilon_2} \exp\left(\left|1.5T'\right|\right) \cdot d\varepsilon_t^p - \sum_{Compressive\ Cycles} \int_{\varepsilon_1}^{\varepsilon_2} \exp\left(\left|1.5T'\right|\right) \cdot d\varepsilon_c^p \tag{7}$$

Similarly, modified critical void growth index ($VGI_{cyclic}^{\prime critical}$) and the modified fracture criterion can be defined as shown below.

$$VGI_{cyclic}^{\prime critical} = VGI_{monotonic}^{critical} \exp\left(-\lambda' \cdot \varepsilon_p^{accumulated}\right) \tag{8}$$

Simplified Cyclic void growth model failure criterion; $VGI'_{cyclic} \geq VGI'^{critical}_{cyclic}$ (9)

The calibration of modified λ' is explained in the next section.

5 Calibration of Modified Damageability Index

It is expected to calibrate modified damageability index λ' for new simplified cyclic void growth model by iteratively changing the value of λ' until the fracture criterion satisfied through the low strain histories obtained from the OpenSees analysis. To do this, an experimental specimen (2B) performed by Shaback [4] was used. The objective is to get the local and global structural response using OpenSees framework for this particular specimen. Same experimental conditions were modeled in the OpenSees and executed the analysis until the experimentally failure cycle is met in the OpenSees model also. Thus, the analysis is capable of giving accurate force – displacement response which can be used as a validation for the numerical model as shown in Fig. 8. Then, the simplified CVGM was implemented while iteratively changing the λ' value until the failure criterion satisfied. The resultant λ' value is distinct to the actual damageability index λ value which is a constant value usually defined upon type of material.

Figures 9 and 10 shows the failure criterion where in Fig. 9, λ' value was assumed as 0.01 and the failure criterion was not satisfied where in Fig. 10, λ' was assumed as 0.018 and that value satisfied the failure criterion.

From this method, different λ' values can be obtained for different geometric properties using various specimens. It is evident that, when sufficient number of data for

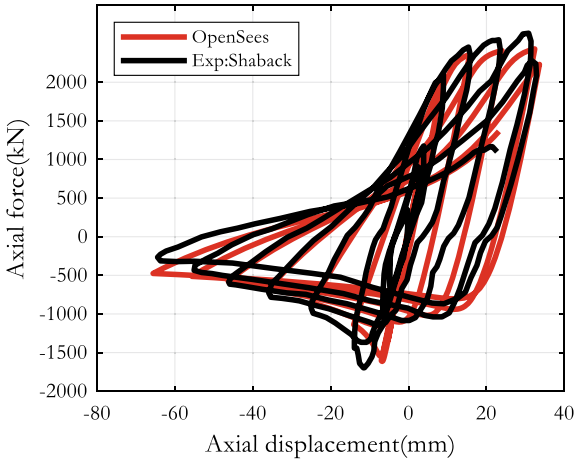

Fig. 8 Force-displacement response of Specimen 2B

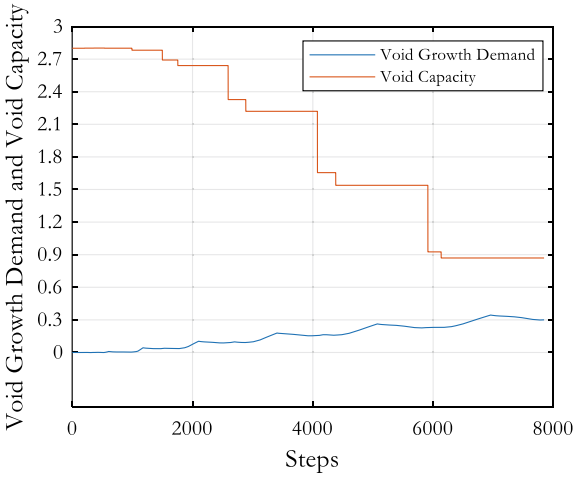

Fig. 9 Failure criterion is not satisfied for $\lambda' = 0.01$

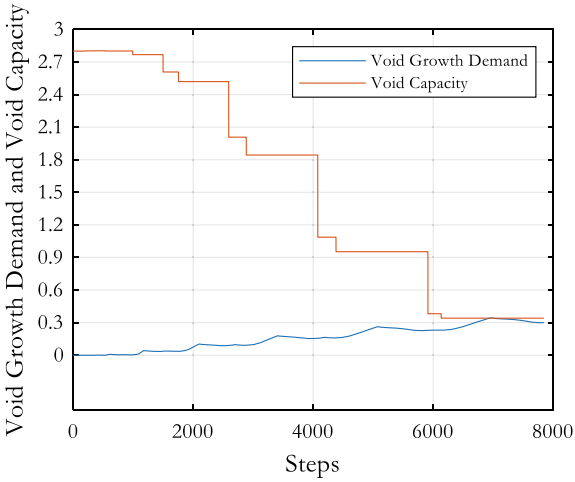

Fig. 10 Failure criterion is satisfied for $\lambda' = 0.018$

λ' is available after being done the aforementioned method for several experimental tests, a relationship can be formed for λ' as a function of brace geometric properties such as slenderness ratio and width to thickness ratio.

6 Conclusions

It was clearly seen that fibre beam column element model utilized within the OpenSees framework can accurately predict the global structural response of the brace. However, it lacks the ability to predict the local response of the brace because

fibre beam column element has been formulated considering the small displacement theory. Hence, the element can not reflect the effect of local buckling and strain concentrations at the middle of the brace. Even though, this problem limits the use of stress-strain histories in predicting the fracture initiation due to ultra-low cycle fatigue using existing CVGM, a modified and a simplified CVGM can be made by changing the damageability index values (λ). Present study shows its potential by calibrating new modified damageability index values for one experiment. In future, it is expected to perform this same analysis to number of experiments and observe the variation of λ' values with respect to the brace geometry. If an expression can be made to calculate this λ' for a certain brace, once the stress-strain history obtained from the OpenSees software analyzed for a particular earthquake is employed within the proposed simplified CVGM, it can be found whether the certain brace is failed under the given earthquake level.

References

1. FEMA F (2000) Recommended seismic design criteria for new steel moment-frame buildings. FEMA-350
2. Kanvinde AM, Deierlein GG (2006) The void growth model and the stress modified critical strain model to predict ductile fracture in structural steels. J Struct Eng 132(12):1907–1918
3. Kanvinde AM, Deierlein GG (2007) Cyclic void growth model to assess ductile fracture initiation in structural steels due to ultra-low cycle fatigue. J Eng Mech 133(6):701–712
4. Shaback JB (2001) Behavior of square HSS braces with end connections under reversed cyclic axial loading. Calgary
5. Spacone E, Filippou FC, Taucer FF (1996) Fibre beam–column model for non-linear analysis of R/C frames: Part I. Formulation. Earthquake Eng Struct Dynam 25(7):711–725
6. Uriz P, Filippou FC, Mahin SA (2008) Model for cyclic inelastic buckling of steel braces. J Struct Eng 134(4):619–628

Incorporation of Disaster Risk Reduction Mechanisms for Flood Hazards into the Greensl® Rating System for Built Environment in Sri Lanka

A. A. S. E. Abeysinghe, C. S. Bandara, C. S. A. Siriwardana, R. Haigh, D. Amarathunga, and P. B. R. Dissanayake

Abstract Global human population continues to boom which consequently necessitates the provision for more buildings. Predominantly in developing countries, these buildings, built to accommodate the influx of more people comply with local and national building laws and regulations which have been outdated and do not resist to natural hazards and rapidly changing natural global trends such as climate change and global warming, etc. Disaster risk in Sri Lanka is increasing mainly due to unplanned urbanization, outdated and poor quality buildings and infrastructure, and the impacts of climate change. This has exposed the community and their economic assets vulnerable to natural hazards such as floods, cyclones, landslides, droughts, coastal erosion and tsunami. Out of those, floods are considered to be the most frequent as well as which destroyed and damaged the highest number of buildings during the period of 1965–2019. As more anthropogenic natural hazards like floods pile up, it is essential that developments, specially buildings which are community shelters, to be disaster resilient and be designed to withstand strains and pressure which will be imposed by future trends. Therefore, sustainable hazard mitigation measures are required to develop a safe, economically feasible, environment-friendly and socially approved growth in Sri Lanka. Although Green Building Council of Sri Lanka (GBCSL) has promoted sustainability and resilience, specifically through reducing resource usage and energy consumption, it has not properly recognized the need of incorporating Disaster Risk Reduction (DRR) mechanisms to withstand against the natural hazards in their GREENSL® Rating System for Built Environment. This research paper is focused on identification of structural and non-structural DRR mechanisms for flood hazards which can be incorporated into the GREENSL® Rating System for Built Environment through refinements to the sub-categories under main 8 categories.

A. A. S. E. Abeysinghe (✉) · C. S. Bandara · P. B. R. Dissanayake
Faculty of Engineering, University of Peradeniya, Peradeniya, Sri Lanka
e-mail: sonali.abeysinghe@eng.pdn.ac.lk

C. S. A. Siriwardana
Faculty of Engineering, University of Moratuwa, Katubedda, Sri Lanka

R. Haigh · D. Amarathunga
University of Huddersfield, Huddersfield, UK

R. Dissanayake et al. (eds.), *ICSECM 2019*, Lecture Notes in Civil Engineering 94,
https://doi.org/10.1007/978-981-15-7222-7_47

Keywords Disaster risk reduction · Flood hazard · Disaster resilient buildings · Climate change · Sustainable buildings

1 Introduction

According to World Health Organization (WHO) [17], every year natural disasters kill around 90,000 people and affect close to 160 million people worldwide. Natural disasters include earthquakes, tsunamis, volcanic eruptions, landslides, hurricanes, floods, wildfires, heat waves and droughts. They have an immediate impact on human lives and often result in the destruction of the physical, biological and social environment of the affected people, thereby having a longer-term impact on their health, well-being and survival. Also according to the report 'Economic losses, Poverty and Disaster—1998 and 2017', published by United Nations system for Disaster Risk Reduction (UNISDR) [5], during the period of 1998 and 2017, climate-related and geophysical disasters have killed 1.3 million people and left a further 4.4 billion injured, homeless, displaced or in need of emergency assistance. While the majority of fatalities were damaged and destroyed due to geophysical events, 91% of all disasters were caused by floods, storms, droughts, heatwaves and other extreme weather events. In 1998–2017, disaster-hit countries experienced direct economic losses valued at US$ 2908 billion, of which climate-related disasters caused US$ 2245 billion or 77% of the total. This is up from 68% (US$ 895 billion) of losses (US$ 1313 billion) reported between 1978 and 1997. Overall, reported losses from extreme weather events rose by 151% between these two 20-year periods.

When it comes to Sri Lankan context, Sri Lanka was considered as the 2nd most affected country from extreme weather events during 2018 (Germanwatch Global climate index). Sri Lanka is considered as a tropical country due to its placement near the equator which experiences high temperatures and frequent rainfalls almost through out the year. Wet zone of Sri Lanka receives over 5000 mm of annual rainfall as the country is located in south west monsoon region whereas northern and eastern lands of the island are usually identified as dry zones due to the mounting barrier of the central highland. Within this background, disasters with hydro-meteorological origin are more common and act as annual events in the country. River floods, urban floods, landslides, cyclones, wildfires are considered as primary hazards with high risk and coastal erosion, tsunami and droughts with medium risk [16]. Table 1 shows Summary of deaths, houses destroyed and damaged, number of affected victims, and losses from main disasters occurred in Sri Lanka during the period of 1965–2019. The most common natural hazards in Sri Lanka include localized and seasonal floods and associated landslides while less frequent but more severe hazards include cyclones, droughts, and tsunamis [16]. Also Sri Lanka was among one of the worst hit countries by the 2004 Indian Ocean Tsunami. According to World Bank estimates, the country's average annual losses are $380 million which is 3% of total government expenditure. Figure 1 shows the breakdown of nationally reported economic losses due to main natural hazards occurred during 1990–2014 in Sri Lanka. Sri Lanka's

Table 1 Summary of deaths, houses destroyed and damaged, affected victims and local losses from main disasters occurred in Sri Lanka (1965–2019)

Hazard/disaster	Deaths	Houses destroyed	Houses damaged	Number of victims	Local losses ($)
Animal attack	1002	197	7715	80,207	0
Coastline and coastal erosion	0	153	437	4137	0
Collapse of building	15	0	1	12	0
Collapse of gabage fill	32	60	22	1782	0
Cyclone	846	18,208	111,565	1,375,005	0
Cyclone and flood	9	13,178	37,371	319,128	0
Drought	0	0	0	20,725,949	0
Earth slip	10	56	168	3043	0
Epidemic	368	0	0	572,644	0
Explosion	1	161	346	7952	0
Fire	108	2078	1043	16,489	7,700,000
Flash flood	6	72	684	8812	0
Flood	707	55,003	186,548	15,068,593	378,500
Forest fire	1	16	19	198	0
Heavy rains	37	689	7583	780,213	0
Landslide	1077	2900	12,026	291,964	1,038,000
Lightning	549	37	595	4014	0
Strong wind	211	7693	104,548	731,571	1,077,900
Tornado	0	58	277	910	0
Tsunami	30,959	57,085	48,069	970,705	16,130,000
Urban flood	0	0	0	155	0

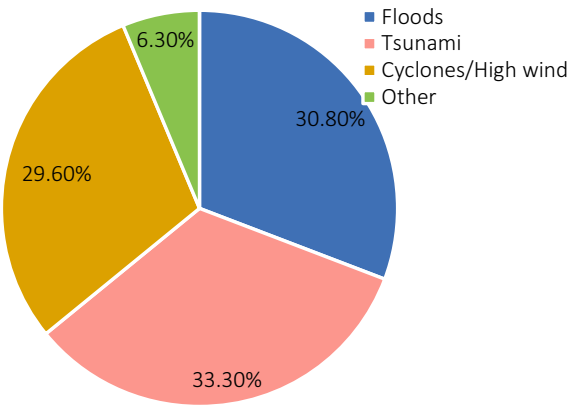

Fig. 1 Nationally reported economic losses

flood risk profile is rising day by day. In the Colombo Metropolitan Region, economic growth and changes in land use are exacerbating flood risk. In 2010, heavy rainfall and flooding affected about 50% of the private sector. In May 2016, Tropical Storm Roanu caused flooding and landslides in 22 out of 25 districts. Over 90 people were killed and damages and losses, per the preliminary post-disaster needs assessment, exceed $570 million. Climate change is expected to increase the frequency and impact of hydro-meteorological hazards. Major flooding in 2010, 2011, 2014, and 2016 exemplifies a 20-year trend [7]. According to the records of Disaster Management Center (DMC) of Sri Lanka and UNISDR [4], floods are considered to be the most frequent, highest number of disasters reported and as well as which destroyed and damaged the highest number of buildings during the period of 1965–2019 in Sri Lanka. Therefore, the focus of this research paper is into the flood hazards of Sri Lanka.

Flood can be defined as the condition in which the land is submerged in water which is normally used to be dry. It can be attributed to an unusual high stage of a river or other water bodies like lakes, oceans etc. during which the water spills over the bank and spread to the adjoining land. The low-lying area adjacent to a river bank is called flood plain, which is formed mainly of the sediments of river and consists of a very fertile soil. For a flat or low-lying land with infiltration or runoff rate lesser than the rate of precipitation, water can accumulate resulting in a flood situation [12]. Due to different natural phenomena like rainfall lasting for a longer period of time, monsoon seasonal rains or tropical cyclones, floods occur in rivers or other drainage systems. In coastal areas, when the water level is high due to some storm and its combines with the natural high tide the water spills over to the adjoining areas causing a flood. In urban areas due to improper drainage system sometimes due to high precipitation water can accumulate on the streets and maybe sometimes comes back into the building through sewers pipes when rainfall is higher than the drainage capacity. Rising rate of population and consequent urbanization leads to deforestation and a high percentage of the paved surface which blocks the infiltration of water in case of precipitation. Lesser infiltration leads to high runoff resulting in rapid and increased hydrographic peak which creates floods [12]. This increasing trend of flood hazards and disaster losses caused to the built environment are mainly due in part to the unprecedented rate of urban growth, increasing dependence on complex infrastructure, unplanned urbanization, outdated and poor quality buildings and infrastructure, and the impacts of climate change that are increasing exposure to anthropogenic and natural hazards [2].

Also, a study conducted by the Asian Institute of Technology in 2012 has investigated the adoption of disaster resilience measures for wind, rain and flood and landslides in the national building codes. This highlights that landslide resistance and flood situations are not considered in the Sri Lankan building codes and consideration of wind effects are also voluntary [3]. A detailed, comprehensive disaster resilient building code could not be found in Sri Lanka. A further study conducted in Sri Lanka during 2014 revealed a lack of adequate regulatory frameworks, unplanned urbanization and city development, outdated building stock and infrastructure which are not a safe condition, unauthorised developments, inappropriate institutional arrangements,

inadequate capacities at the local level, a lack of funding, an inadequacy of qualified human resources, and corruption and unlawful activities [14]. These factors will undermine efforts to increase disaster resilience in the built environment. Built environment consists of infrastructure such as roads, railways, schools, hospitals, phone lines, treatment plants and power generation plants and buildings which includes single storied to high rise commercial and residential shelters. The focus of this research paper is about the buildings in the built environment but not about its infrastructure component. Although GBCSL has promoted sustainability and resilience, specifically through reducing resource usage and energy consumption in buildings, it has not properly recognized the need of incorporating DRR mechanisms to withstand against the natural hazards in their GREENSL® Rating System for Built Environment. Although GBCSL has promoted the green buildings among the Sri Lankan community, the sustainability of those buildings to withstand against strains and pressure which will be imposed by increasing trends of hazards like floods are questionable. Even though the buildings constructed are platinum rated green buildings which have been applied with many greener and sustainable concepts, they are not sustainable if they can not resistant which is simple can be damaged or destroyed against the natural hazards. Therefore incorporation of DRR and disaster resilient mechanisms in to the community shelters which are buildings becomes very important and vital for a sustainable built environment. The DRR mechanisms for flood preparation and mitigation can be categorized into structural (hard) and non-structural (soft) measures. Efficient flood fore-casting warning systems, following laws and regulations and awareness raising etc. come into nonstructural approach whereas small to large scale constructional components added to the buildings to mitigate flood risks and damages are considered to be structural approaches. This research paper is focused on identification of structural and non-structural DRR mechanisms for flood hazards which can be incorporated into the GREENSL® Rating System for Built Environment through refinements to the sub-categories under main 8 categories [8]. Therefore, globally used structural and non-structural measures for flood resistant buildings, applicable to Sri Lankan context are discussed in the following sections of the paper.

2 Structural (Hard) DRR Mechanisms for Flood Preparation and Mitigation

Under this section, the structural measures which have been taken and applied in world wide for flood mitigation and protection will be discussed. When it comes to hard DRR mechanisms, flood performance of buildings can be categorized as, structural performance, material performance and impacts of contamination as well. Around the world, there are many structural mechanisms and approaches are proposed for making the buildings more capable to resist floods.

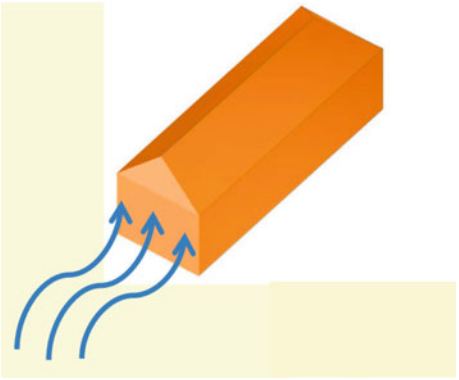

Fig. 2 Shorter side of the building is oriented to face the direction of flooding

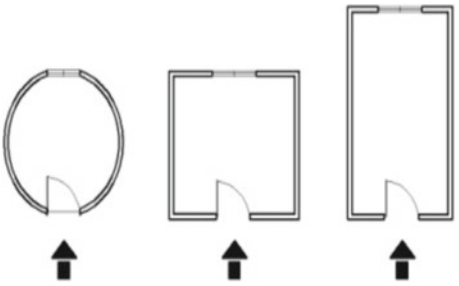

Fig. 3 Placement of openings in the buildings, creating a flow path for water

2.1 Planning Phase of Building Orientation and Placement of Openings

Identify the flood zone and the maximum flood level recorded in the selected location or site, using available sources or by contacting relevant authorities. i.e. Irrigation Department. Then the direction of the flooding is to be identified properly. The it comes to the building plan and its orientation, shorter side of the building shall be oriented to face the direction of the flooding as shown in Fig. 2. Also openings should be placed in line with each other on opposite walls creating a flow path for water as shown in Fig. 3 [11].

2.2 Foundations of the Flood Resistant Buildings

Concrete slabs and foundations are the most suitable foundation type to be used to withstand the natural hazards and pile foundations can be used where problematic soil conditions exist. Buildings should be located via stable foundations on soil strata having no susceptibility for liquefaction due to flooding. Depth of foundation shall be increased as follows;

- The column footings shall be lowered minimum 1.0 m below finished grade.
- Wall footings shall be lowered minimum 0.6 m below grade.

Also flood barrier walls can be designed and introduced as a solution to the threat of flooding at ground levels in storied buildings [11].

2.3 *Rising the Elevation of the Buildings*

Mainly, there are two types of elevated buildings are available as below.

1. The floor elevation shall be raised by increasing the plinth either by building on a higher ground as in Fig. 4 or by creating an elevated ground as shown in Fig. 5. The plinth height shall be minimum 150 mm above the highest recorded flood level in the region.
2. Construct the building on silts where the silts shall be raised up to minimum 150 mm above highest recorded flood level in the region and the maximum unsupported height of silts shall not exceed 3 m. Otherwise an intermediate tie beam shall be provided as shown in Fig. 6.

Here in both options, the elevation of living area is raised above the Base Flood Elevation (B. F. E.) of the respective construction site. The house is raised on some supports which should be sufficiently strong enough to bear the load of the structure and forces acting by the flood water and have ample space for the passage of flow

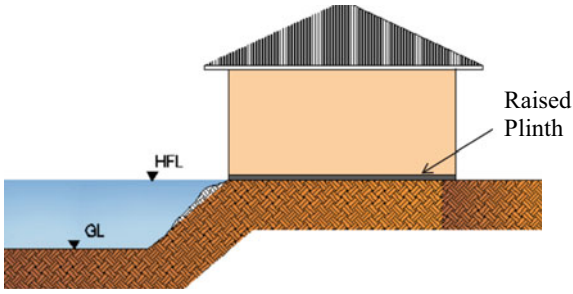

Fig. 4 Plinth level raised by building on higher ground

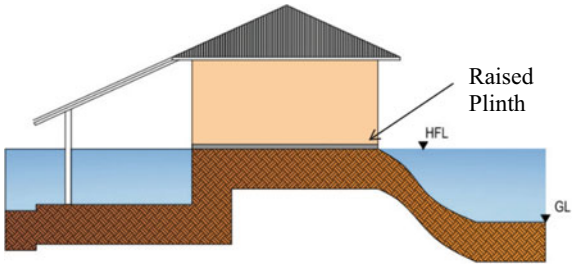

Fig. 5 Plinth level raised by creating an elevated ground

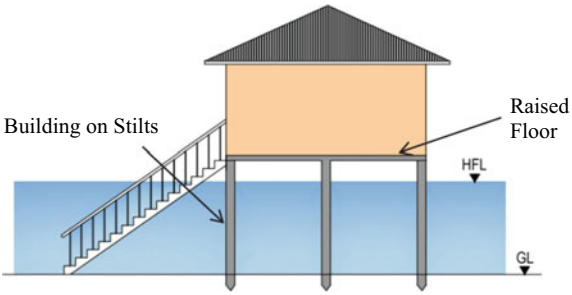

Fig. 6 Plinth level raised by building on silts

in case of flood. For an area with a low probability of flood the space below the living area can be utilized for parking the vehicle, laundry or bathroom etc. The B. F. E. is the water surface level for a flood of 100 years return period. There are many methods available for estimation of flood; for some sites with lesser available data or for sites with no data available at all, regional flood frequency analysis can be used [1].

Existing buildings which can not be elevated also should be retrofitted and improved to be disaster resilient in a way that the basement infills and flood openings can help manage storm water. Converting the lowest floor to nonessential uses like a garage can reduce the flooding impact to living areas.

2.4 Superstructure of the Buildings

Cross walls are the main superstructure type used in the flood resistant buildings as the cross walls can be utilized to strengthen walls against flow of flood water. Figure 7 indicates the placement of cross walls inside the building. Also at least 4 reinforced concrete columns at the four corners of the building are required for the strengthening of the building. For wall lengths exceeding 6 m, an additional intermediate column along that wall should be introduced. These columns are essential for buildings in the coastal zone subject to flooding. Walls should be made as heavy as possible; if hollow blocks are used they should be at least 200 mm thick, and if 100 mm thick walls are used, they should be of solid block work or brickwork. Such walls would provide a basic level of thermal insulation and rain protection too. The sizes of openings on walls should be such that the aggregate width of openings on any wall do not exceed 50% of the width of that wall [11].

2.5 AMPHIBIOUS Buildings

Amphibious buildings can be used in both land and water and they are made in such a way that they are free to float on the flood water and rose with the water level

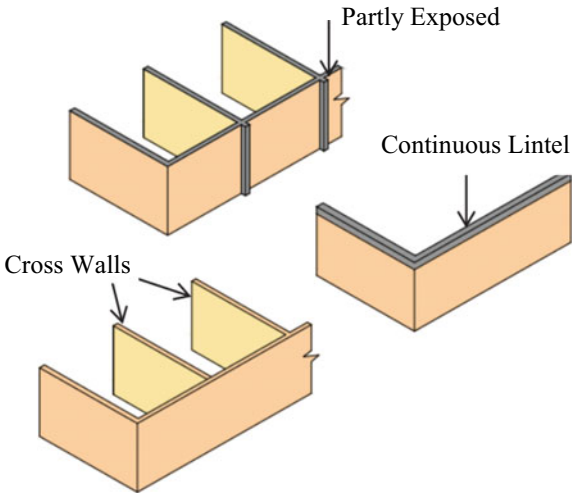

Fig. 7 Cross walls

and comes back to their or original initial position as the flow recedes. Amphibious buildings are mainly constructed for residential purposes as houses around the world in areas such as Maasbommel, Netherlands, and at Raccourci Old River, Louisiana, New Orleans and Bangladesh due to very frequent floods they face. There are major two types of amphibious houses can be found as, boat type and lift type [6].

2.5.1 Boat Type AMPHIBIOUS Buildings

This type of floating building is free to move in both vertical and horizontal directions. The floor of the building is designed to be water tight so the water does not enter from the base to the floor area. The building has an anchor system to stop the house to dislocate from its original position with the flow of water.

2.5.2 Lift Type AMPHIBIOUS Buildings

When it comes to lift type amphibious buildings, these buildings are free to move only in vertical direction in a controlled way along with the rising water level in a flood situation. The building is restrained to move in horizontal direction by guiding columns at the corners. The building remains on ground surface until the flood water starts lifting it up by buoyant forces. Both type of amphibious buildings can be provided with a suitable base to be supported on and to provide sufficient buoyant forces required to initialize the movement. The foundation used in these houses can be termed as buoyant foundation. Underside of the house buoyancy blocks are provided. Buoyancy blocks lift the house in case of flood and can be made of recycled, recapped plastic bottles as well.

2.6 Flood Proof Construction Materials

Building with robust materials which have a high versatility and strength, wind and water resistance, tsunami resistance, fire resistance, energy efficiency and durability. Concrete building systems are especially suited to provide resistance to natural hazards. Concrete doesn't rot or rust even if it is subject to flooding. Concrete has the necessary hardness and mass to resist the high winds and flying debris of high winds. Concrete is fire resistant and non-flammable, which means it can contain fires and will not contribute to the spreading of fire. Reinforced concrete framing systems can be designed to resist the most severe earthquakes without collapse. Therefore, concrete structures are suitable and resist against many natural hazards including floods. Stone, brick, concrete, decay-resistant wood, and water-resistant, fibre-reinforced gypsum sheathing resist flood damage better than materials like plywood, particle board, linoleum, vinyl, carpeting, traditional gypsum, and plaster. Internal walls should be water resilient to withstand floods. For that, materials should be used which will allow fast recovery such as concrete block partitions, lime plaster or magnesium oxide board as finishing skirting is sealed with an internal cavity membrane.

Also, the materials used should be of good quality too, especially since excessive loads may have to be resisted. For binding mortar, the mix proportions should not be leaner than 1:6 cement:sand. For making cement blocks, the proportions should be 1:10 with cement and sand (or quarry dust); it can be made 1:7:10 using cement, sand and 6–8 mm aggregate chips. Blocks should ideally not be used until least 1 month (or even 2 months) after casting, so that most of the shrinkage is over before the block is placed in the wall. For concrete, the quality should be at least grade 20, which can be achieved by using a 1:2:4 mix of cement, sand and coarse aggregate.

2.7 Wall to Floor Junction in a Building

Wall to floor junction is considered to be one of the main component which needs to be designed against floods as it is a major point which water leaks inside the building. There are two options available. Option 1 is, designing of a primary and a secondary layer of waterproofing which includes water tanking below slab to resist water pressure (primary layer) and a cavity drainage for water collection after flood (secondary layer). Second option is utilizing a waterproof concrete again with a primary and secondary layers of waterproofing where primary layer is consist of a concrete slab and wall with water resistant additive and the secondary layer is with a cavity drainage for water collection and removal following a flood.

2.8 Wet Flood Proofing Technique

Wet flood proofing involves the controlled and safe passage of flood water through the lower levels of the building. The building is designed to resist water up to 600 mm in depth after which water is allowed to enter into the property to reduce pressure on the structure. The sewers and water system should be above the water level or should be sealed when the water rises above them to avoid any health hazards. Also sewage system can be designed with a non-return valve while drainage pipes are sealed through the "flood proof layer", covered and locked in concrete to resist lower ground water pressure and to prevent damages from floods. Inspection chambers are fitted with anti-lift lid. All service entry points should be sealed or raised where possible and all electrics appliances and outlets should also be at higher levels above the design flood level. Kitchen units below flood level should be of waterproof materials (plastic or stainless steel hardware) while kitchen unit doors and drawers should also be sealed. The inlets points should be opened well before any pileup of water to avoid pressure at the structure. Also fire protection equipment should be raised in new construction, above the flood level. Automatic opening window panels (flood inlets) are triggered by localized sensors to allow a controlled inundation of flood water into the property [9].

2.9 Building the Lower Levels Water Tight

The walls and openings of the lower levels are sealed to stop the water from penetrating the building. The sealing should be sufficiently strong to bear the forces in the flood conditions acting in the form of lateral forces and uplift thrust of the flood water. The building should be designed by taking all these forces in consideration. Enclosures, sealants, membranes and coatings can be used as main construction materials to make the lower levels water tight. Flood resistant doors should be installed to protect against water entry.

2.10 Post-flood Drainage Systems

Channels, pipes and drains are built into the floor to drain off the water after a flood. Drain connections into man hole are fitted with non-return valve and anti-lift lid. Pipes are fitted with non-return valves to avoid back-flow of sewage as well. A Mechanical Ventilation Heat Recovery (MVHR) system is installed in addition to natural ventilation which will aid drying out after a flood.

2.11 Other Structural Flood Prevention and Mitigation Techniques

- Do relevant checking and monitoring checks of the building structures in specific predetermined periodic intervals (maybe annually), depending on the location of the building, under the monitoring and targeting the resilience of the buildings to withstand against the natural hazards.
- A backup fire safety communication system should be installed in commercial buildings and residential housing apartment complexes. All such high populated and high rise buildings in flood zones should consider having a backup wireless fire communication system, and new large critical buildings must have backup phone and data connections. Mandate the use of storage batteries with a life of at least eight hours to serve buildings' fire and life safety communication systems. Also as another option, can use cogeneration and solar power during blackouts due to natural hazard as a reliable backup power source. Remove barriers which restrict gaining solar energy and increase the allowable roof space for solar panels. Also residential stairwells, hallways and emergency exit ways should be kept lit during blackouts using the generated solar energy.
- In flood prone areas, storm water collection systems which can be integrated to rain water harvesting tanks or storages should be designed and installed to handle greater quantity of rain water. These storm water collection tanks can be installed either on roof tops or as underground mini reservoirs depending on the rainfall data of the site. Also this system can be developed in most of the buildings in urban areas and can integrate each underground mini reservoirs of the buildings and construct an underground water transmission tunnel which can reduce greater amount of flood hazards in urban areas. This concept has been applied by many developed countries like Japan to prevent flood hazards in their major cities.
- The reliance on public water systems should be reduced in case of emergency situations. Installation of redundant emergency networks of water supply and wastewater treatment by creating secondary facilities, redundant transmission-distribution pipelines or multiple water storage facilities. When it comes to solid waste management systems maintained inside the buildings, special care and safeguard should be given to the toxic materials storage units in flood zones. Toxic waste collection bins or stores in flood zones should be stored in a flood proof area which water can not be reached.

3 Non-structural (Soft) DRR Mechanisms for Flood Preparation and Mitigation

There is no flood protection measure guaranteeing complete safety. In many vulnerable areas, sufficient flood protection cannot be reached with the help of structural means only. Hence, further flood risk reduction via non-structural measures is often

indispensable. An optimal, site-specific mix of structural and non-structural measures is being sought. Non-structural flood protection measures include source control, zoning, insurance, flood forecast-warning system, awareness raising and improving information, etc. Few non-structural flood protection measures which can be incorporated in to the GREENSL® Rating System for Built Environment are discussed below.

- Assess site condition before design to evaluate sustainable options by completing and documenting site assessment on following [10];
  - Topography—Contour mapping, unique topographic features, slope stability risk.
  - Hydrology—Flood hazard areas, delineated wetlands, lakes, streams, shorelines, rainwater collection and reuse opportunities and initial water storage capacity of the site, etc.
- Watershed management (source control) modifies formation of floodwater. This concept includes land use and soil conservation to minimize surface runoff, erosion and sediment transport, e. g. by terracing and contour ploughing, vegetation cover management and afforestation. The idea of "catching water where it falls" can be implemented by such measures as enhancing storage of water on the land surface, or underground, e.g. by infiltration [13]. Enhancing retention counteracts such adverse effects of urbanisation as decrease of water storage potential, growth of impermeable area and flood peak, reduction of time-to-peak of a hydrograph. The notion of watershed management is central to the concept of natural flood reduction strategies.
- Check the resilience of the brownfield land for potential hazards before the redevelopment/Increase the resilience of the brownfield land in the brownfield redevelopment stage.
- Incorporation of an emergency handling section to the building user guide which covers the emergency response in potential hazards (Other hazards except fire). Also an emergency preparedness information and instructions manual to be developed for apartment residents and homeowners, including model emergency operating procedures and a building contact directory [15].
- Ensuring the community connectivity and transportation needs during emergency situations through creating alternative connectivity by creating connections with adjourning urban areas.
- Design public open spaces in low disaster risk areas, may be higher elevations to reduce flood risk for disaster resilience which public can gather during a hazard or an emergency situation.
- Introduce flood warning systems and sensors to detect floods and disseminate early warning alerts. For this, a series of water sensors are located outside the property and on entry points, linked to an internal remote alarm. Emergency rescue locations are designated at ground and first floor levels. Automation is essential to allow the various technologies to work in synergy and provide early warning, emergency contact and automatic safety measures. External door sensors

and internal ground level sensor advises off the presence of water. All sensors are connected to a main sounder to give acoustic and visual warning. Potential to connect the main sounder to an automated call system/emergency authority. Flood Emergency Kit to be stored on first floor.

- Awareness raising among general public about natural hazards, prevention and mitigations measures and preparedness mechanisms is a very important aspect. Improving information about floods is badly needed for awareness raising and enhancing the consultative process, which leads to a broadly acceptable flood protection strategy. Only informed stakeholders can make rational decisions about choice of strategies of flood protection, in cost-benefit framework; with the account of sustainability issues. Awareness raising should be an inherent part of a flood preparedness system.
- Input a section or module to the curriculum which is given to qualify as a green building accredited professional as well as a compulsory module for university students in all higher education institutes in Sri Lanka.

4 Conclusions

The most common natural hazards in Sri Lanka include localized and seasonal floods and associated landslides while less frequent but more severe hazards include cyclones, droughts, and tsunamis. Out of those, floods are considered to be the most frequent, highest number of disasters reported and as well as which destroyed and damaged the highest number of buildings during recent past. Therefore it becomes a vital requirement to take necessary steps and DRR mechanisms for flood preparation and mitigation. This paper explains about globally used structural (hard) and non-structural (soft) techniques and mechanisms which can be applied for flood resistant buildings in Sri Lanka. The next step of this research study will be the incorporation of these identified flood mitigation and preparation measures and mechanisms into the GREENSL® Rating System for Built Environment through refinements to the sub-categories under main 8 categories rather than coming up with a new category or a separate code for DRR mechanisms. Also this research will be further extended to the other natural hazards such as landslides, strong winds and storms, etc. that Sri Lanka is more vulnerable into and they will also be incorporated to the rating tool.

References

1. Alam J, Muzzammil M, Khan MK (2016) Regional flood frequency analysis: comparison of L-moment and conventional approaches for an Indian catchment. ISH J Hydraul Eng 22(3):247–253
2. Amaratunga D, Haigh R, Malalgoda C, Keraminiyage K (eds) (2017) Mainstreaming disaster resilience in the construction process: professional education for a resilient built environment.

A report of the CADRE project: Collaborative Action towards Disaster Resilience Education. Available from: www.disaster-resilience.net/cadre.
3. Asian Disaster Preparedness Center (ADPC) (2013) Mainstreaming disaster risk reduction into housing sector in Sri Lanka
4. DesInventar official website by UNISDR, viewed 25 Nov 2019. https://www.desinventar.lk:8081/DesInventar/country_profile.jspcountrycode=sl&lang=EN
5. Economic losses, Poverty and Disaster—1998 and 2017 of UNISDR, viewed 25 Nov 2019. https://www.unisdr.org/we/inform/publications/61119
6. Future–proofing new and existing buildings—flood resilient design and construction technique, Katy Hunter BRE Scotland 28 April 2015. https://www.climatenorthernireland.org/cmsfiles/3-Katy-Hunter---Flood-resilient-design.pdf
7. GFDRR, Sri Lanka, viewed 25 Nov 2019, https://www.gfdrr.org/en/sri-lanka
8. GREENSL® Rating System for Built Environment
9. Guidelines for buildings at risk from natural disasters | A response to the tsunami of 26/12/2004 & A contribution to the task of reconstruction July 2005, Society of Structural Engineers—Sri Lanka
10. Hazard profiles of Sri Lanka | Official website of Disaster Management Centre Sri Lanka, viewed 25 Nov 2019. https://www.dmc.gov.lk/hazard/hazard/Report.html
11. Hazard resilient housing construction manual | Resilient Construction Series No. 1, National Building Research Organization (NBRO)
12. Khan MK, Ahmad S (2017) Flood resistant buildings: a Requirement for sustainable development in flood prone areas
13. Kundzewicz ZW, Takeuchi K (1999) Flood protection and management: quo vadimus? Hydrol Sci J 44:417–432
14. Malalgoda C, Amaratunga D, Haigh R (2014) Challenges in creating a disaster resilient built environment
15. Menzel L, Kundzewicz ZW (2003) Non-structural flood protection—a challenge. In: International conference 'towards national flood reduction strategies', Warsaw, pp 6–13
16. PreventionWeb, Sri Lanka Disaster & Risk Profile, viewed 25 Nov 2019. https://www.preventionweb.net/english/
17. World Health Organization, viewed 25 Nov 2019. https://www.who.intenvironmental_health_emergencies/natural_events/en/

A Case Study on Early Stage Adoption of Lean Practices in Prefabricated Construction Industry

P. A. N. Peiris, F. K. P. Hui, T. Ngo, C. Duffield, and M. G. Garcia

Abstract Prefabricated construction involves the manufacturing of the components off-site or in a separate production facility located on-site. Prefabricated construction industry lends itself easily to new technologies and concepts used in the manufacturing industry. The application of lean concepts to streamline processes by identifying and eliminating wastes in the prefabricated construction is a good example. This paper presents a case study of a real-life industry example of an early-stage adoption of lean practices in prefabricated housing module manufacturer using techniques such as 5S, waste elimination and standard work to improve the productivity of the overall prefabrication process. The challenges of implementing lean practices at a construction setting and possible countermeasures are also presented and discussed. It was observed that even at the early stages of adoption, these lean practices enable better housekeeping, consistent work quality and reliable work processes in the manufacturing facility.

Keywords Lean construction · Prefabrication · Productivity improvement · Layout planning · 5S · Early-stage adoption

1 Introduction

Lean manufacturing is a well-known concept among the manufacturing industry where it is used to add value by providing better, innovative and more satisfying products to the consumers [12]. Use of lean in the construction has recently become increasingly popular with the introduction of prefabrication, a technique with promising outcomes related to high construction speed, low cost and enhanced quality. Apart from the potential to incorporate lean manufacturing techniques in construction, prefabricated building construction is now enhanced with possibilities from emerging technologies such as 3D printing, Building Information Modelling (BIM), Internet of Things (IoT) and Industry 4.0 [19, 22].

P. A. N. Peiris (✉) · F. K. P. Hui · T. Ngo · C. Duffield · M. G. Garcia
University of Melbourne, Parkville, VIC 3010, Australia
e-mail: achini.peiris@unimelb.edu.au

R. Dissanayake et al. (eds.), *ICSECM 2019*, Lecture Notes in Civil Engineering 94,
https://doi.org/10.1007/978-981-15-7222-7_48

The concept of "prefabrication" is based on constructing the components in factories on or off-site and installing them on-site later at the required stages [1, 2, 6]. This has made construction projects more manageable and predictable when compared with in-situ construction [6]. Similar to lean concepts, pre-fabrication has enabled quality assurance, lower costs and minimal waste when compared to traditional construction [13, 14, 17]. Even though prefabrication delivers a significant number of advantages, not all the companies in the industry reap the maximum benefits out of it. There still exist areas that can be improved using lean practices in a way that it will enhance the productivity and efficiency of the work undertaken [7, 11].

Further improvements in the efficiency of prefabricated construction can be accomplished using lean principals for factory floor efficiency and making manufacturing lines more responsive and proactive to at the early construction phases using fundamental lean tools [3, 4]. Henceforth, this case study concentrates on the early stage benefits of implementation of lean practices at a prefabrication housing module manufacturer in Melbourne, Australia.

2 Literature Review

2.1 Enablers and Barriers for Lean Implementation in the Construction Industry

The construction industry, being an important contributor to the economy in a number of countries, is dynamic and open to various opportunities to further improve the productivity and efficiency of the overall work undertaken [3, 15]. Enablers such as management commitment, workforce training and development, willingness to implement lean practices and research and development will lead the companies to successfully initiate the execution of lean principals. Further, ability to introduce sustainable concepts by optimising waste reduction, resource and financial management encourage to utilise the concept of lean construction [3, 4].

However, it is another perception in the industry that lean construction is not as similar or straightforward as generic lean manufacturing [15]. The explanation behind the cognition is that the construction companies trying to adopt lean principals should be able to introduce change to the traditional work practices in the due course. Construction differs from manufacturing due to on-site complex production. Further, most of the construction-related manufacturing is highly customised dislike a production line consisting of a number of identical products [3, 15]. Therefore, the flexibility and willingness to change of the stakeholders involved play a crucial role in successfully implementing lean principals.

2.2 Lean Practices for Prefabrication

Lean manufacturing better fits the prefabrication construction industry due to several reasons. Prefabrication, as the name itself suggests, occurs before the actual construction starts at a manufacturing facility. It can be illustrated as a more controlled environment than the traditional construction site [6]. In the recent past, the effort to introduce "lean" to the construction industry has been increasingly popular due to the demands of environmental, economic sustainability and continuous improvement [20].

2.3 Lean Tools Are Easily Implemented in Early Stages

Some tools of lean are easily implemented during the early stages of lean adoption. 5S and Standard work are two such examples. 5S originally taken from the first letters of the Japanese words Seiri, Seiton, Seiso, Seiketsu, Shitsuke can be roughly translated to Sort, Set-in-order, Shine, Standardise and Sustain [9]. These 5 simple steps help the factory floor in numerous ways to reduce non-value adding activities in the production process. Sorting out what is needed at the workplace and eliminating the unneeded items helps reduce clutter that adds to the inefficiency. Setting in order means to find a 'home' for every essential item at the workplace so it is easy to locate when needed. Shine means to clean up regularly. Standardise is a way of improving the workplace so that there is a common language throughout e.g. colour coding of tools. Finally Sustain really means instilling the discipline in the workplace to feel proud of the 5S efforts and internalising this as part of the company culture [9].

In his seminal work, Ohno [18] writes about the philosophy of value-add and wastes. Waste is considered anything that is not of value and should be eliminated from the factory. Wastes or Muda (無駄) can originate from overproduction, quality issues, excessive processing, excessive motion, excessive transportation, inventory and waiting. It is important to look for opportunities to reduce such wasteful during any improvement processes [18, 21]. Standard work is another key concept in lean philosophy. The idea is that repeated work should result in consistent quality and done within the standard time [5]. Documenting best practices using baseline and standard operating procedures, it provides a baseline for conducting improvement activities. Standard work also includes the element of takt time that the rate at which the product must be produced to meet customers' demand. Another element of standard work is the standard inventory which specifies how much stock is allowable in the production lines. This helps minimise the waste due to over inventory [10].

3 Case Study

This case study involves one of the largest multi-disciplinary companies in Australia, that has recently started its newest sector of prefabricated modular building component manufacturing. The company started with implementing lean tools and principles. This case study will elaborate on the early stage benefits the manufacturing plant has experienced.

Figure 1 presents the wall tiling work carried out for one of the bathroom pods and Fig. 2 elaborates the different components that are involved. It is evident that tiling consists of more than just the act of sticking a tile to a wall as it also involves several supporting activities. To make an efficient production workflow, it is important to determine the non-value adding tasks and to make every effort to eliminate these.

Figure 2 highlights the scope of work involved with "wall tiling" for one of the bathroom pods. As it can be seen, most of the time is spent on cutting the tiles, marking, rework and finding tools. Rework includes the times when the cut-tiles should be readjusted due to space limitations. 5S and Standard work were applied to make these operations more efficient.

The subsections highlight the lean tools implemented and the initial benefits obtained.

3.1 Good Housekeeping

Implementation of 5S in factory floor has helped to reduce the time workers spent on finding material and tools. It has been observed that prior to the implementation, workers can spend roughly around 5–10 min looking for a specific tool or

Fig. 1 Wall tiling

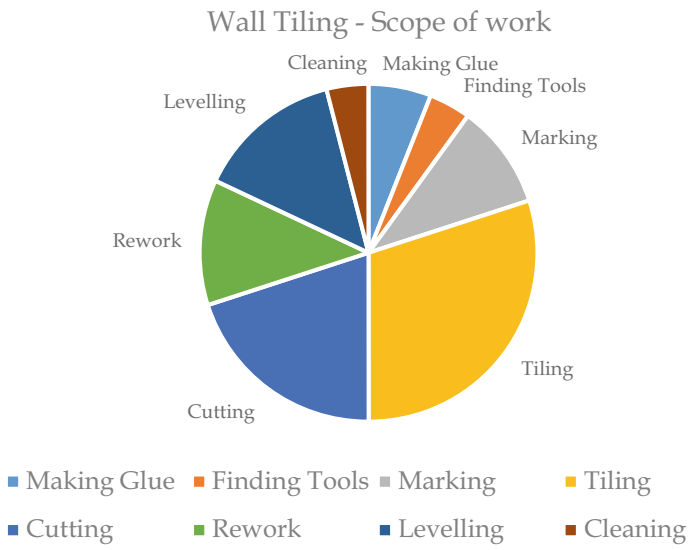

Fig. 2 Activities involved in "wall tiling"

simple material such as tape or a screwdriver. Introducing a trolley to each workstation/worker has improved the productivity by reducing the tool hunting time to <1 min and made the workers proactive as all the required tools can always be found with them. Examples of trolleys are shown in Fig. 3.

Further to that, all required cladding material such as fibre cement sheets and plasterboards have been allocated to designated trolleys sorted as per the project and the pod type. This involves careful layout planning to make sure necessary floor spaces have been allocated for the temporary storage trolleys for the workers to have easy access. This visual management technique, corresponding to Set-in-place, the second S of the 5S, reduced the part hunting time and enhanced the efficiency of installation procedure. Moreover, sorting the component storage significantly reduces the part hunting time, and encourage clarity in the workspace (Fig. 4).

3.2 Implementation of Standard Work

Standardisation through the use of standard work comprise of implementing three elements standard procedures and standard quality, standard time and standard inventory [8, 16].

Standard Procedures has been achieved by well-defined procedures and implementation of proper documentation such as Standard Operating Procedures (SOPs) and Inspection & Test Plans (ITP) for each project are shown in Fig. 7 and 8 respectively. SOPSs and ITPS are made available to the workers through the use of visual

Fig. 3 Sample Trolleys allocated to each workstation/worker

Fig. 4 Sorted items of components required for bathroom pod

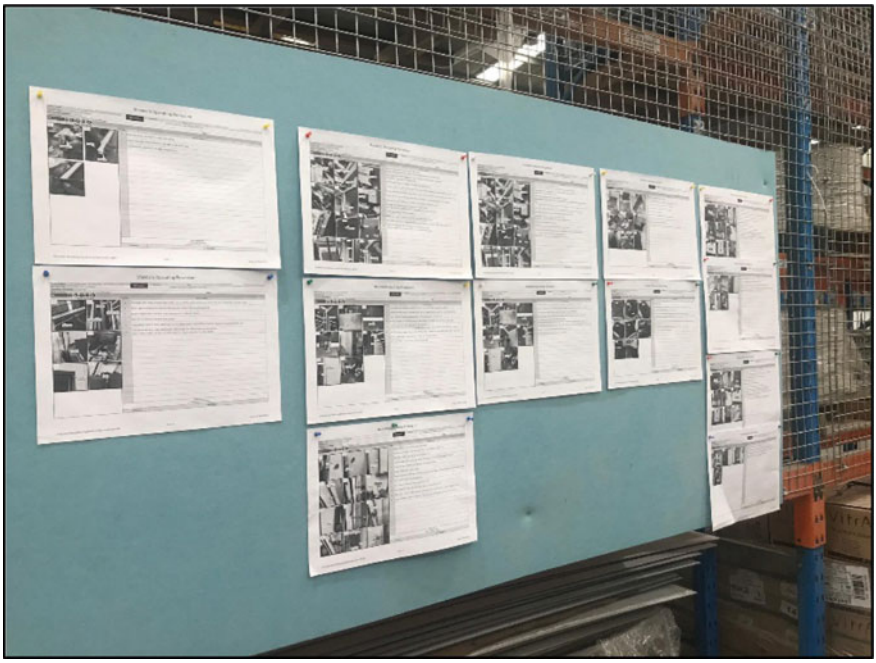

Fig. 5 Visual board—displayed SOPs

boards (see Fig. 5). This reduces the need for hunting for SOPs and would also allow supervisors to emphasize important SOP to the workers. The standard work procedure sometimes requires the design of special jigs and fixtures that helps to simplify work. Figure 6 illustrates a simple tool that is developed to enhance the efficiency of wall cladding. This magnetic clamp will be used when the walls are cladded, to make sure that the cladding material are uniformly glued to the wall frames.

Defining standard procedures provide clarity and ease of knowledge management between the factory floor and the management.

Standard time is achieved by reducing the time spent on labour training while making sure the new recruits obtain enough exposure in completing the job. New workers will be able to refer to the documents to better understand the manufacturing procedure of bathroom pods. This complements the need for excessive hours spent on labour training as the documentation takes them through all the tasks with photographs from previous projects as visual aids. More importantly, the standard time can relate to the takt time or the customer demand [10].

Due to the implementation of these documents, briefing time for the new recruits have been reduced as they have these document to follow while learning and training on the job. As presented in Fig. 5, all these procedures are displayed on wall for better presentation and communication.

Fig. 6 Magnetic clamp

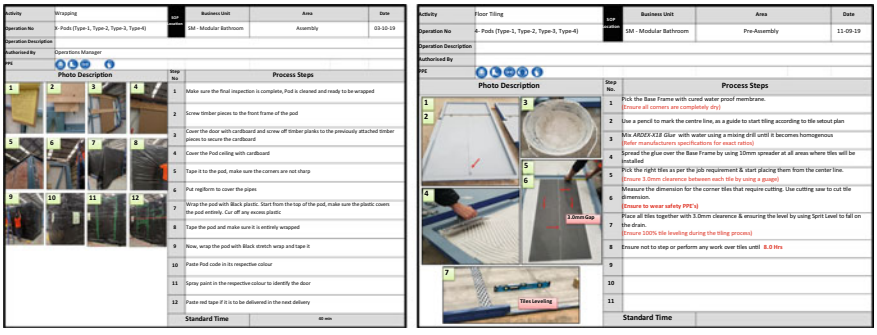

Activity	Wrapping	SOP Number	Business Unit	Area	Date
Operation No	9- Pods (Type-1, Type-2, Type-3, Type-4)		SM - Modular Bathroom	Assembly	03-10-19
Operation Description					
Authorised By	Operations Manager				
PPE					

Photo Description	Step No.	Process Steps
1 2 3 4	1	Make sure the final inspection is complete, Pod is cleaned and ready to be wrapped
	2	Screw timber pieces to the front frame of the pod
	3	Cover the door with cardboard and screw off timber planks to the previously attached timber pieces to secure the cardboard
	4	Cover the Pod ceiling with cardboard
5 6 7 8	5	Tape it to the pod, make sure the corners are not sharp
	6	Put regiform to cover the pipes
9 10 11 12	7	Wrap the pod with Black plastic. Start from the top of the pod, make sure the plastic covers the pod entirely. Cur off any excess plastic
	8	Tape the pod and make sure it is entirely wrapped
	9	Now, wrap the pod with Black stretch wrap and tape it
	10	Paste Pod code in its respective colour
	11	Spray paint in the respective colour to identify the door
	12	Paste red tape if it is to be delivered in the next delivery
		Standard Time 60 min

Activity	Floor Tiling	SOP Number	Business Unit	Area	Date
Operation No	4- Pods (Type-1, Type-2, Type-3, Type-4)		SM - Modular Bathroom	Pre-Assembly	11-09-19
Operation Description					
Authorised By					
PPE					

Photo Description	Step No.	Process Steps
1 2 3 4 5 6 3.0mm Gap 7 Tiles Levelling	1	Pick the Base Frame with cured water proof membrane. (Ensure all corners are completely dry)
	2	Use a pencil to mark the centre line, as a guide to start tiling according to tile setout plan
	3	Mix *ARDEX-X18* Glue with water using a mixing drill until it becomes homogenous (Refer manufacturers specifications for exact ratios)
	4	Spread the glue over the Base Frame by using 10mm spreader at all areas where tiles will be installed
	5	Pick the right tiles as per the job requirement & start placing them from the center line. (Ensure 3.0mm clearence between each tile by using a guage)
	6	Measure the dimension for the corner tiles that require cutting. Use cutting saw to cut tile dimension. (Ensure to wear safety PPE's)
	7	Place all tiles together with 3.0mm clearence & ensuring the level by using Sprit Level to fall on the drain. (Ensure 150% tile leveling during the tiling process)
	8	Ensure not to step or perform any work over tiles until 8.0 Hrs
	9	
	10	
	11	
		Standard Time

Fig. 7 Sample SOP

Standard Quality is achieved through a coordinated quality assurance procedure or an Inspection and Test Plan (ITP)where each work item is logged with a completion date and time (as an example see Fig. 8). A QPIR (Quality Product Inspection Report) sheet is allocated to each pod with the pod code printed, and it will be updated throughout the life cycle of the pod manufacturing process. At the stage of final inspection before wrapping, factory floor manager would cross-check existing status of the pod with the QPIR and log the FQIC (Final Quality Inspection Checklist). This procedure enhances the traceability of any quality-related issues and backtracks the origin of the problem.

Inspection Test Plan

Business Unit		**Level(s)**		**Pod Number**	
Scope	**Supply and Delivery of Modular Bathroom Pods to site**				
Activity	**Pre-assembly, manufacture, delivery and site positioning**				
Contractor (s) *(if applicable)*					
Drawing Numbers applicable	**Floor Plans** **Pod Drawings**				
Inspection Types	**H = Hold Point** *The work cannot proceed until the Engineer or Consultant is able to verify the quality of the completed work and releases the Hold by means of Inspection Request approval.* **W = Witness Point** *is an identified point in the process where the Engineer or Consultant may review, witness, inspect method or process of work. The activities however may proceed* **R = Review Point** **S - Surveillance**				
Inspected By	**C** = Contractor **QA** = Quality Assurance Team **CL** = Client				
Inspection Methods	**V** – Visual Inspections **D** – Dimensional Inspection **F** – Functional Inspection				

Activities	Relevant drawing / specification	Acceptance Criteria/ Verification	Inspection Type *(H, W, R, S)*	Inspected By *(C, QA, CL)*	Inspection Methods *(V, D, F)*	Inspection Sign off and Date	FINAL INSPECTION and Date *(by Operation /Production Manager*
PRE-ASSEMBLY							
Base frame inspection Measure and check the correct dimensions of the base frame.		Actual length: Actual width:	R	C	D D		
Threshold and drain preparation Peel the cover, sand and apply primer to the drain and threshold.		Actual length of threshold:	R	C	D		
		Actual length of drain:	R	C	D		

Fig. 8 Sample ITP format

Having a record of all the tasks that were completed with the person responsible and the date completed, enables swift action to rectify the issues. Further, having this type of standardized procedures encourage the factory floor workers to carefully complete each task and assure the quality before they sign off. Figure 9 shows an application of this in the form of a production monitoring template.

Finally, standard inventory is the pre-determined amount of inventory that is allowable on the shop floor. The implementation and use of trolleys to move and store raw materials as shown in Fig. 4 is a good example of how this was done. Having only the predetermined amount of inventory on the shop floor helps minimise over-production and maximise the use of space for only the materials that is needed.

3.3 Benefits Observed and Improvement Opportunities

Early stage benefits by adopting lean principals in the factory floor can be summarised as in Table 1.

These observed benefits would be further monitored to understand the limitations and opportunities for further improvement. Moreover, the factory is looking at continuing to implement lean principals to gain an overall advantage of production efficiency. The next steps of lean implementation are as listed as follows.

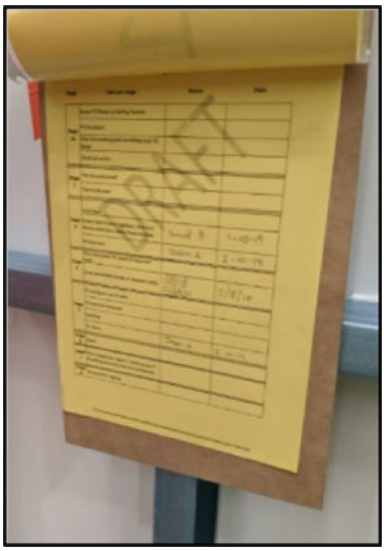

Fig. 9 Production monitoring template

Table 1 Observed early stage benefits

Lean principal	Observed benefits
5S	Reduction of tool hunting time by around 50%
Standard procedures	Ease of knowledge management Reduced labour training time
Standard time	Reduced labour training time
Standard quality	Encourage quality assurance Ease of responsibility assignment Enhanced transparency

Layout planning: This is an ongoing task as there is no perfect layout that can be defined for each of the projects. The production team keep improving the factory floor to better absorb future projects and deliver the components on time as per schedule.

Visual boards: These will be further improved to enhance and encourage better communication.

Toolbox meetings: These will be used in conjunction with the visual boards and to address everyday issues and problems that the factory floor workers face with. The outcomes will be taken into consideration for enhancing worker experience as it will eventually encourage a better working environment.

Housekeeping maintenance: Although the factory floor has had a successful first round of 5S implementation, the challenge is to maintain the ongoing cleanliness.

Some planned activities include regular 5S audits, labour training and awareness sessions and continuous follow-up during tool box meetings.

Further standardisation: This is important as standardisation must be reflected in daily operations. As an example, tools inside the trolleys can be specifically marked so that after every task has been completed they can be allocated to their specific space. This prevents the loss of tools and enhance the ability for finding them as soon as its required. This represents an enormous improvement opportunity.

4 Conclusion

It can be concluded that the adoption of simple lean principles such as 5S and standard work resulted in around 50% total reduction of time spent on non-value adding activities such as looking out for tools and simple materials. Further, standardisation of work-flow produces better quality components with almost nil. Rejection/rework rates from the client. Moreover, it has complemented knowledge management and sharing between different stake holders as everybody involved speaks the same language and have a better understanding on the workflow. Therefore, this case study concludes and proves that adoption of lean principals has the potential of improving the factory floor productivity even at the very early stages.

Acknowledgements The first author would like to acknowledge The University of Melbourne for offering the Melbourne Research Scholarship. This study is sponsored by the Cooperative Research Centres Projects (CRC-P) and the authors would like to acknowledge the support given by Schiavello Group, for the implementations and providing the factory setting. This article was prepared as an industry paper, within the guidelines of the project stated above.

References

1. Azhar S, Lukkad MY, Ahmad I (2013) An investigation of critical factors and constraints for selecting modular construction over conventional stick-built technique. Int J Constr Educ Res 9:203–225
2. Azman MNA, Ahamad MSS, Hussin WMAW (2012) Comparative study on prefabrication construction process. Int Surv Res J (ISrJ) 2:45–58
3. Bayhan HG, Demirkesen S, Jayamanne E (2019) Enablers and barriers of lean implementation in construction projects. IOP Conf Ser: Mater Sci Eng, 471
4. Carvajal-Arango D, Bahamón-Jaramillo S, Aristizábal-Monsalve P, Vásquez-Hernández A, Botero LFB (2019) Relationships between lean and sustainable construction: positive impacts of lean practices over sustainability during construction phase. J Clean Prod 234:1322–1337
5. Feng PP, Ballard G (2008) Standard work from a lean theory perspective. In: Tzortzopoulos P, Kagioglou M (eds) 16th annual conference of the international group for lean construction, 2008/07/16, Manchester, UK, pp 703–712
6. Hong J, Shen GQ, LI Z, Zhang B, Zhang W (2018) Barriers to promoting prefabricated construction in China: a cost–benefit analysis. J Clean Prod 172**:**649–660

7. Hwang B-G, Shan M, Looi K-Y (2018) Key constraints and mitigation strategies for prefabricated prefinished volumetric construction. J Clean Prod 183:183–193
8. India KI (2013) Standardization [Online]. Available: https://kaizeninstituteindia.wordpress.com/2013/12/05/standardization/. Accessed
9. Jackson TL (2009) 5S for healthcare. CRC Press
10. John S (2009) Five missing pieces in your standardized work [Online]. Available: https://www.lean.org/shook/DisplayObject.cfm?o=1320. Accessed
11. Kamali M, Hewage K (2016) Life cycle performance of modular buildings: a critical review. Renew Sustain Energy Rev 62:1171–1183
12. Lai NYG, Wong KH, Halim D, Lu J, Kang HS (2019) Industry 4.0 enhanced lean manufacturing. In: 2019 8th international conference on Industrial technology and management (ICITM), 2–4 March 2019, pp 206–211
13. Li Z, Shen GQ, Xue X (2014) Critical review of the research on the management of prefabricated construction. Habitat Int 43:240–249
14. Lopez D, Froese TM (2016) Analysis of costs and benefits of panelized and modular prefabricated homes. Procedia Eng 145:1291–1297
15. Meng X (2019) Lean management in the context of construction supply chains. Int J Prod Res 57:3784–3798
16. MÍkva M, Prajová V, Yakimovich B, Korshunov A, Tyurin I (2016) Standardization—one of the tools of continuous improvement. Procedia Eng 149:329–332
17. Molavi J, Barral DL (2016) A construction procurement method to achieve sustainability in modular construction. Procedia Eng 145:1362–1369
18. Ōno T (1988) Toyota production system: beyond large-scale production. Productivity Press.
19. Raza Ul Mustafa M, Alaloul WS, Liew MS, Zawawi NAWA, Mohammed BS, Bin Othman I, Latheef M, Bayu Endrayana D, Zulaikha Bt Yusof N (2018) Industry revolution IR 4.0: future opportunities and challenges in construction industry. MATEC Web Conf, p 203
20. Shams Bidhendi S, Goh S, Wandel A (2019) Development of a weighted leanness measurement method in modular construction companies. J Ind Eng Int 15:603–625
21. Womack JP, Jones DT (2003) Lean thinking: banish waste and create wealth in your corporation. Free Press.
22. Xu G, Li M, Chen C-H, Wei Y (2018) Cloud asset-enabled integrated IoT platform for lean prefabricated construction. Autom Constr 93:123–134

Construction Project Managers Graduate Agile Competencies Required to Meet Industry Needs

Paulo Vaz-Serra, Felix Hui, and Lu Aye

Abstract The construction industry is embracing new management challenges to deal with the ever-increasing needs for collaboration, environmental and social responsibilities. Improvements in construction project management competencies are essential to helping the construction sector to embrace the new challenges. Building engineering management capabilities through the correct training are therefore essential. In research involving the twenty-four largest contractors in Australia 'Lean construction' was identified as an important skill to be included in academic programs that has not yet fully been embraced. Contractors are not yet seeing 'lean' and 'agile' methods as important approaches to improve communication within the teams and between projects. This research highlighted that although contractors identified communication as one of the main skills needed to achieve a good performance in project construction management they do not yet recognise that training in lean and agile methodologies will help them to improve communication not only between professionals but between projects and organisations involved in each project in improving business goals.

Keywords Construction management · Lean · Agile · Education · Competencies

P. Vaz-Serra (✉)
Faculty of Architecture, Building and Planning, The University of Melbourne, Parkville, VIC 3010, Australia
e-mail: p.vazserra@unimelb.edu.au

F. Hui
Engineering Management Group, Department of Infrastructure Engineering, Melbourne School of Engineering, The University of Melbourne, Parkville, VIC 3010, Australia

L. Aye
Renewable Energy and Energy Efficiency Group, Department of Infrastructure Engineering, Melbourne School of Engineering, The University of Melbourne, Parkville, VIC 3010, Australia

R. Dissanayake et al. (eds.), *ICSECM 2019*, Lecture Notes in Civil Engineering 94,
https://doi.org/10.1007/978-981-15-7222-7_49

1 Introduction

The construction industry is one of the sectors known to have low productivity [2, 22] and is a sector where adoption of new innovation and new approaches are slow and less effective than in other sectors.

An example is the application of lean construction. It has been more than twenty years since several organisations in the sector reported an adoption of lean methodologies. However, the construction sector still lags behind in a large integration of those methods in spite of the efforts made around the world to help the industry. A good example would be the Institute of Lean Construction which has representations in several countries since the last 20 years. The questions remain why, with all this international genuine interest and political effort, is the concept not fully introduced in a large majority of the construction organisations.

According to some research done recently, one of the best methods to increase adoption for innovation in organisations is through the improved capability of organisations to manage the changes internally in a more efficient way. Research on project outcomes revealed that experienced project managers can create a significant positive difference. The success of construction projects was positively related with applied management skills [5, 16]. In construction, the role of construction project managers in central to achieve the best outcome and the data collected in a recent survey showed that there is a gap between academic courses for construction project managers at a university level and industry expectations for the future graduates [10]. Nowadays changes in technologies, client requirements and management methodologies are continuously changing, and industry needs and expectations towards the skills of future construction project managers are high. Industry requires that academic programmes are prepared to help them for the challenges of the future preparing the young graduates with the right skills. However, the gap between what academia believes that will be the future does not always align with what the industry wants to believe is important. The aim of this article is to highlight the current needs and industry expectation towards the new agile and lean construction approaches. The authors believe that this identification will help to prepare academic degrees to align with industry expectations and to help academia understand where the industry is in innovation and what academics need to do to help industry to be more aware of these important new collaborative methods.

2 Agile Methodologies and Construction Management

Serrador and Pinto [20] studied 1002 projects and highlighted that the adoption of agile methodologies introduced significant improvements in project success, mainly on efficiency and stakeholder satisfaction. The traditional structure of typical project management, as a cascading linear sequence of activities, is relatively simple, easy to

understand and to follow. A model which has been globally accepted as a framework for structured communication between projects and within projects [7].

However, the rapid changes in technologies for planning of resources and focused construction project goals have been recognised as a challenge for these traditional management models [4, 6]. New specific technical and economic requirements for software development are now compulsory and agile project management models have been developed to respond to them.

The description of agility has been accepted through the application of the Agile Manifesto principles and declaration of interdependency to project management [3]. Concepts as "direct communication" and "delivering of value" come up as essential features of agile project management values, principles and attributes [13, 18].

In construction, an additional limitation was identified when transferring agile project management methods due to unusual employment agreements and subcontracting arrangements [13–15]. Some of these non-typical arrangements limit the potential of the adoption of more open and collaborative methods.

Nevertheless, in construction, lean and agile management techniques, like Last Planner System® (LPS) [1, 17] or 'Scrum', have been tested as a novel methodology to help products and processes to developed in a more efficient and collaborative way [19], for improving transparency and better flow of information [21]. Recently, Francis et al. [8] proposed the application of Scrum methodology to construction tendering, developing a Scrum model based on a standard bidding flow to improve team collaborative work during the bid preparation.

The question is who the driver for adoption of more collaborative new methods is; the construction industry that needs to improve their internal methodologies or the external pressures that are pushing the construction industry.

3 Project Construction Managers Skills

Project managers' skillsets have been identified as the main issue to project success. The construction industry relies on the capability and knowledge of their construction project managers to be more efficient, productive and innovative [11]. Recently, Mitcheltree et al. [10] highlighted five main skill areas within the larger main building commercial contractors in Australia for young postgraduate construction project managers: (1) communication (verbal, written, presentation); (2) resilience and persistence; (3) emotional intelligence; (4) commitment to personal development; (5) committed to professional development.

4 Research Methodology for Investigating Management Skills

For the purpose of this investigation only Australian contractors that work in the building environment were studied since usually civil work contractors use experts with civil engineers and engineering management skills to manage their construction projects and this research intended to focus on construction project managers with specific skills in the build environment.

Australian construction industry is regulated by the Victorian Building Authority (VBA) following the building regulations 2018 that defines eight categories of building practitioners [23]: 1—'Building surveyor'; 2—'Building inspector'; 3—'Quantity surveyor'; 4—'Engineer'; 5—'Drafts person'; 6—'Person responsible for a building project' (Project Manager—Domestic); 7—'Erector or supervisor' (temporary structures); 8—Builder (Commercial Builder, Domestic Builder and Demolisher).

Within category 8, 'Builder', large companies in the Commercial Builder's subcategory hire construction project management graduates. Domestic builders and demolishers usually managed their projects with individual registered builders without necessarily feeling the need for hiring graduates or postgraduates in project construction management. One of the reasons is that for smaller organisations their main projects are usually small, and their clients are less demanding. Employing graduates means sometime increasing enterprise overheads costs and the small projects cannot accommodate high overhead costs. Clients of smaller projects also expect lower costs and domestic builders prefer to take some additional construction management risks to keep their competitive bids. Therefore, the research, done on industry needs versus academic courses, was done within the largest commercial building companies who are the main consumers of graduate and postgraduate students.

Nevertheless, a survey sent to 24 Tier 1 Australian contractors (Tier 1 = large contractors) [12], who usually hire construction project management graduates, in 2018, revealed that these employees still do not value collaborative skills like knowledge in lean construction and agile methodologies. The survey targets the 100 biggest Tier 1 contractors (Commercial Builders and Civil works) in Australia published by the HIA-CoreLogic report [9]. From that list, 20 companies were excluded which are not working in projects in the built environment and an additional nine were excluded because they declined to participate. Contacts were made to each company to understand who internally was responsible to prepare the selection criteria to hire young postgraduates. Surprisingly, not all companies have human resources managers and said that the recruitment was done through their senior project construction managers. After the identification of the name and contact person in each company (human resources manager or senior project construction managers) the questionnaires were sent to 71 companies. This process was done during the three months data collection period. Several attempts were done to follow up the initial email sent, by email and by phone, and 24 fully completed questionnaires were returned.

5 Results and Analysis

Of the survey responses returned, most respondents (58%) had over 16 years of experience within the construction industry and worked in recruitment roles for 11 years or more, 29% work in that same company for more than 11 years and 41% are females. Most of the companies (50%) had an annual revenue of $250 mill or more and 75% had overseas activity and have been operating for 21 years or more, 50% have more than 20 construction managers graduates per year and 67% employ 5 or more new graduates.

Regarding the need for collaborative skills only 41% of the respondents believed that subject/courses (depends on different faculties and universities the name of individual units in each degree can be subject or course) in lean construction are important or very important to be included in construction project management postgraduate university degrees. In addition, that number dropped to 25% when be asked for units like sustainability and life cycle analysis.

Interestingly, communication skills (like verbal and presentation) and other personal attributes (resilience and persistence) were ranked as important or very important for more than 91% and 95% respectively. This data is perhaps indicative that the industry is not completely aware that one of the most important attributes of agile methodologies is effectively to improve communication skills not only as personal attributes, but communication between team members, stakeholders and projects.

6 Discussion

Both lean and agile methods emphasize the importance of communication and the effectiveness of communications. In lean methodology, the use of tools such as visual management, 5S standard work, A3 worksheets, Kanban cards are all forms of effective communication tools that aim to enhance the way team members communicate. Lean has also much in common with agile methodologies that aim to communicate effectively so that the team members can respond quickly making their organisations effectively very nimble. One example is the use of the LastPlanner which enhances the ability to respond quickly to changes in production requirements [1]. Lean construction involves the use of such lean tools and agile methods [19]. Lean construction requires a high degree of collaborative and communication skillsets but is ranked not highly in importance by organisations in the survey (41%). However, the same organisations viewed communication and leadership skillsets as important or very important to be included in a Master level degree for more than 91% of the respondents. An explanation for this may be a lack of understanding as to what is “lean construction”, its aims and the use and desired outcomes in the leadership of the new collaborative world. Therefore, there is a need to educate construction organisations that there are productivity tools such as lean construction available

that can help them achieve greater efficiency through enhanced communication and collaboration.

7 Conclusions

This article highlighted the importance of the construction management skills for the success of construction projects. The findings were that learning new skills like lean management can be an important way to improve capability of the construction sector in more sophisticated management methodologies. The survey sent to twenty-four Tier 1 contractors in Australia revealed that lean construction should be include in academic programs but for them it was not so important as personal skills and communication skills. This research identified further opportunities to research in other countries and the reasons why agile methodologies like lean construction are not yet understood by contractors as good ways to improve communication using new IT tools for construction project management.

Acknowledgements This research was supported by the John McIlwraith Foundation Grant—"Construction Project Management, Academic Programs and Industry Needs". The authors acknowledged Dr. David Wilson, Department of Infrastructure Engineering, the University of Melbourne for proof reading the manuscript and improving the language aspects.

References

1. Ballard G (2000) The last planner system of production control. Ph.D. thesis, Univ. Birmingham, Birmingham, United Kingdom http://www.leanconstruction.org (Sep 3, 2003)
2. Barbosa F, Woetzel J, Mischke J, Ribeirinho MJ, Sridhar M, Parsons M, Brown S (2017) Reinventing construction through a productivity revolution. McKinsey Global Institute
3. Beck K, Beedle M, Van Bennekum A, Cockburn A, Cunningham W, Fowler M (2001) The Agile Manifesto [Online]. Available: http://agilemanifesto.org/. Accessed 20 Nov 2019
4. Cervone HF (2011) Understanding agile project management methods using Scrum. OCLC Syst Serv: Int Digit Libr perspect 27:18–22
5. Cooke-Davies T (2002) The "real" success factors on projects. Int J Proj Manag 20(3):185–190
6. Deemer P, Benefield G, Larman C, Vodde B (2012) A lightweight guide to the theory and practice of scrum (version 2.0). Technical report
7. Fernandez DJ, Fernandez JD (2008) Agile project management—Agilism versus traditional approaches. J Comput Inf Syst 49:10–17
8. Francis V, Vaz-Serra P, Ullal A, Nahri A (2018) Can construction bidding practices be improved through use of the scrum project framework? RICS COBRA 2018, London, UK
9. HIA (2017) HIA-CoreLogic construction 100 2016/17. ACT: Housing Industry Association
10. Mitcheltree H, Vaz-Serra P, Carter S, Cameron R (2019) Building sustainable futures: industry perceptions of the key construction project management graduate competencies required to meet industry needs. In: CIB world building congress 2019 Hong Kong SAR, China. 17–21 June 2019
11. Müller R, Turner R (2010) Leadership competency profiles of successful project managers. Int J Proj Manag 28(5):437–448. https://doi.org/10.1016/j.ijproman.2009.09.003

12. Newpoint Advisory (2019) Builder tier system. http://www.newpointadvisory.com/builder-tier-system/. Assessed Nov 2019
13. Owen R, Koskela LJ (2006) An Agile step forward in project management. In: Songer A, Chinowsky P, Carrillo P (eds) 2nd specialty conference on leadership and management in construction, 4th May 2006, Grand Bahama Island, Bahamas, pp 216–224
14. Owen R, Koskela LJ (2006b) Agility in construction. In: 20th IPMA world congress on project management, 15–17 Oct 2006, Shanghai, China, pp 1–4
15. Owen R, Koskela LJ, Henrich G, Codinhoto R (2006) Is agile project management applicable to construction? In: 14th annual conference of the international group for lean construction, 24th July, 2006 Santiago, Chile, pp 51–66
16. Rezvani A, Chang A, Wiewiora A, Ashkanasy NM, Jordan PJ, Zolin R (2016) Manager emotional intelligence and project success: the mediating role of job satisfaction and trust. Int J Proj Manag 34(7):1112–1122
17. Salem O, Solomon J, Genaidy A, Luegring M (2005) Site implementation and assessment of lean construction techniques. Lean Constr J 2(2):1–21
18. Sanchez LM, Nagi R (2001) A review of agile manufacturing systems. Int J Prod Res 39:3561–3600
19. Schwaber K, Sutherland J (2013) The Scrum guide—the definitive guide to Scrum—the rules of the Game. http://scrumguides.org
20. Serrador P, Pinto JK (2015) Does Agile work?—A quantitative analysis of agile project success. Int J Proj Manag 33:1040–1051
21. Streule T, Miserini N, Bartlomé O, Klippel M, de Soto BG (2016) Implementation of Scrum in the construction industry. Procedia Eng 164:269–276
22. Sveikauskas L, Rowe S, Mildenberger J, Price J, Young A (2016) Productivity growth in construction. J Constr Eng Manag 142(10):04016045
23. VBA (2019) Building practitioner registrations, VBA Website https://www.vba.vic.gov.au/building/builder-registrations. Accessed on 28.11.10

Co-created Student Capstone Projects: Case Study of De-Risking Plan for the New Student Precinct

N. Herath, A. Kennedy, F. Taqi, Z. Dahdoule, F. K. P. Hui, and C. Duffield

Abstract Cross disciplinary team learning enhances the team building and collaborative learning process. Engineering capstone subject provides students with different engineering disciplines to work on a live project. This serves them a great learning experience on collaborative learning and team working. Co-created projects provide students to engage in the project during the planning and construction phases. The new student precinct which is a co-created project, was introduced to the students to work on project management capstone subject at the University of Melbourne. This study presents some findings on teaching and learning outcomes of a co-created projects in engineering management. Students develop great team working and project management skills working in this project and they showed higher engagement in the project as they are considered as one of the main key stake holders in the project.

Keywords Co-created projects · Project-based learning · University teaching · Education

1 Introduction

The use of real-world projects in University teaching not only adds realism to the classroom, it also introduces students to the actual unexpected problems that they are likely to encounter when they enter the workforce. Capstone projects and final year projects are particularly suited for the use of such projects. In this paper, we seek to demonstrate how a University capital development project is used as a capstone project for final year engineering management students. Having an internal University project brings about many benefits including access to documentation, convenient access to site, access to industry experts and stakeholders [7]. More importantly, they are also part of a co-creation process that will be described in this paper.

N. Herath (✉) · A. Kennedy · F. Taqi · Z. Dahdoule · F. K. P. Hui · C. Duffield
University of Melbourne, Parkville, VIC 3010, Australia
e-mail: nherath@unimelb.edu.au

R. Dissanayake et al. (eds.), *ICSECM 2019*, Lecture Notes in Civil Engineering 94,
https://doi.org/10.1007/978-981-15-7222-7_50

The University of Melbourne has an ongoing plan to redevelop part of the campus that is more than 100 years old to better cater to a new generation of students [14]. The new capital development collectively called the New Student Precinct (NSP) offers student involvement in co-creation as well as teaching and learning opportunities. The below section describes the background to the project, the involvement of students and the co-creation concept used. This is followed by a detailed description of the case study and initial report on the feedback from the students to date.

2 Background Information and Associated Literature Review

2.1 New Student Precinct Project (NSP)

In 2015, the University of Melbourne recognised the need for a new Student Precinct on the Parkville campus in response to the changing profile and needs of our students and the evolution of the campus itself. The Student Precinct Project will provide an improved student experience through the colocation of student-led student facing services and activities with University provided student services. The Student Precinct project responds to a number of key drivers:

- Alignment of University provided student services with student-led services, activities and amenity;
- End of the functional life of the current Union House Building;
- Reflect the move with over 40% of students studying below Grattan Street;
- Respond to changing student demographics including 50:50 undergraduate and graduate students, and increasing international student numbers; and
- Work with students as co-creators on the Project.

It is envisaged that the New Student Precinct will be a vibrant centre for student activity, where all students have access to social, cultural and community opportunities. The Project will focus on adaptive reuse to create improved amenity for our campus communities as well as two new buildings.

The New Student Precinct Project includes seven buildings and will deliver 37,050 m^2 of new or refurbished internal and external building and landscape space. The site is at the centre of the University's traditional and new student accommodation hubs, making it an ideal location for our 60,000 students to connect. The New Student Precinct has been designed with students at the heart of its thinking. The facilities will deliver the co-location of student services, convenient access to public transport, new Arts and Cultural facilities, increased study space and outdoor space, as well as also delivering on several key University of Melbourne Strategies. Uniquely, the Project has also benefited from the contributions of over 13,500

students who have influenced the direction of the Precinct through our co-creation approach. The Precinct will be completed in stages with main works construction due to begin in 2020.

2.2 Co-creation in the NSP Project

Students are given the opportunity to contribute ideas, experience and expertise to influence and craft the planning and design of the facilities. Partnering with the key stakeholder, the students in this manner ensures that the end-product is user-cantered and fit for purpose [14]. Co-creation activities include online forums and collaborative discussion for the generation of new ideas for the use of space. Examples of these concept design using co-created ideas were published as far back as 2016 [13]. Co-creation also involves activating the students to engage in activities prior to the precinct's completion. This ensures that a healthy and dynamic relationship between the design is tested as it is built.

Co-creation is a concept that is used to create dialogue between key stakeholders for problem-solving [10]. Co-creation of value, value realisation is fundamental and important in construction due to the project location in both social and physical spaces [1]. Some researchers have also argued against co-creation in construction citing disbenefits due to unintended consequences [6] and some citing the inherent asymmetry of power [3, 19] that prompts a need to align interests of the actors conducting the co-creating activities. It is also difficult to determine how dialogues and interactions can be fed into problem solving process or for innovation to take place [11]. The management of expectations and the co-creation process is therefore highly important [8].

The Project is committed to providing students with practical experience and exposure to the project through the integration of teaching and learning opportunities into the project's core activities, and by supporting the use of the project as a 'real-world' case study for curricular subjects across multiple faculties. Providing teaching and learning opportunities for students also supports the project's aim of co-creating the project with students. Through these engagements' students can benefit from the 'real world' experience of working on a major project and feed their ideas, knowledge and aspirations directly into the Project.

The following section describes an assignment that was used as a real-world student project for a capstone subject. A capstone subject is one that integrates theories and concepts learned in the entire course of study. Students are expected to apply these concepts and theories to solve a real-world problem (reference needed).

3 Case Study

Engineering management capstone in University of Melbourne is a Master's degree subject which is open for all engineering discipline students. This subject provides an opportunity for students to work in teams to integrate concepts, principles, models and theories related to engineering and/or project management principles and practice, contract and procurement strategies, finance and management strategy [17]. It will make use of business cases, or simulation of business cases that are relevant to decision making and practice in the engineering management profession

The expected intended learning outcome (ILO) of this subject [16] is:

- Students to be able to work in teams to formulate business cases and proposals for engineering projects to the senior levels or organisation such as Board of Directors.
- Identify key issues encountered in engineering management and/or engineering projects, evaluate among alternative engineering solutions and make recommendations based on best possible project.
- Devise and apply decision criteria to economic and financial analysis outcomes, and use them to make informed decisions as well as to make estimates in budgets.
- To analyse information and organise tasks to create a complete project management plan which may include but not limited to scoping, task definition, cost modelling, budgeting, risk management, procurement, schedule, sequencing of tasks and control measures.
- Demonstrate the ability to comply with legal and other compliance frameworks in the engineering management process.

Since different engineering disciplinary students study this subject, it provides a greater exposure for the students to work in a multi-disciplinary team that is important for their career improvements. Students from Civil, Electrical, mechanical, chemical and bio-medical engineering disciplines work in an industry related project team for one semester which is 12 weeks on an ongoing engineering project. They work as a team to solve an engineering management or project management aspect of the project. The project is unique in design and students aim is to solve the complex problems in a real-world project. Since the project is an ongoing engineering industry project, the industry representatives are involved with the students. The students are expected to have the collaboration with the industry professionals similar to the work they are expected to carry out in the industry. All relevant information for the project is provided for them to perform the tasks.

3.1 The NSP Capstone Project Assignment

Like any major construction projects and capital works, the new Student Precinct has various major construction phases including the master planning, concept design

phase, schematic design, the detailed design phase, the early enabling works phase, and the detailed design phase (interiors and landscape) [15]. The capstone projects designed for this subject aligns with the NSP's construction phase so that students are always facing a real situation that the NSP project would face. In the past, for three semesters, projects have been set around the procurement of design services of major consultant. As the project moved into the tendering of the construction phase, there is a need to de-risk the project. In the actual project, world, this would normally involve the appointment of engineering consultants to consider all forms of risks that might impact the build quality, the timely completion, safety, cost overruns among other things. The de-risking stage is therefore an important stage of the project delivery process [18].

3.2 Project Complexity

The site is complex and constrained with East-West access across the Precinct complicated by built space, narrow walkways and level changes. Traffic across the Precinct is complicated by a 6m level drop north to south. There is street frontage to a main street on the southern boundaries of the historical buildings, noting that the Precinct will include the existing functions of few buildings.

It is intended that the ground plane become increasingly occupiable and trafficable, creating permeability across the site and through a range of mixed-use opportunities including retail, hospitality, student services and informal study space. The site has excellent access to the Melbourne CBD, public transport and local amenities as well as proximity to the Faculties of Engineering as well as neighboring University of Melbourne cultural institutions; Carlton Connect Initiative and The Ian Potter Museum of Art. The site will also be proximate to the new Melbourne Metro station once operational.

3.3 Project Task

Given the complexity of the project, students were asked to prepare a project plan to de-risk the main construction phase of the project. The class assumed the completion of early works in the New Student Precinct site, and that the start of the main contractor tendering phase had commenced. The students were asked to write a report that include and identify any major risks, constraints or issues that may impact the project during the construction phase and confirm the major requirements and key tasks for the contractors and consultants. Further, students should also suggest methods to de-risk the project and provide proposals for methods of work and control, highlighting any innovative measures to be used. Draft resources required to de-risk the project should also be included such as Initial estimate of costs.

3.4 Project Brief and Teaching Considerations

In consideration the design of the capstone subject as well as nominating the project to be used, it is essential that the project is problem-based and project-based [7] as these are the essential experience that employers look for in graduates. Increased realism, professional relevance, involvement in specific roles, report writing [7] and a problem-based pedagogical approach [20] are essential qualities of a good capstone project. Some essential teaching considerations [7] that were considered includes the accessibility of online resources and guidelines, access to industry contacts and industry mentors—all of which was not a problem in this case.

3.5 Team Formation

In order to perform the project, the initial task was to form the student group. The students were given the flexibility to select their team members and it was encouraged to select members depending on the expertise and the experience in each engineering discipline depend on the project objectives. The Ice breaker activity was conducted as an initial step to identify and discuss the potential group members with their interests and experiences.

The NSP project team comprised of 4 members who had couple of years of experience in civil/structural engineering and construction management fields. An experienced tutor was assigned to the group to facilitate and monitor their progress and performance during the project.

4 Results and Discussion

Group projects provides students collaborative work in their learning and this type of projects develop student teamwork skills, leadership skills and encourage them to learn from one another [4]. This project provides students the opportunity to work as a team and use their specialised engineering knowledge into practice in a vibrant environment. This exercise created real industry exposure to students to work with their stake holders in a live project and student engagement in the project was highly evident.

The team was expected to conduct regular meetings among the members on project implementation, as well as with the assigned tutor weekly. Variety of assessment methods such as progress reports, posters, self-reflections, oral presentations and final reports were employed to minimize the limitations in some methods [5]. The progress and the performance of the team was continuously evaluated throughout the semester. The progression of the team was evaluated through progress reports and the achievement of the project was evaluated through a presentation, poster and a final report

at the end of the semester. The final report assessment includes the feasibility and functionality of the project outcome using different project management aspects such as resource manager, change management, sustainability and operational excellence etc.

The team provided 3 progress reports during the semester. The progress report consisted of highlights of major decisions they made, delays, targets against plans, achievements and any problems they faced, and measures taken to overcome those problems. This exercise enables students to a have similar experience as an industry project. Writing progress report is a method of communication and integration of communication modules that helps to increase engineering students' certain aspects of writing skills [12] that engineering students should improve.

The NSP project final report consisted of a managerial, planning and control solution for de-risking the entire project during construction phase. Students provided a risk management plan that includes risk assessment methodology, stakeholder engagement plan, overall methodology plan, project risk management plan and de-risking strategies. Further, they also formulated a detailed risk register, and suggested some prevention action and contingent actions for each risk within the risk registry. Students identified few limitations in the project and some recommendations were provided for implementations. In assessing the progress reports and final report, explanatory and diagnostic feedback was provided together with grades [5].

Students feedback on the project was received at the end of the semester and these demonstrated that, students are happy to be involved with co-created student projects that provide them to have a better insight of what University intentions are to improve the student experience. Students understands the importance of working in this type of projects and they experienced their contributions as stakeholders in the project. Students recognised the importance of cross disciplinary learning which is highly interrelated with team structure, dynamics and collaborative leaning process [9]. The student feedback also reflects some limitations on working in real engineering projects.

5 Conclusion

The paper described a successful implementation of a co-created student project in engineering management capstone subject. Co-created student projects are ideal for capstone subjects as students are already part of the stakeholders in the project. They get an insight of the importance of these type of projects in University education and they understand their role as students in University teaching and learning process. Student engagement was highly noticeable as results that they feel the importance of their contribution to the University teaching and learning process. So, they become more engaged as a result.

References

1. Akaka MA, Vargo SL, Lusch RF (2013) The complexity of context: a service ecosystems approach for international marketing. J Mark Res 21:1–20
2. Barrie SC (2004) Academics' understandings of generic graduate attributes: a framework for assuring quality. Australian Universities Quality Forum, Adelaide, Australia. http://www.auqa.edu.au/auqf/pastfora/2004/program/papers/Barrie.pdf
3. Ballantyne D, Varey RJ (2006) Introducing a dialogical orientation to the service-dominant logic of marketing. In: Lusch RF, Vargo SL (eds) The service-dominant logic of marketing. ME Sharpe, Armonk, pp 224–235
4. Baik C, Harris K-L (2008) Guidelines for effective group projects at the University of Melbourne. Available from: https://melbourne-cshe.unimelb.edu.au/__data/assets/pdf_file/0011/1761176/Guidelines_Group_Projects.pdf
5. CSHE (2003) Assessing learning in Australian Universities. Available from: http://www.ntu.edu.vn/Portals/96/Tu%20lieu%20tham%20khao/Phuong%20phap%20danh%20gia/assessing%20learning.pdf
6. Echeverri P, Skålén P (2011) Co-creation and co-destruction: a practice-theory based study of interactive value formation. Market Theory 11:351–373
7. Holdsworth A, Watty K, Davies M (2009) Developing capstone experiences. Centre for the Study of Higher Education, University of Melbourne
8. Razmdoost K, Mills G (2016) Towards a service-led relationship in project-based firms. Constr Manag Econ 317–334. Received 09 Feb 2015, Accepted 07 Jun 2016, Published online: 22 Jun 2016
9. Othman AR, Hussin, Hilmi, Mustapha, Mazli, and Parman, Setyamartana (2017) Cross-disciplinary team learning in engineering project-based: challenges in collaborative learning. In: 7th World Engineering Education Forum (WEEF), pp 866–871
10. Prahalad CK, Ramaswamy V (2004) Co-creation experiences: the next practice in value creation. J Interact Market 18:5–14
11. Smyth H, Fellows R, Liu A, Tijhuis W (2016) Editorial for the special issue on business development and marketing in construction. Constr Manag Econ 205–217. Published online: 07 Jul 2016
12. Teslenko T, Qi E (2012) Work in progress: integrating writing instruction in engineering courses, IEEE
13. University of Melbourne (2016) Executive summary concept & principles debrief presentation. https://students.unimelb.edu.au/__data/assets/pdf_file/0003/2564463/University-of-Melbourne-Student-Precinct-Revised-Executive-Summary-.pdf. Date accessed 30 October 2019
14. University of Melbourne (2019a) New student precinct, co-creation website. https://students.unimelb.edu.au/student-precinct. Date accessed: 31 October 2019
15. University of Melbourne (2019b) New student precinct, project. https://students.unimelb.edu.au/student-precinct. Date accessed: 31 October 2019
16. University of Melbourne (2019c) ENGM90016 engineering management capstone overview. https://handbook.unimelb.edu.au/2020/subjects/engm90016. Date accessed: 31 October 2019
17. University of Melbourne (2019d) Capstone subjects. https://ask.unimelb.edu.au/app/answers/detail/a_id/4250/~/capstone-subjects. Date accessed: 31 October 2019
18. Walton J, Murphy N, Deobhakta K (2017) De-risking construction projects, presentation at the NZILA Liability discussion group on 5th July 2017. http://www.nzila.org/wp-content/uploads/2017/07/De-Risking-Construction-projects.pdf. Date accessed: 31 October 2019/
19. Vargo SL, Lusch RF (2008) Service-dominant logic: continuing the evolution. J Acad Mark Sci 36:1–10
20. Zolin R (2008) How extreme problem-based learning aids transitioning out. In: Conference presentation, effective teaching and learning conference, Queensland University of Technology, October 2008